

SED

Student Experiment Documentation



Document ID: RX35_APEX_SED_v5-0_24Jun26

Mission: REXUS

Team Name: APEX
Experiment Title: **A**uroral **P**olarization **EX**plorer

Version:	Issue Date:	Document Type:	Valid from:
5.0	**24-06-2026**	**SED**	**24-06-2026**

Issued by:
APEX Student Team

Change Record

Version	Date	Changed Chapters	Remarks
1	19-01-2025	All	Finished Version SED v1-0
2	18-05-2025	 Section 1.1 Section 1.5 Chapter 2 Chapter 3 Chapter 4 Chapter 5 Chapter 6 ?? Chapter B Chapter C	Add List of Figures and List of Tables Updated modeling New members added Updated and reworked requirements Updated WBS, Gantt Chart, Resources, Risk Register Updated everything to latest design Updated requirements and tests Added include PDR feedback Update and elaborate Add engineering drawings, schematics and data sheets
2.1	06-07-2025	Section 4.4 Section 4.5 Appendix F.2	CDR Action 48 CDR Action 47 CDR Action 59
3	28-07-2025	Section 1.5 Chapter 2 and Section 5.1 Chapter 3 Section 4.1 Chapter 4 Section 5.2 Section 6.1.5 Section 7.5 ?? Chapter B Appendix C.2 Appendix C.3 Chapter F	add info on supporting extended team members reword some requirements update add general parts overview design updates testing list updates update and move excess detail to appendix Appendix F.3 add lessons learned include CDR feedback update outreach update designs update designs add appendix chapter for analysis and simulation reports
4	09-11-2025	Section 1.5 Chapter 3 Section 4.5 Section 4.7 Section 5.2 Chapter 6 ?? Chapter B Chapter E Chapter F	update team details update updated CAD and PCB screenshots updated power calculations testing list updates update include IPR feedback update outreach New Test Reports reorganize and update analyses
5	24-06-2026	most sections Chapter 3	change wording to reflect that the experiment has flown updated budget and risk register

continued from previous page

Version	Date	Changed Chapters	Remarks
		Section 4.4	updated pin puller muffler design
		Section 4.5	supplemented renderings with images
		Section 5.2	testing list
		Section 6.3	updated timeline
		Section 7.3	updated and filled in
		Chapter B	update outreach
		Appendix C.3	updated schematics to represent flight hardware
		Chapter E	New Test Reports

Contents

1 Introduction **3**
1.1 Scientific/Technical Background . . . 3
1.1.1 Aurora & Airglow . . . 3
1.1.2 Observation simulation . . . 5
1.2 Mission Statement . . . 6
1.3 Experiment Objectives . . . 7
1.4 Experiment Concept . . . 7
1.5 Team Details . . . 9
1.5.1 Contact Point . . . 9

2 Experiment Requirements and Constraints **10**
2.1 Functional Requirements . . . 10
2.2 Performance Requirements . . . 10
2.3 Operational Requirements . . . 11
2.4 Design Requirements . . . 12
2.5 Constraints . . . 14

3 Project Planning **15**
3.1 Work Breakdown Structure (WBS) . . . 15
3.2 Schedule . . . 21
3.2.1 Project Gantt Chart . . . 21
3.2.2 Social Media and Public Outreach Gantt Chart . . . 26
3.3 Resources . . . 27
3.3.1 Workforce . . . 27
3.3.2 Budget . . . 28
3.3.3 External Support . . . 29
3.4 Outreach Approach . . . 30
3.5 Risk Register . . . 31

4 Experiment Description **34**
4.1 Experiment Setup . . . 34
4.2 Experiment Interfaces . . . 42
4.2.1 Mechanical . . . 42
4.2.2 Electrical . . . 43
4.3 Experiment Components . . . 44
4.4 Mechanical Design . . . 46
4.4.1 Sub-systems of the mechanical design . . . 46
4.4.2 Bearings . . . 47
4.4.3 Camera Mounting . . . 49
4.4.4 Locking Mechanism . . . 50
4.4.5 Detailed Bearing preload Analysis (FEM) . . . 54
4.4.6 Detailed Vibration Analysis (FEM) . . . 55
4.5 Electronics Design . . . 60
4.5.1 Overview . . . 60

4.5.2 Backplane PCB . . . 61
4.5.3 Flight Computer PCB . . . 61
4.5.4 Inertial Measurement Unit (IMU) Sensor PCB . . . 62
4.5.5 Blackbox PCB . . . 63
4.5.6 Blackbox . . . 64
4.5.7 Sun Sensors . . . 64
4.5.8 Magnetometer . . . 67
4.5.9 Motor Driver PCB . . . 68
4.5.10 Encoder . . . 69
4.5.11 Motors . . . 70
4.5.12 Raspberry Adapter PCB . . . 70
4.5.13 Ethernet Switch and Adapter PCB . . . 71
4.5.14 Experiment Cameras . . . 73
4.5.15 Engineering Cameras . . . 73
4.5.16 Battery . . . 74
4.5.17 Radio Silence Concept . . . 76
4.5.18 Cable Reel . . . 76
4.5.19 Electric Shielding . . . 78
4.6 Thermal Design . . . 80
4.6.1 Operating Temperature . . . 80
4.6.2 Thermal FEM Analysis: Setup . . . 81
4.6.3 Thermal FEM Analysis: Results . . . 85
4.7 Power System . . . 86
4.8 Software Design . . . 87
4.8.1 State Machine . . . 88
4.8.2 Mission Control and Communication . . . 91
4.8.3 Raspberry Pi Software . . . 91
4.8.4 Motor Driver Software . . . 92
4.8.5 Attitude Determination . . . 93
4.8.6 Extended Kalman Filter for Attitude Calculation . . . 96
4.8.7 State Estimate . . . 97
4.8.8 Prediction . . . 97
4.8.9 Update . . . 97
4.9 Ground Support Equipment . . . 98
4.9.1 Functionalities . . . 98
4.9.2 Space Weather Monitoring . . . 98

5 Experiment Verification and Testing 99
5.1 Verification Matrix . . . 99
5.2 Verification Plan . . . 113
5.3 Verification Results . . . 121

6 Launch Campaign Preparation 128
6.1 Input for the Campaign / Flight Requirement Plans . . . 128
6.1.1 Dimensions and Mass . . . 128
6.1.2 Ground and Flight Safety Risks . . . 128
6.1.3 Electrical Interfaces . . . 129
6.1.4 Launch Site Requirements . . . 129
6.1.5 Flight Requirements . . . 130
6.1.6 Accommodation Requirements . . . 131
6.2 Preparation and Test Activities at Esrange . . . 131
6.2.1 Aurora Nowcast . . . 132

6.3 Timeline for Countdown and Flight . . . 133
6.4 Post-Flight Activities . . . 133

7 Data Analysis and Results 134
7.1 Data Analysis Plan . . . 134
7.2 Launch Campaign . . . 134
7.2.1 Flight preparation activities as they happened during the launch campaign 134
7.2.2 Flight performance/Flight report . . . 137
7.2.3 Aurora conditions on launch day . . . 138
7.2.4 Form and Amount of Data . . . 140
7.2.5 Possible failures and malfunctions, failure analysis . . . 141
7.2.6 Power consumption and Thermal behavior of the experiment . . . 145
7.2.7 Recovery (condition of experiment, re-usability, damages) . . . 145
7.2.8 Post-flight activities . . . 146
7.3 Results . . . 147
7.4 Input to Campaign Report . . . 151
7.5 Lessons Learned . . . 152

List of Figures v

List of Tables ix

Acronyms xi

Glossary xiii

References xiv

Appendix A: Experiment Reviews 155

Appendix B: Outreach and Media Coverage 156
B.1 APEX Video Series Part 1 . . . 156
B.2 Flyer . . . 157
B.3 Logo . . . 158
B.4 Newsletter . . . 159
B.5 Text on the TU-Graz Website . . . 159
B.6 Motion Expo Graz 2025 . . . 161
B.7 Article in Krone . . . 161
B.8 Recruitment Presentations . . . 162
B.9 Space Week St. Paul . . . 162
B.10 Unite! Network . . . 162
B.11 Article about APEX on the Webpage of the IWF (Space Research Center Austria) 163
B.12 Exhibitor at Graz in Space 2025 . . . 163
B.13 APEX Experiment and Post Flight presentation . . . 163
B.14 Yuri's night 2026 . . . 165
B.15 APEX Launch Video . . . 165
B.16 Lange Nacht der Forschung (Austrian long night of Sciences) 2026 . . . 165
B.17 27th ESA Symposium on European Rockets and Balloons in Trondheim, Norway 166

Appendix C: Additional Technical Information 169
C.1 Detailed Structural and Mechanical Calculations . . . 169
C.2 Engineering Drawings . . . 169
C.3 Electric Schematics . . . 196

C.4 PCB - Layout . . . 252
C.5 Datasheets . . . 252

Appendix D: Checklists **254**

Appendix E: Detailed Test Reports **255**
E.1 Minimal Prototype Test . . . 255
E.2 Optical Filter Transmissivity Degradation due to Vacuum Outgassing . . . 258
E.3 Locking Tests . . . 261
E.4 Mass Measurement . . . 278
E.5 Vibration Test . . . 279
E.6 Attitude Determination Test and Area Pointing Test . . . 290
E.7 Long Duration Test . . . 292
E.8 Flight Simulation . . . 293
E.9 Data Storage Endurance . . . 294
E.10 System Alignment Test . . . 297
E.11 Optical Polarization Test . . . 298
E.12 Gimbal Camera Test . . . 301
E.13 Arming Test . . . 305
E.14 Power Supply Test . . . 306
E.15 Blackbox Test . . . 307
E.16 Thermal Convection Test . . . 307

Appendix F: Analysis and Simulation **309**
F.1 Thermal Analysis . . . 310
F.2 Aurora Simulation . . . 311
F.3 Launch Time Analysis . . . 312
F.4 Pin Puller Calculations . . . 315
F.5 Motor Speed Calculations . . . 321
F.6 FEMA Reports . . . 324
List of Figures . . . 362
List of Tables . . . 364

Preface

The REXUS/BEXUS programme is realised under a bilateral Agency Agreement between the Deutsches Zentrum für Luft- und Raumfahrt (DLR) and the Swedish National Space Agency (SNSA). The Swedish share of the payload has been made available to students from other European countries through a collaboration with the European Space Agency (ESA). EuroLaunch, a cooperation between the Swedish Space Corporation (SSC) and the Mobile Raketen Basis (MORABA) of DLR, is responsible for the campaign management and operations of the launch vehicles. Experts from DLR, SSC, ZARM and ESA provide technical support to the student teams throughout the project. REXUS and BEXUS are launched from SSC, Esrange Space Center (Esrange) in northern Sweden.

Auroral Polarization EXplorer (APEX) was an experiment developed by a team of students from the University of Technology Graz, Austria. It aimed to demonstrate polarimetric measurements of the aurora borealis from above the atmosphere. APEX flew aboard REXUS 35 as part of cycle 16 of the Swedish-German program REXUS/BEXUS.

This document contains all relevant available information regarding APEX; including the experiment's objectives and requirements, a breakdown of the experiment design and the nosecone modification, design verification procedures, scientific background and a timeline. Technical documents that pertain to the design are also included for reference as appendix sections.

Abstract

The dancing bands of the aurorae, commonly known as polar lights, have long fascinated humanity. While being a spectacular natural light show, aurorae give a unique scientific opportunity to explore the interaction between Earth's magnetosphere and the solar wind. One of the lesser-understood phenomena in plasma physics is the polarization of auroral emissions.

In 2008, Lilensten et al. discovered the polarization of the red emission line using ground-based measurements. While other studies have continued to investigate the topic through measurements directly from aurora [Lilensten et al. (2008, 2013, 2015), Bosse et al. (2022)] and under laboratory conditions [Bourgeois et al. (2022)], several unanswered questions and interests persist.

The Auroral Polarization EXplorer (APEX) aimed to demonstrate polarimetric measurements of the aurora borealis from above the atmosphere. This shall be done outside Earth's atmosphere to avoid the influence of Rayleigh and/or Mie scattering on the measurements. The main part of the instrument was a three-axis stabilized camera platform capable of measuring up to two different auroral emission lines at a time. The combination of the gained data with the rocket's attitude and the position of the auroral oval at the time of the launch was planned to give a 3D origin of the measured emission, providing valuable input for the processes in Earth's thermosphere.

1 Introduction

1.1 Scientific/Technical Background

One of the lesser-understood phenomena in plasma physics is the polarization of auroral emissions. Lilensten et al. [1] discovered that the red emission line is polarized using ground-based measurements. While other studies have continued to investigate the topic through measurements directly from aurorae [1], [2], [3], [4] and under laboratory conditions [5], several unanswered questions and interests persist.

The origin of the polarization, for instance, is still unclear. Quantum mechanical models forbid the polarization of the green emission line at their origin [6]. Nevertheless, observations suggest a polarized green line [4]. Another reason for the interest is that auroral polarization parameters can help to constrain models of the thermosphere [2] and further be used for space weather studies [7]. Further, processes suggested by Bosse et al. [8], namely the polarization of light by ionospheric currents, could also apply to airglow, polarizing it as well. So far, only earthbound observations have been made, and the effect of Rayleigh and/or Mie scattering of auroral light on the observation could not be determined [1], [8]. Therefore, Auroral Polarization EXplorer (APEX) was planned to contribute to the study of the auroral line polarization, confirming or disproving results from previous ground-based observations.

1.1.1 Aurora & Airglow

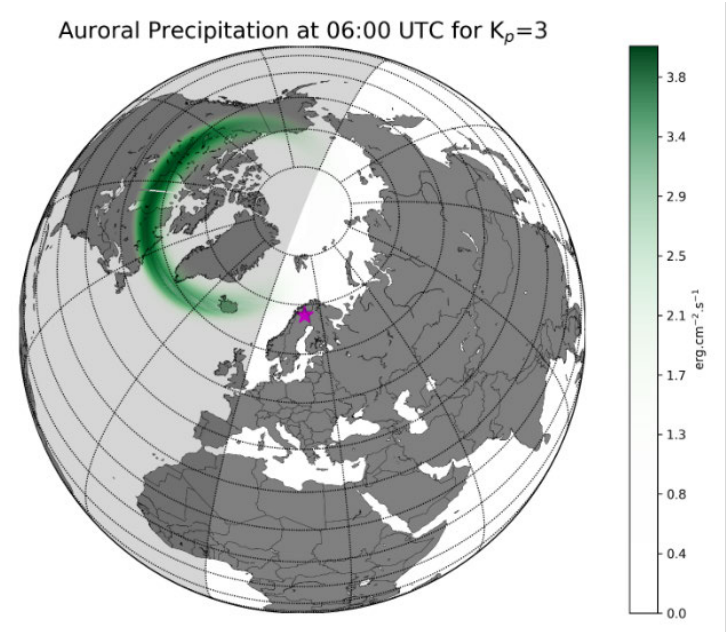


Figure 1.1: Electron precipitation rate of the auroral oval at 06:00 UTC with a Kp index of 3. Kiruna is marked by a purple star. Model by Zhang and Paxton [9]

Aurora emissions are caused by energetic charged particles hitting the upper atmosphere. Due to the structure of Earth's magnetic field, this occurs in an oval around the poles called the auroral oval. Figure 1.1 shows the averaged electron precipitation rate. How electrons dissipate their energy when encountering the atmosphere is modeled according to [10], [11]. From this, we can calculate the volume emission rates of the aurora as shown in Figure 1.2. As the exact time of launch and the space weather conditions at that time were not known in advance, analysis was conducted for different conditions to estimate the required exposure times and target region. Further detail can be found in Section 4.9.2 and Appendix F.2.

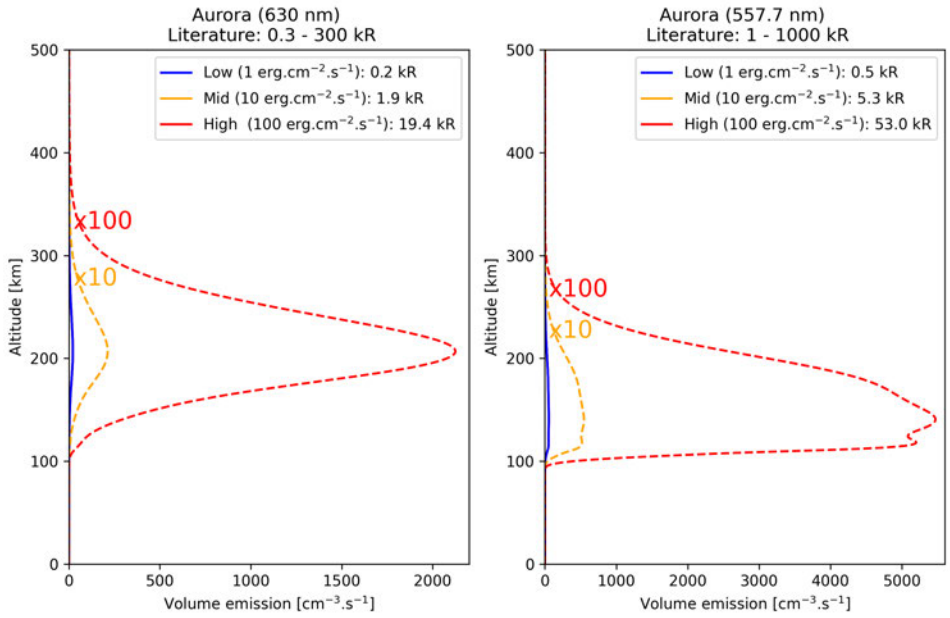


Figure 1.2: Calculated aurora volume emission rates (altitude profile) for the 630 nm (red) and 557.7 nm (green) line for three cases of low (1 erg/cm^2/s), medium (10 erg/cm^2/s) and high (100 erg/cm^2/s) electron precipitation rates.

Airglow is an emission of light by the atmosphere. On the dayside (dayglow), it is stimulated by solar UV radiation, photoelectrons, thermally by neutral particles, ions and electrons, and chemical reactions [12]. On the nightside, a fainter nightglow is present, stimulated by the background of energetic particles. Airglow volume emission rates are taken from literature [12], [13], [14]. Further analysis on the variability of dayglow depending on the solar zenith angle or solar EUV and UV flux were conducted.

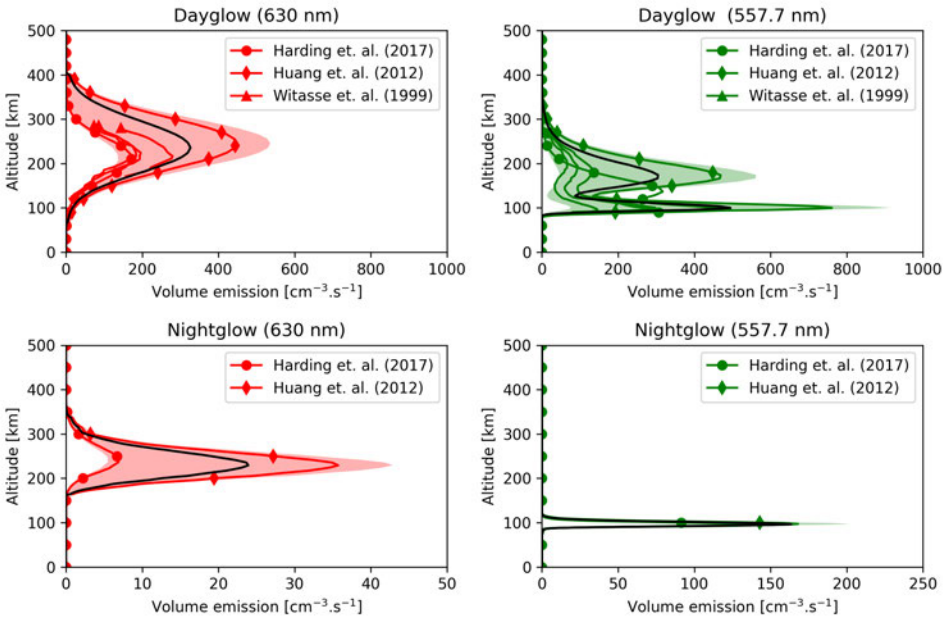


Figure 1.3: Volume emissions rates for dayglow and nightglow for the red and green emissions lines. Data taken from [12], [13], [14]

1.1.2 Observation simulation

To get a preliminary observation simulation, the volume emission rates of aurora (with a simulated 1% polarization signal) and airglow (unpolarized) (Figures 1.2 and 1.3) are integrated along a line of sight. The resulting simulated image for the example conditions of 06:00 UTC and Kp 3 is shown in Figure 1.4. Binning pixel down to a spatial resolution of 3 by 3 degrees (comparable to pervious ground-based observation) reduces the uncertainty in the degree of polarization (Q/I) low enough to enable concluding on the presence (or not) of auroral polarization at the 1% level (see Figure 1.5). Considering an entrance aperture radius of 5 mm for the lens, exposure times of 3 to 6 s are required to achieve this accuracy. This analysis were carried out for various geomagnetic conditions and different times of day (and night). Further notes on how the models were used on launch day to conduct an aurora nowcast are found in Section 6.2.1.

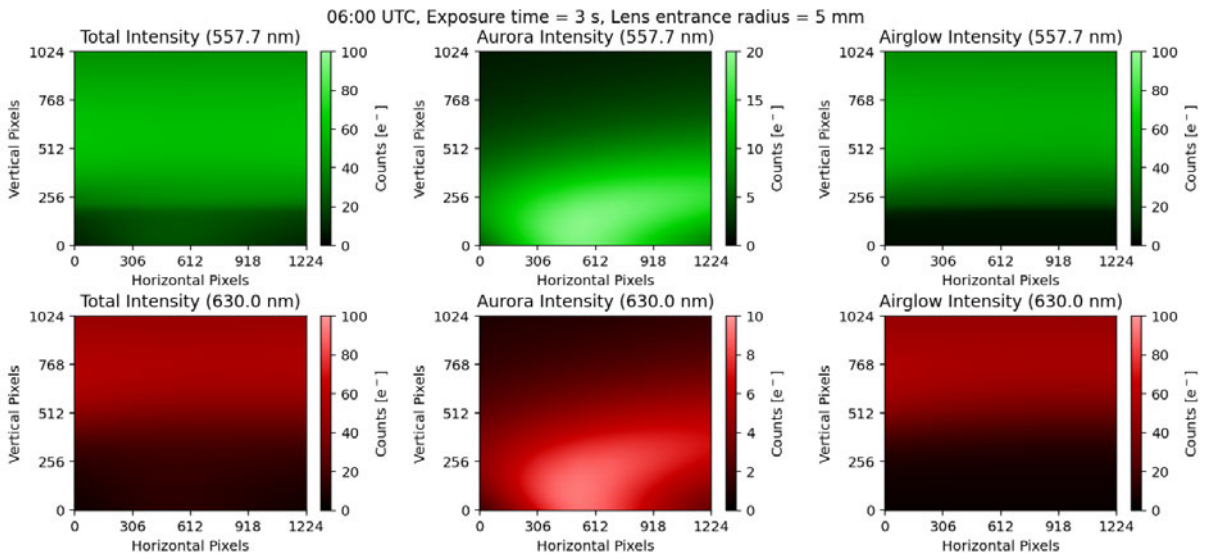


Figure 1.4: Observation simulation of a 3 s exposure at 06:00 UTC with Kp 3. The images in the middle and right column show the contributions of aurora and airglow respectively for the red and green emission lines. The combined signal is shown on the left.

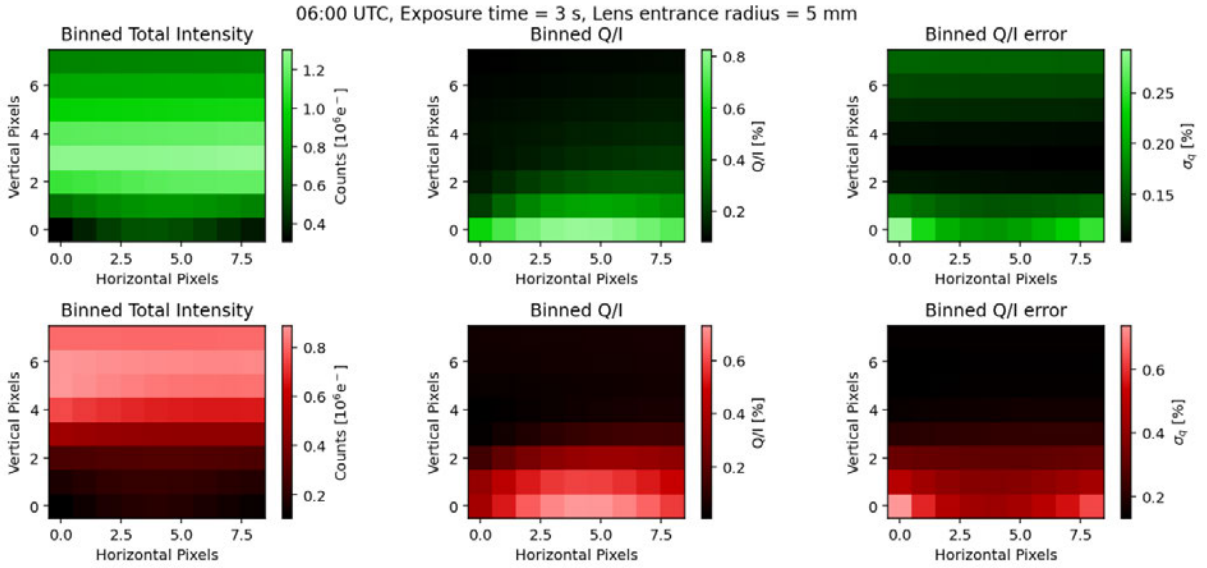


Figure 1.5: Observation simulation of a 3 s exposure at 06:00 UTC with Kp 3 with pixel binning. Left column shows the total intensity, middle the degree of polarization Q/I and the right column the Q/I error

1.2 Mission Statement

Auroral Polarization EXplorer aimed at achieving the first polarimetric measurements of the aurora borealis from above the atmosphere. Former studies have only been conducted via ground-based measurements [1], [2], [3], [4]. These studies noted the importance of obtaining measurement data from above the atmosphere to avoid scattering processes and their effect on polarization. Therefore, we planned to perform the first measurements of aurora/dayglow polarization from a sounding rocket.

1.3 Experiment Objectives

Scientific Objectives

Obj.1: Measure the total intensity, amount of linear polarization and angle of linear polarization of the auroral oval; equivalent to measuring the first three Stokes parameters

Obj.2: Measure at least one emission line of the auroral oval/airglow layer and at best two

Technical Objectives

Fulfilling the scientific objective with a sufficient signal-to-noise ratio requires a long exposure time. This comes with multiple technical challenges:

Obj.3: Design a (multi-) camera system being able to measure the first three Stokes parameters and filter the wavelengths of interest

Obj.4: Design of a three-axis stabilized camera system that tracks the target region during the flight.

Obj.5: Implement a tracking software using multiple sensor inputs (e.g. sun tracker, gyro and magnetometer data) to keep the camera pointed during the duration of each exposure.

Obj.6: Store the collected data to retrieve it after landing.

The expected emissions were a mixture of aurora and/or airglow emissions, depending on geomagnetic conditions and the time of launch. Because a launch at a specific time with significant aurora activity cannot be guaranteed, this mission was designed as a demonstrator mission. Its success is assured when the technical objectives are met (even though no aurora measurement was conducted).

Furthermore, measurements of the polarization of thermospheric airglow have not been performed from the ground nor from space, and therefore holds scientific interest. It is to be noted that the measurement of the thermosphere dayglow also requires a 3-axis stabilized gimbal, as the camera must remain in the same attitude during one exposure.

1.4 Experiment Concept

The experiment was based on polarization cameras mounted at the top of the three-axis stabilized gimbal.

Two PHX050S1-P/Q cameras (see Figure 1.6) with on-chip polarization filters (Sony IMX264MZR/MYR CMOS) were used. Groups of four pixels have linear polarization filters placed on the CMOS, at 0°, 45°, 90° and 135° respectively. This can be seen in Figure 1.7. Each camera were preceded by a narrow band filter for the 557.7 nm (green) and 630.0 nm (red) emission lines respectively (10 nm full width at half maximum).



Figure 1.6: Image of the polarization camera

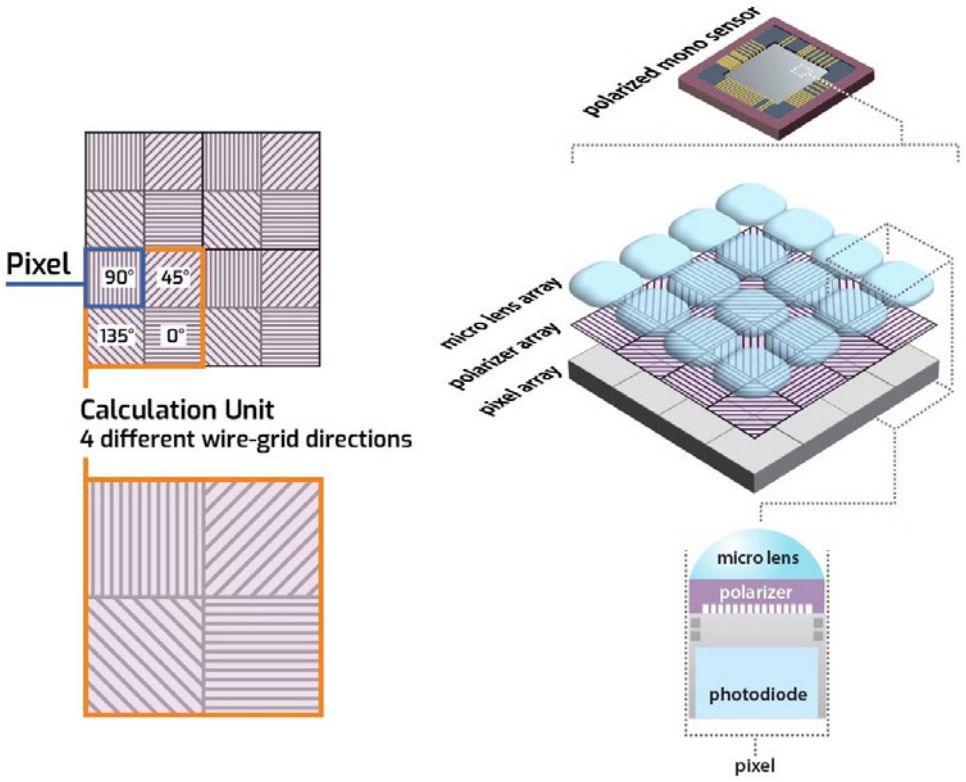


Figure 1.7: Pixel Array Scheme

The measured intensities for each of the four polarization angles were planned to be used to get the desired Stokes parameters: S_0, S_1 and S_2. The measurement of the degree of circular polarization in the light, represented by S_3, was not included in this experiment.

In addition to this, one more camera without on-chip polarization filters was included for outreach purposes and to provide a context-reference image of the observation.

1.5 Team Details

1.5.1 Contact Point

Postal Address: Aerospace Team Graz (ASTG)
Graz University of Technology
Infeldgasse 16b / ICEG094
8010 Graz
Austria

Team Email Address: APEX@astg.at

2 Experiment Requirements and Constraints

AD 1: Applicable Document Rexus User Manual

2.1 Functional Requirements

F-1 : The experiment shall be able to image a target region of the auroral oval and airglow layer. (Obj. 1, Obj. 2, Obj. 3, Obj. 4, Obj. 5) (formerly: F-1+F-2)

F-2 : The experiment shall measure the intensity, degree and angle of linear polarization of the incoming 557.7 nm light. (Obj. 1, Obj. 2) (formerly: F-3)

F-3 : The experiment shall measure the intensity, degree and angle of linear polarization of the incoming 630 nm light. (Obj. 1, Obj. 2) (formerly: F-4)

F-4 : The experiment shall provide unpolarized footage in the VIS spectrum of the target region and its immediate surroundings (Used as reference footage). (Created) (formerly: F-5)

F-5 : The experiment shall be able to track the observation target by compensating for attitude changes. (Obj. 5)

F-6 : The experiment shall be able to acquire an initial attitude at start of observation. (Obj. 5)

F-7 : The experiment shall be able to 2-way communicate with the ground station via the Telecommand System during countdown. (Created) (formerly: F-14)

F-8 : The experiment shall be able to downlink data via the Rexus Service module during flight. (Created)

F-9 : Any moveable part shall be constrained (locked) in all axis during ascent. (Created)

F-10 : The experiment shall be able to store scientific data onboard. (Obj. 6)

F-11 : The experiment shall be able to store housekeeping data onboard. Housekeeping data includes timestamps, states, sensor data, attitude and gimbal positions (Obj. 6)

F-12 : The experiment should downlink science data during descent. (Created)

2.2 Performance Requirements

P-1 : The Degree of Linear Polarization shall be resolved with a resolution of 1% at 2-sigma (F-2, F-3) (formerly: P-1)

P-2 : APEX shall be able to expose the camera sensors for at least a 4 s duration. (P-1) (formerly: P-3)

P-3 : APEX shall have a minimum resolution of 3° (P-1) (formerly: P-4)

P-4 : The experiment shall be able to keep a stable pointing direction within 1° (Root-Mean-Square of Azimuth & Elevation) over the duration of the exposure (4 s). (F-5, P-3) (formerly: P-5)

P-5 : The initial attitude error at start of experiment shall be less than 5 ° (in a cone around the true attitude) (F-6)

P-6 : The relative attitude change shall be evaluated at least every 20 milli seconds (with 50 Hz) (P-5)

P-7 : The gimbal shall be able to move 420 ° in the rotation axis (P-5) (formerly: P-6)

P-8 : The cameras shall be able to move 420 ° in the rotation axis (P-5) (formerly: P-7)

P-9 : The camera shall have a range of motion 200 ° in its pitch direction (P-5) (formerly: P-8)

P-10 : Every Axis shall be able to accelerate with 120 °/s² (P-5)

P-11 : Every Axis shall be able to rotate with at least 360 °/s (P-5)

P-12 : APEX shall log the Housekeeping data transmitted over the CAN bus at least every 100 milli second (F-11) (formerly: P-9)

P-13 : The experiment shall be able to write 12 MB per second to the scientific data blackbox (F-10)

P-14 : The reference image camera shall record images with a frequency of 10 FPS (F-4)

P-15 : The reference image camera shall have a resolution of at least 1080 x 1080 pixel (F-4)

P-16 : The reference image camera shall have a field of view equal or larger than 50 ° (F-4)

2.3 Operational Requirements

O-1 : The experiment shall operate autonomously during flight. (Created) (formerly: O1)

O-2 : The experiment shall accept a request for radio silence at any time while on the launch pad. (AD 1 - Chapter 7.10)

O-3 : The gimbal shall move in safe position during descent phase to reduce the likelihood of damage to cameras (Created)

O-4 : The experiment shall be able to enter a secure mode after landing (pyros and sensitive equipment shall be disabled). (AD 1 - Chapter 3.5.4)

O-5 : The experiment shall be able to unlock the gimbal autonomously after Nosecone Separation. (Created)

O-6 : The experiment shall operate in a testing mode allowing the testing of the cameras via the 2 way communication prior to lift off (Created)

O-7 : Pyro shall be short circuited until Integration (SSC Regulations)

O-8 : Pyros shall be short circuited with a manually removable shunt during integration (ReBF tag) (SSC Regulations) (formerly: New)

2.4 Design Requirements

D-1 : The center of mass of the camera subsystem shall align with the gimbal rotation axis to within 20mm once mounted (AD 1 - Chapter 5.12) (formerly: D3)

D-2 : The mounting structure shall be able to withstand 20g of longitudinal acceleration during Launch (AD 1 - Chapter 5.10) (formerly: D4)

D-3 : The gimbal structure shall be able to withstand 20g of acceleration in all directions during the reentry phase (AD 1 - Chapter 5.10)

D-4 : The gimbal shall withstand vibration profile of REXUS flight (Defined in Qualification and Acceptance according to Table 10.2 in AD 1: REXUS Manual (AD 1 - Chapter 10.3) (formerly: D5)

D-5 : The experiment shall be able to withstand the expected loads during prelaunch handling (Low shock movement in 1 g environment in arbitrary orientation) (Created)

D-6 : The data storage shall survive a nominal landing with 8m/s (D-28) (formerly: D19)

D-7 : The data storage shall be able to survive -30° C after landing (D-28) (formerly: D20)

D-8 : The data storage shall be able to survive being submerged in molten snow after landing (D-28) (formerly: D21)

D-9 : Design shall not exceed a mass of 7,5 kg (C - 1) (formerly: D7)

D-10 : The total cell capacity shall be well below 20 Wh (AD 1 - Chapter 7.11.2) (formerly: D6)

D-11 : The batteries shall be accessible by using one tool in under 10 minutes in the case of no nosecone or other experiment section attached (Created) (formerly: D17)

D-12 : Batteries shall be used to overcome the power limitations of the RXSM supply line. (Created) (formerly: D18)

D-13 : Batteries should be calculated with a maximum of 80% capacity used (AD 1 - Chapter 7.11.1) (formerly: D26)

D-14 : The APEX power management system shall be able to use voltages between 24 and 36 V (AD 1 - Chapter 7.7.4) (formerly: D22)

D-15 : The mean power drawn by the experiment per service line shall not exceed 30 W (AD 1 - Chapter 7.7.4)

D-16 : The experiment shall not consume more than 3 Amps for more than 500ms from the Rexus Service Line. (AD 1 - Chapter 7.7.4) (formerly: D23)

D-17 : The experiment shall not consume more than 20 Amps for more than 100us from the Rexus Service Line. (AD 1 - Chapter 7.7.4) (formerly: D24)

D-18 : The experiment shall limit feedback ripples over the power line to a maximum of 100mVpp (AD 1 - Chapter 7.7.4) (formerly: D25)

D-19 : All metal parts of the experiment shall be connected to a common ground (AD 1 - Chapter 7.13.5)

D-20 : The transmittance of the optical system shall be not degraded by more than 10 % by the vacuum environment at apogee (P1) (formerly: D33)

D-21 : The science cameras shall be aligned within 1° (P-6)

D-22 : The reference camera shall be aligned within 5° with the science cameras (F-4)

D-23 : The Attitude shall be given as the quaternion between Earth Centered Inertial (ECI)-frame and body frame (Created)

D-24 : The body frame of the gimbal shall be aligned with the body frame of the rocket (AD 1 - Chapter 4.2)

D-25 : Every axis shall be able to move independently (F-1) (formerly: F15)

D-26 : The pyro system shall be triggered by a REXUS Pyro line (Created)

D-27 : The Pyrotechnic Gas Generator (E- Match) shall have a no fire current of >= 1 A (Esrange Safety Manual (ESM) v10, §5.3.4)

D-28 : The Pyrotechnic Gas Generator (E- Match) shall have an all fire current of <= 10 A (Created)

D-29 : The Pyrotechnic Gas Generator (E- Match) shall have an internal resistance of no more than 2.2 Ohm (Created)

D-30 : The pyrotechnic pin puller shall retain/contain all solid parts larger than 10mm³ (e.g. plastic latches, pyro bolt) (Created)

D-31 : Reaction forces from gas outlets should be minimized by using at least two openings located symmetrically on the module. (AD 1 - Chapter 5.4)

D-32 : The gimbal shall use HELICOIL thread inserts with M5 for the connection to the baseplate (AD 1 - Chapter 5.1)

D-33 : The screws connecting the Gimbal to the baseplate shall be : Hexagon socket head cap screw (ISO 4762, DIN 912), M5 x 16 mm, Material: Steel 8.8 galvanized (AD 1 - Chapter 5.1)

D-34 : The tightening torque for the M5 screws connecting gimbal and baseplate shall be 7 Nm. (AD 1 - Chapter 5.1)

D-35 : The Raspberry Adapter PCB shall be accessible by removing no more than 6 screws with the same tool (Created) (formerly: D12)

D-36 : The Flight computer PCB shall be accessible by removing no more than 6 screws with the same tool (Created) (formerly: D13)

D-37 : Sun Sensor and Magnetometer PCBs shall be replaceable with no more than 6 screws with the same tool (Created) (formerly: D14)

D-38 : The experiments electrical interface shall be the D-SUB 15 male connector. (AD 1 - Chapter 7.7.1) (formerly: D15)

D-39 : The pins of the D-SUB 15 connector shall use the pin layout defined in the REXUS manual (D-15) (formerly: D16)

D-40 : APEX should be connected by either an optocoupler device or a relay to the REXUS signal lines (AD 1 - Chapter 7.7.6)

D-41 : The REXUS signal lines shall not be connected to a microcontroller directly (AD 1 - Chapter 7.7.7)

D-42 : Sun Sensor PCBs shall be connected to the Flight Computer PCB via CAN Bus (Created)

D-43 : APEX should produce a vibrational level of less than 5 x 10^-5 g_rms (0 - 25 Hz) (AD 1 - Chapter 5.11)

D-44 : The modules internal thermal dissipation shall not heat up the outer structure more than 10 °C about ambient temperature, tolerance is ± 5 °C. (AD 1 - Chapter 6.1.5.1)

D-45 : The modules internal thermal dissipation shall not heat up the parts close to or in contact with the feed-through cable to more than +70 °C. (AD 1 - Chapter 6.1.5.2)

D-46 : The modules internal thermal dissipation shall not heat up parts facing other modules to more than +50°C (AD 1 - Chapter 6.1.5.3)

D-47 : The heat transport by convection shall be limited in such a way that the air temperature at the module interfaces does not exceed the ambient temperature by more than 10 °C. (AD 1 - Chapter 6.1.5.4)

D-48 : The mounting structure shall provide sufficient thermal capacity and conductivity to keep the temperature in the specified operating temperature range of -10°C to 55°C (AD 1 - Chapter 10.2) (formerly: D2)

D-49 : The Gimbal shall function in the vacuum environment of 80 km altitude (AD 1 - Chapter 10.1)

D-50 : The payload structure shall not be used as signal or power return (AD 1 - Chapter 7.14)

D-51 : The center frequency of the emission lines shall be within the full width half max of the filters. (F-2, F-3) (formerly: P-2)

D-52 : The filter full width half max shall be smaller equal to 20 nm (F-2, F-3)

D-53 : The housekeeping data shall contain timestamps, states, sensor data, attitude and gimbal positions (F-12) (formerly:)

D-54 : The Blackbox PCB shall be accessible by removing no more than 6 screws with the same tool (Created)

D-55 : The Experiment Blackbox shall be accessible by removing no more than 6 screws with the same tool (Created)

D-56 : Magnetometer PCBs shall be connected to the Flight Computer PCB via SPI (Created)

2.5 Constraints

C-1 : The experiment shall not exceed a mass of 7.5 kg (REXUS)

C-2 : SI Units shall be used for calculations (AD 1 - Chapter 9.2)

C-3 : For structural analysis, values from ESA Material Handbooks, Werkstoffhandbuch der Deutschen Luftfahrt, Metallic Materials Properties Development and Standardization (MMPDS) Handbook, Etc. shall be used (AD 1 - Chapter 9.3)

C-4 : APEX shall request the permission of photos/videos publication to the following authorities: SSC and Lantmäteriet (AD 1 - Chapter 11.4)

3 Project Planning

3.1 Work Breakdown Structure (WBS)

The Work Breakdown Structure (WBS) is split into five major parts: Gimbal, Ground Testing Equipment, Testing, Project Management and Outreach. The Gimbal and Ground Testing Equipment WBS concern themself with the design, ordering, and manufacturing of the Gimbal and the Ground Support Equipment, as well as the Ground Testing Equipment. The testing WBS separates all the tests depending on the required subsystems for the test.

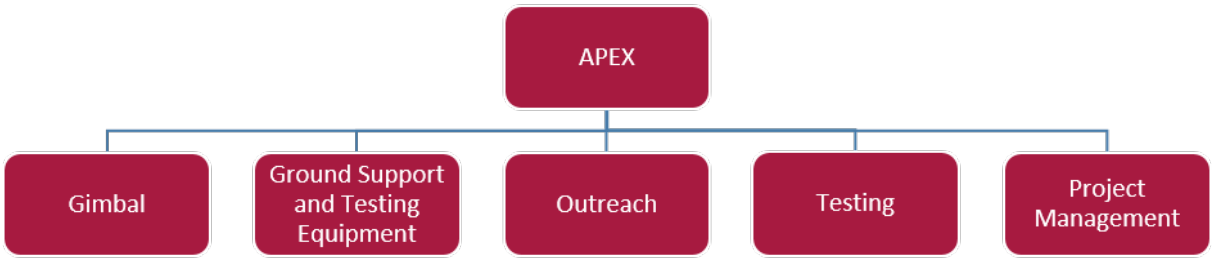


Figure 3.1: WBS of APEX.

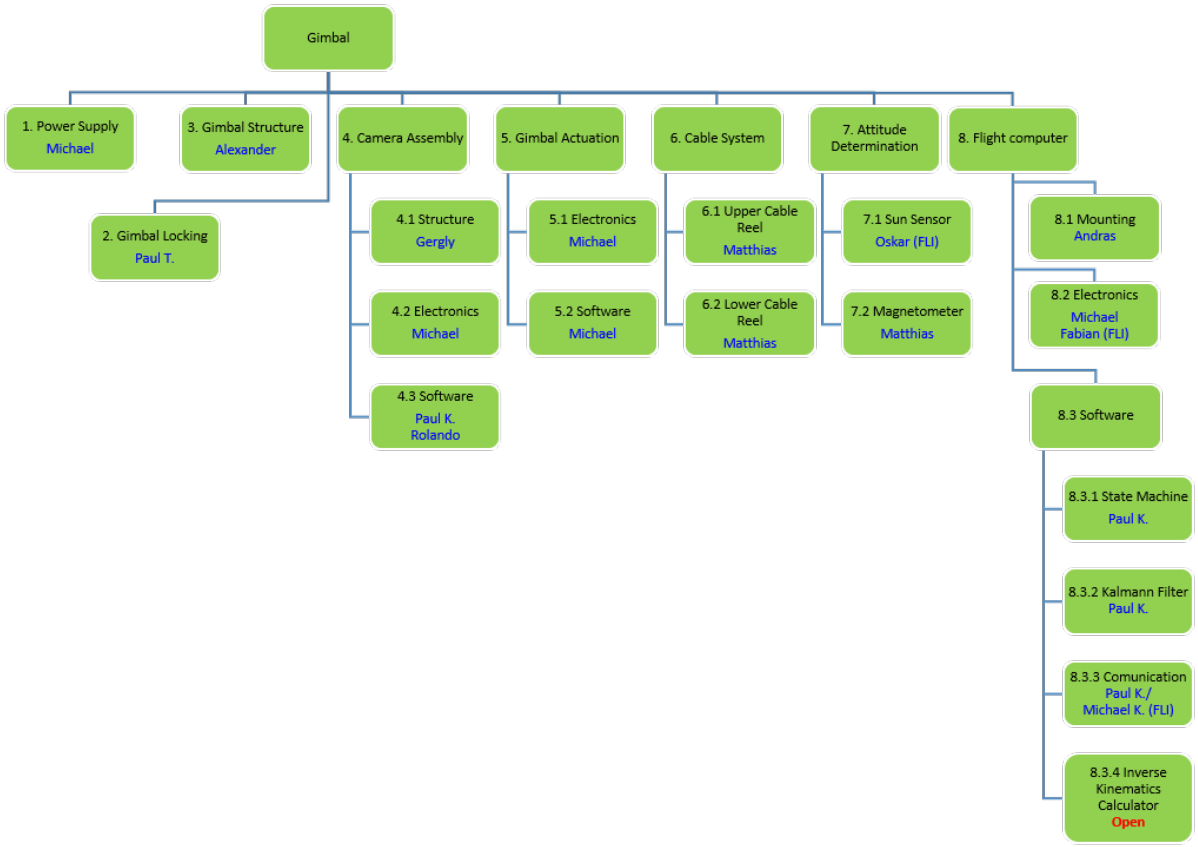


Figure 3.2: WBS of the Gimbal Hardware. Each Block contains a sublevel consisting of design, ordering, and manufacturing not shown here.

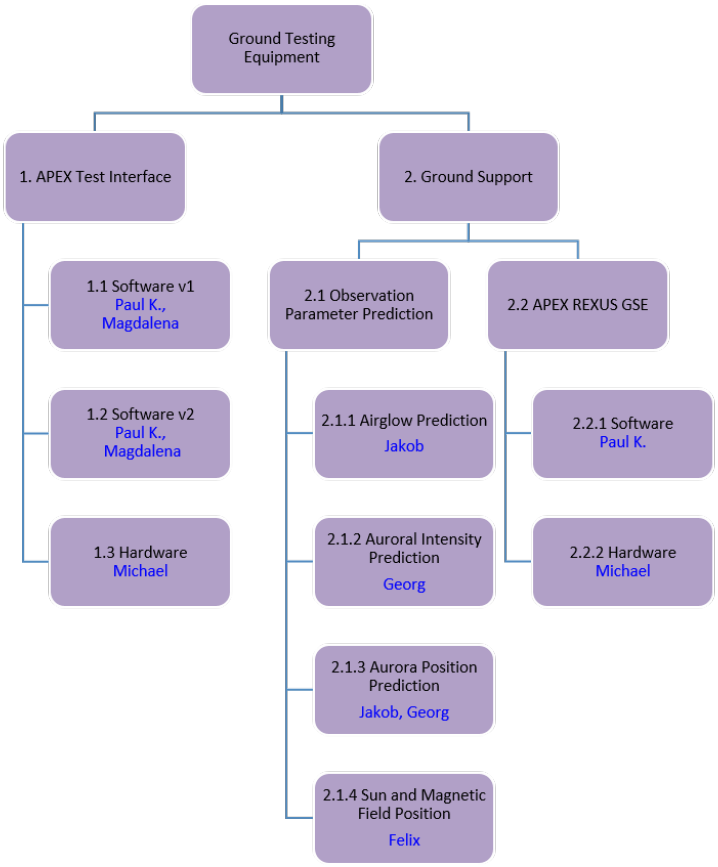


Figure 3.3: WBS of the Ground testing Equipment.Each Block contains a sublevel consisting of design, ordering, and manufacturing not shown here.

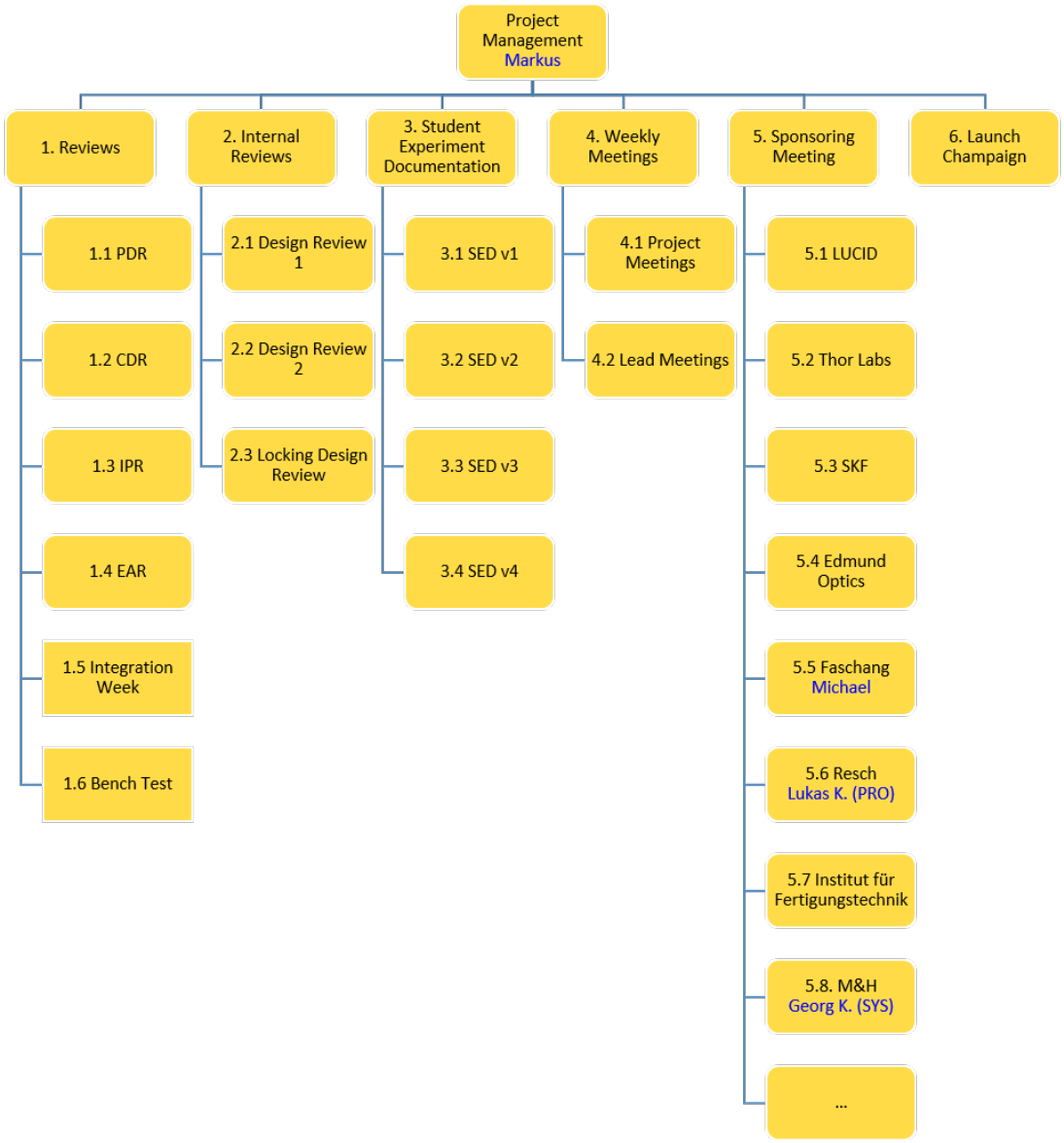


Figure 3.4: WBS for the Project Management

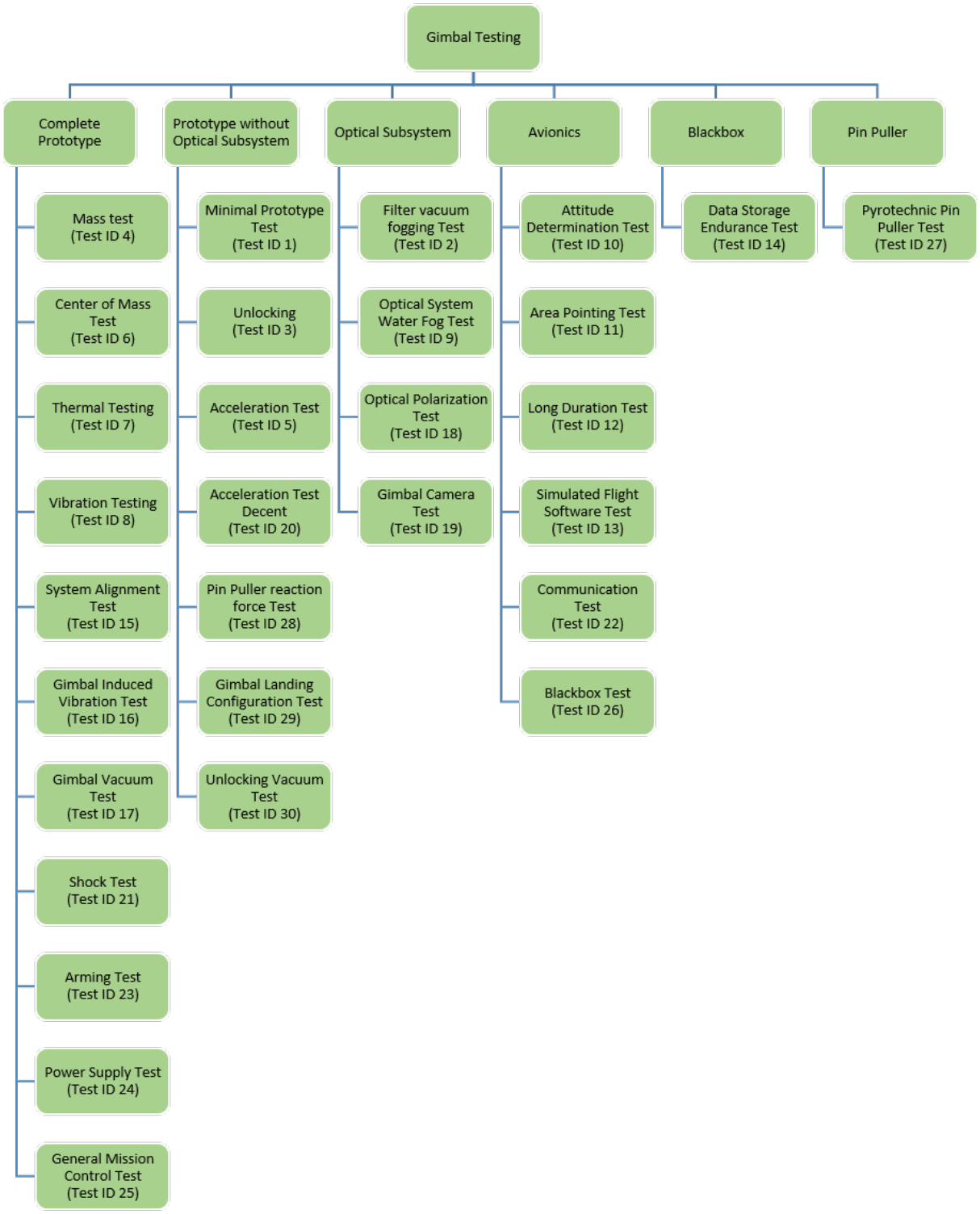


Figure 3.5: WBS of the testing and verification.

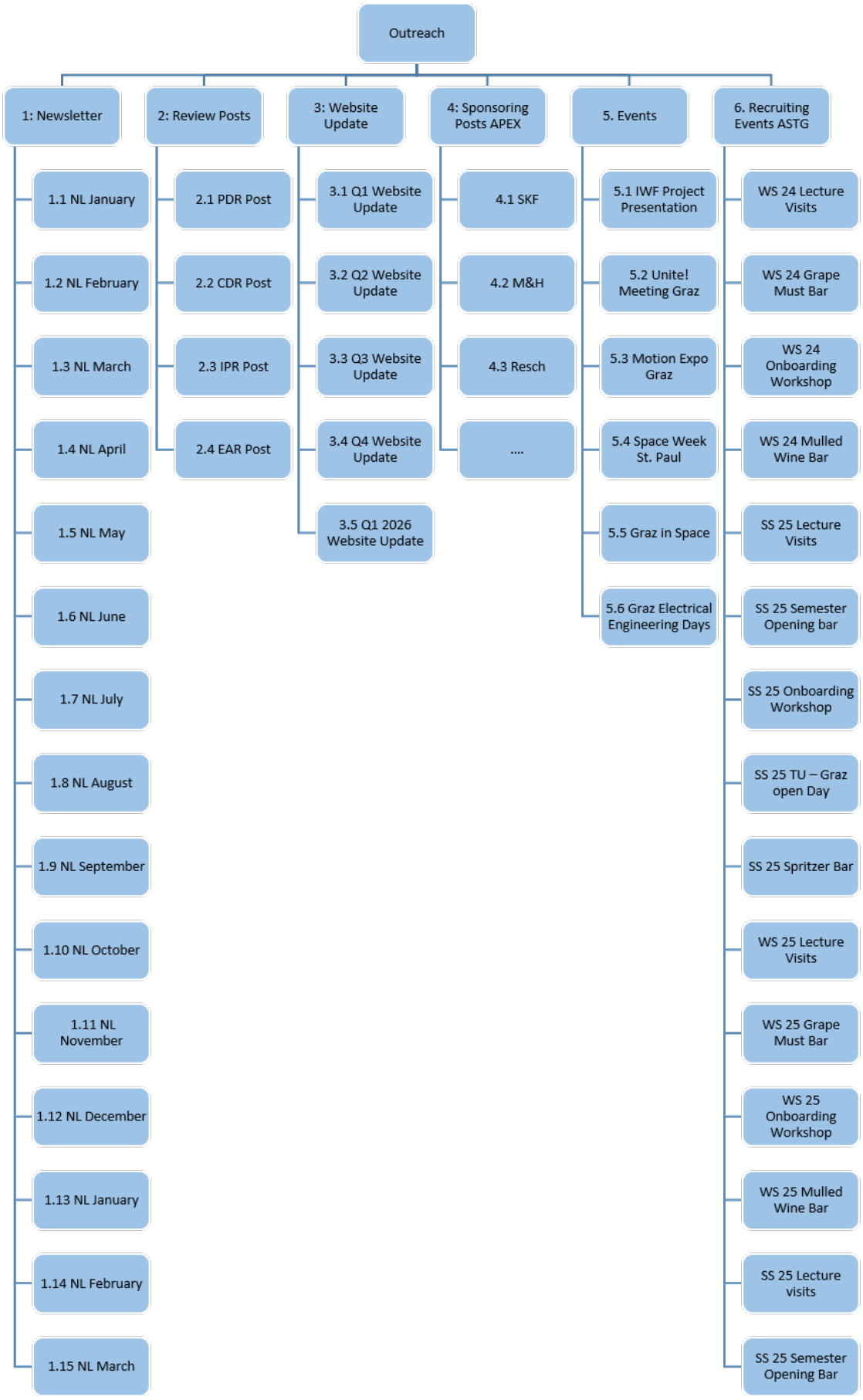
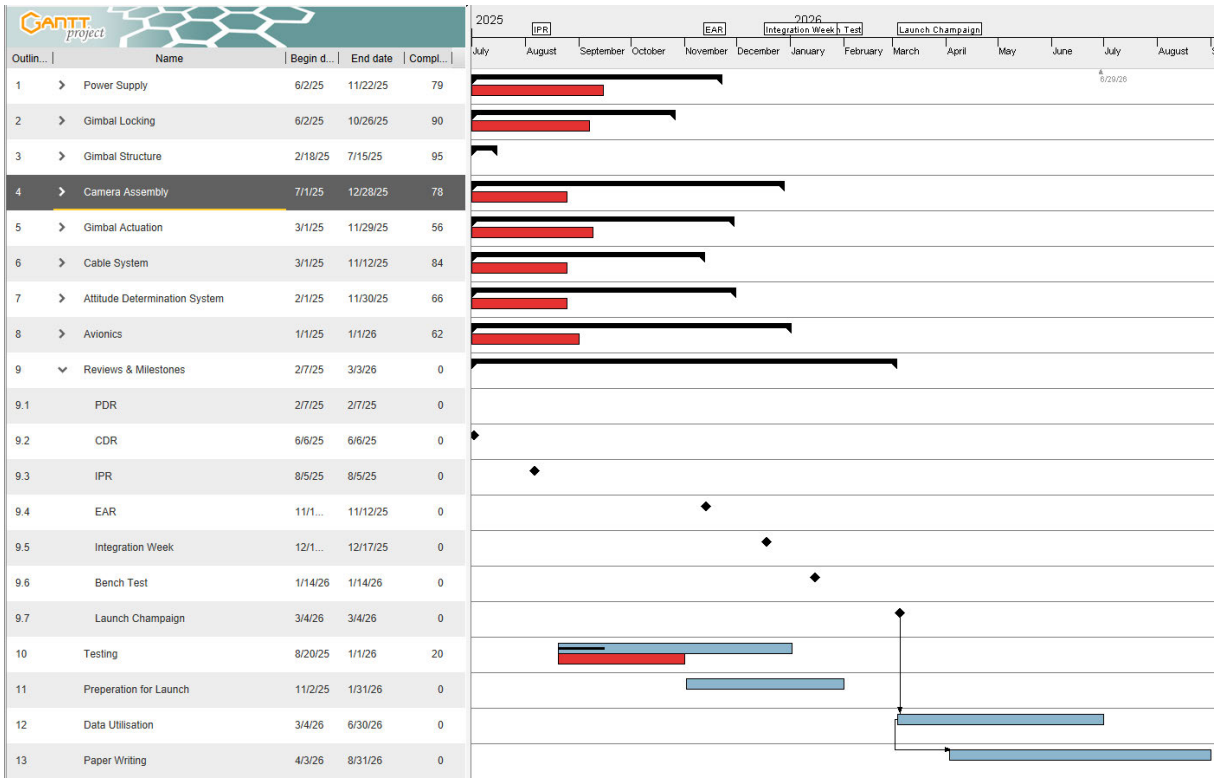


Figure 3.6: WBS for the Project Outreach and Recruting

3.2 Schedule

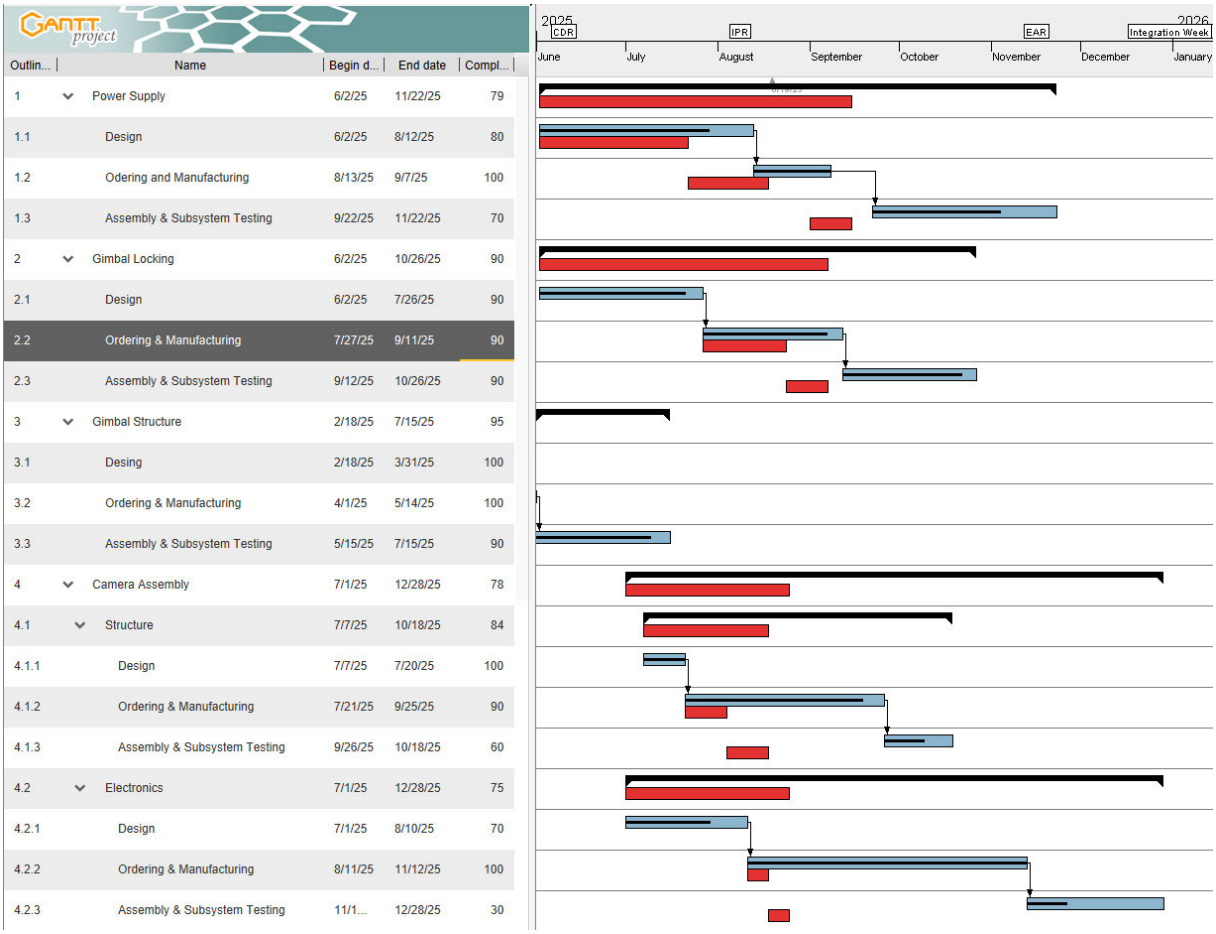
3.2.1 Project Gantt Chart

The Gantt chart for the project APEX is split into two parts and covers the time between February 2025 and July 2026. The red line gives the Baseline delivered at the IPR. The Test ID in the combined GANTT and testing list (Figure 3.12 to Figure 3.15) encodes, in addition, the status in the colour. Red is for scheduled but date not confirmed, green indicates finished successfully, blue indicates scrubbed tests, and yellow indicates scheduled and confirmed.



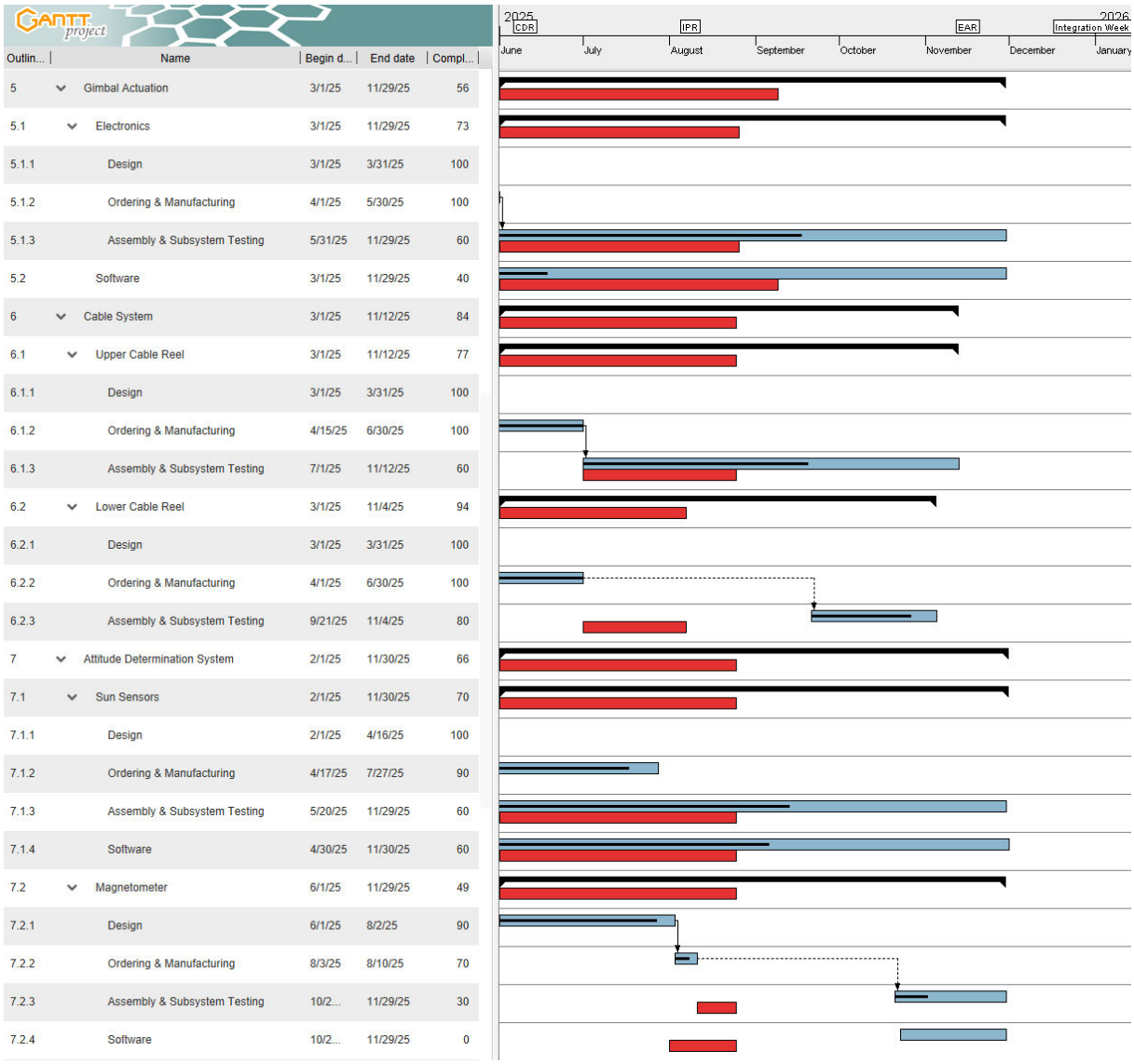
Outlin...	Name	Begin d...	End date	Compl...
1	Power Supply	6/2/25	11/22/25	79
2	Gimbal Locking	6/2/25	10/26/25	90
3	Gimbal Structure	2/18/25	7/15/25	95
4	Camera Assembly	7/1/25	12/28/25	78
5	Gimbal Actuation	3/1/25	11/29/25	56
6	Cable System	3/1/25	11/12/25	84
7	Attitude Determination System	2/1/25	11/30/25	66
8	Avionics	1/1/25	1/1/26	62
9	Reviews & Milestones	2/7/25	3/3/26	0
9.1	PDR	2/7/25	2/7/25	0
9.2	CDR	6/6/25	6/6/25	0
9.3	IPR	8/5/25	8/5/25	0
9.4	EAR	11/1...	11/12/25	0
9.5	Integration Week	12/1...	12/17/25	0
9.6	Bench Test	1/14/26	1/14/26	0
9.7	Launch Champaign	3/4/26	3/4/26	0
10	Testing	8/20/25	1/1/26	20
11	Preperation for Launch	11/2/25	1/31/26	0
12	Data Utilisation	3/4/26	6/30/26	0
13	Paper Writing	4/3/26	8/31/26	0

Figure 3.7: Reduced GANTT Chart for the full Project Duration



Outlin...	Name	Begin d...	End date	Compl...
1	Power Supply	6/2/25	11/22/25	79
1.1	Design	6/2/25	8/12/25	80
1.2	Odering and Manufacturing	8/13/25	9/7/25	100
1.3	Assembly & Subsystem Testing	9/22/25	11/22/25	70
2	Gimbal Locking	6/2/25	10/26/25	90
2.1	Design	6/2/25	7/26/25	90
2.2	Ordering & Manufacturing	7/27/25	9/11/25	90
2.3	Assembly & Subsystem Testing	9/12/25	10/26/25	90
3	Gimbal Structure	2/18/25	7/15/25	95
3.1	Desing	2/18/25	3/31/25	100
3.2	Ordering & Manufacturing	4/1/25	5/14/25	100
3.3	Assembly & Subsystem Testing	5/15/25	7/15/25	90
4	Camera Assembly	7/1/25	12/28/25	78
4.1	Structure	7/7/25	10/18/25	84
4.1.1	Design	7/7/25	7/20/25	100
4.1.2	Ordering & Manufacturing	7/21/25	9/25/25	90
4.1.3	Assembly & Subsystem Testing	9/26/25	10/18/25	60
4.2	Electronics	7/1/25	12/28/25	75
4.2.1	Design	7/1/25	8/10/25	70
4.2.2	Ordering & Manufacturing	8/11/25	11/12/25	100
4.2.3	Assembly & Subsystem Testing	11/1...	12/28/25	30

Figure 3.8: GANTT Chart for the Gimbal Part 1



Outlin...	Name	Begin d...	End date	Compl...
5	Gimbal Actuation	3/1/25	11/29/25	56
5.1	Electronics	3/1/25	11/29/25	73
5.1.1	Design	3/1/25	3/31/25	100
5.1.2	Ordering & Manufacturing	4/1/25	5/30/25	100
5.1.3	Assembly & Subsystem Testing	5/31/25	11/29/25	60
5.2	Software	3/1/25	11/29/25	40
6	Cable System	3/1/25	11/12/25	84
6.1	Upper Cable Reel	3/1/25	11/12/25	77
6.1.1	Design	3/1/25	3/31/25	100
6.1.2	Ordering & Manufacturing	4/15/25	6/30/25	100
6.1.3	Assembly & Subsystem Testing	7/1/25	11/12/25	60
6.2	Lower Cable Reel	3/1/25	11/4/25	94
6.2.1	Design	3/1/25	3/31/25	100
6.2.2	Ordering & Manufacturing	4/1/25	6/30/25	100
6.2.3	Assembly & Subsystem Testing	9/21/25	11/4/25	80
7	Attitude Determination System	2/1/25	11/30/25	66
7.1	Sun Sensors	2/1/25	11/30/25	70
7.1.1	Design	2/1/25	4/16/25	100
7.1.2	Ordering & Manufacturing	4/17/25	7/27/25	90
7.1.3	Assembly & Subsystem Testing	5/20/25	11/29/25	60
7.1.4	Software	4/30/25	11/30/25	60
7.2	Magnetometer	6/1/25	11/29/25	49
7.2.1	Design	6/1/25	8/2/25	90
7.2.2	Ordering & Manufacturing	8/3/25	8/10/25	70
7.2.3	Assembly & Subsystem Testing	10/2...	11/29/25	30
7.2.4	Software	10/2...	11/29/25	0

Figure 3.9: GANTT Chart for the Gimbal Part 2



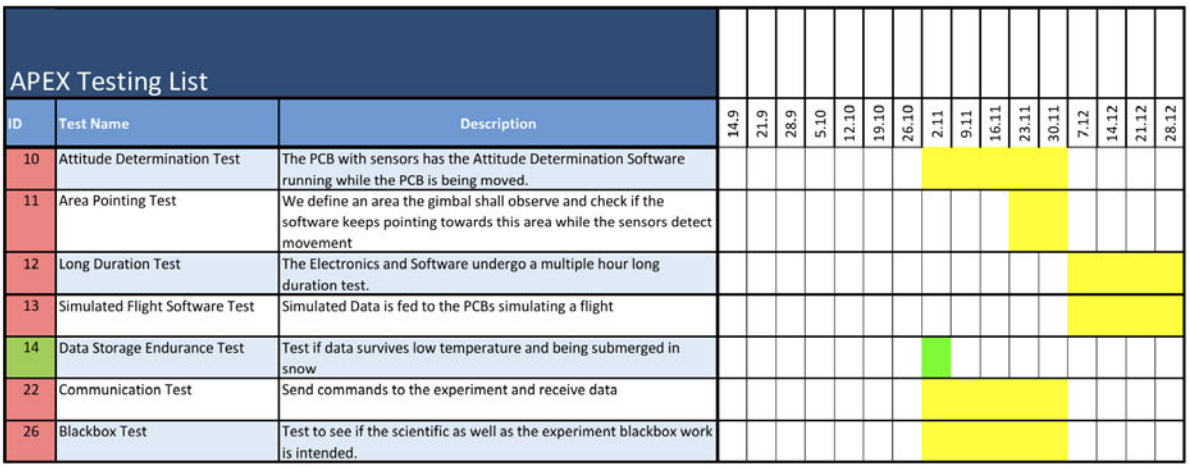
Outlin...	Name	Begin d...	End date	Compl...
8	Avionics	1/1/25	1/1/26	62
8.1	Mounting	6/1/25	11/22/25	70
8.1.1	Design	6/1/25	7/26/25	90
8.1.2	Ordering & Manufacturing	7/27/25	11/8/25	70
8.1.3	Assembly & Subsystem Testing	11/9/25	11/22/25	0
8.2	Electronics	3/2/25	12/7/25	78
8.2.1	Design	3/2/25	9/12/25	100
8.2.2	Ordering & Manufacturing	7/1/25	10/19/25	90
8.2.3	Assembly & Subsystem Testing	7/20/25	12/7/25	40
8.3	Software	1/1/25	1/1/26	50
8.3.1	State Machine	5/20/25	6/18/25	100
8.3.2	Attitude Determination (Kalman Fi...	1/1/25	12/31/25	60
8.3.3	Communication	7/1/25	12/3/25	60
8.3.4	Inverse Kinematics Calculator	7/27/25	1/1/26	10

Figure 3.10: GANTT Chart for the Gimbal Part 3



Outline...	Name	Begin date	End date	Compl...
1	APEX Test Interface	5/20/25	12/4/25	59
1.1	Software v1	6/2/25	9/26/25	80
1.2	Software v2	9/29/25	12/4/25	0
1.3	Hardware	5/20/25	6/27/25	100
1.3.1	Design	5/20/25	6/6/25	100
1.3.2	Ordering & Manufacturing	6/9/25	6/27/25	100
2	Groudn Support	3/3/25	1/2/26	66
2.1	Assembly & Subsystem Tes...	6/30/25	8/4/25	100
2.2	Obseervation Prediction Par...	3/3/25	1/2/26	75
2.2.1	Airglow Prediction	3/3/25	1/2/26	80
2.2.2	Auroral Intensity Prediction	6/2/25	1/1/26	80
2.2.3	Aurora Position Prediction	7/1/25	1/2/26	80
2.2.4	Sun and Mag. Field Predi...	9/1/25	10/22/25	20
2.3	APEX-REXUS GSE	10/1/25	12/2/25	0
2.3.1	Software	10/1/25	12/2/25	0
2.3.2	Hardware	10/1/25	12/2/25	0

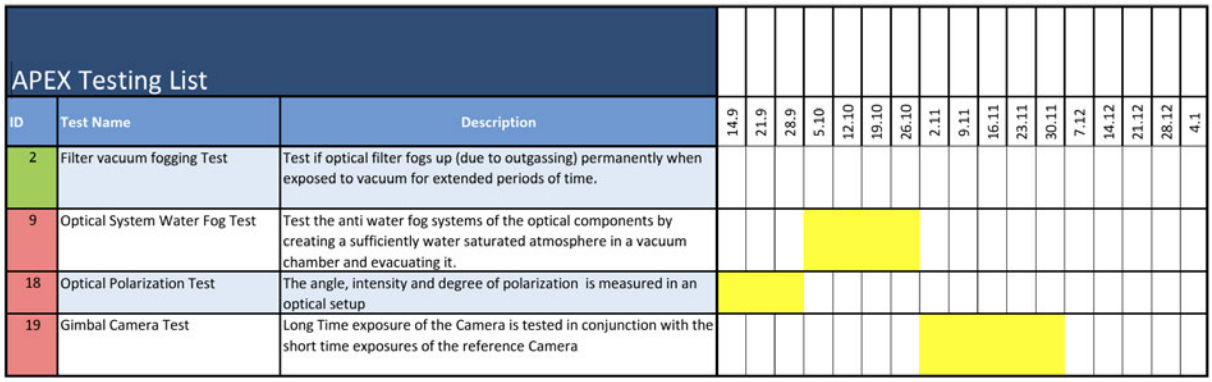
Figure 3.11: GANTT Chart for the GSE



APEX Testing List

ID	Test Name	Description
10	Attitude Determination Test	The PCB with sensors has the Attitude Determination Software running while the PCB is being moved.
11	Area Pointing Test	We define an area the gimbal shall observe and check if the software keeps pointing towards this area while the sensors detect movement
12	Long Duration Test	The Electronics and Software undergo a multiple hour long duration test.
13	Simulated Flight Software Test	Simulated Data is fed to the PCBs simulating a flight
14	Data Storage Endurance Test	Test if data survives low temperature and being submerged in snow
22	Communication Test	Send commands to the experiment and receive data
26	Blackbox Test	Test to see if the scientific as well as the experiment blackbox work is intended.

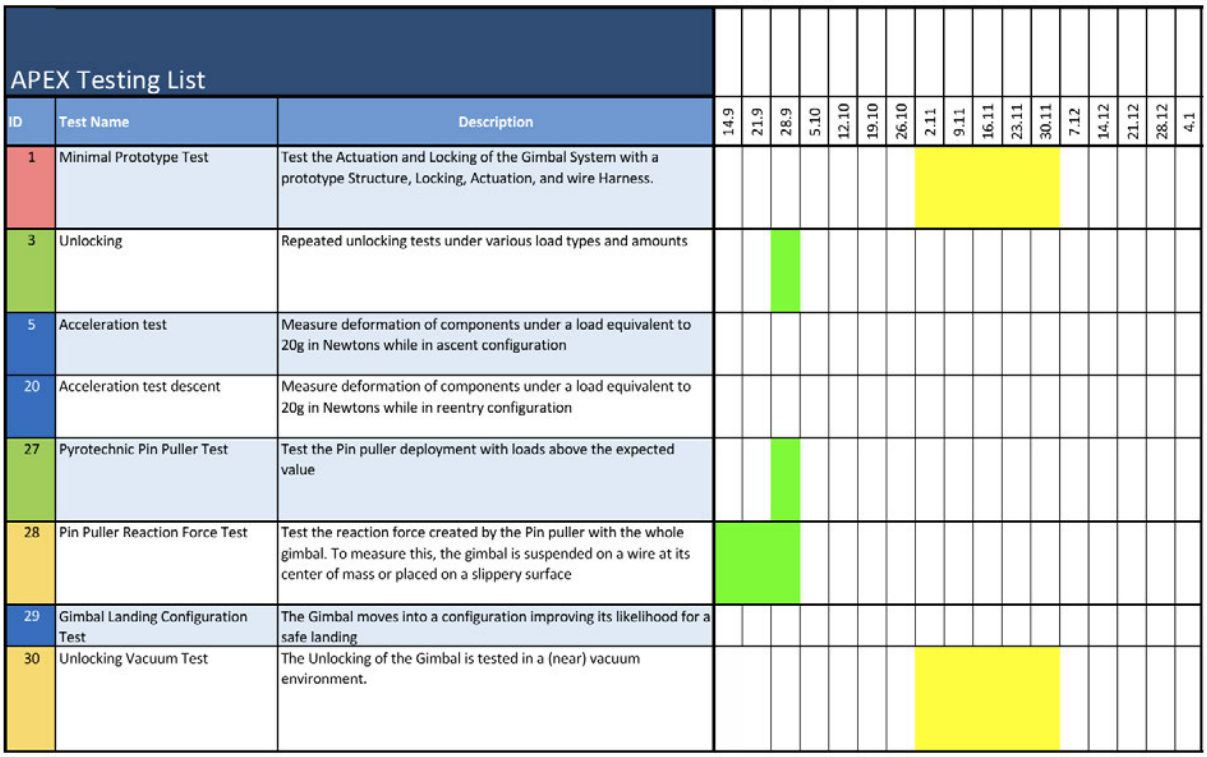
Figure 3.12: GANTT of the Tests with the Avionics system and Blackbox.



APEX Testing List

ID	Test Name	Description
2	Filter vacuum fogging Test	Test if optical filter fogs up (due to outgassing) permanently when exposed to vacuum for extended periods of time.
9	Optical System Water Fog Test	Test the anti water fog systems of the optical components by creating a sufficiently water saturated atmosphere in a vacuum chamber and evacuating it.
18	Optical Polarization Test	The angle, intensity and degree of polarization is measured in an optical setup
19	Gimbal Camera Test	Long Time exposure of the Camera is tested in conjunction with the short time exposures of the reference Camera

Figure 3.13: GANTT of the Tests with the Optical Subsystem.



APEX Testing List

ID	Test Name	Description
1	Minimal Prototype Test	Test the Actuation and Locking of the Gimbal System with a prototype Structure, Locking, Actuation, and wire Harness.
3	Unlocking	Repeated unlocking tests under various load types and amounts
5	Acceleration test	Measure deformation of components under a load equivalent to 20g in Newtons while in ascent configuration
20	Acceleration test descent	Measure deformation of components under a load equivalent to 20g in Newtons while in reentry configuration
27	Pyrotechnic Pin Puller Test	Test the Pin puller deployment with loads above the expected value
28	Pin Puller Reaction Force Test	Test the reaction force created by the Pin puller with the whole gimbal. To measure this, the gimbal is suspended on a wire at its center of mass or placed on a slippery surface
29	Gimbal Landing Configuration Test	The Gimbal moves into a configuration improving its likelihood for a safe landing
30	Unlocking Vacuum Test	The Unlocking of the Gimbal is tested in a (near) vacuum environment.

Figure 3.14: GANTT of the Tests without Optical Subsystem and the Pin Puller.

APEX Testing List

ID	Test Name	Description
4	Mass test	Measuring the weight of the entire assembly
6	Center of mass test	Measurement of the center of gravity of the whole assembly on all rotational axes
7	Thermal Vacuum Testing	Measuring the temperature of the gimbal inside a vacuum chamber after 180s of runtime
8	Vibration test	Vehicle level 1 Sine and Random Vibrations, with frequency search before and after. In thrust axis only. Vehicle level 1 Sine and Random Vibrations, with frequency search before and after. In thrust axis. Vehicle level 1 Random Vibrations, with frequency search before and after. In lateral axis.
15	System Alignment Test	Tests the alignment of the System with static pointing
16	Gimbal induced Vibration Test	The full Gimbal is actuated with acceleration sensors attached to the base plate to measure induced vibration
17	Gimbal Vacuum Test	The full Gimbal is operated in a Vacuum Chamber (both motors and Videos)
21	Shock test	Test the full Gimbal against schock
23	Arming Test	Test pyro short circuiting.
24	Power Supply Test	Test the power supply of the whole system for endurance.
25	General Mission Control Test	Test to see if all buttons in the mission control are working as intended.
31	Thermal Convection Test	The Gimbal is covered by a chamber simulating the nosecone volume, while the bottom of the module is thermally isolated against the ground below. Prelaunch Tests are done to test thermal increase of air temperature until it stabilizes

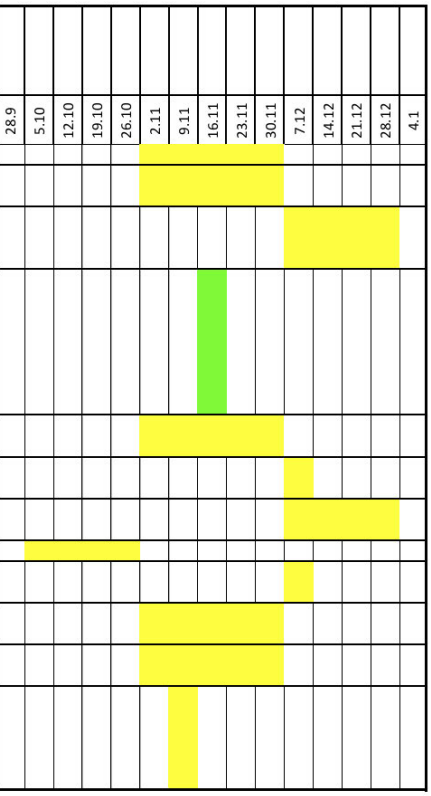
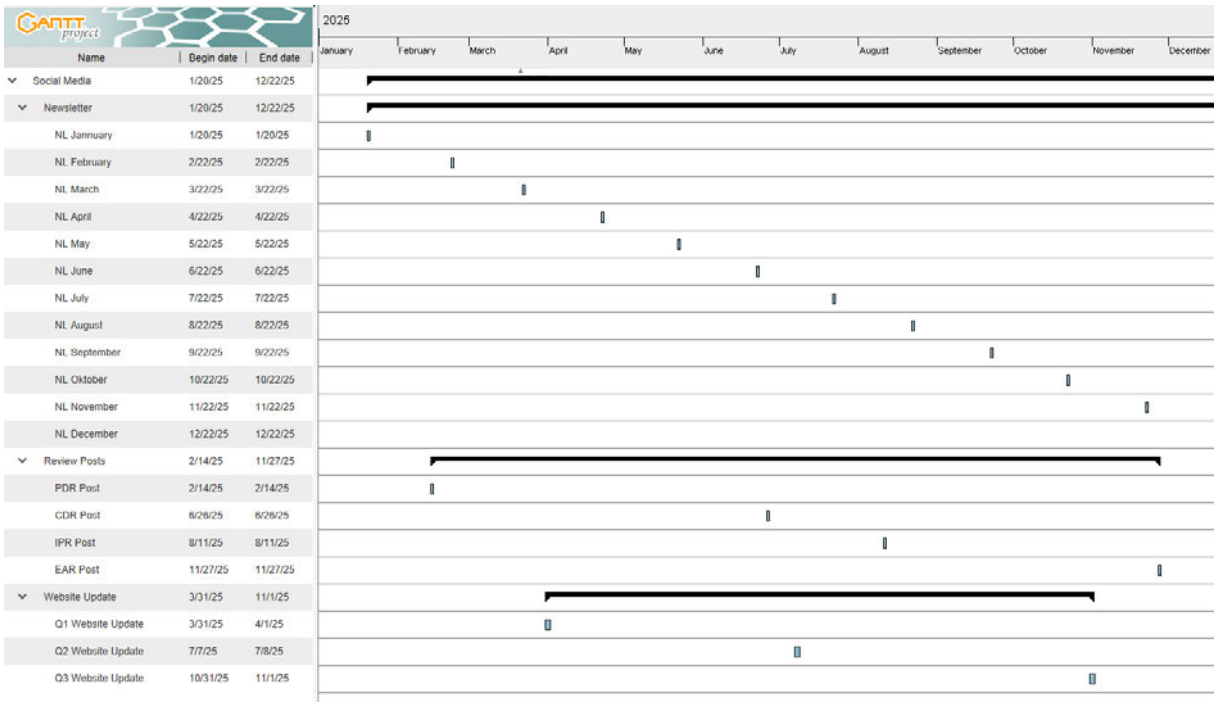


Figure 3.15: GANTT of the Tests with full System.

3.2.2 Social Media and Public Outreach Gantt Chart

The following Gantt chart includes all planned newsletters, publications, and social media posts. Posts of opportunity are not shown, as they have no posting date yet.



3.3 Resources

3.3.1 Workforce

Table 3.1 shows the estimates of hours available split by task per month. A bar diagram representation can be seen in Figure 3.16. It shows a relatively constant availability, with only a significant reduction in availability around the Christmas holidays. Furthermore, both the end of June and the end of January show slight dips due to the exam period. Note, that, due to the Austrian University exam system, many exams are spread out over the whole semester, reducing the impact during the nominal ”exam phases”.

Table 3.1: Hours per month available split into the different work fields.

PM	Project Management	ELEC	Electronics Engineering
SE	System Engineering	SOFT	Software Engineering
SC	Science	MECH	Mechanical Engineering

Per Month	Jun	Jul	Aug	Sep	Oct	Nov	Dec	Jan	Feb	Mar
PM	17.5	24	24	24	14	24	24	24	24	24
SE	51.5	61.4	68	64	57.5	67	55.4	46	53	54
SC	56	62.8	82	72	75	75	57.2	47	76	74
ELEC	74.5	110	109	90	55	44	44	44	54	64
SOFT	46.5	48.8	56	54	44	37	34.4	34	44	40
MECH	107	108	89	89	119.5	128	82	90	95	95
Total	353	415	428	393	365	375	297	285	346	351

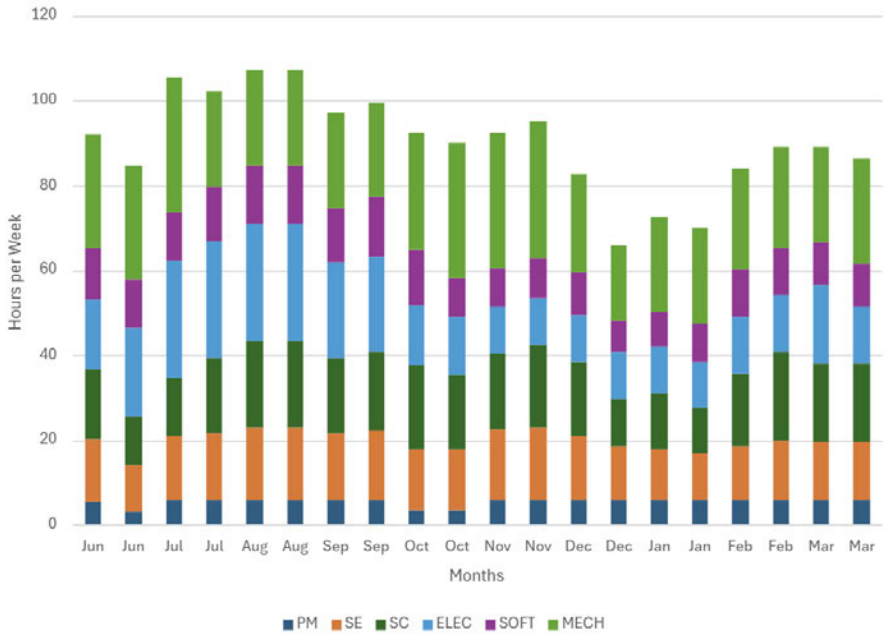


Figure 3.16: Time resources diagram in hours per week on a half-monthly basis. The values can be seen summed up for months in Table 3.1. A month is considered to be 4 weeks.

The APEX experiment was carried out by students from the Aerospace Team Graz (ASTG). In this respect, additional members of the ASTG provided help and feedback on design, manufacturing, and public outreach/sponsoring, debugging, and reviews.

To mitigate remaining shortcomings in the work force, targeted recruiting allowed to find new members in areas where a need had arisen. Our capability to do so was already demonstrated during the last year as we successfully recruited four mechanical engineers and two scientists.

3.3.2 Budget

The Aerospace Team Graz has received a grant from the national funding agency (FFG, Forschungs Förderungs Gesellschaft), with a share of 15 000 € for the REXUS project APEX. The call for the FFG Fund was" Nationale Vernetzungsplattformen 2024", our fund has the number "FFG Nr: 919566" with the shorttitle "ASTG 2024-2027"

Costs not covered by the above funding were be provided by ASTG, which receives monetary sponsoring each year besides the material ones mentioned in the next section. An estimate of the cost of the materials and if they have been sponsored in previous projects of the ASTG can be seen in Table 3.2.

Table 3.2: Estimate of the costs for the Project. Legend for the sponsored (Sp.) column,: 1: fully sponsored in previous projects, sponsor still active; 2: partially sponsored in previous projects, sponsor still active; 3: sponsoring denied; 4: part of the costs will be paid by the students

Item	**Amount with spares**	**Estimated Cost total** (with margin)	**Estimated Costs after Sponsoring**	**Payed**	**Sp.**
Metal Parts Material	n.A.	1000	300	441.72 €	2
Carbon Tube	2	200	200	85,76 €	
Machining of Metal Parts	n.A.	6000	1000	757.29 €	1
Motors	6	600	600	621.23 €	3
Screws, Pins, etc	n.A.	300	300	148.39 €	
Camera Polarization	3	2500	2500	2010 €	3
Camera Public Outreach	2	1000	0	Sponsored	1
Filters	4	1000	1000	967.76 €	2
Lenses	5	1500	0	Sponsored	1
Gimbal Electronics	3	1300	1100	1307.25 €	2
PCB	4	500	200	431.51 €	2
Bearings	2	2000	0	Sponsored	2
Pyroactuation	2	500	100	Sponsored	1
Tools	n.A.	500	300	85,9 €	
total material		18900	7800	6856.81	
travel					
Student training week	1S	500	0	Payed by the Students	4
PDR	2S	800	0	Payed by the Students	4
ITW	1S	500	150	Payed by the Students	4
Bench Test	1S	400	150	Payed by the Students	4
Sponsor visits	n.A.	500	500	not needed	4
Launch	8S	8400	6600	8300	4
Outreach					
APEX-Stickers	n.A.	100	100	70	
Post Flight Event	n.A.	300	0	Sponsored	1
Testing and Shipping					
Shaker Test	n.A.	3000	0	Sponsored	
Shipping	n.A.	800	800	Not needed	
total		41400	18300	15226.81 €	

3.3.3 External Support

The project team had access to the laboratories of the Space Research Institute (IWF) Graz (thermal vacuum chamber, thermal chamber, soldering infrastructure including vapor-phase soldering and PCB washing machine, cleanroom for electronic and mechanical assembly).

Furthermore, the Project Team had access to all the ASTG infrastructures. These include a soldering room, a mechanical workshop and assembly rooms. In addition to internal manufacturing capabilities, the APEX team had access the wide network of sponsors of Aerospace Team Graz, who have the capability to manufacture even complex mechanical parts.

Companies already sponsoring the ASTG. E.g., Magna Aerospace, Peak Technology, AT&S, and STMicroelectronics, among others, which, in previous projects of the ASTG, have fully sponsored manufacturing capabilities and materials or given us significant discounts.

Furthermore, new companies were constantly added to this list.

3.4 Outreach Approach

As a project of the ASTG, APEX was included in the association's marketing activities. These include the presentation of in-progress prototypes and posters at national and international exhibitions. Regular posts on social media (Instagram, Facebook, Linkedin) of ASTG kept the sponsors and the public up-to-date on our activities.

Outreach activities included:

- Monthly articles in the newsletter of the ASTG
- Social Media Posts after every review: (PDR, CDR, IPR, EAR)
- Coverage of the launch event: (Multiple posts on Social Media)
- Coverage of the visit of REXUS team SPECTRE in Austria (May 2025)
- Coverage of the Project Presentation

Outreach social media posts of opportunity included:

- Posts when presenting APEX on exhibitions
- Posts of working parts of the experiment. These posts did not follow a schedule, as they depend on the social media schedule of the association as a whole and the test's suitability.
- YouTube explanation short videos. Concepts for 5 videos exist with the first already being posted. Due to the large amount of work associated with each video the work and resource schedule allows for no commitment on these videos.
- YouTube video of the Launch campaign. Similar to before, the amount of resources necessary for a video does not allow for a commitment.

Shortly after the launch campaign, a project presentation was held at the Space Research Institute to show the sponsors and interested parties the preliminary results of the project.

Table 3.3: APEX Social Media Links

Website	`https://astg.at/projects/apex`
Instagram	`https://www.instagram.com/aerospaceteamgrazofficial/`
LinkedIn	`https://www.linkedin.com/company/aerospace-team-graz`
YouTube	`https://www.youtube.com/@aerospaceteamgraz4009`

3.5 Risk Register

For the preliminary risk analysis, the project team used the template provided by REXUS.

Risk ID
TC – technical/implementation
MS – mission (operational performance)
SF – safety
VE – vehicle
PE – personnel
PM – project management
EN – environmental

Probability (P)
A. Minimum – Almost impossible to occur
B. Low – Small chance to occur
C. Medium – Reasonable chance to occur
D. High – Quite likely to occur
E. Maximum – Certain to occur, maybe more than once

Severity (S)
1. Negligible – Minimal or no impact
2. Significant – Leads to reduced experiment performance
3. Major – Leads to failure of subsystem or loss of flight data
4. Critical – Leads to experiment failure or creates minor health hazards
5. Catastrophic – Leads to termination of the REXUS and/or BEXUS program, damage to the vehicle or injury to personnel

The rankings for probability (P) and severity (S) are combined to assess the overall risk classification, ranging from very low to very high, and are colored green, yellow, orange, or red according to the SED guidelines. **Note:** Cells in the "Risk and consequence column" have been left free if they simply implement the prevention and/or mitigation actions from the line above to ease readability.

E	low	medium	high	very high	very high
D	low	low	medium	high	very high
C	very low	low	low	medium	high
B	very low	very low	low	low	medium
A	very low	very low	very low	very low	low
	1	2	3	4	5

Figure 3.17: Risk Matrix with the probability on its y-axis and severity on its x-axis, following the SED guidelines.

Risk	ID2	Risk & Consequence	P	S	P x S	Prevention and/or Mitigation Action
TC	10	Damage to flight ciritcal comonents	B	4	B4	- Full flight spare - Transportation Box
TC	11		A	4	A4	- Acceptable Risk: no action
TC	20	Failure of the power management system resulting in a tripping of the REXUS fuse	C	4	C4	- Extensive testing of the system - Optional addition of batteries and detaching the power draw of the motors form the REXUS power supply system
TC	21		A	4	A4	- Acceptable Risk: no action
TC	30	Failure of the Black Box to record flight data	C	4	C4	- Extensive testing of the System
TC	31		B	4	B4	- Implementation of a secondary Black Box
TC	32		A	4	A4	- Acceptable Risk: no action
MS	10	Failure of the experiment to initialize the target area	B	4	B4	- Back up Mode to scan the sky if no target area available - Extensive Testing of the Initialization System
MS	11		B	2	B2	- Acceptable Risk: no action
MS	20	Failure of the locking mechanism to deploy	C	4	C4	- Testing of the deployment Mechanism after shaker test
MS	21		A	4	A4	- Acceptable Risk: no action
MS	30	No Aurora observable due to time of launch or unlucky space weather	C	4	C4	- Back up Mode to scan the sky if no target area available
MS	31		C	1	C1	- Acceptable Risk: no action
MS	40	Gimbal beeing stuck due to a frozen mechanism	C	4	C4	- Require Heeting of the nose cone section prior to launch - Motors and Actuaturs are designed with sufficient marging to pull free of a slightly frozen system
MS	41		A	4	A4	- Acceptable Risk: no action
MS	50	Failure of on of the polarization Cameras	B	4	B4	- Test of the Cameras in relevant environment
MS	51		A	4	A4	- Acceptable Risk: no action
SF	10	Personal fingers gets injured by moving gimbal during ground testing	C	4	C4	- Emergency Stop on the test Box taking the power of the experiment
SF	11		A	4	A4	- Acceptable Risk: no action
SF	20	Ignitorn of the Pyrotechic E-Match during handeling	C	4	C4	- Transport the E-Matches in an ESD protected box seperate from any sources of electrical energy (e.g. batteries) - Shortcircuit the E-Match druning installation in all steps were possible - Personal and workplace is grounded during assembled
SF	21		A	4	A4	- Acceptable Risk: no action

VE	10	Detachment of parts from the gimbal damaging the rocket	C	5	C5	- Performing of a System Level FMECA to identify Subsystem Risks - Performing of shaker tests
VE	11		A	5	A5	- Acceptable Risk: no action
VE	20	Early deployment of the Locking resulting in a free rotating gimbal during Accent	C	5	C5	- Pyros are actuated by the REXUS Service Module - Pyros are seperated from any Student designed electronics
VE	21		A	5	A5	- Acceptable Risk: no action
PE	10	Critical team members leafing the project prematurely	C	4	C4	- Multiple people working on the same task - Timely recruiting of new Members - Creation of Hand Over Documents - Recruting emergency Work Power from the ASTG Association
PE	11		C	2	C2	- Acceptable Risk: no action
PM	10	Delays in the delivery of machined parts	B	4	B4	- Ordering of components early (Februar) - Definition of Deadlines to seek alternative solutions - Find back up solutions/suppliers
PM	11		B	2	B2	- Acceptable Risk: no action
PM	20	Delay of the delevery of the cameras	C	4	C4	- Ordering of components early (Februar) - Include the long lead time (up to 2 months in the Gantt)
PM	21		B	4	B4	- Acceptable Risk, though one of the most critical components
EV	10	Fogging up of optic componsents	B	4	B4	- Design Heater elements to avoid fogging problems - Add desicant to the Nosecone to reduce Moister - Test for fogging up problems in the Vakkum Chamber
EV	11		A	4	A4	- Acceptable Risk: no action
EV	20	Damage to storage due to water at landing point	B	4	B4	- Harden Black box against Water - Test Black box in Water environment
EV	21		B	2	B2	- Acceptable Risk, though one of the most critical components

4 Experiment Description

4.1 Experiment Setup

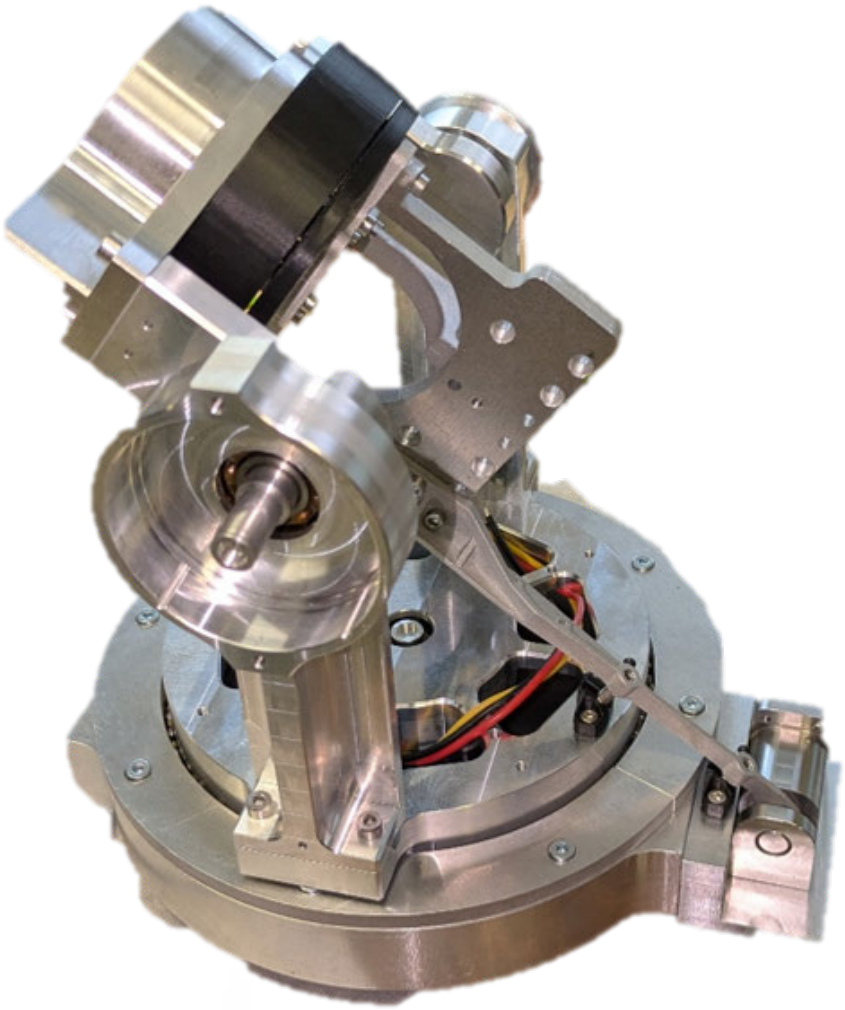


Figure 4.1: First manufactured parts of the Gimbal

APEX consisted of four main parts:

- the Camera Assembly,
- the Gimbal Stage,
- the REXUS Bulk Head,
- the Gimbal Flight Computer.

The following shall give a short overview of the Experiment, with additional information found through Chapter 4.

The Camera Assembly was the measurement stage of the Experiment. It held two scientific cameras with their optics and optical filters. The optical filter preselected the wavelength range each of the cameras can observe, and with it, the spectral emission line of the aurora under investigation. The measurement of the polarization itself happened on the camera chip with an array of differently oriented linear polarization filters. The camera assembly held an additional third camera, which acted as a reference camera. It had a field of view of 60.6° (f= 8.5 mm) compared to the 30.9° (f = 16 mm) of the science cameras, and no filter. The cameras were connected to a switch housed below the cameras in the Camera assembly with a Gigabit Ethernet connection. The camera assembly was attached to the camera roll motor and the locking arm.

The Gimbal Stage was the core of the gimbal, including the three motors plus their respective bearing, responsible for the movement of the Camera Assembly in 3 axes. The motors were actuated with the Motor Driver PCB situated in the heart of the Gimbal Stage on top of the first movable stage. This allowed the Motor Driver PCB a connection to each motor without the need to feed the cable through the cable reels. The cable reels were situated around the two roll axes, and connected the Flight Computer with the motor driver and the Raspberry Pi Computer with the camera switch in the Camera Assembly. The last part connected to the bottom of the Gimbal Stage was the locking mechanism responsible for locking the system during ascent.

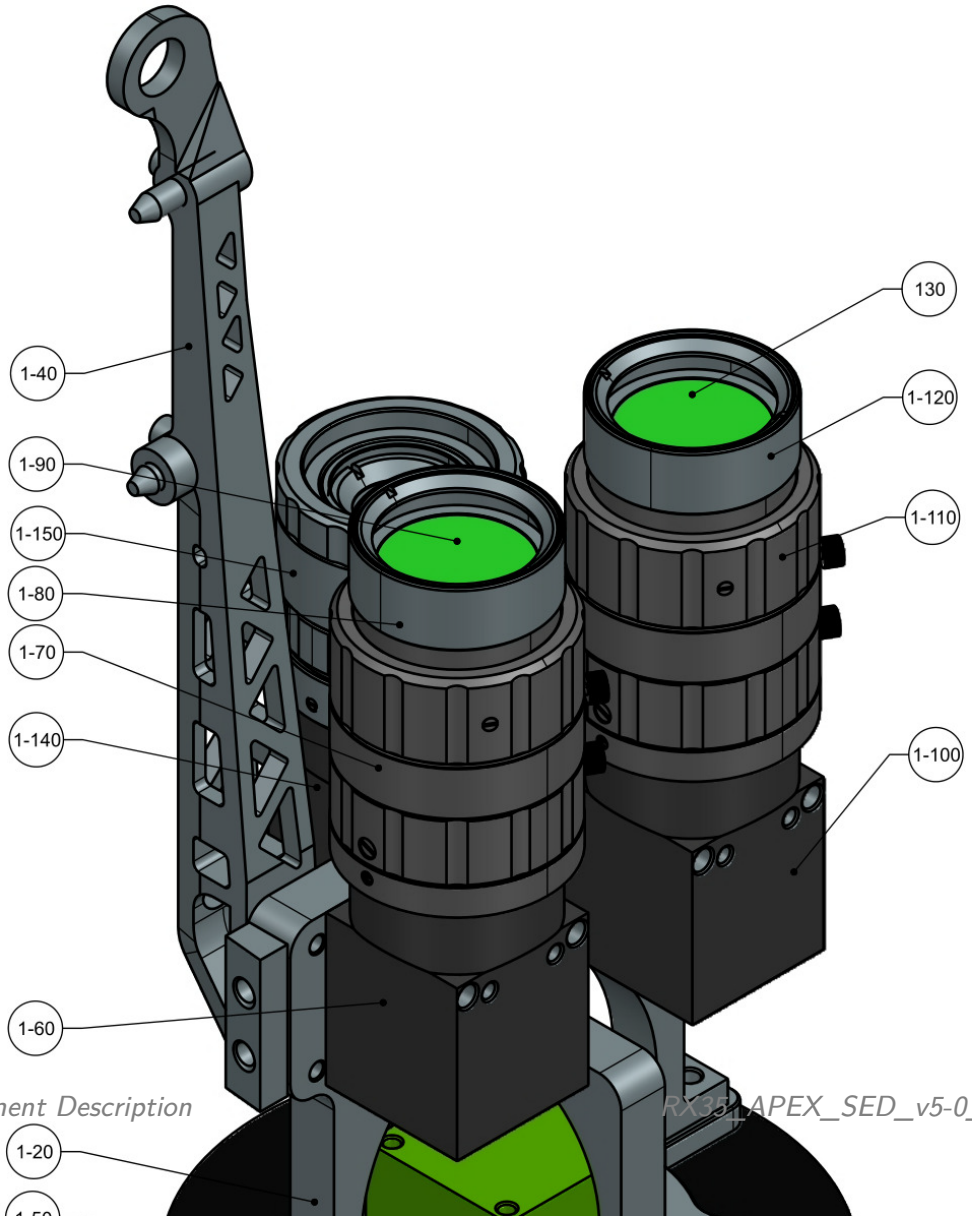
Mounted to the REXUS Bulk Head were the Gimbal itself and the Flight Computer, the battery housing, the sun sensors for the Attitude Determination System, as well as the Magnetometer and the engineering camera. A total of 8 sun sensors were used, 6 facing radially outward and 2 facing up. The engineering camera was placed so that its field of view includes both the gimbal locking and the gimbal itself.

Below the Bulk Head sat the Flight Computer, housed in an aluminium structure. It consisted of the flight computer PCB itself, the Raspberry Pi computer, the black boxes for the scientific data, and the housekeeping data, as well as a backplane connecting the other PCBs and acting as a communication interface.

Their block diagram can be seen in Figures 4.2, 4.4, 4.6 and 4.10. Table 4.1 shows the mass estimates of the gimbal, the current-best-estimate based on the current design files, as well as the mass with margin based on the initial estimate.

Table 4.1: Mass Budget of the Gimbal. Margin of 1.1 was applied to parts modeled with the correct material in the CAD, Margin of 1.25 was applied to modeled parts with PCBs, Margin of 1.5 was applied to not modeled parts. Note: Due to time restrictions, relocking parts have not been implemented.

Object	**Mass [g]**	**Margin**	**Mass with Margin [g]**
Camera Assembly	690	1.1	759
Base Assembly	866	1.1	952.6
Rotating Assembly	1628	1.1	1790.8
Swivel Assembly	954	1.1	1049.4
Sun Sensors	170	1.1	187
Pinpuller	394	1.1	433.4
Relocking	–	–	–
Avionics Box	700	1.25	875
Batteries	536	1.25	670
Runcam	61	1.1	67.1
Magnetometer	37	1.1	40.7
Total	**6036**		**6825**
Rexus Module	4448	1	4448
Total + Rexus Module	**10484**		**11273**



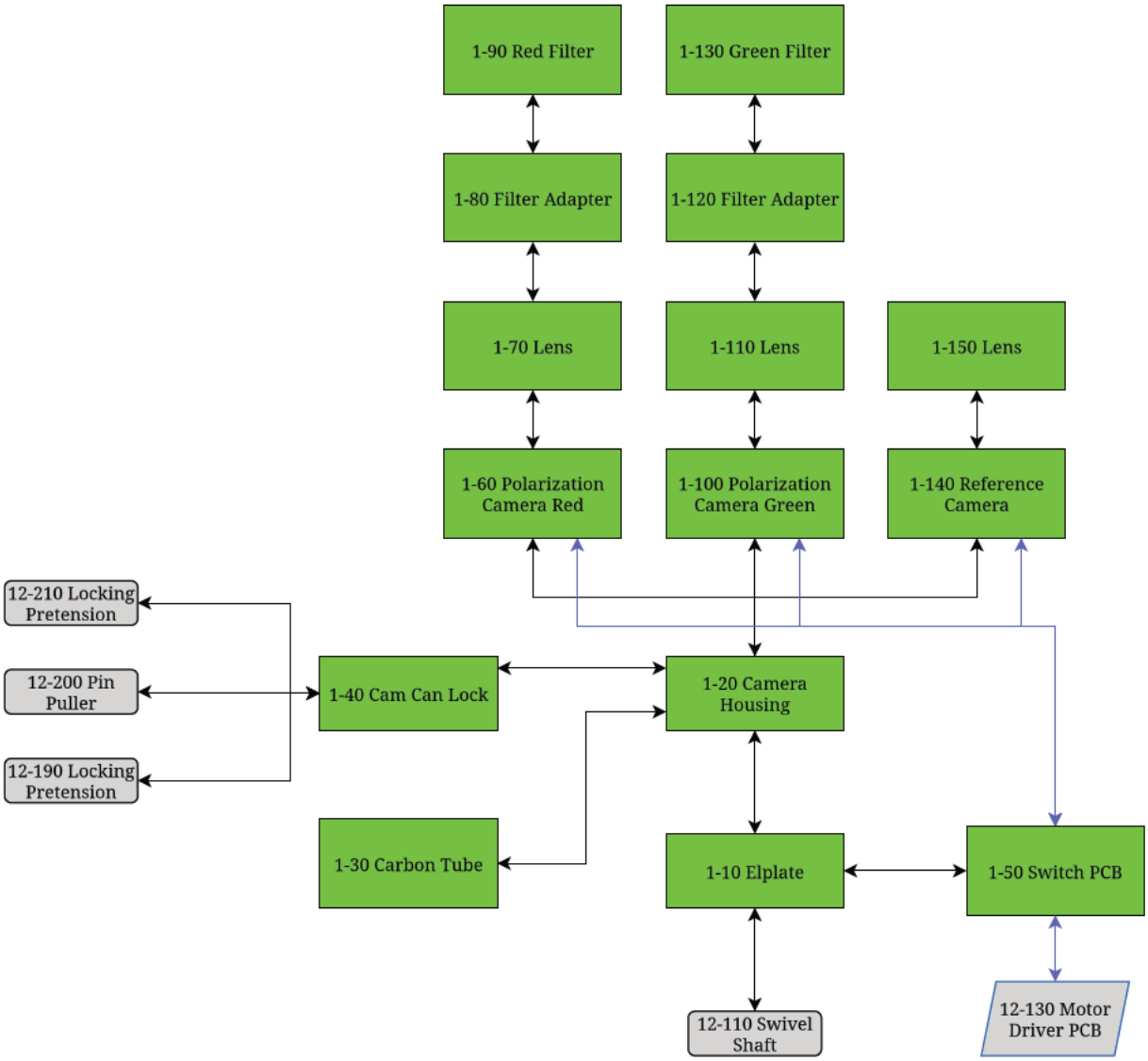
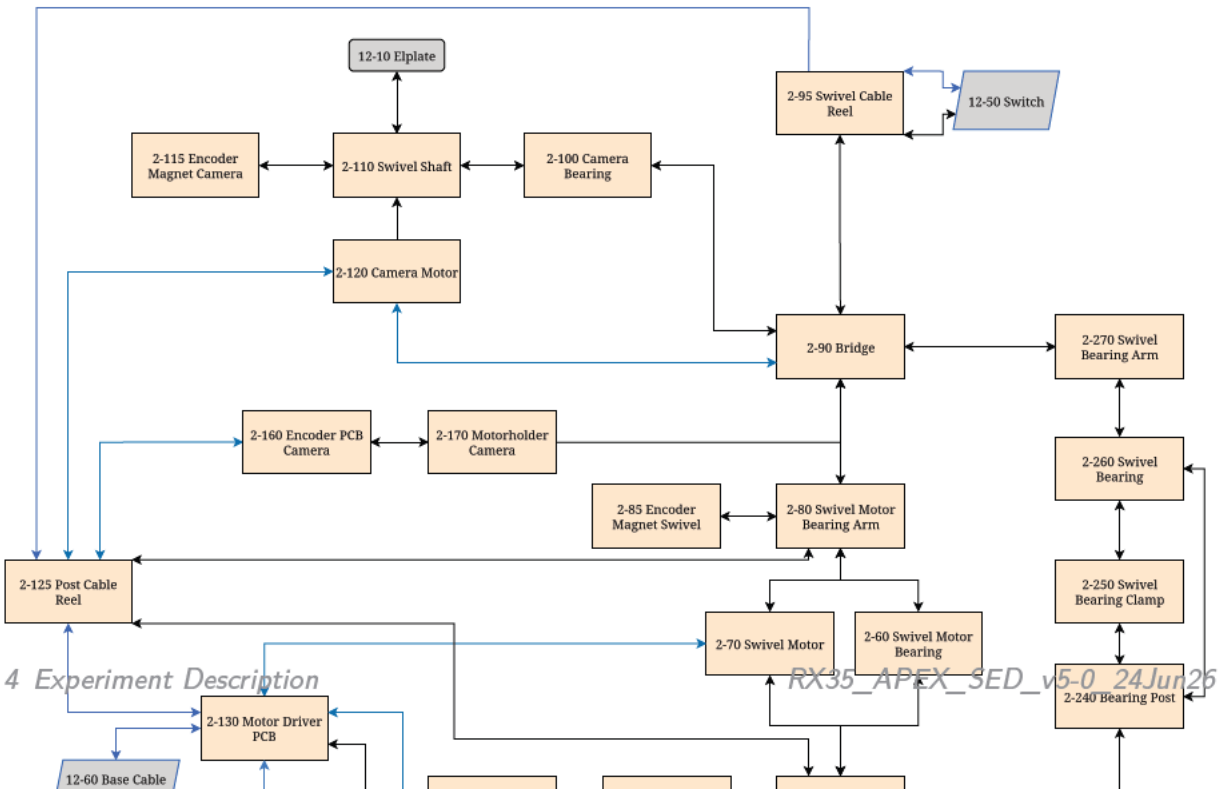


Figure 4.2: Block diagram of the Camera Assembly. Blue lines indicate electrical connections, black mechanical.



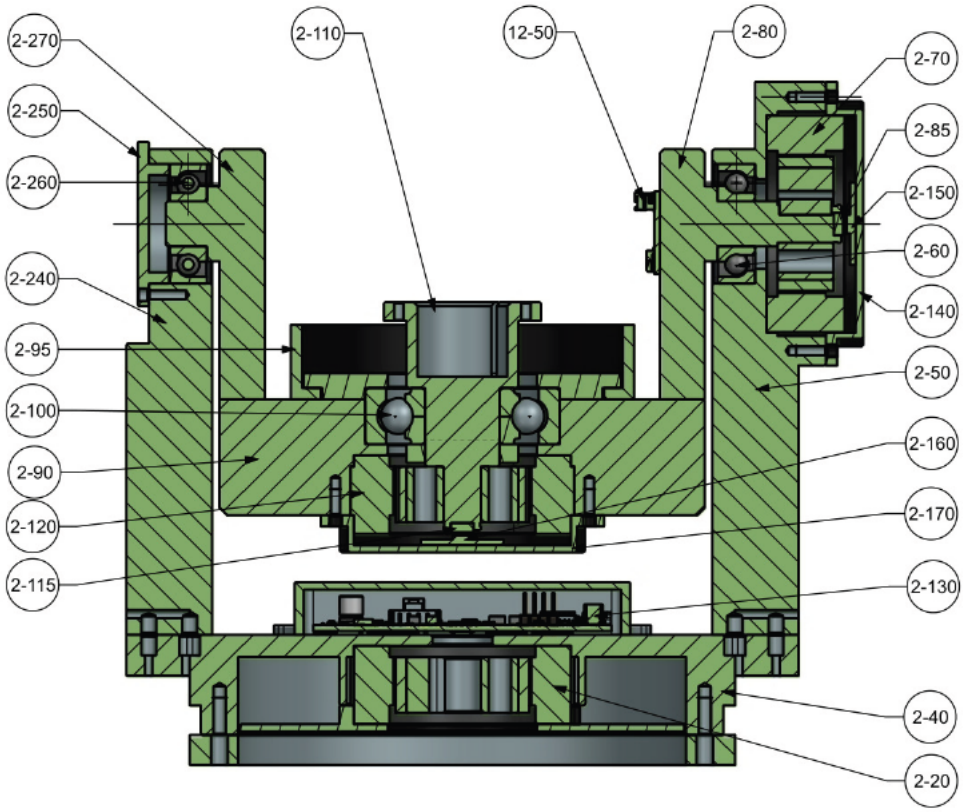


Figure 4.5: Model of the Gimbal Stage, part 1 labeled with part ids from the block diagram Figure 4.4

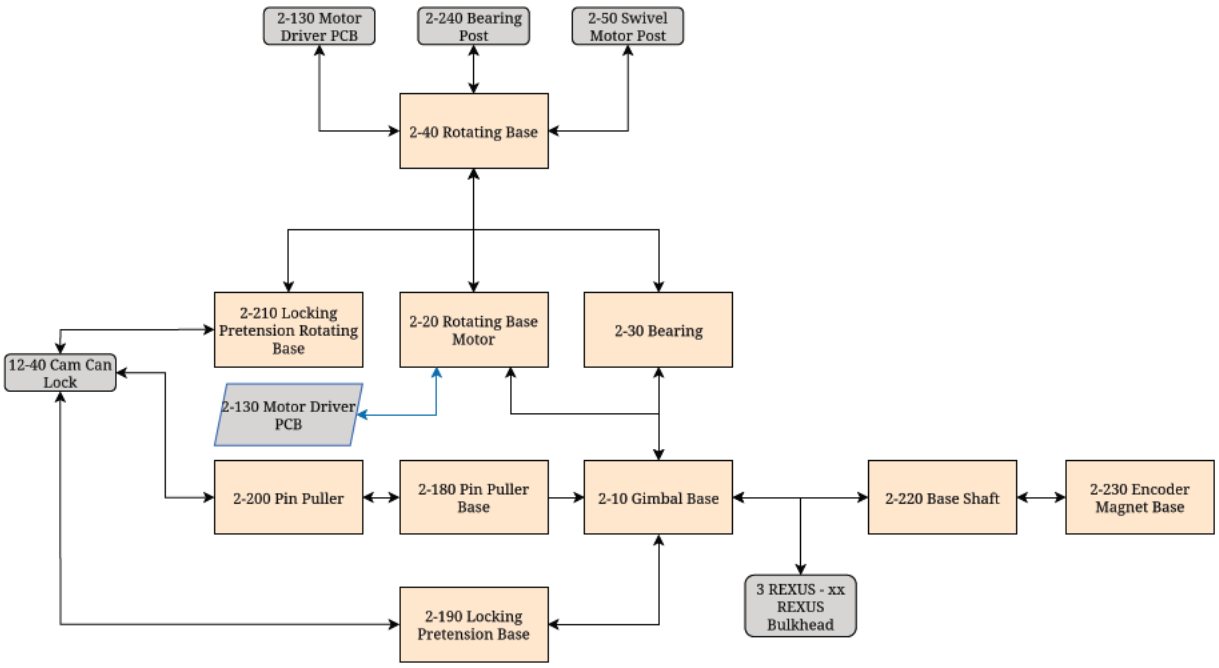


Figure 4.6: Block diagram of the Gimbal Stage, part 2, below rotating base. Blue lines indicate electrical connections, black mechanical.

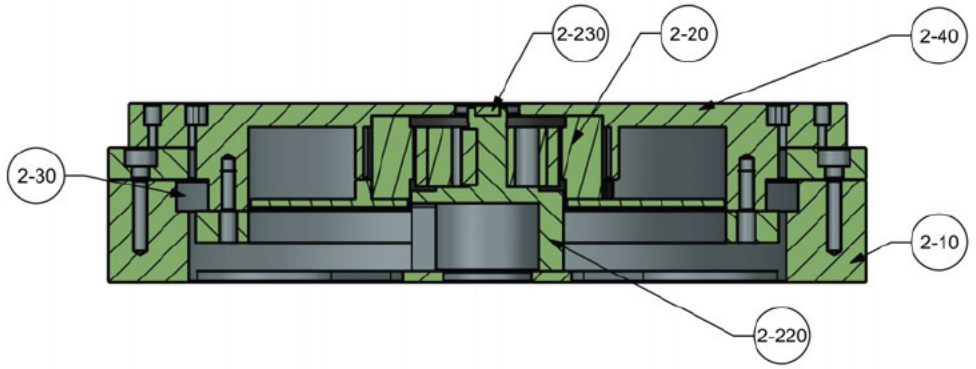


Figure 4.7: Model of the Gimbal base labeled with part ids from the block diagram Figure 4.6

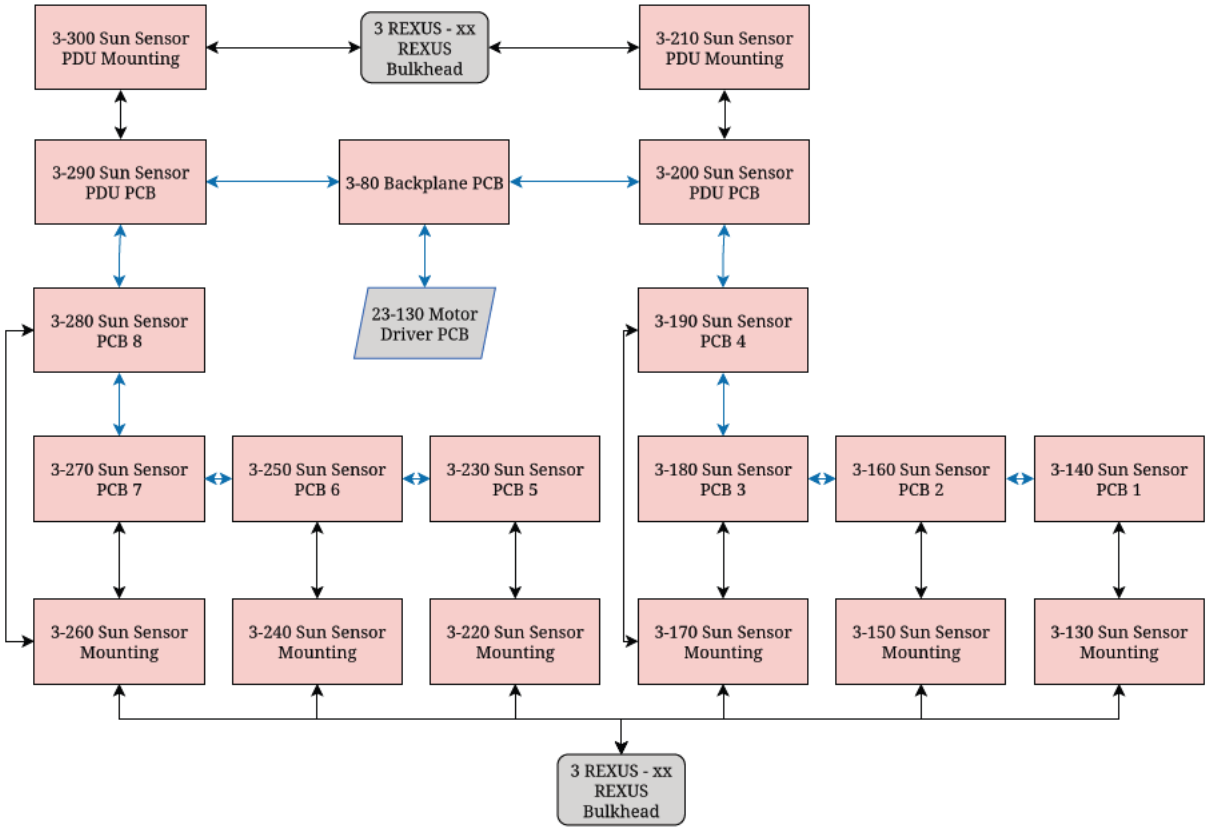


Figure 4.8: Block diagram of the Gimbal Electronics part 1. Blue lines indicate electrical connections, black mechanical.

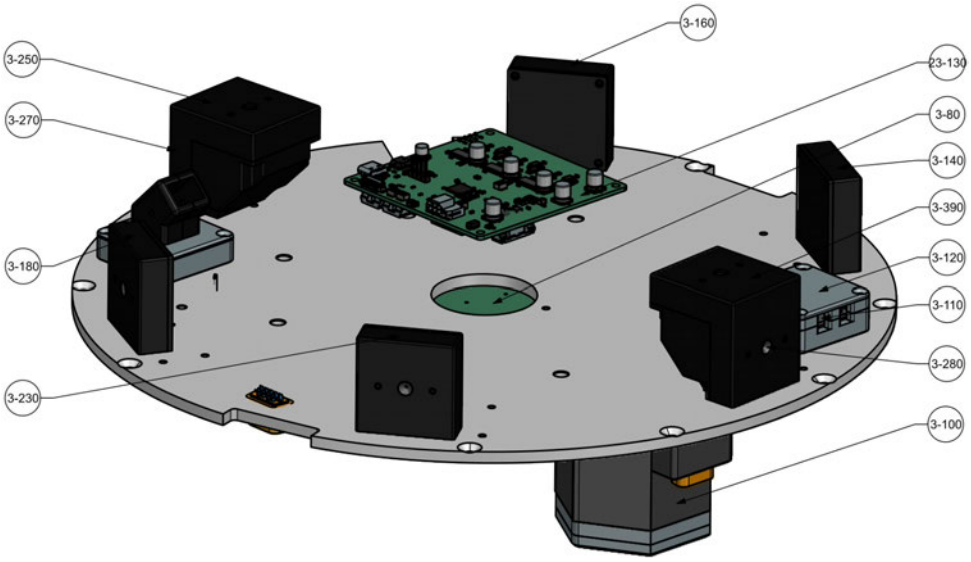


Figure 4.9: Model of the Gimbal base electronics labeled with part ids from the block diagram Figure 4.8

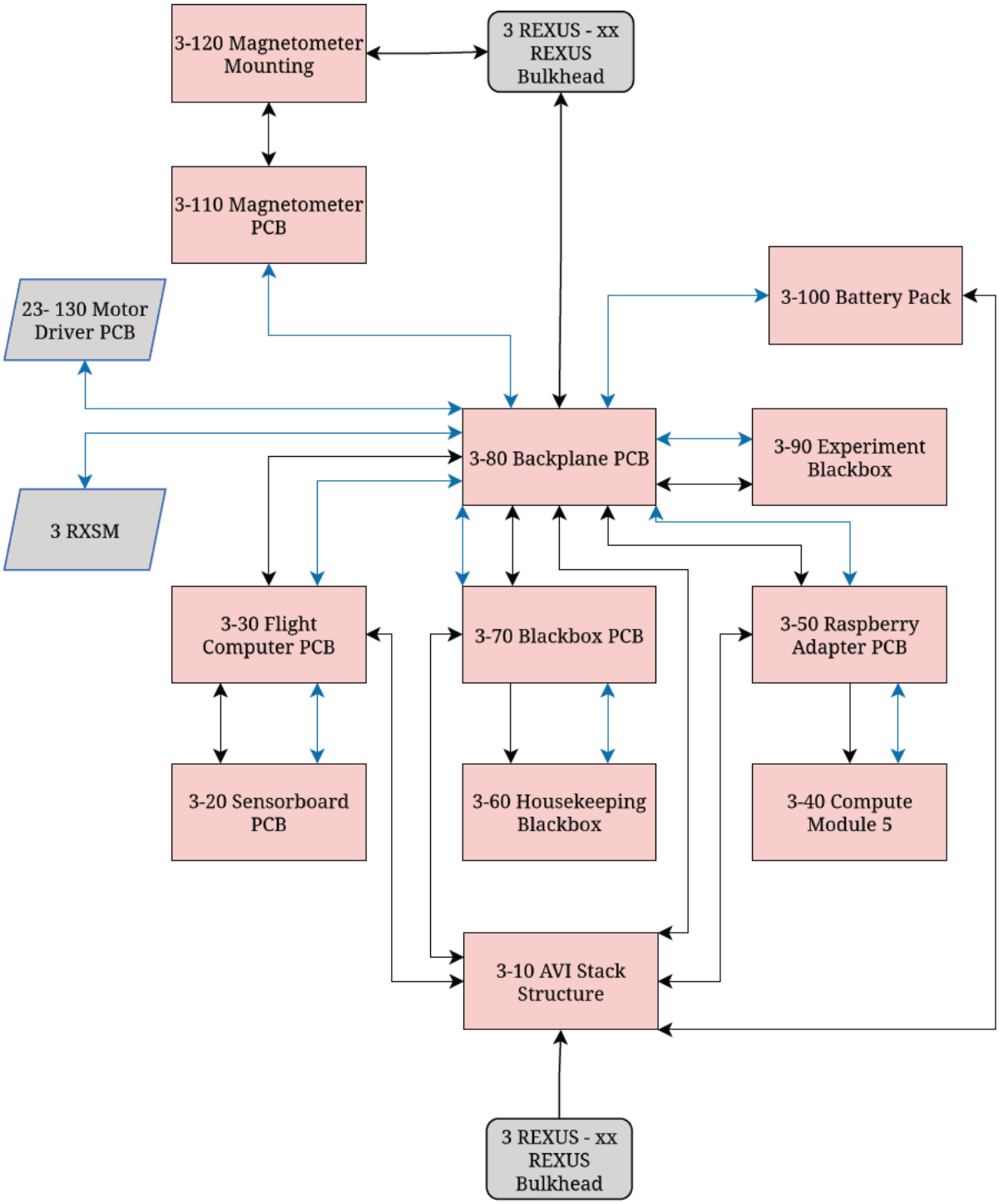


Figure 4.10: Block diagram of the Gimbal Electronics part 2. Blue lines indicate electrical connections, black mechanical.

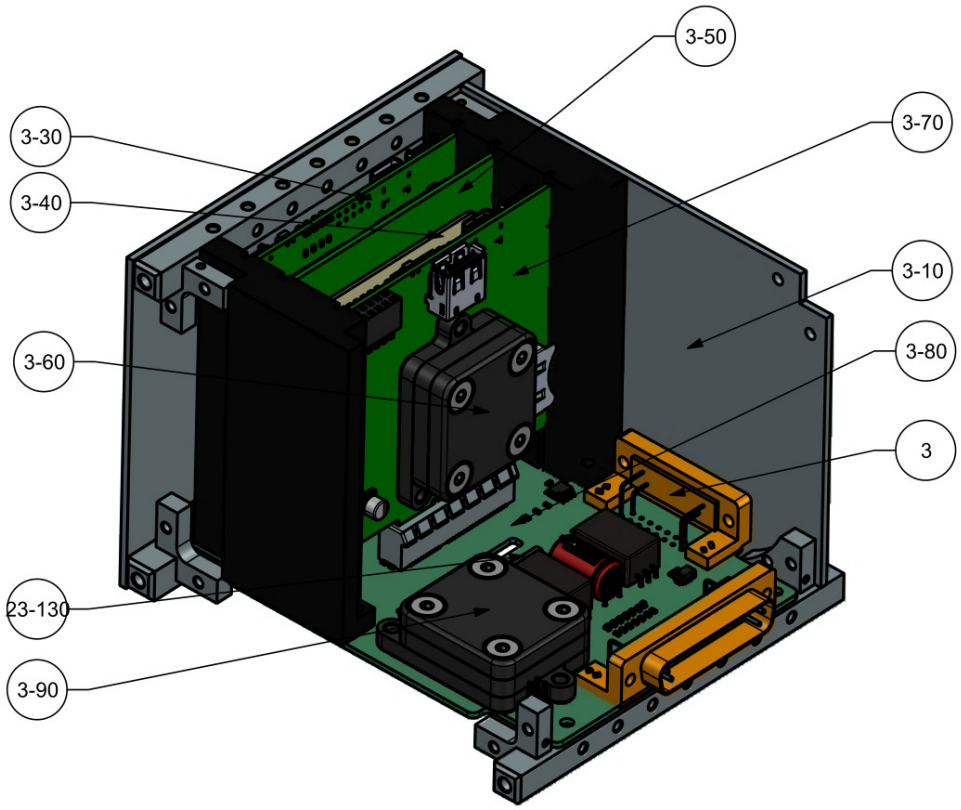


Figure 4.11: Model of the Avionics box labeled with part ids from the block diagram Figure 4.10

4.2 Experiment Interfaces

4.2.1 Mechanical

The gimbal will be secured to the rocket using 8 Hexagon socket head cap screw (ISO 4762), M5 x 16 mm (up to 20 mm possible). The gimbal will be mounted to ensure its main axis aligns with the rocket's rotational axis.

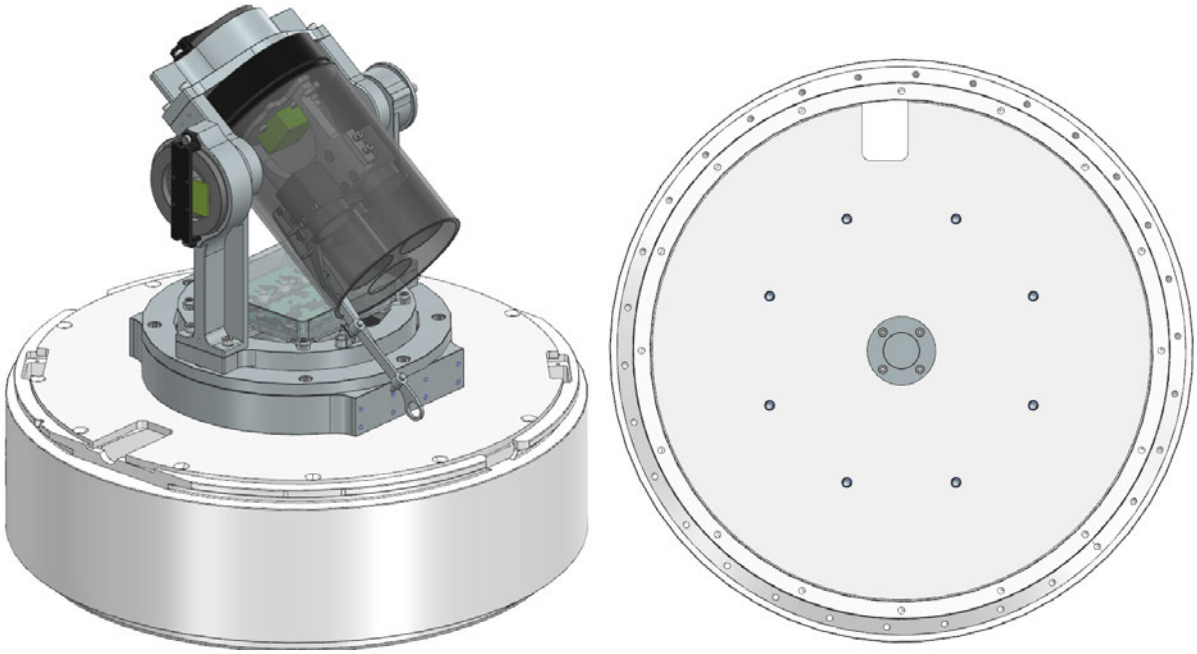


Figure 4.12: Gimbal mounted on REXUS

4.2.2 Electrical

The experiment used a 15-pin D-Sub connector as an interface toward the RXSM; the signals transferred through this interface are specified in Table 4.2. The two power lines on pins 1 & 9 and 8 & 15 supplied the experiment. The charging line was used to charge the experiment batteries. The signals SODS, SOE, and LO were connected and used to transition between different mission states. The EXP in and out lines were connected to communicate with the Ground Station over the RXSM.

Table 4.2: The RXSM D-SUB connector pin configuration

Pin	Pin Name	Usage notes
1	+28 V	Experiment Power
2	Charging (28 V/1 A)	Not available with new RXSM
3	SODS	Connected and used
4	SOE	Connected and used
5	LO	Connected and used
6	EXP out +	Non-inverted experiment data to RXSM
7	EXP out -	Inverted experiment data to RXSM
8	28 V Ground	Power Ground
9	+28 V	Experiment Power
10	n.c.	Not connected
11	n.c.	Not connected
12	Charging Return	Not available with new RXSM
13	EXP in +	Non-inverted experiment data to the experiment
14	EXP in -	Inverted experiment data to the experiment
15	28 V Ground	Power Ground

4.3 Experiment Components

Parts are listed in Tables 4.4 to 4.6. Weights are summarized in Table 4.1. Mass in dimensions is summarized in Section 6.1.1

Table 4.3: Experiment mass and volume, *Mass without bulkhead

Experiment mass (in kg)	6.036*
Experiment dimensions (in mm):	265x190x340
Experiment expected Centre of Gravity (COG) position:	x,y<3mm, z=87mm from connectorplate

Table 4.4: Parts List Camera Housing

Nr	**Part**	**Amount (Spares)**	**Cost**	**Supplier**
1-10	Elpalate	1(1)		ASTG
1-20	Camera Housing	1(1)		ASTG
1-30	Carbon Tube	1(1)		ASTG
1-40	Cam Can Lock	1(1)		M&H
1-50	Switch PCB	1(2)	100€ pp	ASTG
1-60 1-100	Polarization Cameras	2 (1)	1000 € pp	Lucid
1-70 1-110	Lens	2 (1)	Sponsored	Edmund Optics
1-80 1-120	Filter Adapter	2 (2)		ASTG
1-90	Red Filter	1 (1)	180 € pp	Thorlabs
1-130	Green Filter	1 (1)	180 € pp	Thorlabs
1-140	Reference Camera	1 (0)	Sponsored	Lucid
1-150	Lens	1 (0)	Sponsored	Edmund Optics

Table 4.5: Parts List Gimbal Structure

Nr	**Part**	**Amount (Spares)**	**Cost**	**Supplier**
2-10	Gimbal Base	1 (1)		IFT
2-20 2-70 2-120	Motor	3 (2)	100€ pp	Cubemars
2-30	Bearing	1 (1)	664 € pp	SKF
2-40	Rotating Base	1 (1)		Resch
2-50	Swivel Motor Post	1 (1)		Resch
2-60 2-260	Swivel Bearing	2 (2)	22,49 € pp	SKF
2-80	Bearing Arm	1 (1)		Resch
2-85 2-115	Encoder Magnet Swivel	2 (2)		
2-90	Bridge	1 (1)		Resch
2-95	Swivel Cable Reel	1 (1)		ASTG, IFT
2-100	Camera Bearing	1 (1)	55,55 € pp	SKF
2-110	Swivel Shaft	1 (1)		Resch
2-130	Motor Driver PCB	1 (?)		ASTG
2-140 2-170	Motorholder Swivel	2 (4)		ASTG
2-150 2-160	Encoder PCB Swivel	2 (2)	15,80€	Mouser
2-180	Pin Puller Base	1 (1)		IFT
2-190	Locking Pretension Base	1 (1)		ASTG
2-200	Pin Puller			
2-210	Locking Pretension Rotating Base	1 (1)		ASTG
2-220	Base Shaft			Resch
2-230	Encoder Magnet Base	1 (1)		
2-240	Bearing Post	1 (1)		IFT
2-250	Swivel Bearing Clamp	1 (1)		IFT
2-270	Swivel Bearing Arm	1 (1)		Resch

Table 4.6: Parts List Gimbal Electronics

Nr	Part	Amount (Spares)	Cost	Supplier
3-10	AVI Stack Structure	1(1)		ASTG
3-20	Sensorboard PCB	1(1)		ASTG
3-30	Flight Comupter PCB	1(1)		ASTG
3-40	Compute Module 5	1 (1)	45 € pp	Raspberry PI
3-50	Raspberry Adapter PCB	1(1)		ASTG
3-60	Housekeeping Blackbox	1(1)		ASTG
3-70	Blackbox PCB	1(1)		ASTG
3-80	Backplane PCB	1(1)		ASTG
3-90	Experiment Blackbox	1(1)		ASTG
3-100	Battery Pack	1(1)		ASTG
3-110	Magnetometer PCB	1(1)		ASTG
3-120	Magnetometer Mounting	1 (3)		ASTG
3-130 3-150 3-220 3-240	Sun Sensor Mounting horizontal	4 (10)		ASTG
3-140 3-160 3-180 3-190 3-230 3-250 3-270 3-280	Sun Sensor PCB	8 (10)		ASTG
3-170 3-260	Sun Sensor Mounting horizontal & vertical	2 (5)		ASTG
3-200 3-290	Sun Sensor PDU PCB	2(2)		ASTG
3-210 3-300	Sun Sensor PDU Mounting	2 (5)		ASTG

4.4 Mechanical Design

4.4.1 Sub-systems of the mechanical design

The gimbal's mechanical assembly consisted of the following sub-systems:

- The base: mounted to the bulk head
- The rotating platform: Includes The Motordriver PCB
- The swivel: in between the rotating platform and the camera housing
- The camera housing: housing the cameras
- The locking mechanism

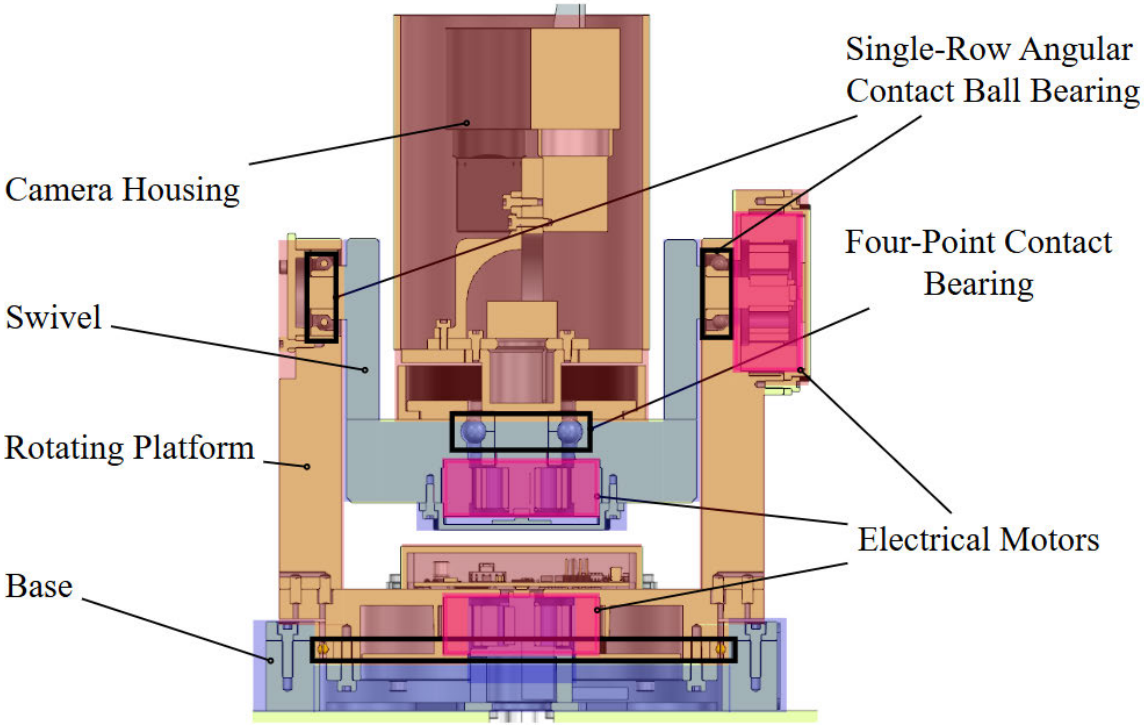


Figure 4.13: Main mechanical components of the gimbal design

4.4.2 Bearings

Motors without integrated bearings were selected in order to avoid potential issues associated with unspecified motor bearings.

For the base, a four-point contact ball bearing (Reali-Slim thin section bearing from SKF, KDN.K14008XP0) is employed. These bearings are well-suited for this application, as they can accommodate both axial and radial loads. Due to the relatively large diameter of this bearing, tight tolerances are required. The selected bearing fulfills this requirement, offering high accuracy and ensuring smooth operation. It is preloaded via an interference fit on the inner ring.

For the swivel, two single-row angular contact ball bearings (SKF, 7201 BEGAP) are used. They are installed in an X-orientation and preloaded with 300 N using a combination of shims (DIN 988) and axial screws.

The final bearing, which supports the camera housing, is a four-point contact bearing (SKF, QJ 304 MA). Due to its split inner ring, it is preloaded using a shaft nut. This configuration allows for precise axial preloading without introducing play.

The safety factor of the bearings is well above 60 for the weakest bearing, as the design was driven by the following specific requirements:

- Low weight
- Zero ball clearance
- Conformance to size and geometry constraints

These requirements significantly limited the selection of suitable bearings. As a result, the bearings chosen for the design are considerably stronger than actually necessary for the expected loads.

Additionally, the bearing with the narrowest operating temperature range is the Reali-Slim model, specified for temperatures between −55 °C and 120 °C.

Another critical aspect of the mechanism is the type of lubrication the bearings. Currently, the lubrication used in the bearings is being evaluated. In case it cannot withstand the environmental condition of the mission, it will be substituted with commercially available “Space Grease” (e.g., Braycote 601EF, −80 °C to 200 °C, space rated). Proper lubrication of all moving parts will be implemented to maintain performance and reliability under operational conditions.

During initial assembly of the gimbal, it was observed that two bearing fits were too tight. The first issue occurred with the upper four-point contact split-ring bearing (SKF QJ 304 MA), where the shaft fit for the inner ring was excessively tight. To correct this, the shaft surface was lightly ground using sandpaper on a lathe to achieve proper clearance. Since the inner ring is secured with a shaft nut, this adjustment did not significantly affect performance.

The second issue involved the lower thin-section four-point bearing (KDN.K14008XP0). According to the manufacturer, a press fit on the inner diameter is required to achieve the specified preload, with a recommended interference of 56 µm to 78 µm on the shaft. This was implemented as intended. The outer diameter was designed as a transition fit, but the bearing could not be installed without excessive force. It is assumed that the tight press fit on the inner ring caused a slight deformation or expansion of the outer ring, increasing its effective diameter. To compensate, the housing bore for the outer ring was carefully ground using sandpaper to enable easier installation. As a result, the lower bearing still requires some heat treatment for assembly, but the required force is significantly reduced, and rotational resistance has improved, allowing the motors to operate the gimbal effectively.

4.4.3 Camera Mounting

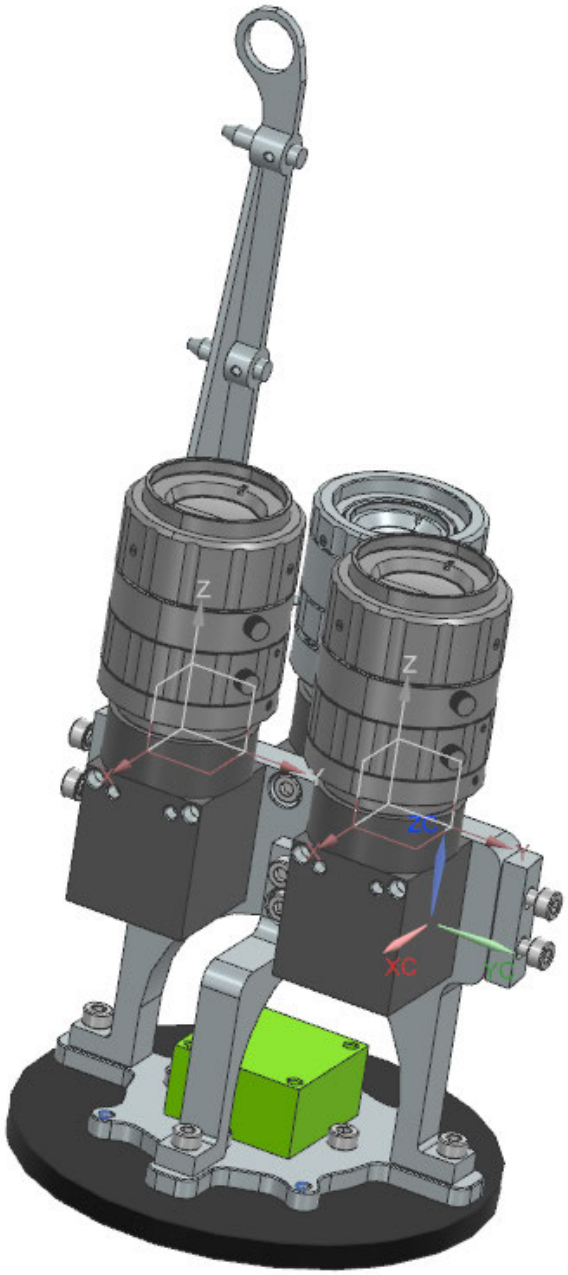


Figure 4.14: Rendering of the camera mounting

The camera will be mounted to the rest of the system using an aluminum plate, reinforced with a supporting leg. This upper structure is also the securing point for the locking arm. To ensure the stability of the cameras, each of them is secured with three screws to the structure, and the structure is attached to the gimbal with a connector plate in between, which also serves as the mounting point for the camera electronics. The whole structure is balanced around the rotating axis, to reduce strain on motors. Aluminum offers a compromise between thermal conductivity, weight, rigidity, and cost, all of which are relevant factors, since the mounting structure needs to serve as a heat sink for the cameras and provide a strong mechanical interface. The lenses will be installed using the C-mount thread of the cameras and secured with glue (e.g. loctite).

4.4.4 Locking Mechanism

Function

The function of the locking mechanism is to secure the gimbal in all axes without electrical power during ascent. After ascent, it must be unlocked and cause minimal interference to other systems. The new design features a single locking arm with three points of contact on the gimbal and is locked using a pyrotechnic pin puller.

Mode of operation

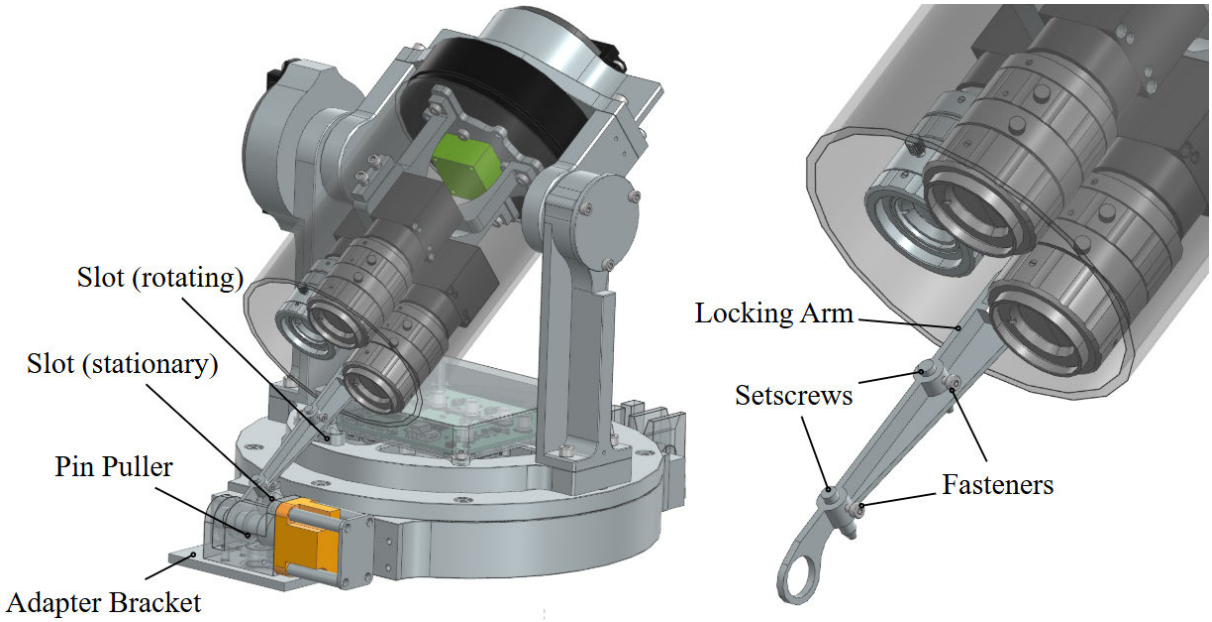


Figure 4.15: Locking mechanism components

The locking arm is permanently attached to the camera mounting structure and held down with a pin puller which locks the swivel axis.

To prevent rotation and any play in the structure, a setscrew with a conical tip is pressed down onto a V-shaped slot (stationary). The rotating plate of the gimbal would now only be indirectly constrained through two sets of bearings; to address this, the rotating plate features a second setscrew- and slot(rotating).

By torquing the setscrews to a set amount, the reaction forces on all points of contact are defined: This ensures sufficient pre-load on points of contact without causing too much shear load on the pin puller. After torquing the setscrews, they are secured with fasteners

To unlock the system after ascent: Two pyrotechnic charges are fired, and the pin is retracted. The gimbal then swivels up under motor power and is ready for operation.

Re-locking

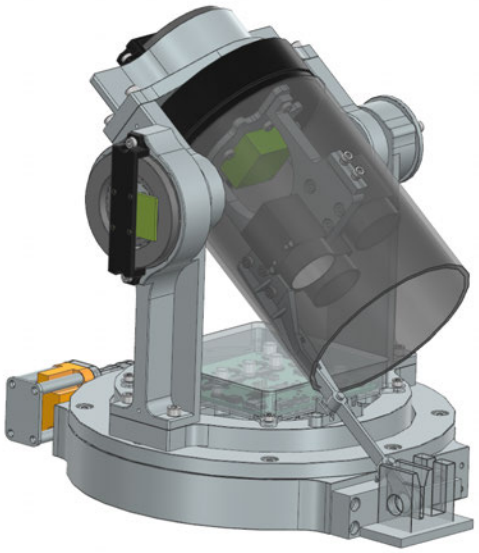


Figure 4.16: Gimbal in re-locked position

After gimbal operation it is not required, but desirable to orient the gimbal such that damage to expensive parts is minimized upon descent. The locking arm additionally serves as a re-locking structure. After operation the locking arm slots into a latch on the opposite side of the pin puller under motor power.

Pyrotechnic Pin Puller (Legacy Design)

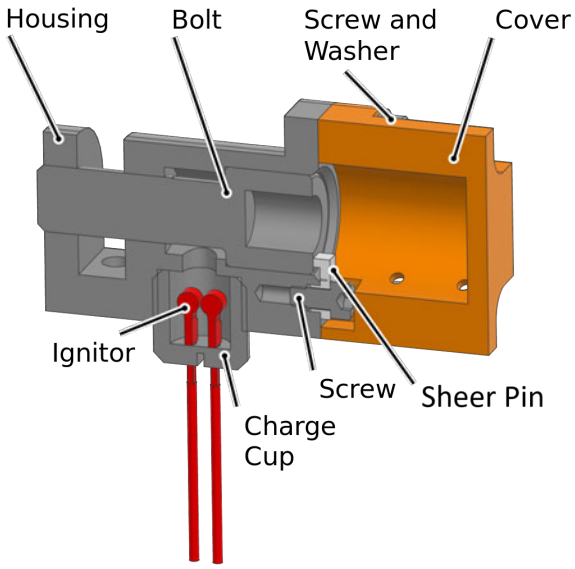


Figure 4.17: Pin puller components

The depicted pin puller is a legacy model from the aerospace team's recovery module. This is the latest model used in our SRAD and has gone through 5 iterations. There is documented testing

proving reliable operation under a shear load of 300 N on the bolt.

The design features two pyrotechnic gas generators that are actuated in parallel for redundancy, they are inserted in a threaded charge cup. The cover consists of flexible 3D print (TPU). It functions as a shock absorber and bolt catch. Premature unlocking is prevented by a sheer pin that breaks away under bolt force.

For refurbishing:

- The charge cup is reusable
- Gas generators are sponsored and supplies
- The cover and Sheer pin are 3D printed in house
- The housing and charge cup are cleared of residue after use

With refurbishing taking 15-30 minutes, this allows for extensive testing of the mechanism.

Pin Puller Design for Apex

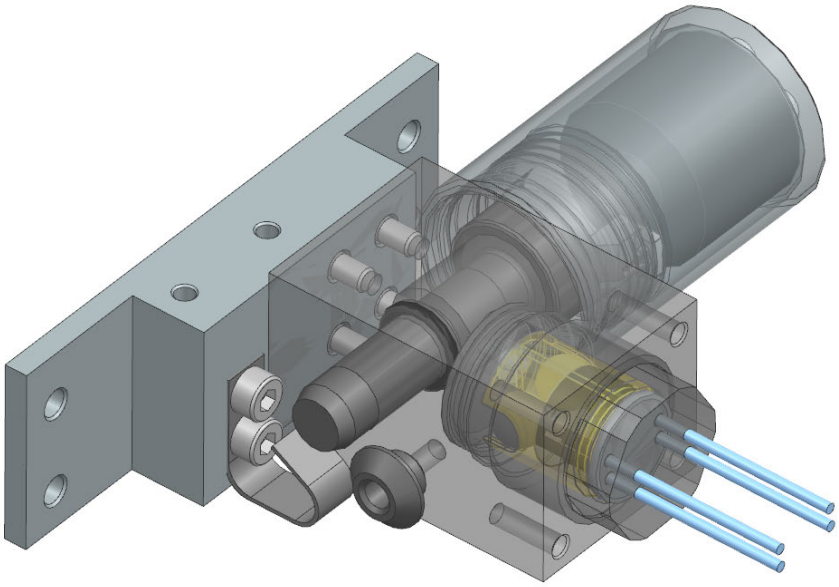


Figure 4.18: Current Design

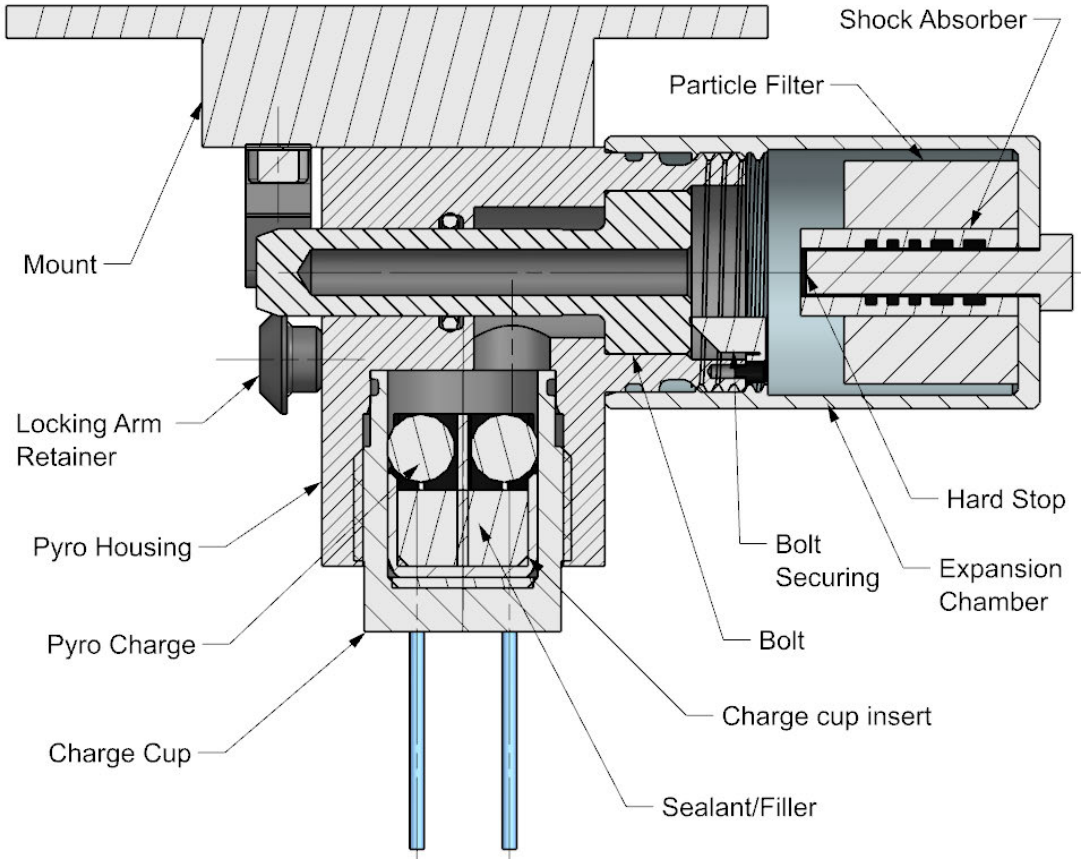


Figure 4.19: Current Concept Cross-section

The current design features a expansion chamber which is screwed onto the pin puller housing. There is a dynamic seal around the bolt and static seals for the charge cup and expansion chamber.

Version used for flight: Hard stop for bolt length reduced and shock absorbing sealing putty on top of TPU shock absorbing tip. with 5 layers of kapton tape to mitigate the thread inside the bolt shearing through the shock absorbing putty. Particle filter: 5 felt cut-outs with a hole around the bolt stopper.

The priority of this design iteration was safety while testing, and reducing emitted particles to a minimum.

Overview of aspects:

- The overall design is meant to control exhaust; Block any sparks, and (slow down/depressurize) gas to the point any smoke particles pass through a fine filter layer situated right before exhaust vent ports in a controlled matter
- Gas generators with sufficient no-fire current
- Larger charge cup (M 20 Thread) able to fit two gas generators, and allowing for thicker material leading to a structural safety factor of 4.0 (permanent deformation) and Total material failure safety factor 10.6 see Appendix F.4
- The Initial dead space/has been reduced and Pressure area on the bolt enlarged to overcome additional friction due to the dynamic bolt seal. The operational safety factor for unlocking is 4.3 see Appendix F.4

- The charge cup insert is now 2-part epoxy resin , sealing off the electrical connection for charges and allowing slight modulation of the initial expansion volume
- A leaf spring additionally pre-loading the locking arm, ensuring the pin cannot reenter the hole in the locking arm
- The Leaf Spring additionally allows for an unlocked state signal due to the motor encoders picking up the change in swivel angle of the gimbal (1 to 3 degrees)
- The expansion chamber allows many combinations of baffles/filters/shock absorbers and is easy to install (flexibility for rapid design change if needed)
- Only structural/pressure components are made of steel, separate from the adapter/pin catcher which reduces weight

4.4.5 Detailed Bearing preload Analysis (FEM)

As mentioned in Section 4.4.2, the two single-row angular contact ball bearings (SKF, 7201 BEGAP) are installed in an X-orientation and preloaded with 300 N.

The affected components of the gimbal are the two arms and the structure of the swivel assembly. A separate FEM analysis was performed for each of these parts. On each part, a preload force of 300 N was applied at the respective bearing interface.

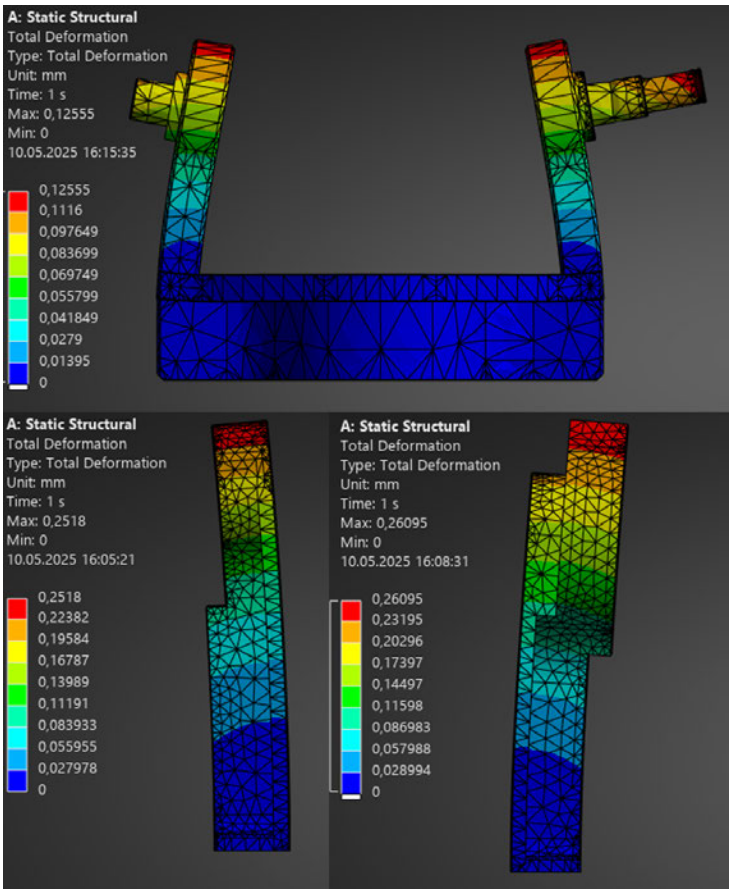


Figure 4.20: Deformation of the effected parts

The total deformation is within an acceptable range. In addition, it is symmetric, which helps to preserve the rotational axis of the camera housing.

4.4.6 Detailed Vibration Analysis (FEM)

Finite Element Method (FEM) simulations were performed with ANSYS. Since the vibration loads occur during the rocket's ascent, the simulation was performed in the "locked" state.

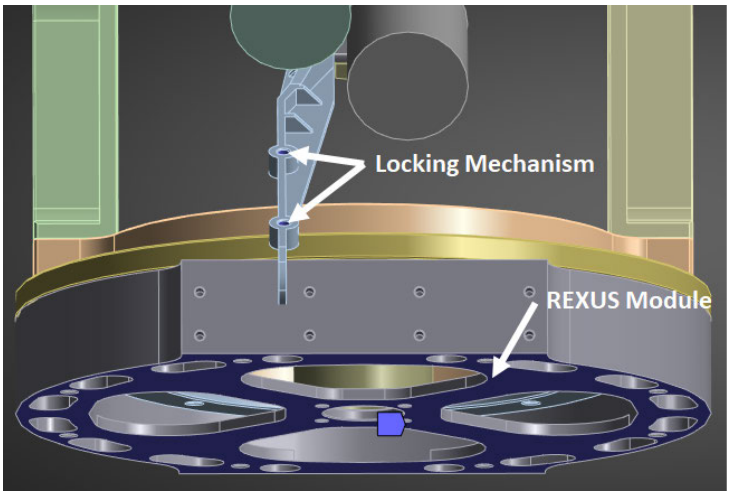


Figure 4.21: Fix points of the "locked" state for the FEM Analysis

To make the analysis feasible, the assembly was simplified by removing all screws and standard components. The bearings were replaced with simplified cylindrical shapes. To simulate the behavior of the bearings, the contacts between the cylindrical bearing representations and adjacent parts were changed from "bonded" to "frictional" with a friction coefficient of $\mu = 0.005$.

The vibration tests were based on the requirements outlined in the RX-UserManual-v7 (Table 10-2). For the sine load case, a "Harmonic Response" analysis was used. For random loads, the "Random Vibration" analysis was applied.

Each simulation yielded results regarding equivalent (von-Mises) stress. The structure is made of aluminum EN AW-6082, with an assumed maximum yield strength of approximately 260 MPa.

Natural Frequencies

First, the natural frequencies of the eigenmodes were determined using the "Modal" analysis system. The table below lists the natural frequencies of the individual modes.

Table 4.7: Natural frequencies of the eigenmodes.

Eigenmode	Natural Frequency [Hz]
1	237.65
2	268.48
3	308.44
4	400.97
5	546.42
6	682.38

Sine Vibration

As previously mentioned, the "Harmonic Response" analysis in ANSYS was used for this simulation. The parameters specified in the RX-UserManual-v7 (Table 10-2) (here Table 4.8) are as follows:

Table 4.8: Sine Vibration, Table 10-2 from the RX-UserManual-v7

Vehicle Level One		**Vehicle Level Two**	
Sweep Rate: 4 oct./min.		Sweep Rate: 4 oct./min.	
Test Profile:		*Test Profile:*	
3.0 in./s	10–144 Hz	3.84 in./s	5–24 Hz
7.0 g	144–2000 Hz	1.53 g	24–110 Hz
		3.50 g	110–800 Hz
		10.0 g	800–2000 Hz
THRUST AXIS ONLY		**THRUST AXIS ONLY**	

The maximum stress typically occurs at the natural frequencies (eigenvalues) of the structure (Table 4.7). Since these natural frequencies lie between approximately 200 Hz and 700 Hz, the simulation was limited to this frequency range. The "Vehicle Level One" test profile specifies a maximum load of 7.0 g along the thrust axis only (Table 4.8).

To avoid unrealistically high stress values (on the order of 10^5 MPa), a damping ratio of 0.001 was introduced into the analysis settings. A damping ratio between 0.001 and 0.003 corresponds to very low damping, assuming clean, rigid joints without friction. This represents a worst-case scenario.

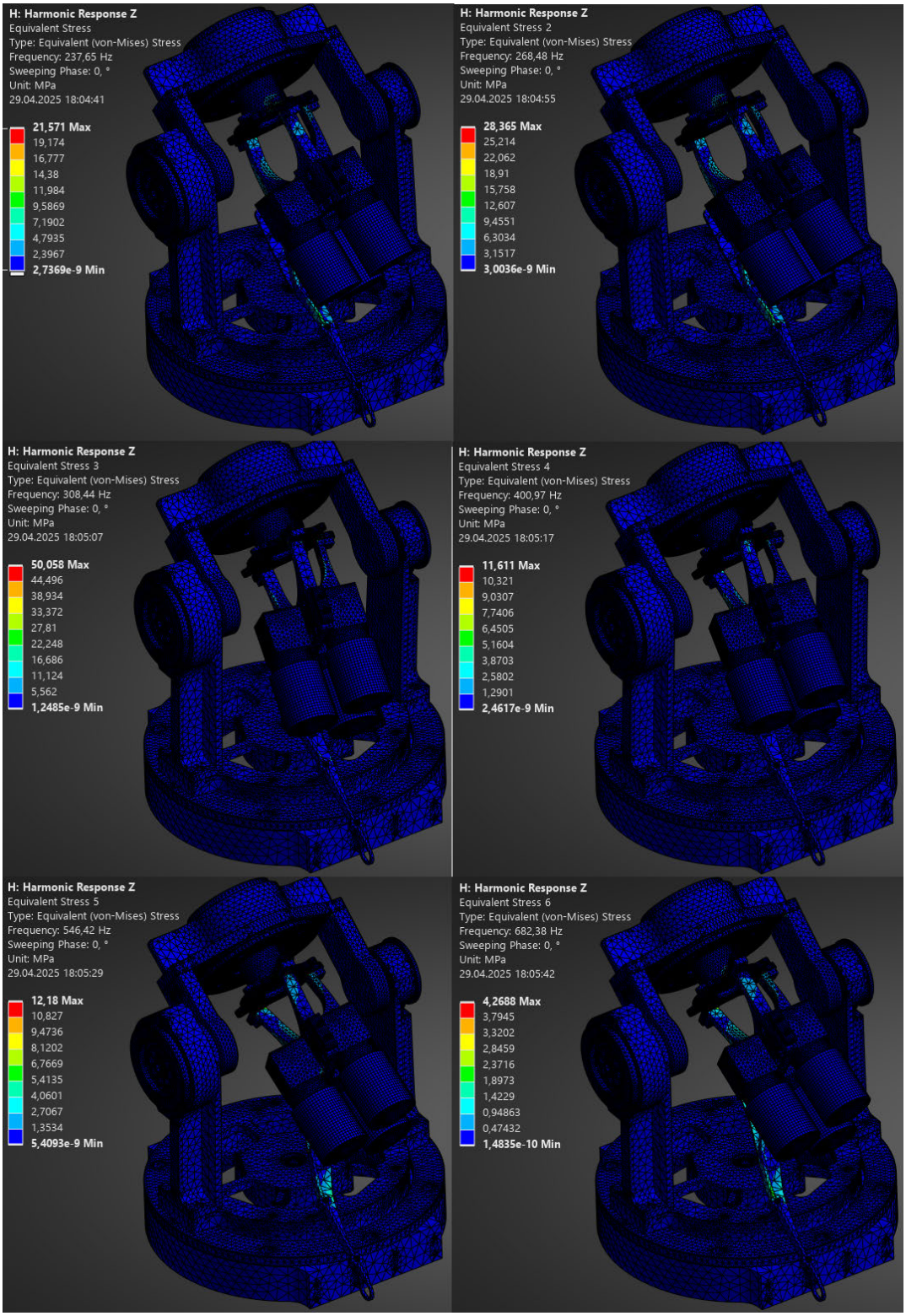


Figure 4.22: Sine Vibration analysis result at natural frequencies in thrust axis Z

According to the analysis results, the highest stress occurs at eigenmode 3 (Table 4.7), which is at 308.44 Hz. The maximum stress is located on the frame of the camera housing and reaches 50 MPa. Given the yield strength of aluminum 6082 at 260 MPa, this results in a safety factor of approximately 7.

The total deformation in eigenmode 3 is well below 0.05 mm on the locking arm, which is the

critical area.

Random Vibrations

The random vibrations for all axes were evaluated based on the parameters specified in the RX-UserManual-v7 (Table 10-2):

Vehicle Level One	**Vehicle Level Two**
Duration: 20 sec./axis	Duration: 10 sec./axis
Thrust Axis Spectrum:	*Spectrum:*
10.0 grms	12.7 grms
0.051 g^2/Hz 20–2000 Hz	0.01 g^2/Hz 20 Hz
Lateral Axis Spectrum:	0.10 g^2/Hz 1000 Hz
7.60 grms	(on 1.8 dB/oct. slope)
0.029 g^2/Hz 20–2000 Hz	0.10 g^2/Hz 1000–2000 Hz
	SAME IN ALL AXES

Table 4.9: Random Vibration, Table 10-2 from the RX-UserManual-v7

The lateral axes are X and Y, while the thrust axis is Z. Only one direction was simulated at a time. Additionally, it was not possible to specify a load duration of 20 seconds per axis. As a result, the analysis was performed as a static equivalent load case rather than a time-dependent simulation.

Similar to the Sine simulation, only the parameters from the ”Vehicle Level One” profile were used, as they are expected to exert the highest stress on the gimbal.

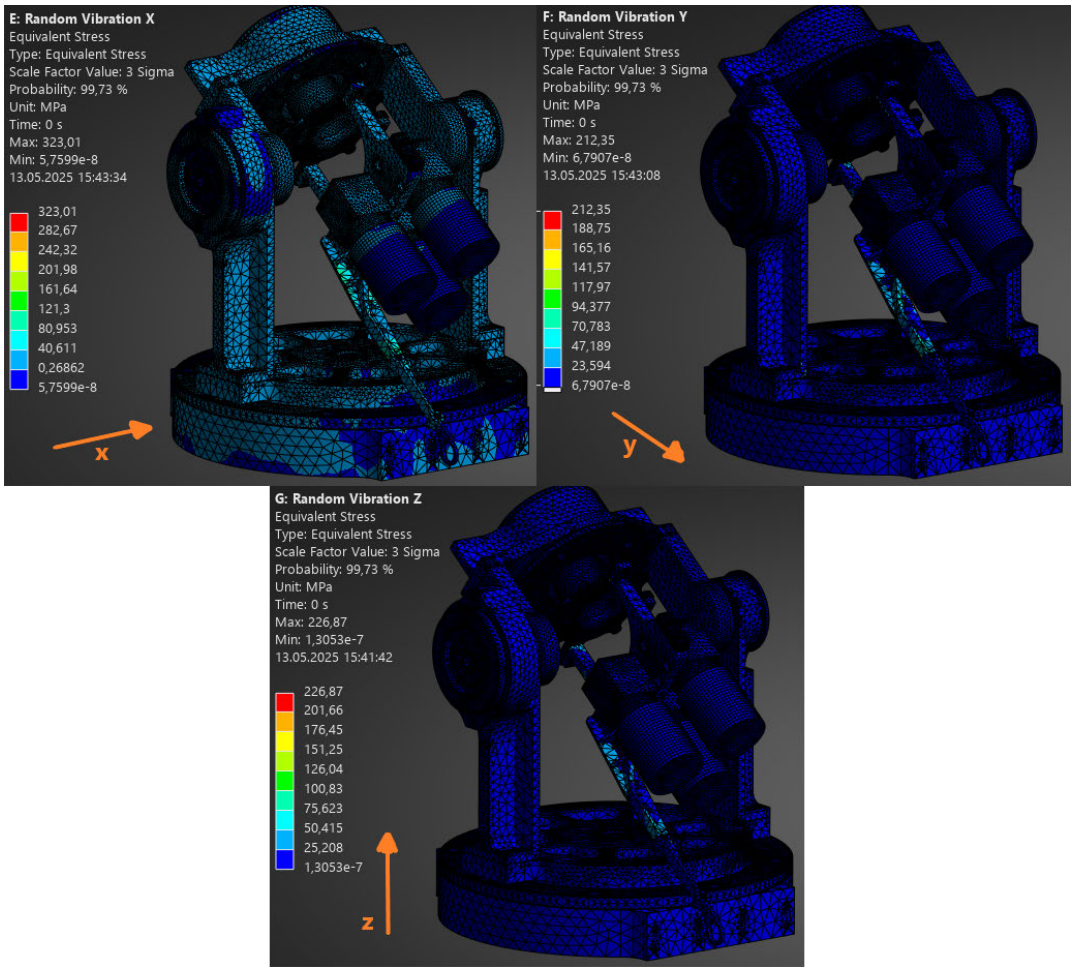


Figure 4.23: Equivalent stress (von-Mises) from the random vibration analysis along the X, Y, and Z axes, shown with a 3σ scaling factor.

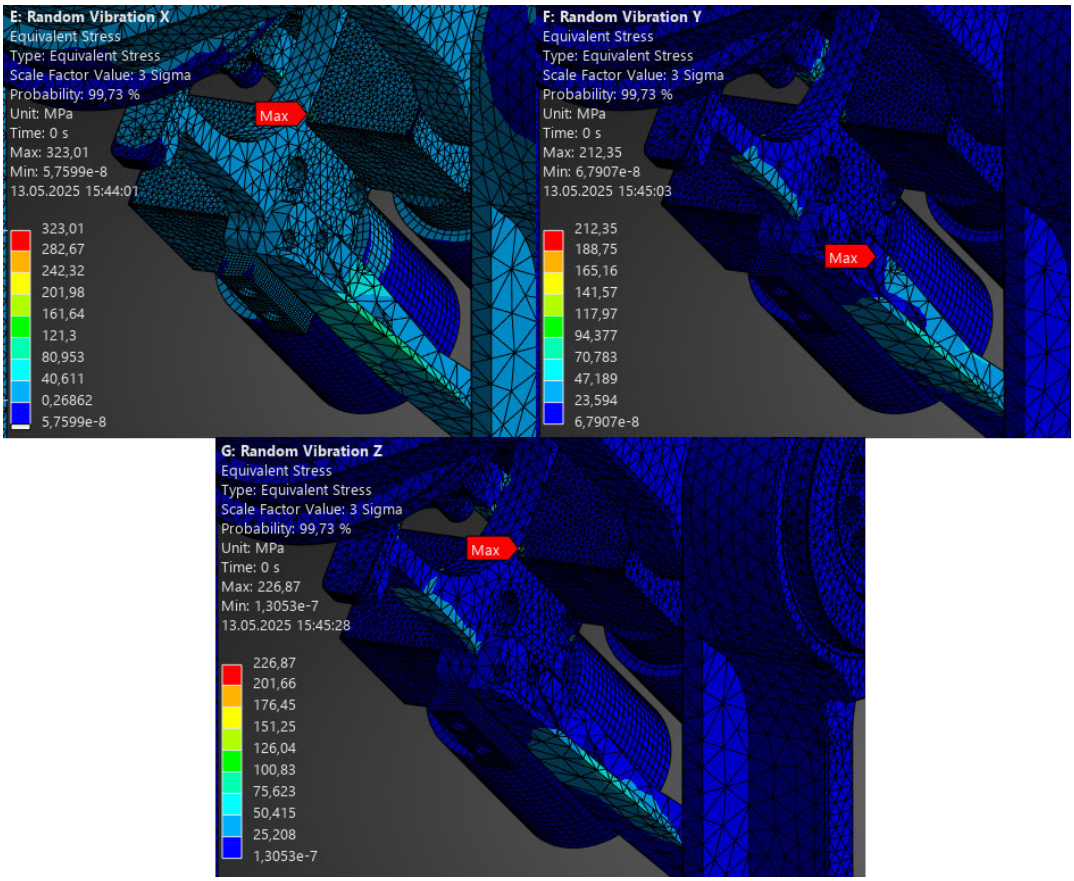


Figure 4.24: Max. point of equivalent stress of the random vibrations along the X, Y, and Z axes.

The results from Figure 4.23 show that the highest stress occurs along the X-axis, reaching 323 MPa. However, this value appears to be a meshing error, as indicated in Figure 4.24. The reason to suspect an error is that the region of maximum stress is extremely small and physically unrealistic.

If this anomaly is disregarded, the locking arm is the component subjected to the highest stress, which does not exceed 130 MPa. This remains well below the yield strength of aluminum EN AW-6082, which is 260 MPa.

The total deformation is also within acceptable limits, staying below 0.05 mm on the locking arm. However, for the X-axis, deformation reaches up to 0.1 mm.

4.5 Electronics Design

4.5.1 Overview

The electronics for the experiment consisted of several components, which are explained in the sections below. The block diagram (Figures 4.8 and 4.10) shows the location and interconnection of all the individual components.

4.5.2 Backplane PCB

The Backplane PCB acted as the interconnect between the RXSM and all other experiment electronic components. It featured three PCIe slots for the FC PCB, the black-box PCB, and the Raspberry Adapter PCB. This simplified the overall system integration while ensuring a reliable connection. The Backplane PCB was mounted with an aluminum support structure to the bulkhead. Additional 3D prints mounted to the aluminum side panels and the Backplane PCB secured the slotted PCBs. The PCBs were secured in place with the top aluminum panel that held down the PCBs with an additional 3D-printed part. The housing for the electronics is further explained in Section 4.5.19.

Connectors on the Backplane PCB included the D-SUB 15 connector to the RXSM interface, the connectors to the Sun Sensor PCBs, and the FFC cable that is wired over the cable reel to the Motor Driver PCB. A D-SUB 25 connector served as a shielded interconnect for the Magnetometer PCB, the battery, and the engineering camera. The blackbox for the experiment data was mounted directly onto the Backplane PCB.

The power distribution with the integrated battery charging and monitoring circuit was also located on the Backplane PCB. This task was realized by a combined buck-boost battery charger, the LTC4020.

The design for this PCB heavily related to the other ASTG's rocket projects Backplane PCB. The battery charging circuit was flight-proven in ASTG's 2024 and 2025 EuRoC rocket.

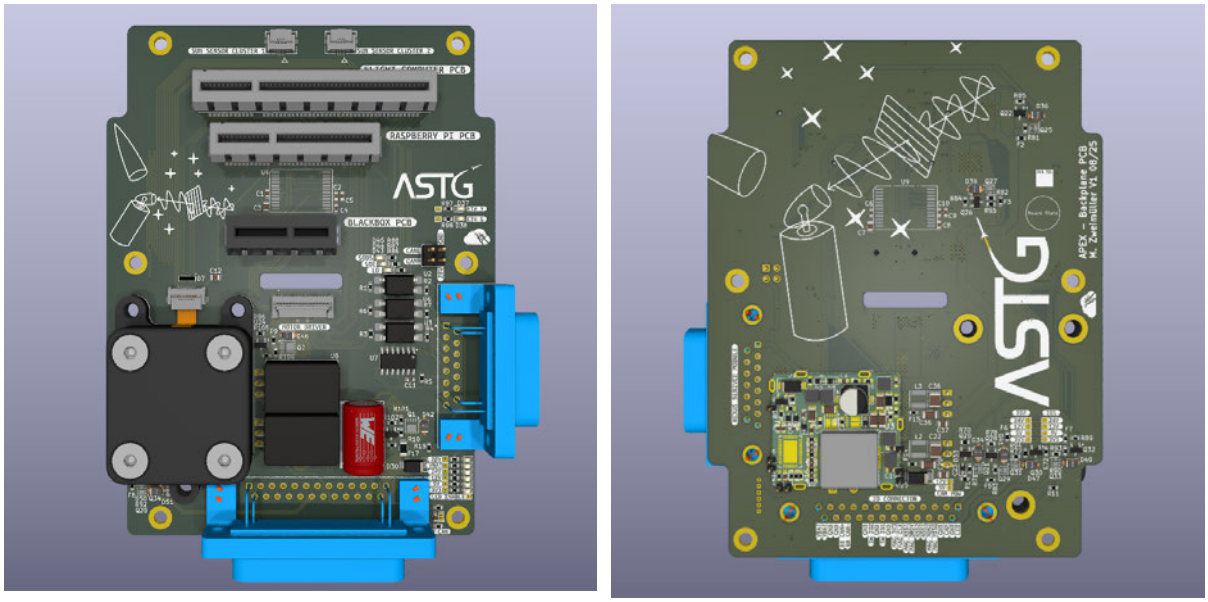


Figure 4.25: Backplane PCB Front and Backside

4.5.3 Flight Computer PCB

The FC PCB was the 5th revision of the ASTGs rocket main FC PCB and had already been flight-tested several times. The main microcontroller was an STM32H745ZIT processor. With its two cores, it can handle the workload of calculating the attitude in real-time as well as all other tasks relevant during flight. Figure **??** shows the front and back side of the Main Flight Computer PCB.

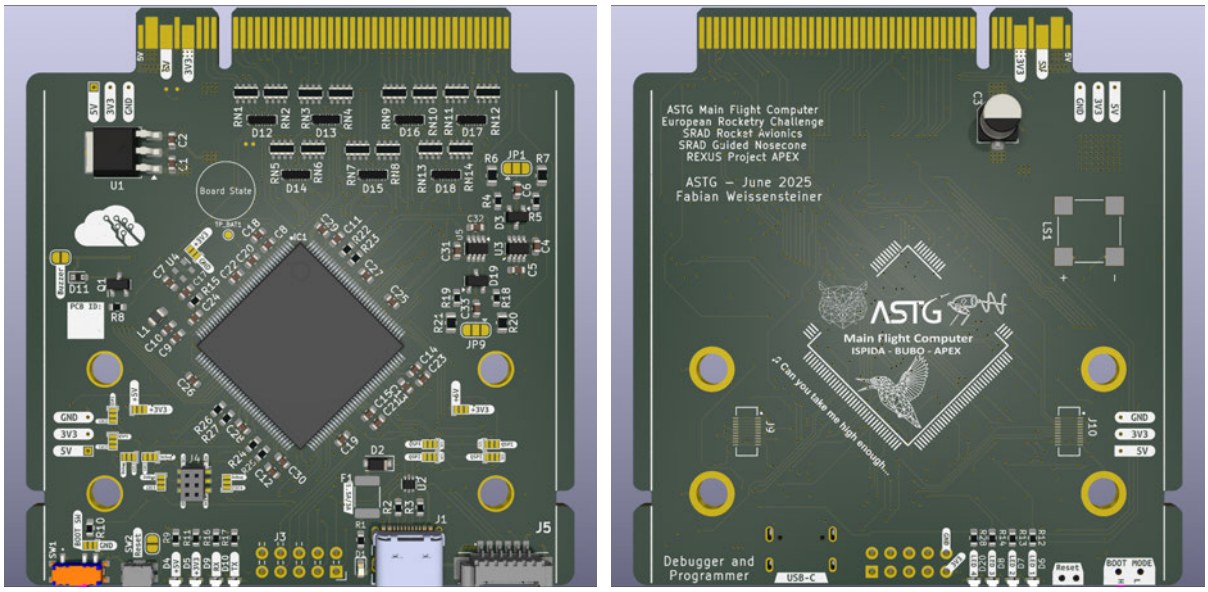


Figure 4.26: Flight Computer PCB Front and Backside

4.5.4 Inertial Measurement Unit (IMU) Sensor PCB

This PCB was a HAT on the FC PCB. Two fully separated IMU channels featured redundancy for sensor data. The board was connected to the FC PCB via four M3 screws and Slim-Stack board-to-board connectors from Molex. For the experiments operation relevant sensors were the BMI088 IMU, and the IAM-20380 gyroscope. As the PCB was designed by the ASTG and also used for the 2025 rocket project, barometers and accelerometers were also included in the circuit. The mounted sensors included:

- BMI088 by Bosch Sensortec: 6DoF IMU with 3 axis accelerometer and 3-axis gyroscope and built-in temperature sensor
- IAM-20380 Gyroscope by TDK InvenSense
- AIS2IH1 Accelerometer
- BMP390 Barometer by Bosch Sensortec
- MS5607 Barometer by TS Connectivity

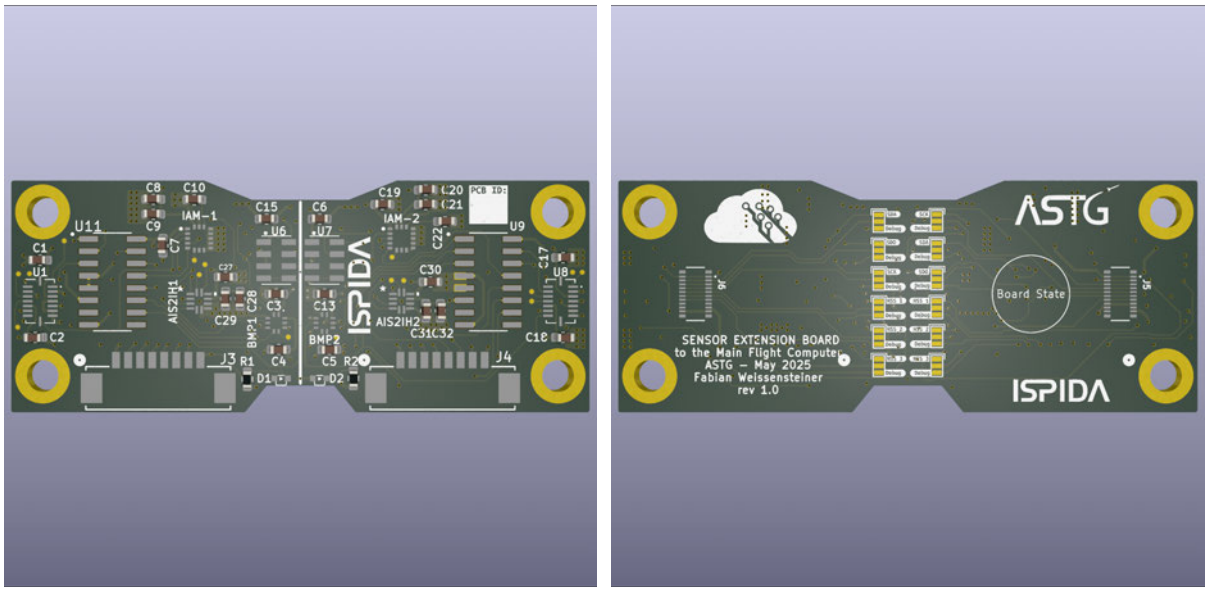


Figure 4.27: IMU Sensor PCB Front and Backside

4.5.5 Blackbox PCB

This PCB was used for storing the housekeeping data generated by the main flight computer and other sensors. With its own microprocessor, it can record and save all data transmitted over the CAN bus.

A PCIe card-style interface served as the connection to the Backplane PCB, the same way as the FC PCB and the Raspberry Adapter PCB.

The Blackbox, described in Section 4.5.6, was connected to the Blackbox PCB with a custom FPC connector and three M3 screws and had been flight-tested several times.

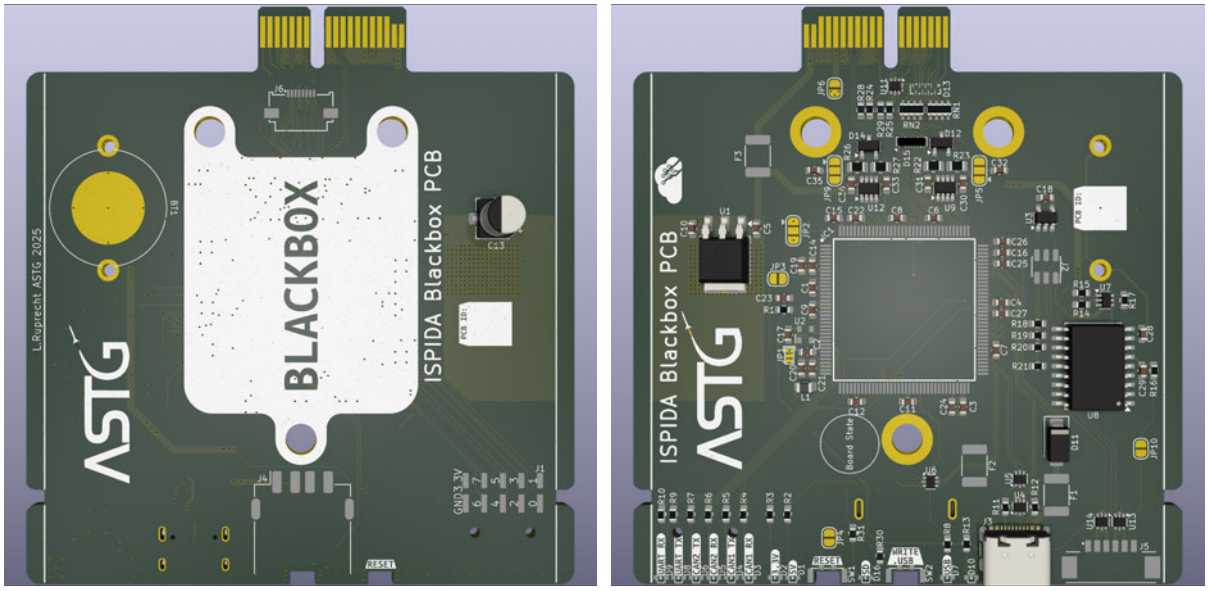


Figure 4.28: Blackbox PCB Front and Backside

4.5.6 Blackbox

The Blackbox was a custom-built enclosure for a micro-SD card. The casing consisted of several carbon layers connected together by three M4 screws. This Blackbox ensured that all collected data is not lost after a crash-landing. Two of these Blackboxes could be found in the experiment. One Blackbox, the Experiment Blackbox, was mounted directly onto the Backplane PCB by three M3 screws. It served as an external SD storage for the Compute Module 5 and therefore houses all the generated polarization images of the experiment cameras. The second, the Housekeeping Blackbox, was mounted on the Blackbox PCB as described in Section 4.5.5.

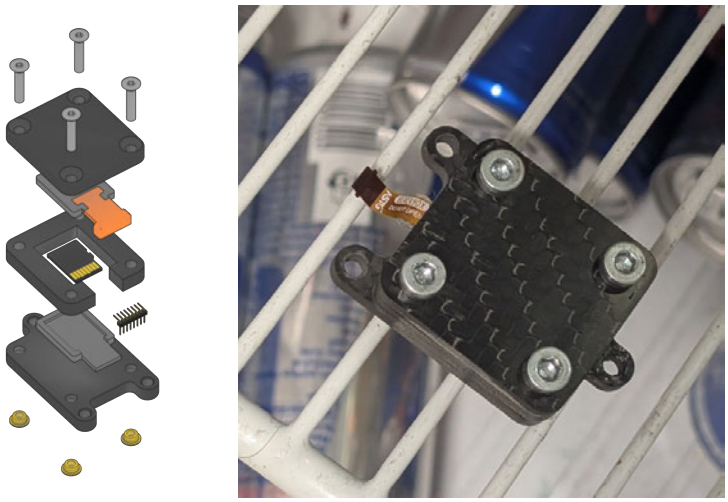


Figure 4.29: Explosion View of Blackbox (left) and Blackbox during thermal testing (right).

4.5.7 Sun Sensors

The design of the sun sensor PCBs was a modified version of the FS1 sun sensor design of the Aalto University in Finland. Changes include:

- A different microprocessor with integrated operational amplifiers for the two-dimensional photodiode S5990-01 from Hamamatsu
- communication over CAN bus

In total, eight sun sensor PCBs were mounted in the configuration seen in Figure 4.30 below (or in Figure 4.47 as mounted on the hardware).

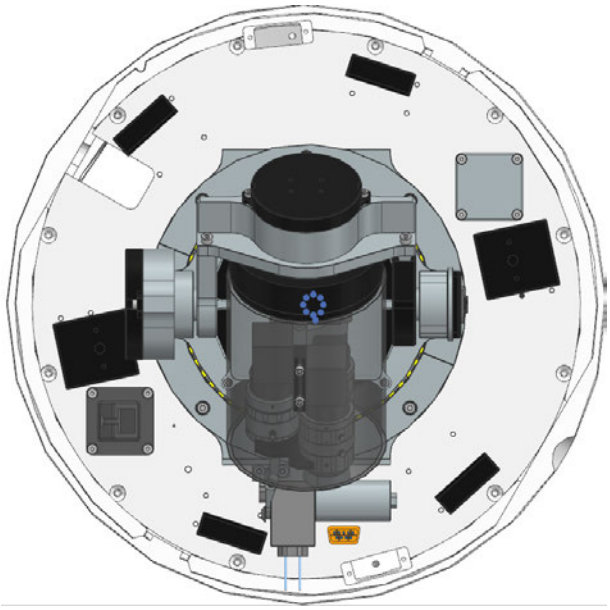


Figure 4.30: Mounting of Sun Sensors

The PCBs were interconnected by COTS FFC cables. The front and backside of the Sun Sensor PCB, and the Pinhole cover can be seen in Figure 4.31 and Figure 4.32 respectively.

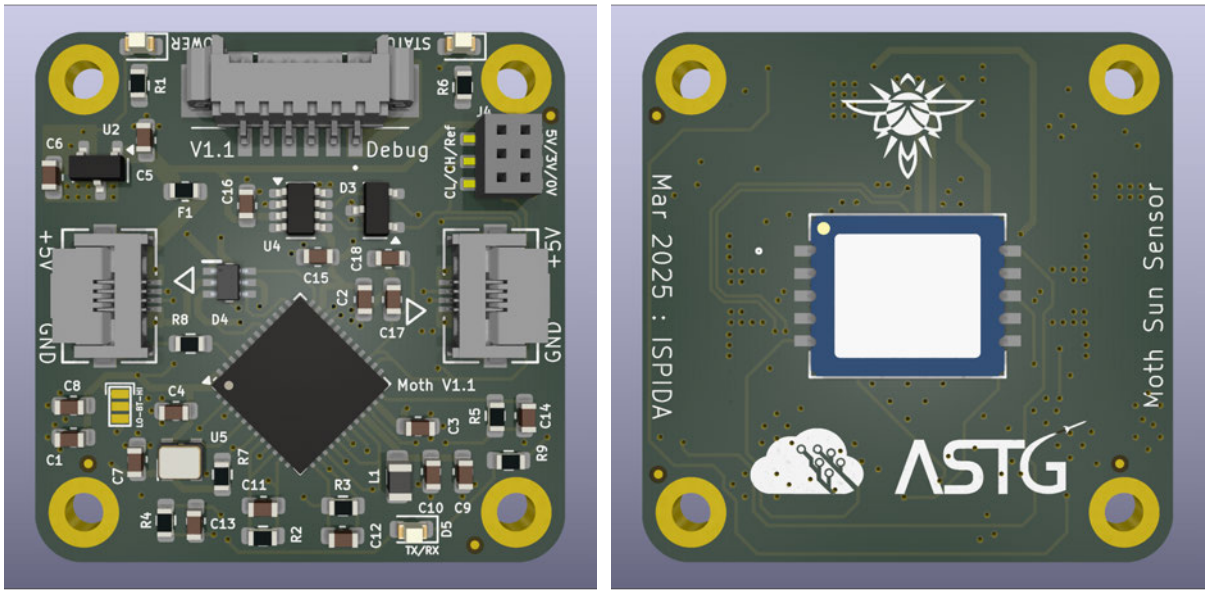


Figure 4.31: Sun Sensor PCB Front and Backside

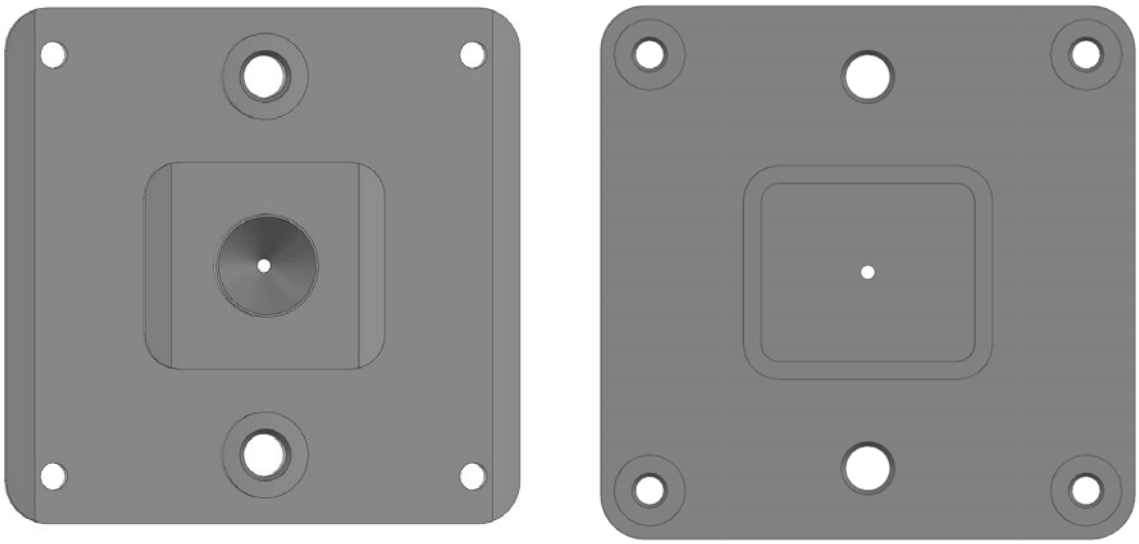


Figure 4.32: Sun Sensor Pinhole Cover PCB Front and Backside

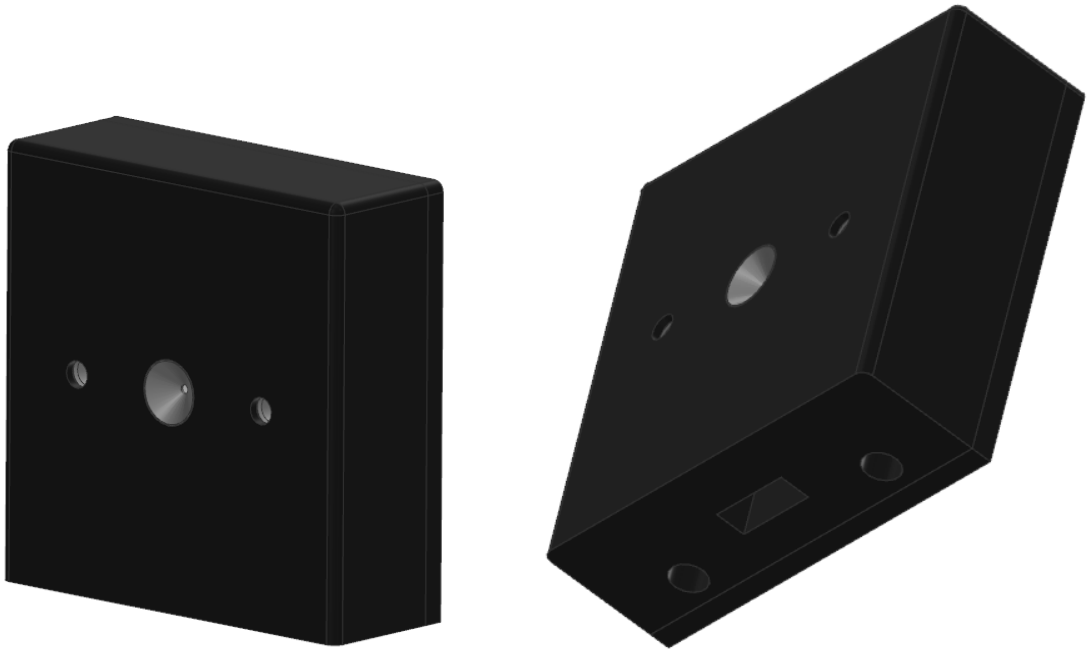


Figure 4.33: Sun Sensor Mounting Single Front Side

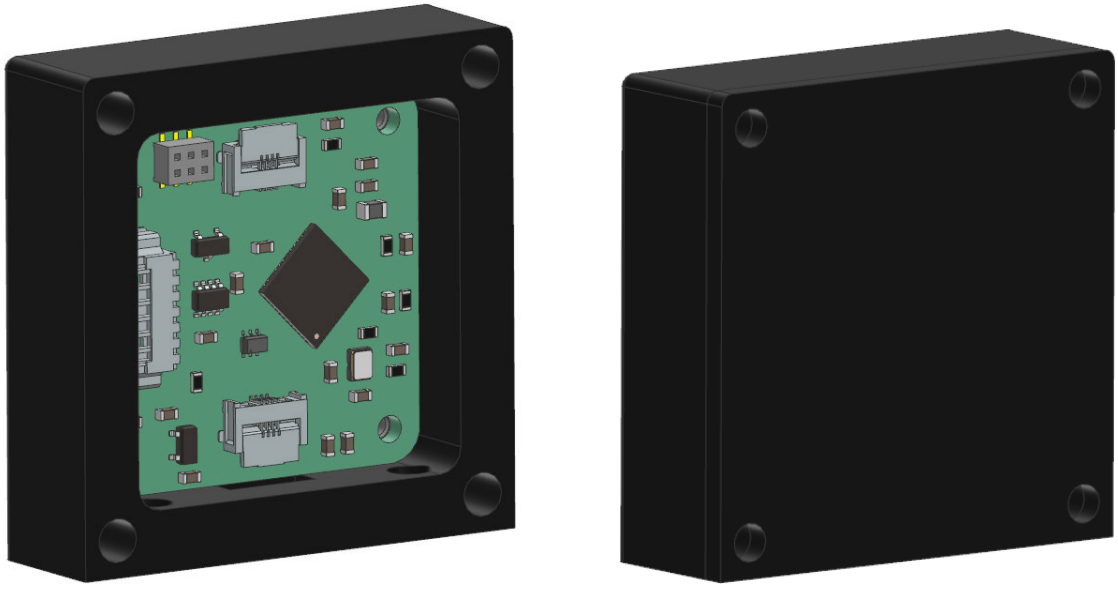


Figure 4.34: Sun Sensor Mounting Single Back Side

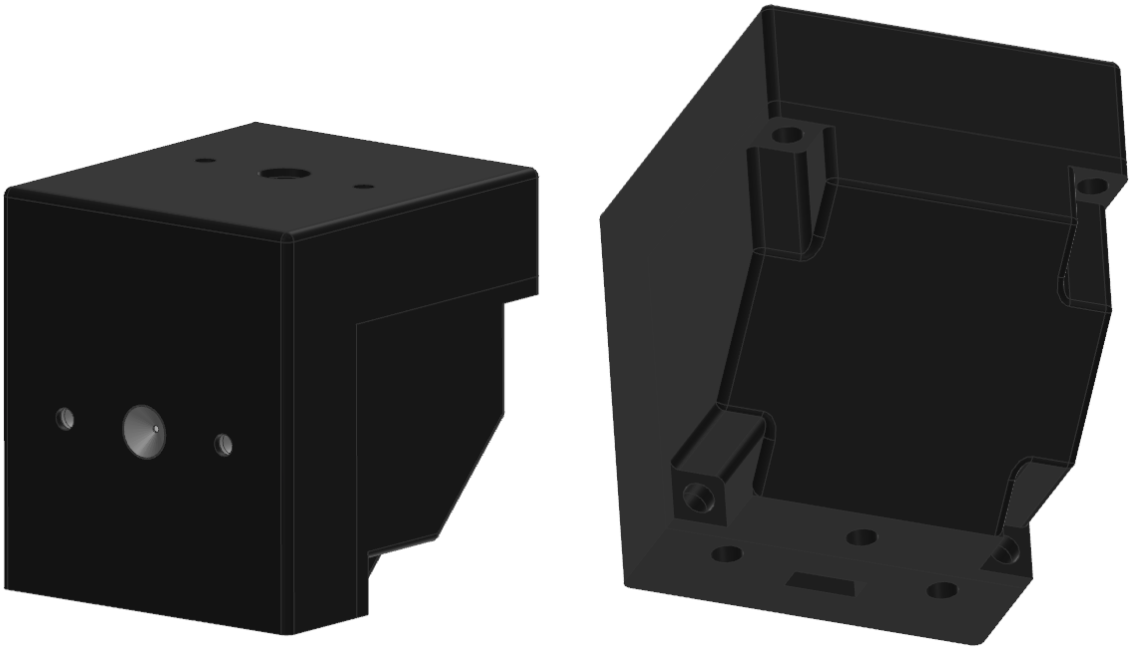


Figure 4.35: Sun Sensor Mounting Double

4.5.8 Magnetometer

The Magnetometer PCB featured an RM3100 sensor from PNI Sensor and was connected to the Backplane PCB over a cable connection via SPI. It was a standalone PCB so that it could be mounted apart from other parts that emit electromagnetic interference. The sensor was a magneto-inductive type and consisted of three coils and an ASIC that controlled the circuit and handled the SPI communication. It was housed in an aluminum enclosure with a 3D-printed wall and carbon top plate similar to the engineering camera's housing as seen in Figure 4.37.

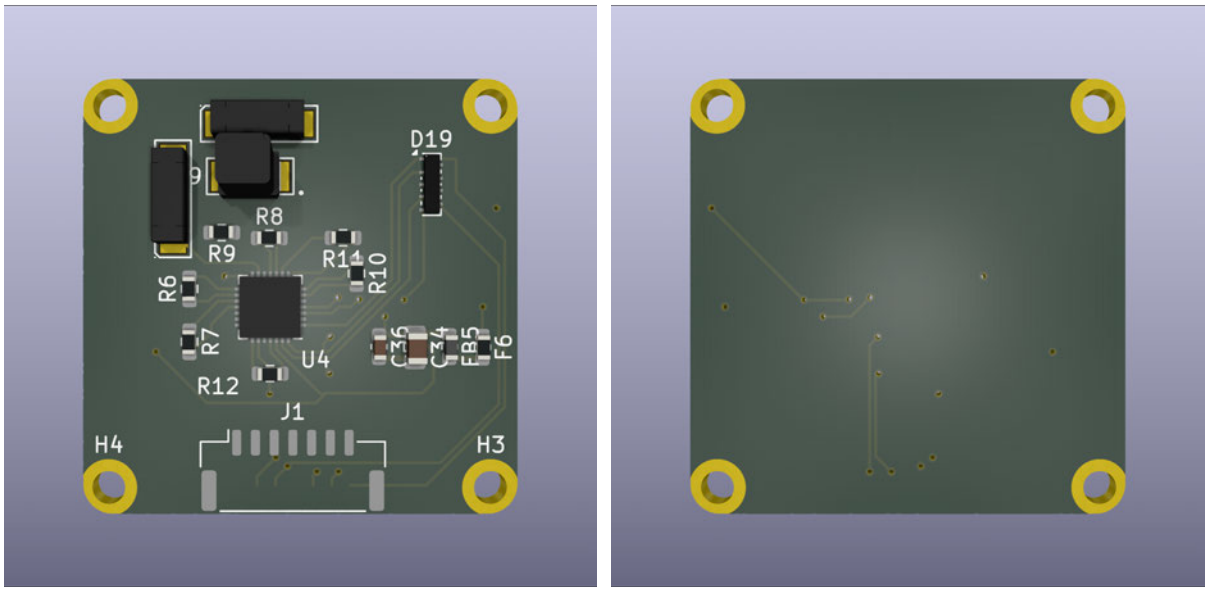


Figure 4.36: Magnetometer PCB Front and Backside

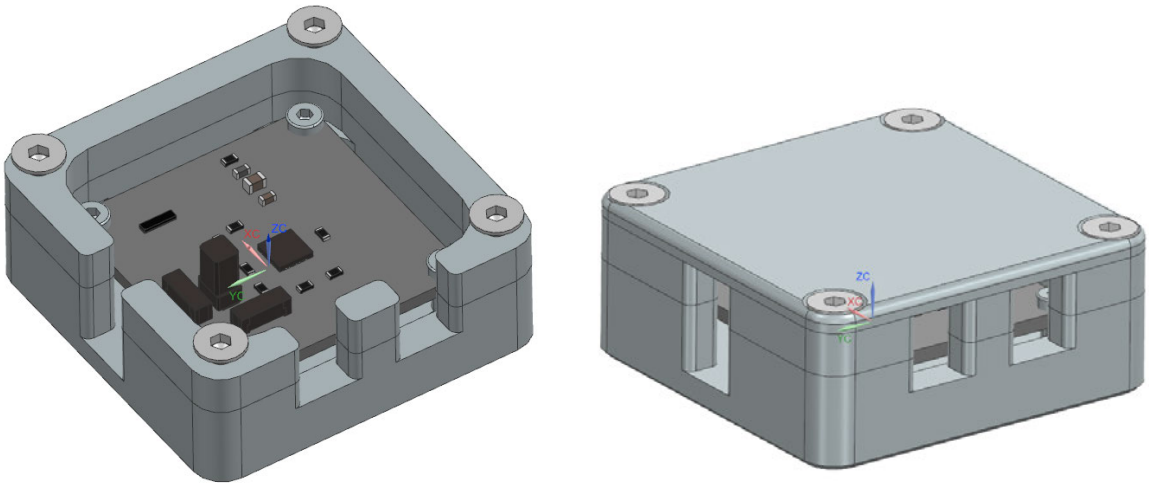


Figure 4.37: Magnetometer mounting

4.5.9 Motor Driver PCB

The Motor Driver PCB was responsible for actuating the three BLDC motors and used the feedback from the position sensors in a closed-loop control algorithm. A more detailed explanation of the FOC algorithm and the closed-loop control is given in Section 4.8.4. To mitigate voltage ripples and interferences due to the switching currents of the drivers, an additional filtering circuit was implemented. The main components of the PCB included:

- 3 DRV8313 BLDC drivers
- 2 connectors for AS5048A absolute magnetic encoders
- 1 directly mounted encoder on the back side of the PCB
- 2 inline current sensing op-amps for every driver

- feedthrough for Ethernet connection between Raspberry Pi and Ethernet Switch
- CAN interface
- STM32H725 microcontroller

The front and back side of the Motor Driver PCB can be seen in Figure 4.38.



Figure 4.38: Motor Driver PCB Front and Backside

4.5.10 Encoder

Three AS5048A magnetic encoders were used to determine the current absolute position of every axis. Those sensors measured the magnetic field changes of a rotating, small diametrically magnetized (two-pole) magnet placed on the rotor with a resolution of 14 bits, which equals an accuracy of 0.05°. The encoders were connected to the Motor Driver PCB over SPI. The cross-sectional view of the recommended mounting can be seen in Figure 4.39.

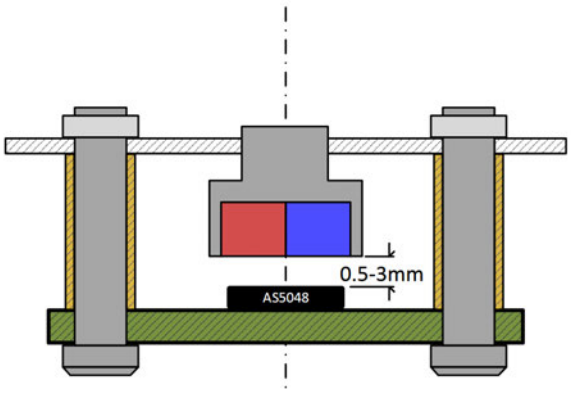


Figure 4.39: Recommended mounting. Crosscut of AS5048 and Magnet.

4.5.11 Motors

Three BLDC motors were used to move the gimbal in each of the three axes. The used motors were Cubemars RI-60 Frameless Inrunner. They had a frameless design for better integration without built-in bearings, so that individual bearings, which could be preloaded, could be integrated. The motor specifications can be seen in Table 4.10 below. The three phases of each of the motors were connected to the Motor Driver PCB, which delivered the sinusoidal control signals. Figure 4.40 shows the motor with the rotor, consisting of the metal ring with the magnets, on the left side and the stator with the coils on the right side.

Table 4.10: Motor Specification

Rated Voltage	24-48V
Rated Torque	0.57Nm
Pole Pairs	14
Kt (Nm/A)	0.1



Figure 4.40: Cubemars RI60 Inrunner Motor

4.5.12 Raspberry Adapter PCB

The Raspberry Adapter PCB was a custom IO-board that breaks out several interfaces from the Compute Module 5. The Compute Module 5 was mounted by 4 M2.5 screws and connected by two Amphenol 100pin 0.4mm pitch connectors to the Adapter PCB. A SPI to CAN chip enabled communication from the Compute Module 5 to the FC PCB via CAN-FD.

The Compute Module 5 was supplied by 5 V from the Backplane PCB.

The images generated by the experiment cameras and transmitted to the Compute Module 5 were planned to be saved on the Experiment Blackbox, which was configured as an external SD storage for the Compute Module 5. The Raspberry Adapter PCB had a PCIe card-style interface so that it could be connected to the Backplane PCB the same way as the FC PCB and the Blackbox PCB. Figure 4.41 shows the front and back side of the Compute Module 5.

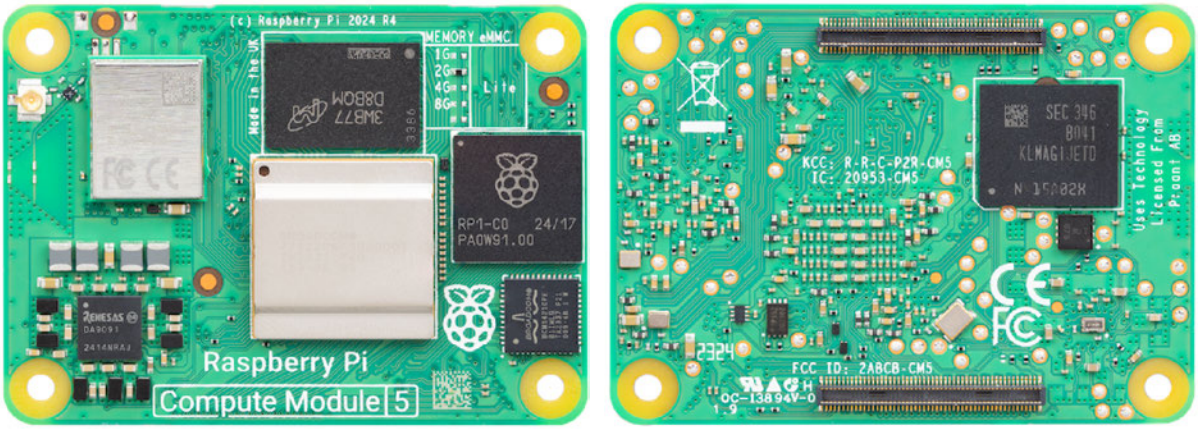


Figure 4.41: Raspberry Pi Compute Module 5 Front and Backside

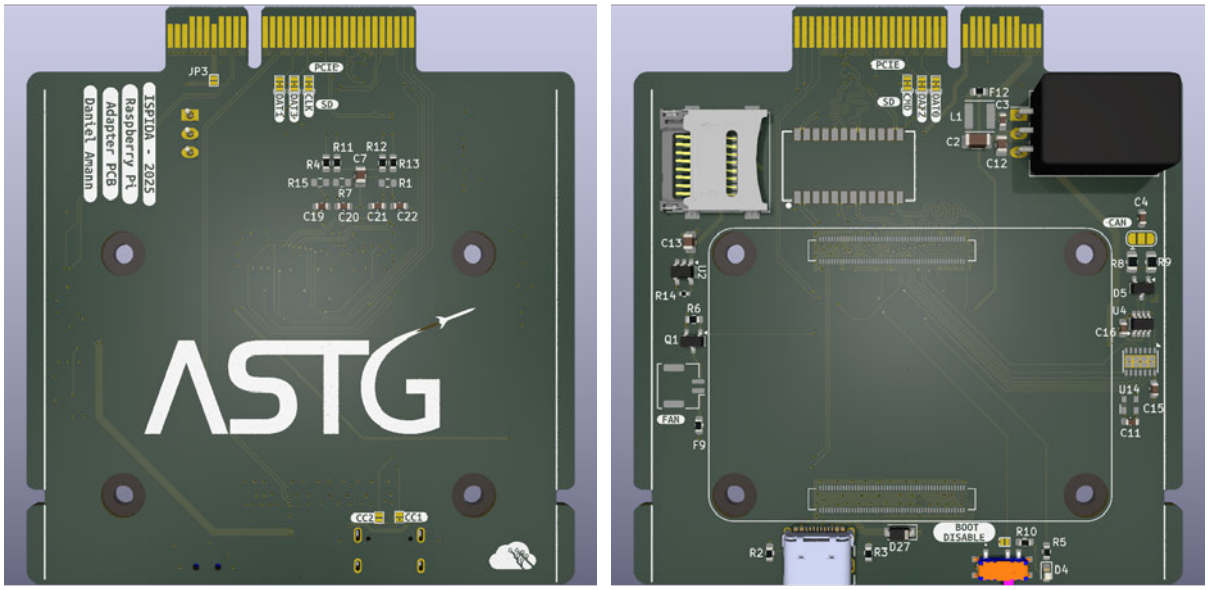


Figure 4.42: Raspberry Adapter PCB Front and Backside

4.5.13 Ethernet Switch and Adapter PCB

To connect more than one camera to the Raspberry Pi over Ethernet, an Ethernet switch was needed. The Gigablox Nano from Botblox was a small-sized Gigabit Ethernet switch with four ports. A custom-designed adapter board stacked on top of the Ethernet switch broke out the FFC connectors to the three cameras and a fourth connector to the Raspberry Pi. Figure 4.43 shows the front side of the Gigablox Nano Ethernet Switch. The back side of the PCB had the connection to the adapter board. The adapter board was a custom PCB that had three FFC connectors for the experiment cameras and two more connectors on the backside for the Ethernet Switch and the connector to the Motor Driver PCB. The mounting of the components in the Gimbal can be seen in Figure 4.45.

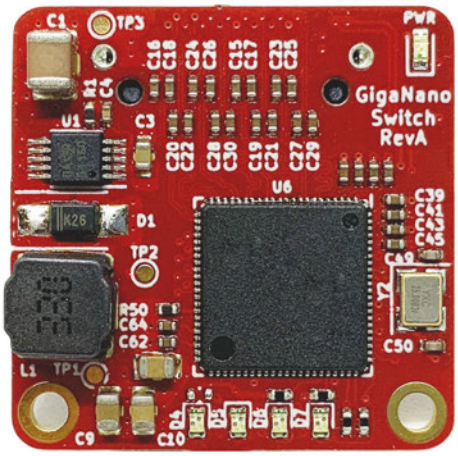


Figure 4.43: GigaBlox Nano Ethernet Switch

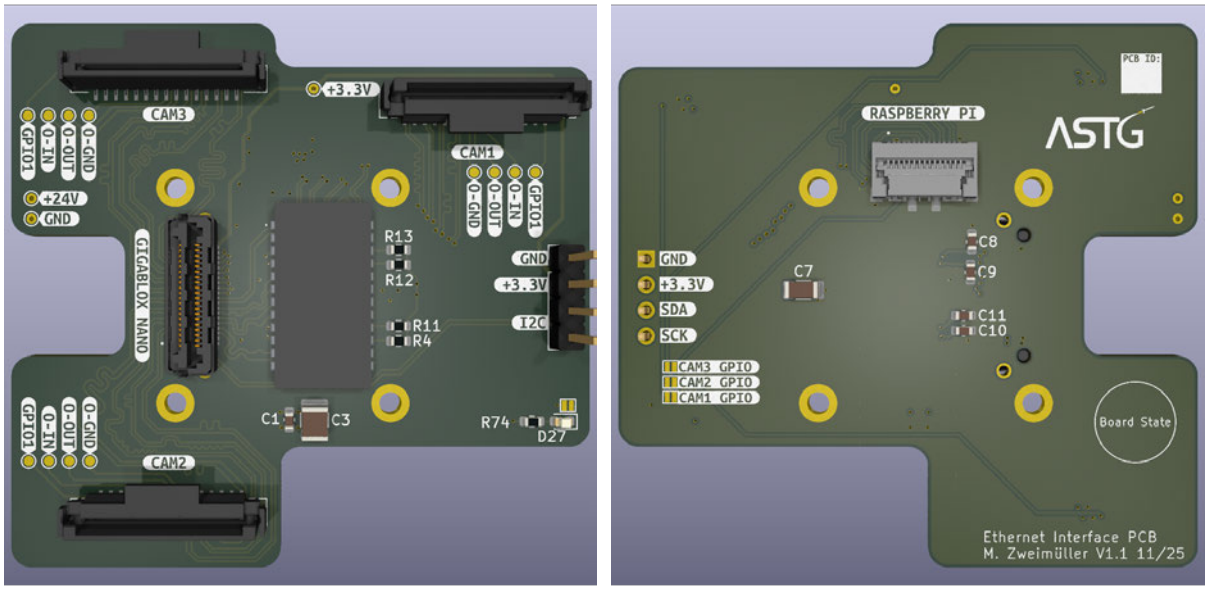


Figure 4.44: Ethernet Switch Adapter PCB Front and Backside

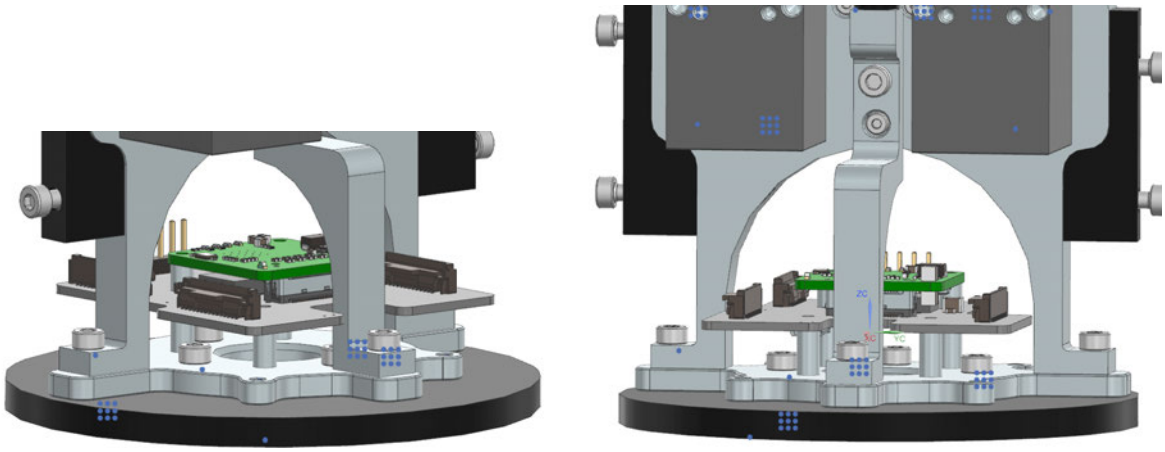


Figure 4.45: Ethernet Switch and Adapter Mounting

4.5.14 Experiment Cameras

The two main experiment cameras were LUCID Phoenix PHX050S1-PC-FFC with the Sony IMX264MZR polarization monochrome sensor. The third camera, the PHX050S-CC-FFC with an RGB IMX264 sensor, was planned to be used as a public outreach and context camera. The cameras featured an FFC connector as their electrical interface. Instead of using the RJ-45 connector, which would have taken up a lot of unnecessary space, the more compact FFC connectors were used. Two different kind of lenses were mounted on the cameras. The EO C Series Lens 2/3" 16 mm with a horizontal field of view of 30 degrees was mounted on the two experiment, polarization, cameras. The EO C Series Lens 2/3" 8.5mm, with a horizontal field of view of 60 degrees was mounted on the context camera.

The routing between the Experiment Cameras and the Raspberry PI happened over the Backplane PCB and the bottom Cable Reel, onto the Motor Driver PCB and from there to the upper Cable Reel and the Ethernet Switch, the Adapter and the individual Cameras.

4.5.15 Engineering Cameras

An engineering camera was mounted on the bulkhead so that the FOV included the operating gimbal with the locking mechanism and the background of the Earth and sky. A Runcam Split 4 used in many ASTG rockets before, was used for this task. It could simultaneously stream, record and save video on the internal SD card. The video output of the camera was connected to a BNC connector, where the REXUS TV channel was then connected. The lens was housed in a 3D-printed structure seen in Figure 4.46. The PCB was mounted on the top side of the bulkhead (see Figure 4.47) and housed in an aluminum structure also seen in Figure 4.46.

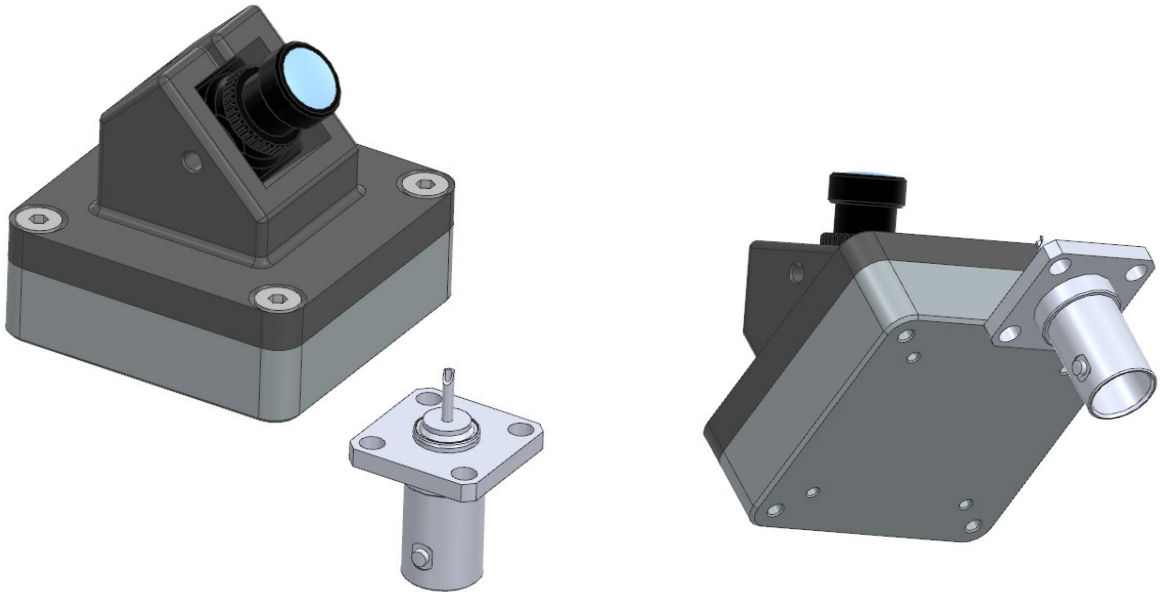


Figure 4.46: Engineering Camera Mounting
Runcam Split 4 with Enclosure and TV-Channel Connector

4.5.16 Battery

To overcome the maximum current limitations of the REXUS power system, an additional battery was implemented. A 7s1p (7 in series connected cells) configuration of LiFePo4 cells with an individual cell capacity of 1200mAh resulted in a total energy of 27.72 Wh. The battery pack is custom-built and has its own COTS Battery Management PCB. With an individual voltage of 3.65 V when fully charged and 3.3 V at nominal charge per Cell, the resulting battery voltage resulted in 25.2 V and 23.1 V respectively. The worst-case power consumption in Section 4.7 shows that 6.432 Wh are used from the Battery, which fulfills the 80% capacity requirement.

The battery was assembled as a quickly exchangeable pack with a D-SUB9 connector, connecting directly to the D-SUB25 connector of the Backplane PCB and was mounted on the Bulkhead with an aluminum support plate and M3 threaded rods (see Figure 4.54 for a hardware image). Figure 4.48 shows the explosion view of the battery with its individual cells and the mounting.

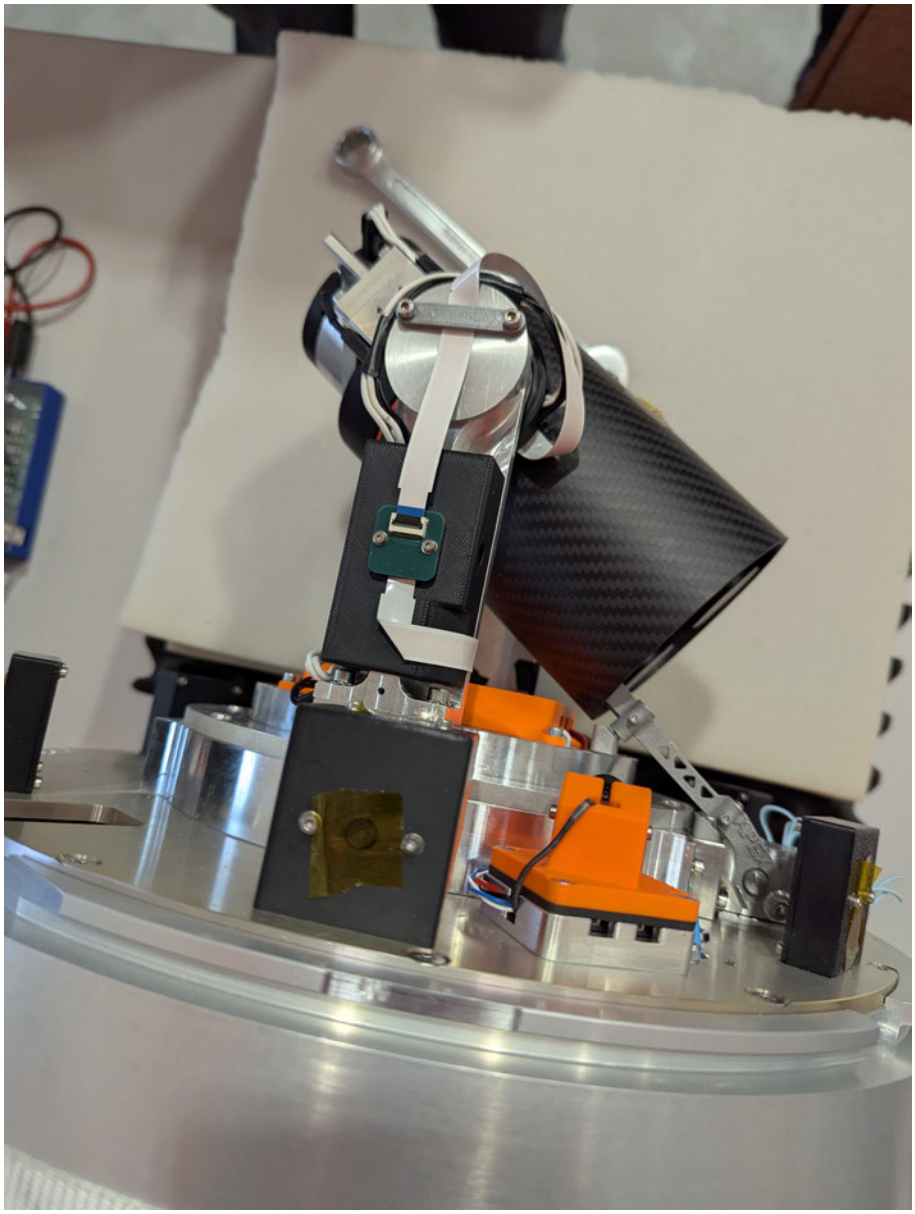


Figure 4.47: Image of the Sun-sensor(s) (in black 3D print and Engineering Camera (orange 3D print) mounted on the bulkhead with the gimbal.

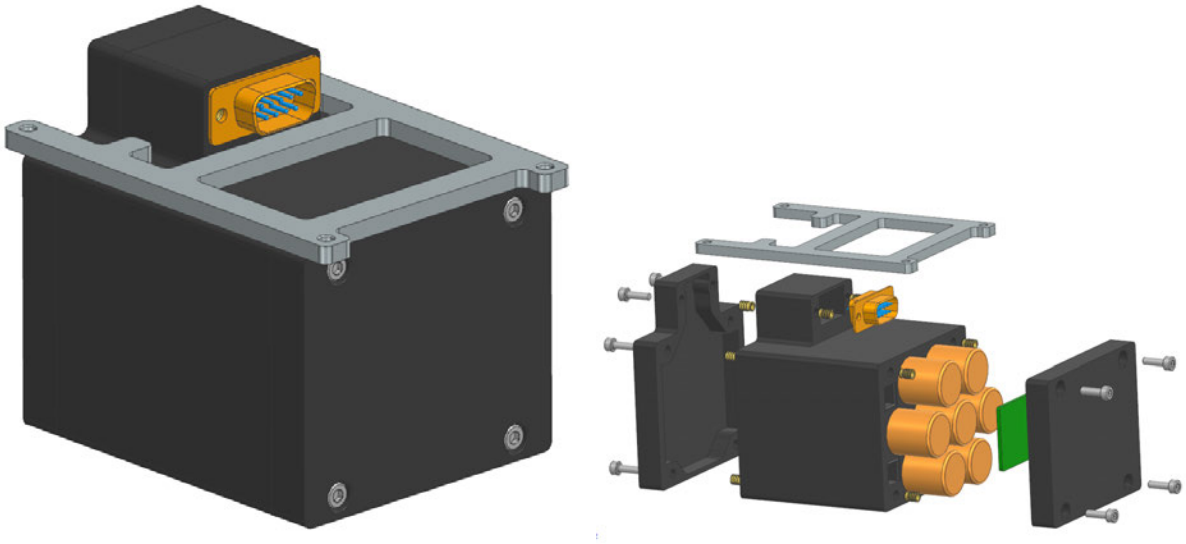


Figure 4.48: Battery in assembled and explosion view

4.5.17 Radio Silence Concept

Due to the use of Batteries in the experiment, the system had to adhere to Radio Silence announced by the Operations Officer during launch preparations. The system had to be completely dead, so when the power is turned off by the RXSM, an extra NMOS and PMOS circuit between the battery output and the system input will switch off the battery power. The circuit for this concept can be seen in Figure 4.49 below.

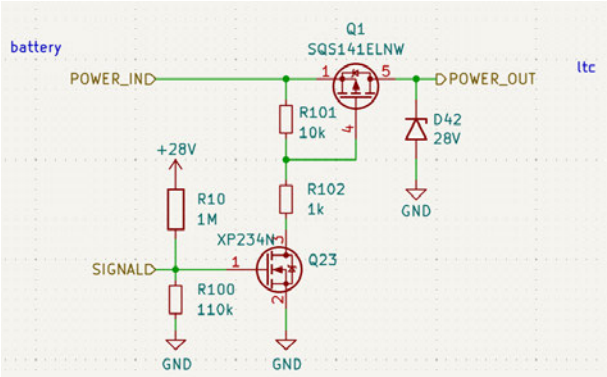


Figure 4.49: Circuit for Radio Silence with two MOSFETs

4.5.18 Cable Reel

To transmit power between the different rotational stages, coiled FFC cables were used. The FFC cables were commercially available cables. To mitigate the use of lots of connectors in between the Backplane PCB and the different rotational stages, the cables were folded at the end points as seen in Figure 4.50.



Figure 4.50: Coiled and folded FFC cable

To enable more than one rotation without straining the cables, they had a length of 300 mm. They had a pitch of 0.5 mm resulting in a height of 13 mm for the lower cable reel with 25 contacts and 8 mm for the upper cable reel with 15 contacts. By their rating, they limited the maximum transmitted current at 0.5 A per contact, so seven contacts each were used for power and ground for the lower Cable Reel for a maximum current of 3.5 A, and three contacts each were used for power and ground on the upper Cable Reel to transmit a maximum of 1.5 A.

Two Cable Reels were integrated, one was connecting the base to the rotational stage and the other connects the swivel to the camera. The coiled cables were enclosed in a 3D-printed structure to minimize movement in the vertical axis. The cabling connecting the rotational stage and the swivel stage was realized by regular silicon cables wrapped with a cable sleeve and routed over the top of the arm with a short slack to enable rotation without straining the cables. To mitigate tangling cables, they were fixed to the arms with a support structure seen in Figure 4.51

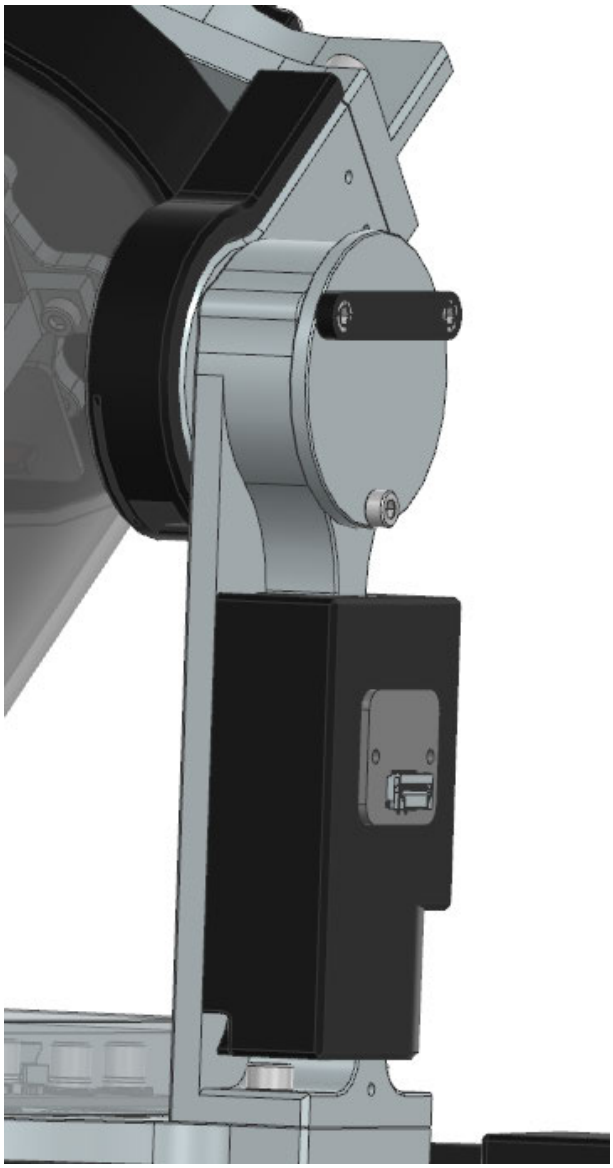


Figure 4.51: 3D printed support structure for Cable Loop. The hardware implementation can be seen in Figure 4.47 on the gimbal in the background.

4.5.19 Electric Shielding

To minimize the electric noise produced by PCBs and motors, they were covered with electrically conductive shielding. For the Motor Driver PCB, the swivel motor and the camera motor, these shields consisted of 3D printed covers, either electroplated or covered with metal foil (see Figure 4.52).

Figure 4.53 shows the mounting and shielding for the main electronic components. The structure consisted of four CubeSat corner pillars that have already been manufactured for previous ASTG CubeSats. With sufficient spares available, reusing them for the structure saved both cost and time. The side panels were 2 mm aluminium panels and could be manufactured by the team with waterjet cutting. Additional 3D printed supports were holding the PCBs in place.

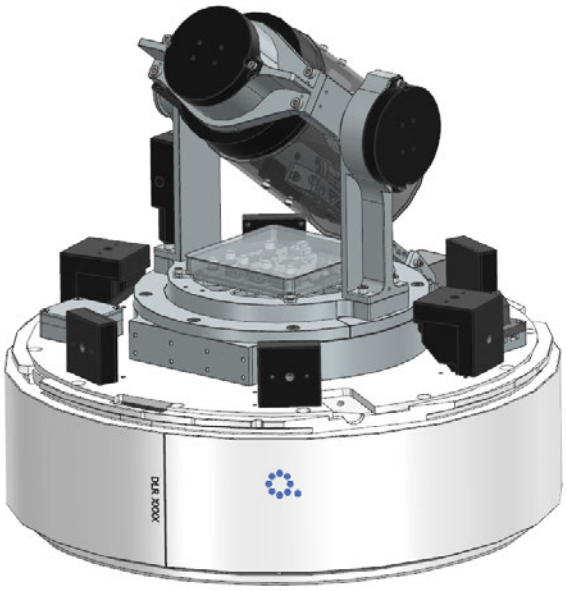


Figure 4.52: The motor and the motor driver PCB were covered by conductive 3D printed covers to minimize electromagnetic emission.

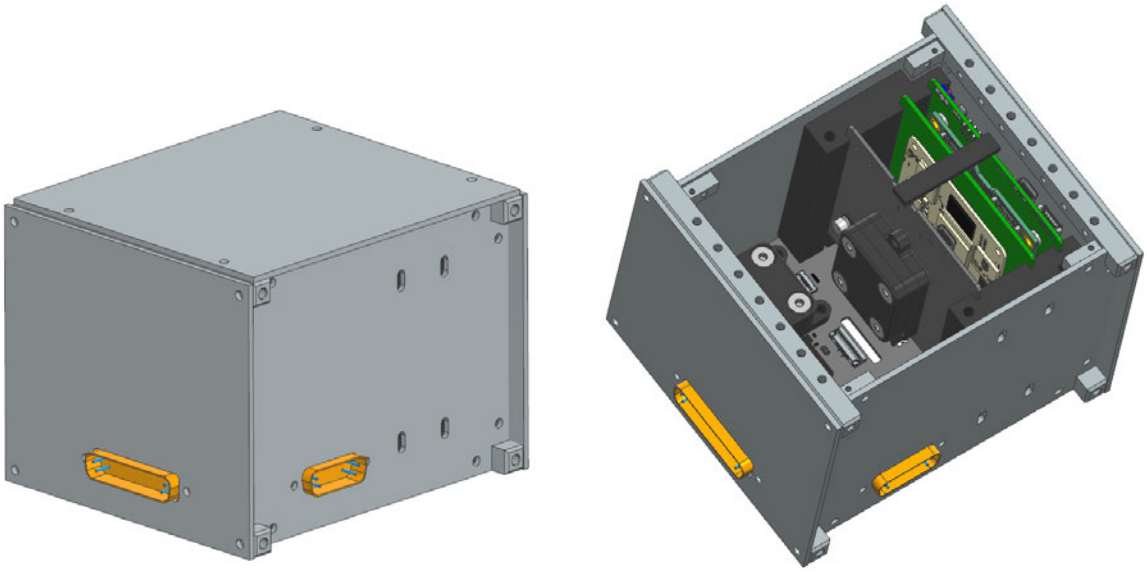


Figure 4.53: Aluminum housing of the Avionics. The box consisted of repurposed aluminum struts with aluminum side panels.

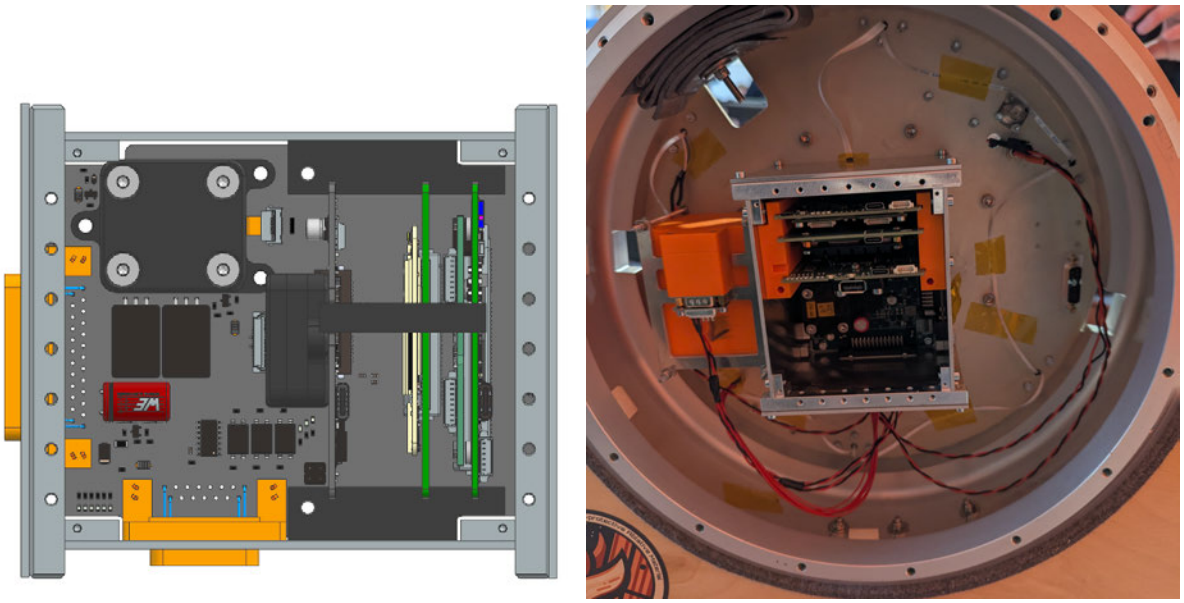


Figure 4.54: [
Top Down View of Avionics Stack (left) next to an image from below the bulkhead (right). Next to the Stack the batteries pack is visible in orange. To the bulkhead the cables for the sun sensors and the engineering camera are taped. In the upper left corner a lead weight for balancing the rocket (mounted by the launch provider) can be seen.

4.6 Thermal Design

4.6.1 Operating Temperature

The following table shows the operating temperature ranges of all temperature-critical components. Regarding the storable temperature range, the cameras and motors were rated to withstand cooling down to −30 °C.

Table 4.11: Operating Temperature Ranges of Components

Component	**min. T [°C]**	**max. T [°C]**
3D Print (ASA)	-30	85
Bearings	-55	120
Motor	-20	50
Space Grease	-80	200
Camera	-20	55
Lens	-20	60
Filter	-20	60
Motor Driver PCB	-20	85
Backplane PCB	-20	85
Raspberry Pi Compute Module 5	-20	85
Ethernet Switch	-20	80
Flight Computer PCB	-20	85
IMU Sensor PCB	-40	85
Sun Sensor PCB	-20	60
Magnetometer PCB	-40	85
Encoder	-40	125
Battery	-20	60
E-Match	-40	71
Range	**-20**	**50**

The safe operating temperature range of the components was between -20 °C and 50 °C. Since the temperature inside the unheated launcher housing was expected to range from -30 °C to +25 °C, a heater was required during launch to ensure safe operation of all components.

4.6.2 Thermal FEM Analysis: Setup

For this analysis, the *Transient Thermal* module in ANSYS was used, enabling temperature evaluation over a specified time frame.

The simulation parameters were defined as follows: the operation time was set to 120 s, and the initial temperature was set to 20 °C. This temperature represents a worst-case scenario, as the heater unit on the rocket is designed to maintain the experiment temperature above 0 °C.

Only the mechanical structure and its associated heat sources were included in the model. Electrical cables have not been considered. The included heat sources are:

- Motors: 3 × 12 W (24 V, 0.5 A) (maximum power draw)
- Cameras: 3 × 2.5 W
- Solar radiation: 1360 W/m^2
- Thermal radiation: ambient temperature of 200 K with an emissivity of 0.2 (milled aluminum)

The heat generated by the motors was applied to the surfaces of the stators, where the copper windings are located. For the cameras, heat was applied directly to their external surfaces. Radiative heat exchange was modeled on all external surfaces of the gimbal. Solar radiation was applied only to the surfaces exposed to sunlight, those primarily those facing opposite the direction the cameras are pointed.

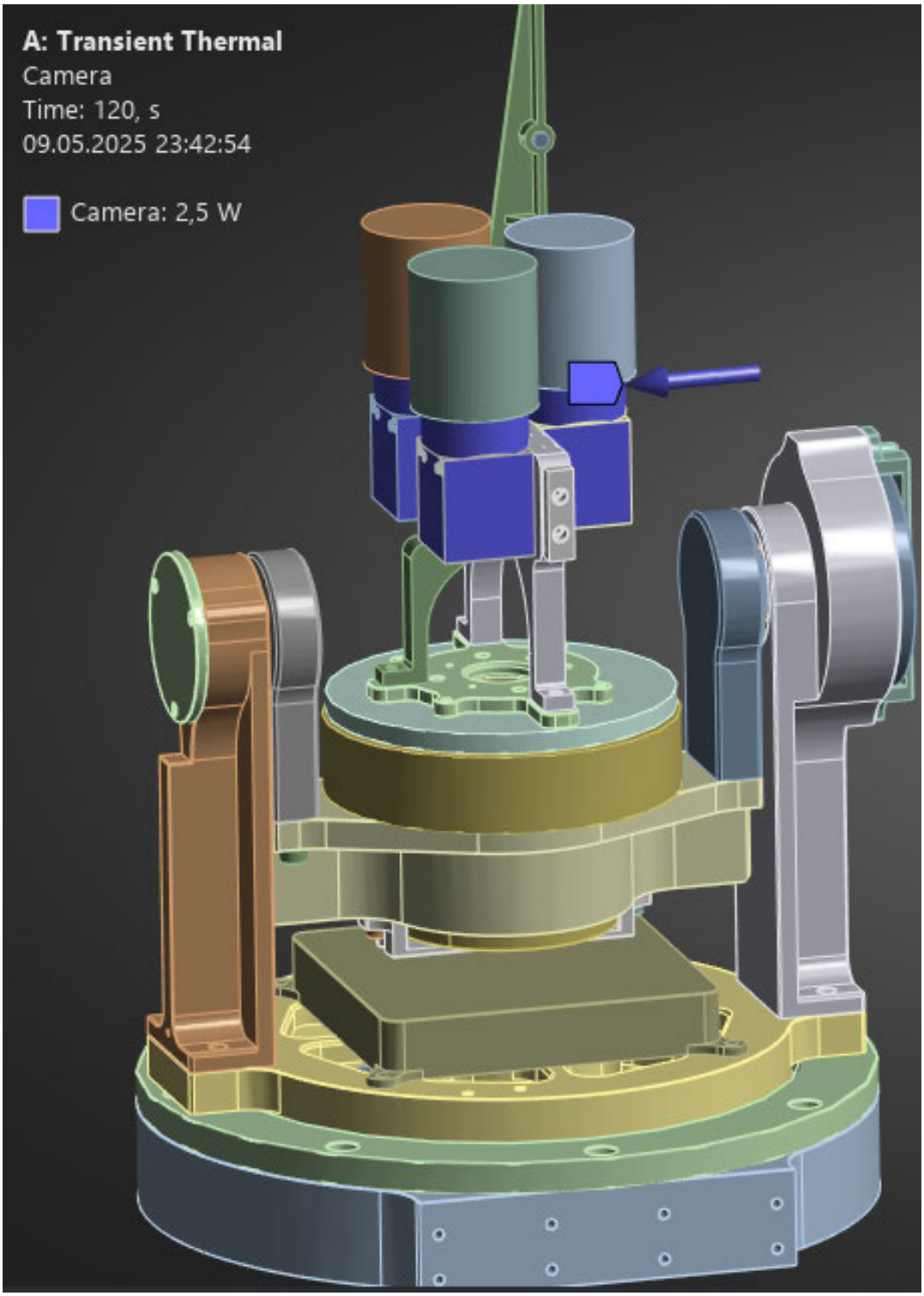


Figure 4.55: Heat source of camera

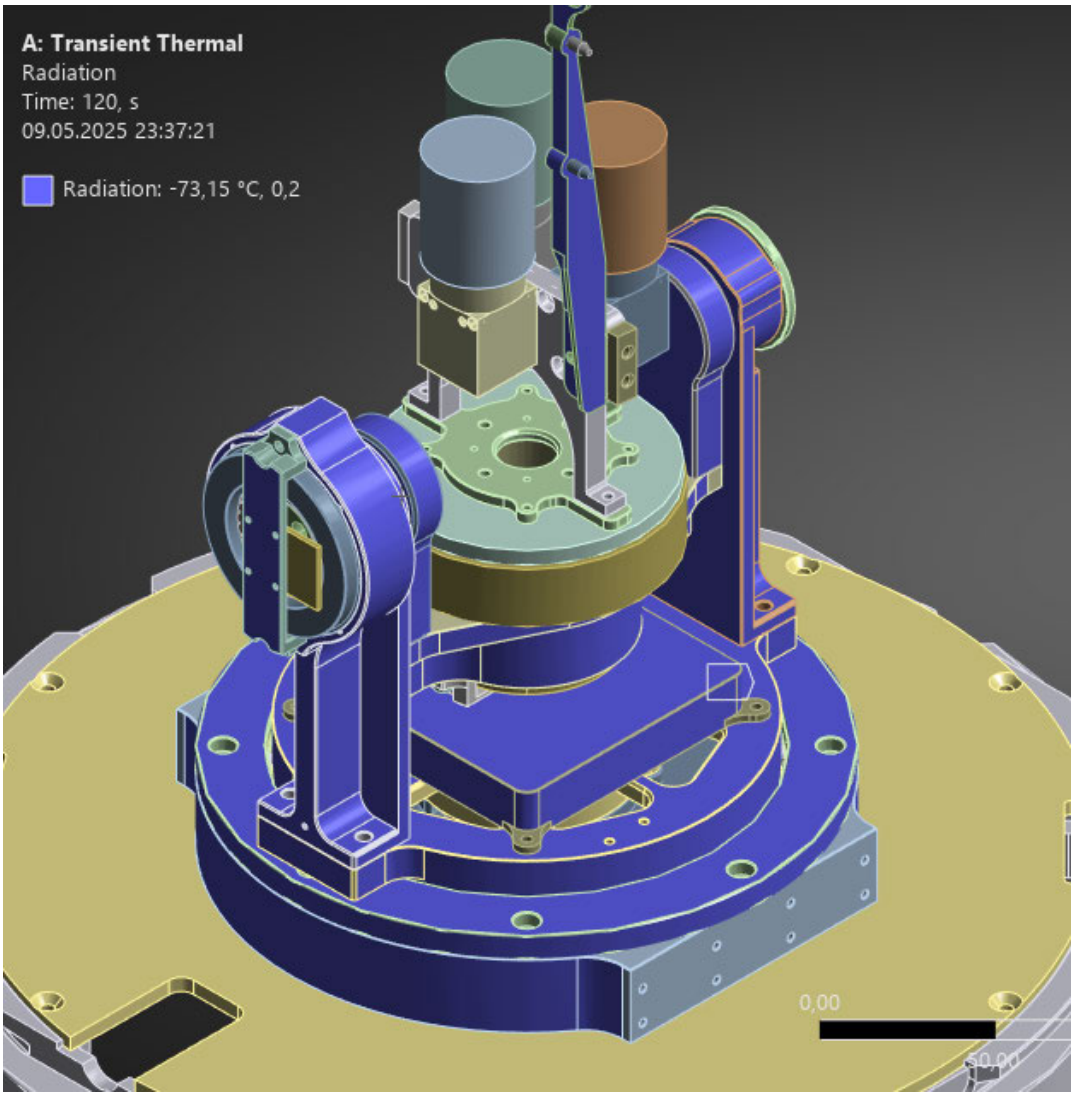


Figure 4.56: Outer surfaces for thermal radiation

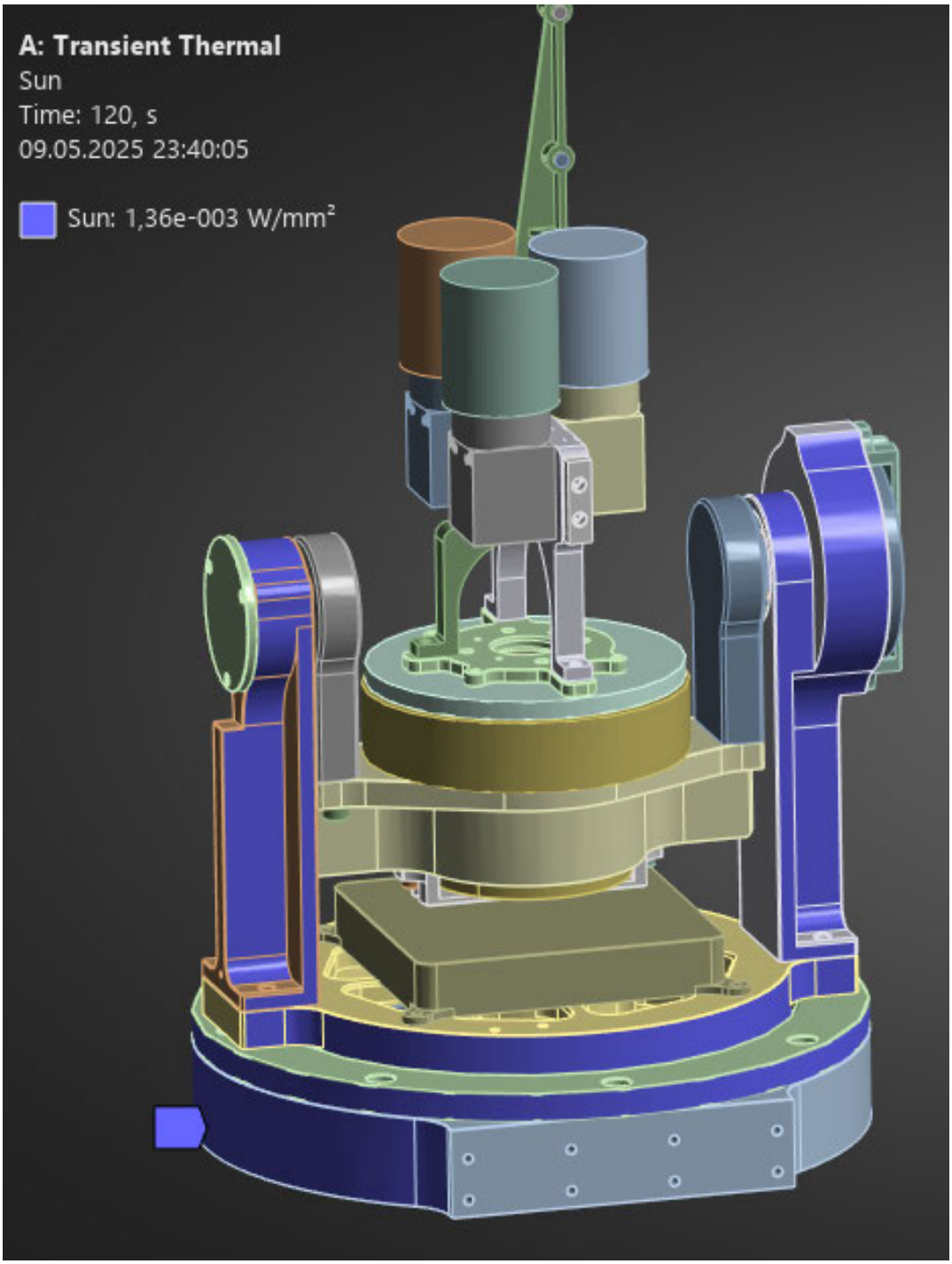


Figure 4.57: Surfaces where sun shines onto

4.6.3 Thermal FEM Analysis: Results

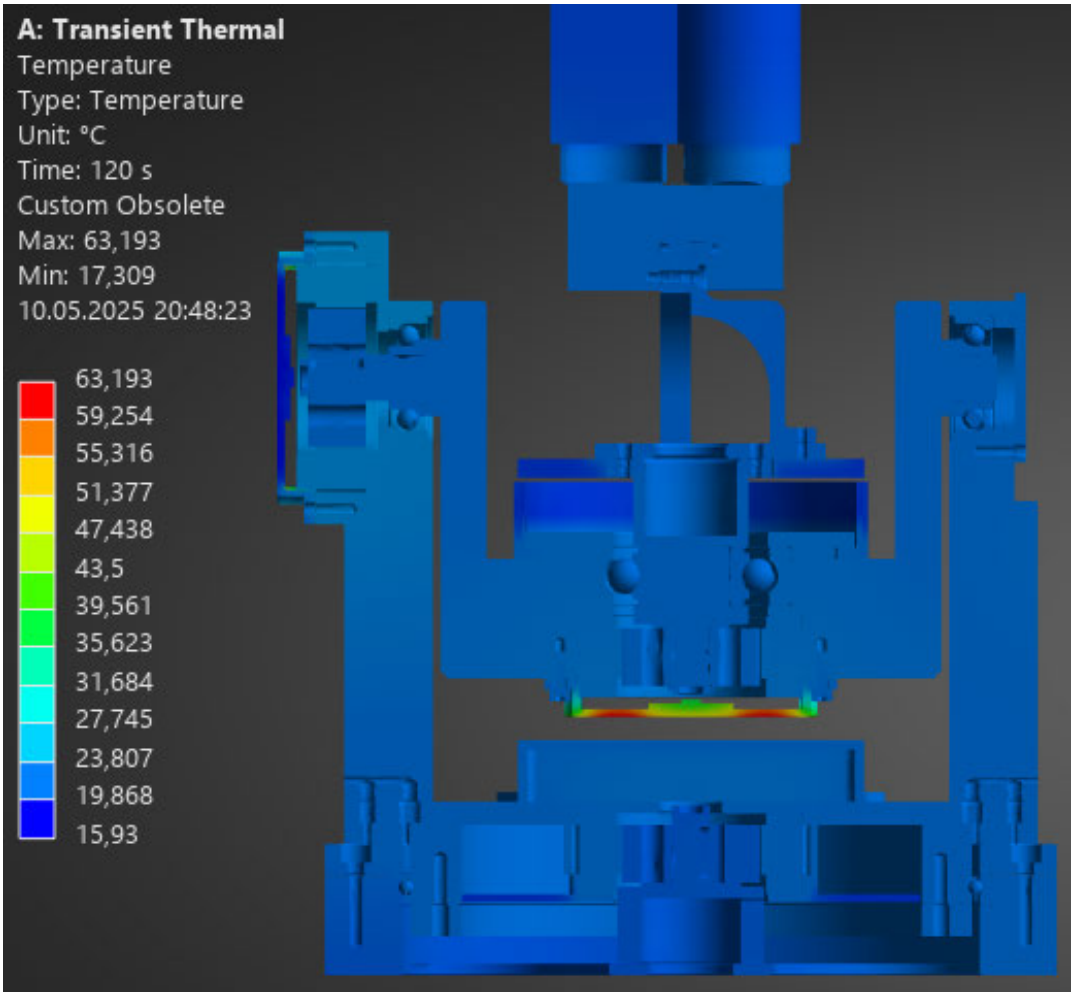


Figure 4.58: Results of the thermal Simulation

The simulation shows that the 3D-printed component holding the motor encoder PCB experiences significant heating due to solar exposure during the 120-second operation period. To mitigate this, it may be advisable to either switch to a more heat-resistant 3D printing material or replace the component with an aluminium version. Using aluminium would improve thermal conductivity and help dissipate the heat more effectively.

The figure below illustrates the thermal distribution if the component were made from aluminium EN AW-6082 instead of 3D-printed ASA.

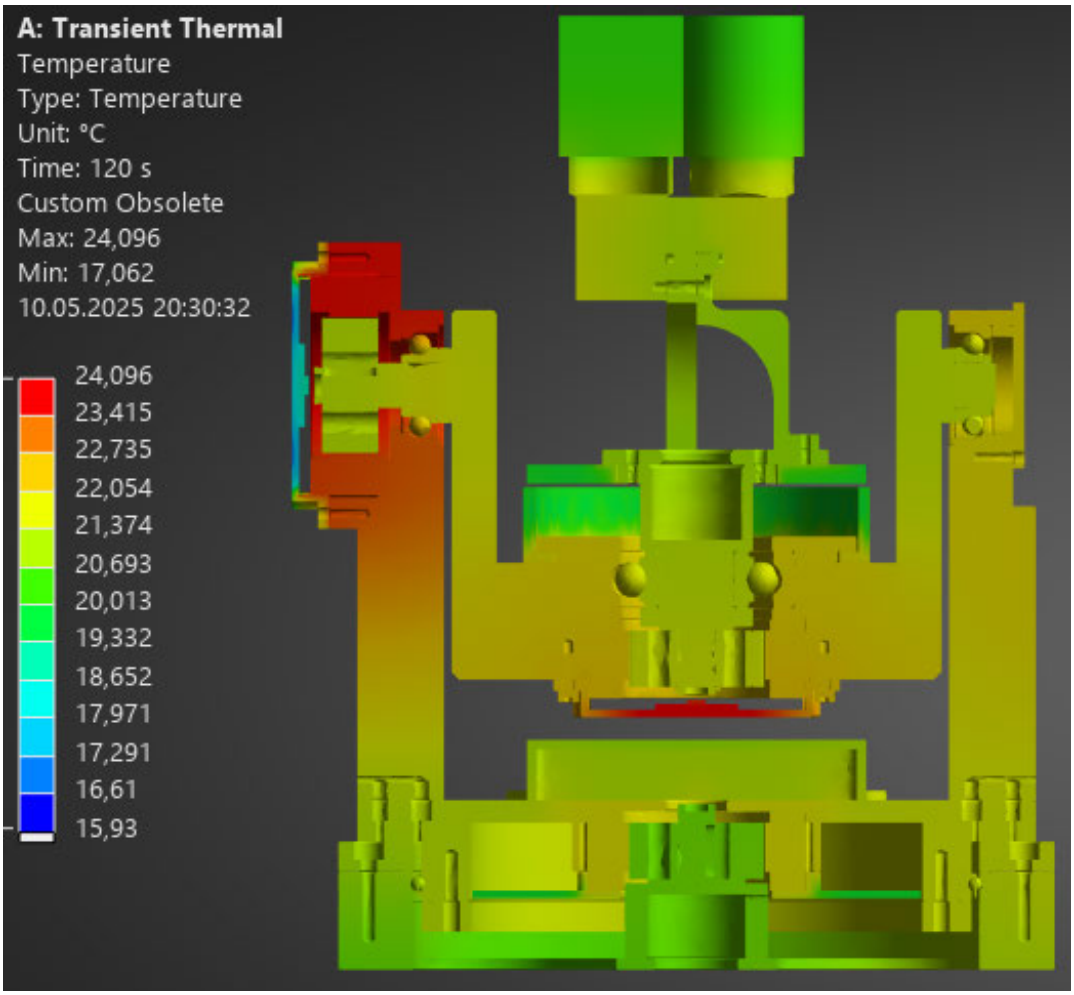


Figure 4.59: Simulation result using aluminium EN AW-6082 instead of 3D-printed ASA

The results show that, apart from the motor encoder PCB holder, the temperature change was less than ±5 °C. More importantly, almost no temperature rise was measured at the connection to the REXUS module.

The generated heat from the wires and other electronic components was not included in this result. However, since these components consume significantly less power compared to the motors and cameras, the overall temperature increase would likely remain nearly the same if they were included.

4.7 Power System

The table below shows the projected power consumption by the experiment. The columns show five different time windows: pre-launch to internal battery on, internal battery on to liftoff, liftoff to nosecone deployment, nosecone deployment to parachute deployment, and parachute deployment to touchdown.

INFO: The needed capacity was calculated without the 90% efficiency margin.

Table 4.12: Worst case power consumption
Columns show different time windows, in $T \pm$ seconds

Component	**T:** −600, −300	−300, +0	+0, +61	+61, +380	+380, +600
Flight Computer @ 3.3V	0.3A	0.3A	0.3A	0.3A	0.3A
Raspberry PI CM5 @ 5V	0.4A	0.4A	0.9A	0.9A	0.9A
Cameras @ 24V	0.3A	0.3A	0.3A	0.3A	0.3A
Ethernet Switch @ 24V	0.01A	0.01A	0.04A	0.04A	0.04A
Motor Driver @ 3.3V	0.1A	0.1A	0.2A	0.2A	0.1A
Motors @ 24V	0A	0A	0A	1.5A	0A
Current	1.11A	1.11A	1.74A	3.24A	1.64A
Current drawn 28V line	1A	1A	1A	1A	1A
Current drawn internal battery (24V)	0.11A	0.11A	0.74A	2.24A	0.64A
Power consumption	10.76W	10.76W	14.31W	50.31W	13.98W
Total Power (90% efficiency)	11.84W	11.84W	15.74W	55.34W	15.38W
Needed Capacity from RXSM	0.083Ah	0.083Ah	0.017Ah	0.089Ah	0.061Ah
Needed Energy from RXSM	2.33Wh	2.33Wh	0.48Wh	2.49Wh	1.71Wh
Needed Capacity from internal battery	0.009Ah	0.009Ah	0.013Ah	0.198Ah	0.039Ah
Needed Energy from internal battery	0.220Wh	0.220Wh	0.301Wh	4.752Wh	0.939Wh

4.8 Software Design

The software of APEX ran on different components namely: Flight Computer which is split into the flight computer main core and flight computer sensor core, raspberry pi, motor driver, housekeeping blackbox, sun sensors and the Mission Control. The Flight Computer was the main compute unit and interfaces via the flight computer main core with the service module and the Controller Area Network (CAN) bus and thus to the rest of the experiment as seen in Figure 4.60. It received commands and REXUS signals from the service module and sends commands to the rest of the system which is described in more detail in Section 4.8.2. The flight computer sensor core's task was to read sensor data from the sensor boards as well as the magnetometers while feeding the attitude determination described in Section 4.8.5. Due to every sun sensor being connected to the CAN bus their data needed to be transmitted from the flight computer main core to the flight computer sensor core. The housekeeping blackbox waqs designed to record everything that gets transmitted on the CAN bus. The motor driver was the interface between Flight Computer and the gimbals motors to actuate them in the way the flight computer main core calculated it beforehand. For actuation of the cameras, as well as handling the data generated by the cameras, a raspberry pi was used as described in Section 4.8.3.

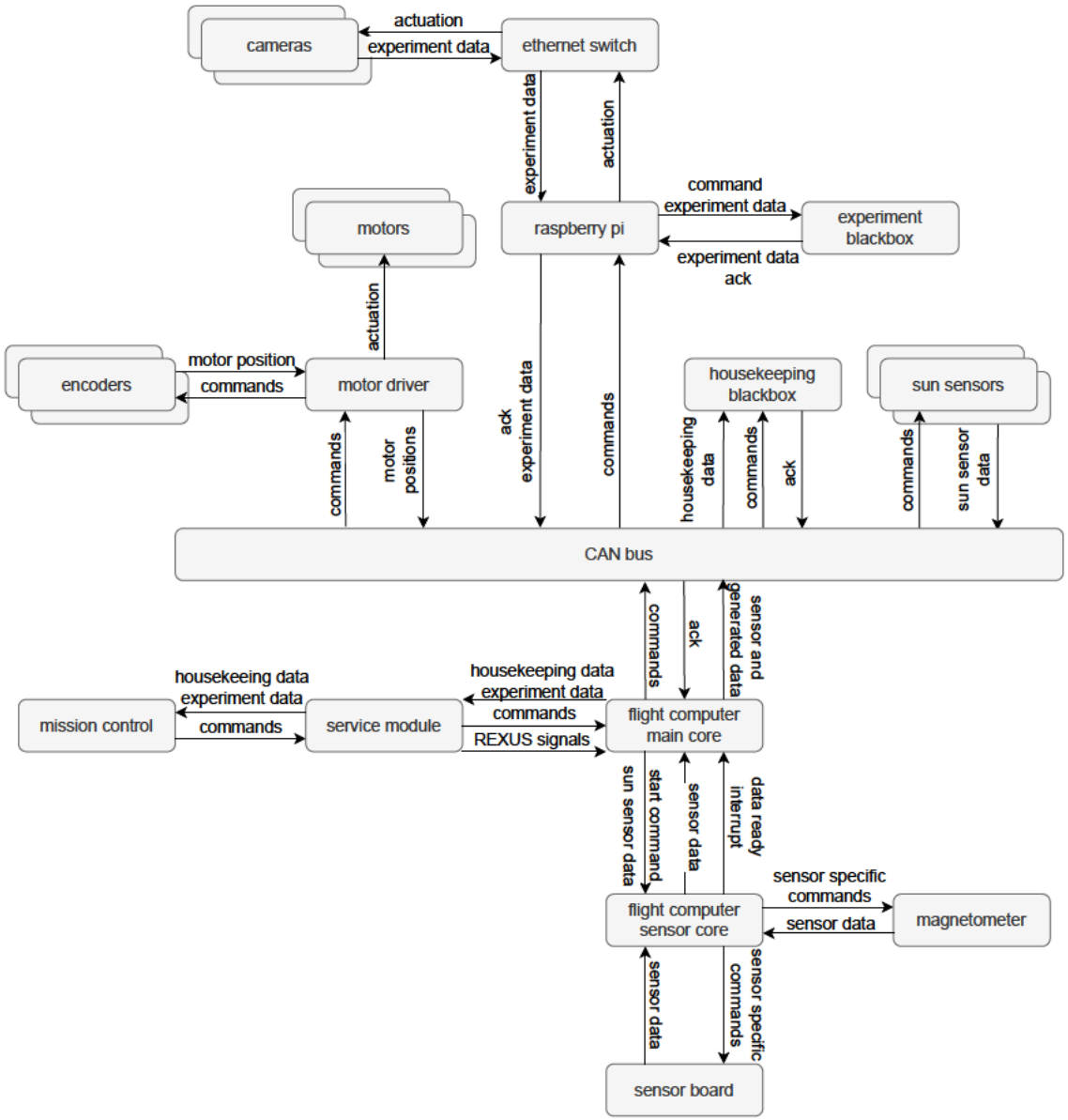


Figure 4.60: Data flow diagram of APEX

4.8.1 State Machine

The state machine ran on the flight computer main core and tracked what the experiment has to do in each given phase. Figure 4.61 presents the state machine with all its transitions. Most of the transitions were carried out by one or two Mission Control commands. During the mission the state machine relied on the Lift Off, Start Off Experiment and Start Of Data Storage signals to transition into the next state. For testing proposes the state machine could be set back into the idle state from every state.

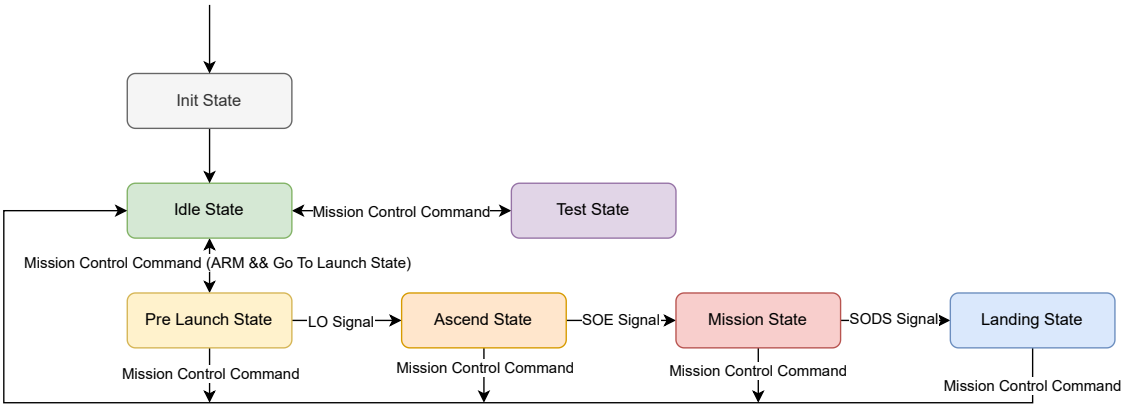


Figure 4.61: The state machine used with all transitions

Init State

The init state was the first state being executed after the Flight Computer powers on and executes the initialization sequence. Its task wast to first initialize communication with the CAN bus as well as Mission Control, then tell the blackboxes to initialize its memory to then initialize all sensors of the experiment. After this was done it would automatically transition into the idle state.

Idle State

The idle state was used to wait until the REXUS rocket finished its internal tests. During the idle state commands could be send to the experiment and data generated by the sensors was sent to Mission Control. From the idle state the system could transition into the test state as well as pre launch state. For the later two Mission Control commands (i.e. one arming command before each critical command) were needed to not transition there by accident.

Test State

The test state was used to test various abilities of the experiment. This state could be quickly expanded to whatever checks the pre launch check list required. In this state the experiment would also send back housekeeping data. From this state the system could go back into the idle state.

Pre Launch State

During the pre launch state the system would await the lift off of REXUS. With the Lift Off signal by the service module the system would transition into the ascend state while a Mission Control command could get it back into idle.

Ascend State

During the ascend state REXUS would ascend until nosecone ejection where the experiment would then receive the Start Of Experiment signal to go into the mission state or with a Mission Control command back to idle. Additionally to sending data to the Mission Control, housekeeping data was also designed to be stored on the blackbox.

Mission State

The mission state as seen in Figure 4.62 was responsible for all experiment operations between nosecone ejection and rocket heading to the ground again. First the attitude determination was initialized and started which would run on the second core of the Flight Computer. It is described more detailed in Section 4.8.5. The states task on the CM7 core was to calculate an exposure movement. If no image was being taken by the experiment, the path would be send to the motor driver which would then actuate the gimbal into the start position and notify the Flight Computer. Then the Flight Computer would broadcast to the system to start a exposure. This means themotor driver would actuate the motors to follow the calculated path and the raspberry pi would capture a picture. The housekeeping data that was generated here was designed to be stored on the blackbox as well as sent to the Mission Control. From this state the system could transition into the landing state by the Start Of Data Storage signal by the service module or into the idle state by a Mission Control command.



Figure 4.62: The mission state with its routine and transitions

Landing State

During the landing state, images were planed to be transmitted to the Mission Control while REXUS was descending, continuing until the connection would be lost. At the start of this task, the motor driver was designed to receive a command to park the gimbal in a safe position, minimizing the risk of camera damage upon touchdown. After sending this command, the task would repeatedly transmit housekeeping data and store it on the blackbox. Additionally, in every cycle, the Flight Computer would request a picture, originally taken during the mission state, from the Raspberry Pi, as described in Section 4.8.3, and forward it to the Mission Control.

4.8.2 Mission Control and Communication

The Mission Control was split into three components: the control panel, a data panel and a database. The control panel used a graphical presentation to send commands to the experiment and was built on the javascript framework Vue.js. The data panel on the other hand used the open source visualization software Grafana which displayd data sent from the experiment and was stored onto a postgres database. These components were all heritage systems by the ASTG and run on a docker to create the possibility that every member of the team could startup the Mission Control. The communication between Mission Control, Flight Computer and on the CAN bus worked on the protocol Tel-Talk which was also a heritage system by the ASTG. Tel-Talk was a serialization/deserialization library similar to protobuf, but optimized for packet size. Included features were fragmentation, checksums, commands with ack, log messages. For communication between Mission Control and Flight Computer this protocol needed to be transformed into and from the REXUS telecommand.

4.8.3 Raspberry Pi Software

The raspberry pi had three functionalities as seen in Figure 4.63. The main two were actuating the cameras to get experiment data and then save it on the experiment blackbox. For testing purposes a picture could be taken and directly sent over the Flight Computer to the Mission Control to confirm the cameras were working properly. During descent as described in Section 4.8.1 the raspberry could send cropped pictures to the Flight Computer to then send them to the Mission Control.

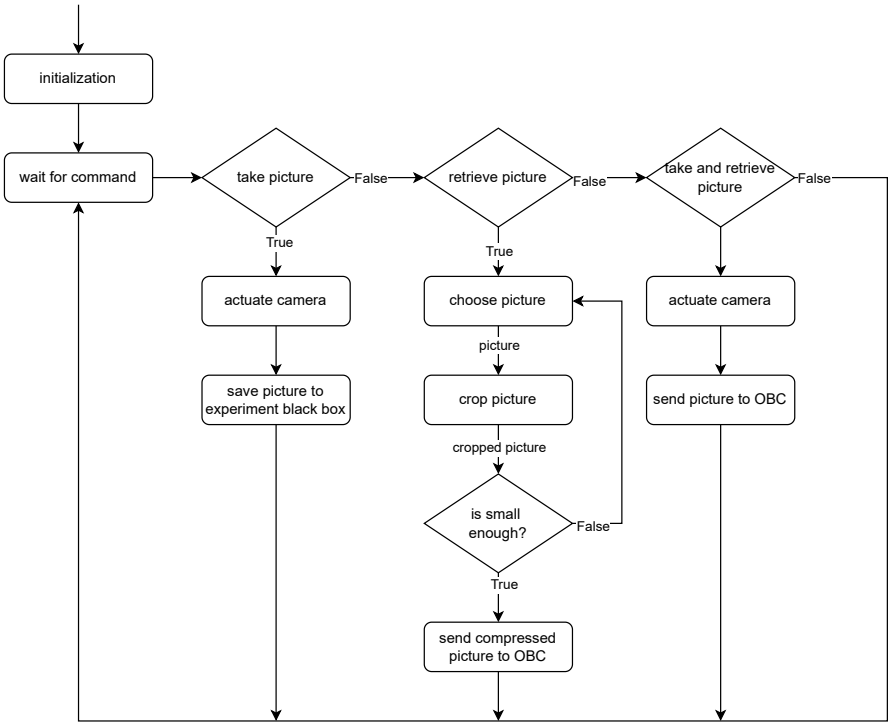


Figure 4.63: Raspberry Pi software diagram

4.8.4 Motor Driver Software

The Motor Driver Software was part of the Motor Driver PCB and ran on the STM32H725 MCU. The entire software for this driver was based on the open-source library stm32-FOC, which implements the FOC algorithm for BLDC motors. An SPI driver was custom-written for the position sensor. To obtain accurate speed data at a high data rate, the sensor signal was filtered using an alpha-beta filter.

After unlocking the Pin Puller, the Motor Driver would move to its initial position. Upon receiving valid target positions from the Flight Computer, the coordinates would be stored in a list, and the Motor Driver would execute linear movements between them. If a commanded move would exceed the allowed physical range (where the Locking Arm would interfere with the Sun Sensors or Bulkhead), the movement would be automatically halted at the boundary of the safe range.

Figure 4.64 illustrates the three nested PID loops that comprise the FOC. The innermost loop controlled the phase currents of the motor, the middle loop managed velocity control, and the outer loop regulated the position.

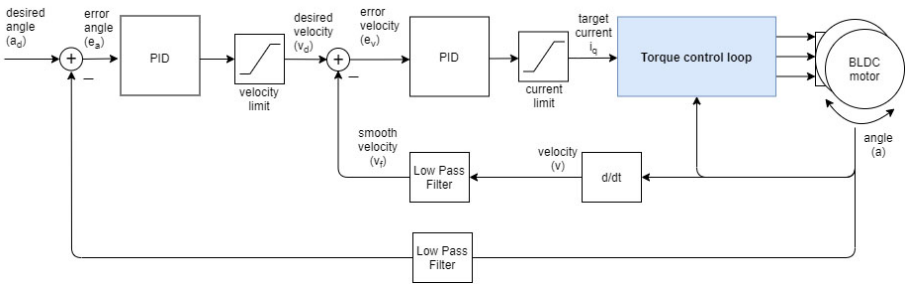


Figure 4.64: Position Control Loop

One of the primary challenges in establishing reliable position control was tuning the PID parameters of the FOC control loop. The majority of issues arose during the tuning of the speed controllers, as the cable reels physically restricted movement. To resolve this, system identification was performed using MATLAB, which ultimately provided feasible PID values.

4.8.5 Attitude Determination

The Camera Assembly needed to have a certain pointing-accuracy according to the requirements. The Gimbal Base Plate was aligned with the Rocket. Through the Gimbal Stage, a relative attitude between the Gimbal Base Plate and the Camera Assembly could be achieved.

Earth Centered Inertial-Frame

For Attitude Determination, the identification of the vectors $\vec{S}$ (Sun-Vector), and $\vec{B}$ (Magnetic-Field-Vector) was required. These Vectors are known in the Earth Centered Inertial-Frame (ECI) J2000.

$$\begin{aligned} \text{Origin:} &\quad \text{Center of Mass of Earth} \\ \hat{e}_z: &\quad \text{Earth's rotation axis at 1 January 2000} \\ \hat{e}_x: &\quad \text{Mean Vernal Equinox} \\ \hat{e}_y: &\quad \hat{e}_z \times \hat{e}_x \end{aligned}$$

A general vector in the ECI-Frame shall be denoted as $\vec{a}_{\text{ECI}}$.

Body-Frame

The Sensors were mounted in the same reference frame as the Gimbal Base Plate. This frame shall be aligned with the Rockets Bodyframe and a vector represented in this frame shall be denoted as $\vec{a}_{\text{b}}$.

Attitude-Quaternion

Since $\vec{S}_{\text{ECI}}$ and $\vec{B}_{\text{ECI}}$ is known, one can determine the quaternion $\bar{\mathbf{q}}^b_{\text{ECI}}$ which represents the rotation from the body-frame in the ECI-frame. The principle behind this conversion is the so-called QUEST (Quaternion Estimator Algorithm). The derivation presented in this section follows the formulation of the QUEST-Algorithm as described by [15], unless otherwise stated.

This algorithm is designed to minimize a cost function, or finding an optimal $\hat{\mathbf{A}}_{\text{opt}}$, so that it minimizes

$$L(\hat{\mathbf{A}}) = \frac{1}{2}\sum_{i=1}^{n} a_i |\hat{\mathbf{W}}_i - \hat{\mathbf{A}}\hat{\mathbf{V}}_i|,$$

where $\hat{\mathbf{A}}^{3\times3}$ is the rotation matrix between two coordinate-Frames (ECI-Frame and Bodyframe), $\hat{\mathbf{V}}_i$ are reference vectors and $\hat{\mathbf{W}}_i$ are observation vectors. a_i are non-negative weights, so that $\sum_{i=1}^{n} a_i = 1$. We define a gain function $g(\hat{\mathbf{A}})$, so that $g(\hat{\mathbf{A}}) = 1 - L(\hat{\mathbf{A}}) = \sum_{i=1}^{n} = a_i \hat{\mathbf{W}}_i^T \hat{\mathbf{A}} \hat{\mathbf{V}}_i$. This function is constructed so that it has a maximum where the loss-function has a minimum. Utilizing the trace of a matrix, we can rewrite the gain-function to

$$g(\hat{\mathbf{A}}) = \sum_{i=1}^{n} \operatorname{tr}(\hat{\mathbf{W}}_i^T \hat{\mathbf{A}} \hat{\mathbf{V}}_i) = \operatorname{tr}(\hat{\mathbf{A}}\hat{\mathbf{B}}^T),$$

Where $\hat{\mathbf{B}}^T$ is the transpose of the **attitude profile matrix** $\hat{\mathbf{B}} = \sum_{i=1}^{n} a_i \hat{\mathbf{W}}_i \hat{\mathbf{V}}_i^T$. The quaternion $\bar{\mathbf{q}}$ represents the rotation between the two frames and is defined as follows. Note, that we use the **scalar-first**-convention.

$$\bar{\mathbf{q}} = \begin{bmatrix} q \\ \mathbf{Q} \end{bmatrix} = \begin{bmatrix} \cos\frac{\theta}{2} \\ \hat{\mathbf{X}} \sin\frac{\theta}{2} \end{bmatrix},$$

where $\hat{\mathbf{X}}$ is the axis of rotation and θ is the angle in which the frame is rotated about $\hat{\mathbf{X}}$.

Since the quaternion $\bar{\mathbf{q}}$ is a *versor*, it must satisfy the unit norm constraint:

$$\bar{\mathbf{q}}^T \bar{\mathbf{q}} = \|\mathbf{Q}\|^2 + q^2 = 1,$$

where $\mathbf{Q} \in \mathbb{R}^3$ is the vector part and $q \in \mathbb{R}$ is the scalar part of the quaternion.

The attitude matrix $\mathbf{A}$ corresponding to the quaternion $\bar{\mathbf{q}}$ is given by:

$$\mathbf{A}(\bar{\mathbf{q}}) = (q^2 - \mathbf{Q}\cdot\mathbf{Q})\mathbf{I} + 2\mathbf{Q}\mathbf{Q}^T + 2q[\mathbf{Q}]_\times,$$

where $\mathbf{I}$ is the 3×3 identity matrix, and $[\mathbf{Q}]_\times$ denotes the **skew-symmetric matrix** associated with $\mathbf{Q}$:

$$[\mathbf{Q}]_\times = \begin{bmatrix} 0 & Q_3 & -Q_2 \\ -Q_3 & 0 & Q_1 \\ Q_2 & -Q_1 & 0 \end{bmatrix}$$

The gain function $g(\bar{\mathbf{q}})$, originally defined in matrix form, can be expressed using quaternion components as:

$$g(\bar{\mathbf{q}}) = (q^2 - \mathbf{Q}\cdot\mathbf{Q})\operatorname{tr}(\mathbf{B}^T) + 2\operatorname{tr}(\mathbf{Q}\mathbf{Q}^T\mathbf{B}^T) + 2q\operatorname{tr}([\mathbf{Q}]_\times \mathbf{B}^T),$$

Finally, this expression simplifies compactly to:

$$g(\bar{\mathbf{q}}) = \bar{\mathbf{q}}^T \mathbf{K} \bar{\mathbf{q}},$$

where $\mathbf{K} \in \mathbb{R}^{4\times4}$ is the symmetric *K-matrix* derived from the minimization problem and is defined as follows:

$$\mathbf{K} = \begin{bmatrix} \mathbf{S} - \sigma\mathbf{I} & \mathbf{Z} \\ \mathbf{Z}^T & \sigma \end{bmatrix},$$

where the scalar σ, the symmetric matrix $\mathbf{S}$, and the vector $\mathbf{Z}$ are auxiliary quantities defined by:

$$\begin{aligned}\sigma &= \mathrm{tr}(\mathbf{B}),\\ \mathbf{S} &= \mathbf{B} + \mathbf{B}^T,\\ \mathbf{Z} &= \sum_{i=1}^{n} a_i \left(\hat{\mathbf{W}}_i \times \hat{\mathbf{V}}_i\right),\end{aligned}$$

with $\hat{\mathbf{W}}_i$ and $\hat{\mathbf{V}}_i$ being unit vectors measured in the body and ECI frames respectively, and a_i denoting weighting factors.

We define an extended gain function using Lagrange multipliers:

$$g'(\bar{\mathbf{q}}) = \bar{\mathbf{q}}^T \mathbf{K} \bar{\mathbf{q}} - \lambda \bar{\mathbf{q}}^T \bar{\mathbf{q}}.$$

Maximization of $g'(\bar{\mathbf{q}})$ under the unit norm constraint yields:

$$\mathbf{K}\bar{\mathbf{q}} = \lambda \bar{\mathbf{q}}.$$

Hence, the function $g(\bar{\mathbf{q}})$ is maximized when $\bar{\mathbf{q}}_{\text{opt}}$ is the eigenvector of $\mathbf{K}$ associated with the largest eigenvalue $\lambda_{\max}$:

$$\mathbf{K}\bar{\mathbf{q}}_{\text{opt}} = \lambda_{\max}\bar{\mathbf{q}}_{\text{opt}}.$$

This implies that for any eigenvalue λ,

$$\lambda = \sigma + \mathbf{Z} \cdot \mathbf{Y},$$

where $\mathbf{Y}$ is the **Gibbs vector**, also known as the **Rodrigues vector**, defined as:

$$\mathbf{Y} = \frac{\mathbf{Q}}{q} = \hat{\mathbf{X}} \tan\left(\frac{\theta}{2}\right).$$

We can also write the quaternion as:

$$\bar{\mathbf{q}} = \frac{1}{\sqrt{1 + |\mathbf{Y}|^2}} \begin{bmatrix} \mathbf{Y} \\ 1 \end{bmatrix}.$$

Substituting into the gain expression, we obtain the eigenvalue equation:

$$\lambda = \sigma + \mathbf{Z}^T \left[(\lambda + \sigma)\mathbf{I} - \mathbf{S}\right]^{-1} \mathbf{Z},$$

which is equivalent to the characteristic equation of $\mathbf{K}$.

Using the **Cayley-Hamilton theorem**, we can eliminate the Gibbs vector and express the characteristic equation as:

$$\lambda^4 - (a + b)\lambda^2 - c\lambda + (ab + c\sigma - d) = 0,$$

where the constants are defined as:

$$
\begin{aligned}
a &= \sigma^2 - \kappa, \\
b &= \sigma^2 + \mathbf{Z}^T\mathbf{Z}, \\
c &= \Delta + \mathbf{Z}^T\mathbf{S}\mathbf{Z}, \\
d &= \mathbf{Z}^T\mathbf{S}^2\mathbf{Z}, \\
\sigma &= \frac{1}{2}\mathrm{tr}(\mathbf{S}), \\
\kappa &= \mathrm{tr}(\mathrm{adj}(\mathbf{S})), \\
\Delta &= \det(\mathbf{S}).
\end{aligned}
$$

To solve for λ, we apply the **Newton-Raphson method**, using the normalized weight sum as an initial guess:

$$
\lambda_{t+1} \leftarrow \lambda_t - \frac{f(\lambda)}{f'(\lambda)} = \lambda_t - \frac{\lambda^4 - (a+b)\lambda^2 - c\lambda + (ab + c\sigma - d)}{4\lambda^3 - 2(a+b)\lambda - c}.
$$

Typically, for attitude estimation accuracies better than 1 arc-minute, one iteration using 64-bit floating-point precision is enough.

Final Attitude Quaternion

The optimal quaternion representing the attitude is then:

$$
\bar{\mathbf{q}}_{\mathrm{opt}} = \frac{1}{\sqrt{\gamma^2 + |\mathbf{X}|^2}} \begin{bmatrix} \mathbf{X} \\ \gamma \end{bmatrix},
$$

with:

$$
\begin{aligned}
\mathbf{X} &= (\alpha\mathbf{I} + \beta\mathbf{S} + \mathbf{S}^2)\mathbf{Z}, \\
\gamma &= (\lambda + \sigma)\alpha - \Delta, \\
\alpha &= \lambda^2 - \sigma^2 + \kappa, \\
\beta &= \lambda - \sigma.
\end{aligned}
$$

Note: This expression may become indeterminate if both γ and $\mathbf{X}$ vanish. This occurs only when the rotation angle equals π and $\mathbf{X}$ does not vanish alone.

The QUEST algorithm provides an initial estimate for the Extended Kalman filter, which provides a continuous state estimate. It fuses magnetometer, sun, and gyroscope sensors together. More information can be found in Section 4.8.6.

4.8.6 Extended Kalman Filter for Attitude Calculation

The goals of the extended Kalman filter for attitude calculation was to fuse all sensors present, namely magnetometers, gyros, and sun sensors but also consider the gyros bias caused by its drift as well as the sun sensors bias. This work used the Multiplicative Extended Kalman Filter (MEKF), which functions with the quaternion based representation of attitude.

4.8.7 State Estimate

The state vector of the MEKF is

$$\delta \boldsymbol{x} = \begin{bmatrix} \delta \boldsymbol{\alpha} \\ \delta \boldsymbol{\beta} \end{bmatrix}, \tag{4.1}$$

where $\delta\boldsymbol{\alpha}$ is the state of the errorquaternion $\delta \boldsymbol{q}(\boldsymbol{\alpha}) = [1, \alpha_1/2, \alpha_2/2, \alpha_3/2]$, which is the differential rotation between the state $k-1$ and the state k. $\delta\beta$ is the error state of the gyroscope bias. It is defined as $\delta\beta = \beta - \hat{\beta}$, where β is the true gyroscope bias and $\hat{\beta}$ is the bias estimation. The linearized process model of the MEKF is given by

$$\delta \dot{x} = \hat{F}\delta x + \hat{G}\omega \tag{4.2}$$

$$\delta \dot{x} = \begin{bmatrix} -[\hat{\omega}]_\times & -\mathbf{I}_{3\times3} \\ \mathbf{0}_{3\times3} & \mathbf{0}_{3\times3} \end{bmatrix} \begin{bmatrix} \delta\alpha \\ \delta\beta \end{bmatrix} + \begin{bmatrix} -\mathbf{I}_{3\times3} & \mathbf{0}_{3\times3} \\ \mathbf{0}_{3\times3} & \mathbf{I}_{3\times3} \end{bmatrix} \begin{bmatrix} \eta_\nu \\ \eta_u \end{bmatrix}, \tag{4.3}$$

where $\hat{F}$ is the linearized dynamics of the system. η_ν is the gyro-noise and η_u is the noise of the gyro bias drift.

4.8.8 Prediction

The prediction step starts with the quaternion kinematic equation

$$\mathbf{q}_{k|k-1} = \mathbf{q}_{k-1|k-1} + \frac{1}{2} \begin{bmatrix} q_0 & -q_1 & -q_2 & -q_3 \\ q_1 & q_0 & -q_3 & q_2 \\ q_2 & q_3 & q_0 & -q_1 \\ q_3 & -q_2 & q_1 & q_0 \end{bmatrix}_{k-1|k-1} \begin{bmatrix} 0 \\ \omega_1 \\ \omega_2 \\ \omega_3 \end{bmatrix} \Delta t. \tag{4.4}$$

The estimation of the state covariance for the MEKF can be written as

$$P_{k|k-1} = \Phi_k P_{k-1|k-1} \Phi_k^T + Q_k, \tag{4.5}$$

with $\Phi_k = \mathbf{I}_{6\times6} + \mathbf{F}_k \Delta t$ denoting the Euler integration step of the state model and

$$\mathbf{Q}_k = \begin{bmatrix} (\sigma_v^2 \Delta t + \frac{1}{3}\sigma_u^2 \Delta t^3)\mathbf{I}_{3\times3} & -\frac{1}{2}\sigma_u^2 \Delta t^2 \mathbf{I}_{3\times3} \\ -\frac{1}{2}\sigma_u^2 \Delta t^2 \mathbf{I}_{3\times3} & \sigma_u^2 \Delta t \mathbf{I}_{3\times3} \end{bmatrix} \tag{4.6}$$

4.8.9 Update

The measurement model is the rotation matrix associated with the estimated quaternion $\mathbf{R}(\mathbf{q}_{k|k-1})$ times the known reference vectors $\mathbf{r}_i$, for $i = 1, \ldots, n$. It is expressed as

$$\mathbf{h}_k = \begin{bmatrix} \mathbf{R}(\mathbf{q}_{k|k-1})^T \mathbf{r}_1 \\ \vdots \\ \mathbf{R}(\mathbf{q}_{k|k-1})^T \mathbf{r}_n \end{bmatrix}. \tag{4.7}$$

To calculate the Kalman Gain, the equation is

$$\mathbf{K}_k = \mathbf{P}_{k|k-1} \mathbf{H}_k^T (\mathbf{H}_k \mathbf{P}_{k|k-1} \mathbf{H}_k^T + \mathbf{R}_k)^{-1}, \tag{4.8}$$

with

$$\mathbf{H}_k = \begin{bmatrix} [\mathbf{R}(\mathbf{q}_{k|k-1})^T \mathbf{r}_1]_\times \\ \vdots \\ [\mathbf{R}(\mathbf{q}_{k|k-1})^T \mathbf{r}_n]_\times \end{bmatrix} \tag{4.9}$$

being the measurement Jacobian, constructed from the cross-product matrices of the predicted measurement vectors $\mathbf{R}(\mathbf{q}_{k|k-1})\mathbf{r}_i$ for $i = 1, \dots, n$. The updated error state vector in the MEKF is

$$\delta\mathbf{x}_{k|k} = \mathbf{K}_k(\mathbf{z}_k - \mathbf{h}_k) = \begin{bmatrix} \delta\alpha_1 \\ \delta\alpha_2 \\ \delta\alpha_3 \\ \delta\beta_1 \\ \delta\beta_2 \\ \delta\beta_3 \end{bmatrix}_{k|k} . \tag{4.10}$$

$\mathbf{z}_k$ is the measurement vector containing the attitude measurements. From this error state vector, the updated error quaternion $\delta\mathbf{q}_{k|k}$ is formed using the first three entries of the error state vector, so that

$$\delta\mathbf{q}_{k|k} = \begin{bmatrix} 1 \\ \frac{1}{2}\delta\alpha_1 \\ \frac{1}{2}\delta\alpha_2 \\ \frac{1}{2}\delta\alpha_3 \end{bmatrix} . \tag{4.11}$$

The a posteriori quaternion is calculated by multiplying the a priori estimation with the updated error quaternion, giving

$$\mathbf{q}_{k|k} = \mathbf{q}_{k|k-1}\delta\mathbf{q}_{k|k}. \tag{4.12}$$

Finally, the a posteriori covariance is

$$\mathbf{P}_{k|k} = (\mathbf{I} - \mathbf{K}_k\mathbf{H}_k)\mathbf{P}_{k|k-1}. \tag{4.13}$$

4.9 Ground Support Equipment

4.9.1 Functionalities

The Mission Control displayed data generated by sensors and calculations. Furthermore, it was able to send commands to transition into Idle State, Test State and Ground State as seen in States. In the Test State the operator could start predefined tests. During Idle State and Ground State, it was possible to upload the necessary setup information used during Mission State. The communication happened over the D-SUB 15 connector, as stated in the REXUS manual. In addition, the Ground Support Equipment could be connected directly to the experiment for testing purposes.

4.9.2 Space Weather Monitoring

The space weather conditions were be monitored to model the expected brightnesses of aurora and dayglow emissions and the position of the auroral oval. This provided observation parameters such as the required camera gain and target region, which was uploaded to the experiment before launch. Further details about the aurora model can be found in Section 1.1. Notes on the monitoring activity before launch can be found in Section 6.2.1. The conditions as observed on launch day are described in Section 7.2.3.

5 Experiment Verification and Testing

5.1 Verification Matrix

Abbreviations used in the following tables:

- A: Analysis
- R: Review of Design
- I: Inspection
- T: Testing
- AD 1: Rexus User Manual

Table 5.1: Verification Matrix for Functional Requirements

ID	Requirement Text	Method	Applicable Documents	Status	Results
F-1	The experiment shall be able to image a target region of the auroral oval and airglow layer.	R, A	Analysis ID: 01	R - Done March 2025 A - Done, November 2025	Verified
F-2	The experiment shall measure the intensity, degree and angle of linear polarization of the incoming 557.7 nm light.	R, T	Test ID: 18	R - Done March 2025 T - Verified Feb. 2026	Verified
F-3	The experiment shall measure the intensity, degree and angle of linear polarization of the incoming 630 nm light.	R, T	Test ID: 18	R - Done March 2025 T - Verified Feb. 2026	Verified
F-4	The experiment shall provide unpolarized footage in the VIS spectrum of the target region and its immediate surroundings (Used as reference footage).	R, A	Analysis ID: 02	R - Done March 2025 A - Verified, see SED Appendix F	Verified
F-5	The experiment shall be able to track the observation target by compensating for attitude changes.	R, T	Test ID: 10	R - Done March 2025 T - Done, March 2026	Verified
F-6	The experiment shall be able to acquire an initial attitude at start of observation.	R, T	Test ID: 11	R - Done March 2025 TT - Done, March 2026	Verified

ID	Requirement Text	Method	Applicable Documents	Status	Results
F-7	The experiment shall be able to 2-way communicate with the ground station via the Telecommand System during countdown.	R, T	Test ID: 22	R - Done March 2025 T - Verified, See EAR Report Appendix A	Verified
F-8	The experiment shall be able to downlink data via the Rexus Service module during flight.	R,T	Test ID: 22	R - Done March 2025 T - Done, November 2025	Verified
F-9	Any moveable part shall be constrained (locked) in all axis during ascent.	R,A,T	Analysis ID: 03 Test ID: 3	R - Done March 2025 A - Verified, see SED Appendix F T - Verified, November 2025	Verified
F-10	The experiment shall be able to store scientific data onboard.	R, T	Test ID: 26	R - Done March 2025 T - Verified during launch campaign	Verified
F-11	The experiment shall be able to store housekeeping data onboard. Housekeeping data includes timestamps, states, sensor data, attitude and gimbal positions	R,T	Test ID: 26	R - Done March 2025 T - Failed, prior and during launch operations	Not Verified
F-12	The experiment should downlink science data during descent.	R, T	Test ID: 22	R- Done June 2025 T-Failed, as experiment data downlink was not implemented	Not Verified

Table 5.3: Verification Matrix for Performance Requirements

ID	Requirement Text	Method	Applicable Documents	Status	Results
P-1	The Degree of Linear Polarization shall be resolved with a resolution of 1% at 2-sigma	A, T	Analysis ID: 4 Test ID: 18	A - Done, November 2025 T - A full test could not be performed, only a partial verification with simulations was possible	Not Verified
P-2	APEX shall be able to expose the camera sensors for at least a 4 s duration.	R, T	Test ID: 19	R - Done March 2025 T - Requirement was shifted to 3 s as updated calculations on the scientific side allowed for it. 3 s exposure demonstrated during launch campaign.	Verified
P-3	APEX shall have a minimum resolution of 3°	A	Analysis ID: 1	Performance could not be accessed as the resolution is very dependent on the signal strength of the aurora. The camera pixel resoltion was with 2024 pixel for ~30 FOV sufficient for this requirement to be in theory verified	Retired

ID	Requirement Text	Method	Applicable Documents	Status	Results
P-4	The experiment shall be able to keep a stable pointing direction within 1° (Root-Mean-Square of Azimuth & Elevation) over the duration of the exposure (4 s).	R, T	Test ID: 11	R - Done March 2025 T - Done in Februar 2026, pointing accuracy was not measured	Not Verified
P-5	The initial attitude error at start of experiment shall be less than 5 ° (in a cone around the true attitude)	R,A, T	Analysis ID: 10 Test ID: 11	R - Done July 2025 A - Done, December 2025 T - Done in Februar 2026, pointing accuracy was not measured	Not Verified
P-6	The relative attitude change shall be evaluated at least every 20 milli seconds (with 50 Hz)	R, T	Test ID: 10	R - Done March 2025 T - Open	Pending
P-7	The gimbal shall be able to move 420 ° in the rotation axis	R, T	Test ID: 1	R - Done March 2025 T - Done Feb 2026	Verified
P-8	The cameras shall be able to move 420 ° in the rotation axis	R, T	Test ID: 1	R - Done March 2025 T - Done Feb 2026	Verified
P-9	The camera shall have a range of motion 200 ° in its pitch direction	R, T	Test ID: 1	R - Done March 2025 T - Done Feb 2026	Verified
P-10	Every Axis shall be able to accelerate with 120 °/s²	A, T	Analysis ID: 5 Test ID: 1	A - Verified, see SED Appendix F T - Done Feb 2026	Verified
P-11	Every Axis shall be able to rotate with at least 360 °/s	A, T	Analysis ID: 5 Test ID: 1	A - Verified, see SED Appendix F T - Done Feb 2026	Verified
P-12	APEX shall log the Housekeeping data transmitted over the CAN bus at least every 100 milli second	R, T	Test ID: 12	R - Done March 2025 T - Done Feb 2026	Verified

ID	Requirement Text	Method	Applicable Documents	Status	Results
P-13	The experiment shall be able to write 12 MB per second to the scientific data blackbox	A, T	Test ID: 26	A - not verified, as the full transmission chain proved difficult to model T - Failed, as the science data blackbox did not work	Not Verified
P-14	The reference image camera shall record images with a frequency of 10 FPS	R, T	Test ID: 19	R - Done June 2025 T - Done Feb 2026	Verified
P-15	The reference image camera shall have a resolution of at least 1080 x 1080 pixel	R		R - Done June 2025	Verified
P-16	The reference image camera shall have a field of view equal or larger than 50 °	R		R - Done June 2025	Verified

Table 5.5: Verification Matrix for Operational Requirements

ID	Requirement Text	Method	Applicable Documents	Status	Results
O-1	The experiment shall operate autonomously during flight.	R, T	Test ID: 13	R - Done March 2025 T - Done, February 2026	Verified
O-2	The experiment shall accept a request for radio silence at any time while on the launch pad.	R, T	Test ID: 24	R - Done March 2025 T - Done, November 2025	Verified
O-3	The gimbal shall move in safe position during descent phase to reduce the likelihood of damage to cameras	R,T	Test ID: 29	Retiered due to lack of time a ”safe position” was not implemented	Retired

ID	Requirement Text	Method	Applicable Documents	Status	Results
O-4	The experiment shall be able to enter a secure mode after landing (pyros and sensitive equipment shall be disabled).	R, T		Verified on Vehicel level as the power of the pyros and experiment was taken prior to landing	Verified
O-5	The experiment shall be able to unlock the gimbal autonomously after Nosecone Separation.	R, T	Test ID: 3	R - Done August 2025 T - Done, September 2025	Verified
O-6	The experiment shall operate in a testing mode allowing the testing of the cameras via the 2 way communication prior to lift off	R,T	Test ID: 25	Retiered due to lack of time no comunication between science camera feed and ground station could be implemented	Retired
O-7	Pyro shall be short circuited until Integration	R,I		R - Done March 2025 I - Checklist with item to short-circuited ignitor pins with Wargo Clamp	Verified
O-8	Pyros shall be short circuited with a manually removable shunt during integration (ReBF tag)	R,T	Test ID: 23	R - Done March 2025 T - Done, December 2025	Verified

Table 5.7: Verification Matrix for Design Requirements

ID	Requirement Text	Method	Applicable Documents	Status	Results
D-1	The center of mass of the camera subsystem shall align with the gimbal rotation axis to within 20mm once mounted	A, T		A -CAD - Model Data verified with weight measurement of sub component provided a sufficient approximation of the center of mass.	Verified
D-2	The mounting structure shall be able to withstand 20g of longitudinal acceleration during Launch	A, T	Test ID: 5	A -Verified, see SED Section 04.04 T - Scrubbed, deemed not measurable	Retired
D-3	The gimbal structure shall be able to withstand 20g of acceleration in all directions during the reentry phase	A,T	Test ID: 20	A-Verification for launch stresses was deemed sufficient T - Scrubbed, deemed not measurable	Retired
D-4	The gimbal shall withstand vibration profile of REXUS flight (Defined in Qualification and Acceptance according to Table 10.2 in AD 1: REXUS Manual	A, T	Test ID: 8	A -Verified, see SED Section 04.04 T-Done, November 2025	Verified
D-5	The experiment shall be able to withstand the expected loads during prelaunch handling (Low shock movement in 1 g environment in arbitrary orientation)	R		R - Done March 2025	Verified
D-6	The data storage shall survive a nominal landing with 8m/s	R, T	Test ID: 14	Blackbox is below the bulkhead acting as mechanical shield	Retired
D-7	The data storage shall be able to survive -30° C after landing	R, T	Test ID: 14	R - Done March 2025 T - Done, See Test ID 14	Verified

ID	Requirement Text	Method	Applicable Documents	Status	Results
D-8	The data storage shall be able to survive being submerged in molten snow after landing	R, T	Test ID: 14	R - Done March 2025 T - Done, See Test ID 14	Verified
D-9	Design shall not exceed a mass of 7,5 kg	A, T	Analysis ID: 6 Test ID: 4	A - Verified, SED section 04.01 T - Done, final mass with NCA 10.76kg	Verified
D-10	The total cell capacity shall be well below 20 Wh	R, A	Analysis ID: 8	Retired after discussion with Moraba September 2025	Retired
D-11	The batteries shall be accessible by using one tool in under 10 minutes in the case of no nosecone or other experiment section attached	R, I		R - Done in September 2025 I - Done, Dec 2025	Verified
D-12	Batteries shall be used to overcome the power limitations of the RXSM supply line.	R, T	Test ID: 24	R - Done in June 2025 T - Done, see Test ID 24	Verified
D-13	Batteries should be calculated with a maximum of 80% capacity used	R, A	Analysis ID: 8	R - Done in September 2025 A - Done, see SED chapter 4.5	Verified
D-14	The APEX power management system shall be able to use voltages between 24 and 36 V	R, T	Test ID: 24	R - Done in June 2025 T - Done, see Test ID 24	Verified
D-15	The mean power drawn by the experiment per service line shall not exceed 30 W	R, T	Test ID: 24	R - Done in June 2025 T - Done, see Test ID 24	Verified
D-16	The experiment shall not consume more than 3 Amps for more than 500ms from the Rexus Service Line.	R, T	Test ID: 24	R - Done in June 2025 T - Done, see Test ID 24	Verified
D-17	The experiment shall not consume more than 20 Amps for more than 100us from the Rexus Service Line.	R, T	Test ID: 24	R - Done in June 2025 T - Done, see Test ID 24	Verified

ID	Requirement Text	Method	Applicable Documents	Status	Results
D-18	The experiment shall limit feedback ripples over the power line to a maximum of 100mVpp	R, T	Test ID: 24	R - Done in June 2025 T - Done, see Test ID 24	Verified
D-19	All metal parts of the experiment shall be connected to a common ground	R, T	Test ID: 24	R - Done in June 2025 T - Done, see Test ID 24	Verified
D-20	The transmittance of the optical system shall be not degraded by more than 10 % by the vacuum environment at apogee	T	Test ID: 2	T - Verified	Verified
D-21	The science cameras shall be aligned within 1°	R, T	Test ID: 15	R - Done March 2025 T - Done, See Test ID 15	Verified
D-22	The reference camera shall be aligned within 5° with the science cameras	R, T	Test ID: 15	R - Done March 2025 T - Done, See Test ID 15	Verified
D-23	The Attitude shall be given as the quaternion between Earth Centered Inertial (ECI)-frame and body frame	R		R - Done July 2025	Verified
D-24	The body frame of the gimbal shall be aligned with the body frame of the rocket	R		R - Done July 2025	Verified
D-25	Every axis shall be able to move independently	R, T	Test ID: 1	R - Done March 2025 T - Done, January 2026	Verified
D-26	The pyro system shall be triggered by a REXUS Pyro line	R, T		R - Done March 2025 T - Done during hot Bench test, see SED chapter 7.2	Verified
D-27	The Pyrotechnic Gas Generator (E- Match) shall have a no fire current of >= 1 A	R, T	Test ID: 27	R - Done in June 2025 T - COTS Part, verified by manufacturer	Verified

ID	Requirement Text	Method	Applicable Documents	Status	Results
D-28	The Pyrotechnic Gas Generator (E- Match) shall have an all fire current of <= 10 A	R, T	Test ID: 27	R - Done in June 2025 T - COTS Part, verified by manufacturer	Verified
D-29	The Pyrotechnic Gas Generator (E- Match) shall have an internal resistance of no more than 2.2 Ohm	R, T	Test ID: 27	R - Done in June 2025 T - COTS Part, verified by manufacturer	Verified
D-30	The pyrotechnic pin puller shall retain/contain all solid parts larger than 10mm³ (e.g. plastic latches, pyro bolt)	R, T	Test ID: 27	R - Done March 2025 T - Verified, Test Report 27	Verified
D-31	Reaction forces from gas outlets should be minimized by using at least two openings located symmetrically on the module.	R, T	Test ID: 28	Retired, was replaced with a test checking for the reaction force	Retired
D-32	The gimbal shall use HELICOIL thread inserts with M5 for the connection to the baseplate	R, I			Retired
D-33	The screws connecting the Gimbal to the baseplate shall be : Hexagon socket head cap screw (ISO 4762, DIN 912), M5 x 16 mm, Material: Steel 8.8 galvanized	R, I		Retiered, as to constraining for the system design	Retired
D-34	The tightening torque for the M5 screws connecting gimbal and baseplate shall be 7 Nm.	R, I		R - Done in March 2025 Retiered, Experts suggest ”Hand tightening for a less damage to threads”	Verified
D-35	The Raspberry Adapter PCB shall be accessible by removing no more than 6 screws with the same tool	R, I		R - Done March 2025 I - Done, Dec 2025	Verified

ID	Requirement Text	Method	Applicable Documents	Status	Results
D-36	The Flight computer PCB shall be accessible by removing no more than 6 screws with the same tool	R, I		R - Done March 2025 I - Done, Dec 2025	Verified
D-37	Sun Sensor and Magnetometer PCBs shall be replaceable with no more than 6 screws with the same tool	R, I		R - Done March 2025 I - same tool, but more screws for both sun sensors and Magnetometer (8 instead of 6)	Not Verified
D-38	The experiments electrical interface shall be the D-SUB 15 male connector.	R, I		R - Done June 2025 I - Done October 2025	Verified
D-39	The pins of the D-SUB 15 connector shall use the pin layout defined in the REXUS manual	R, I		R - Done June 2025 I - Done, November 2025	Verified
D-40	APEX should be connected by either an optocoupler device or a relay to the REXUS signal lines	R, I		R - Done June 2025 I - Done September 2025	Verified
D-41	The REXUS signal lines shall not be connected to a microcontroller directly	R, I		R - Done June 2025 I - Done September 2025	Verified
D-42	Sun Sensor PCBs shall be connected to the Flight Computer PCB via CAN Bus	R, I		R - Done March 2025 I - Done, Dec 2025	Verified

ID	Requirement Text	Method	Applicable Documents	Status	Results
D-43	APEX should produce a vibrational level of less than 5 x 10^-5 g_rms (0 - 25 Hz)	A, T	Test ID: 16	A - Deemed unfeasible within the scope of the project T - Influence of the vibration of the experiment on the environment were deemed sufficiently low as minimal vibration could be observed during groundtesting	Retired
D-44	The modules internal thermal dissipation shall not heat up the outer structure more than 10 °C about ambient temperature, tolerance is ± 5 °C.	A, T	Analysis ID: 9 Test ID: 7	A - Verified, see SED Appendix F T -Retiered, as subsystem tests of the camera system, analysis and test 31 was deemed sufficient	Verified
D-45	The modules internal thermal dissipation shall not heat up the parts close to or in contact with the feed-through cable to more than +70 °C.	R, T	Test ID: 7	A - Verified, see SED Sect. 4.6.3 T -Retiered, as subsystem tests of the camera system, analysis and test 31 was deemed sufficient	Verified

ID	Requirement Text	Method	Applicable Documents	Status	Results
D-46	The modules internal thermal dissipation shall not heat up parts facing other modules to more than +50°C	A, T	Analysis ID: 9 Test ID: 7	A - Verified, see SED Sect. 4.6.3 T -Retiered, as subsystem tests of the camera system, analysis and test 31 was deemed sufficient	Verified
D-47	The heat transport by convection shall be limited in such a way that the air temperature at the module interfaces does not exceed the ambient temperature by more than 10 °C.	T	Test ID: 31	T - Done, December 2025	Verified
D-48	The mounting structure shall provide sufficient thermal capacity and conductivity to keep the temperature in the specified operating temperature range of -10°C to 55°C	A, T	Analysis ID: 9 Test ID: 7	A - Verified, see SED Sect. 4.6.1 T -Retiered, as subsystem tests of the camera system, analysis and test 31 was deemed sufficient	Verified
D-49	The Gimbal shall function in the vacuum environment of 80 km altitude	T	Test ID: 17	T - Retiered as previous payloads on rexus rockets did not report problems with their electronics due to vaccuum	Retired
D-50	The payload structure shall not be used as signal or power return	R, I		R - Done March 2025 I - Done, January 2026	Verified
D-51	The center frequency of the emission lines shall be within the full width half max of the filters.	R, I		R - Done March 2025 I - June 2025	Verified

ID	Requirement Text	Method	Applicable Documents	Status	Results
D-52	The filter full width half max shall be smaller equal to 20 nm	R, T	Test ID: 18	R - Done March 2025 T - Not verified, Jan 2026, increased to 40 nm after test	Not Verified
D-53	The housekeeping data shall contain timestamps, states, sensor data, attitude and gimbal positions	R, T	Test ID: 12 Test ID: 13 Test ID: 22 Test ID: 25 Test ID: 26	R - Done November 2025 T - Done, December 2025	Verified
D-54	The Blackbox PCB shall be accessible by removing no more than 6 screws with the same tool	R, I		Over constrained the System.	Retired
D-55	The Experiment Blackbox shall be accessible by removing no more than 6 screws with the same tool	R, I		Over constrained the System. Final Design uses 8 screws	Retired
D-56	Magnetometer PCBs shall be connected to the Flight Computer PCB via SPI	R, I		R - Done June 2025 I - Done, November 2025	Verified

Table 5.9: Verification Matrix for Constraints

ID	Requirement Text	Method	Applicable Documents	Status	Results
C-1	The experiment shall not exceed a mass of 7.5 kg	R			Verified
C-2	SI Units shall be used for calculations	R			Verified
C-3	For structural analysis, values from ESA Material Handbooks, Werkstoffhandbuch der Deutschen Luftfahrt, Metallic Materials Properties Development and Standardization (MMPDS) Handbook, Etc. shall be used	R			Verified

ID	Requirement Text	Method	Applicable Documents	Status	Results
C-4	APEX shall request the permission of photos/videos publication to the following authorities: SSC and Lantmäteriet	R			Verified

5.2 Verification Plan

Test ID	Test 1
Test Name	Minimal Prototype Test
Test Location	ASTG Workshop
Tested Item	Prototype without optical subsystem, but stand in for optical subsystem
Description	Test the Actuation and Locking of the Gimbal System with a prototype Structure, Locking, Actuation, and wire Harness.
Test Campaign Date	28.02.2026
Status	Completed
Requirements	P-7, P-8, P-9, P-10, P-11,
Prerequisite Tests	3

Test ID	Test 2
Test Name	Filter vacuum fogging Test
Test Location	ASTG Workshop
Tested Item	Optical Subsystem
Description	Test if optical filter fogs up (due to outgassing) permanently when exposed to vacuum for extended periods of time.
Test Campaign Date	13.01.2025
Status	Completed
Requirements	D-20,
Prerequisite Tests	

Test ID	Test 3
Test Name	Unlocking
Test Location	ASTG Workshop
Tested Item	Prototype without optical subsystem, but stands in for optical subsystem
Description	Repeated unlocking tests under various load types and amounts
Test Campaign Date	28.09.2025
Status	Completed
Requirements	F-9, O-5,
Prerequisite Tests	27

Test ID	Test 4
Test Name	Mass test
Test Location	ASTG Workshop
Tested Item	Complete Prototype
Description	Measuring the weight of the entire assembly
Test Campaign Date	November
Status	Completed
Requirements	D-9,
Prerequisite Tests	

Test ID	Test 5
Test Name	Acceleration test
Test Location	ASTG Workshop
Tested Item	Prototype without optical subsystem
Description	Measure deformation of components under a load equivalent to 20g in Newtons while in ascent configuration
Test Campaign Date	2025-08-03 00:00:00
Status	Retired
Requirements	D-2,
Prerequisite Tests	

Test ID	Test 6
Test Name	Center of mass test
Test Location	ASTG Workshop
Tested Item	Complete Prototype
Description	Measurement of the center of gravity of the whole assembly on all rotational axes
Test Campaign Date	November
Status	Retired
Requirements	D-1,
Prerequisite Tests	

Test ID	Test 7
Test Name	Thermal Vacuum Testing
Test Location	IWF
Tested Item	Complete Prototype
Description	Measuring the temperature of the gimbal inside a vacuum chamber after 180s of runtime
Test Campaign Date	December
Status	Retired
Requirements	D-44, D-45, D-46, D-48,
Prerequisite Tests	

Test ID	Test 8
Test Name	Vibration test
Test Location	TU Graz
Tested Item	Complete Prototype
Description	Vehicle level 1 Sine and Random Vibrations, with frequency search before and after. In thrust axis only. Vehicle level 1 Sine and Random Vibrations, with frequency search before and after. In thrust axis. Vehicle level 1 Random Vibrations, with frequency search before and after. In lateral axis.
Test Campaign Date	20.11.2025
Status	Completed
Requirements	D-4,
Prerequisite Tests	

Test ID	Test 9
Test Name	Optical System Water Fog Test
Test Location	ASTG Workshop
Tested Item	Optical Subsystem
Description	Test the anti water fog systems of the optical components by creating a sufficiently water saturated atmosphere in a vacuum chamber and evacuating it.
Test Campaign Date	October
Status	Retired
Requirements	
Prerequisite Tests	

Test ID	Test 10
Test Name	Attitude Determination Test
Test Location	ASTG Workshop
Tested Item	Complete Prototype + Mission Control
Description	The PCB with sensors has the Attitude Determination Software running while the PCB is being moved.
Test Campaign Date	November
Status	Completed
Requirements	F-5,
Prerequisite Tests	

Test ID	Test 11
Test Name	Area Pointing Test
Test Location	ASTG Workshop
Tested Item	Complete Prototype + Mission Control
Description	We define an area the gimbal shall observe and check if the software keeps pointing towards this area while the sensors detect movement
Test Campaign Date	End of Nov.
Status	Completed
Requirements	F-6, P-4, P-5,
Prerequisite Tests	1,10, 15

Test ID	Test 12
Test Name	Long Duration Test
Test Location	ASTG Workshop
Tested Item	Flight Computer
Description	The Electronics and Software undergo a multiple hour long duration test.
Test Campaign Date	December
Status	Completed
Requirements	D-53,
Prerequisite Tests	24

Test ID	Test 13
Test Name	Simulated Flight Software Test
Test Location	ASTG Workshop
Tested Item	Flight Computer
Description	Simulated Data is fed to the PCBs simulating a flight
Test Campaign Date	November
Status	Completed
Requirements	O-1, O-4, D-53,
Prerequisite Tests	

Test ID	Test 14
Test Name	Data Storage Endurance Test
Test Location	ASTG Workshop
Tested Item	Blackbox
Description	Test if data survives low temperature and being submerged in snow
Test Campaign Date	08.11.2025
Status	Completed
Requirements	D-6, D-7, D-8,
Prerequisite Tests	

Test ID	Test 15
Test Name	System Alignment Test
Test Location	ASTG Workshop
Tested Item	Complete Prototype
Description	Tests the alignment of the System with static pointing
Test Campaign Date	November
Status	Completed
Requirements	D-21, D-22,
Prerequisite Tests	

Test ID	Test 16
Test Name	Gimbal induced Vibration Test
Test Location	ASTG Workshop
Tested Item	Complete Prototype
Description	The full Gimbal is actuated with acceleration sensors attached to the base plate to measure induced vibration
Test Campaign Date	8.12.2025
Status	Completed
Requirements	D-43,
Prerequisite Tests	1

Test ID	Test 17
Test Name	Gimbal Vacuum Test
Test Location	ASTG Workshop
Tested Item	Complete Prototype
Description	The full Gimbal is operated in a Vacuum Chamber (both motors and Videos)
Test Campaign Date	December
Status	Retired
Requirements	D-49,
Prerequisite Tests	1

Test ID	Test 18
Test Name	Optical Polarization Test
Test Location	ASTG Workshop
Tested Item	Optical Subsystem
Description	The angle, intensity and degree of polarization is measured in an optical setup
Test Campaign Date	September
Status	Completed
Requirements	F-2, F-3, P-1,P-3,
Prerequisite Tests	19

Test ID	Test 19
Test Name	Gimbal Camera Test
Test Location	ASTG Workshop
Tested Item	Optical Subsystem
Description	Long time exposure of the science cameras is tested in conjunction with the short time exposure of the reference camera
Test Campaign Date	November
Status	Completed
Requirements	P-2, P-14,
Prerequisite Tests	

Test ID	Test 20
Test Name	Acceleration test descent
Test Location	ASTG Workshop
Tested Item	Prototype without optical subsystem
Description	Measure deformation of components under a load equivalent to 20g in Newtons while in reentry configuration
Test Campaign Date	nan
Status	Retired
Requirements	D-3,
Prerequisite Tests	

Test ID	Test 21
Test Name	Shock test
Test Location	ASTG Workshop
Tested Item	Complete Prototype
Description	Test the full Gimbal against schock
Test Campaign Date	October
Status	Retired
Requirements	
Prerequisite Tests	1

Test ID	Test 22
Test Name	Communication Test
Test Location	ASTG Workshop
Tested Item	Flight Computer
Description	Send commands to the experiment and receive data
Test Campaign Date	November
Status	Completed
Requirements	F-7, F-8, F-12, D-53,
Prerequisite Tests	

Test ID	Test 23
Test Name	Arming Test
Test Location	ASTG Workshop
Tested Item	Complete Prototype
Description	Test pyro short circuiting.
Test Campaign Date	ITW
Status	Completed
Requirements	O-8,
Prerequisite Tests	

Test ID	Test 24
Test Name	Power Supply Test
Test Location	ASTG Workshop
Tested Item	Complete Prototype
Description	Test the power supply of the whole system for endurance.
Test Campaign Date	November
Status	Completed
Requirements	O-2,
Prerequisite Tests	

Test ID	Test 25
Test Name	General Mission Control Test
Test Location	ASTG Workshop
Tested Item	Complete Prototype + Mission Control
Description	Test to see if all buttons in the mission control are working as intended.
Test Campaign Date	November
Status	Completed
Requirements	O-6, D-53,
Prerequisite Tests	22

Test ID	Test 26
Test Name	Blackbox Test
Test Location	ASTG Workshop
Tested Item	Complete Prototype
Description	Test to see if the scientific as well as the experiment blackbox work is intended.
Test Campaign Date	November
Status	Completed
Requirements	F-10, F-11, P-13,, D-53,
Prerequisite Tests	

Test ID	Test 27
Test Name	Pyrotechnic Pin Puller Test
Test Location	ASTG Workshop
Tested Item	Pin Puller
Description	Test the Pin puller deployment with loads above the expected value
Test Campaign Date	28.09.2025
Status	Completed
Requirements	D-27, D-28, D-29, D-30,
Prerequisite Tests	

Test ID	Test 28
Test Name	Pin Puller Reaction Force Test
Test Location	ASTG Workshop
Tested Item	Prototype without optical subsystem, but stand in for optical subsystem
Description	Test the reaction force created by the Pin puller with the whole gimbal. To measure this, the gimbal is suspended on a wire at its center of mass or placed on a slippery surface
Test Campaign Date	September
Status	Retired
Requirements	D-31,
Prerequisite Tests	1

Test ID	Test 29
Test Name	Gimbal Landing Configuration Test
Test Location	ASTG Workshop
Tested Item	Prototype without optical subsystem
Description	The Gimbal moves into a configuration improving its likelihood for a safe landing
Test Campaign Date	nan
Status	Retired
Requirements	O-3,
Prerequisite Tests	

Test ID	Test 30
Test Name	Unlocking Vacuum Test
Test Location	ASTG Workshop
Tested Item	Prototype without optical subsystem, but stands in for optical subsystem
Description	The Unlocking of the Gimbal is tested in a (near) vacuum environment.
Test Campaign Date	November
Status	Completed
Requirements	
Prerequisite Tests	3

Test ID	Test 31
Test Name	Thermal Convection Test
Test Location	ASTG Workshop
Tested Item	Complete Prototype
Description	The Gimbal is covered by a chamber simulating the nosecone volume, while the bottom of the module is thermally isolated against the ground below. Prelaunch Tests are done to test thermal increase of air temperature until it stabilizes
Test Campaign Date	2nd Week Nov.
Status	Completed
Requirements	D-47,
Prerequisite Tests	

5.3 Verification Results

Test ID	1
Test Name	Minimal Prototype Functionality and Kinematic Test
Verified item	Mechanical prototype assembly utilizing mass/inertia simulators in lieu of the final optical subsystem flight hardware.
Test description	Empirical evaluation of the actuation dynamics, closed-loop control, and mechanical locking/unlocking mechanisms of the Gimbal System. The assembly includes the primary structural frame, hold-down and release mechanisms, localized actuation components, and the preliminary wire harness.
Expected Result	**Success:** Unrestricted kinematic movement across all designated rotational degrees of freedom (DoF) matching operational envelope requirements, alongside 3 consecutive, flawless mechanical unlocking cycles. **Partial Success:** Consistent actuation across all axes with minor angular positioning deviations, or minor mechanical resistance noted during a subset of the unlocking cycles.
Obtained results	The multi-axis gimbal structure was actively controlled across all three independent rotational axes. Uniform motion was achieved within the structurally and electronically defined boundary limits without binding.
Overall conclusion	**Successfully Verified** — The structural integrity, kinematic boundaries, and primary actuation mechanisms conform to initial design criteria.

Test ID	16
Test Name	Gimbal-Induced Structural Vibration Test
Verified item	Integrated Minimal Prototype Assembly
Test description	Dynamic actuation of the integrated gimbal system across various angular velocity profiles, utilizing ultra-sensitive acceleration sensors rigidly mounted to the base plate to characterize and quantify induced micro-vibrations and structural resonance.
Expected Result	**Success:** Measured structural vibrations induced into the base interface remain strictly below the allowable threshold of $5 \times 10^{-5}\,\mathrm{g_{rms}}$ across the critical frequency spectrum of 0 to 25 Hz. **Partial Success:** Qualitative and quantitative ground-based assessment shows no major tactile or audible structural oscillations during unconstrained, non-isolated bench testing throughout the full spatial range of motion.
Obtained results	During non-isolated ambient ground laboratory testing, no severe macro-vibrations or abnormal acoustic resonances were detected across the operating spectrum. However, precision micro-g verification remains unquantified due to ambient facility noise floor limitations.
Overall conclusion	**Partially Verified** — Qualitative structural stability is validated for nominal operations; high-fidelity isolation testing is required for quantitative compliance.

Test ID	02
Test Name	Optical Filter Transmittance Degradation due to Vacuum Outgassing
Verified item	Optical Color Filter
Test description	Measure transmissivity before and after the filter is placed in a sustained vacuum in order to determine the effect of outgassing on filter transmissivity
Expected Result	**Sucess:** Measureable effect, but not critically strong **Partial Sucess:** No measurable effect would necessitate further tests to confirm
Obtained results	Transmissivity degradation was obtained to be $6.3\,\% \pm 0.7\,\%$ after 1 h in a vacuum equivalent to an altitude of 51 km
Overall conclusion	Successfully verified

Test ID	03
Test Name	Unlocking
Verified item	Prototype without optical subsystem, but stands in for optical subsystem
Test description	Repeated unlocking tests under various load types and amounts
Expected Result	**Success :** At least 3 consecutive unlockings of the Gimbal System. At least one of them must be with both ignitors firing simultaneously, and one with only one ignitor firing. **Partial Success:** -
Obtained results	Summary in a few sentences of the overall result of the test.
Overall conclusion	Successfully verified

Test ID	27
Test Name	Pyrotechnic Pin Puller Test
Verified item	Pin Puller
Test description	Test the Pin puller deployment with loads above the expected value
Expected Result	**Success :** At least 3 consecutive unlockings, with no solid parts larger than 10mm^3 escaping the pin puller. At least one of them must be with both igniters firing simultaneously, and one with only one ignitor firing **Partical Success:**-
Obtained results	Tested successfully with both 2 and 1 ignitor, no soot could be observed on paper towels aligned with potential exit paths.
Overall conclusion	Successfully verified

Test ID	28
Test Name	Pin Puller Reaction Force Test
Verified item	Prototype without optical subsystem, but stand in for optical subsystem
Test description	Test the reaction force created by the Pin puller with the whole gimbal. To measure this, the gimbal is suspended on a wire at its center of mass or placed on a slippery surface.
Expected Result	**Success :** The force created by the pin puller is quantified of below a limit of 1 Ns. **Partical Sucess:**-
Obtained results	Retired, as the impulse exerted during other tests by the pin puller on the system was deemed small enough to not result in excessive unwanted tumble rate during the flight of the system.
Overall conclusion	Retiered

Test ID	30
Test Name	Unlocking Vacuum Test
Verified item	Prototype without optical subsystem, but stands in for optical subsystem
Test description	The Unlocking of the Gimbal is tested in a (near) vacuum environment.
Expected Result	**Success :** Unlocking is demonstrated in a vacuum environment of 10 Pascal after being there for 120 s. At least 2 consecutive successful tests **Partical Success:** -
Obtained results	Tested in the Vacuum chamber with success at a pressure of ≈20 mbar. Could not fulfill the vacuum requirement of 10 Pa.
Overall conclusion	Partially verified

Test ID	4
Test Name	Mass test
Verified item	Complete Prototype
Test description	Measuring the weight of the entire assembly
Expected Result	**Sucess:** The assembly has a mass of less than 7.5 kg **Partial Sucess:**-
Obtained results	The mass of APEX without nosecone adapter was weight at 6.22 kg
Overall conclusion	Successfully verified

Test ID	6
Test Name	Center of mass test
Verified item	Complete Prototype
Test description	Measurement of the center of gravity of the whole assembly on all rotational axes
Expected Result	**Sucess:** The centers of masses are within 20 mm of the respective axes of rotation. **Partical Sucess:**-
Obtained results	Retired as CAD - Model Data verified with weight measurement of sub component provided a sufficient approximation of the center of mass.
Overall conclusion	Retired

Test ID	8
Test Name	Shaker Test
Verified item	Gimbal without Carbon Tube
Test description	Vehicle level 1 Sine and Random Vibrations, with frequency search befor and after. In thrust axis. Vehicel level 1 Random Vibrations, with frequency search befor and after. In lateral axis.
Expected Result	**Sucess:** No shift of eigenfrequency during testing **Partial Sucess:** Minor shift in eigenfrequency
Obtained results	14Hz loss for thrust axis. No frequenzy loss for lateral axis.
Overall conclusion	Successful

Test ID	10
Test Name	Attitude Determination
Verified item	the whole experiment (system level test)
Test description	The PCB with sensors has the Attitude Determination Software running while the PCB is being moved.
Expected Result	**Success:** The attitude is calculated correctly every 20 ms. **Partial Success:** -
Obtained results	The Attitude Determination system was verified for a few distinct static directions with a simulated sun (flash light). No dynamic tests were successfully performed.
Overall conclusion	Partially verified
Authority	Michael Zweimüller

Test ID	11
Test Name	Area Pointing
Verified item	the whole experiment (system level test)
Test description	We define an area the gimbal shall observe and check if the software keeps pointing towards this area while the sensors detect movement.
Expected Result	**Success:** The system successfully points towards goal area while moving the system. **Partial Success:** -
Obtained results	The Area pointing was tested for a few distinct static directions with a simulated sun (flash light), in wich the camera pod pointed in the expected direction. No dynamic tests were successfully performed. The pointing accuracy was not measured.
Overall conclusion	Partially verified
Authority	Felix Arch

Test ID	12
Test Name	Long Duration Test
Verified item	complete prototype
Test description	The Electronics and Software undergo a multiple hour long duration test.
Expected Result	**Success:** The Avionics system is powered for at least 2 hours without failure. **Partical Success:**-
Obtained results	The experiment ran during testing for more than 45 minutes uninterrupted. A longer test was deemed unnecessary because of the missions duration.
Overall conclusion	Successfully verified

Test ID	13
Test Name	Flight Simulation
Verified item	Kalman Filter and Attitude Determination
Test description	The Attitude Determination Framework was tested using simulated test-data under different sensor configurations and noise and bias levels.
Expected Result	**Sucess:** The Kalman Filter shall be able to determine the attitude of the bodyframe within an error-margin of below 1°.
Obtained results	The Kalman Filter was able to determine the attitude of the bodyframe within an error-margin of below 1°.
Overall conclusion	Successfully verified
Authority	Felix Arch

Test ID	14
Test Name	Data Storage Endurance
Verified item	Blackbox data storage endurance
Test description	The storage medium is exposed to sub-zero temperatures (approximately -10°C to -15°C) for 30 minutes and snow submersion-like conditions to simulate post-landing recovery conditions.
Expected Result	**Success:** All stored data remains intact and fully retrievable after exposure to all test conditions without corruption or loss.
Obtained results	Summary in a few sentences of the overall result of the test.
Overall conclusion	Successfully verified

Test ID	15
Test Name	System Alignment Test
Verified item	Gimbal without Carbon Tube
Test description	Test the alignment of the System with static pointing
Expected Result	**Success :** The science cameras are aligned within 1° and the reference camer shall be aligned whithin 5° with the science cameras **Partial Success:**Cameras align to the camera housing
Obtained results	Measuring of Camera housing alignments are within 1° of the camera holder plate
Overall conclusion	Partially successful

Test ID	18
Test Name	Optical Polarization Test
Verified item	Optical Subsystem
Test description	The angle, intensity and degree of polarization is measured in an optical setup
Expected Result	**Success :** The Degree of Linear Polarization is resolved with a resolution of 1% at 2-sigma, **Partial Success:-**
Obtained results	The spectrum of the Filter was measured wit a spectrometer. Other parameters or a combination of spectral and polarization measurement were not performed due to a lack in time. This was deemed acceptable, as the optical subsystem is COTS.
Overall conclusion	Partially verified

Test ID	19
Test Name	Gimbal Camera Test
Verified item	Subsystem and flight hardware test
Test description	Long time exposure of the science cameras is tested in conjunction with the short time exposure of the reference camera
Expected Result	**Sucess:** Long time exposures of 3 seconds for both science cameras are possible in conjunction with 10 Hz exposures of the reference camera **Partial Sucess:** -
Obtained results	Simultaneous initialization and operation of polarization and reference cameras were validated across both subsystem and flight hardware levels. Metadata latency was identified during flight hardware testing. Due to project timing constraints, mitigation strategies remain recommended for future implementations.
Overall conclusion	Succesfully verified

Test ID	23
Test Name	Arming Test
Verified item	Complete Prototype
Test description	Test pyro short circuiting.
Expected Result	**Success:** Pyro channel is short-circuited when ”remove before flight”-tag is inserted and open when the tag is removed **Partial Success:-**
Obtained results	The short circuit resistance of the short circuit connector was measured at below 0.1 Ohm
Overall conclusion	Successfully verified

Test ID	24
Test Name	Power Supply Test
Verified item	the whole experiment
Test description	Test the power supply of the whole system for endurance.
Expected Result	**Success :** The power supply does not collapse during testing. Current, voltage and power limits are not exceeded. Request for Radio Scilence is accepted
Obtained results	Measuring of the voltages and currents during operation showed no peaks or crashes in the power supply. Input voltages between 24 and 36V were accepted without issues. Mean power draw at 28W.
Overall conclusion	Successfully verified
Authority	Michael Zweimüller

Test ID	26
Test Name	Blackbox Test
Verified item	Complete Prototype
Test description	Test to see if the scientific as well as the experiment blackbox work is intended.
Expected Result	**Sucess:** Both blackboxes are able to write data with the desired speeds. **Partial Sucess:-**
Obtained results	During launch operations, neither the scientific data blackbox nor the flight computer blackbox were able to recorded data
Overall conclusion	Not verified

Test ID	31
Test Name	Thermal Convection Test
Verified item	Complete Prototype
Test description	The Gimbal is covered by a chamber simulating the nosecone volume, while the bottom of the module is thermally isolated against the ground below. Prelaunch Tests are done to test thermal increase of air temperature until it stabilizes
Expected Result	**Success:** The air temperature at the module interfaces does not exceed the ambient temperature by more than 10 °C. Ambient Temperature for the Test is assumed with 20°C. **Partial Success:-**
Obtained results	The Avionics system was run for extended period of time with a closed bottom without a noticeable increase in temperature. Test was performed without temperature measurement.
Overall conclusion	Partially verified

6 Launch Campaign Preparation

6.1 Input for the Campaign / Flight Requirement Plans

6.1.1 Dimensions and Mass

Table 6.1: Experiment mass and volume, *Mass without bulkhead

Experiment mass (in kg)	6.036*
Experiment dimensions (in mm):	265x190x340
Experiment expected Centre of Gravity (COG) position:	x,y<3mm, z=87mm from connectorplate

6.1.2 Ground and Flight Safety Risks

Risk	Key Characteristics	Mitigation
Flight of Lithium Iron Phosphate Batteries	Type: LiFePo4 Number of: 7 Total Capacity: 600 mAh	Batteries will be tested in thermal vacuum to 0.5 mbar under expected mechanical, electrical and thermal load.
Premature Ignition of the Pyrotechnic E-Matches as Gas Generators for Pin Puller (Locking Device).	Type: Pyrotechnic Fuse Head No-fire current: $\leq$ 1 A / 5min All-fire current: $\geq$ 5 A / 50 ms ESD immunity: 500 pF / 500 Ω / $\pm$25 kV (0.6 Joule) Pressure after ignition (3.5 ccm bomb): 25 - 45 bar (mean value)	The fuse heads (also referred to as e-matches) are shunted during and after installation, arming is done with by Pulling a shunt; The Pin Puller Housing is constructed so that only gas and very small particulates (i.e. smoke) can escape in event of a missfire

6.1.3 Electrical Interfaces

Table 6.2: Electrical interfaces

REXUS Electrical Interfaces		
Service module interface required? Yes/No		
	Number of service module interfaces:	1
	TV channel required? Yes If yes, when is it required:	after NC deployment until parachute deployment
Up-/Downlink (RS-422) required? Yes		
	Data rate - downlink (max and average):	30Kbit/s
	Data rate - uplink (max and average):	0
Power system: Service module power required? Yes		
	Peak power and current consumption:	28W and 1A
	Average power and current consumption:	28W and 1A
	Total power and current consumption after lift-off (until T+600 s	$W \cdot h$ and $A \cdot h$
	Power ON	600s before lift-off
	Power OFF	600s after lift-off
	Battery recharging through service module:	Yes
Experiment signals: Signals from service module required? Yes/No (specify if they are related to flight events e.g. nosecone separation, etc.		
	LO:	Yes
	SOE:	@ Nosecone Deployment
	Pyro(s):	3s after Nosecone Deployment
	SODS:	180 s after SOE

6.1.4 Launch Site Requirements

Table 6.3: Launch site requirements

Category	**Item**	**Amount**
Workstation		
	Table	2
	Chair	6
	Power extension	3
	External Monitors	2
	Power cable for External Monitors	2
	HDMI Cable for External Monitors	2
	Power supply, 0-30 V	1
	Soldering Station	1
Measurement Instruments		
	Multimeter	1
	Oscilloscope	1
	Inbus Set	1
Consumables		
Chemicals		
	Isopropyl alcohol	100 mL

6.1.5 Flight Requirements

Table 6.4: Flight Requirements

De-spun/spinning	De-Spun
Weather conditions during countdown	Space Weather conditions that produce Aurora are preferred. No specific conditions for Earth weather.
Module temperature during countdown	15 °C to 30 °C
Launch window	Variable see Appendix F.3 Early March: starting 06:15 UTC Late April: starting 02:05 UTC End see Table 6.5

Table 6.5 shows a breakdown of our scientific and technical objectives and at which time of the day they can be fulfilled. This is based on the analysis presented in Appendix F.2, for the 20th of March 2026 with Kp 4 auroral condition. Obj. 3 and 6 are achievable independent of daytime. Obj 4 and 5 are achievable if there is sunlight and the sun is 10° above the horizon. Obj. 2 is split for red and green emission lines and for airglow. For Kp index of 4, the error for the weaker red emission line never goes below the error threshold. For further details see Appendix F.2 and Figure F.2.3.

Similar analyses were be produced for the first attempted launch date for the range of possible geomagnetic conditions and launch times. See Section 7.2.3.

Table 6.5: Possibility of the fulfillment of the scientific and technical objectives, calculated for the March 20th, with a Kp index of 4 and 4 s of exposure time. The blue line marks the earliest possible launch time ar 05:00 UTC based on the elevation of the Sun in the sky. All times UTC
Green .... full fulfillment achievable (Error $< 0.3\%$ for green emission, $< 0.5\%$ for red emission)
Yellow .... still achievable with degradation (Error $< 0.4\%$ for green emission)
Orange .... nearly achievable (Error $< 0.5\%$ for green emission, $< 0.7\%$ for red emission)
Red ..... not achievable (Error $> 0.5\%$ for green emission, $> 0.7\%$ for red emission)

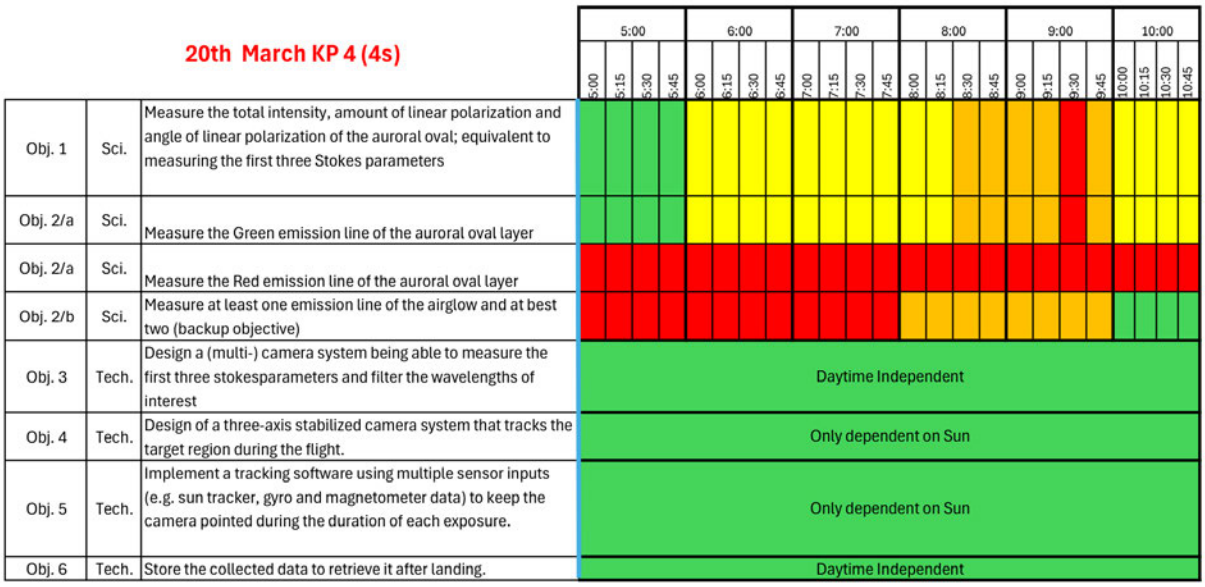


Table 6.6: Flight Requirements on timeline events

Yo-yo de-spin	before start of experiment
Motor separation	before start of experiment
Nosecone ejection	before start of experiment

6.1.6 Accommodation Requirements

APEX was mounted in the nosecone of the rocket. As the experiment used magnetometers for the initial attitude determination, an electromagnetically low-noise environment was required. If not possible, an environment with a stable predictable noise source was preferred over a randomly fluctuating one. Because APEX used a gimbal to stabilize its exposures, it was also preferable if mechanically noisy experiments are installed further away from the nosecone, to reduce parasitic vibration level. Short, known bursts of mechanical vibration were preferred over random extended vibrations.

6.2 Preparation and Test Activities at Esrange

Note: The following list is was the planed list prior to arrival in Kiruna.

Time	Main Task	Description	Responsible	Duration	Comment
T-2 days	Casting of charge cups	The pyrotechnic e-matches used to deploy the locking system must be cast into the charge cups with resin.		2 h	
T-2 days	Assembly Muffler	The Muffler of the locking system is assembled		2 h	
T-1 days	Locking System Test	The Locking System is tested for functionality after transport to Kiruna		2 h	
T-2 days	Camera assembly	The Cameras are screwed to the gimbal assembly after having been transported separately to the gimbal		1 h	
T-2 days	Camera alignment Test	The Camera alignment is tested and documented		2 h	
T-2 days	Sun Sensor Calibration	The Direction of the Sun Sensor is calibrated after Transport to Kiruna		2 h	
T-2 days	Gimbal Pointing Test	The Gimbal Pointing is tested with a preprogrammed test path		4 h	
T-0.5 days	Locking Assembly for Launch	Assemble the locking as final preparation before the launch		1 h	

6.2.1 Aurora Nowcast

The space weather and geomagnetic conditions was continuously monitored before launch. The current Kp index serves as the main input for the aurora model. This provided an estimate of the current position and intensity of the auroral oval (Figure 1.1). Images from all-sky camera stations were planed to be used to get data about the current aurora activity. The predictive power of space weather forecasts is even more limited than Earth weather forecasts. If there is a solar storm in transit, there might be a significant auroral enhancement at some point in the next 12 to 24 hours. Solar storms occur more frequently near the maximum of the 11-year solar cycle, which was during 2024/2025. However, whether one could expect strong aurora activity on launch day was a matter of luck.

6.3 Timeline for Countdown and Flight

Table 6.7: Timeline for the countdown and flight

Time [s]	**Signal**	**Function**
T-600s	POWER ON	Experiment switched on
T+0s	LO	
T+1:21 min	V-B (2) APEX	Start APEX Engineering Camera Transmission
T+1:23 min		Nosecone Deployment
T+1:25 min	Pyro	Unlocking of Gimbal
T+1:25 min	SOE	Attitude and Motor contorller is started
T+3:30 min	SODS	Power is taken from the Motors Software enters landing state Section 4.8.1

6.4 Post-Flight Activities

7 Data Analysis and Results

7.1 Data Analysis Plan

The images for each emission line were planned to be analyzed to extract the Stokes parameters: S_0, S_1 and S_2. S_0 can be measured directly as it represents the total intensity. S_1 and S_2 can be calculated by subtracting the horizontal and vertical and the diagonal and antidiagonal components, respectively. The measurement of the degree of circular polarization in the light, represented by S_3, was not included in this experiment. If stable exposures would have been taken, it may have been possible to calculate and remove the dayglow background signal. It would have been necessary to use pixel binning to resolve the degree of polarization with sufficient precision. The housekeeping logs of the ADS and the reference images of the white light camera could have aided in interpreting the images.

7.2 Launch Campaign

7.2.1 Flight preparation activities as they happened during the launch campaign

Preparation of Locking System and charge cup Casting

This section lists the actions taken to prepare the locking system and casting the charge cups. The charge-cups were filled with as per checklist, with the main difference being that instead of the usual polyurethane a slightly harder version dispensed from a dual syringe (Type WIKO® REPAIR 90 SOFT UF POLYOL) was used. The change of material was already verified in tests prior to the campaign. The change was due to the new polyurethane being significantly easier in handling (no need for measuring and premixing of components, no need for oven to harden, lower risk of dangerous spills as the isocyanate was contained in the syringe during the full filling process), at the cost of worse mechanical properties (harder, therefore less shock absorbent; harder to remove after tests from the charge cup). A total of 4 cups were filled, with two being marked for launch.

Preparation of the muffler which functions to filter soot and contains the following;

- ASA 3D printed hard stop attached with a bolt with a snap-on 3d printed flexible shock absorbing tip. with a small square of sealing putty and 5 layers of Teflon tape facing the bolt.

The same checklist was used as in testing with only very minor changes. These are the actions taken while preparing the pin-puller on the final test as well as campaign;

- Cleaning Pin Puller internals
- Lubricating surfaces in contact with combustion materials to ease cleaning for reuse
- Testing alignment of all parts by inserting pin into arm and checking for proper movement
- Attaching a bolt retaining shear pin
- Inspecting muffler internals



Figure 7.1: One of the sun sensor covers with a broken thread insert (left) compared to its replacement part (right).

- Pretensioning the locking arm using:
  1. 0.15 Nm for the Pin closest to the Camera mount
  2. 0.15 Nm for the Pin closest to the Pin puller
  3. again 0.15 Nm for the Pin closest to the Camera
- Fix the Arm pretension screws with the worm Screws from the side
- Checking ignitors for proper resistance and continuity with housing
- Screwing in charge cup before test and flight
- Connect ignitors to rocket

Mechanical fixes and Changed 3D-Prints

Since work was performed on the flight computer, the avionics box had to be opened. Consequently, all screws on this box were secured with Loctite after final assembly. Furthermore, all D-Sub connectors were also secured with Loctite.

As there were issues getting both black boxes working, all the data, housekeeping, and experiment data were instead saved on the Raspberry Pi SD card mounted in the standard SD card holder on the PCB. The SD card was secured with 5-minute epoxy to mitigate vibration effects from the launch on the spring contacts.

After Benchtest in Oberpfaffenhofen, the Engineering Camera was screwed back together without any additional securing. So before the flight, the SD card was formatted, and the PCB was secured with Loctite.

During sun sensor hardware servicing (see below), the inserts in two sun sensor covers got damaged (once the insert holding in the pin hole, once the insert facing the bulkhead). Both sun sensor covers were replaced with identical spare parts. Figure 7.1 shows the broken and replacement parts for one sun-sensor on a scale.

Update of Sun Sensor Software

The sun sensors received only two small software patches during the launch campaign, as in terms of functionality, the software was already complete and calibrated. The first one was an update of the teltalk library. This was done to make sure that all (new or updated) commands and data packets can be received and sent correctly. The last patch was an update to the CAN bus timing settings, as we had a lot of issues with reflections on the sun sensor CAN bus line. This ended up fully fixing the reflection issue, but unfortunately there was no more time to upload this patch to the built-in sun sensors.

Update of Sun Sensor Hardware

The sun sensor system received the following hardware updates during and before the launch campaign.

- One broken and a few working FFC cables were replaced
- The system was reconfigured to use only 6 sun sensor nodes (the ones that were looking up were disabled and disconnected)
- The special sun sensor node with an additional power adapter was replaced with a spare (since the number of active nodes dropped, less power was needed)
- A cracked sensor housing cover was replaced with a new one
- Two sun sensor enclosures were replaced, as some of the brass screw inserts broke during disassembly

Update of Raspberry PI Software

Several modifications were made to the Raspberry Pi software and boot sequence to resolve operational difficulties. Initially, the boot process stalled while attempting to establish a network connection, preventing the initialization of mission-critical services; this dependency was subsequently removed to ensure autonomous startup.

During ground testing, sudden power cycles resulted in SD card file system corruption. To mitigate this risk, a graceful shutdown command was implemented to ensure data integrity prior to any planned system resets. Furthermore, the camera communication software was refactored to utilize multi-threading, enabling the concurrent saving of multiple images and improving overall data throughput.

Finally, the default camera exposure time and gain parameters were adjusted to act as a fail-safe, ensuring viable image capture in the event of an up-link loss from the Ground Control Station.

Testing of Full System

The system was tested using the same checklist and procedures planned for pre-launch operations. During the test, predefined settings for the Sun, magnetic field, and aurora were entered, allowing the expected gimbal movement to be predicted and used to verify the correct operation of the algorithm.

The gimbal was initially kept in an unlocked state while positioned as it would be during flight when locked. After the system was set to the PRE LAUNCH state, the REXUS signals were triggered in the same sequence expected during the actual flight. The experiment went into the correct states during this.

Once the experiment received the SOE signal, the gimbal moved to the expected orientation, captured an image, and then returned to its base position. This process repeated continuously until the SODS signal was received, at which point power to the motors was cut.

Two benchtests were conducted at the campaign. A cold-open and a hot-closed. For the cold open, our experiment was placed upright to mitigate gravity effects on the gimbal's rotational axes and reduce the force on the motors. A flashlight served as our sun and was placed next to a sun sensor. For the cold-open test, the locking arm was held in place by hand and released after SOE was received to simulate an unlocking.

For the hot-closed test, the different experiment modules were screwed together, and the pyros were installed. The rocket was oriented on the bench so that the HARTS hatch and experiment could eject from the rocket, and, for APEX, the pyro release would minimize gimbal movement. A flashlight was placed again in front of a sun sensor, and the full timeline was performed.

Both tests concluded successfully; the gimbal moved as it should in a stationary attitude and the science cameras captured pictures. Additionally, the hold-down and release mechanism released as planned. After receiving SODS, the motor movement was turned off. Data was received during both tests without any issues at the mission control.

7.2.2 Flight performance/Flight report

The following list gives a rough indication of the flight timeline and the relevant events for APEX

- t-9 min: Startup of the APEX experiment
- t-8 min: No connection between the experiment and the Ground Station (Laptop) on Student side can be established. The student team decides to ask the Payload operator to power circle the experiment, at the risk of not properly shutting the raspberry pi down.
- t-7 min: After power circling still no connection. The payload operator confirms that they receive data from the experiment, the error must be on ground station side. Unplugging and restarting the Ground Station software fixes the connection issue.
- t-6 min: The pointing parameters are entered in the system. The precalculate Sun-vector is given for a start time of 7:02, as per schedule.
- t-4 min: Values are entered and sent to the ground system, operators recheck the values for correctness
- t-0: Liftoff at 7:02 LT
- t+1:23 min : Nosecone deploys
- t+1:25 min : The locking Pyros fire, unlocking the gimbal
- t+1:30 min: The ADS system tries to calculate the Attitude of the Experiment
- t+1:50 min: First attempt to stabilize. The Gimbal can be seen thrashing around violently for a few seconds on the video feed of the engineering camera, after which the motor-controller returns it very controlled back to the initial position.
- t+2 to t+3 min: three more attempts as stabilization, each with the same effect.
- t+3:30 : End of Experiment. The power of the motor is taken.



Figure 7.2: Four images taken by the engineering camera of APEX. From the top left starting, the first shows the gimbal in the stored position in the nosecone, illuminated by the service light in the bulkhead. Image two shows the gimbal in the waiting position, image three and four while trying to stabilize the image.

Figure 7.2 shows four snapshots of the flight. A supercut of the full video can be found on Youtube: `https://www.youtube.com/watch?v=0MmMdWRgxWo&t=3s`.

7.2.3 Aurora conditions on launch day

We followed the checklist for auroral conditions as outlined on both launch attempts of RX35 on Monday, 9th March and Tuesday, 10th March. In addition, we checked all available resources starting five days prior to gain a better understanding of the expected conditions during the launch campaign. All checks and estimates were performed on both days equally; for clarity, we document only the conditions for the launch day of RX35, Tuesday, 10th March. Simulations were conducted for 9th March for all possible space weather conditions, and not repeated for 10th March because they are computationally expensive. The resulting parameters such as the target direction don't change significantly from day to day.

Determination of Kp-Index

All available resources for estimating geomagnetic activity showed a low overall activity. There were no flares detected within the five-day pre-launch campaign checks, as well as no Coronal Mass Ejections that could impact the space weather at Earth. As shown in Figure 7.3, the conditions between 00:00UTC and 03:00UTC were favorable with a G-scale index around 5-6. Yet for the time of the launch window, this dropped significantly. Local Kp indices from Kiruna, Northern Finland and Greenland showed a value of 1-2.

Target Vector and Camera gain determination

In order to predict the direction of highest auroral emission we run the auroral simulation for the Kp 1 and 2. From this prediction of the APEX FOV (Fig. 7.4) we determine the maximum brightness of the green line at an azimuthal angle which we use for the determination of the target

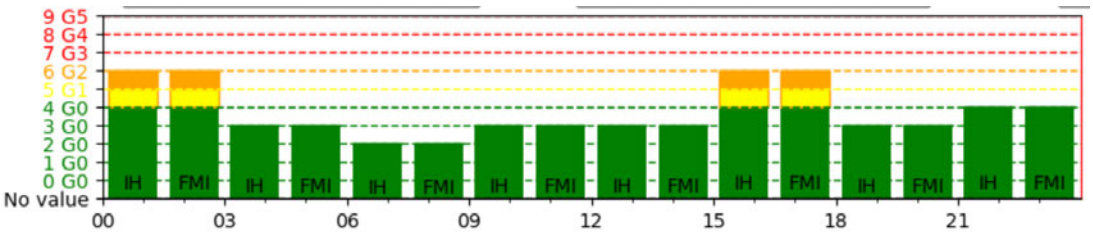


Figure 7.3: NOAA Space Weather scale for Tuesday, 10th March. The Inner Heliosphere (IH) Model Within the Space Weather Modelling Framework, the Inner Heliosphere (IH) component simulates space weather from 20 solar radii out to the orbit of Earth (and beyond). FMI (Finnish Meteorological Institute) acts as the primary space weather research and operational centre in Northern Europe.

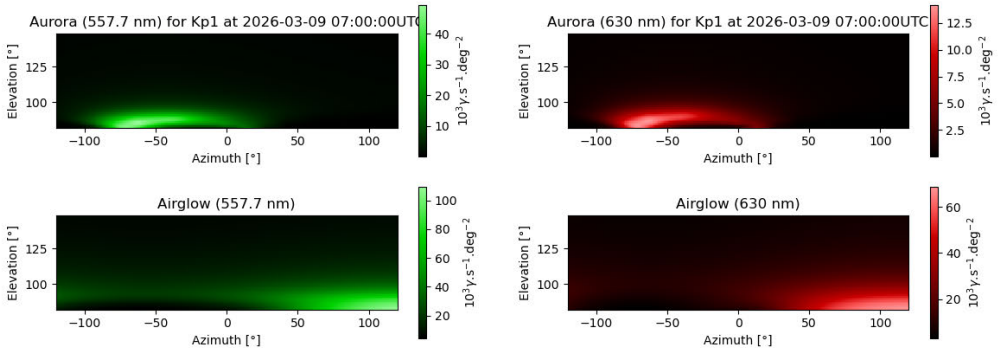


Figure 7.4: Auroral and Airglow observation simulation for Monday, 9th March and Kp 1. Azimuth of 0° points north.

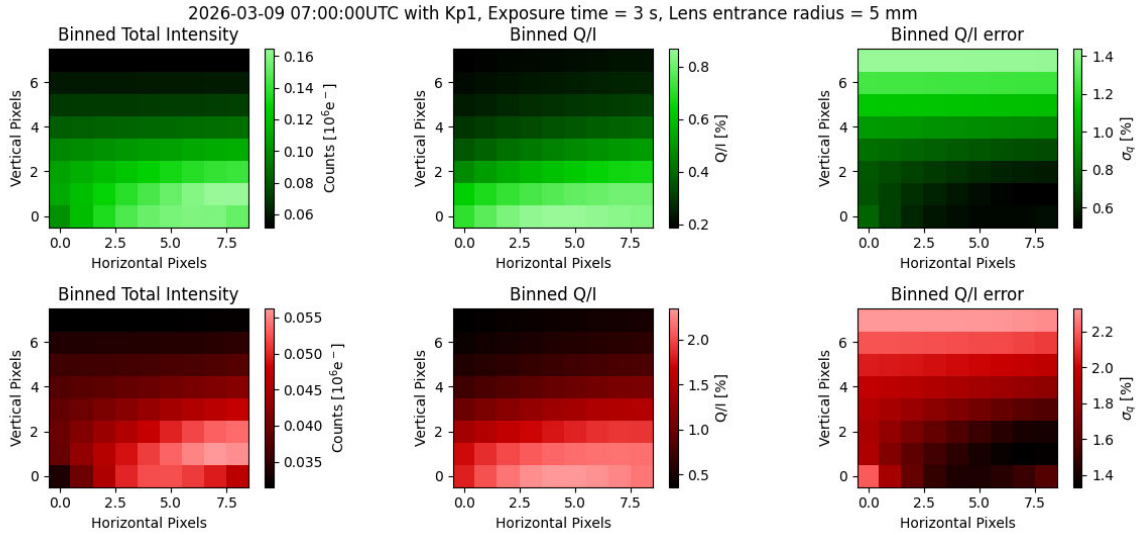


Figure 7.5: Binned total intensity, Binned Q/I and Binned Q/I Errors for our expected observational and camera parameters (3 second exposure time and 5 mm lens radius).

Table 7.1: Camera Gains sent to mission control dependent on launch time.

Possible Launch time	06:00LT	07:00LT
	Gain [dB]	Gain [dB]
Green Science Camera (C1)	26	27
Reference Camera (C2)	5	5
Red Science Camera (C3)	33	33

vector. We also simulate the expected measurements based on the observational parameters determined and our camera specifications.

With that we determine the best target vector at 2026-03-10 07:02 UTC to be:

$$\begin{pmatrix} x_{ECI} \\ y_{ECI} \\ z_{ECI} \end{pmatrix} = \begin{pmatrix} -0.96647 \\ -0.17624 \\ 0.18674 \end{pmatrix}$$

Based on all the estimated values we set the camera gains to the values seen in Table 7.1.

7.2.4 Form and Amount of Data

A total of 2,234,978 data points were received through the experiment downlink. Since the black box malfunctioned, no data could be recovered from it. The received data included both raw sensor measurements and calculated values generated by the algorithms used to actuate the gimbal.

After extraction from the mission control database, the data was reformatted into a CSV file to allow easier processing and analysis.

The science cameras took a total of 4 exposures, which could be recovered after landing from the SD - card of the raspberry pi.

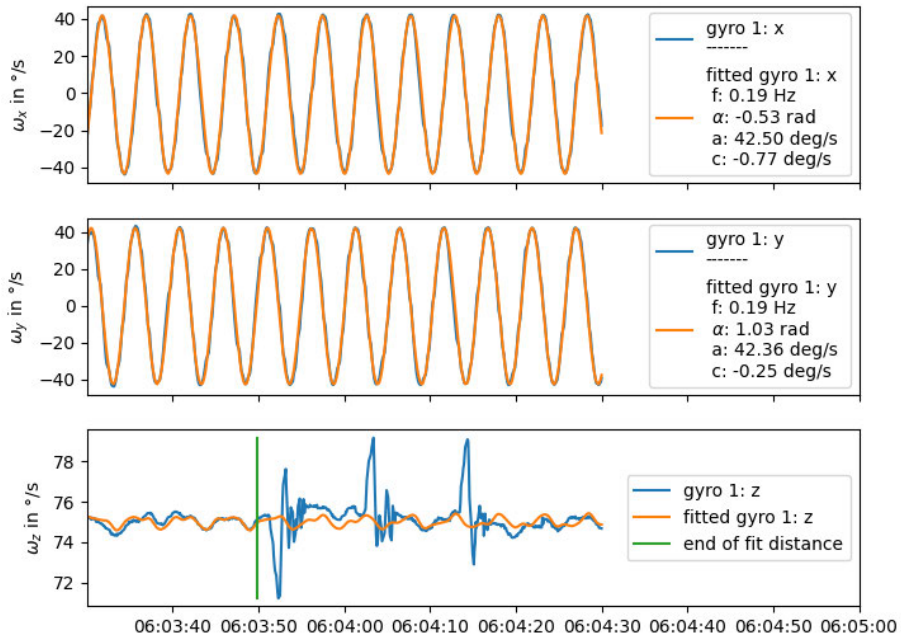


Figure 7.6: Measured and fitted gyro rates of the experiment phase, measured in the rocket body frame. The x - axis is given in UT. Fit parameters for the simple single sinus fit in x and y direction are given.

7.2.5 Possible failures and malfunctions, failure analysis

The video feed of the engineering camera showed already prior to touchdown that the likelihood of successful observations was very low. This was as the Gimbal could be seen trashing around radically during observations. This combined with the high tumble rate observed made it very unlikely, that the cameras stayed focused on the same point for a sufficiently long time frame. In this subsection we shall explore possible causes in more detail.

Gyroscopes and Magnetometer

We check the gyroscopic data and magnetometer data for consistency with both the observed and expected. We start by extracting the gyro data and plotting it in a body center frame of reference, shown in Figure 7.6. As can be seen, we measure an extremely height residual role rate of roughly 70 °/s in combination with a tumbling in the other two axes in the order of 40 °/s. We fitted the x and y component of the gyro data with a sinus to up-sample the measured values for later use, their parameters can be seen in the plot legend. As the z component was more complex but also essentially flat, with fitted only the beginning (up to the green line) with 3 added sinus functions. The high measured tumble rate is confirmed by the observed tumble rate in the video of the engineering camera. The consistence form (clean sinus in x and y, essentially flat in z) gives confidence in the correctness of the values.

We use the up-sampled gyro values to rotate the magnetic field vector measured from the body frame of the rocket to an arbitrary earth fixed system. We decide the z component to be aligned with the positive magnetic b_z component, as this gives us roughly up (reminder, that the magnetic field close to earths North pole is mostly in the negative b_z direction, as it is a magnetic south pole). For the rotation, solve the Euler equations in quaternions by integrating the rotation rates, following the approach of [16]. The quaternions were transformed into rotation matrices

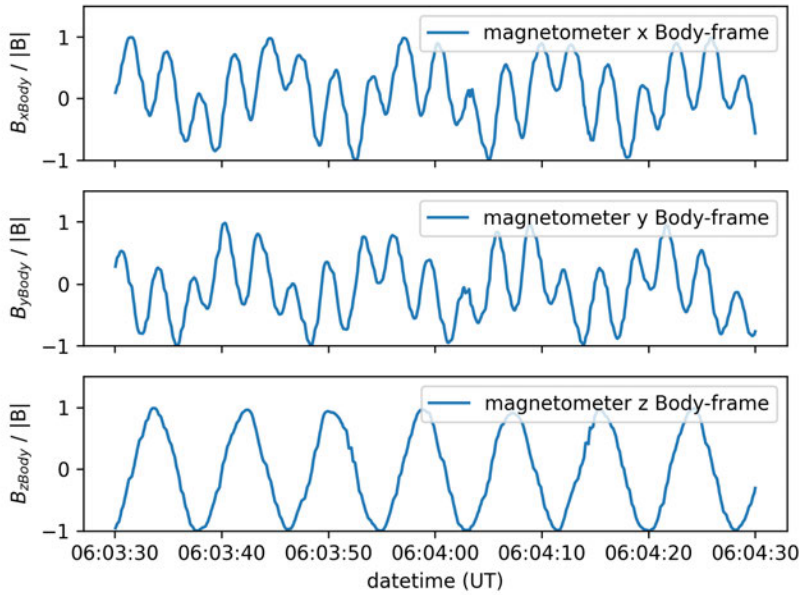


Figure 7.7: Magnetic field measured in the rocket body frame, normalized with the total magnetic field.

using the *Rotation* package form *scipy.spatial.transform* and its inverse applied to the magnetic field vector in the body frame.

While Figure 7.7 shows the magnetic field in the body frame of the rocket, Figure 7.8 shows the magnetic field rotated to the earth fixed frame. The magnetic field was fitted with a line in all three axis, and the line slope is shown in the plots legend. Notably, the de-rotation does a good job pointing the magnetic field vector in the same direction, both validating the gyro data and the magnetic field data. Further, while we observe fluctuations in the magnetic field data likely due to electromagnetic influences (i.e. the gimbal motors), the fluctuations are relatively small and fast, easily to smooth out by the Kalman filter. Lastly the slope gives an indication for the drift rate of the gyros during the measurement. The drift rates shifts the magnetic field vector by 17 °/min, a significant value over the whole experiment duration (roughly 2 minutes) and an indication that accurate sun sensor values are needed for repeated observations of the same targe area.

Sun Sensors

The sun sensors had two main issues during the launch campaign. The first one was a software configuration problem, which involved the CAN bus system - we had severe reflection problems on the CAN bus that connected all of the sun sensors and the flight computer. When all 8 sensors were connected together, about half of them would crash in terms of communication capabilities. And if the configuration of the sensors was changed (even when the cables were kept the exact same), different nodes would die, while the ones that did not work before would begin to communicate properly with the flight computer. All of this was caused by a bad CAN bus bit timing configuration. Before, it was sampling the data bits at about 60% of the single data bit time, while a recommended value is at about 80%. At 60% the reflections had large enough amplitudes, so that they interfered with the actual data that was being transferred. But if we sample the bus at 80% of the bit time, most of the reflections have been attenuated enough so that they no longer interfere with the signal. The configuration file was updated to meet these

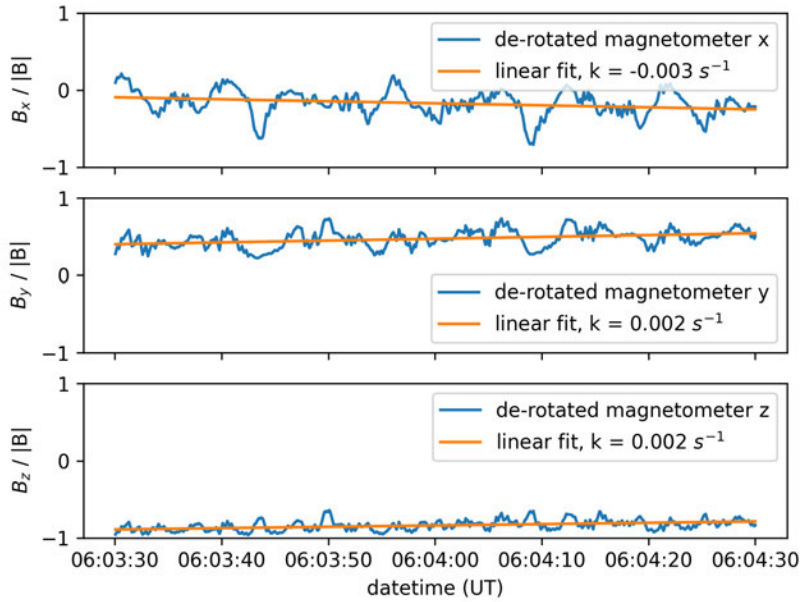


Figure 7.8: Magnetic field rotated to an earth fixed frame, chosen as the z axis being aligned with the negative magnetic field. The rotated measurements are fitted with a line. Note that the magnetic field shown is normalized.

criteria and it was able to fix the reflection issue, but unfortunately the software patch could not be pushed to the sun sensors, as the experiment preparation time ran out.

The second issue was hardware related and involved the sun sensor covers themselves. After analysis the data from all sun sensors post launch, about half of them had a much smaller field of view when compared to the expected field of view of about 120 degrees. This was caused by 3D-printed cover design. The plastic part of the pinhole was drilled with the same drill diameter that was used for the metal insert below it, and since the plastic part is a lot thicker than the metal one, the light would be almost fully blocked by the geometry when it hit the pinhole at a large angle. This created dead-zones between the sensors and caused major issues for the Kalman filter's attitude determination during flight. Figure 7.9 shows the measured combined sun vector in the body frame of the rocket. The colors indicate the different sun sensors. Figure 7.10 shows the measured sun vector in the body frame compared with the sun vector taken at the start of the plot and propagated with the rotation matrices calculated as described in the previous mini-section.

Kalman Filter

The Kalman filter fused measurements from the gyroscope, sun sensors, and magnetometer to estimate the attitude of the bulkhead with respect to the ECI reference frame. However, the filter exhibited significant limitations in achieving reliable attitude estimation during the experiment. Since a detailed post-flight assessment of the filter performance under actual flight conditions is difficult due to the limited availability of representative data, the following analysis focuses on identifying the most likely causes based on the subsystem development and pre-flight testing campaign.

The gyroscope and magnetometer measurements showed good performance throughout the testing campaign and provided reliable attitude information. In contrast, the sun sensors did not deliver usable measurements, primarily because their field of view was insufficient to consistently detect

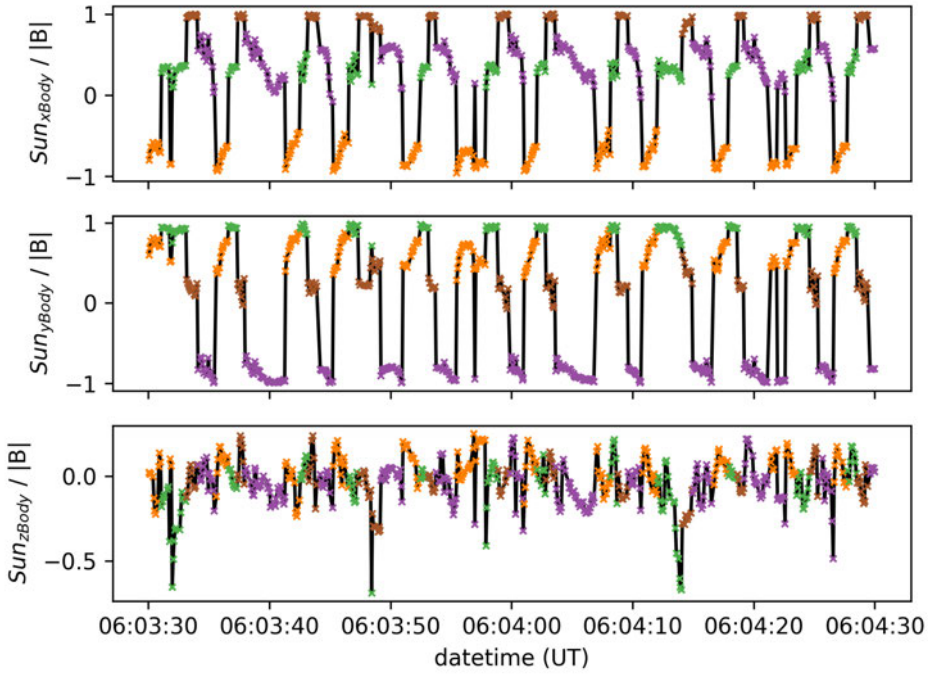


Figure 7.9: Observed sun vector in the rocket body frame. The colors indicate the sensor currently observing. Note that only 4 sensors were working, hence only four colors are plotted.

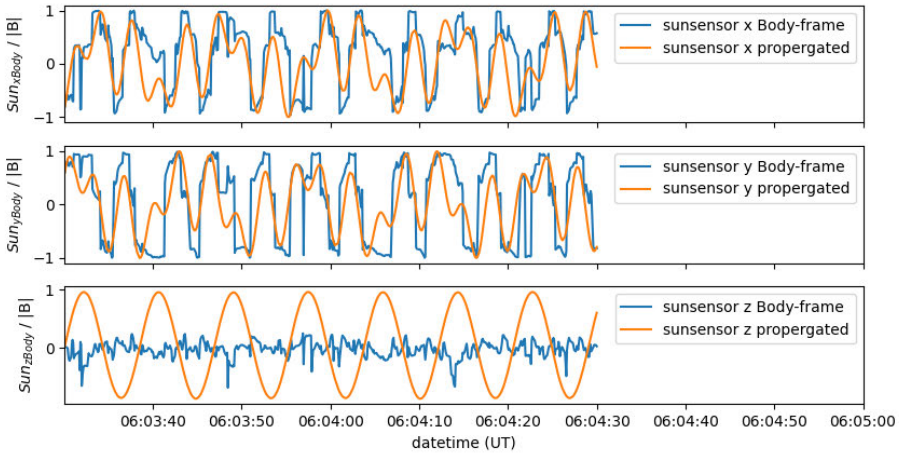


Figure 7.10: Observed sun vector in the rocket body frame. Overplotted is the sun vector at the beginning of the data series propagated with the gyro data.

the simulated sun source. The main limitation of the attitude determination subsystem was the lack of dedicated time for filter validation. Testing of the Kalman filter depended on several other subsystems and components that were themselves still under development. As a result, nearly every test campaign was affected by changing sensor characteristics, incomplete hardware, or modifications to the software architecture. This significantly complicated debugging and filter tuning, since sensor fusion performance is inherently dependent on both the quality of the sensor data and the accuracy of the associated uncertainty models.

During the performed tests, the basic functionality of the system could be validated. In particular, the correspondence between the incident direction of the simulated sun source and the resulting gimbal motion was verified, and the general attitude representation and axis conventions were confirmed. However, only limited validation of the kinematic behavior was possible. Due to the restricted dynamic range and the continuously evolving system configuration, the tests were largely limited to verifying sensor orientation, rotation directions, and coarse attitude behavior under low-dynamic conditions. The available test data were insufficient to adequately validate the dynamic performance of the attitude determination subsystem.

For future developments, a dedicated test setup for the attitude determination and Kalman filtering subsystem should be prepared early in the project. In particular, an air-bearing platform should be used to enable realistic rotational motion and independent subsystem validation. Sufficient time must also be allocated for filter tuning and characterization of sensor uncertainties. Since sensor fusion performance depends strongly on stable and well-characterized sensor inputs, meaningful filter validation can only be performed once the sensor suite and associated hardware have reached a mature and stable state.

Black Boxes

The primary black box, designed to monitor all CAN bus traffic, was functional at the hardware level; however, due to time constraints, the flight software could not be fully verified prior to launch. Consequently, during the flight, the black box only recorded its own transmitted packets and failed to capture telemetry from the other network nodes. Additionally, the Raspberry Pi was originally designed to utilize a dedicated black box enclosure for its primary SD card (which houses the operating system and mission data). However, for unknown reasons, the SD card experienced data corruption after a power cycle of the experiment. As a contingency, the SD card was relocated directly to the onboard Raspberry Pi PCB slot and mechanically secured with epoxy for flight protection. The Raspberry Pi was able to record all mission-critical data during the flight.

7.2.6 Power consumption and Thermal behavior of the experiment

The temperature readings from all sensors did not show realistic data. This was not really a focus of the experiment, and there were many other open to-dos before the flight that took higher priority. The current consumption of the two sensors, one for the battery and one measuring the total current consumption, showed that the worst-case current consumption was not exceeded. A maximum of 1.5A continuous was measured during operation, with a constant of 1A at 28V from the Service Module, and the rest coming from the battery.

7.2.7 Recovery (condition of experiment, re-usability, damages)

Figure 7.11 to Figure 7.13 show the APEX experiment directly after the flight. Notably, the bulkhead was unscrewed from the nosecone adapter ring for transport, requiring that most of the experiment arrived in a bag. Inspection of the Experiment showed fortunately no major

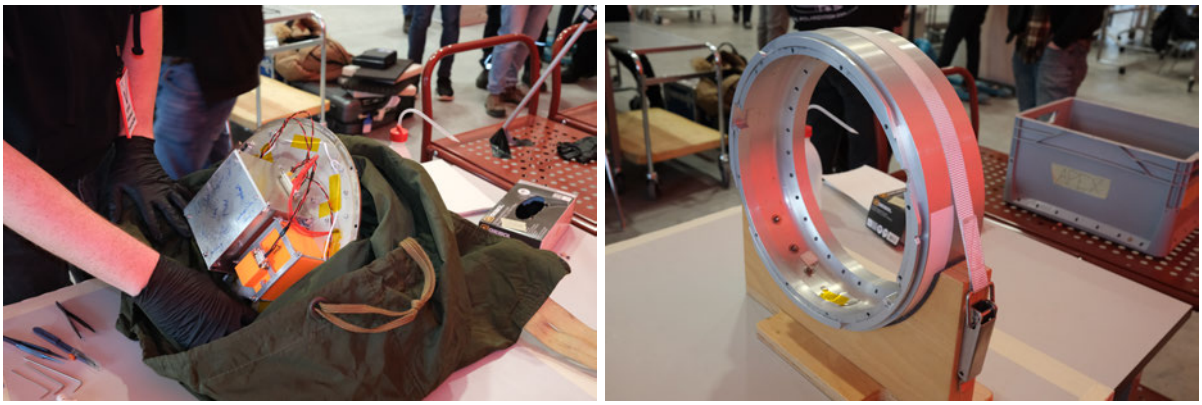


Figure 7.11: State of the gimbal as hand over to the student team by MORABA after the flight. The left image shows the Gimbal and Flightcomputer still mounted to the Bulkhead transported in a Sack, the right image the separately delivered nosecone adapter ring.

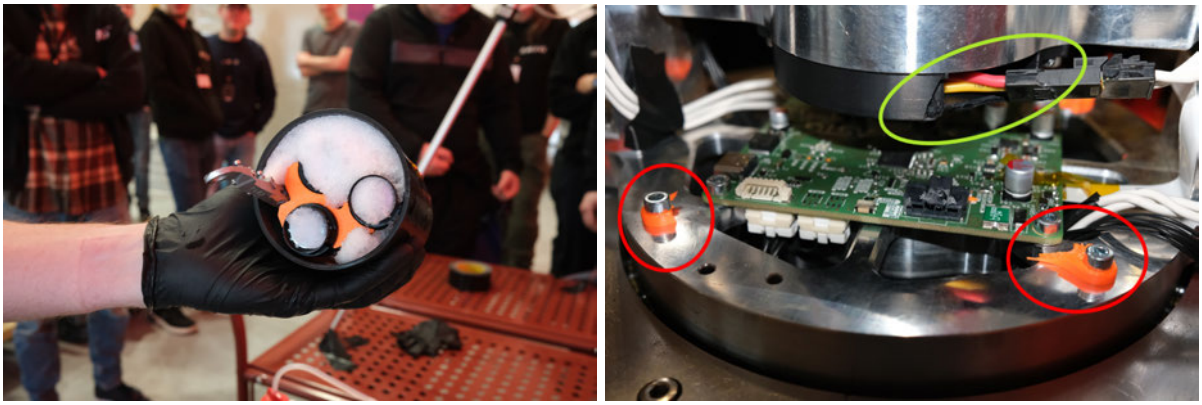


Figure 7.12: Post-flight status of the camera-can (left side) and the motor controller. The front of the camera can after recovery showed no visible damage. On the motor controller side, the 3D-Print covering the PCB (circled in red) was broken and lost (the event can be observed in the uncut engineering camera feed). Further, the 3D-Print covering the camera role motor can be seen damaged from the landing (circled in green).

damage. Multiple 3D - Printed covers were broken or missing, but those were designed as easy to replace parts. The most notable damage was that the screws connecting the camera can to the Gimbal (see Figure 7.13) were torn out. But this could be fixed by rebutting the threads, allowing for a full refurbishment of the flight model. The refurbished flight model was demonstrated moving through a pre-programmed motor path after the flight on multiple outreach occasions (See Chapter B for more information).

7.2.8 Post-flight activities

Disassembly and Packing

After the inspection the flight computer and the electronics were disassembled (Figure 7.14). This was done to access the SD cards of both the raspberry pi holding the scientific data, and the engineering camera. In addition, all electronics were quickly rinsed with Isopropyl alcohol to remove the moisture of the snow and prevent degradation. Further the pin puller was disassembled

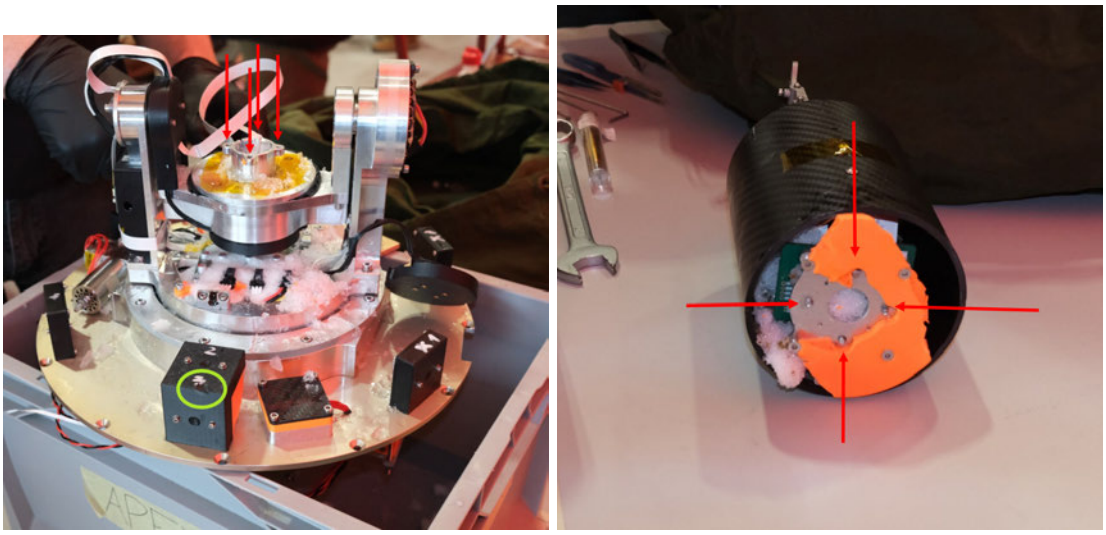


Figure 7.13: The gimbal (left) and the other side of the camera can (right) post flight. The two parts were delivered separately to the team. The four red arrows show the screws and their corresponding threads that ripped during landing. The only other damage that can be observed on the gimbal is multiple dents in the sun sensor 3D print (one is circled in green) where the Locking Arm hit them during the reentry phase (As can be observed in the engineering camera video).

to access the state of the muffler and to verify that all pyros fired properly. The inspection showed no difference to ground tests.

As the experiment was largely undamaged, packing was eased as the bulkhead with the attached gimbal and flight computer was simply packed back into its transport box. Before that, the cameras were unscrewed from the camera can and stored separately, to better shield them during transportation (Although the camera can had proven to be a very good impact protection.).

7.3 Results

Scientific Results

Following the launch, the images recorded by the science cameras were investigated for potential data. Figure 7.15 shows one of the recorded images and the corresponding pixel statistic. As can be seen, every pixel is equally saturated (i.e. has a DN of 255). This means that event sophisticated de-convolution methods are not capable to extract information from the observations. Figure 7.17 shows the only image recoded by the camera can that has distinguishable features. It was recoded by the reference camera which took the image with an exposure time of 0.1 s, at the start of an attempted stabilization. Visible is earth limb, as well as the locking arm of the gimbal.

Engineering Results

The engineering results can be largely seen as a great success. Firstly, the locking system of APEX was able to firstly restrain the payload during launch, and then unlock allowing for the free movement of the gimbal. Further, the gimbal was able to move in all axis, even after the harsh vibration environment after launch. Further, the motor-controller had control authority over the gimbal during the flight phase, demonstrated by recovering the gimbal after every failed stabilization attempt and bringing it back into the default waiting position. During the



Figure 7.14: Disassembled post flight to access electronic parts.

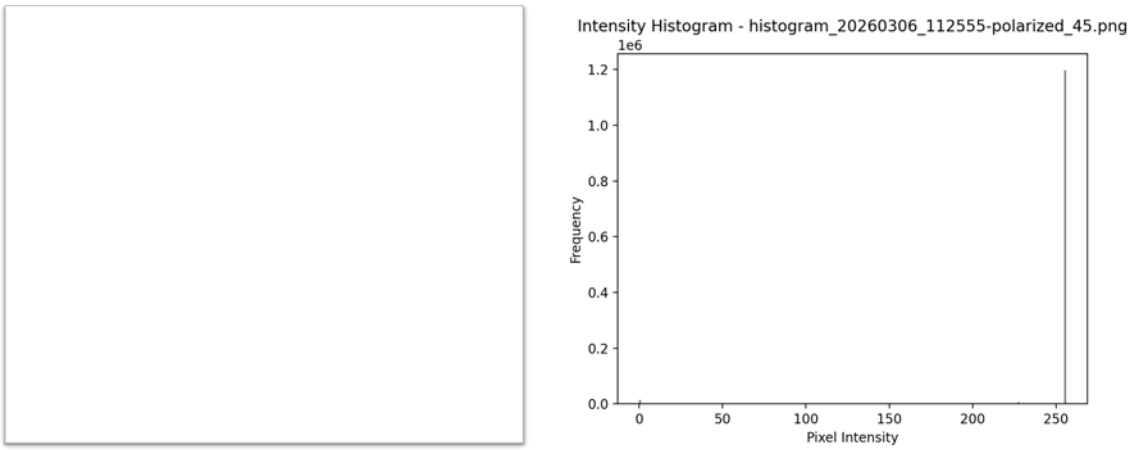


Figure 7.15: The left image shows one of the observations taken by the Science Camera, the right image shows the histogram taken from the image. As can be seen, all pixels are saturated (single peak at pixel intensntiy = 255).

attempts at stabilization the science cameras and the reference camera recorded images, which were correctly transmitted via the upper and lower cable reel and stored on the Raspberry Pi, as proven by Figure 7.17. Partial attitude was provided by the magnetometer and gyroscopes, as the cross-calibration (see Figure 7.8) shows. Unfortunately, a full attitude could not be measured due to problems with the sun sensors (see from more details). Further, due to a very limited calibration campaign, some of the technical requirements could be only qualitatively verified, not quantitatively. This qualitatively analysis was in great part only possible due to engineering camera, filming the gimbal actuation. Lastly, the sensor data (gyro, magnetometer, ...) measured was successfully handed over to the REXUS - rocket, down-linked and than recoded by the APEX ground station.



Figure 7.16: The members of team APEX during launch campaign in front of REXUS 36. (Note, the APEX payload flew with RX 35, but due to a late role-out no photos were made). Image credit: Thomas Schleuß



Figure 7.17: Image taken by the reference camera with 0.1 s exposure time. Visible is the limb of earth (lower left half) and the locking arm (right upper half). Text was added in image editing software

7.4 Input to Campaign Report

The first days of the campaign were used by team APEX to update the software of the payload, recalibrate the motor controllers and prepare the locking system including the casting of the pyrotechnic charge cups. Due to issues with the hardware, the full three days were used to bring the payload in a flight ready state. Following the preparation, the payload successful participated in the ground bench test. Known issues after the Ground testing was the loss of 4 out of the 8 sun-sensor due to electrical problems, as well as the risk of loss of data in the case of repeated uncontrolled shut-off of the raspberry pi. The first issue was accounted for in code, while the second was dealt with by the introduction of proper shutdown procedures during testing.

During the launch, video footage filmed by the onboard engineering camera showed the successful deployment of the nosecone and the unlocking of the gimbal. After unlocking, the gimbal tried to stabilize the cameras for four times. The video footage streamed down already showed the gimbal thrashing around during stabilization, paired with an unusual high tumble rate of the rocket (The earth could be seen rapidly moving through the camera frame). After each stabilization attempt, the gimbal recovered to its default position, before trying again.

Post flight analysis of the rotation rates measured by the onboard gyros showed indeed a residual role rate of 70 °/s and a tumble rate of up to 40 °/s in the other tow axis. Magnetometer data verified the measured rates. This in combination with the already compromised sun-sensor suite lead to the attitude determination not being able to correctly predict the current rotation of the rocket and correct for it. While multiple images where taken by the science cameras during the flight, no observation delivered scientific results due to overexposure of every image.

7.5 Lessons Learned

As some members of the APEX Project Team have worked for multiple years on Students Project in the ASTG, many lessons concerning Student Groups as a whole and working on a project without compensations have been learned prior to the APEX Project. This includes the possibility of delays due to miscommunication of priorities within the team or with sponsors, or just bad luck. Therefore, the following list includes both more general notions learned already in past projects and new things learned during REXUS. After this list a second list will focus on REXUS exclusive lessons learned

- Manufacturing of Metal Parts takes 4-6 Weeks after the manufacturer has the drawings AND the material
- Some manufacturers might require you to acquire material, which might add 2 weeks to the delivery time
- Manufacturing and Testing PCBs might take longer than expected. A rough estimate of 2 - 3 weeks for Manufacturing and Testing for a Complex PCB per person helping seems to be a good estimate.
- As a result, make sure you have sufficient electrical engineers capable of handling PCB production/testing.
- Be aware that inexperienced mechanical engineers might take 1 week to produce a manufacturing drawing (and 1 further to include the feedback on it).
- Let an experienced engineer check the manufacturing drawing, to avoid getting back wrongly manufactured parts.
- Check the lead time of Components, they might be at least 6 weeks.
- Check if the price of Components includes already tax or not.
- Assume a delivery fee of up to 50 € for many components below half a kilo of weight.
- Always check if you can get a component sponsored. It takes you 20 min to write the mail. You might get surprised.
- Writing a report takes at least 2 weeks.
- People rarely finish a report before an internal deadline. It is still good to have an internal deadline though.
- Hold internal Reviews to review Hardware. (Independent of if there exist external Reviews). Your peers will find the errors you have not seen better than many experts, and will not shy away from parading you for them.
- Use the resources you have. Especially, ask people with expert knowledge.
- Test as you fly, fly as you test. If you just did not test something this day because it worked all the time before, it WILL NOT work.
- Have Checklists for everything. Spare Parts, Setup Procedures, Abort Situations. If necessary, have a checklist for checklists.
- Have de-scoping options in mind, so that you know which things are necessary and which are nice to have.
- Make sure to keep meetings as short as possible while as long as necessary. If possible, shift in detail discussion after a meeting in small groups.

- BUT, make sure these follow up meetings take place. I.e. make sure the planned participants already agree in the large group meeting on at least a rough time slot.

REXUS-specific:

- Create your SED in Overleaf. This allows multiple people to work on it at the same time
- It is smart to use Python programs to translate EXCEL table to Latex. This allows to have more information in a single EXCEL table than any table in the SED needs on its own (e.g. the Requirements and their verifications). Further, calling updating only the EXCEL sheet and than using the Python program to create the output avoids problems with synchronization of information in different tables of the SED.
- Try to find problems in your design prior to a review. Ask the expert jury for anything that might bother them. This might give you a day to find the prove that you can solve this problem (Or there is actually no Problem at all).
- Have a prototype prior to CDR. The time between CDR and IPR (2 months) is to short for much to do.
- When creating a GANT Chart/ Timeline, focus on the important Deadlines and critical paths more than on small details.
- Consequently, an Excel sheet with all important parts can already be a great GANTT chart, especially for yourself.
- When creating a GANTT Chart, be aware that nearly everything will slip except the critical paths (As you can not allow them to slip).
- Communicate your science goals multiple times throughout the program, so that everyone is on the same page
- Check your science goals at least twice after defining them (at CDR and at IPR). There might be stuff not fully formulated you did not know as important back than that suddenly is very problematic.
- Ensure to have a framework to test your software prior to full hardware development, as this can be delayed (and your programmers cannot work otherwise)

REXUS Launch Campaign-specific:

- Realize that you have only 2 days to finish all experiment preparation on the campaign before the bench tests: Design your experiment accordingly. This includes
  - All Ports to update software or Debug electronics are placed in a way to be accessible by removing at most a single panel.
  - Be especially careful with 3D Printed covers with inserts used as Covers => after they have been locked down with screwglue, the insert might loosen when you try to unscrew them.



Figure 7.18: Overall conclusion of the mission

List of Figures

1.1 Auroral Oval (Kp 3) . . . 3
1.2 Aurora Volume Emission Rates . . . 4
1.3 Airglow Volume Emission Rates . . . 5
1.4 Observation Simulation . . . 6
1.5 Observation Simulation binned . . . 6
1.6 Image of the polarization camera . . . 8
1.7 Pixel Array Scheme . . . 8

3.1 Work Breakdown Structure . . . 15
3.2 Gimbal WBS . . . 16
3.3 Ground testing Equipment WBS . . . 17
3.4 Project Management WBS . . . 18
3.5 Testing WBS . . . 19
3.6 Outreach WBS . . . 20
3.7 Reduced GANTT chart . . . 21
3.8 GANTT for Gimbal Part 1 . . . 22
3.9 GANTT for Gimbal Part 2 . . . 23
3.10 GANTT for Gimbal Part 2 . . . 24
3.11 GANTT for GSE . . . 24
3.12 GANTT for Tests Avionics . . . 25
3.13 GANTT for Tests Optical System . . . 25
3.14 GANTT for Test without Optical System . . . 25
3.15 GANTT for Test with full System . . . 26
3.16 Time Resource Diagram . . . 27
3.17 Risk Matrix . . . 31

4.1 First manufactured parts of the Gimbal . . . 34
4.3 Camera Assembly labeled . . . 36
4.2 Block Diagram Camera Assembly . . . 37
4.4 Block Diagram Gimbal Stage 1 . . . 37

4.5 Gimbal Stage 1 labeled . . . 38
4.6 Block Diagram Gimbal Stage 2 . . . 38
4.7 Gimbal Base labeled . . . 39
4.8 Block Diagram Gimbal Electronics 1 . . . 39
4.9 Gimbal electronics labeled . . . 40
4.10 Block Diagram Gimbal Electronics . . . 41
4.11 Avionics box labeled . . . 42
4.12 Interface . . . 43
4.13 Components . . . 47
4.14 Rendering of the camera mounting . . . 49
4.15 Locking mechanism components . . . 50
4.16 Gimbal in re-locked position . . . 51
4.17 Pin puller components . . . 51
4.18 Current Design . . . 52
4.19 Current Concept Cross-section . . . 53
4.20 Deformation of the effected parts . . . 54
4.21 Fix points of the ”locked” state for the FEM Analysis . . . 55
4.22 SINE Vibration . . . 57
4.23 Random Vibrations . . . 59
4.24 Random Vibrations . . . 60
4.25 Backplane PCB Front and Backside . . . 61
4.26 Flight Computer PCB Front and Backside . . . 62
4.27 IMU Sensor PCB Front and Backside . . . 63
4.28 Blackbox PCB Front and Backside . . . 63
4.29 Blackbox . . . 64
4.30 Mounting of Sun Sensors . . . 65
4.31 Sun Sensor PCB Front and Backside . . . 65
4.32 Sun Sensor Pinhole Cover PCB Front and Backside . . . 66
4.33 Sun Sensor Mounting Single Front Side . . . 66
4.34 Sun Sensor Mounting Single Back Side . . . 67
4.35 Sun Sensor Mounting Double . . . 67
4.36 Magnetometer PCB Front and Backside . . . 68
4.37 Magnetometer mounting . . . 68
4.38 Motor Driver PCB Front and Backside . . . 69

4.39 Recommended mounting. Crosscut of AS5048 and Magnet. 69
4.40 Cubemars RI60 Inrunner Motor 70
4.41 Raspberry Pi Compute Module 5 Front and Backside 71
4.42 Raspberry Adapter PCB Front and Backside 71
4.43 GigaBlox Nano Ethernet Switch 72
4.44 Ethernet Switch Adapter PCB Front and Backside 72
4.45 Ethernet Switch and Adapter Mounting 73
4.46 Engineering Camera Mounting Runcam Split 4 with Enclosure and TV-Channel Connector 74
4.47 Image: Sun-sensor and Engineering Camera 75
4.48 Battery in assembled and explosion view 76
4.49 Circuit for Radio Silence with two MOSFETs 76
4.50 Coiled and folded FFC cable 77
4.51 3D printed support structure for Cable Loop. The hardware implementation can be seen in Figure 4.47 on the gimbal in the background. 78
4.52 Motor and Motor driver PCB cover 79
4.53 Aluminum housing of the Flight Computer 79
4.54 AVI Stack image 80
4.55 Heat source of camera 82
4.56 Outer surfaces for thermal radiation 83
4.57 Surfaces where sun shines onto 84
4.58 Thermal Simulation Results 85
4.59 Thermal simulation aluminium 86
4.60 State Machine 88
4.61 State Machine 89
4.62 State Machine 90
4.63 Raspberry Pi 92
4.64 93

7.1 Replacement 3D Sun Sensor Cover 135
7.2 Launch Impressions 138
7.3 NOAA Space Weather scale for Tuesday, 10th March 139
7.4 Auroral and Airglow observation simulation 139
7.5 Observation Simulations, binned 140
7.6 Gyro rates of experiment phase 141
7.7 Magnetic field measured in the rocket body frame 142

7.8 Magnetic field rotated to an earth fixed frame 143
7.9 Observed sun vectors 144
7.10 Observed sun vectors 2 144
7.11 APEX after Flight 146
7.12 Post-flight Camera-Can and Motor Controller 146
7.13 Post-flight Gimbal 147
7.14 Disassembled Experiment 148
7.15 Science Camera Observation 149
7.16 APEX with RX36 150
7.17 APEX Refcam Image 150
7.18 APEX Great Success 154

List of Tables

3.1 Hours per Month 27
3.2 Project Budget Breakdown 29
3.3 APEX Social Media Links 30

4.1 Mass Budget 36
4.2 The RXSM D-SUB connector pin configuration 43
4.3 Experiment mass and volume 44
4.4 Parts List Camera Housing 44
4.5 Parts List Gimbal Structure 45
4.6 Parts List Gimbal Electronics 46
4.7 Natural frequencies of the eigenmodes. 55
4.8 Vibration Test Parameters 56
4.9 Random Vibration, Table 10-2 from the RX-UserManual-v7 58
4.10 Motor Specification 70
4.11 Operating Temperature Ranges of Components 81
4.12 Power Consumption 87

5.1 Verification Matrix for Functional Requirements 99
5.3 Verification Matrix for Performance Requirements 100
5.5 Verification Matrix for Operational Requirements 103
5.7 Verification Matrix for Design Requirements 104
5.9 Verification Matrix for Constraints 112

6.1 Experiment mass and volume 128
6.2 Electrical interfaces 129
6.3 Launch site requirements 129
6.4 Flight Requirements 130
6.5 Objective fulfillment 2026-03-20 131
6.6 Flight Requirements on events 131
6.7 Countdown Timeline 133

7.1 Camera Gains sent to mission control dependent on launch time. 140

Acronyms

ADS Attitude Determination System.

APEX Auroral Polarization EXplorer.

ASIC Application-specific Integrated Circuit.

ASTG Aerospace Team Graz.

BEXUS Balloon EXperiments for University Students.

BLDC Brushless DC.

CAN Controller Area Network.

CDR Critical Design Review.

CMOS Complementary metal oxide semiconductor.

COG Centre of Gravity.

COTS Commercial-off-the-shelf.

DLR Deutsches Zentrum für Luft- und Raumfahrt.

EAR Experiment Acceptance Review.

ESA European Space Agency.

Esrange Esrange Space Center.

EuRoC European Rocketry Challenge.

EUV Extreme Ultraviolet.

FC Flight Computer.

FFC Flet Flax Cable.

FFG National Funding Agency Austria (Forschungs Förderungs Gesellschaft).

FOC Field Oriented Control.

FPC Flexible Printed Circuit Board.

FWHM full width at half maximum.

HAT Hardware Attached on Top.

IMU Inertial Measurement Unit.

IPR Integration Progress Review.

ITW Integration and Testing Week.

IWF Space Research Institute.

Kp planetary K index.

LO Lift Off.

LOS Line-of-sight.

MORABA Mobile Raketen Basis.

PCB Printed Circuit Board.

PCIe Peripheral Component Interconnect Express.

PDR Preliminary Design Review.

REXUS Rocket EXperiments for University Students.

RXSM REXUS Service Module.

SNSA Swedish National Space Agency.

SODS Start Of Data Storage.

SOE Start Of Experiment.

SPECTRE SPacE proof of Composite Tape-springs boom on REXUS Experiment.

SPI Serial Peripheral Interface.

SSC Swedish Space Corporation.

TU Graz University of Technology Graz.

UTC Coordinated Universal Time.

UV Ultraviolet.

WBS Work Breakdown Structure.

ZARM Zentrums für angewandte Raumfahrttechnologie und Mikrogravitation.

Glossary

blackbox Hardened data storage device designed to survive ballistic impacts.

flight computer main core The CM7 core of the STM32 used on the experiment,.

flight computer sensor core The CM4 core of the STM32 used on the experiment for reading sensor data and calculating its kalman filter,.

Mission Control Facility to manage launch and test operations.

motor driver The system responsible to control the motors present in the gimbal,.

raspberry pi The unit processing data generated by the cameras,.

REXUS/BEXUS Program allowing students from European universities to carry out experiments on research rockets and balloons.

Stokes parameters Set of 4 parameters, describing the polarization state of light.

thermosphere Layer of the atmosphere with a positive temperature gradient, between 80 km-600 km altitude.

References

[1] J. Lilensten et al., "Polarization in aurorae: A new dimension for space environments studies," *Geophysical Research Letters*, vol. 35, no. 8, 2008. DOI: https://doi.org/10.1029/2007GL033006 [Online]. Available: https://agupubs.onlinelibrary.wiley.com/doi/abs/10.1029/2007GL033006

[2] Lilensten Jean et al., "The thermospheric auroral red line polarization: confirmation of detection and first quantitative analysis," *J. Space Weather Space Clim.*, vol. 3, A01, 2013. DOI: 10.1051/swsc/2012023 [Online]. Available: https://doi.org/10.1051/swsc/2012023

[3] Lilensten Jean et al., "The auroral red line polarisation: modelling and measurements," *J. Space Weather Space Clim.*, vol. 5, A26, 2015. DOI: 10.1051/swsc/2015027 [Online]. Available: https://doi.org/10.1051/swsc/2015027

[4] Bosse Léo et al., "The polarisation of auroral emissions: A tracer of the E region ionospheric currents," *J. Space Weather Space Clim.*, vol. 12, p. 17, 2022. DOI: 10.1051/swsc/2022014 [Online]. Available: https://doi.org/10.1051/swsc/2022014

[5] S. Bourgeois et al., "Laboratory Experiments Confirm the Polarization of Auroral Emissions," *Geophysical Research Letters*, vol. 49, no. 13, e2022GL098707, 2022. DOI: https://doi.org/10.1029/2022GL098707 [Online]. Available: https://agupubs.onlinelibrary.wiley.com/doi/abs/10.1029/2022GL098707

[6] V. Bommier, S. Sahal-Bréchot, J. Dubau, and M. Cornille, "The theoretical impact polarization of the O I 6300 Å red line of Earth aurorae," *Annales Geophysicae*, vol. 29, no. 1, pp. 71–79, Jan. 2011, ISSN: 1432-0576. DOI: 10.5194/angeo-29-71-2011

[7] J. Lilensten, C. Simon-Wedlund, M. Barthélémy, J. Moen, R. Thissen, and D. A. Lorentzen, "Considering the polarization of the oxygen thermospheric red line for space weather studies," *Space Weather*, vol. 4, no. 11, 2006. DOI: https://doi.org/10.1029/2006SW000228 [Online]. Available: https://agupubs.onlinelibrary.wiley.com/doi/abs/10.1029/2006SW000228

[8] L. Bosse et al., "At the source of the polarisation of auroral emissions: experiments and modeling," *Journal of Space Weather and Space Climate*, vol. 12, p. 7, Apr. 2022, ISSN: 2115-7251. DOI: 10.1051/swsc/2022004

[9] Y. Zhang and L. Paxton, "An empirical Kp-dependent global auroral model based on TIMED/GUVI FUV data," *Journal of Atmospheric and Solar-Terrestrial Physics*, vol. 70, no. 8-9, pp. 1231–1242, Jun. 2008, ISSN: 13646826. DOI: 10.1016/j.jastp.2008.03.008

[10] T. Sergienko and V. Ivanov, "A new approach to calculate the excitation of atmospheric gases by auroral electrons," *Annales Geophysicae*, vol. 11, pp. 717–727, Apr. 1993.

[11] C. Simon-Wedlund, H. Lamy, B. Gustavsson, T. Sergienko, and U. Brändström, "Estimating energy spectra of electron precipitation above auroral arcs from ground-based observations with radar and optics," *Journal of Geophysical Research: Space Physics*, vol. 118, no. 6, pp. 3672–3691, Jun. 2013, ISSN: 2169-9380. DOI: 10.1002/jgra.50347

[12] O. Witasse, J. Lilensten, C. Lathuillère, and P.-L. Blelly, "Modeling the OI 630.0 and 557.7 nm thermospheric dayglow during EISCAT-WINDII coordinated measurements," *Journal of Geophysical Research: Space Physics*, vol. 104, no. A11, pp. 24 639–24 655, 1999. DOI: https://doi.org/10.1029/1999JA900260 [Online]. Available: https://agupubs.onlinelibrary.wiley.com/doi/abs/10.1029/1999JA900260

[13] B. J. Harding et al., "The MIGHTI Wind Retrieval Algorithm: Description and Verification," *Space Science Reviews*, vol. 212, no. 1-2, pp. 585–600, Oct. 2017, ISSN: 0038-6308. DOI: 10.1007/s11214-017-0359-3

[14] Y. Huang, J. J. Makela, and G. R. Swenson, "Simulations of imaging Fabry–Perot interferometers for measuring upper-atmospheric temperatures and winds," *Applied Optics*, vol. 51, no. 17, p. 3787, Jun. 2012, ISSN: 1559-128X. DOI: 10.1364/AO.51.003787

[15] M. D. Shuster and S.D. Oh, "Three-Axis Attitude Determination from Vector Observations," English, *Journal of Guidance and Control*, vol. 4, Jan. 1981.

[16] F. J. Arch, *Attitude determination algorithms and modelling for small satellite platforms*, Graz, Nov. 2025. DOI: 10.3217/djbp7-ejw48

Appendix A: Experiment Reviews

Appendix B: Outreach and Media Coverage

Table B.0.1: APEX Social Media Links

Website	`https://astg.at/projects/apex`
Instagram	`https://www.instagram.com/aerospaceteamgrazofficial/`
LinkedIn	`https://www.linkedin.com/company/aerospace-team-graz`
YouTube	`https://www.youtube.com/@aerospaceteamgraz4009`

B.1 APEX Video Series Part 1

In June 2024 the first part of a theoretical 5-part long short-video series explaining the science behind APEX was produced and posted on the ASTG YouTube and Instagram channels.

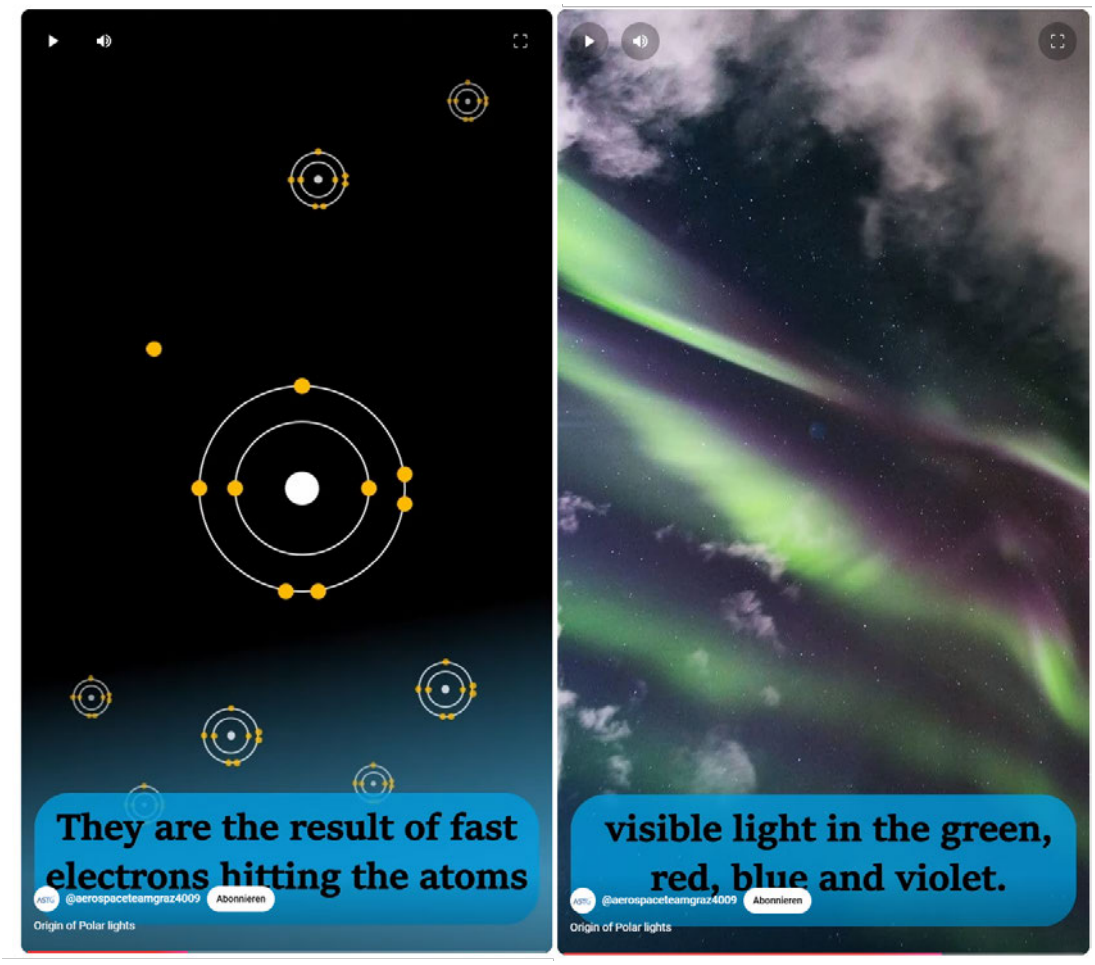


Figure B.1.1: Screen shot of the APEX Video Series Part 1 to be found under https://www.youtube.com/shorts/TAScfFPIxUw.

B.2 Flyer

The APEX project is included on the ASTG's flyer, last updated in May 2024. This can be seen in Figure B.2.2. Note that the last update was prior to the acceptance of APEX into the REXUS/BEXUS program, hence why SNSA, DLR and ESA are not listed as sponsors.





Figure B.2.2: ASTG Flyer from May 2024

B.3 Logo

The Team has designed a logo for the APEX project for use in internal as well as public presentations, to be printed on APEX Merchandise and to be printed as stickers. The Merchandise is for members only, whereas the stickers are also publicly distributed. The logo can be seen in Figure B.3.3.



Figure B.3.3: The APEX Logo

B.4 Newsletter

The APEX Project is covered in our monthly Newsletter, which, as of May 2025, has 249 recipients. The demographic mostly consists of our partners in the industry and (former) members. An example text can be seen in Figure B.4.4.

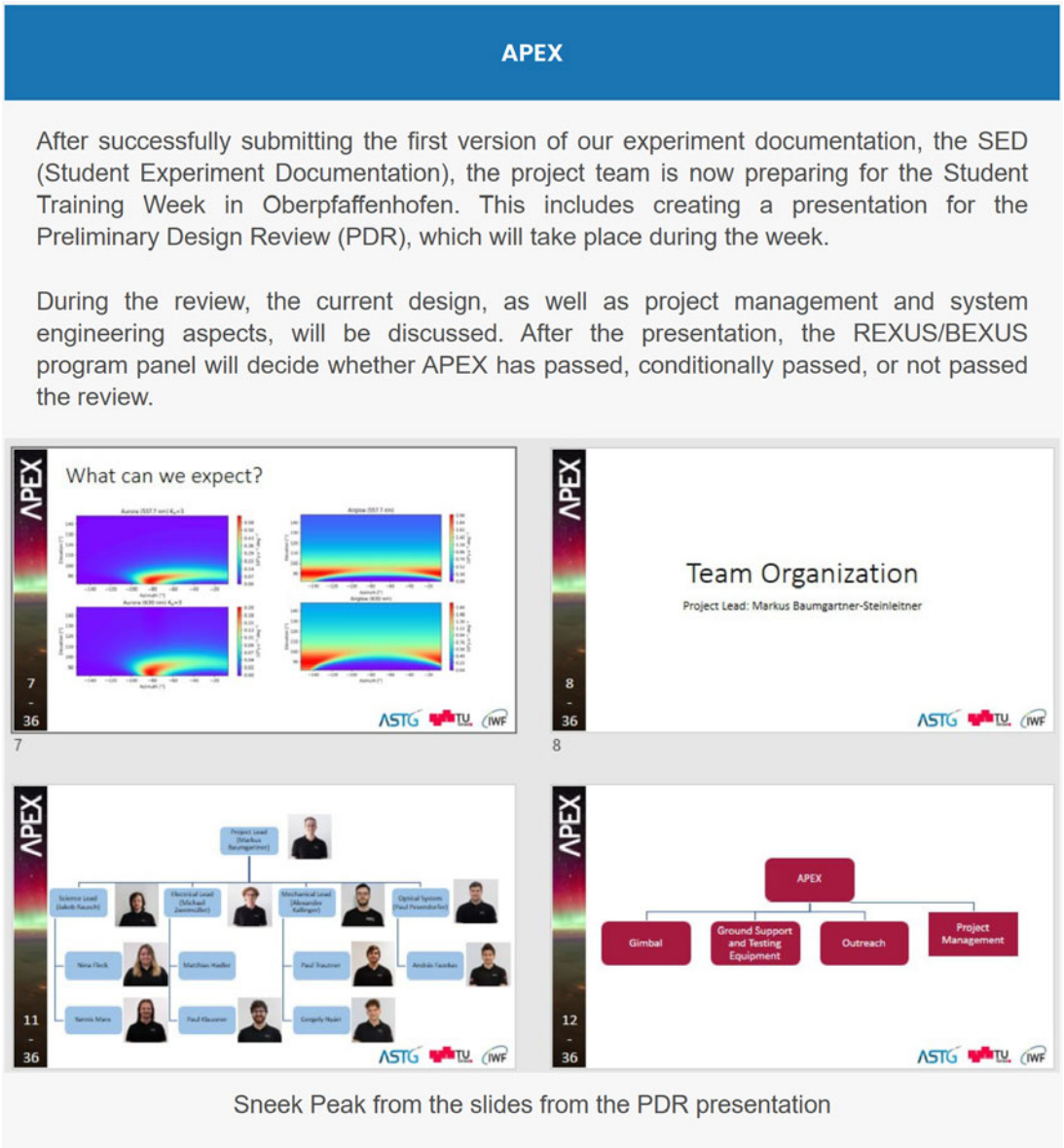


Figure B.4.4: Excerpt of the Newsletter from February 2025

B.5 Text on the TU-Graz Website

The ASTG is also featured on the Website of TU Graz.



Figure B.5.5: https://www.tugraz.at/studium/studieren-an-der-tu-graz/studierende/studieren-denteams/wettbewerbs-und-fokusteams/aerospace-team-graz.

B.6 Motion Expo Graz 2025

ASTG was present at the Motion Expo in the exhibition center Graz from March 13th to 15th. Members were present to inform about our projects, including APEX. APEX also features a paragraph on the large Poster as seen in the Background of Figure B.6.6. The Event attracted an estimated 21000 visitors in total.



Figure B.6.6: ASTG's exhibition at Motion Expo Graz 2025

B.7 Article in Krone

The ASTG was featured in an article by "Kronenzeitung", a well-known newspaper in Austria, on May 6th 2025. A paragraph of the article talks about APEX and also names SNSA,DLR and ESA.

https://www.krone.at/3769942

B.8 Recruitment Presentations

In the process of ASTG's semiannual recruitment process, we hold numerous presentations during university lectures in two different universities in Graz. In the last recruitment phase in October, around ten in-lecture presentations were held. Every presentation includes at least one slide about APEX, however an emphasis is placed on one of the projects depending on the subject matter.

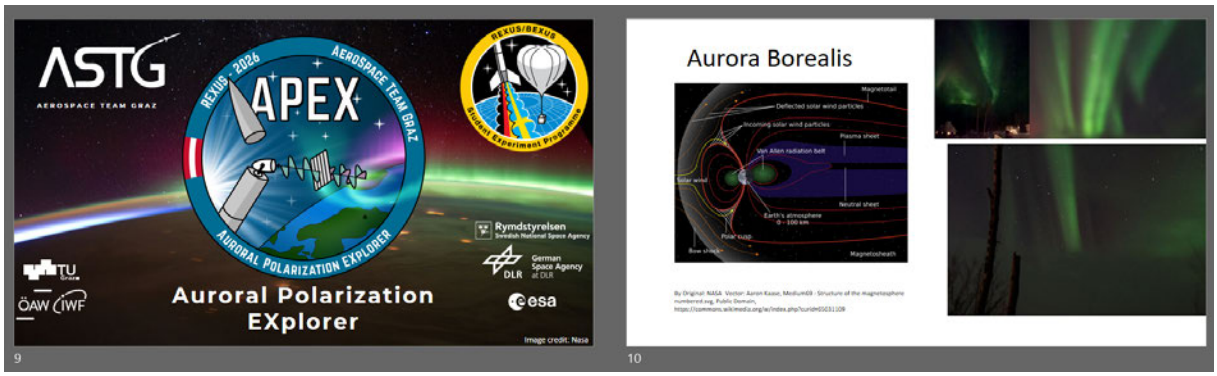


Figure B.8.7: One of the Presentation Slides showing APEX

B.9 Space Week St. Paul

In February 2024, the Carinthian town of St. Paul played host to an event named "Space Week", which mostly served to educate students in the region on recent developments in the space sector, but also other STEM topics. ASTG was represented by a small group. A short introduction presentation was held in front of local press and officials. A total of twelve presentations were held in front of students in two different schools in the region.

B.10 Unite! Network

In early April, ASTG was visited by two fellow student teams - WARR from Munich and SPECTRE from Stockholm. Team SPECTREs visit was part of an exchange program that was supported by the Unite! network. We showed our guests around our workshop and office. All the teams held presentations about their projects. Team SPECTRE talked about their experiences in the REXUS program. All this facilitated talks and discussions between the teams about their experiments with rocketry. The visits were concluded by a dinner (Figure B.10.8) where discussions naturally continued.

To further promote the visit, the staff of Unite! network at the TU-Graz cut a short video clip of the workshop day. The video was posted on Instagram under https://www.instagram.com/p/DKZWgMwNzxE/. Further, the Video was posted on YouTube in an extended Version including end cards acknowledging the agency. (Note: These end cards were also meant to be part of the Instagram video. Unfortunately, it was posted by the Unite! Staff, before we could give feedback, although it was agreed upon.)



Figure B.10.8: Teams SPECTRE, WARR and ASTG at dinner for unite! meetup

B.11 Article about APEX on the Webpage of the IWF (Space Research Center Austria)

To promote the cooperation of the ASTG and the IWF in the REXUS/BEXUS program, an article was included on the website of the IWF in the young researcher section. It lists the main goals of the APEX - Projects. Link: `https://www.oeaw.ac.at/iwf/forschung/nachwuchsprogramm/yrp-astg`

B.12 Exhibitor at Graz in Space 2025

Graz in Space took place on October 4th and 5th at the IWF - Graz (Graz Space Science Research Center). During the two days, over 15 different lectures on the advances of the IWF were presented to an audience from the general Public. The Aerospace Team Graz participated as an exhibitor, showing one of our rockets as well as hardware of the APEX Program, combined with a Poster explaining the APEX Mission (Figure B.12.10

B.13 APEX Experiment and Post Flight presentation

In order to present the result of the launch champaign, the APEX team hosted a ”APEX Experiment and Post Flight presentation” at the Institute for Space science (IWF) in Graz. Invited were supporters and sponsors as well as members and Alumni of the Aerospace Team Graz (see Figure B.13.11). The goal of the presentation was, beside showing the successes of the past two years to motivate a new team of students to participate in REXUS/BEXUS.

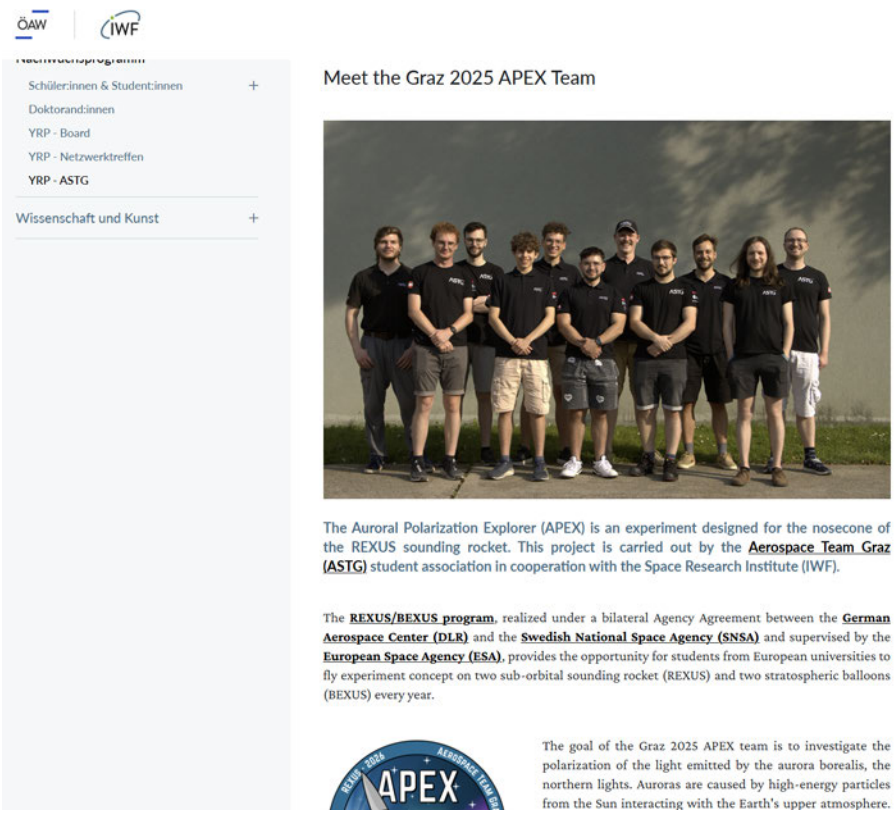


Figure B.11.9: Screenshot of the IWF Website

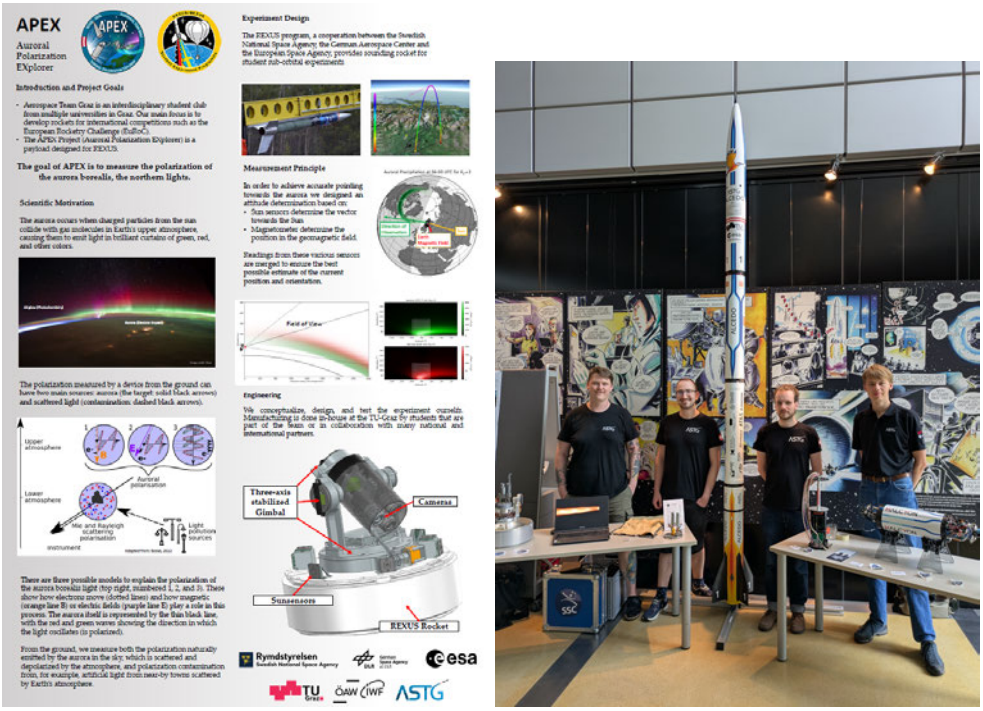


Figure B.12.10: Left: Poster presented at Graz in Space describing the APEX Mission. Right: The presenters from both APEX-Project and the Ispida Rocket Project.



Figure B.13.11: APEX Experiment and Post Flight presentation

B.14 Yuri's night 2026

On April 12, 1961, cosmonaut Yuri Gagarin became the first person to fly into space. This event is celebrated around the world every year. In Austria, the Artemis Association was hosting "Yuri's Night" at the Vienna Planetarium on April 12, 2026. The ASTG APEX team was there showing off our flight hardware.

B.15 APEX Launch Video

Shortly after its debut in the "APEX Experiment and Post Flight presentation" a supercut Video of the APEX engineering camera with the parachute camera of the REXUS rocket (provided by MORABA) was published on Youtube (`https://www.youtube.com/watch?v=0MmMdWRgxWo&t=4s`). The video was further promoted on Instagram. Figure B.15.13 shows a screenshot from the Video, further screenshots can be found in Section 7.3.

B.16 Lange Nacht der Forschung (Austrian long night of Sciences) 2026

As the years before, the Aerospace Team Graz presented at the Austrians long night of science hold biyearly. Over the duration of 6 hours members presented the projects of the ASTG, the rocket projects and the REXUS project APEX to hundreds of visitors of all ages. Presented was among other the refurbished flight model of APEX, which was programmed to follow a pre-programmed path. Figure B.16.14 shows the presenting team as well as the exhibits from the ASTG, APEX can be seen to the left of the image.

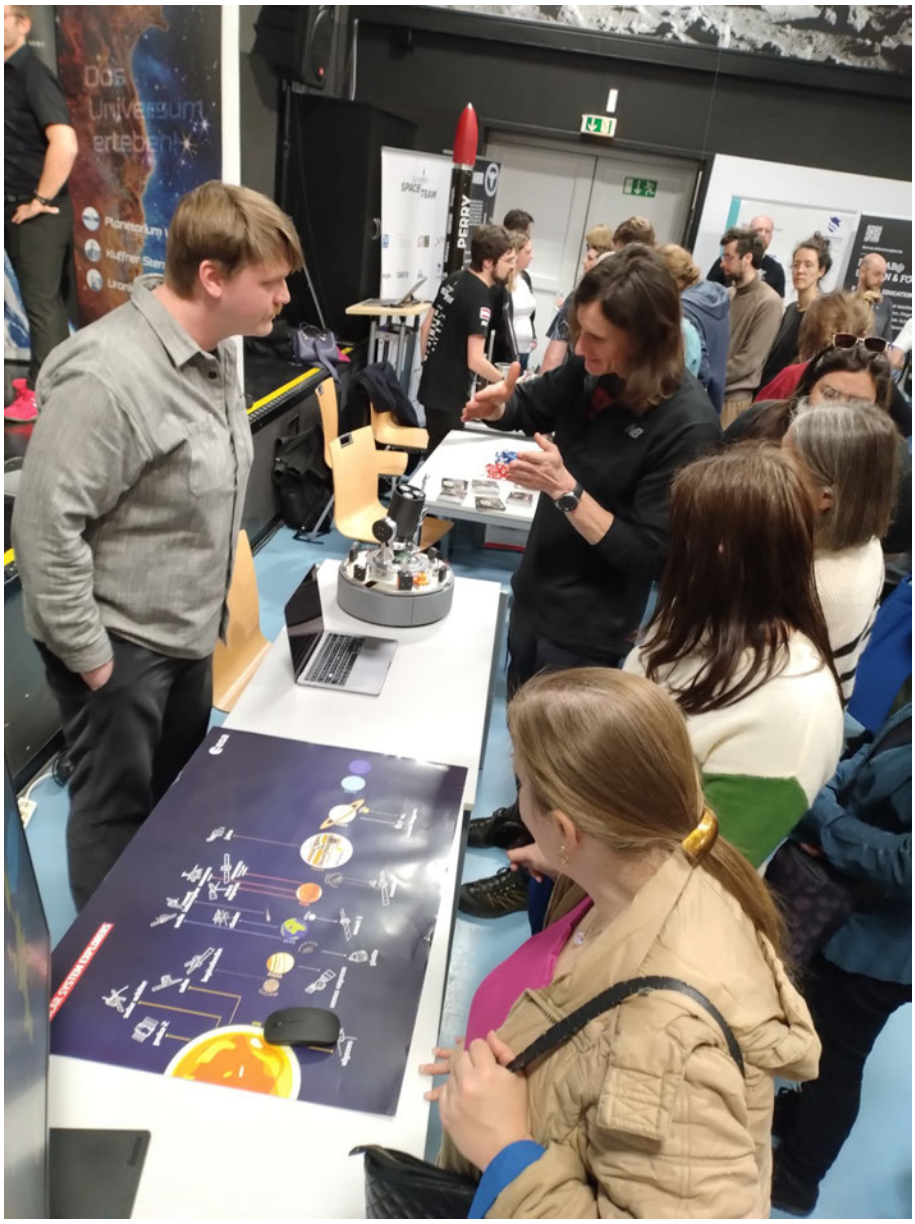


Figure B.14.12: APEX at Yuri's night

B.17 27th ESA Symposium on European Rockets and Balloons in Trondheim, Norway

As crowning last Public Outreach event (at least within the time frame of the last version of the SED) four members of APEX participated in the *27th ESA Symposium on European Rockets and Balloons in Trondheim, Norway*. The members participated with two talk and two posters, outlining the mission, the science behind, the technical implementation and the mission results. The Abstract book can be found under `https://custom-eur.cvent.com/559ED04F91884F02A58E7EF44ABF0E8B/files/2a0fe8ac6a5d441e8d765ccaedb4958e.pdf`. Figure B.17.15 shows the members during their presentations (Poster presenters had to present as part of a PICO pitch).

- Presentation by Markus Baumgartner-Steinleinter:

  THE AURORAL POLARIZATION EXPLORER (APEX), A REXUS 35 MISSION TO

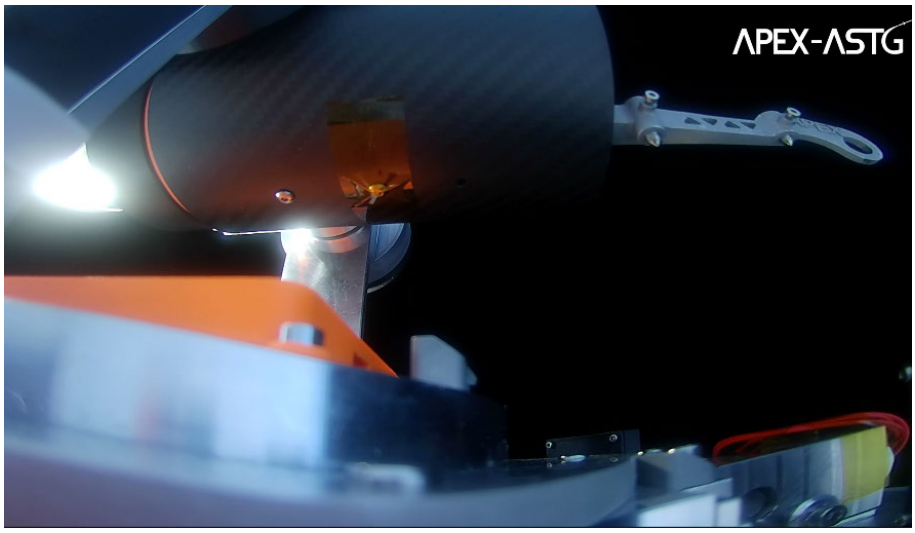


Figure B.15.13: APEX supercut Video

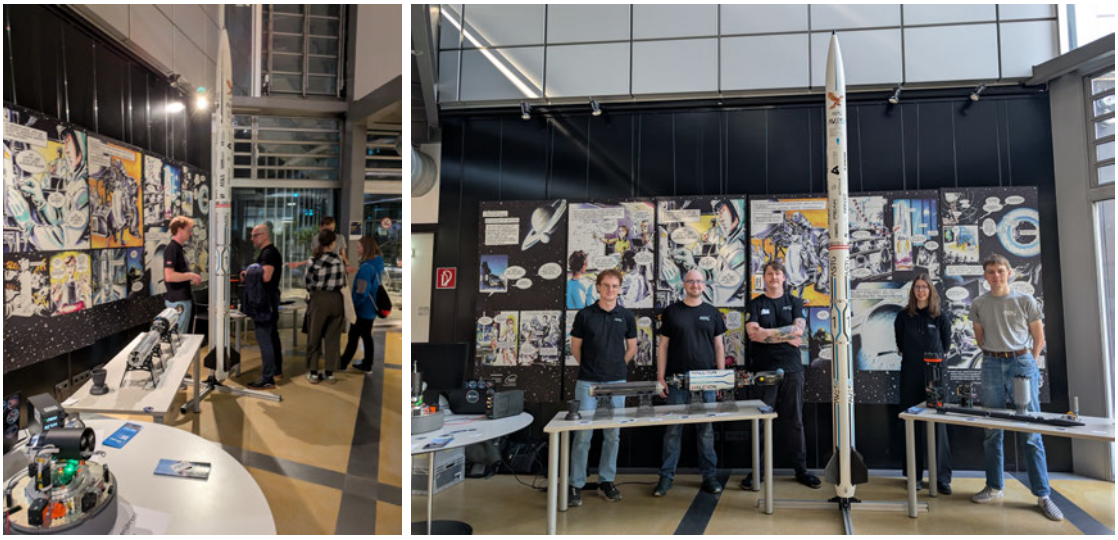


Figure B.16.14: APEX as part of the ASTG both at the Austrian long night of Sciences 2026.



Figure B.17.15: Members of APEX presenting at ESA Symposium

STUDY THE POLARIZATION OF THE AURORA BOREALIS

- Presentation by Georg Blüthner:

  POLARIMETRIC MEASUREMENTS OF AURORAL EMISSIONS, AT AURORAL HEIGHTS

- Poster by Jakob Rausch:

  AIRGLOW VARIABILITY AS SEEN BY MATS IN PREPARATION FOR THE REXUS EXPERIMENT APEX

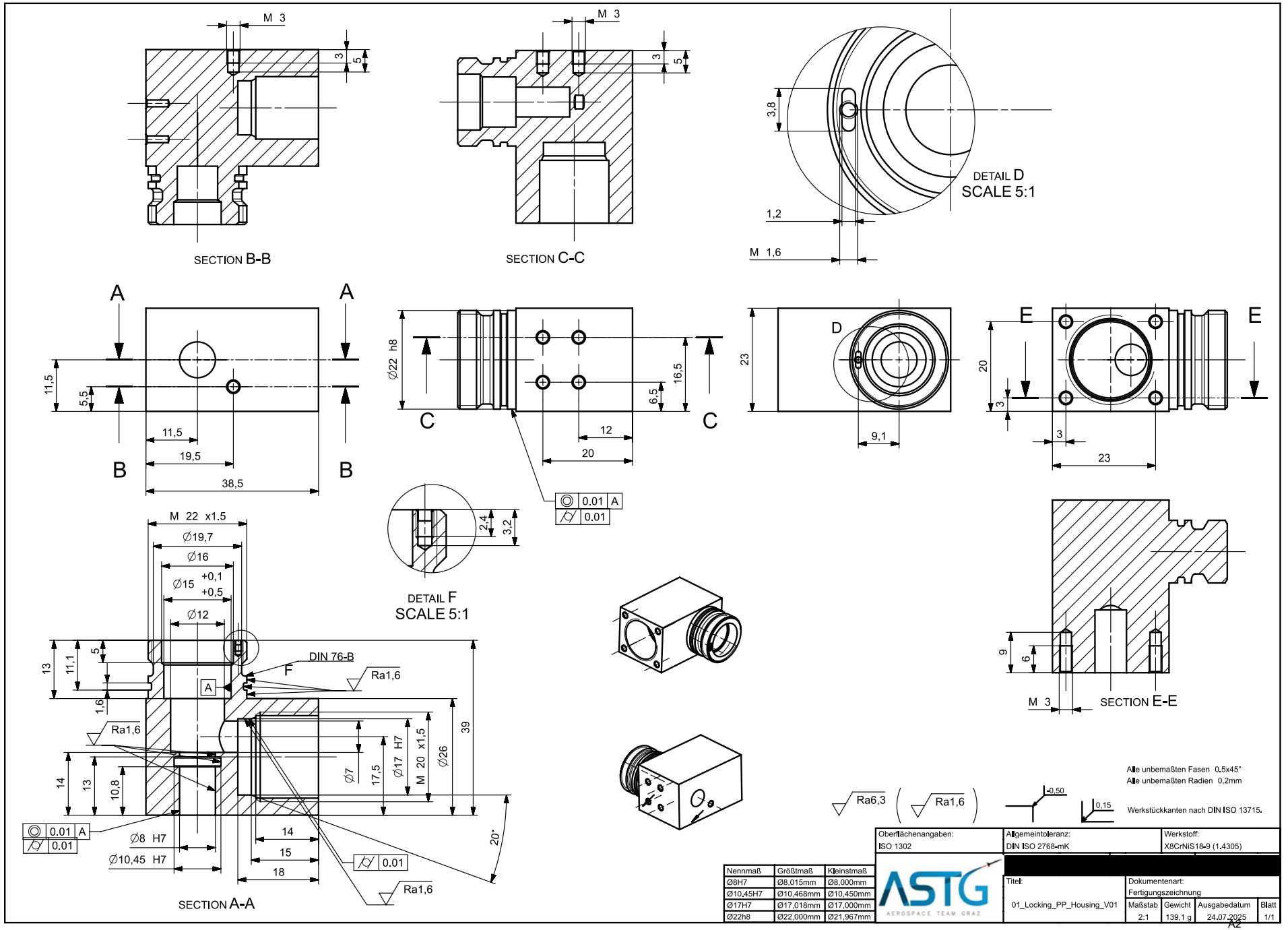
- Poster by Michael Zweimüller:

  THE ENGINEERING OF THE AURORAL POLARIZATION EXPLORER (APEX), A REXUS 35 MISSION

Appendix C: Additional Technical Information

C.1 Detailed Structural and Mechanical Calculations

C.2 Engineering Drawings



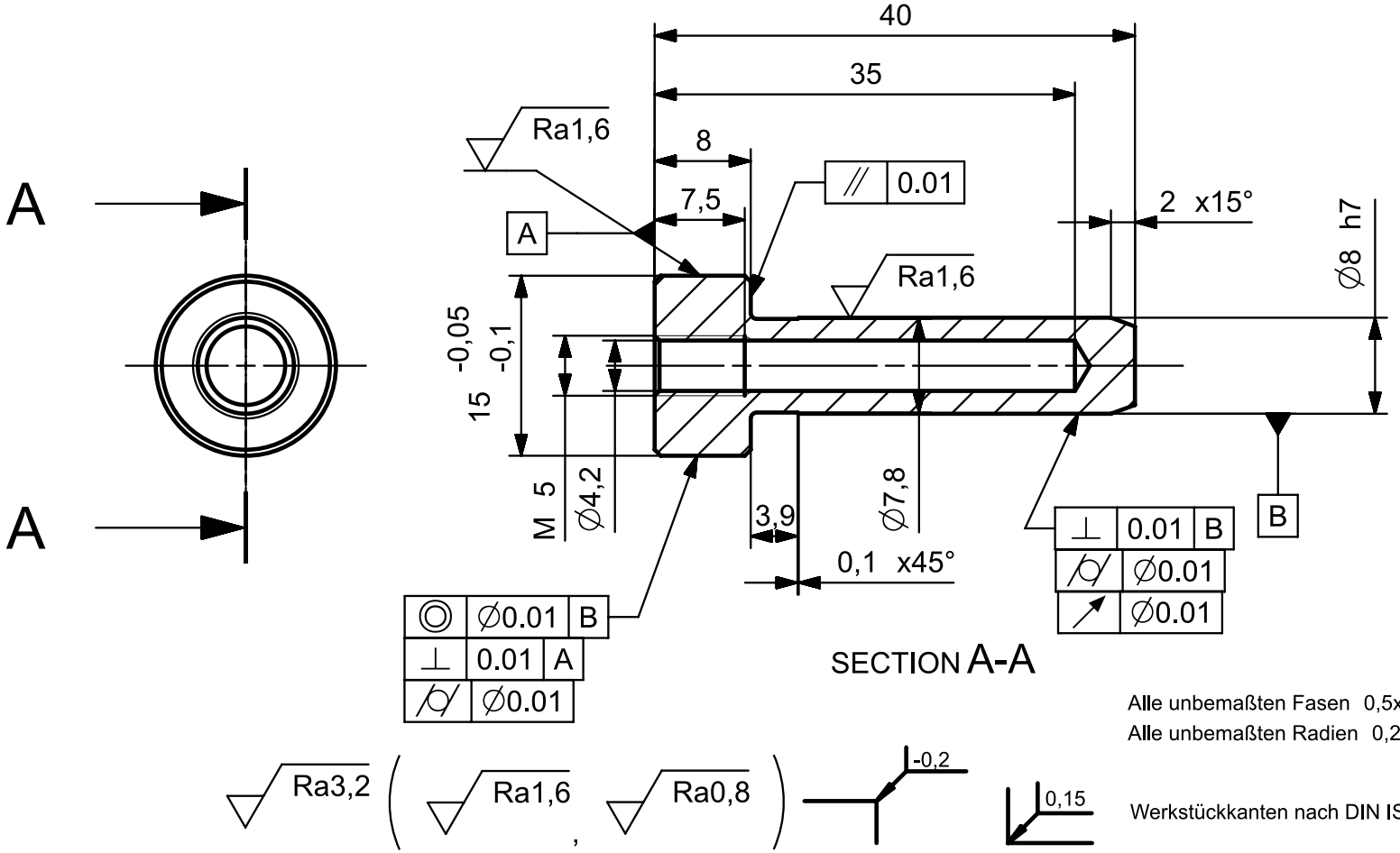
Nennmaß	Größtmaß	Kleinstmaß
Ø8H7	Ø8,015mm	Ø8,000mm
Ø10,45H7	Ø10,468mm	Ø10,450mm
Ø17H7	Ø17,018mm	Ø17,000mm
Ø22h8	Ø22,000mm	Ø21,967mm

Oberflächenangaben:	Allgemeintoleranz:	Werkstoff:
ISO 1302	DIN ISO 2768-mK	X8CrNiS18-9 (1.4305)

ASTG AEROSPACE TEAM GRAZ

Titel:	Dokumentenart:			
01_Locking_PP_Housing_V01	Fertigungszeichnung			
	Maßstab	Gewicht	Ausgabedatum	Blatt
	2:1	139,1 g	24.07.2025	1/1

A2



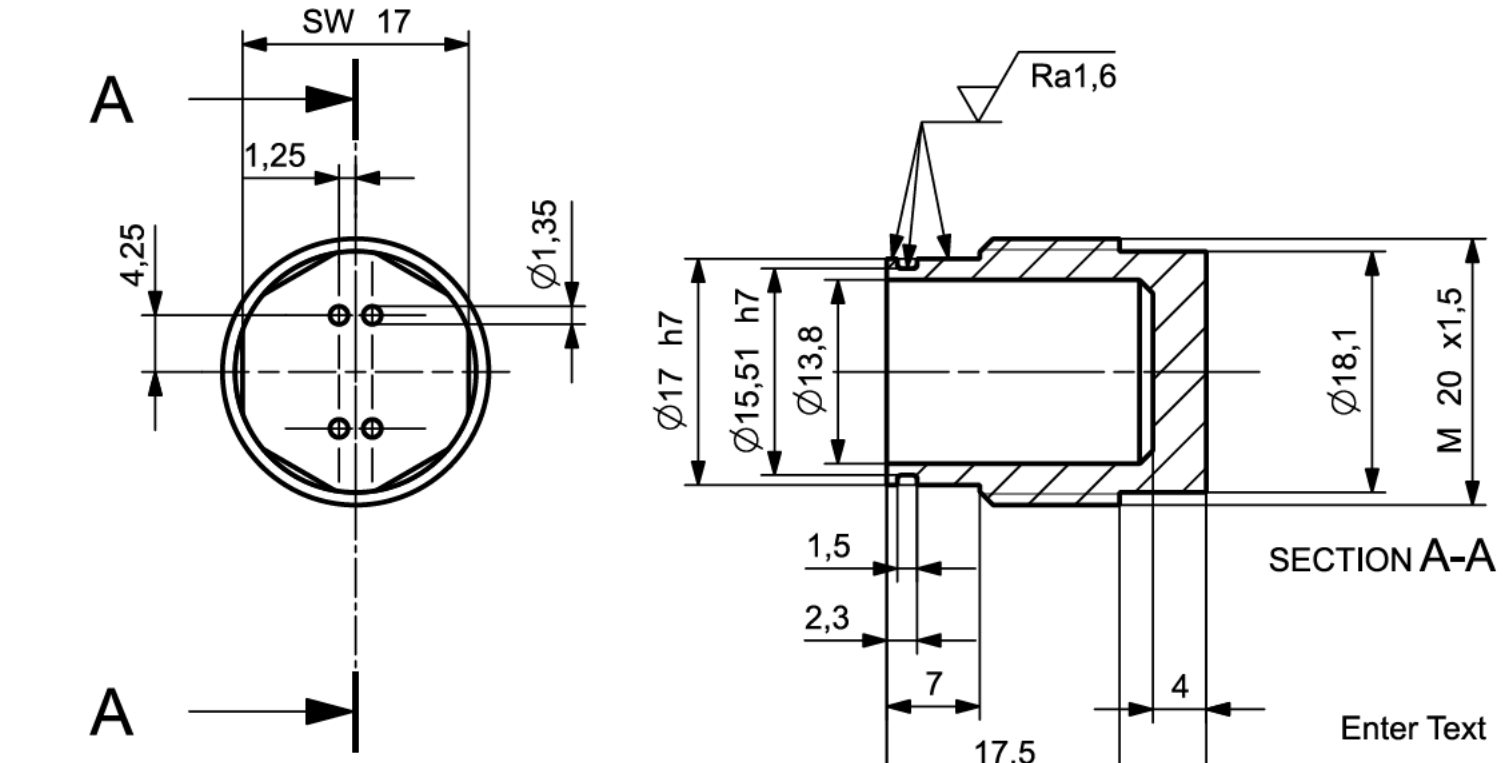
Anzahl 2#

Oberflächenangaben:	Allgemeintoleranz:	Werkstoff:
ISO 1302	DIN ISO 2768-mK	X8CrNiS18-9 (1.4305)

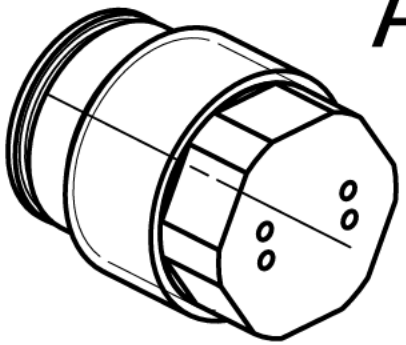
Nennmaß	Größtmaß	Kleinstmaß
Ø8h7	8,000mm	7,985mm

AEROSPACE TEAM GRAZ

Titel:	Dokumentenart:			
01_Locking_PP_Bolt_V01	Fertigungszeichnung			
	Maßstab	Gewicht	Ausgabedatum	Blatt
	21	19,5 g	25.07.2025	1/1



Anzahl 2#



Ra6,3 (Ra1,6)

-0,50

0,15

Alle unbemaßten Fasen 0,5x45°
Alle unbemaßten Radien 0,2mm

Werkstückkanten nach DIN ISO 13715.

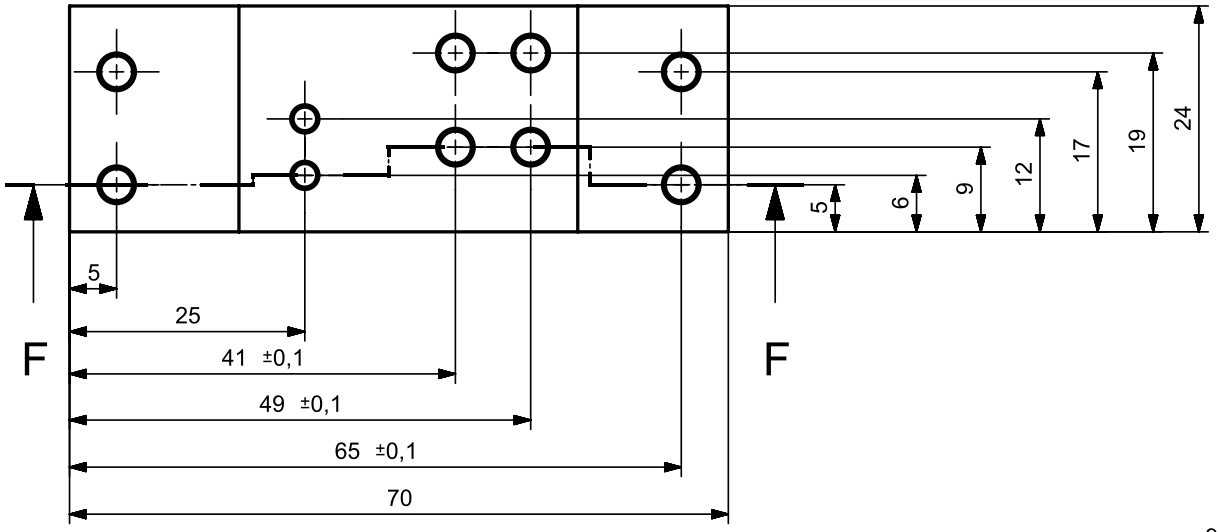
Nennmaß	Größtmaß	Kleinstmaß
Ø15,51h7	15,510mm	15,492mm
Ø17h7	17,000mm	16,982mm

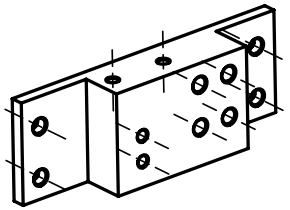
ASTG
AEROSPACE TEAM GRAZ

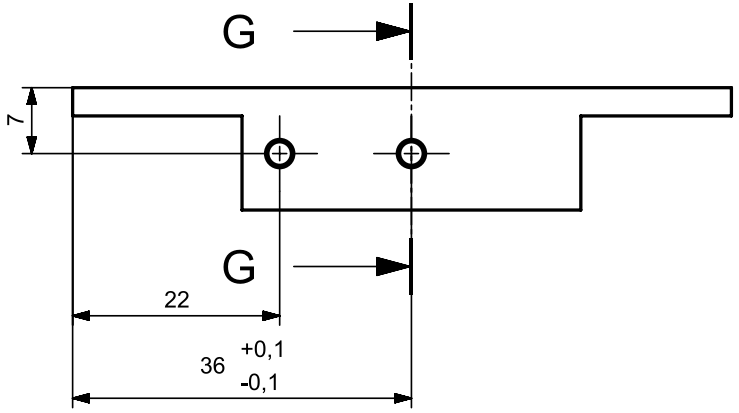
Oberflächenangaben:	Allgemeintoleranz:	Werkstoff:
ISO 1302	DIN ISO 2768-mK	X8CrNiS18-9 (1.4305)

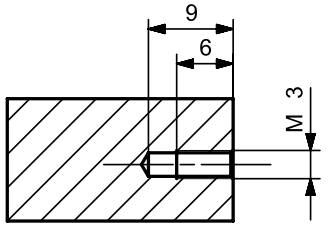
[redacted]

Titel:	Dokumentenart:			
01_Locking_Charge_Cup_V01	Fertigungszeichnung			
	Maßstab	Gewicht	Ausgabedatum	Blatt
	2:1	27,0 g	24.07.2025	1/1

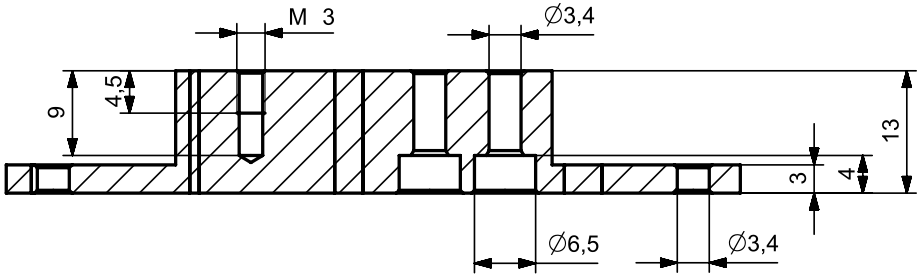








SECTION G-G



SECTION F-F

Alle unbemaßten Fasen 0,5x45°
Alle unbemaßten Radien 0,2mm

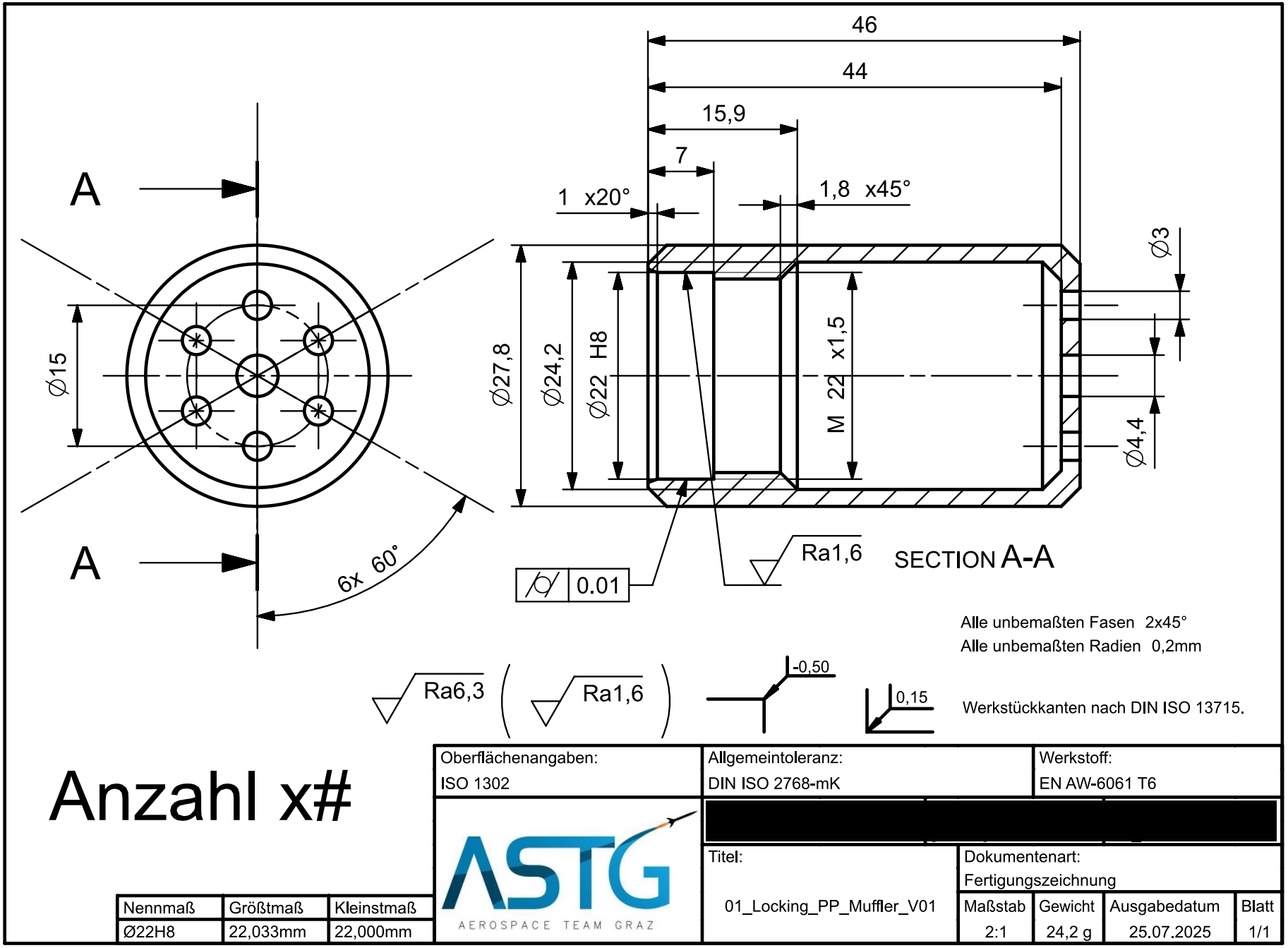
Ra6,3

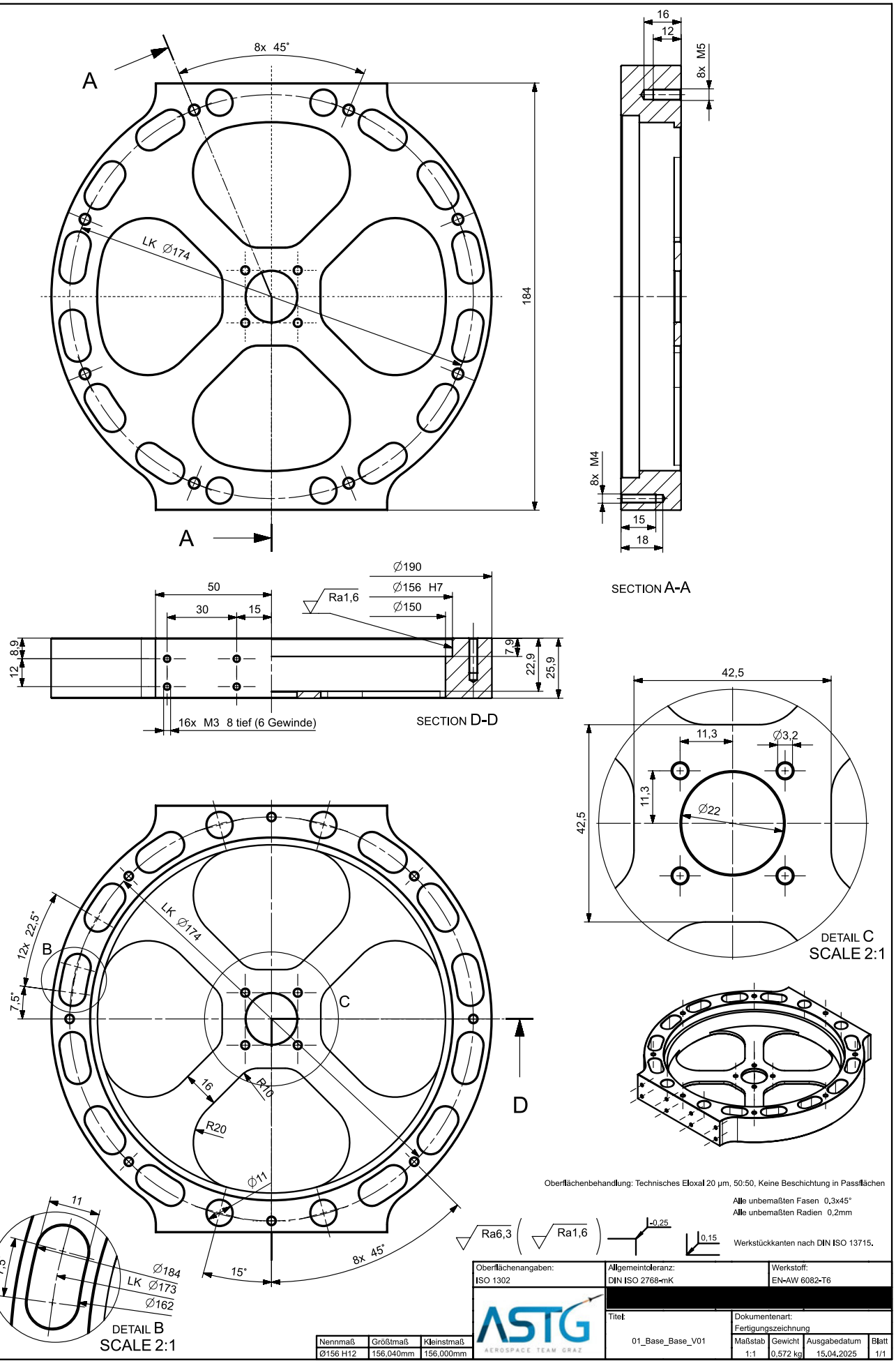
-0,50

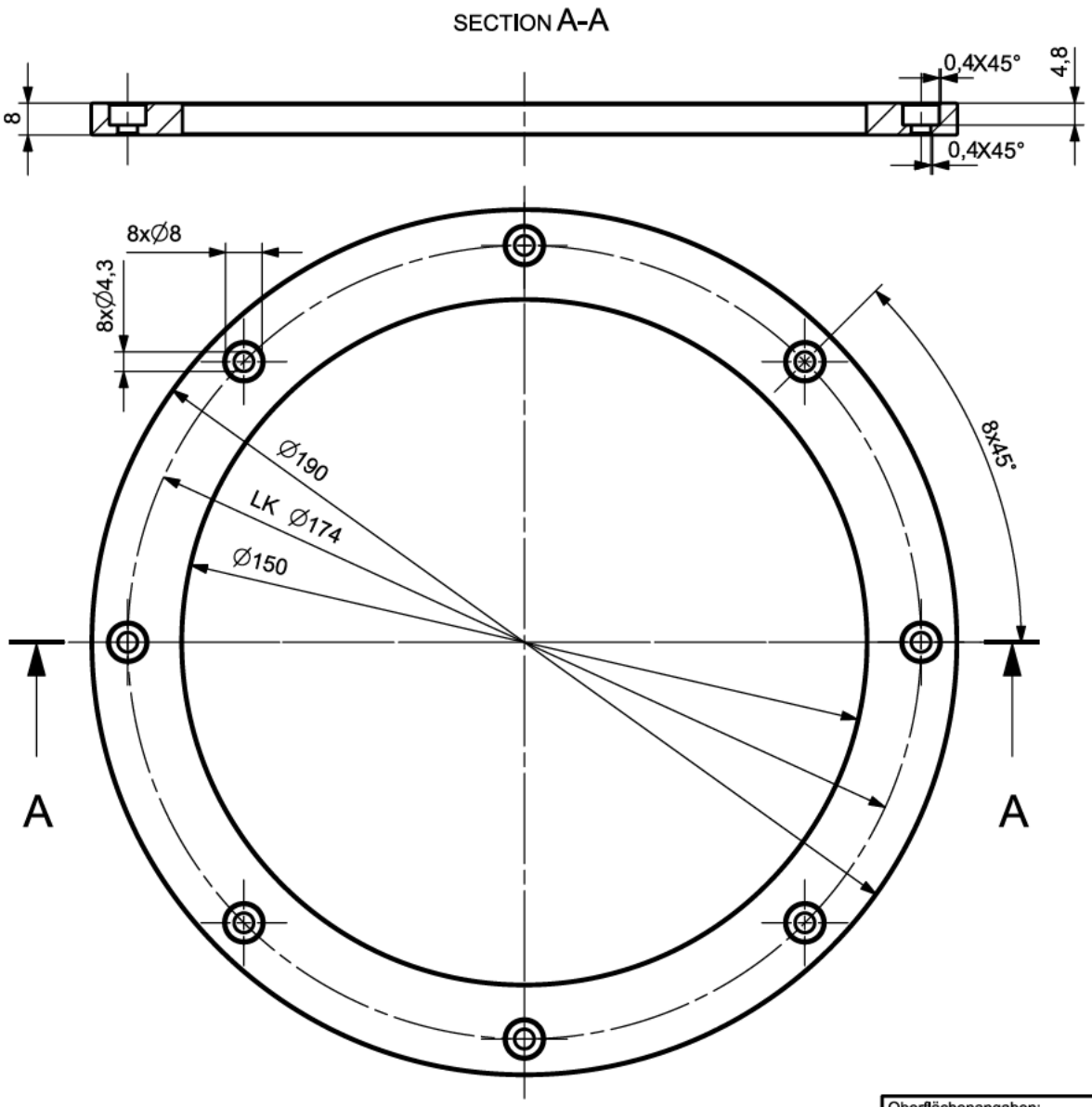
0,15

Werkstückkanten nach DIN ISO 13715.

Oberflächenangaben: ISO 1302	Allgemeintoleranz: DIN ISO 2768-mK	Werkstoff: EN AW-6061 T6			
ASTG AEROSPACE TEAM GRAZ	[redacted]				
	Titel: 01_Locking_PP_Mount_V01	Dokumentenart: Fertigungzeichnung			
		Maßstab 2:1	Gewicht 97,3 g	Ausgabedatum 25.07.2025	Blatt 1/1


46
44
15,9
7
1 x20°
1,8 x45°
A
A
Ø15
6x 60°
Ø27,8
Ø24,2
Ø22 H8
M 22 x1,5
Ø3
Ø4,4
0.01
Ra1,6
SECTION A-A
Alle unbemaßten Fasen 2x45°
Alle unbemaßten Radien 0,2mm
Ra6,3
Ra1,6
-0,50
0,15
Werkstückkanten nach DIN ISO 13715.
Anzahl x#
Oberflächenangaben:
ISO 1302
Allgemeintoleranz:
DIN ISO 2768-mK
Werkstoff:
EN AW-6061 T6
ASTG
AEROSPACE TEAM GRAZ
Titel:
01_Locking_PP_Muffler_V01
Dokumentenart:
Fertigungszeichnung
Maßstab
2:1
Gewicht
24,2 g
Ausgabedatum
25.07.2025
Blatt
1/1
Nennmaß
Ø22H8
Größtmaß
22,033mm
Kleinstmaß
22,000mm


8x 45°
A
LK Ø174
184
A
16
12
8x M5
8x M4
15
18
SECTION A-A
Ø190
Ø156 H7
Ø150
Ra1,6
50
30
15
12
8,9
7,9
22,9
25,9
16x M3 8 tief (6 Gewinde)
SECTION D-D
42,5
11,3
Ø3,2
11,3
Ø22
42,5
DETAIL C
SCALE 2:1
12x 22,5°
7,5°
B
C
D
R10
R20
16
Ø11
15°
8x 45°
11
7,5°
Ø184
LK Ø173
Ø162
DETAIL B
SCALE 2:1
Oberflächenbehandlung: Technisches Eloxal 20 µm, 50:50, Keine Beschichtung in Passflächen
Alle unbemaßten Fasen 0,3x45°
Alle unbemaßten Radien 0,2mm
Ra6,3
Ra1,6
-0,25
0,15
Werkstückkanten nach DIN ISO 13715.
Oberflächenangaben: ISO 1302
Allgemeintoleranz: DIN ISO 2768-mK
Werkstoff: EN-AW 6082-T6
Titel: 01_Base_Base_V01
Dokumentenart: Fertigungszeichnung
Maßstab 1:1
Gewicht 0,572 kg
Ausgabedatum 15.04.2025
Blatt 1/1
Nennmaß Ø156 H12
Größtmaß 156,040mm
Kleinstmaß 156,000mm



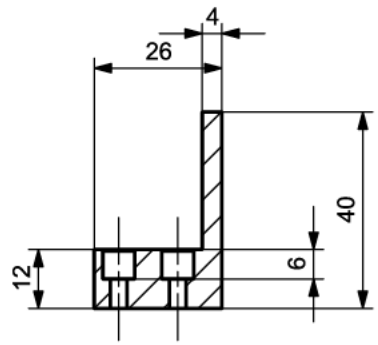
Alle unbemaßten Fasen 0,3x45°
Alle unbemaßten Radien

-0,25

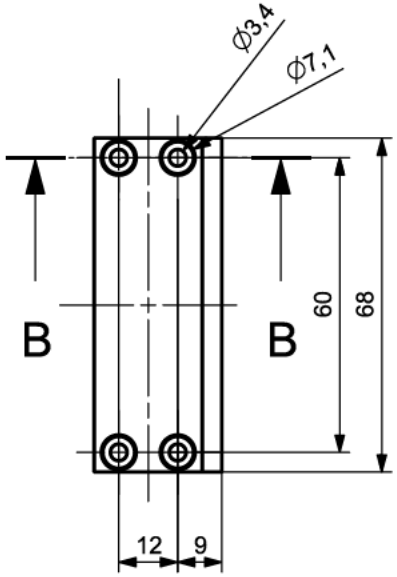
0,15

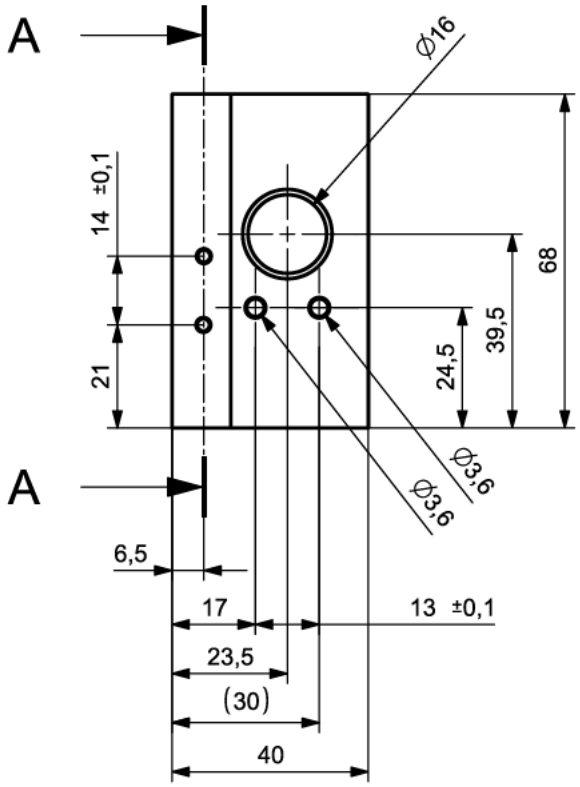
Werkstückkanten nach DIN ISO 13715.

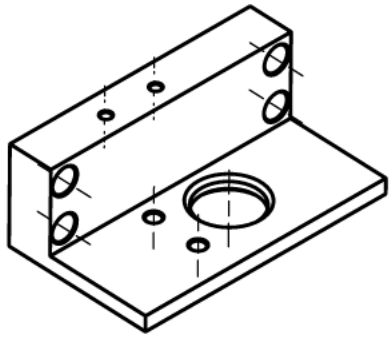
Oberflächenangaben: ISO 1302	Allgemeintoleranz: DIN ISO 2768-mK		Werkstoff: EN-AW 6082-T6	
ASTG AEROSPACE TEAM GRAZ	[redacted]			
	Titel: Base_BearingClamp_V01	Dokumentenart: Fertigungszeichnung		
		Maßstab 1:2	Gewicht 0,196kg	Ausgabedatum 03.04.2025	Blatt 1/1

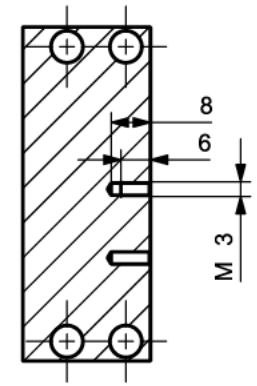


SECTION B-B









SECTION A-A

Alle unbemaßten Fasen -
Alle unbemaßten Radien -

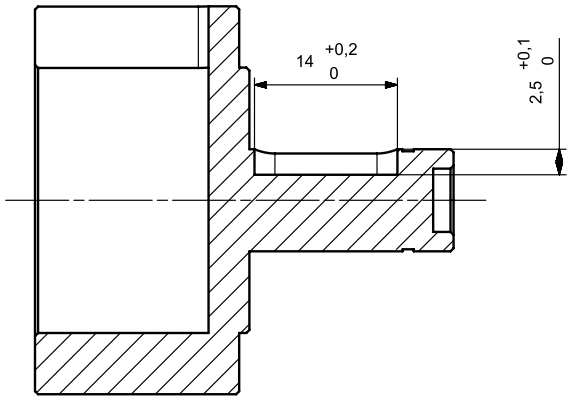
Ra 6,3 | -0,50 | 0,15

Werkstückkanten nach DIN ISO 13715.

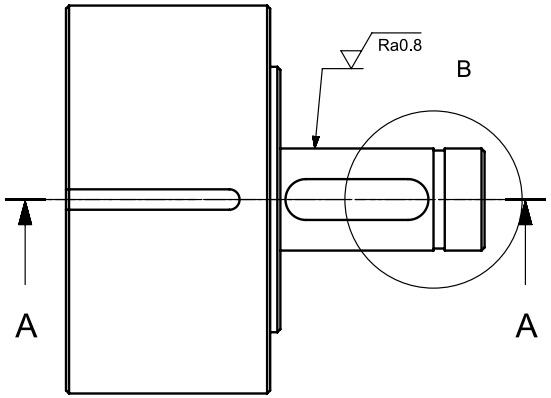
Oberflächenangaben:	Allgemeintoleranz:	Werkstoff:
ISO 1302	DIN ISO 2768-mK	EN-AW 6082-T6

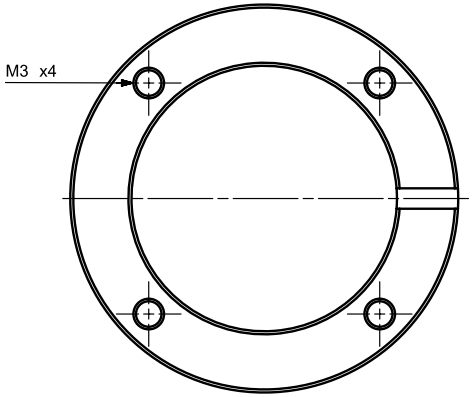
ASTG AEROSPACE TEAM GRAZ

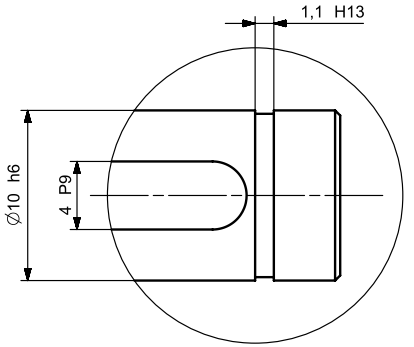
Titel:	Dokumentenart:			
01_Base_Preliminary_PP_adapter	Fertigungszeichnung			
	Maßstab	Gewicht	Ausgabedatum	Blatt
	1:1	0,073 kg	08.04.2025	1/1



SECTION A-A







DETAIL B
SCALE 5:1

Oberflächenbehandlung: Technisches Eloxal 20 µm, 50:50, Keine Beschichtung in Passflächen

Alle unbemaßten Fasen 0.3x45°
Alle unbemaßten Radien 0,2mm
Alle unbemaßten Dimensionen aus .STP

Werkstückkanten nach DIN ISO 13715.

Ra3,2 (Ra0,8)

-0,25

0,15

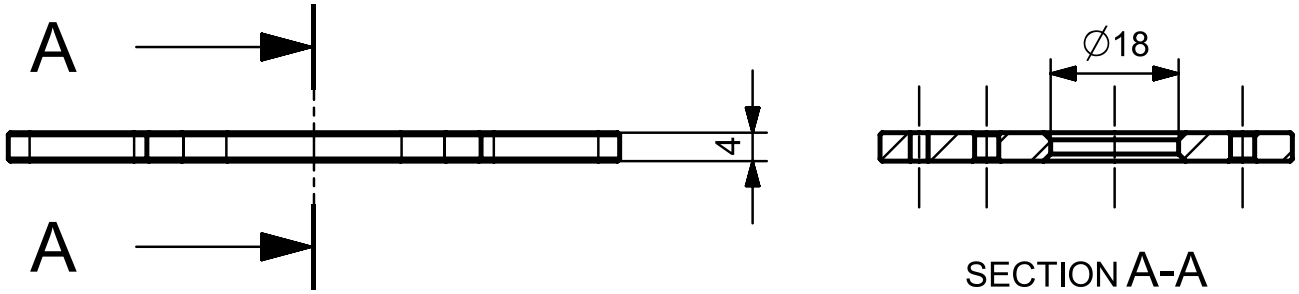
Nennmaß	Größtmaß	Kleinstmaß
1,1 H13	1,240mm	1,100mm
4 P9	3,988mm	3,958mm
∅10 h6	∅10,000mm	∅9,991mm

Oberflächenangaben:	Allgemeintoleranz:	Werkstoff:
ISO 1302	DIN ISO 2768-mK	EN-AW 6082-T6

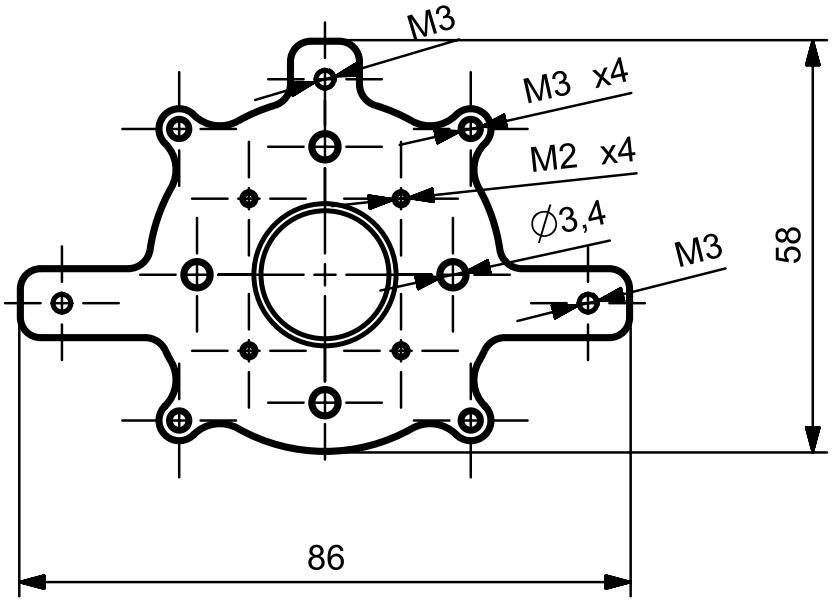
ASTG AEROSPACE TEAM GRAZ

[redacted]

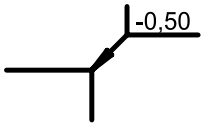
Titel:	Dokumentenart:			
01_Base_Shaft_V01	Fertigungszeichnung			
	Maßstab	Gewicht	Ausgabedatum	Blatt
	3:1	0,041 kg	31.03.2025	1/1

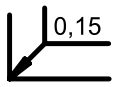


SECTION A-A



Alle unbemaßten Fasen 0.3x45°
Alle unbemaßten Radien 0,2mm





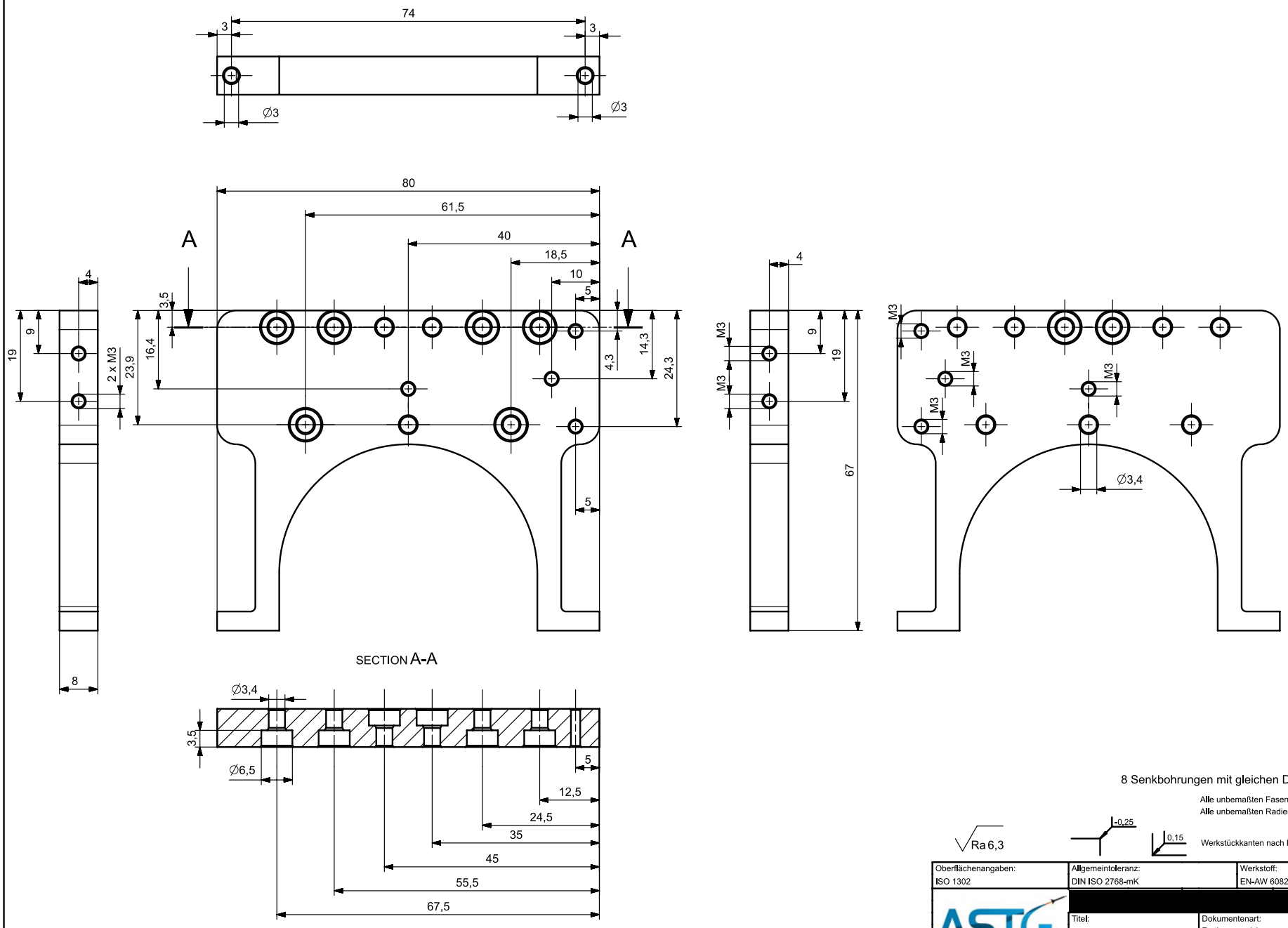
Werkstückkanten nach DIN ISO 13715.

Oberflächenangaben:	Allgemeintoleranz:	Werkstoff:
ISO 1302	DIN ISO 2768-mK	[WERKSTOFF]

Nennmaß	Größtmaß	Kleinstmaß
Ø33h12	33,000mm	32,750mm

ASTG AEROSPACE TEAM GRAZ

Titel:	Dokumentenart:			
[TITEL]	[DOKUMENTENART]			
	Maßstab	Gewicht	Ausgabedatum	Blatt
	1:1	-kg	dd.mm.yyyy	1/1



8 Senkbohrungen mit gleichen Dimensionen

Alle unbemaßten Fasen 0.3x45°
Alle unbemaßten Radien 0,2mm

Ra 6,3

-0,25

0,15

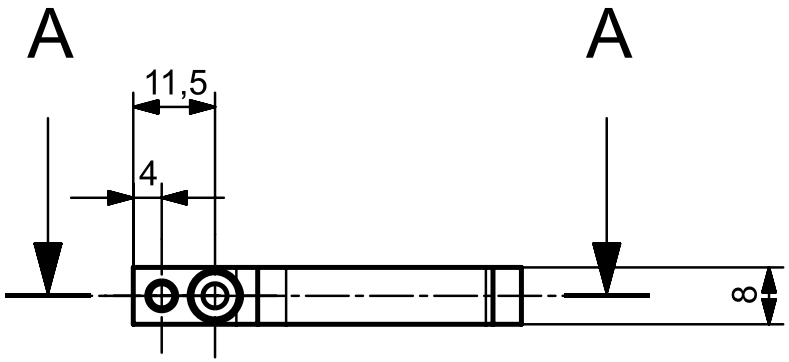
Werkstückkanten nach DIN ISO 13715.

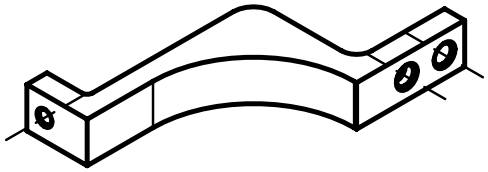
Oberflächenangaben:	Allgemeintoleranz:	Werkstoff:
ISO 1302	DIN ISO 2768-mK	EN-AW 6082-T6

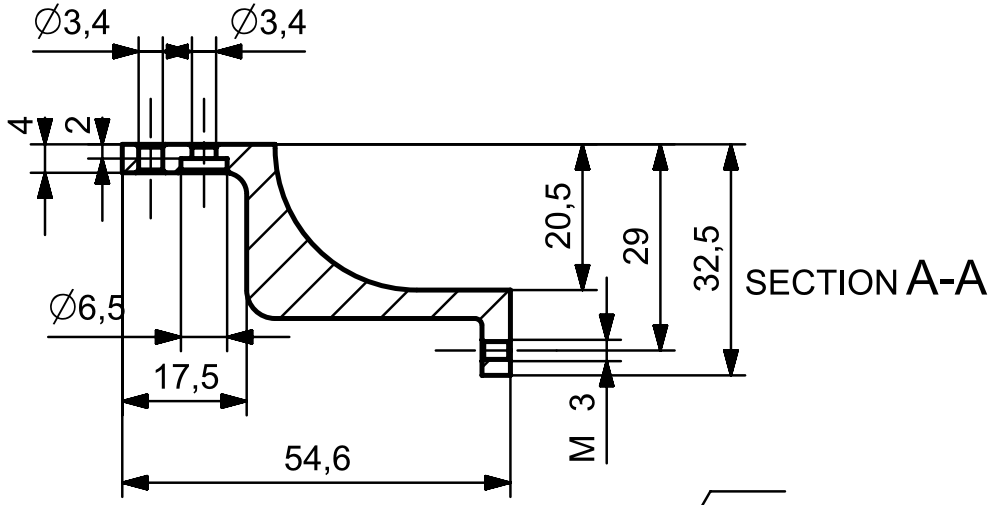
ASTG AEROSPACE TEAM GRAZ

[redacted]

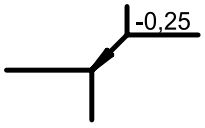
Titel:	Dokumentenart:			
01_Camera_Housing3_Housing_V02	Fertigungszeichnung			
	Maßstab	Gewicht	Ausgabedatum	Blatt
	2:1	0,061 kg	01.04.2025	1/1

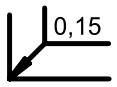






Ra 6,3





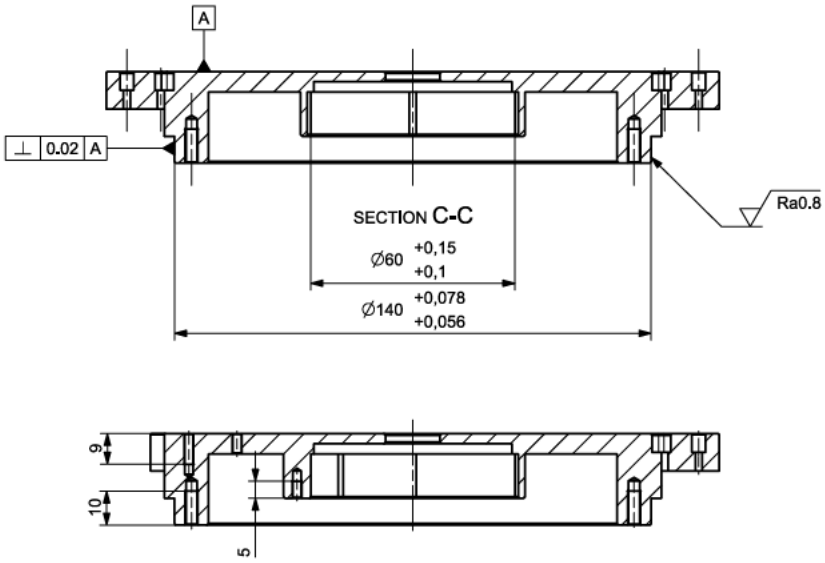
Alle unbemaßten Fasen 0.3x45°
Alle unbemaßten Radien 0,2mm

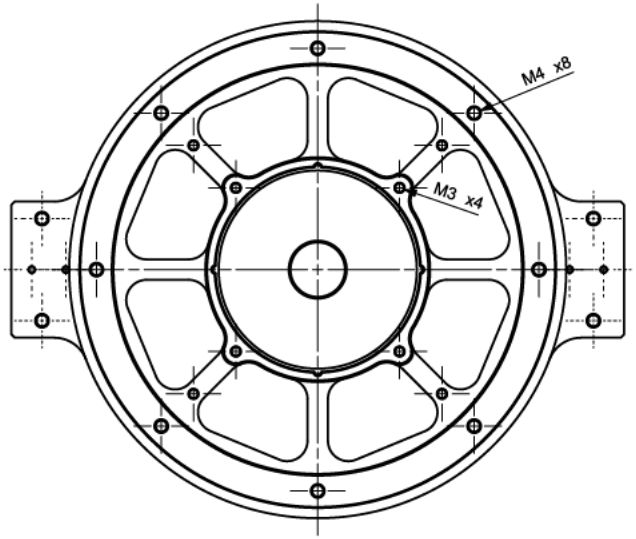
Werkstückkanten nach DIN ISO 13715.

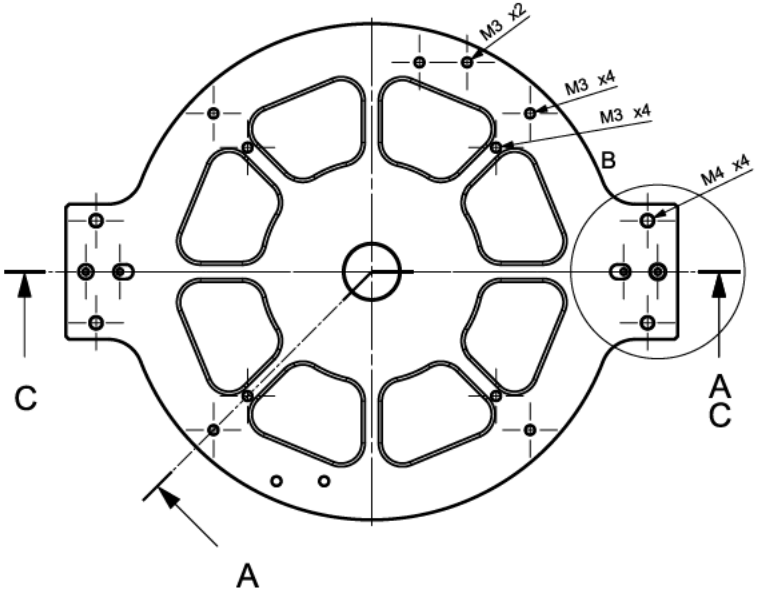
Oberflächenangaben:	Allgemeintoleranz:	Werkstoff:
ISO 1302	DIN ISO 2768-mK	EN-AW 6082-T6

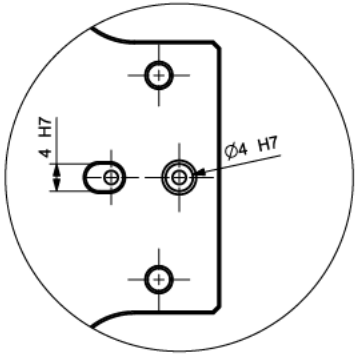
ASTG AEROSPACE TEAM GRAZ

Titel:	Dokumentenart:			
01_Camera_Housing3_Support	Fertigungszeichnung			
	Maßstab	Gewicht	Ausgabedatum	Blatt
	1:1	8,6 g	01.04.2025	1/1









DETAIL B
SCALE 2:1

Oberflächenbehandlung: Technisches Eloxal 20 µm, 50:50, Keine Beschichtung in Passflächen

Alle unbemaßten Fasen 0,3x45°
Alle unbemaßten Radien 0,2mm
Alle unbemaßten Dimensionen aus .STP

Werkstückkanten nach DIN ISO 13715.

Ra3,2 (Ra0,8) -0,25 0,15

Oberflächenangaben:	Allgemeintoleranz:	Werkstoff:
ISO 1302	DIN ISO 2768-mK	EN-AW 6082-T6

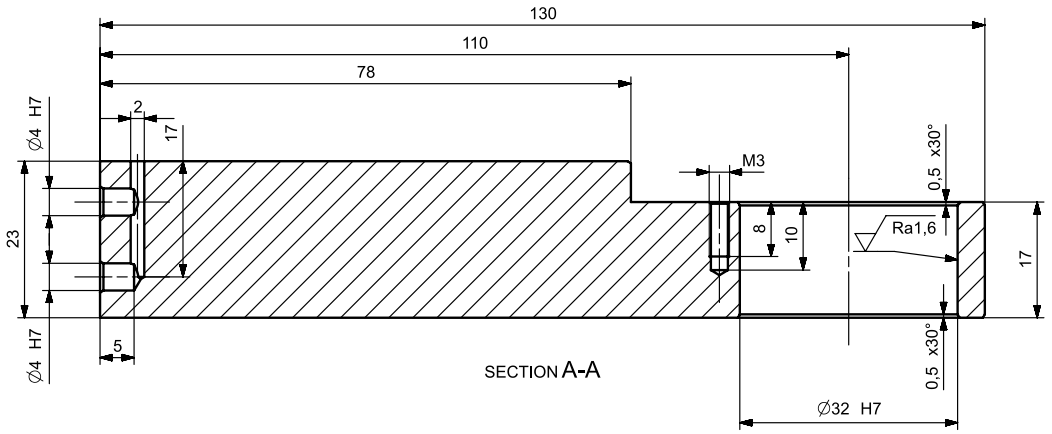
ASTG AEROSPACE TEAM GRAZ

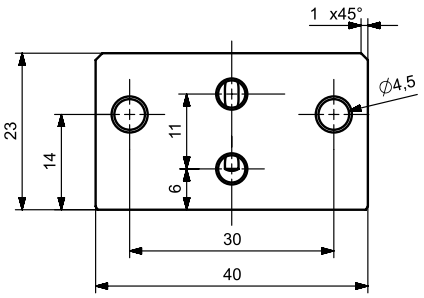
Titel: 01_Rotating_Base_V01

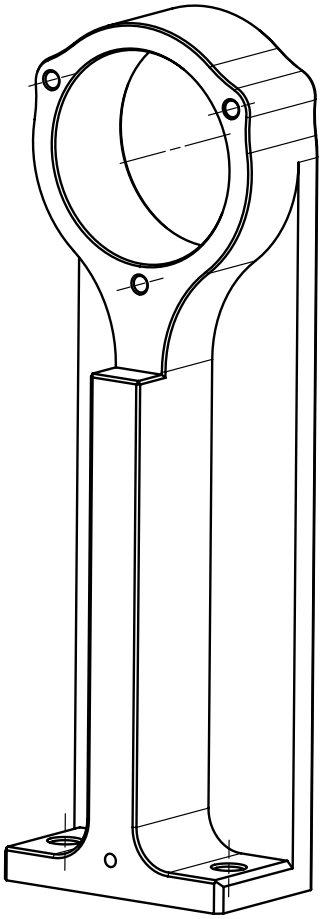
Dokumentenart: Fertigungszeichnung

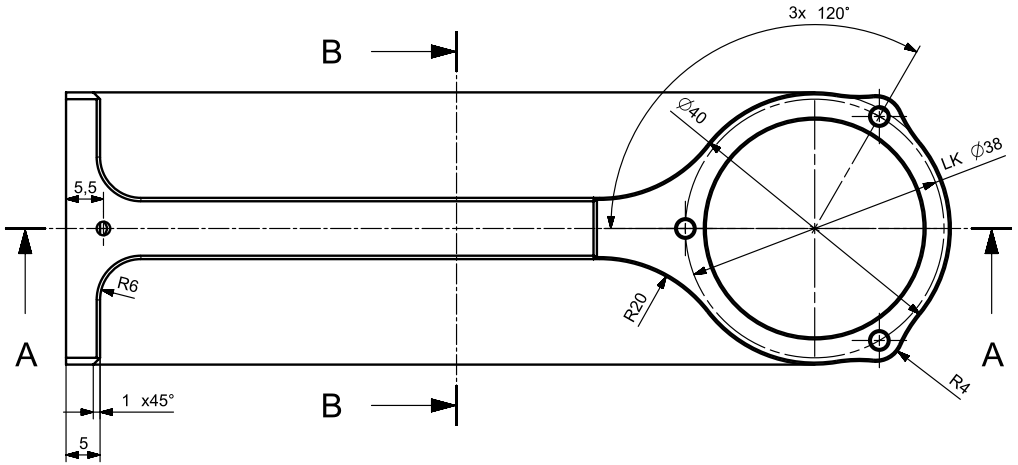
Maßstab	Gewicht	Ausgabedatum	Blatt
1:1	0,504 kg	31.03.2025	1/1

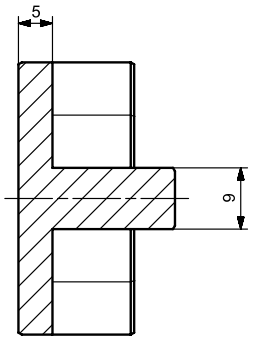
Nennmaß	Größtmaß	Kleinstmaß
4 H7	4,012mm	4,000mm











SECTION B-B

Alle unbemaßten Fasen 0.3x45°
Alle unbemaßten Radien 0,2mm

Ra6,3 (Ra1,6) -0,25 0,15

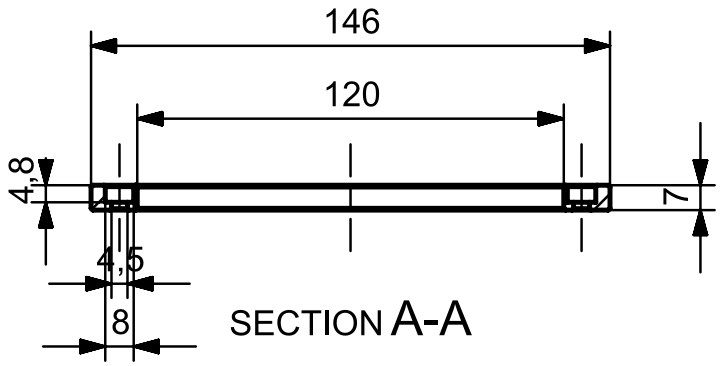
Werkstückkanten nach DIN ISO 13715.

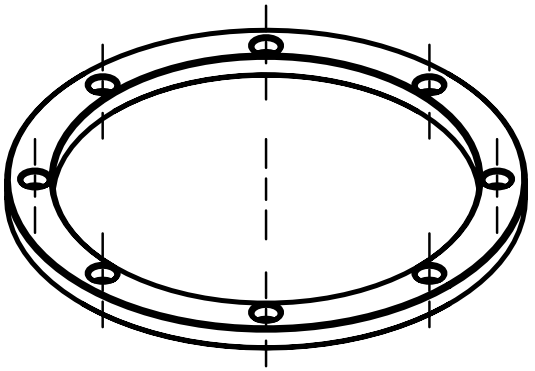
Oberflächenangaben:	Allgemeintoleranz:	Werkstoff:
ISO 1302	DIN ISO 2768-mK	EN-AW 6082-T6

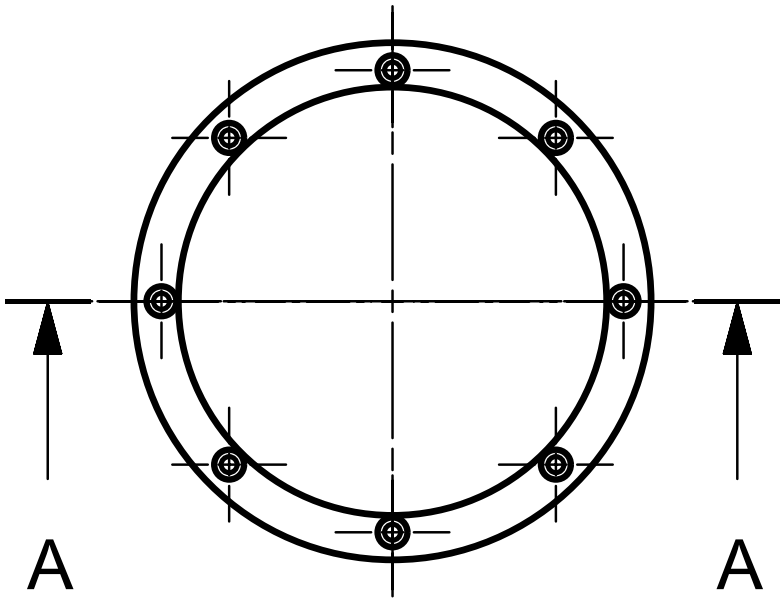
Nennmaß	Größtmaß	Kleinstmaß
Ø4 H7	4,012mm	4,000mm
Ø32 H7	32,025mm	32,000mm

ASTG AEROSPACE TEAM GRAZ

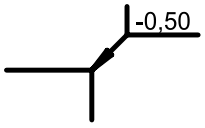
Titel:	Dokumentenart:			
	Fertigungszeichnung			
01_Rotating_BearingArm_V01	Maßstab	Gewicht	Ausgabedatum	Blatt
	2:1	0,119kg	03.04.2025	1/1

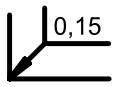






Alle unbemaßten Fasen 0.5x45°
Alle unbemaßten Radien 0,2mm





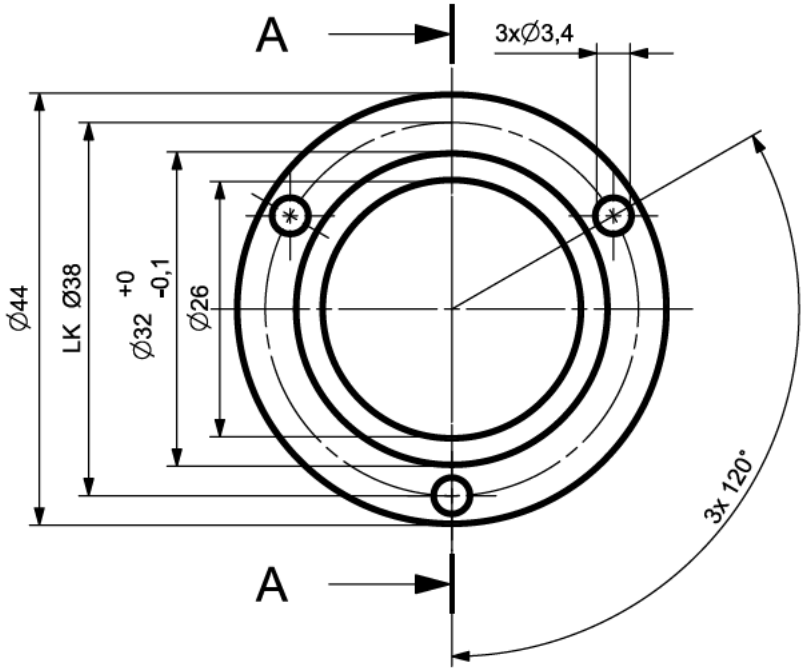
Werkstückkanten nach DIN ISO 13715.

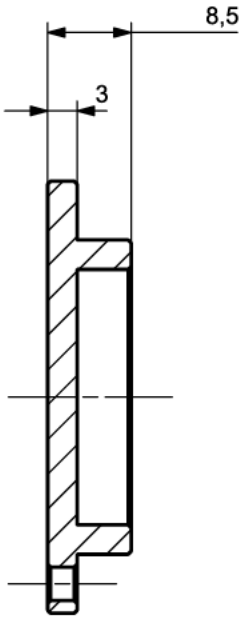
Oberflächenangaben:	Allgemeintoleranz:	Werkstoff:
ISO 1302	DIN ISO 2768-mK	[WERKSTOFF]

Nennmaß	Größtmaß	Kleinstmaß
Ø33h12	33,000mm	32,750mm

ASTG AEROSPACE TEAM GRAZ

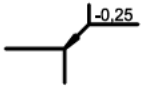
Titel:	Dokumentenart:			
[TITEL]	[DOKUMENTENART]			
	Maßstab	Gewicht	Ausgabedatum	Blatt
	1:1	-kg	dd.mm.yyyy	1/1





SECTION A-A

Alle unbemaßten Fasen 0,3x45°
Alle unbemaßten Radien

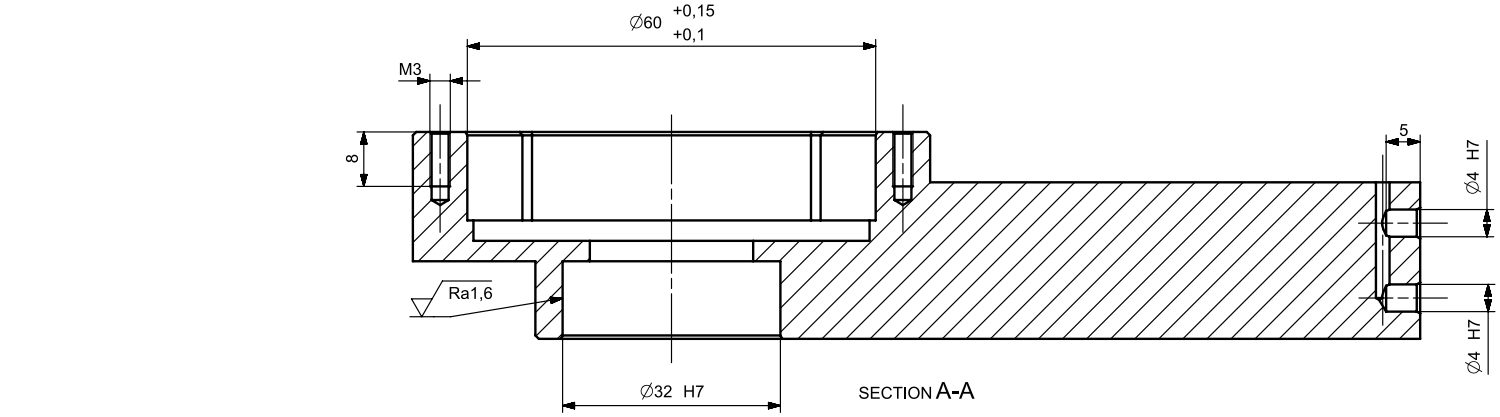


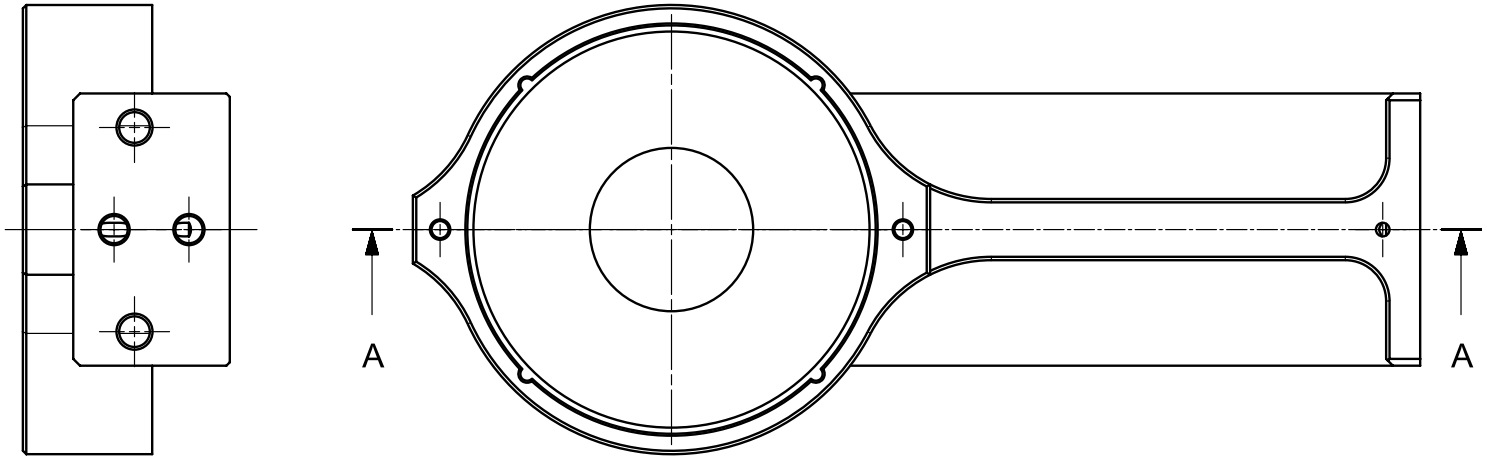
Werkstückkanten nach DIN ISO 13715.

Oberflächenangaben:	Allgemeintoleranz:	Werkstoff:
ISO 1302	DIN ISO 2768-mK	EN-AW 6082-T6

ASTG AEROSPACE TEAM GRAZ

Titel:	Dokumentenart:			
01_Rotating_BearingClamoSmall_V01	Fertigungszeichnung			
	Maßstab	Gewicht	Ausgabedatum	Blatt
	2:1	0,016kg	03.04.2025	1/1





Oberflächenbehandlung: Technisches Eloxal 20 µm, 50:50, Keine Beschichtung in Passflächen

Alle unbemaßten Fasen 0.3x45°
Alle unbemaßten Radien 0,2mm
Alle unbemaßten Dimensionen aus .STP

Werkstückkanten nach DIN ISO 13715.

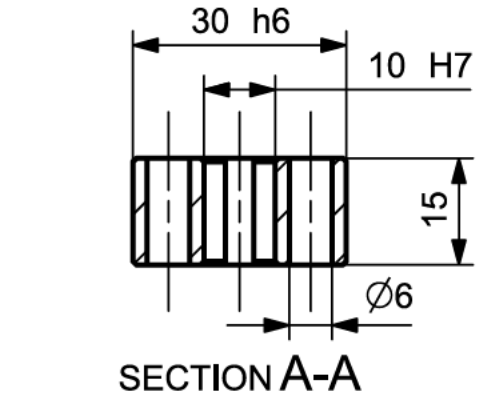
Ra3,2 (Ra1,6) -0,25 0,15

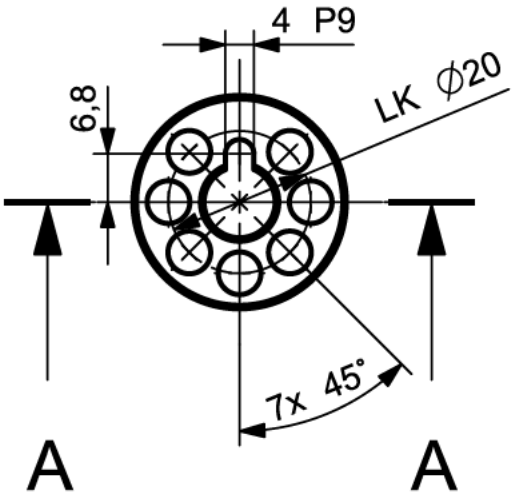
Oberflächenangaben:	Allgemeintoleranz:	Werkstoff:
ISO 1302	DIN ISO 2768-mK	EN-AW 6082-T6

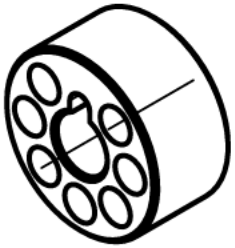
Nennmaß	Größtmaß	Kleinstmaß
∅4 H7	∅4,012mm	∅4,000mm
∅32 H7	∅32,025mm	∅32,000mm

ASTG AEROSPACE TEAM GRAZ

Titel:	Dokumentenart:			
01_Rotating_MotorArm_V01	Fertigungszeichnung			
	Maßstab	Gewicht	Ausgabedatum	Blatt
	2:1	0,177 kg	31.03.2025	1/1

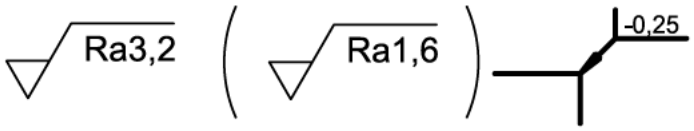






Oberflächenbehandlung: Technisches Eloxal 20 µm, 50:50, Keine Beschichtung in Passflächen

Alle unbemaßten Fasen 0.3x45°
Alle unbemaßten Radien 0,2mm



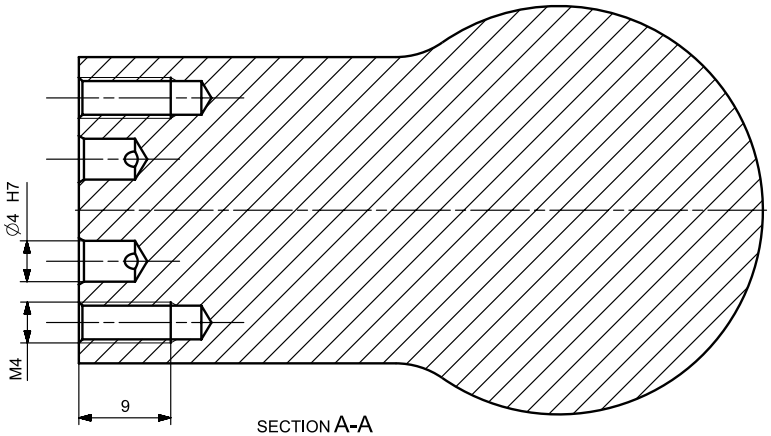
Werkstückkanten nach DIN ISO 13715.

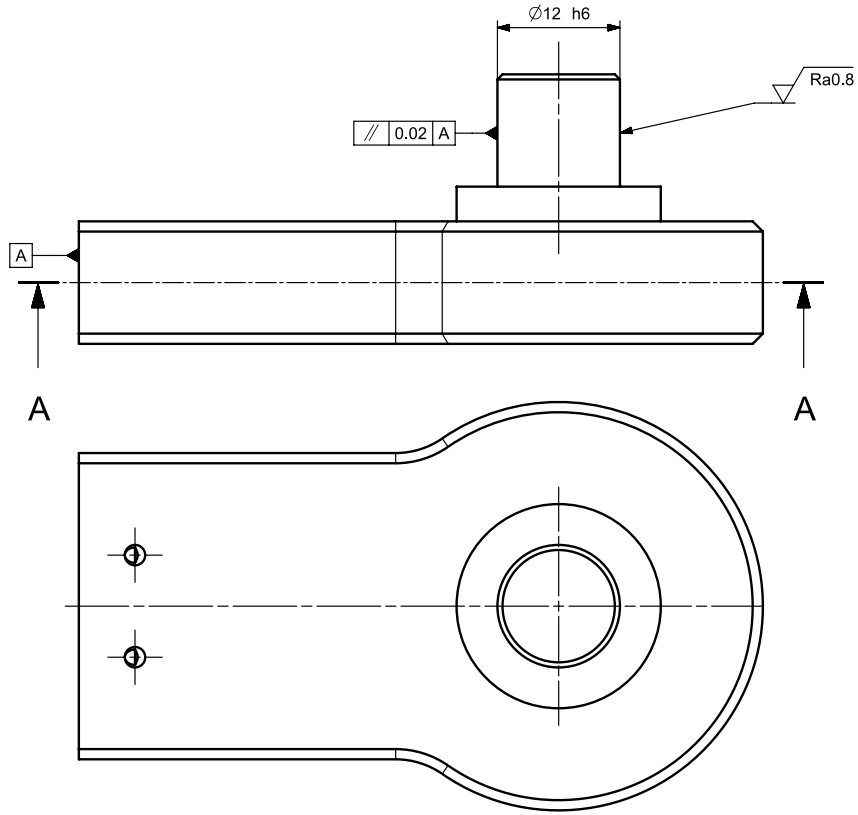
Nennmaß	Größtmaß	Kleinstmaß
4 P9	3,988mm	3,958mm
Ø10 H7	10,015mm	10,000mm
Ø30 h6	29,987mm	30,000mm

Oberflächenangaben:	Allgemeintoleranz:	Werkstoff:
ISO 1302	DIN ISO 2768-mK	EN-AW 6082-T6

ASTG AEROSPACE TEAM GRAZ

Titel:	Dokumentenart:			
01_Rotating_RotorBuchse_V01	Fertigungszeichnung			
	Maßstab	Gewicht	Ausgabedatum	Blatt
	1:1	0,017 kg	03.04.2025	1/1





Oberflächenbehandlung: Technisches Eloxal 20 µm, 50:50, Keine Beschichtung in Passflächen

Ra3,2 (Ra0,8)

-0,25

0,15

Alle unbemaßten Fasen 0,3x45°
Alle unbemaßten Radien 0,2mm
Alle unbemaßten Dimensionen aus .STP

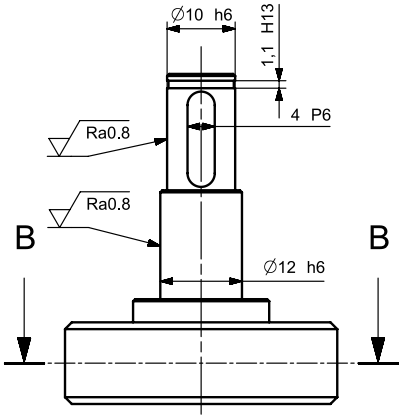
Werkstückkanten nach DIN ISO 13715.

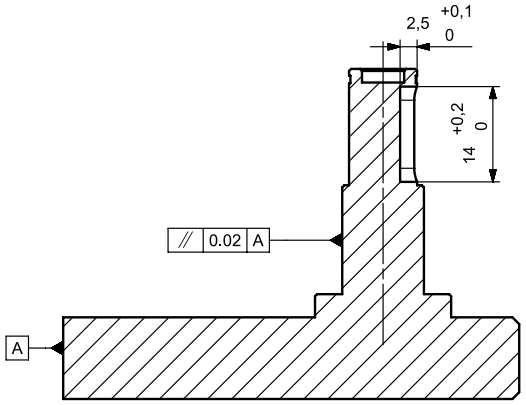
Nennmaß	Größtmaß	Kleinstmaß
Ø4 H7	Ø4,012mm	Ø4,000mm
Ø12 h6	Ø12,000mm	Ø11,989mm

Oberflächenangaben:	Allgemeintoleranz:	Werkstoff:
ISO 1302	DIN ISO 2768-mK	EN-AW 6082-T6

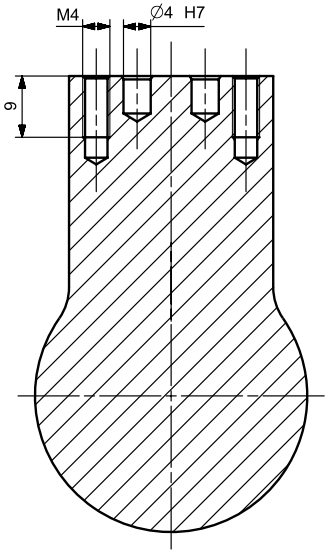
ASTG AEROSPACE TEAM GRAZ

Titel:	Dokumentenart:			
01_Swivel_BearingArm_V01	Fertigungszeichnung			
	Maßstab	Gewicht	Ausgabedatum	Blatt
	3:1	0,051 kg	26.03.2025	1/1

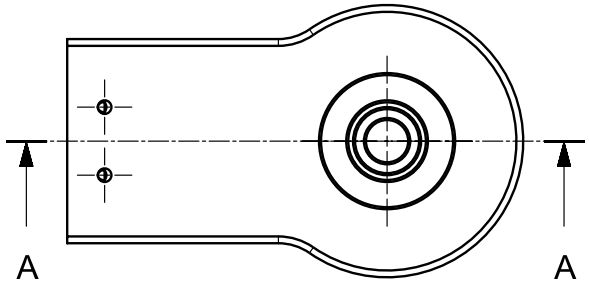




SECTION A-A



SECTION B-B



Oberflächenbehandlung: Technisches Eloxal 20 µm, 50:50, Keine Beschichtung in Passflächen

Alle unbemaßten Fasen 0.3x45°
Alle unbemaßten Radien 0,2mm
Alle unbemaßten Dimensionen aus .STP

Werkstückkanten nach DIN ISO 13715.

Ra3,2 (Ra0,8)

-0,25

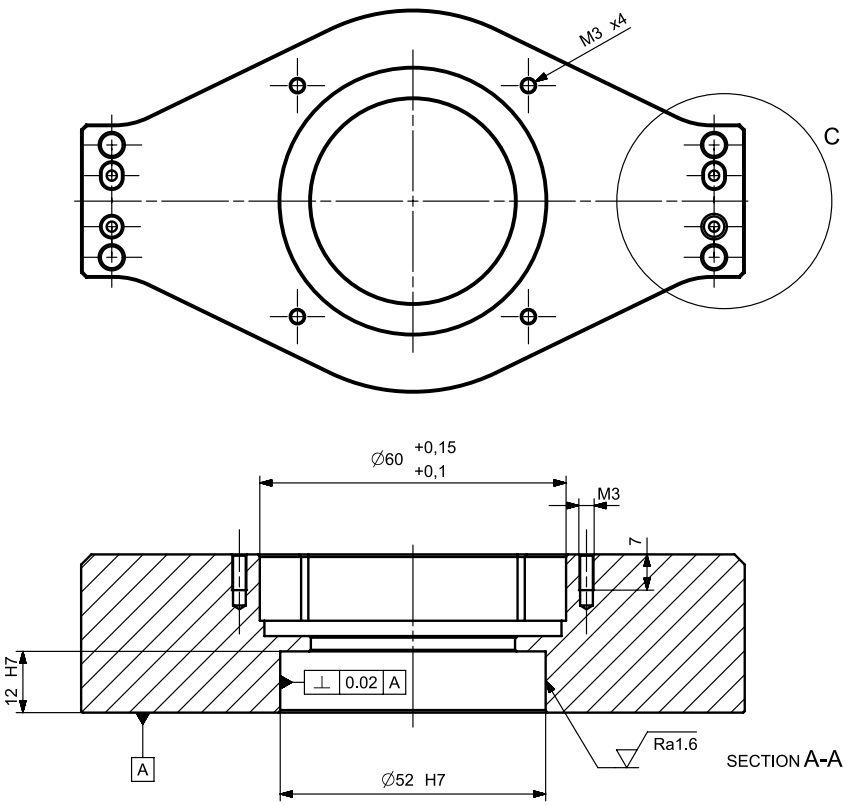
0,15

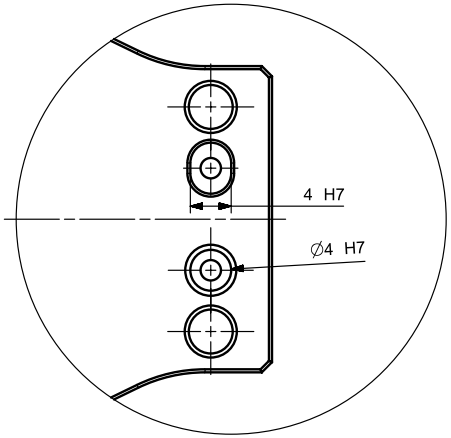
Nennmaß	Größtmaß	Kleinstmaß
1,1 H13	1,240mm	1,100mm
4 P6	3,988mm	3,958mm
∅4 H7	∅4,012mm	∅4,000mm
∅10 h6	∅10,000mm	∅9,991mm
∅12 h6	∅12,000mm	∅11,989mm

Oberflächenangaben:	Allgemeintoleranz:	Werkstoff:
ISO 1302	DIN ISO 2768-mK	EN-AW 6082-T6

ASTG AEROSPACE TEAM GRAZ

Titel:	Dokumentenart:			
01_Swivel_MotorArm	Fertigungszeichnung			
	Maßstab	Gewicht	Ausgabedatum	Blatt
	2:1	0,056 kg	31.03.2025	1/1





DETAIL C
SCALE 3:1

Oberflächenbehandlung: Technisches Eloxal 20 µm, 50:50, Keine Beschichtung in Passflächen

Alle unbemaßten Fasen 0,3x45°
Alle unbemaßten Radien 0,2mm
Alle unbemaßten Dimensionen aus .STP

Werkstückkanten nach DIN ISO 13715.

Ra3,2 (Ra0,8)

-0,25

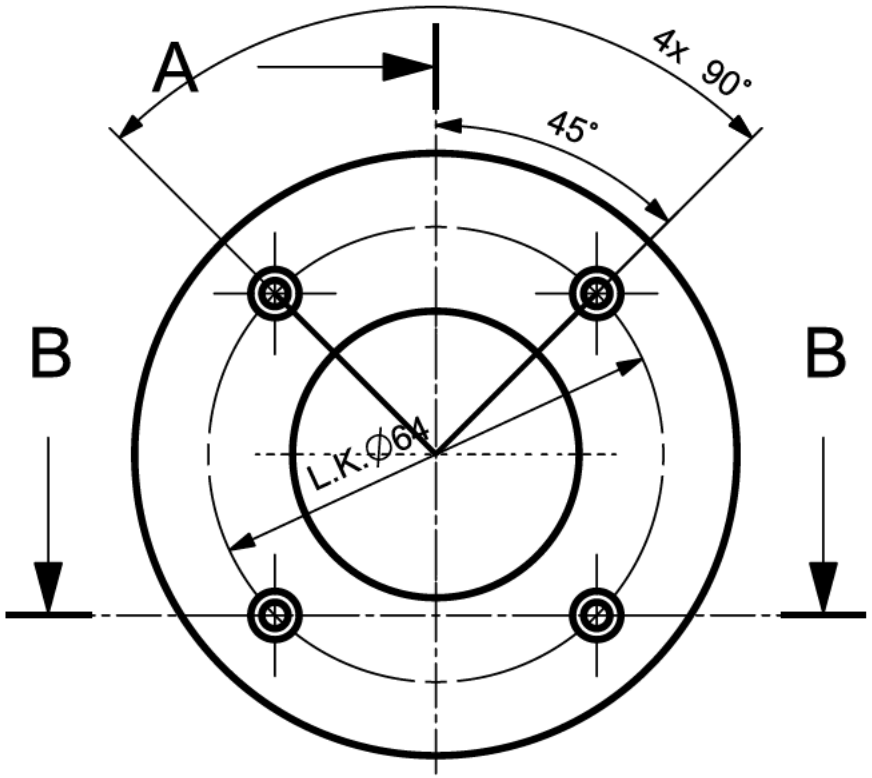
0,15

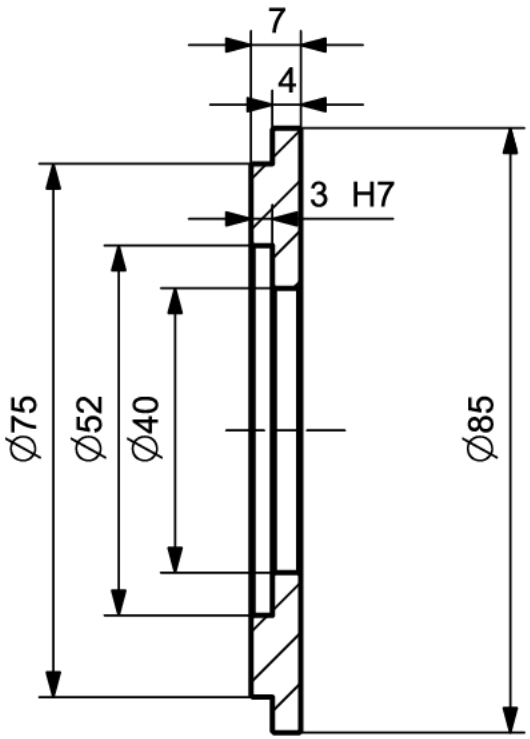
Oberflächenangaben:	Allgemeintoleranz:	Werkstoff:
ISO 1302	DIN ISO 2768-mK	EN-AW 6082-T6

Nennmaß	Größtmaß	Kleinstmaß
4 H7	4,012mm	4,000mm
12 H7	12,018mm	12,000mm
∅52 H7	∅52,030mm	∅52,000mm

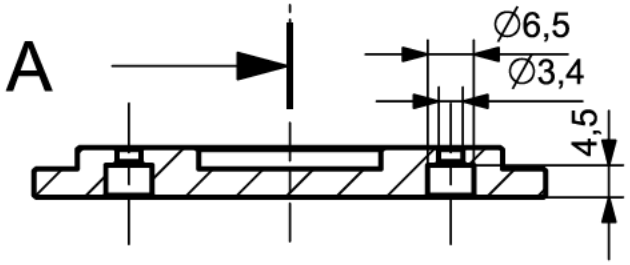
ASTG AEROSPACE TEAM GRAZ

Titel:	Dokumentenart:			
01_Swivel_Bridge_V01	Fertigungszeichnung			
	Maßstab	Gewicht	Ausgabedatum	Blatt
	3:2	0,181 kg	31.03.2025	1/1



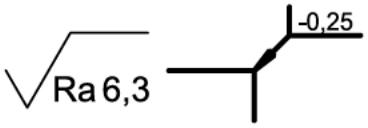


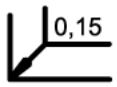
SECTION A-A



SECTION B-B

Alle unbemaßten Fasen 0.3x45°
Alle unbemaßten Radien 0,2mm





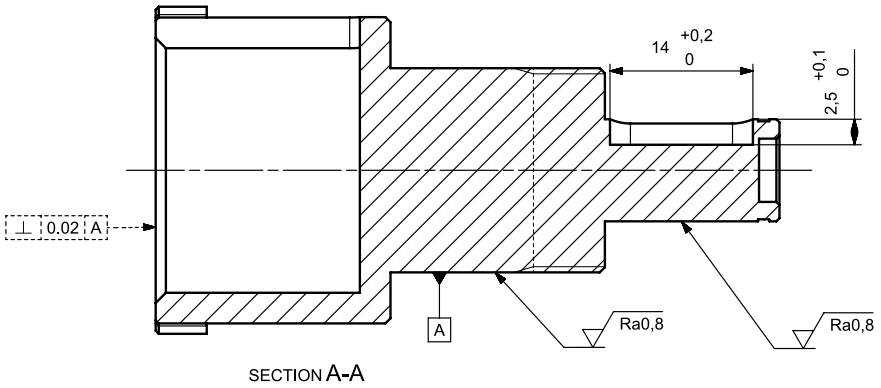
Werkstückkanten nach DIN ISO 13715.

Oberflächenangaben:	Allgemeintoleranz:	Werkstoff:
ISO 1302	DIN ISO 2768-mK	EN-AW 6082-T6

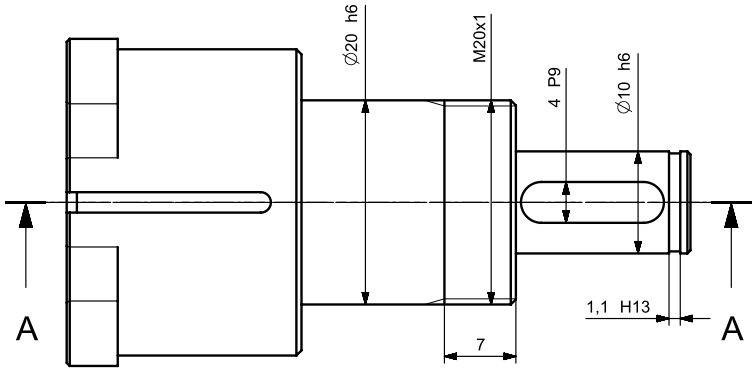
Nennmaß	Größtmaß	Kleinstmaß
3 H7	3.010mm	3.000mm

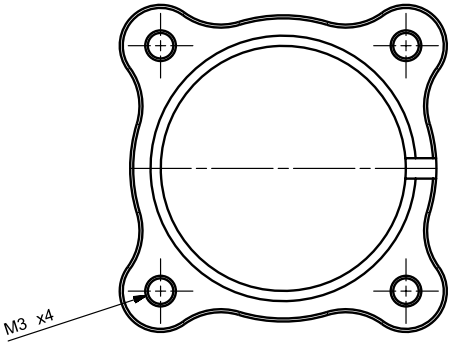
ASTG AEROSPACE TEAM GRAZ

Titel:	Dokumentenart:			
01_Swivel_Cablereel_V01	Fertigungszeichnung			
	Maßstab	Gewicht	Ausgabedatum	Blatt
	1:1	65 g	01.04.2025	1/1



SECTION A-A





Oberflächenbehandlung: Technisches Eloxal 20 µm, 50:50, Keine Beschichtung in Passflächen

Alle unbemaßten Fasen 0.3x45°
Alle unbemaßten Radien 0,2mm
Alle unbemaßten Dimensionen aus .STP

Werkstückkanten nach DIN ISO 13715.

Ra3,2 (Ra0,8)

-0,25

0,15

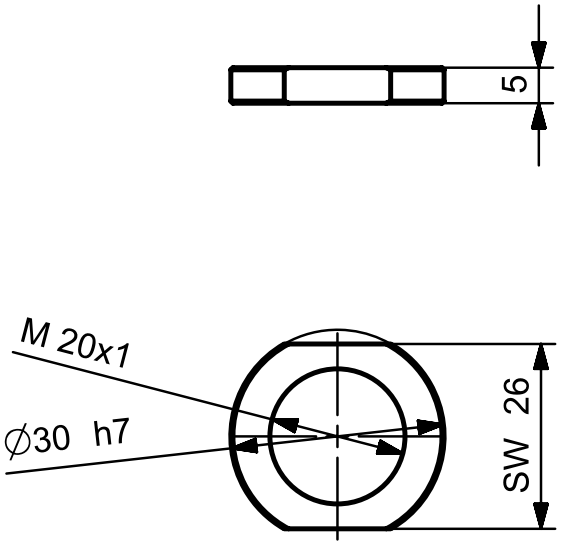
Oberflächenangaben:	Allgemeintoleranz:	Werkstoff:
ISO 1302	DIN ISO 2768-mK	EN-AW 6082-T6

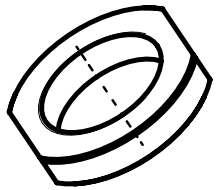
Nennmaß	Größtmaß	Kleinstmaß
1,1 H13	1,240mm	1,100mm
4 P9	3,988mm	3,958m
Ø10 h6	Ø10,000mm	Ø9,991mm
Ø20 h6	Ø20,000mm	Ø19,987mm

ASTG AEROSPACE TEAM GRAZ

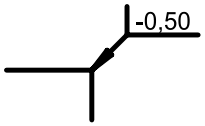
[redacted]

Titel:	Dokumentenart:			
01_Swivel_ShaftC3_V01	Fertigungszeichnung			
	Maßstab	Gewicht	Ausgabedatum	Blatt
	2:1	0,042 kg	31.03.2025	1/1





Alle unbemaßten Fasen 0,3x45°
Alle unbemaßten Radien 0,2mm



Werkstückkanten nach DIN ISO 13715.

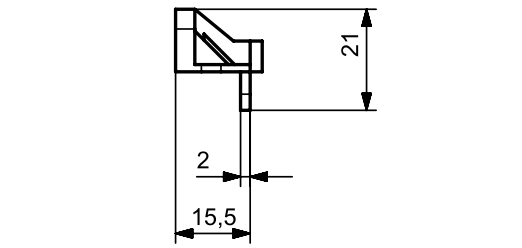
Stückzahl: 1

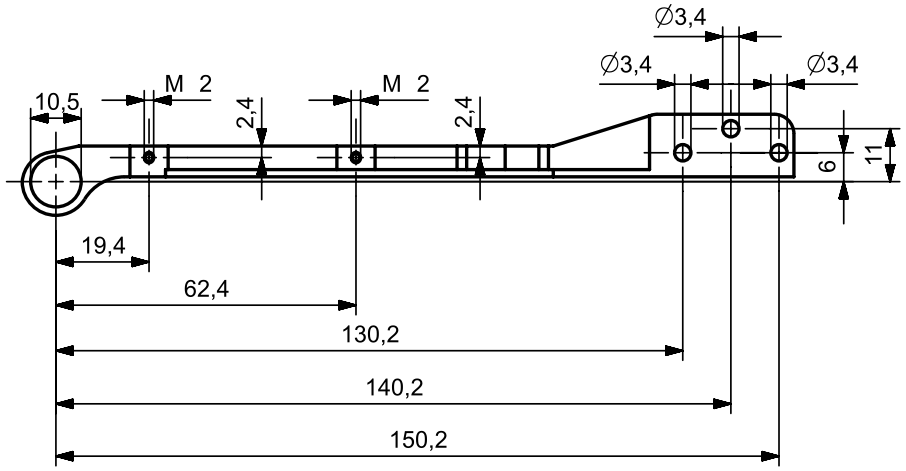
Oberflächenangaben:	Allgemeintoleranz:	Werkstoff:
ISO 1302	DIN ISO 2768-mK	EN-AW 6082-T6

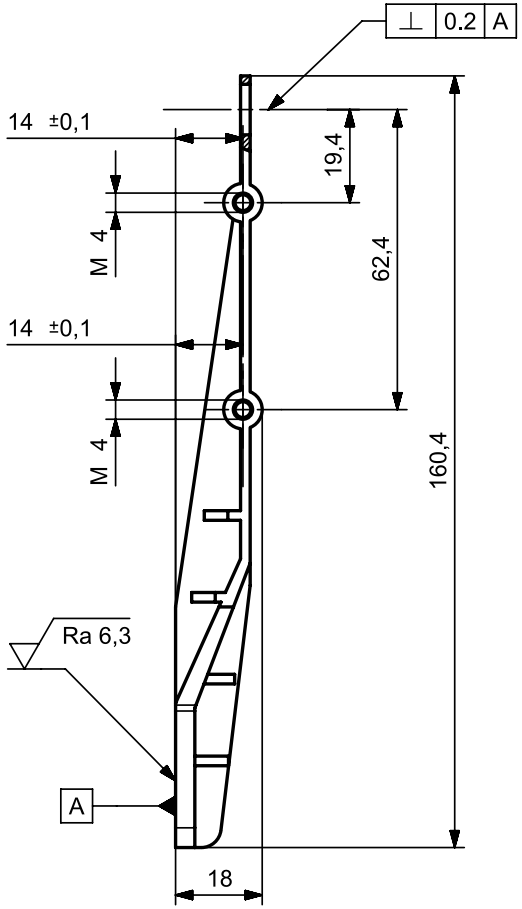
Nennmaß	Größtmaß	Kleinstmaß
30h7	30,000mm	39,967mm

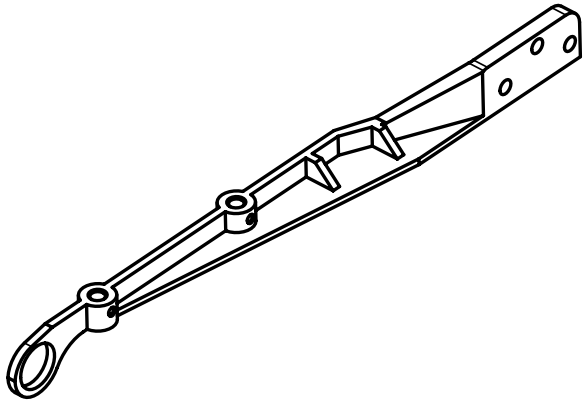
ASTG AEROSPACE TEAM GRAZ

Titel:	Dokumentenart:			
Swivel_Shaftnut	Fertigungszeichnung			
	Maßstab	Gewicht	Ausgabedatum	Blatt
	1:1	-kg	dd.mm.yyyy	1/1









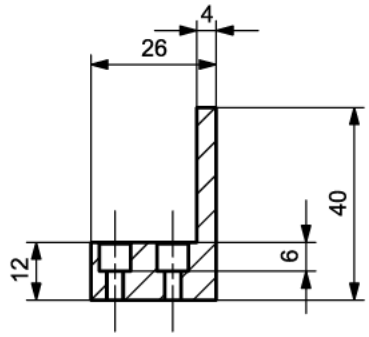
1. Stck.

Fehlende Maße aus .stp Datei
Alle unbemaßten Fasen -
Alle unbemaßten Radien -

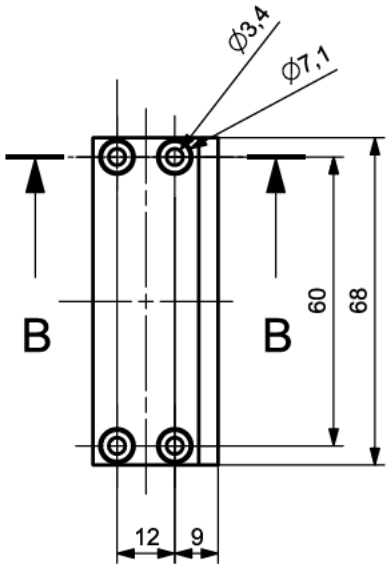
Ra 6,3 -0,50 0,15

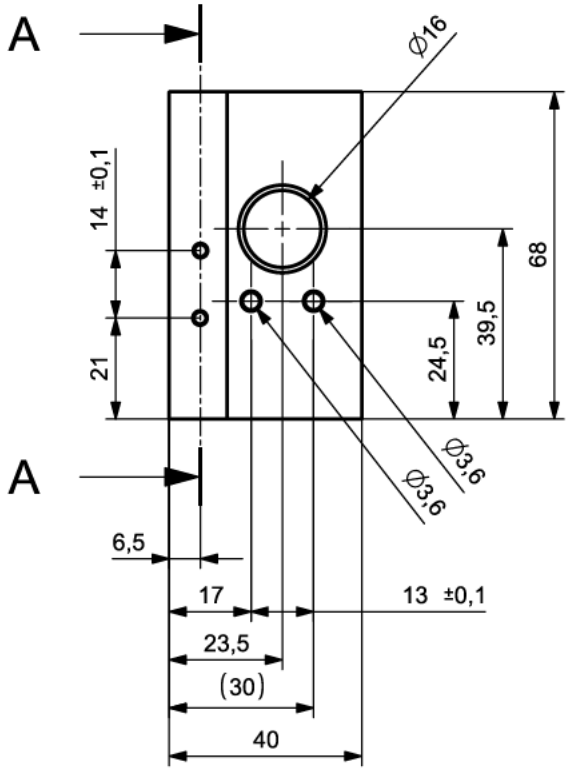
Werkstückkanten nach DIN ISO 13715.

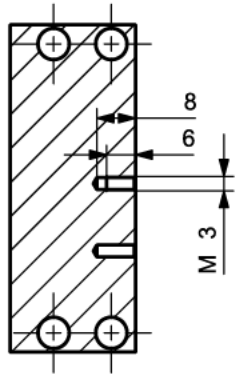
Oberflächenangaben: ISO 1302	Allgemeintoleranz: DIN ISO 2768-mK	Werkstoff: Generic Aluminium			
ASTG AEROSPACE TEAM GRAZ	Titel: 01_Locking_CamCanLock_V01	Dokumentenart: Fertigungszeichnung			
		Maßstab 1:1	Gewicht 15.1 g	Ausgabedatum 19.03.2025	Blatt 1/1



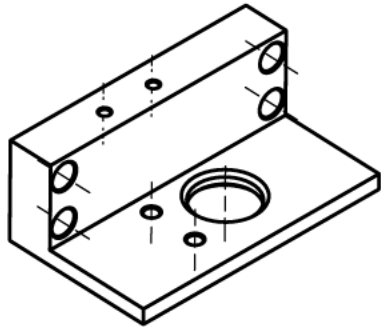
SECTION B-B







SECTION A-A



Ra 6,3

-0,50

0,15

Alle unbemaßten Fasen -
Alle unbemaßten Radien -

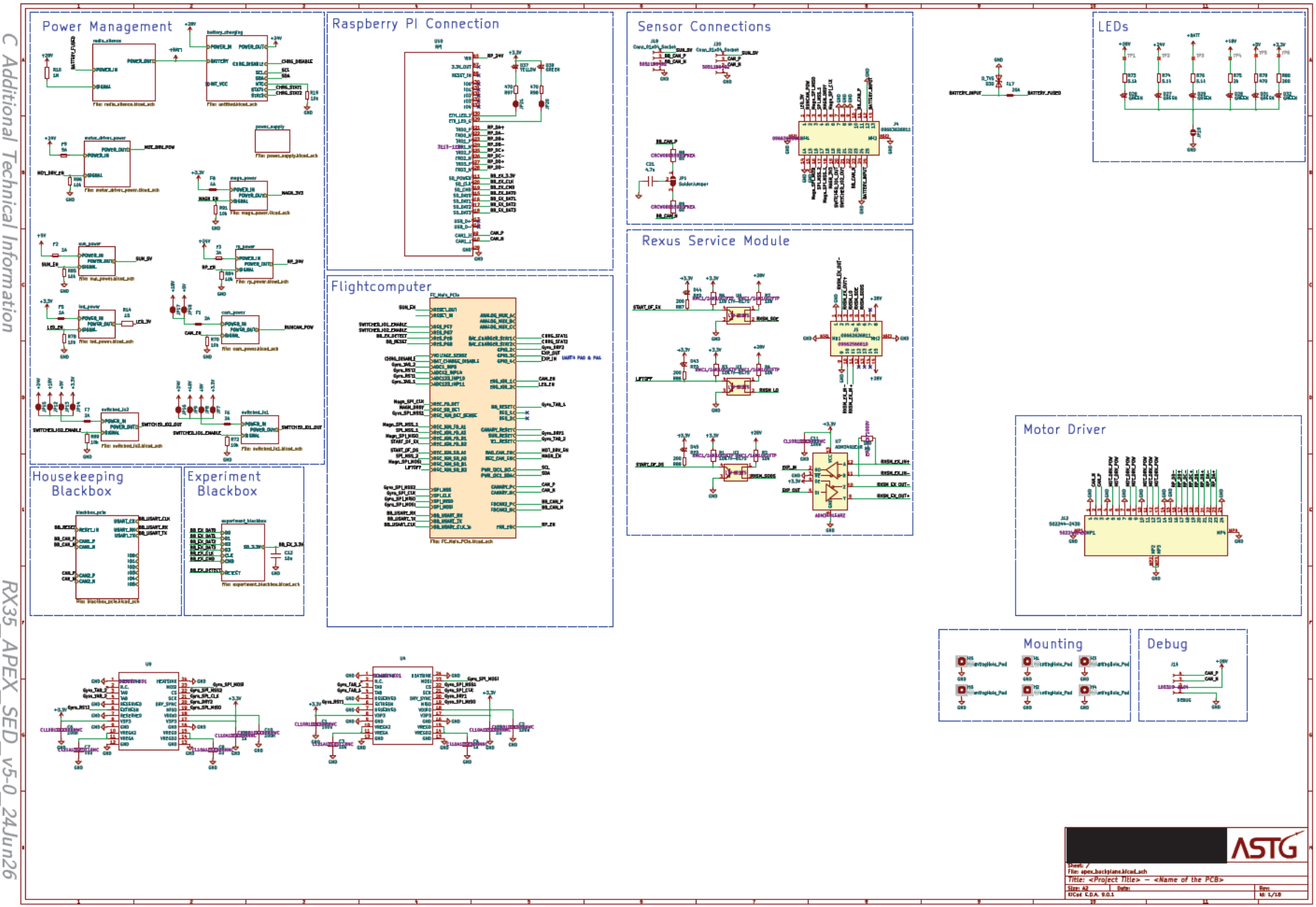
Werkstückkanten nach DIN ISO 13715.

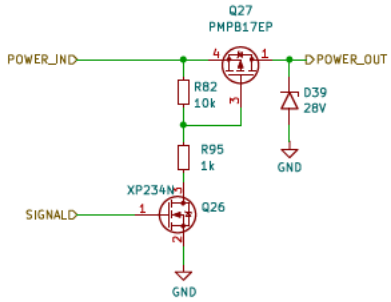
Oberflächenangaben:	Allgemeintoleranz:	Werkstoff:
ISO 1302	DIN ISO 2768-mK	EN-AW 6082-T6

ASTG
AEROSPACE TEAM GRAZ

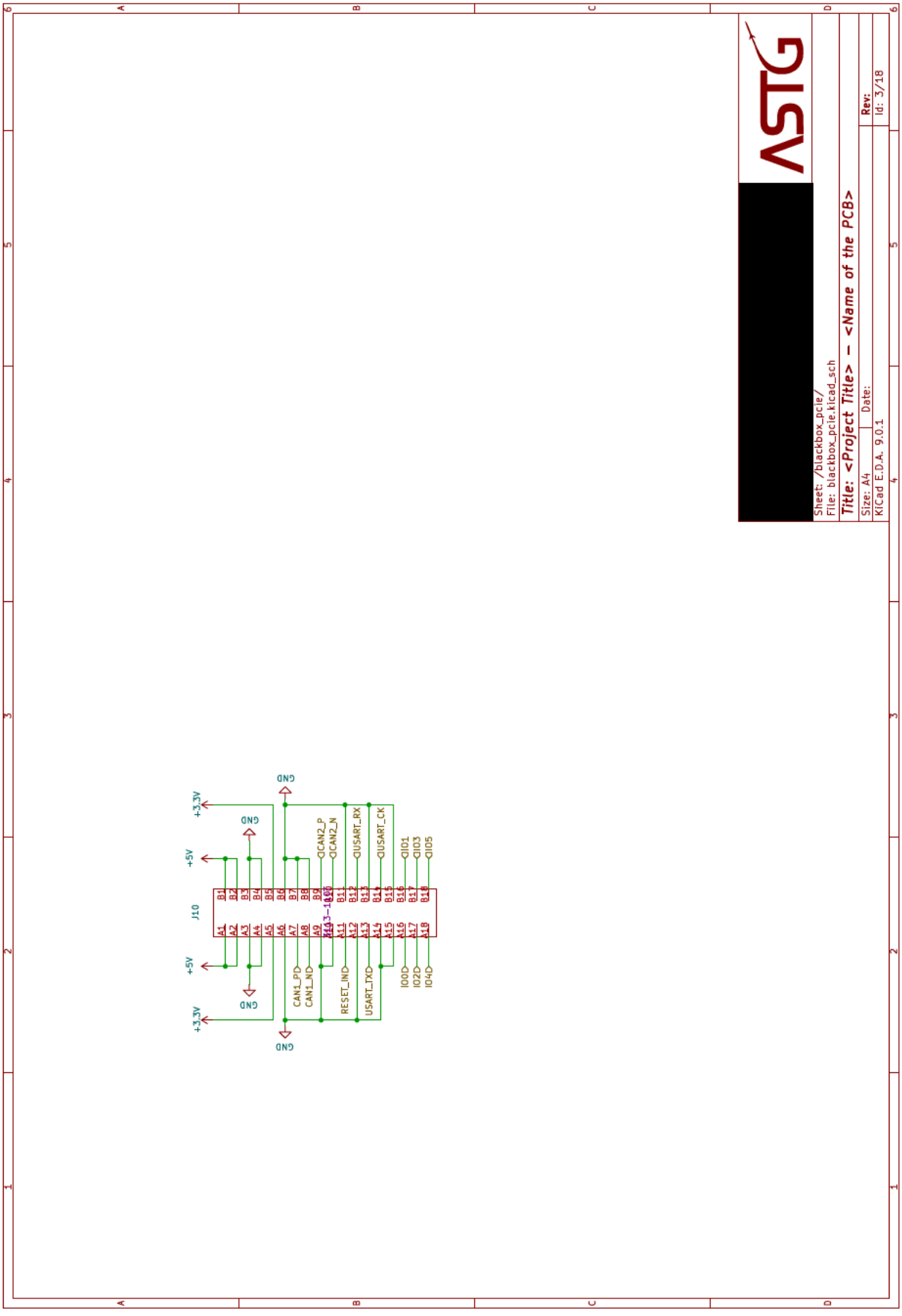
Titel:	Dokumentenart:			
01_Base_Preliminary_PP_adapter	Fertigungszeichnung			
	Maßstab	Gewicht	Ausgabedatum	Blatt
	1:1	0,073 kg	08.04.2025	1/1

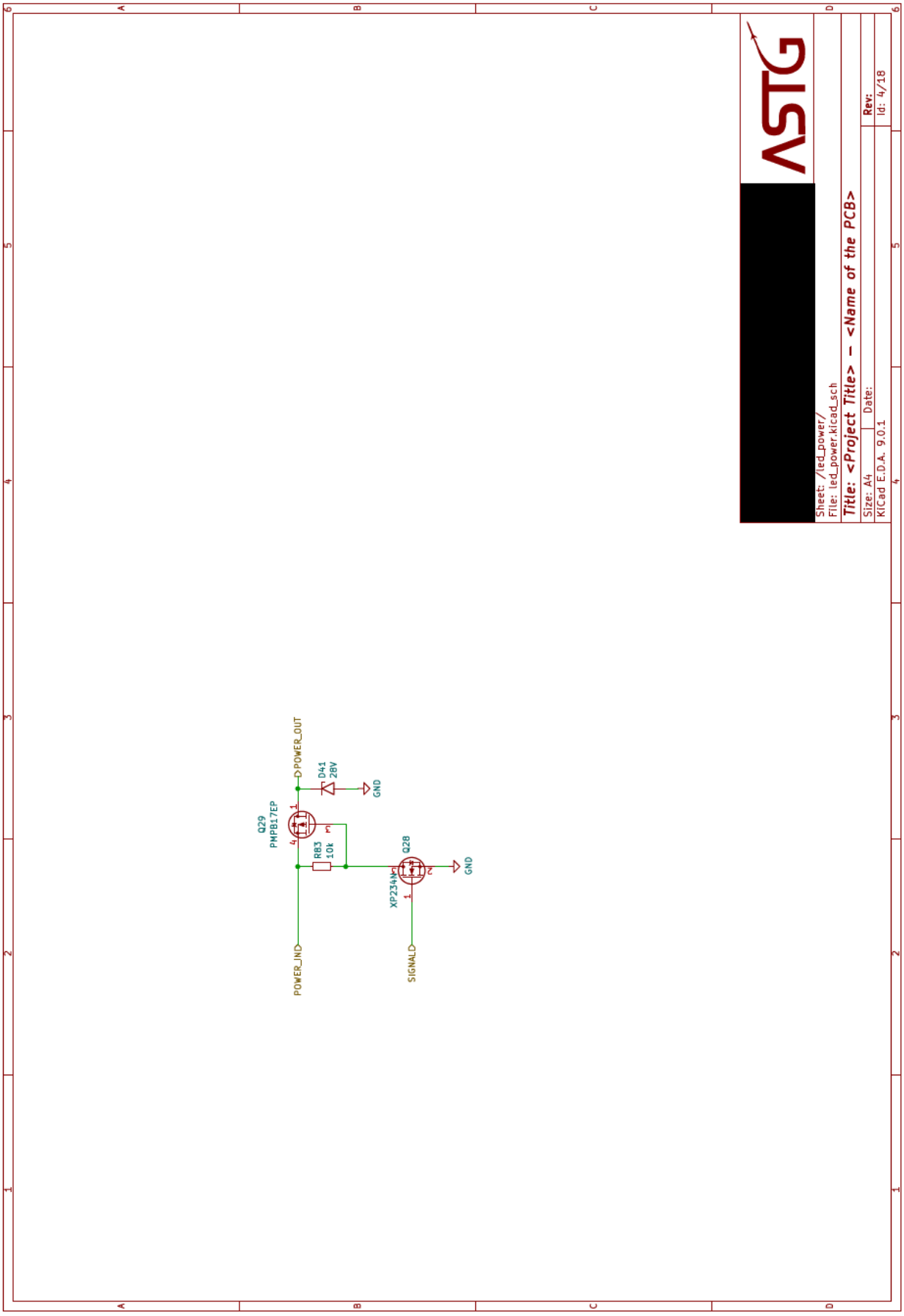
C.3 Electric Schematics

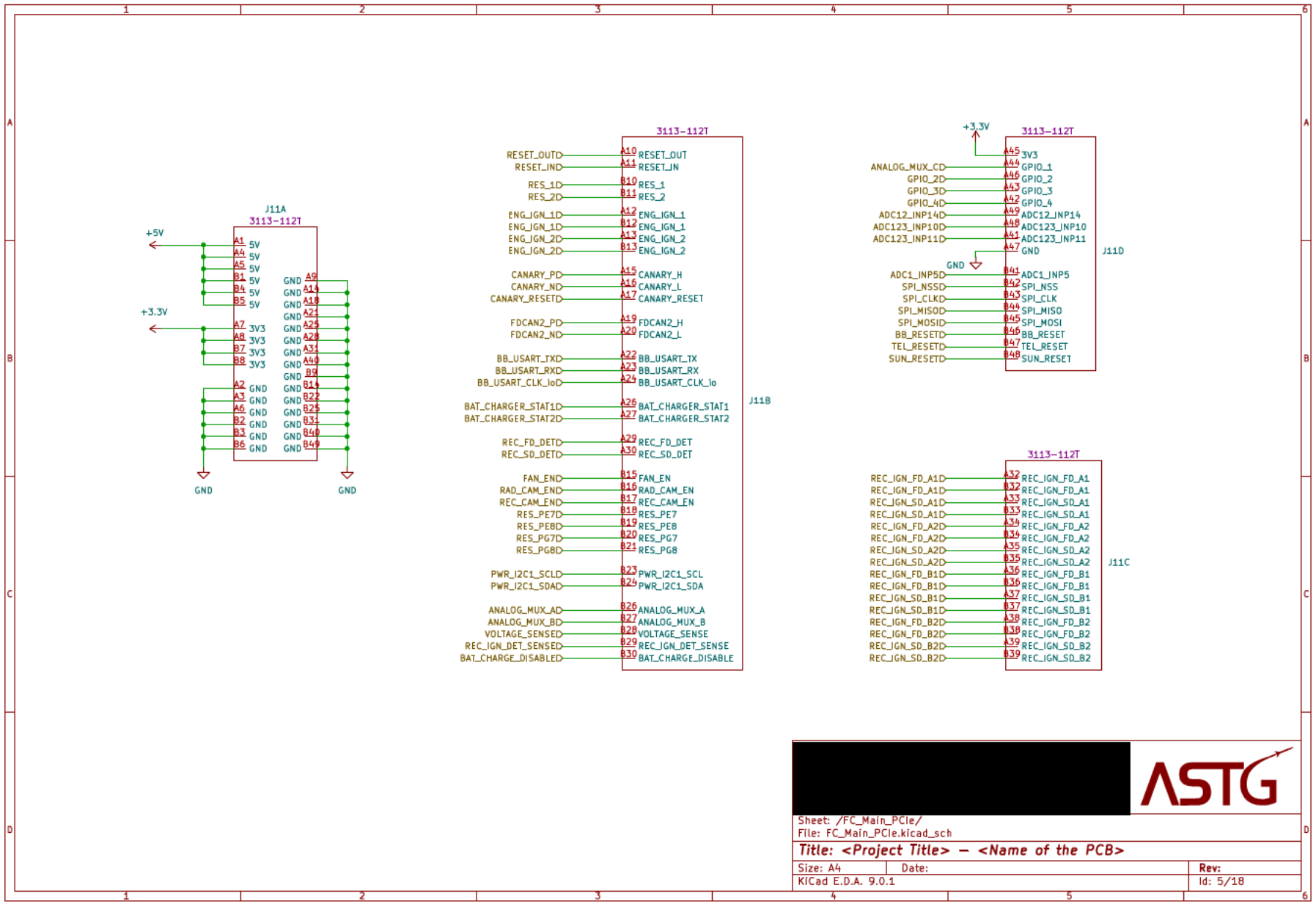

Power Management
Raspberry PI Connection
Sensor Connections
LEDs
Flightcomputer
Rexus Service Module
Housekeeping Blackbox
Experiment Blackbox
Motor Driver
Mounting
Debug
ASTG



Sheet: /rp_power/	
File: rp_power.kicad_sch	
Title: <Project Title> – <Name of the PCB>	
Size: A4	Date:
KiCad E.D.A. 9.0.1	Id: 2/18


ASTG
[redacted]
Sheet: /blackbox_pcie/
File: blackbox_pcie.kicad_sch
Title: <Project Title> – <Name of the PCB>
Size: A4
Date:
Rev:
KiCad E.D.A. 9.0.1
Id: 3/18
J10
+3.3V
+5V
GND
CAN2_P
CAN2_N
USART_RX
USART_CK
IO1
IO3
IO5
CAN1_PD
CAN1_ND
RESET_IND
USART_TXD
IO0D
IO2D
IO4D

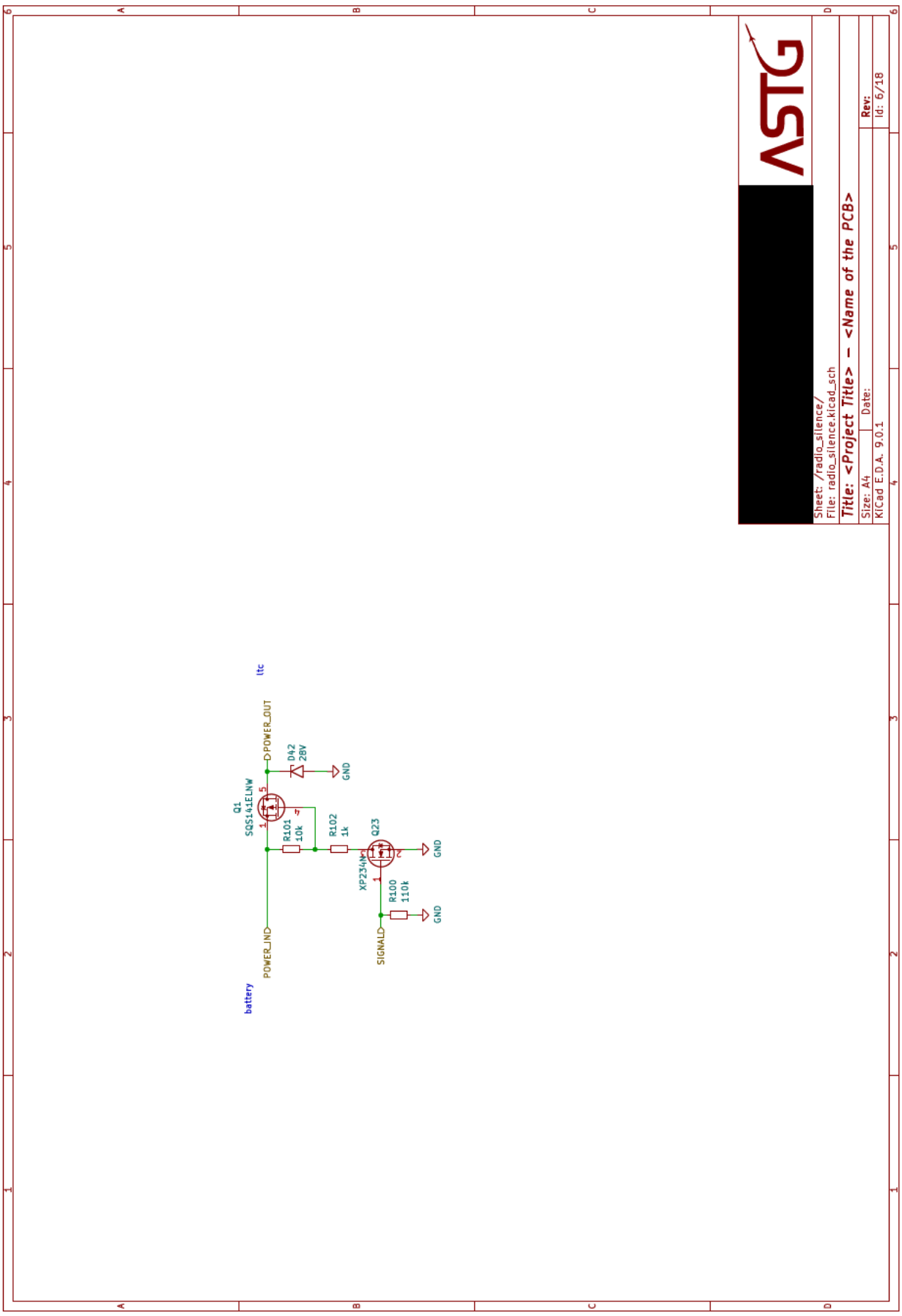

ASTG
[redacted]
Sheet: /led_power/
File: led_power.kicad_sch
Title: <Project Title> – <Name of the PCB>
Size: A4
Date:
Rev:
KiCad E.D.A. 9.0.1
Id: 4/18
POWER_OUT
D41
28V
GND
Q29
PMPB17EP
R83
10k
Q28
XP234W
GND
POWER_IND
SIGNALD

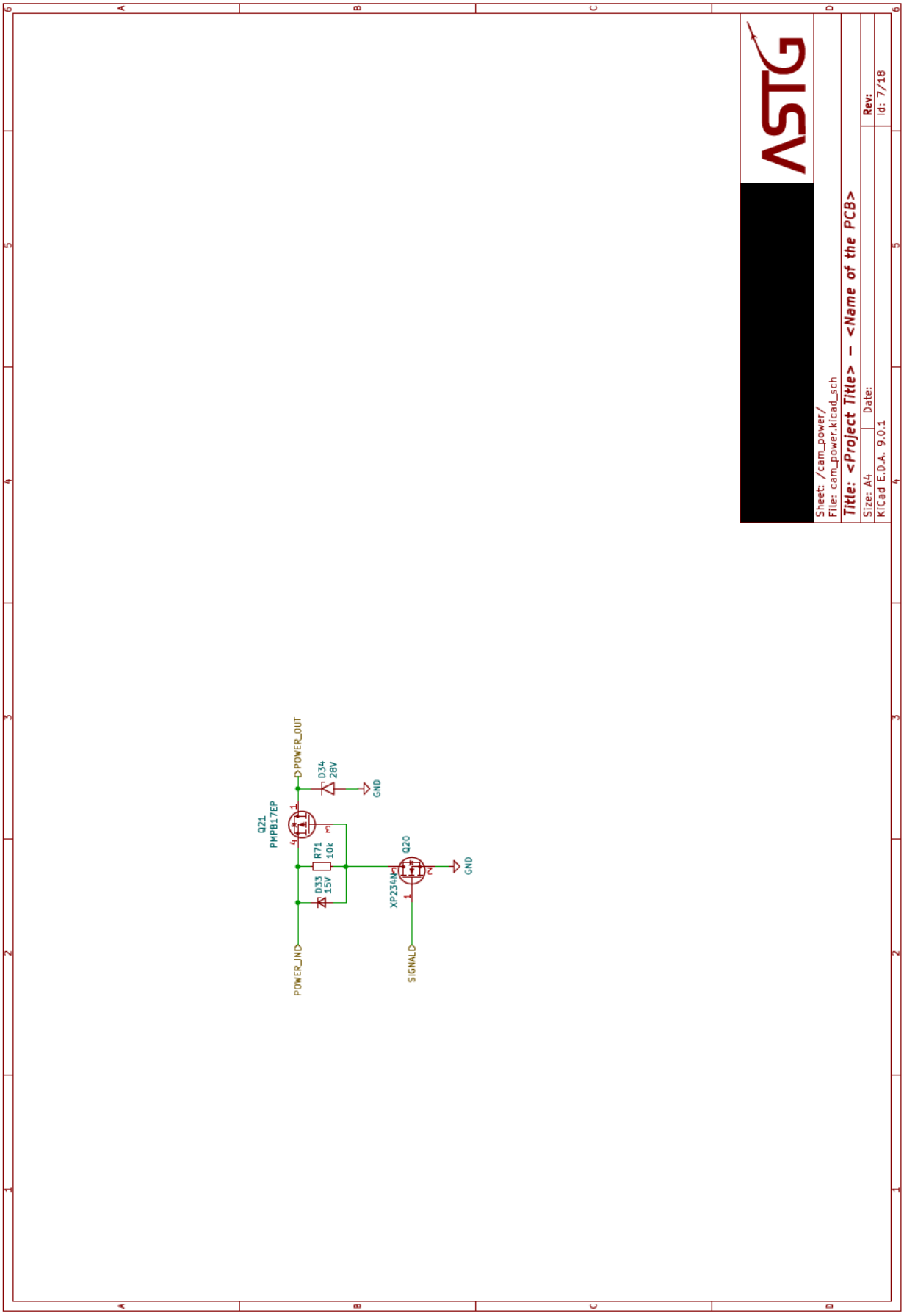


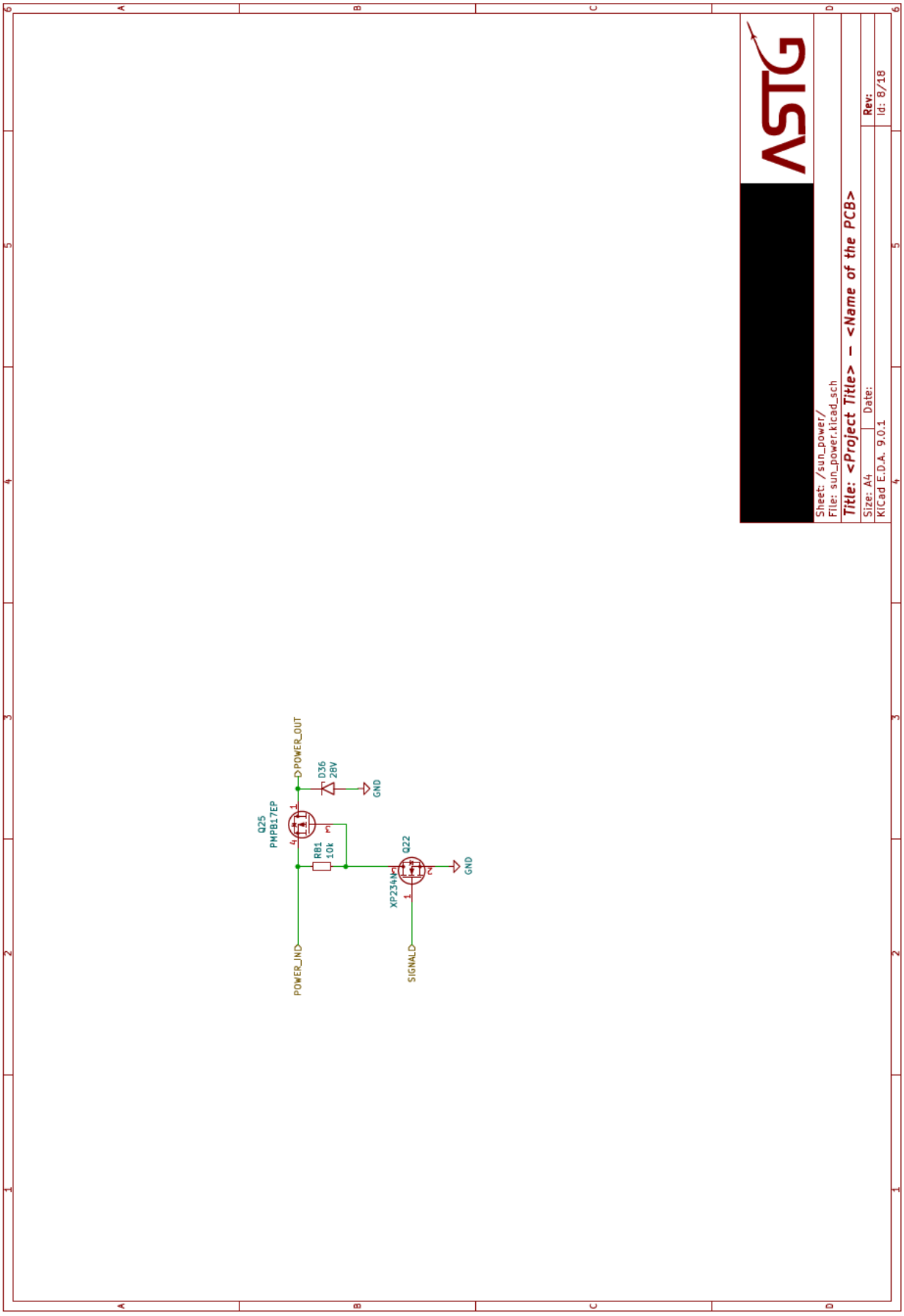
Sheet: /FC_Main_PCIe/
File: FC_Main_PCIe.kicad_sch

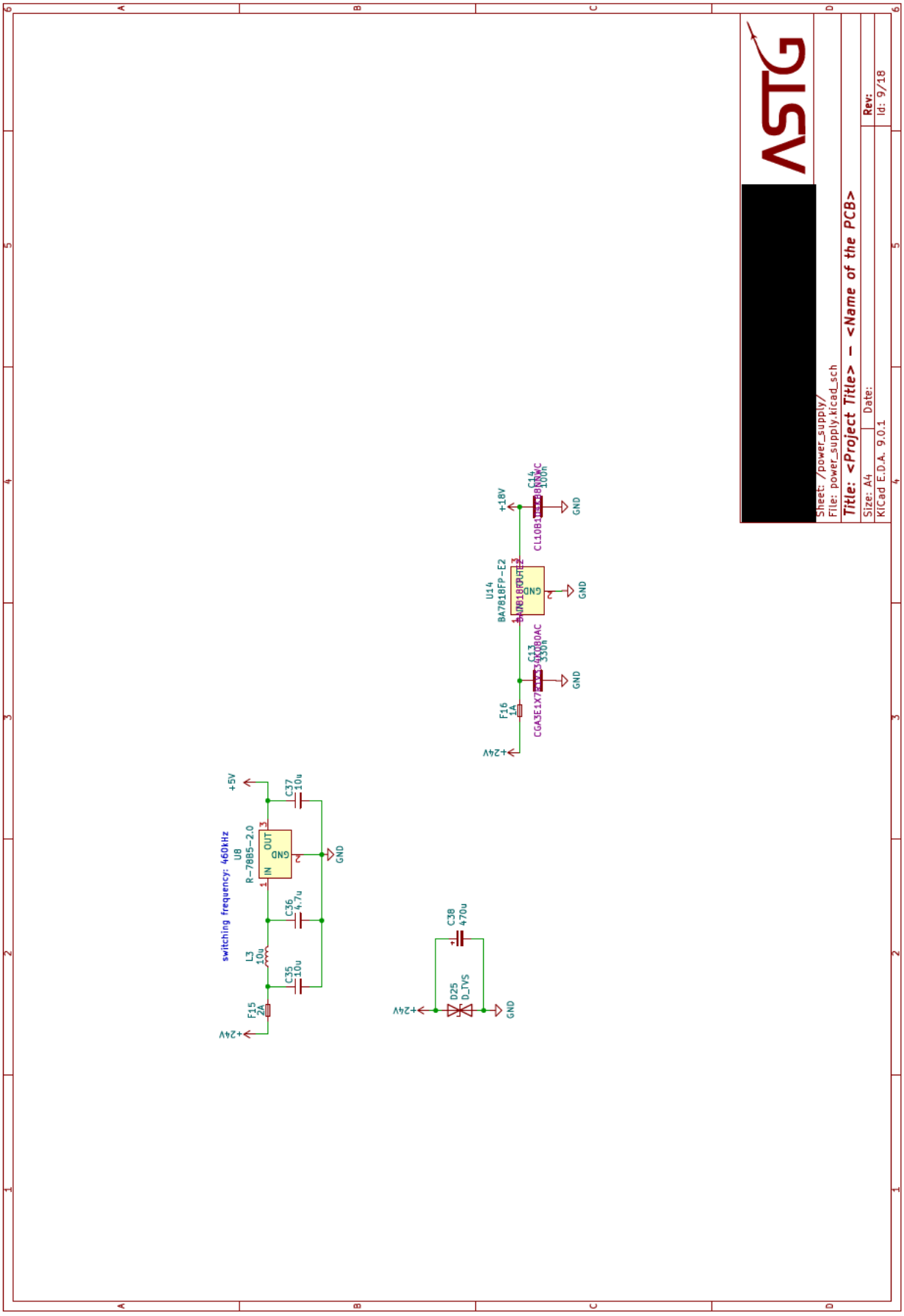
Title: <Project Title> – <Name of the PCB>

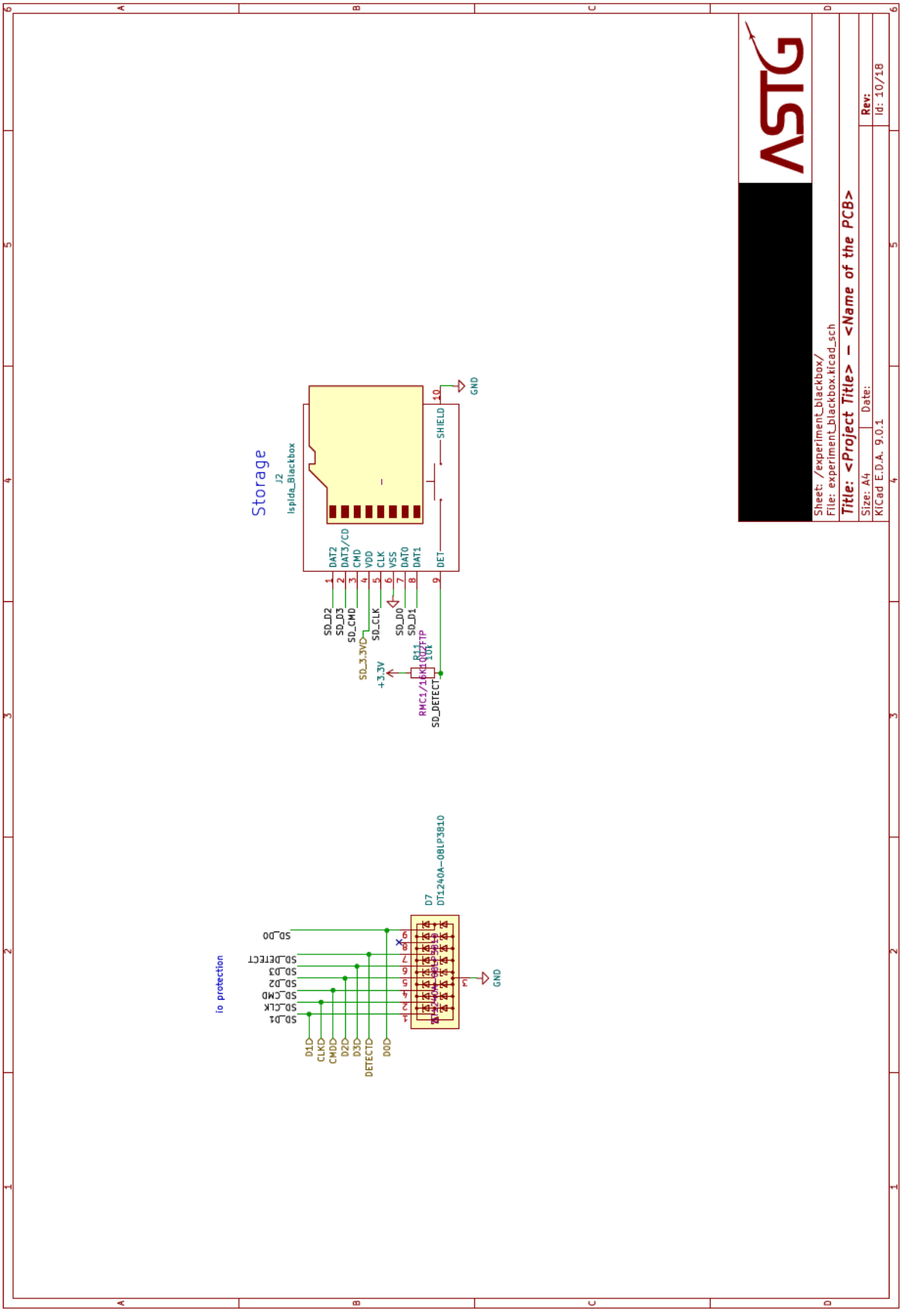
Size: A4	Date:	Rev:
KiCad E.D.A. 9.0.1		Id: 5/18

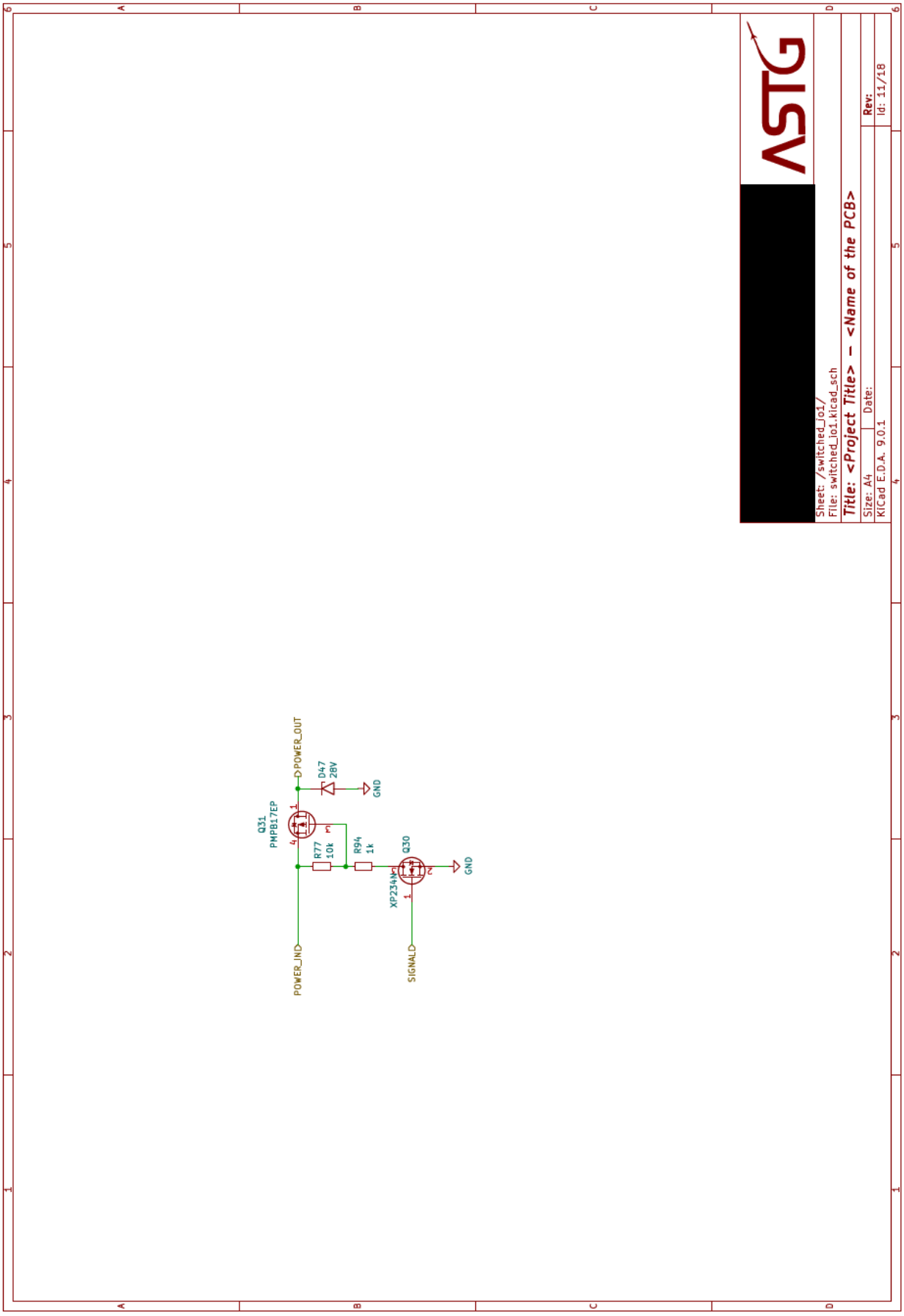

ASTG
[redacted]
Sheet: /radio_silence/
File: radio_silence.kicad_sch
Title: <Project Title> – <Name of the PCB>
Size: A4
Date:
Rev:
KiCad E.D.A. 9.0.1
Id: 6/18
ltc
POWER_OUT
D42
28V
GND
Q1
SQS141ELNW
R101
10k
R102
1k
Q23
XP234M
R100
110k
GND
GND
POWER_IND
SIGNAL
battery

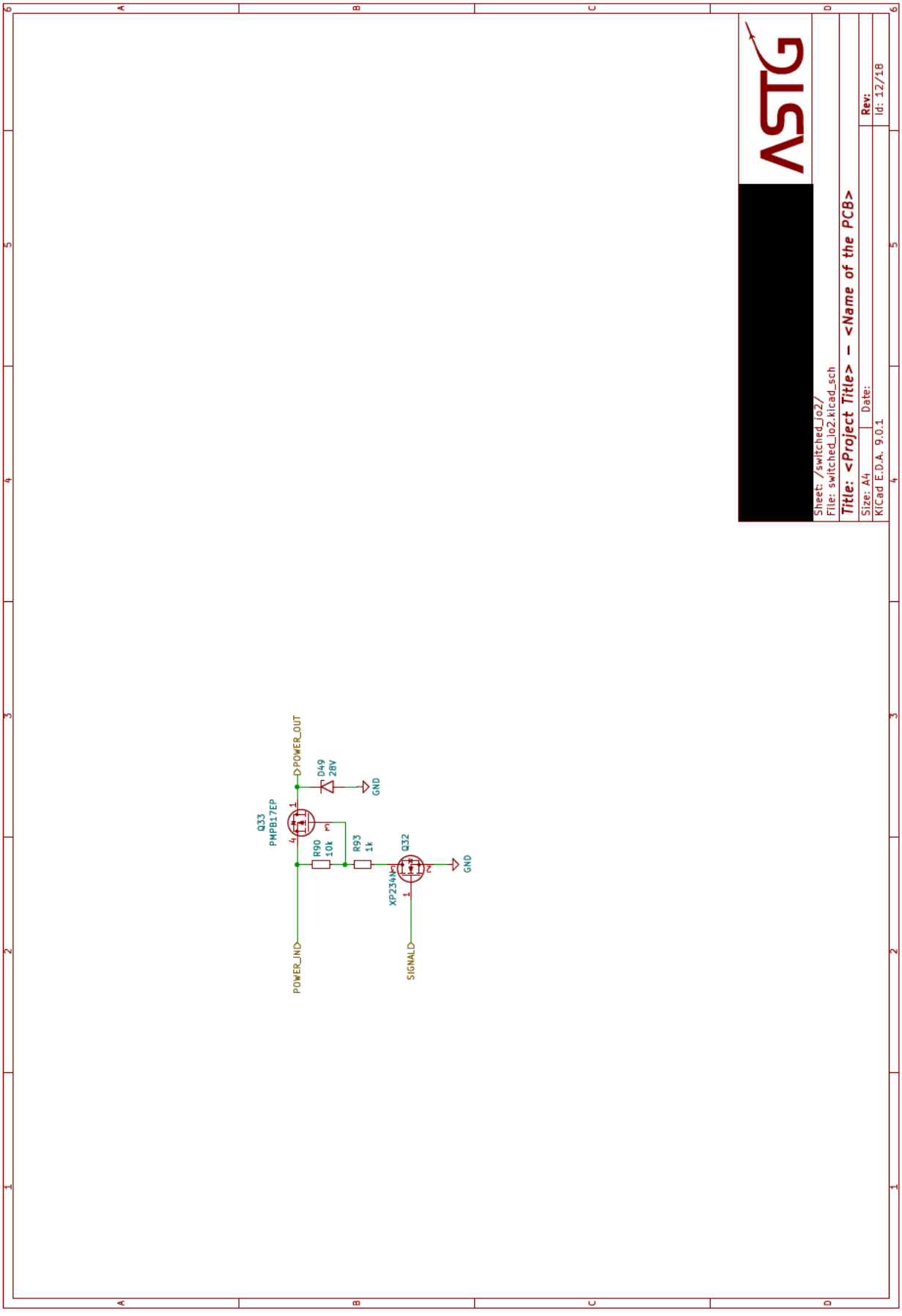

POWER_OUT
D34
28V
GND
Q21
PMPB17EP
R71
10k
D33
15V
Q20
XP234W
GND
POWER_IND
SIGNALD
Sheet: /cam_power/
File: cam_power.kicad_sch
Title: <Project Title> – <Name of the PCB>
Size: A4
Date:
Rev:
KiCad E.D.A. 9.0.1
Id: 7/18

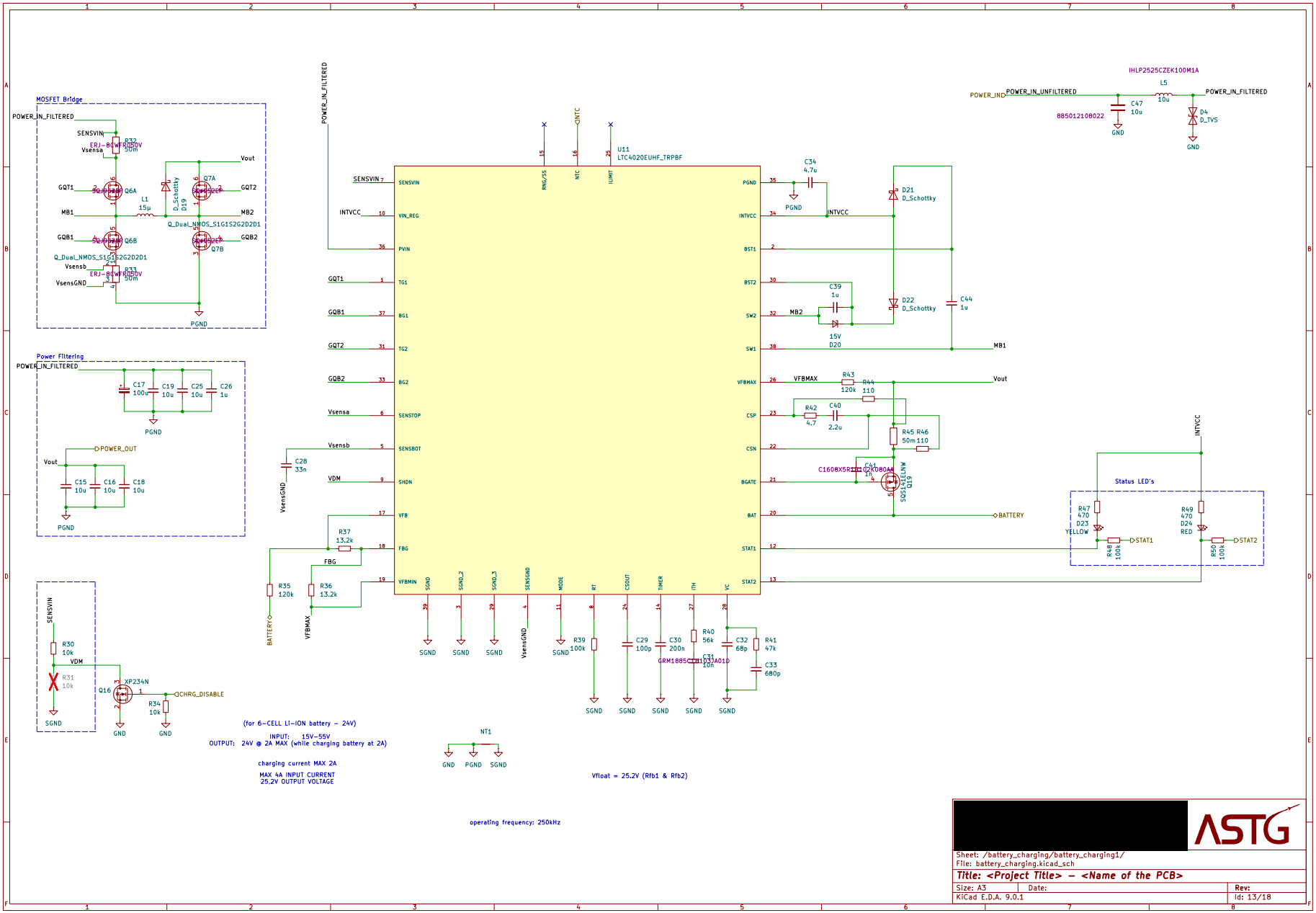

POWER_OUT
D36
28V
GND
Q25
PMPB17EP
R81
10k
Q22
XP234W
GND
POWER_IND
SIGNALD
Sheet: /sun_power/
File: sun_power.kicad_sch
Title: <Project Title> – <Name of the PCB>
Size: A4
Date:
Rev:
KiCad E.D.A. 9.0.1
Id: 8/18

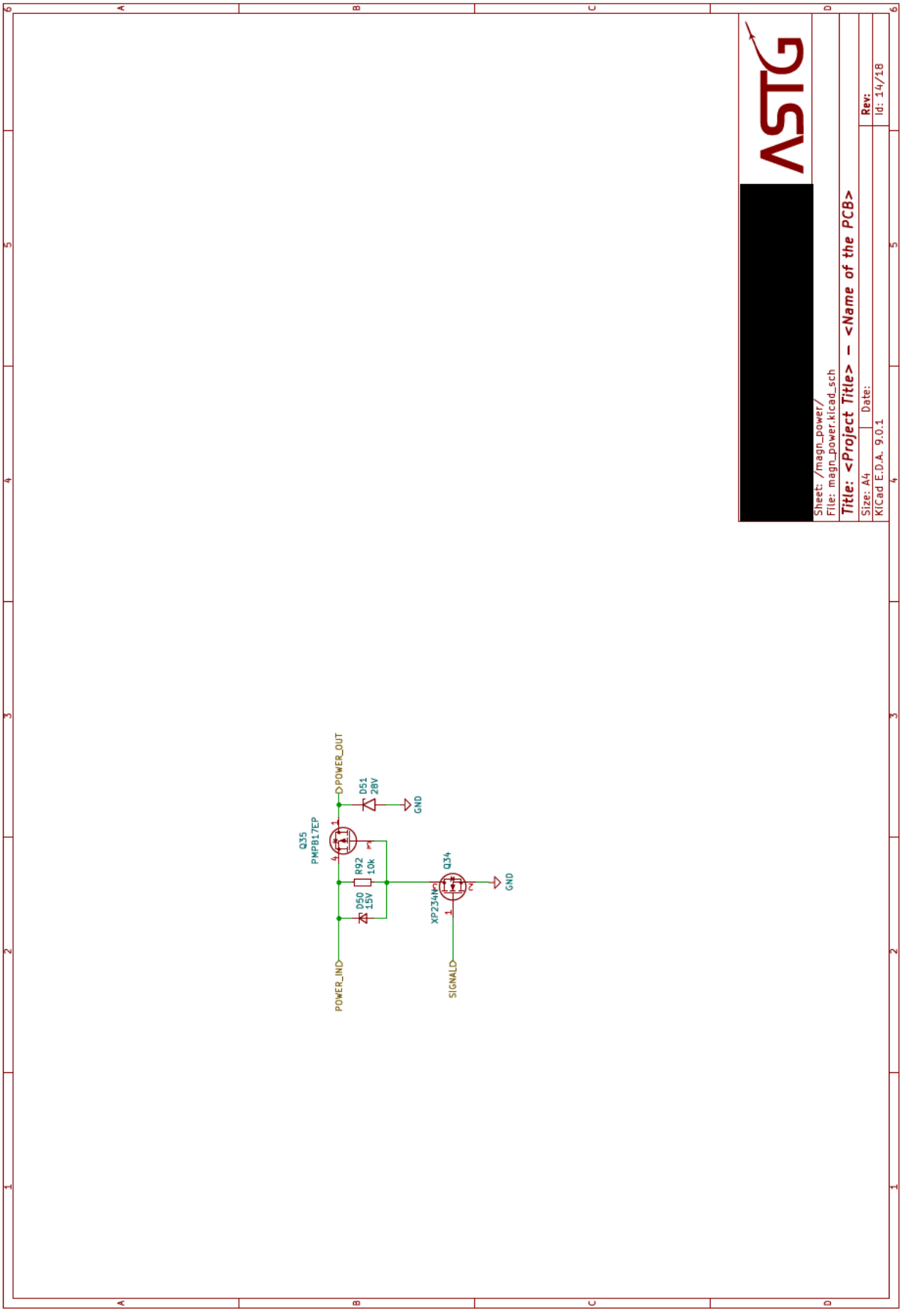

Sheet: /power_supply/
File: power_supply.kicad_sch
Title: <Project Title> – <Name of the PCB>
Size: A4
Date:
Rev:
KiCad E.D.A. 9.0.1
Id: 9/18
+18V
GND
U14
BA7818FP-E2
F16
1A
+24V
switching frequency: 460kHz
U8
R-7885-2.0
+5V
C37
10u
C36
4.7u
C35
10u
L3
10u
F15
2A
C38
470u
D25
D_TVS

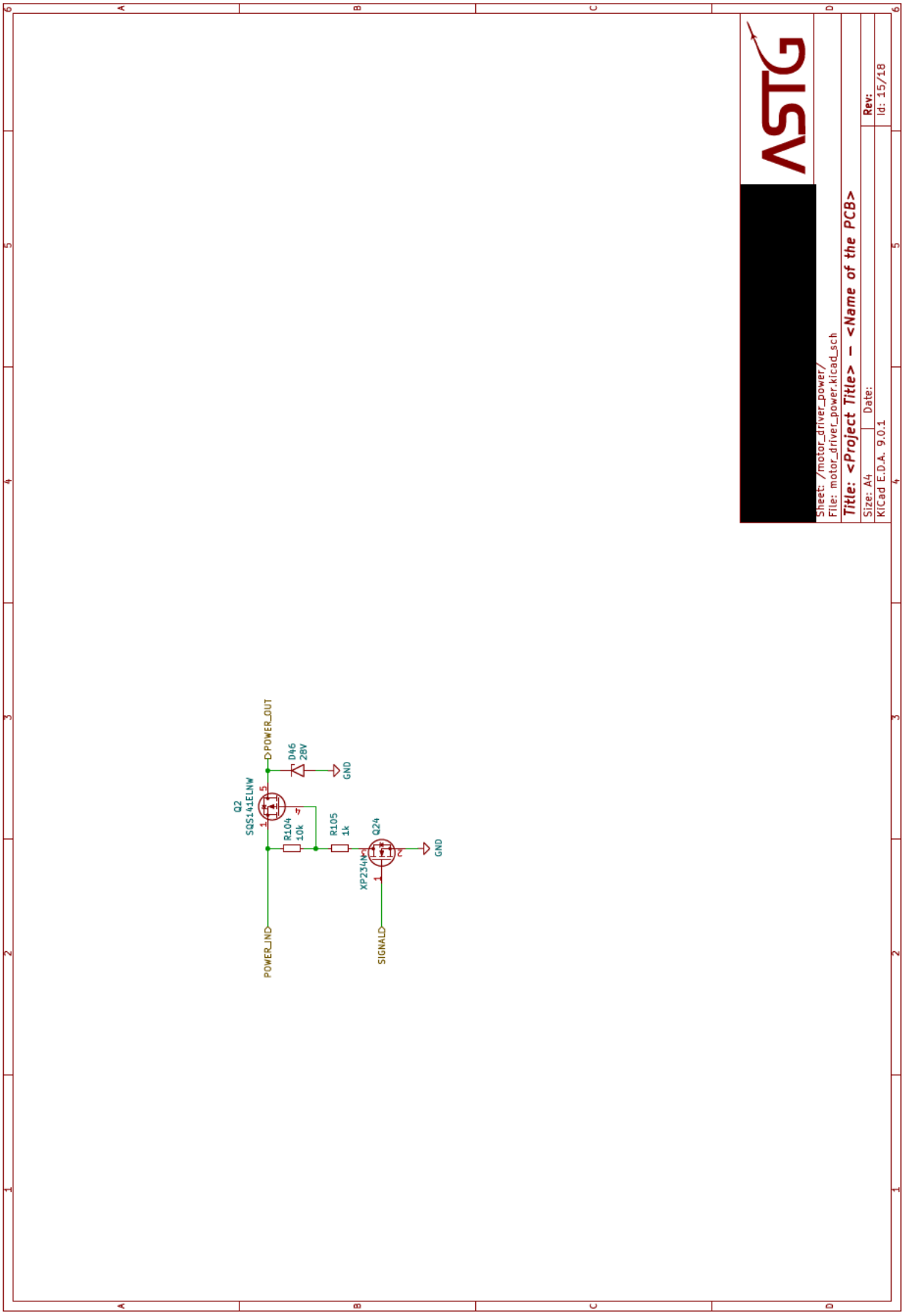

Storage
J2
Isplda_Blackbox
DAT2
DAT3/CD
CMD
VDD
CLK
VSS
DAT0
DAT1
DET
SHIELD
GND
SD_D2
SD_D3
SD_CMD
SD_3.3VO
SD_CLK
SD_D0
SD_D1
+3.3V
RMC1/16K1 R17
10K
SD_DETECT
D7
DT1240A-08LP3810
io protection
SD_D0
SD_DETECT
SD_D3
SD_D2
SD_CMD
SD_CLK
SD_D1
D1D
CLKD
CMDD
D2D
D3D
DETECTD
D0D
GND
Sheet: /experiment_blackbox/
File: experiment_blackbox.kicad_sch
Title: <Project Title> -- <Name of the PCB>
Size: A4
Date:
Rev:
KiCad E.D.A. 9.0.1
Id: 10/18

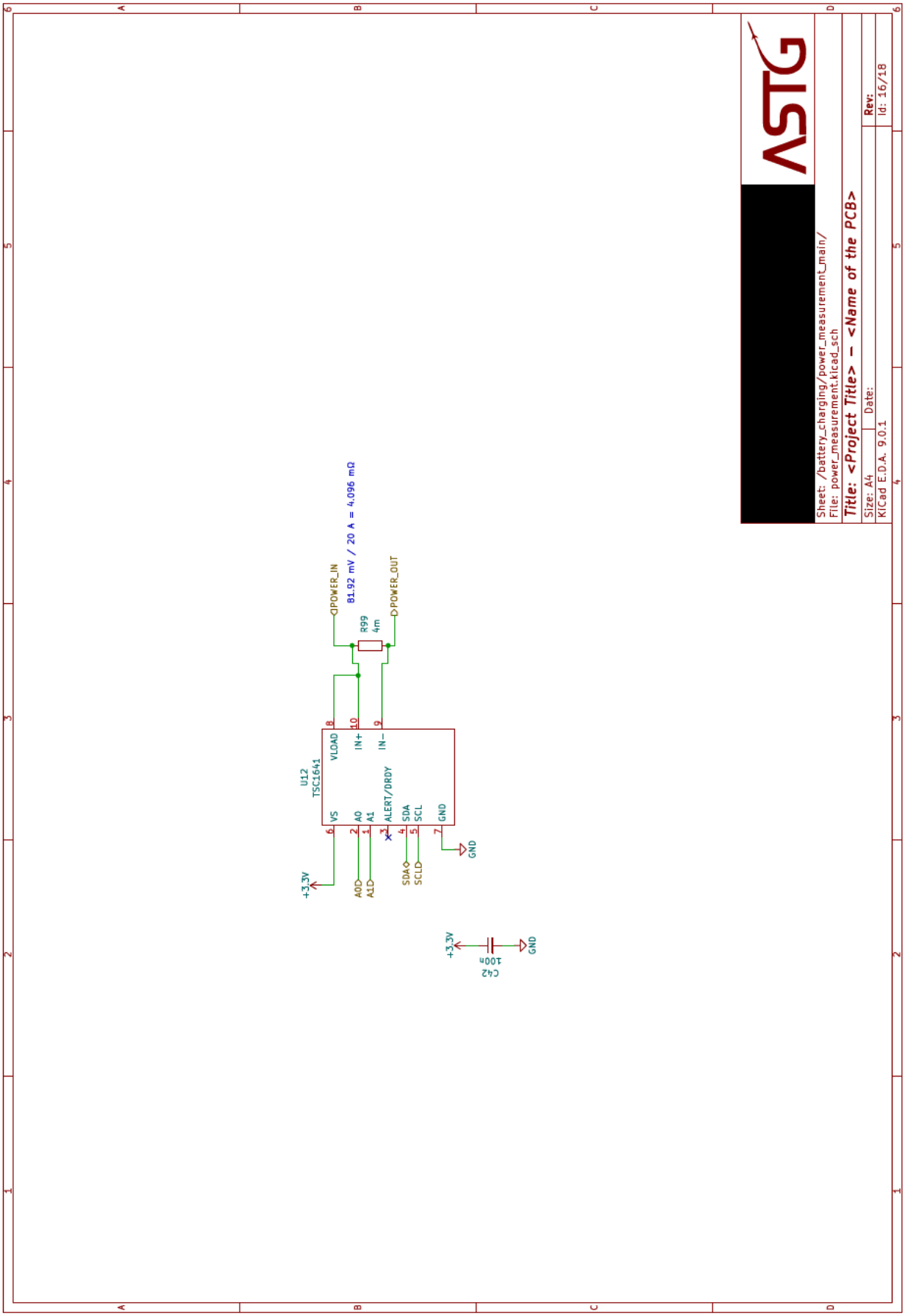

ASTG
[redacted]
Sheet: /switched_io1/
File: switched_io1.kicad_sch
Title: <Project Title> – <Name of the PCB>
Size: A4
Date:
Rev:
KiCad E.D.A. 9.0.1
Id: 11/18
POWER_OUT
D47
28V
GND
Q31
PMPB17EP
R77
10k
R94
1k
Q30
XP234W
GND
POWER_IND
SIGNALD

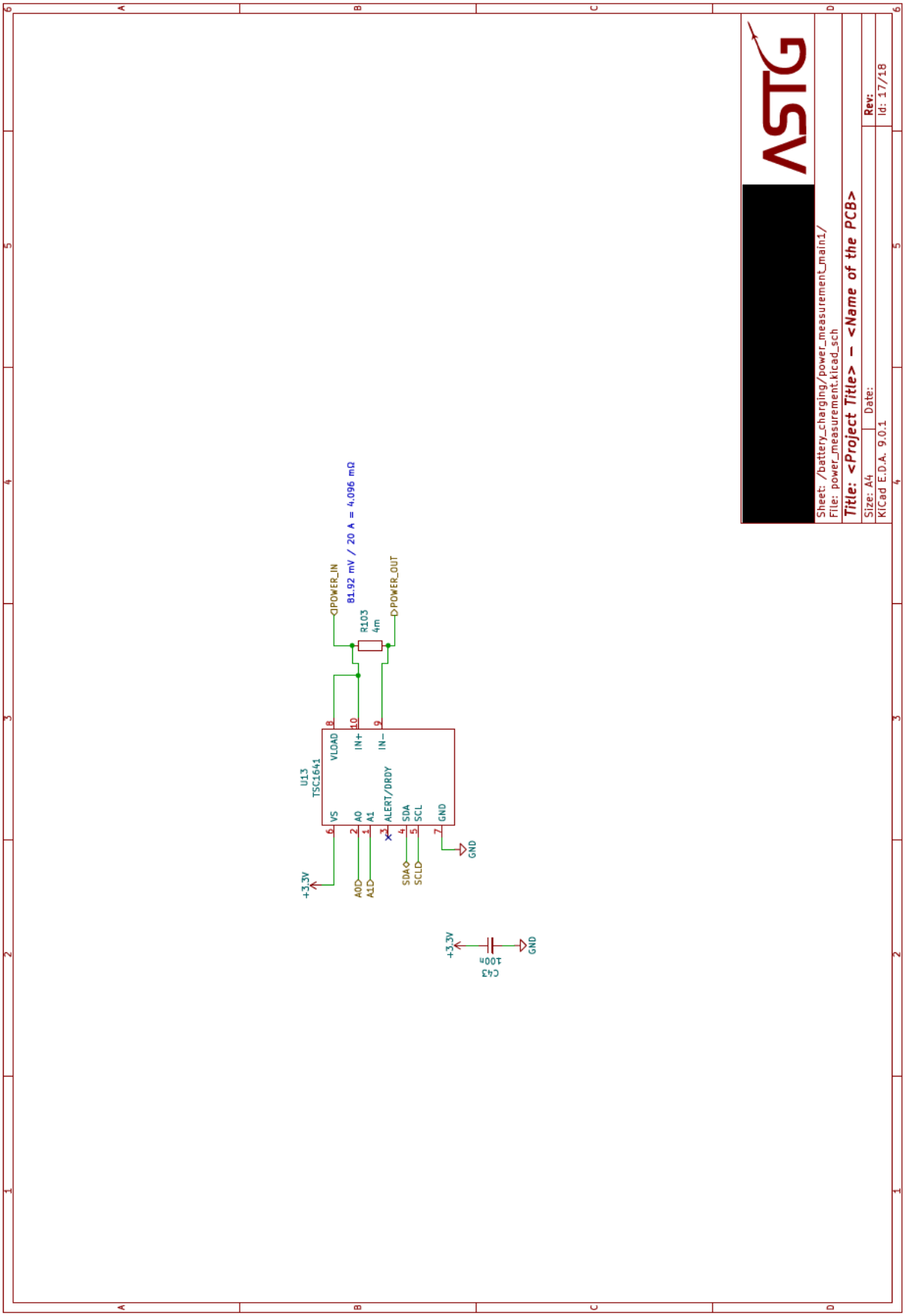

ASTG
Sheet: /switched_io2/
File: switched_io2.kicad_sch
Title: <Project Title> – <Name of the PCB>
Size: A4
Date:
Rev:
KiCad E.D.A. 9.0.1
Id: 12/18
POWER_OUT
D49
28V
GND
Q33
PMPB17EP
R90
10k
R93
1k
Q32
XP234W
GND
POWER_IND
SIGNALD

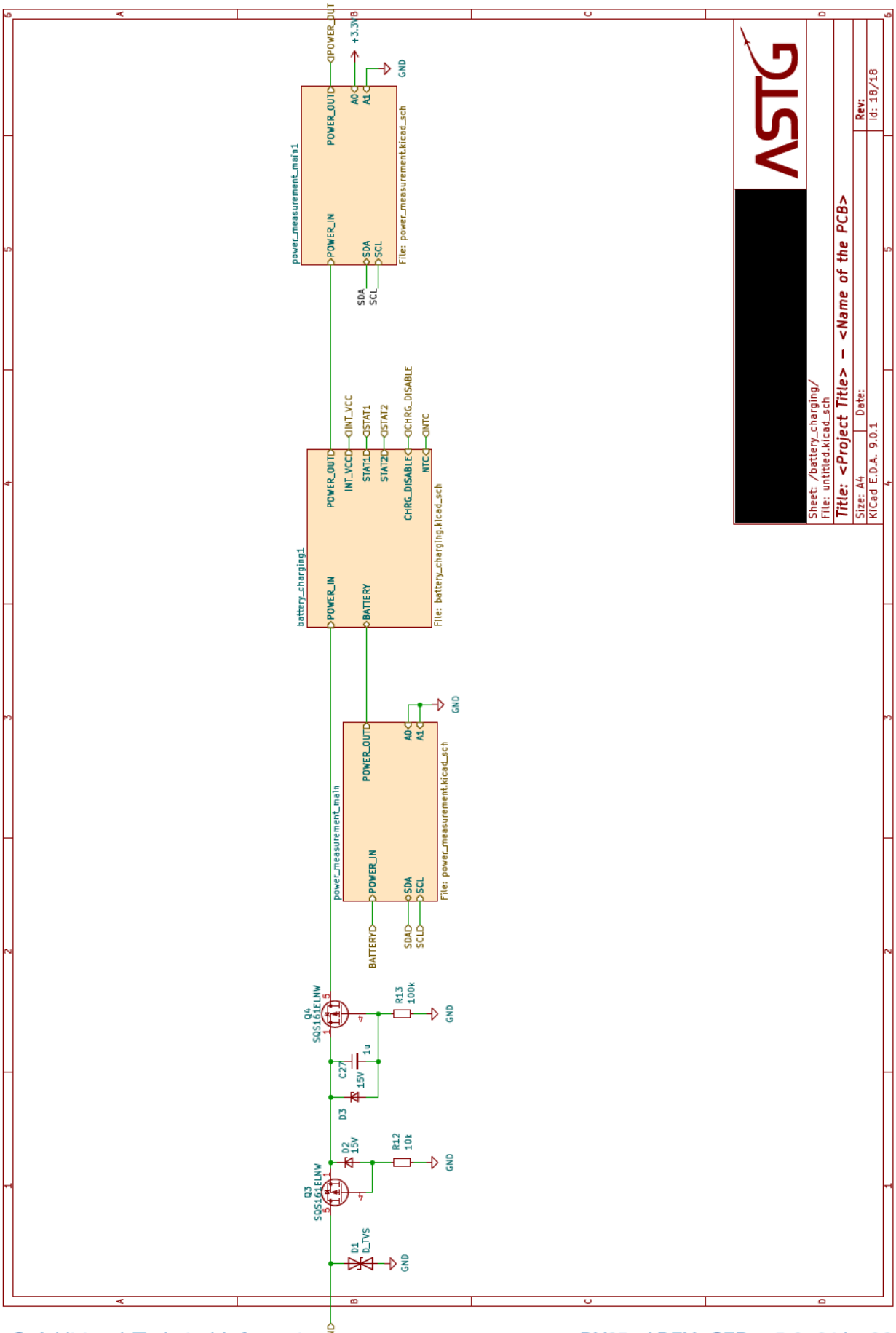

MOSFET Bridge
Power Filtering
U11
LTC4020EUHF_TRPBF
IHLP2525CZEK100M1A
Status LED's
(for 6-CELL LI-ION battery - 24V)
INPUT: 15V-55V
OUTPUT: 24V @ 2A MAX (while charging battery at 2A)
charging current MAX 2A
MAX 4A INPUT CURRENT
25.2V OUTPUT VOLTAGE
Vfloat = 25.2V (Rfb1 & Rfb2)
operating frequency: 250kHz
Sheet: /battery_charging/battery_charging1/
File: battery_charging.kicad_sch
Title: <Project Title> - <Name of the PCB>
Size: A3
Date:
Rev:
KiCad E.D.A. 9.0.1
Id: 13/18

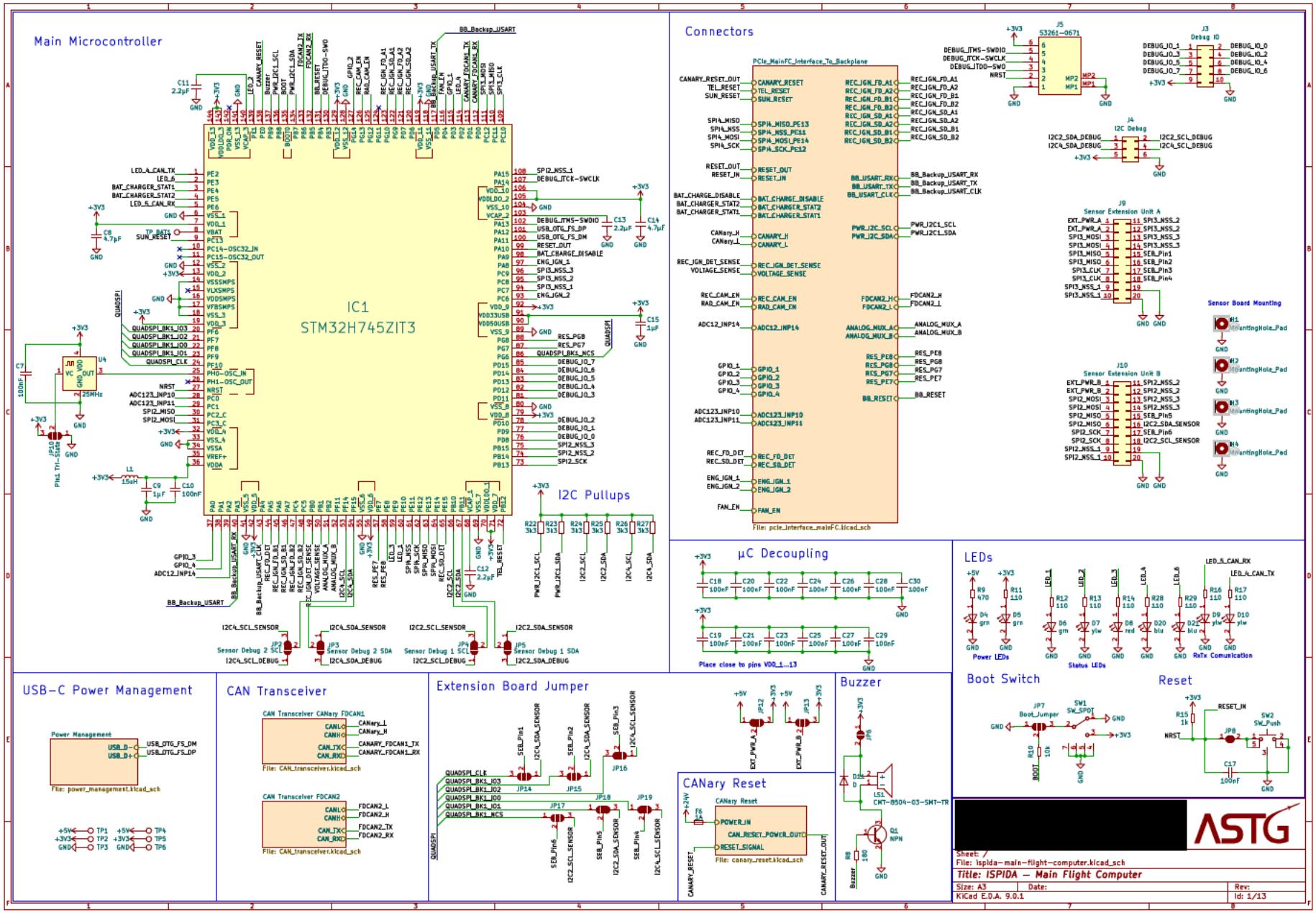

ASTG
[redacted]
Sheet: /magn_power/
File: magn_power.kicad_sch
Title: <Project Title> – <Name of the PCB>
Size: A4
Date:
Rev:
KiCad E.D.A. 9.0.1
Id: 14/18
POWER_OUT
D51
28V
GND
Q35
PMPB17EP
R92
10k
D50
15V
Q34
XP234M
GND
POWER_IND
SIGNALD


ASTG
[redacted]
Sheet: /motor_driver_power/
File: motor_driver_power.kicad_sch
Title: <Project Title> -- <Name of the PCB>
Size: A4
Date:
Rev:
KiCad E.D.A. 9.0.1
Id: 15/18
POWER_OUT
D46
28V
GND
Q2
SQS141ELNW
R104
10k
R105
1k
Q24
XP234N
GND
POWER_IND
SIGNAL_D


ASTG
Sheet: /battery_charging/power_measurement_main/
File: power_measurement.kicad_sch
Title: <Project Title> – <Name of the PCB>
Size: A4
Date:
Rev:
KiCad E.D.A. 9.0.1
Id: 16/18
POWER_IN
81.92 mV / 20 A = 4.096 mΩ
R99
4m
POWER_OUT
U12
TSC1641
VLOAD
IN+
IN–
VS
A0
A1
ALERT/DRDY
SDA
SCL
GND
+3.3V
A0
A1
SDA
SCL
GND
+3.3V
C42
100n
GND

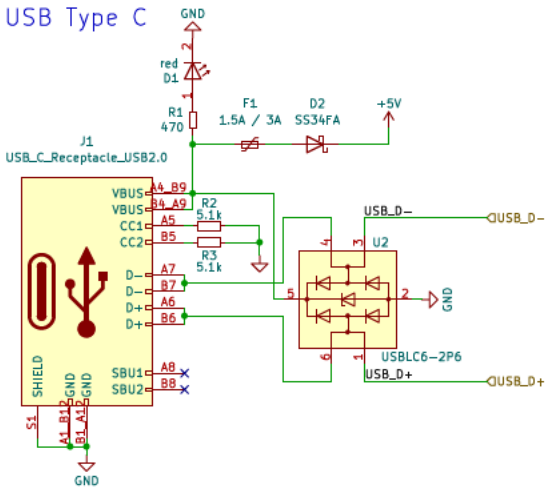

ASTG
Sheet: /battery_charging/power_measurement_main1/
File: power_measurement.kicad_sch
Title: <Project Title> -- <Name of the PCB>
Size: A4
Date:
Rev:
KiCad E.D.A. 9.0.1
Id: 17/18
81.92 mV / 20 A = 4.096 mΩ
POWER_IN
POWER_OUT
R103
4m
U13
TSC1641
VLOAD
IN+
IN-
VS
A0
A1
ALERT/DRDY
SDA
SCL
GND
+3.3V
A0D
A1D
SDAD
SCLD
C43
100n

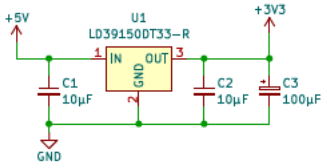

POWER_OUT
+3.3VB
GND
power_measurement_main1
POWER_IN
POWER_OUT
A0
A1
SDA
SCL
File: power_measurement.kicad_sch
battery_charging1
INT_VCC
STAT1
STAT2
CHRG_DISABLE
NTC
File: battery_charging.kicad_sch
power_measurement_main
BATTERY
BATTERY
SDA
SCL
Q4
SQS161ELNW
R13
100k
C27
1u
15V
D3
D2
15V
R12
10k
Q3
SQS161ELNW
D1
D_TVS
ASTG
Sheet: /battery_charging/
File: untitled.kicad_sch
Title: <Project Title> – <Name of the PCB>
Size: A4
Date:
Rev:
KiCad E.D.A. 9.0.1
Id: 18/18


Main Microcontroller
IC1
STM32H745ZIT3
Connectors
PCIe_MainFC_Interface_To_Backplane
File: pcie_interface_mainFC.kicad_sch
J5
53261-0671
J3
Debug IO
J4
I2C Debug
J9
Sensor Extension Unit A
J10
Sensor Extension Unit B
Sensor Board Mounting
I2C Pullups
µC Decoupling
Place close to pins VDD_1...13
LEDs
Power LEDs
Status LEDs
RxTx Comunication
Boot Switch
Reset
USB-C Power Management
File: power_management.kicad_sch
CAN Transceiver
CAN Transceiver CANary FDCAN1
CAN Transceiver FDCAN2
File: CAN_transceiver.kicad_sch
Extension Board Jumper
Buzzer
CANary Reset
File: canary_reset.kicad_sch
Sheet: /
File: ispida-main-flight-computer.kicad_sch
Title: ISPIDA - Main Flight Computer
Size: A3
Date:
Rev:
KiCad E.D.A. 9.0.1
Id: 1/13

Hierarchical Sheet
Sheet: Power Management
File: power_management.kicad_sch
Hierarchical Main Sheet: ispida-main-flight-computer.kicad_sch

Same Sheets: –
Power Supply and Regulator





ASTG

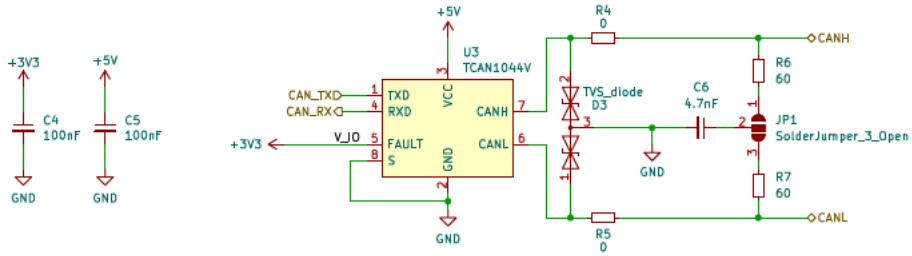
Sheet: /Power Management/
File: power_management.kicad_sch

Title: ISPIDA – Main Flight Computer

Size: A4	Date:	Rev:
KiCad E.D.A. 9.0.1		Id: 2/13

Hierarchical Sheet
Sheet: CAN Transceiver CANary FDCAN1
File: CAN_transceiver.kicad_sch
Hierarchical Main Sheet: ispida-main-flight-computer.kicad_sch

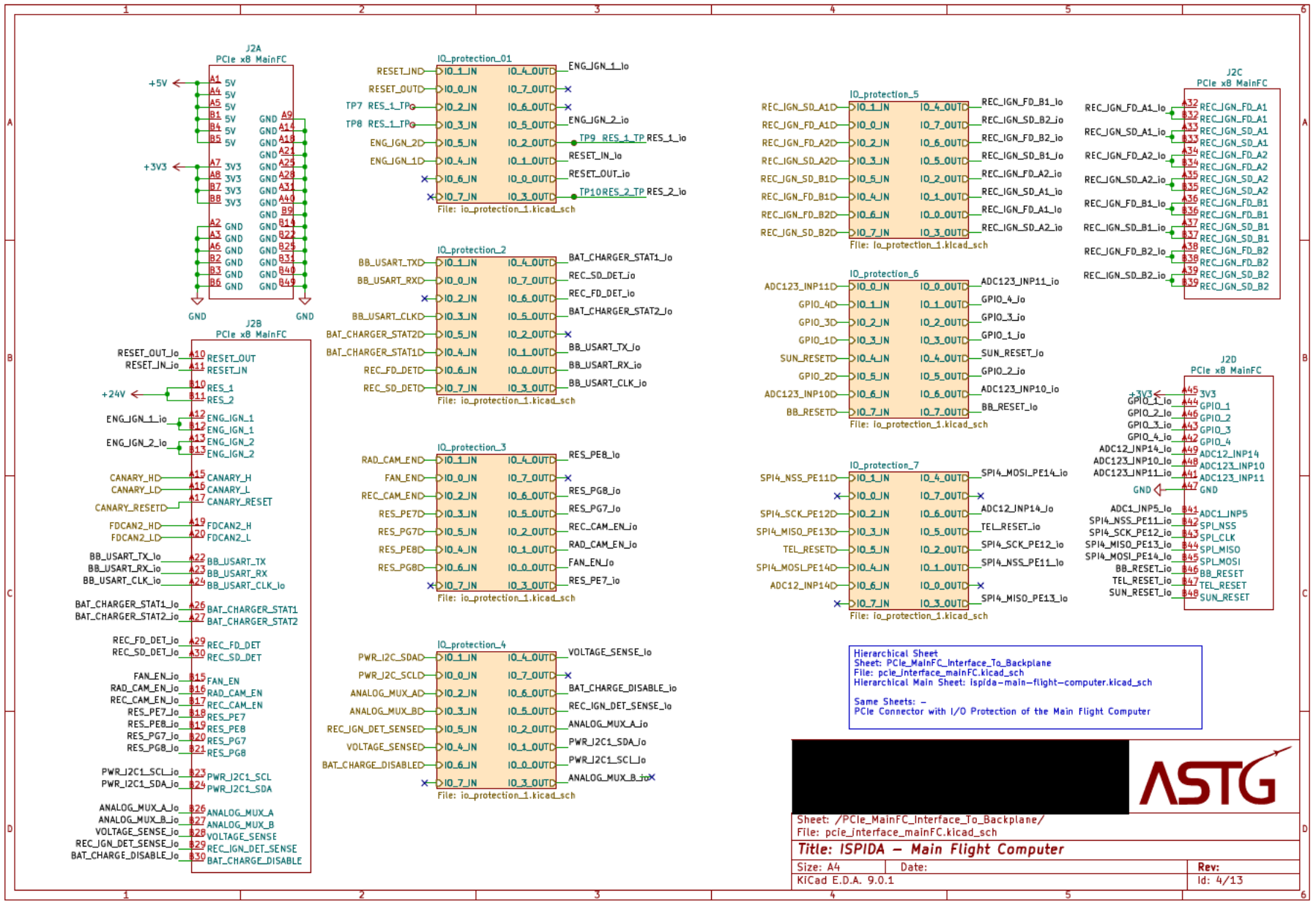
Same Sheets: Id 3 & Id 12
CAN Transceiver Circuit with possible Terminal Resistor



Sheet: /CAN Transceiver CANary FDCAN1/
File: CAN_transceiver.kicad_sch

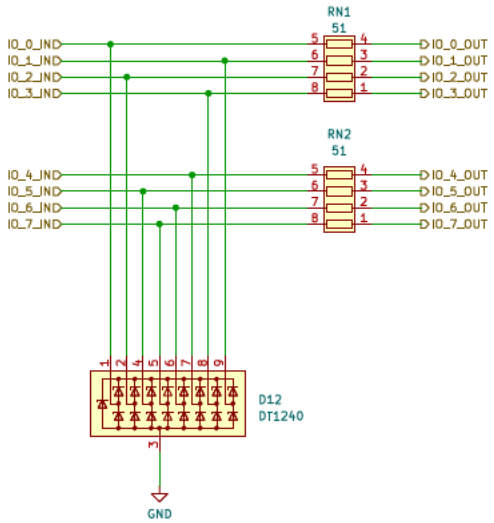
Title: ISPIDA – Main Flight Computer

Size: A4	Date:	Rev:
KiCad E.D.A. 9.0.1		Id: 3/13


J2A
PCIe x8 MainFC
+5V
+3V3
GND
J2B
PCIe x8 MainFC
RESET_OUT_Io
RESET_IN_Io
+24V
ENG_IGN_1_Io
ENG_IGN_2_Io
CANARY_HD
CANARY_LD
CANARY_RESETD
FDCAN2_HD
FDCAN2_LD
BB_USART_TX_Io
BB_USART_RX_Io
BB_USART_CLK_Io
BAT_CHARGER_STAT1_Io
BAT_CHARGER_STAT2_Io
REC_FD_DET_Io
REC_SD_DET_Io
FAN_EN_Io
RAD_CAM_EN_Io
REC_CAM_EN_Io
RES_PE7_Io
RES_PE8_Io
RES_PG7_Io
RES_PG8_Io
PWR_I2C1_SCL_Io
PWR_I2C1_SDA_Io
ANALOG_MUX_A_Io
ANALOG_MUX_B_Io
VOLTAGE_SENSE_Io
REC_IGN_DET_SENSE_Io
BAT_CHARGE_DISABLE_Io
IO_protection_01
RESET_IND
RESET_OUTD
TP7 RES_1_TPo
TP8 RES_1_TPo
ENG_IGN_2D
ENG_IGN_1D
ENG_IGN_1_Io
ENG_IGN_2_Io
TP9 RES_1_TP
RES_1_Io
RESET_IN_Io
RESET_OUT_Io
TP10RES_2_TP
RES_2_Io
File: io_protection_1.kicad_sch
IO_protection_2
BB_USART_TXD
BB_USART_RXD
BB_USART_CLKD
BAT_CHARGER_STAT2D
BAT_CHARGER_STAT1D
REC_FD_DETD
REC_SD_DETD
BAT_CHARGER_STAT1_Io
REC_SD_DET_Io
REC_FD_DET_Io
BAT_CHARGER_STAT2_Io
BB_USART_TX_Io
BB_USART_RX_Io
BB_USART_CLK_Io
File: io_protection_1.kicad_sch
IO_protection_3
RAD_CAM_END
FAN_END
REC_CAM_END
RES_PE7D
RES_PG7D
RES_PE8D
RES_PG8D
RES_PE8_Io
RES_PG8_Io
RES_PG7_Io
REC_CAM_EN_Io
RAD_CAM_EN_Io
FAN_EN_Io
RES_PE7_Io
File: io_protection_1.kicad_sch
IO_protection_4
PWR_I2C_SDAD
PWR_I2C_SCLD
ANALOG_MUX_AD
ANALOG_MUX_BD
REC_IGN_DET_SENSED
VOLTAGE_SENSED
BAT_CHARGE_DISABLED
VOLTAGE_SENSE_Io
BAT_CHARGE_DISABLE_Io
REC_IGN_DET_SENSE_Io
ANALOG_MUX_A_Io
PWR_I2C1_SDA_Io
PWR_I2C1_SCL_Io
ANALOG_MUX_B_Io
File: io_protection_1.kicad_sch
IO_protection_5
REC_IGN_SD_A1D
REC_IGN_FD_A1D
REC_IGN_FD_A2D
REC_IGN_SD_A2D
REC_IGN_SD_B1D
REC_IGN_FD_B1D
REC_IGN_FD_B2D
REC_IGN_SD_B2D
REC_IGN_FD_B1_Io
REC_IGN_SD_B2_Io
REC_IGN_FD_B2_Io
REC_IGN_SD_B1_Io
REC_IGN_FD_A2_Io
REC_IGN_SD_A1_Io
REC_IGN_FD_A1_Io
REC_IGN_SD_A2_Io
File: io_protection_1.kicad_sch
IO_protection_6
ADC123_INP11D
GPIO_4D
GPIO_3D
GPIO_1D
SUN_RESETD
GPIO_2D
ADC123_INP10D
BB_RESETD
ADC123_INP11_Io
GPIO_4_Io
GPIO_3_Io
GPIO_1_Io
SUN_RESET_Io
GPIO_2_Io
ADC123_INP10_Io
BB_RESET_Io
File: io_protection_1.kicad_sch
IO_protection_7
SPI4_NSS_PE11D
SPI4_SCK_PE12D
SPI4_MISO_PE13D
TEL_RESETD
SPI4_MOSI_PE14D
ADC12_INP14D
SPI4_MOSI_PE14_Io
ADC12_INP14_Io
TEL_RESET_Io
SPI4_SCK_PE12_Io
SPI4_NSS_PE11_Io
SPI4_MISO_PE13_Io
File: io_protection_1.kicad_sch
J2C
PCIe x8 MainFC
J2D
PCIe x8 MainFC
+3V3
GND
ADC1_INP5_Io
SPI4_NSS_PE11_Io
SPI4_SCK_PE12_Io
SPI4_MISO_PE13_Io
SPI4_MOSI_PE14_Io
BB_RESET_Io
TEL_RESET_Io
SUN_RESET_Io
Hierarchical Sheet
Sheet: PCIe_MainFC_Interface_To_Backplane
File: pcie_interface_mainFC.kicad_sch
Hierarchical Main Sheet: ispida-main-flight-computer.kicad_sch
Same Sheets: -
PCIe Connector with I/O Protection of the Main Flight Computer
ASTG
Sheet: /PCIe_MainFC_Interface_To_Backplane/
File: pcie_interface_mainFC.kicad_sch
Title: ISPIDA - Main Flight Computer
Size: A4
Date:
Rev:
KiCad E.D.A. 9.0.1
Id: 4/13

Hierarchical Sheet
Sheet: IO_protection_01
File: io_protection_1.kicad_sch
Hierarchical Main Sheet: ispida-main-flight-computer.kicad_sch

Same Sheets: Id 5 - Id 11
I/O Protection Circuit of the Main Flightcomputer PCIe Connector



[redacted]

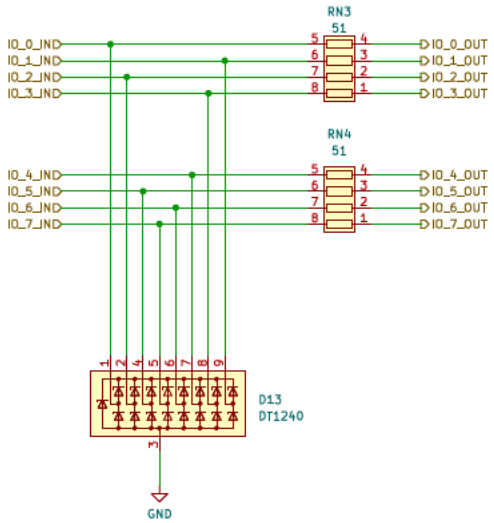
Sheet: /PCIe_MainFC_Interface_To_Backplane/IO_protection_01/
File: io_protection_1.kicad_sch

Title: ISPIDA - Main Flight Computer

Size: A4	Date:	Rev:
KiCad E.D.A. 9.0.1		Id: 5/13

Hierarchical Sheet
Sheet: IO_protection_2
File: io_protection_1.kicad_sch
Hierarchical Main Sheet: ispida-main-flight-computer.kicad_sch

Same Sheets: Id 5 - Id 11
I/O Protection Circuit of the Main Flightcomputer PCIe Connector



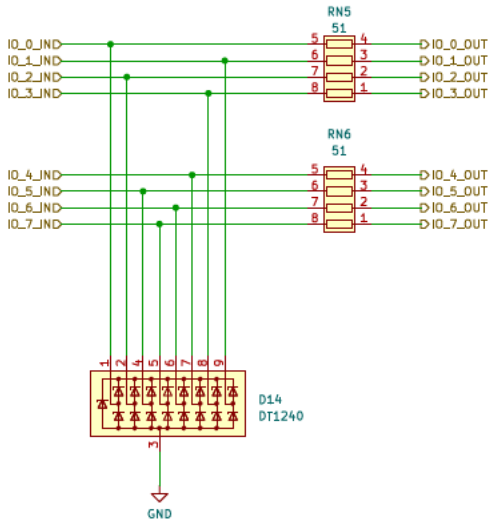
Sheet: /PCIe_MainFC_Interface_To_Backplane/IO_protection_2/
File: io_protection_1.kicad_sch

Title: ISPIDA - Main Flight Computer

Size: A4	Date:	Rev:
KiCad E.D.A. 9.0.1		Id: 6/13

Hierarchical Sheet
Sheet: IO_protection_3
File: io_protection_1.kicad_sch
Hierarchical Main Sheet: ispida-main-flight-computer.kicad_sch

Same Sheets: Id 5 - Id 11
I/O Protection Circuit of the Main Flightcomputer PCIe Connector



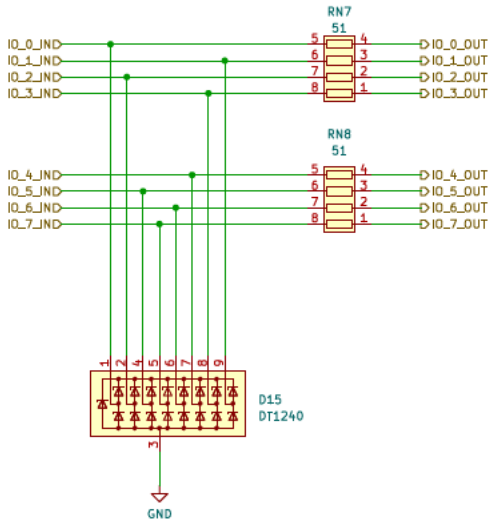
Sheet: /PCIe_MainFC_Interface_To_Backplane/IO_protection_3/
File: io_protection_1.kicad_sch

Title: ISPIDA - Main Flight Computer

Size: A4	Date:	Rev:
KiCad E.D.A. 9.0.1		Id: 7/13

Hierarchical Sheet
Sheet: IO_protection_4
File: io_protection_1.kicad_sch
Hierarchical Main Sheet: ispida-main-flight-computer.kicad_sch

Same Sheets: Id 5 - Id 11
I/O Protection Circuit of the Main Flightcomputer PCIe Connector



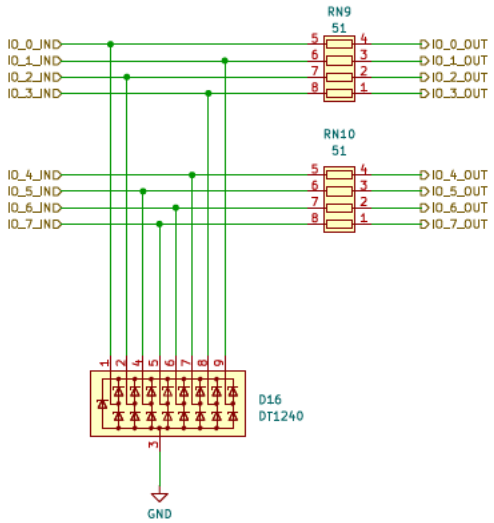
Sheet: /PCIe_MainFC_Interface_To_Backplane/IO_protection_4/
File: io_protection_1.kicad_sch

Title: ISPIDA - Main Flight Computer

Size: A4	Date:	Rev:
KiCad E.D.A. 9.0.1		Id: 8/13

Hierarchical Sheet
Sheet: IO_protection_5
File: io_protection_1.kicad_sch
Hierarchical Main Sheet: ispida-main-flight-computer.kicad_sch

Same Sheets: Id 5 - Id 11
I/O Protection Circuit of the Main Flightcomputer PCIe Connector



[redacted]

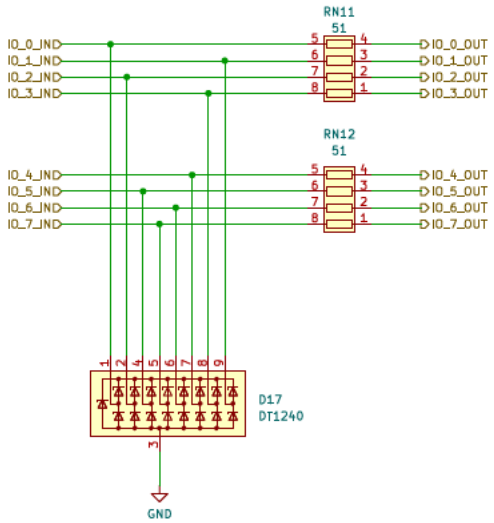
Sheet: /PCIe_MainFC_Interface_To_Backplane/IO_protection_5/
File: io_protection_1.kicad_sch

Title: ISPIDA - Main Flight Computer

Size: A4	Date:	Rev:
KiCad E.D.A. 9.0.1		Id: 9/13

Hierarchical Sheet
Sheet: IO_protection_6
File: io_protection_1.kicad_sch
Hierarchical Main Sheet: ispida-main-flight-computer.kicad_sch

Same Sheets: Id 5 - Id 11
I/O Protection Circuit of the Main Flightcomputer PCIe Connector



[redacted]

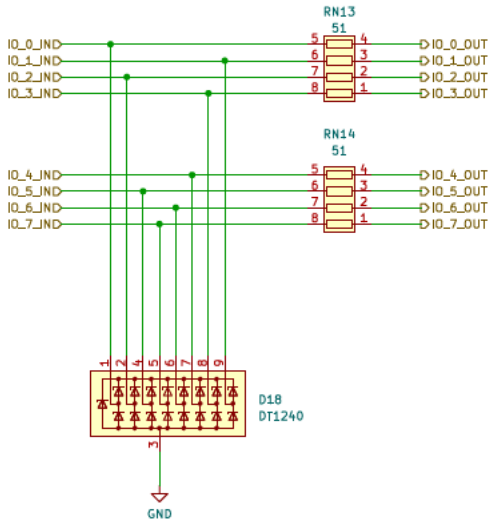
Sheet: /PCIe_MainFC_Interface_To_Backplane/IO_protection_6/
File: io_protection_1.kicad_sch

Title: ISPIDA - Main Flight Computer

Size: A4	Date:	Rev:
KiCad E.D.A. 9.0.1		Id: 10/13

Hierarchical Sheet
Sheet: IO_protection_7
File: io_protection_1.kicad_sch
Hierarchical Main Sheet: ispida-main-flight-computer.kicad_sch

Same Sheets: Id 5 - Id 11
I/O Protection Circuit of the Main Flightcomputer PCIe Connector



[redacted]

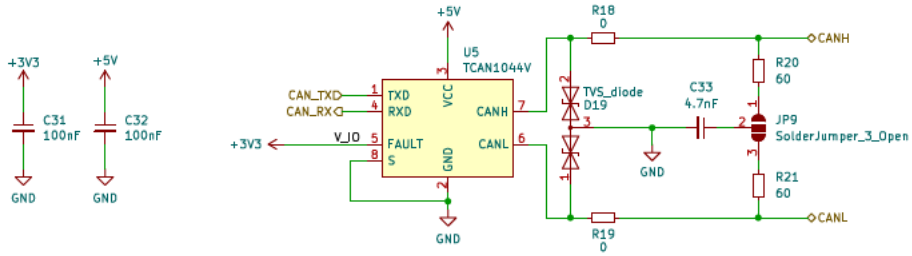
Sheet: /PCIe_MainFC_Interface_To_Backplane/IO_protection_7/
File: io_protection_1.kicad_sch

Title: ISPIDA - Main Flight Computer

Size: A4	Date:	Rev:
KiCad E.D.A. 9.0.1		Id: 11/13

Hierarchical Sheet
Sheet: CAN Transceiver FDCAN2
File: CAN_transceiver.kicad_sch
Hierarchical Main Sheet: ispida-main-flight-computer.kicad_sch

Same Sheets: Id 3 & Id 12
CAN Transceiver Circuit with possible Terminal Resistor



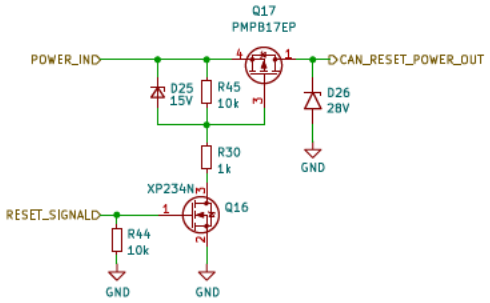
Sheet: /CAN Transceiver FDCAN2/
File: CAN_transceiver.kicad_sch

Title: ISPIDA – Main Flight Computer

Size: A4	Date:	Rev:
KiCad E.D.A. 9.0.1		Id: 12/13

Hierarchical Sheet
Sheet: CANary Reset
File: canary_reset.kicad_sch
Hierarchical Main Sheet: ispida-main-flight-computer.kicad_sch

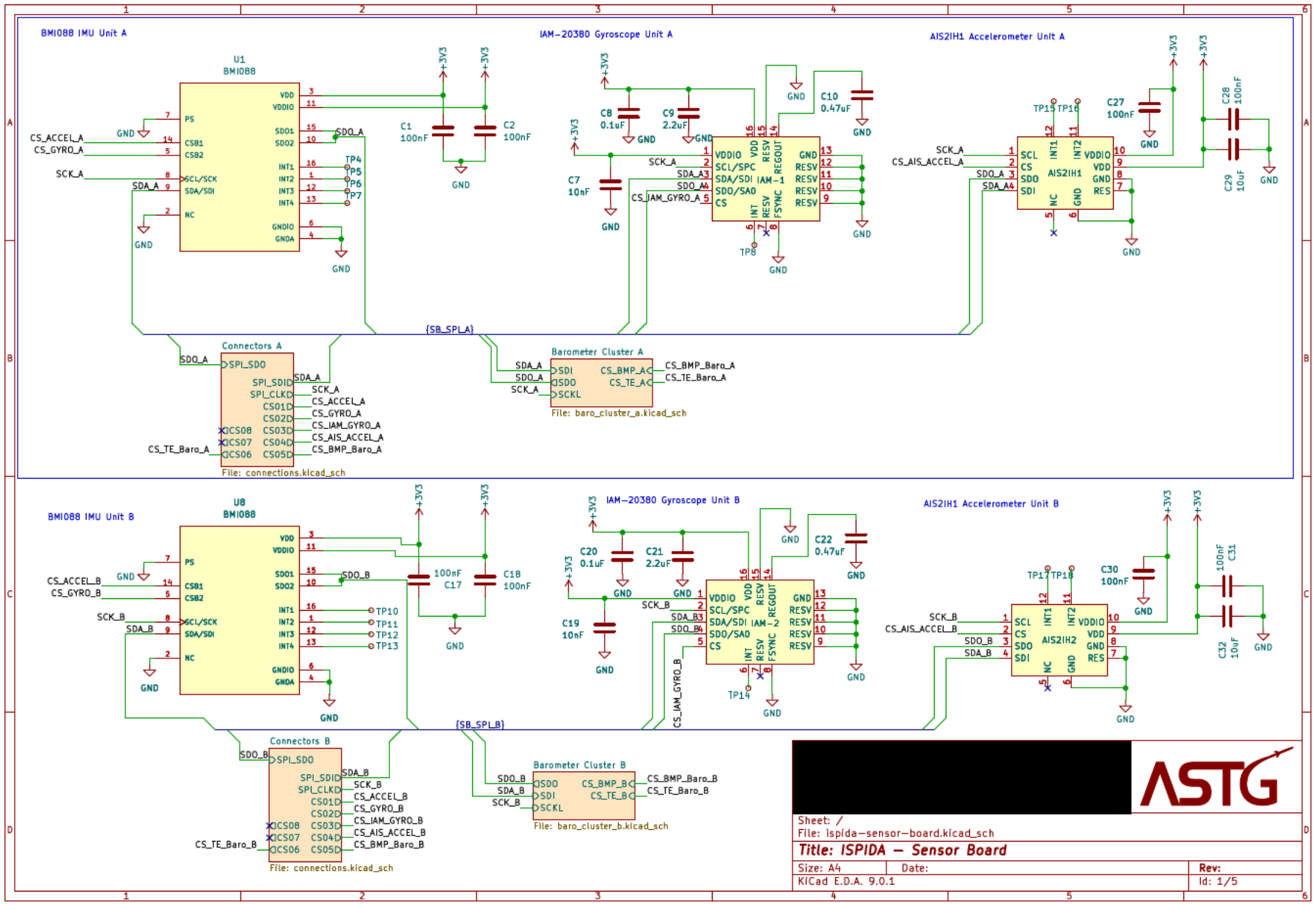
Same Sheets: -
Digital Out Circuit for Canary Reset

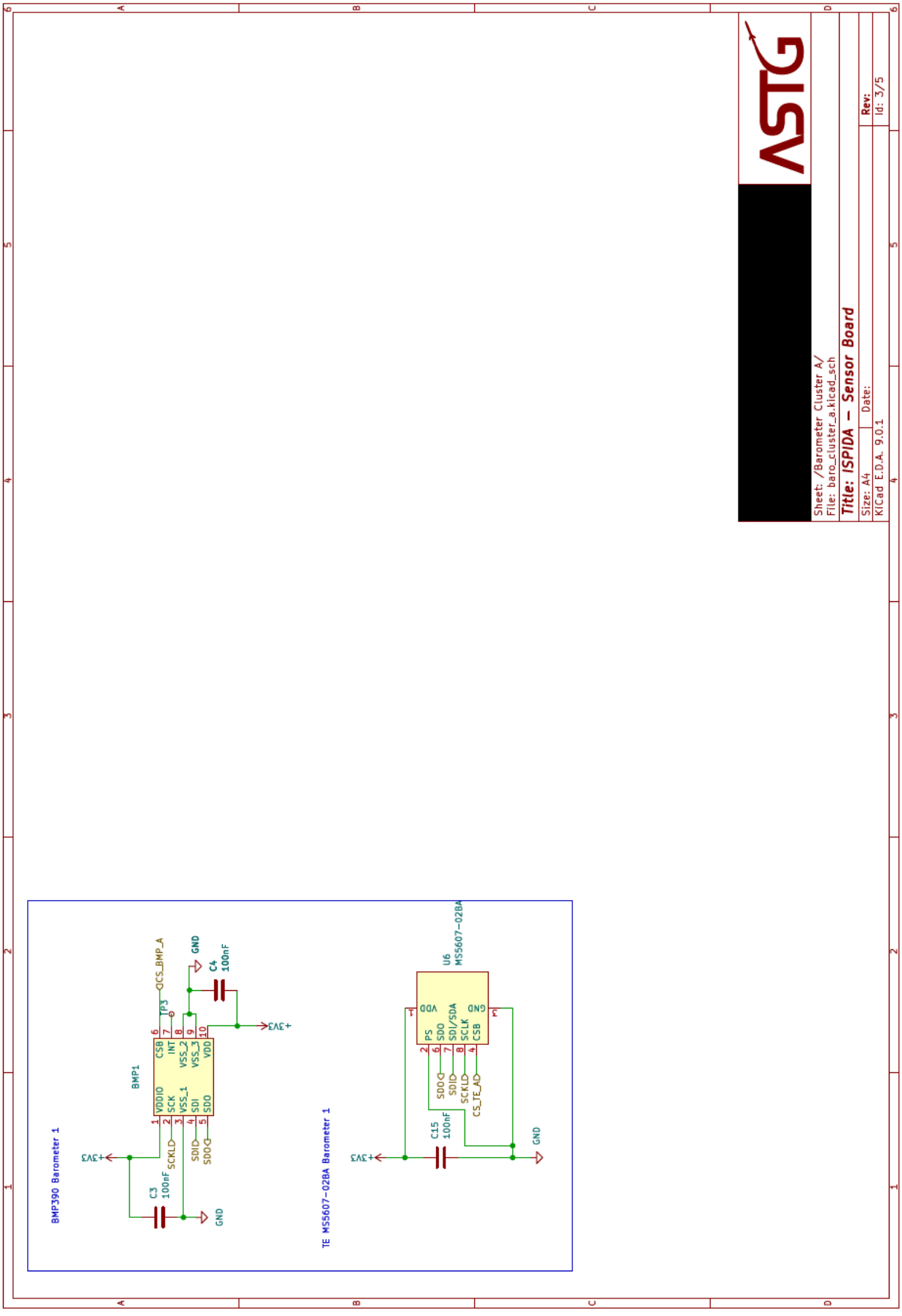


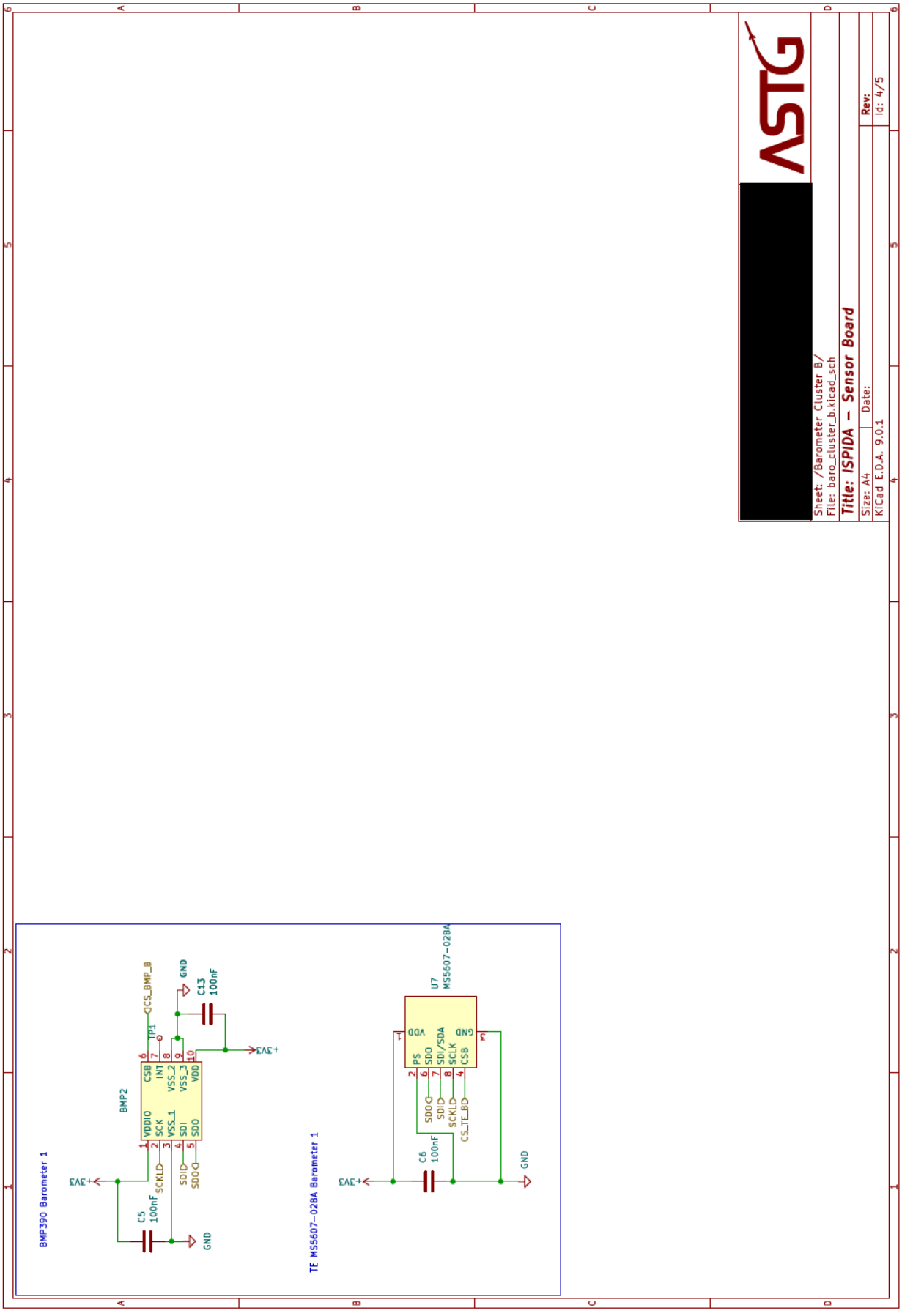
Sheet: /CANary Reset/
File: canary_reset.kicad_sch

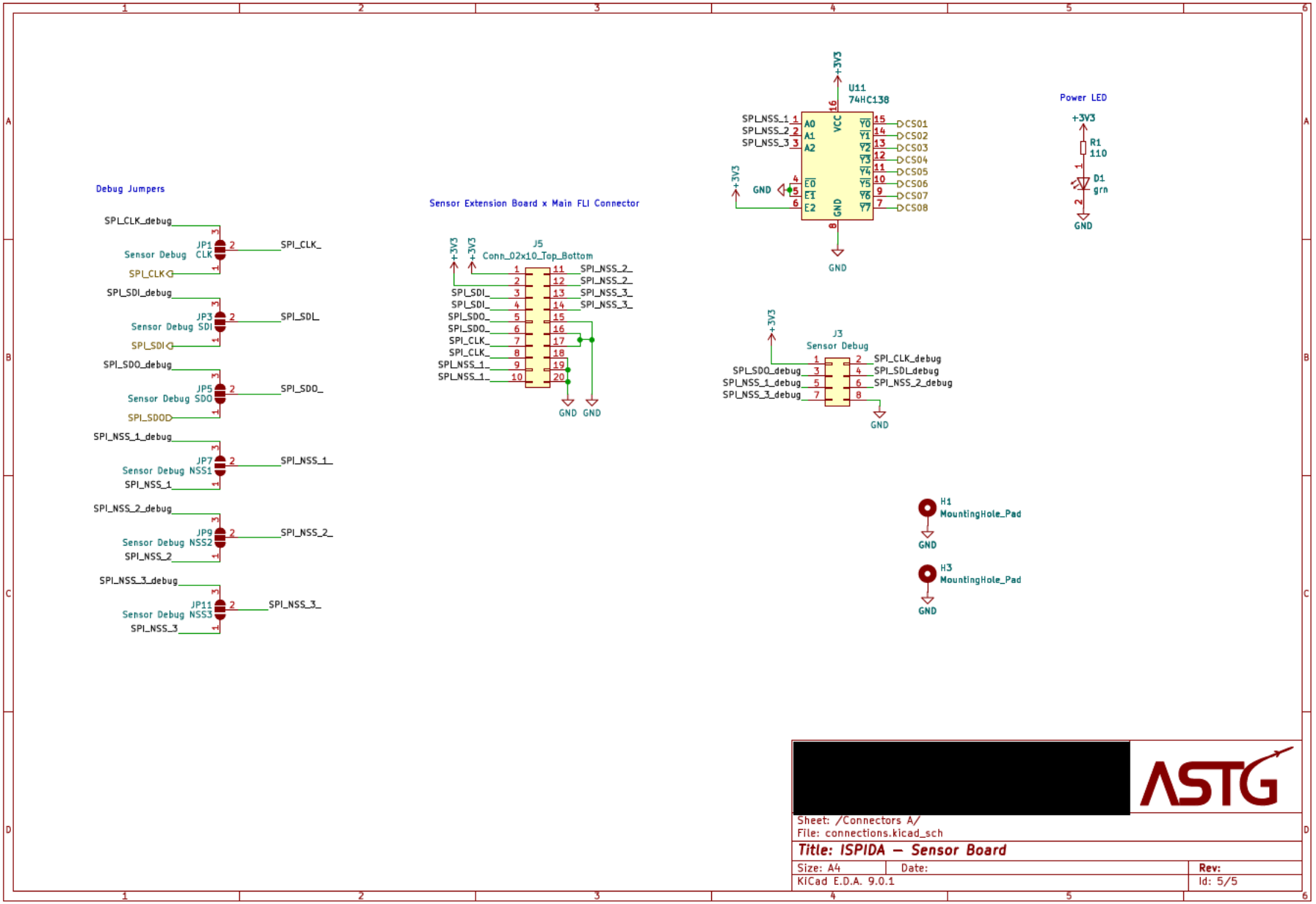
Title: ISPIDA - Main Flight Computer

Size: A4	Date:	Rev:
KiCad E.D.A. 9.0.1		Id: 13/13


BMI088 IMU Unit A
U1
BMI088
IAM-20380 Gyroscope Unit A
AIS2IH1 Accelerometer Unit A
Connectors A
File: connections.kicad_sch
Barometer Cluster A
File: baro_cluster_a.kicad_sch
{SB_SPI_A}
BMI088 IMU Unit B
U8
BMI088
IAM-20380 Gyroscope Unit B
AIS2IH1 Accelerometer Unit B
Connectors B
File: connections.kicad_sch
Barometer Cluster B
File: baro_cluster_b.kicad_sch
{SB_SPI_B}
ASTG
Sheet: /
File: ispida-sensor-board.kicad_sch
Title: ISPIDA – Sensor Board
Size: A4
Date:
Rev:
KiCad E.D.A. 9.0.1
Id: 1/5


Sheet: /Barometer Cluster A/
File: baro_cluster_a.kicad_sch
Title: ISPIDA – Sensor Board
Size: A4
Date:
Rev:
KiCad E.D.A. 9.0.1
Id: 3/5
BMP390 Barometer 1
BMP1
VDDIO
SCK
SCKLD
VSS_1
SDI
SDIO
SDO
SDOO
CSB
INT
VSS_2
VSS_3
VDD
TP3
CCS_BMP_A
C3
100nF
C4
100nF
GND
+3V3
TE MS5607-02BA Barometer 1
U6
MS5607-02BA
VDD
PS
SDO
SDI/SDA
SCLK
CSB
GND
SDOO
SDIO
SCKLD
CS_TE_AD
C15
100nF

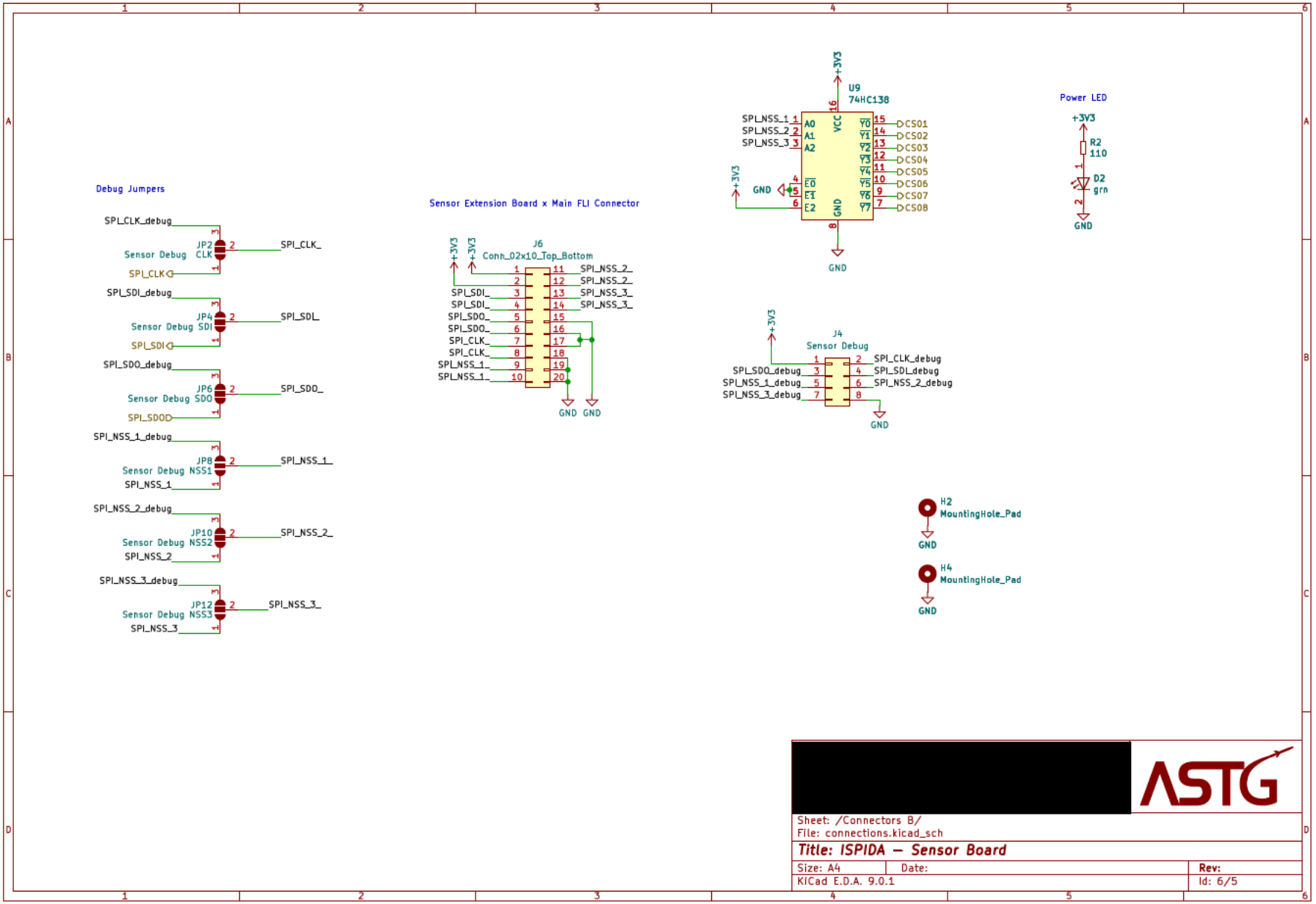

BMP390 Barometer 1
BMP2
VDDIO
SCK
VSS_1
SDI
SDO
CSB
INT
VSS_2
VSS_3
VDD
TP1
CS_BMP_B
GND
C13
100nF
+3V3
C5
100nF
SCKLD
SDIO
SDOO
TE MS5607-02BA Barometer 1
U7
MS5607-02BA
PS
SDO
SDI/SDA
SCLK
CSB
GND
C6
100nF
CS_TE_BD
Sheet: /Barometer Cluster B/
File: baro_cluster_b.kicad_sch
Title: ISPIDA – Sensor Board
Size: A4
Date:
Rev:
KiCad E.D.A. 9.0.1
Id: 4/5

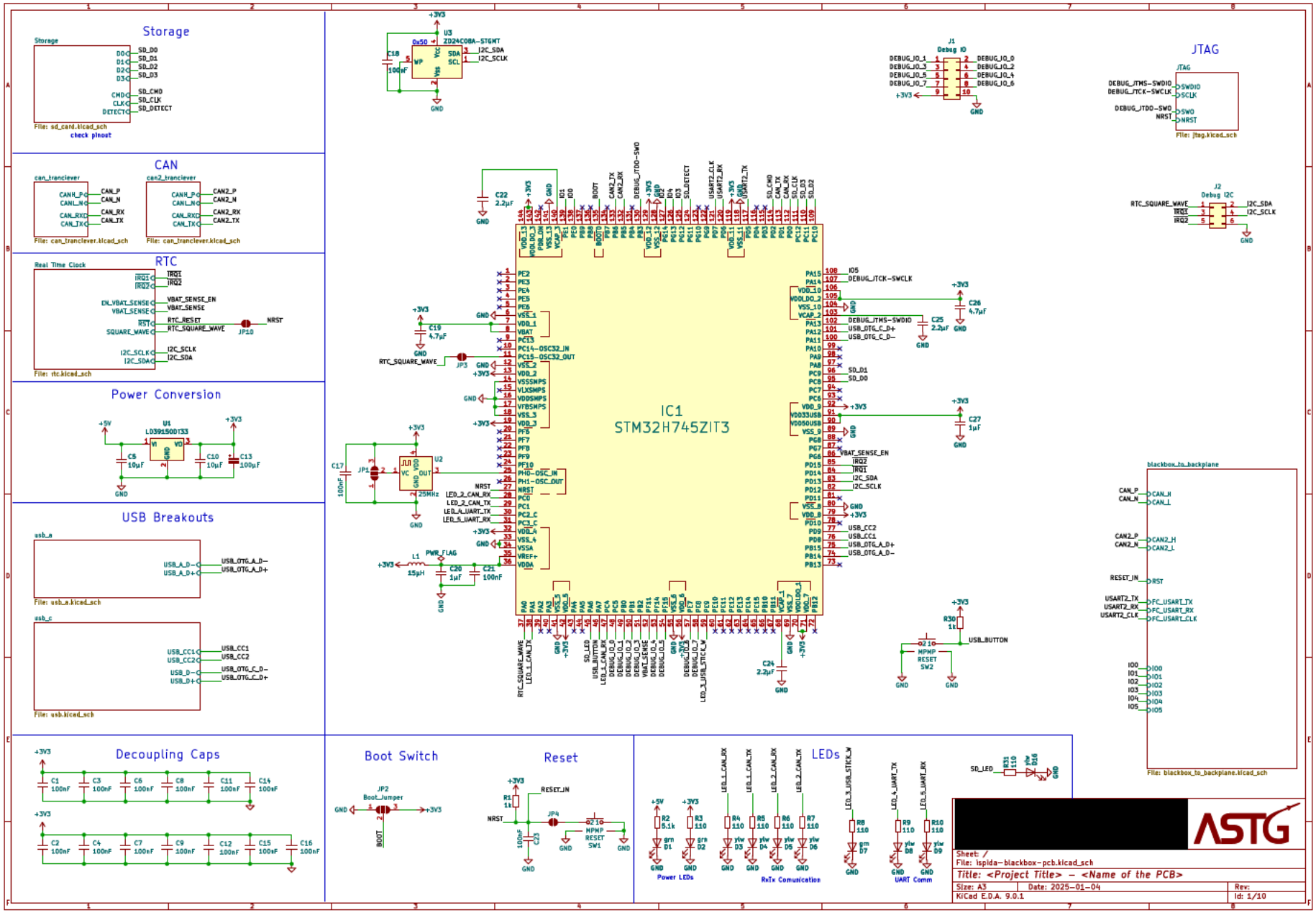


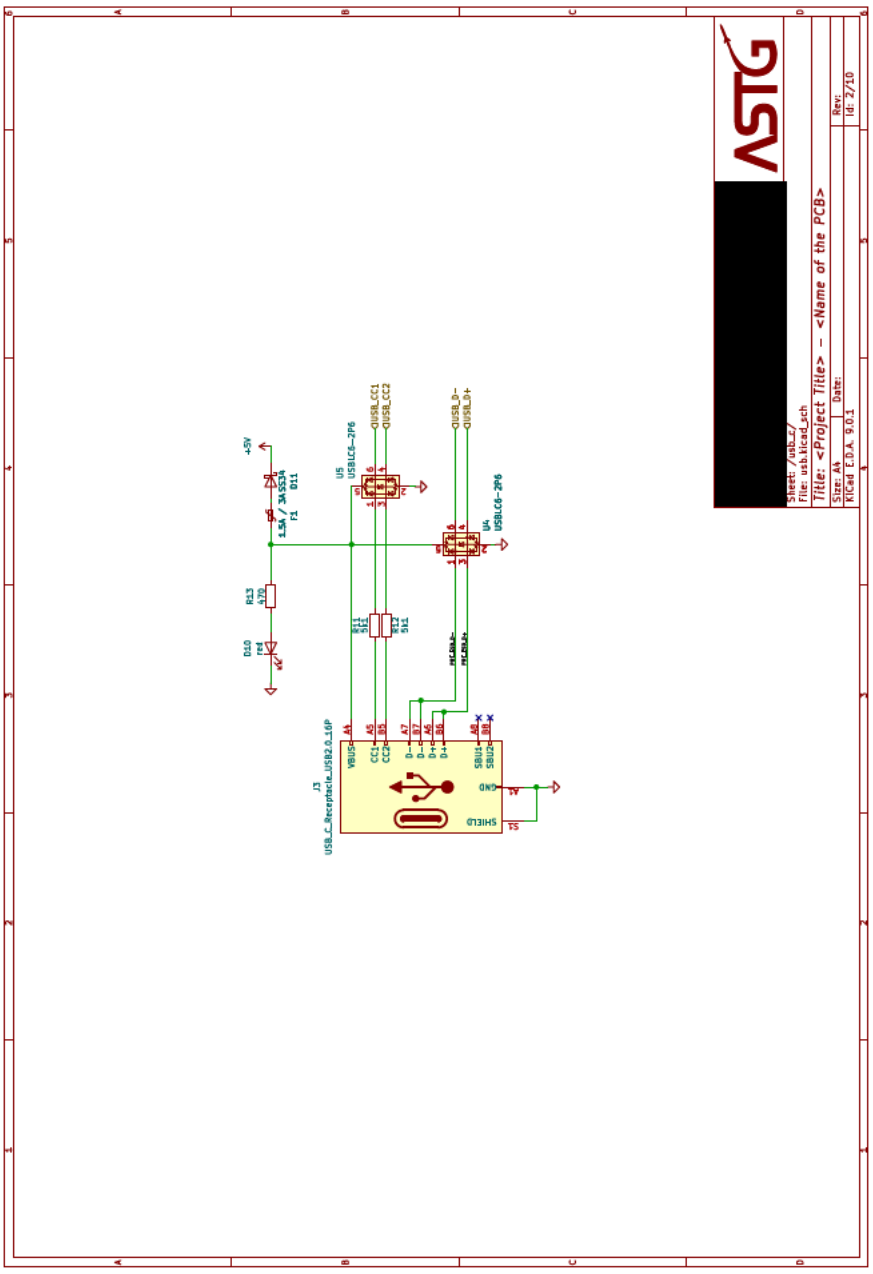
Sheet: /Connectors A/
File: connections.kicad_sch

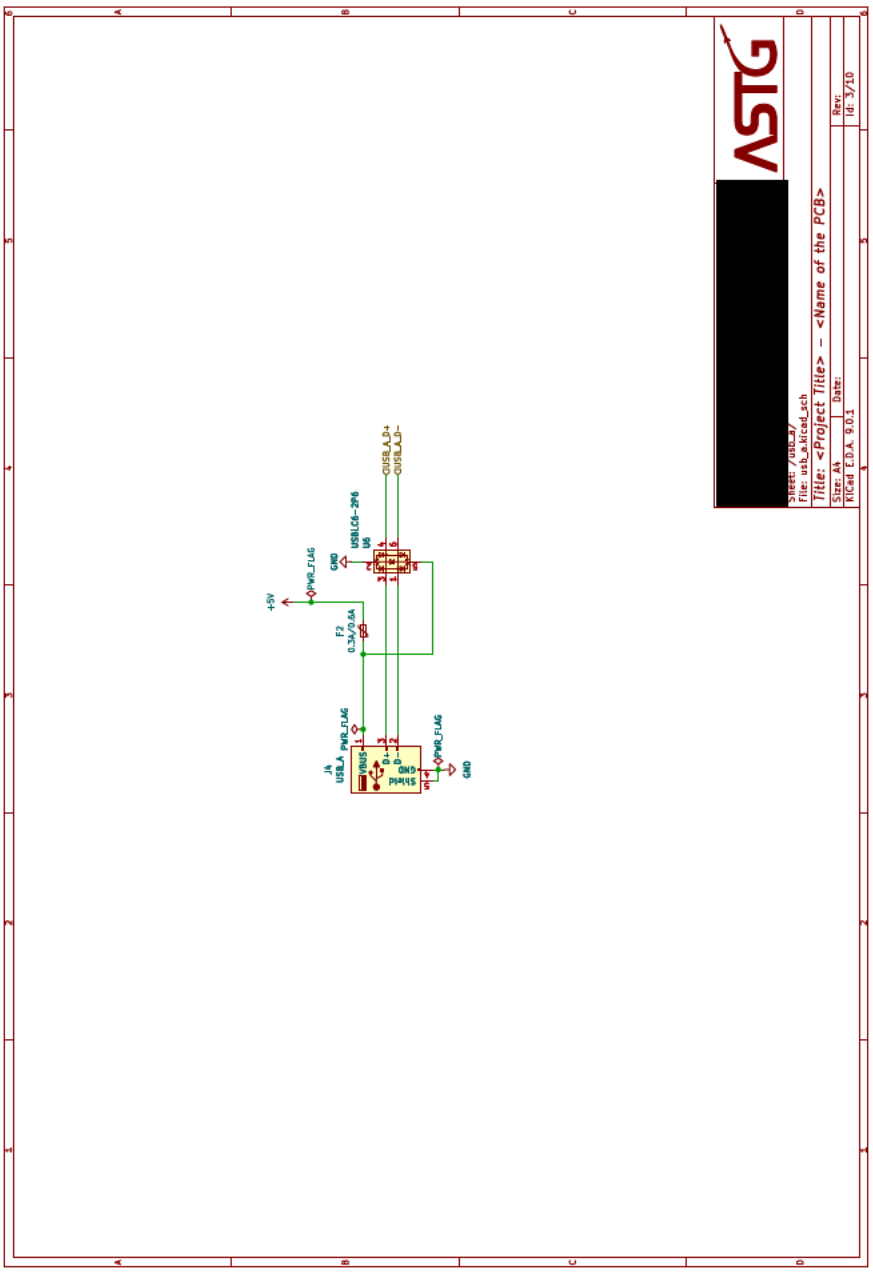
Title: ISPIDA – Sensor Board

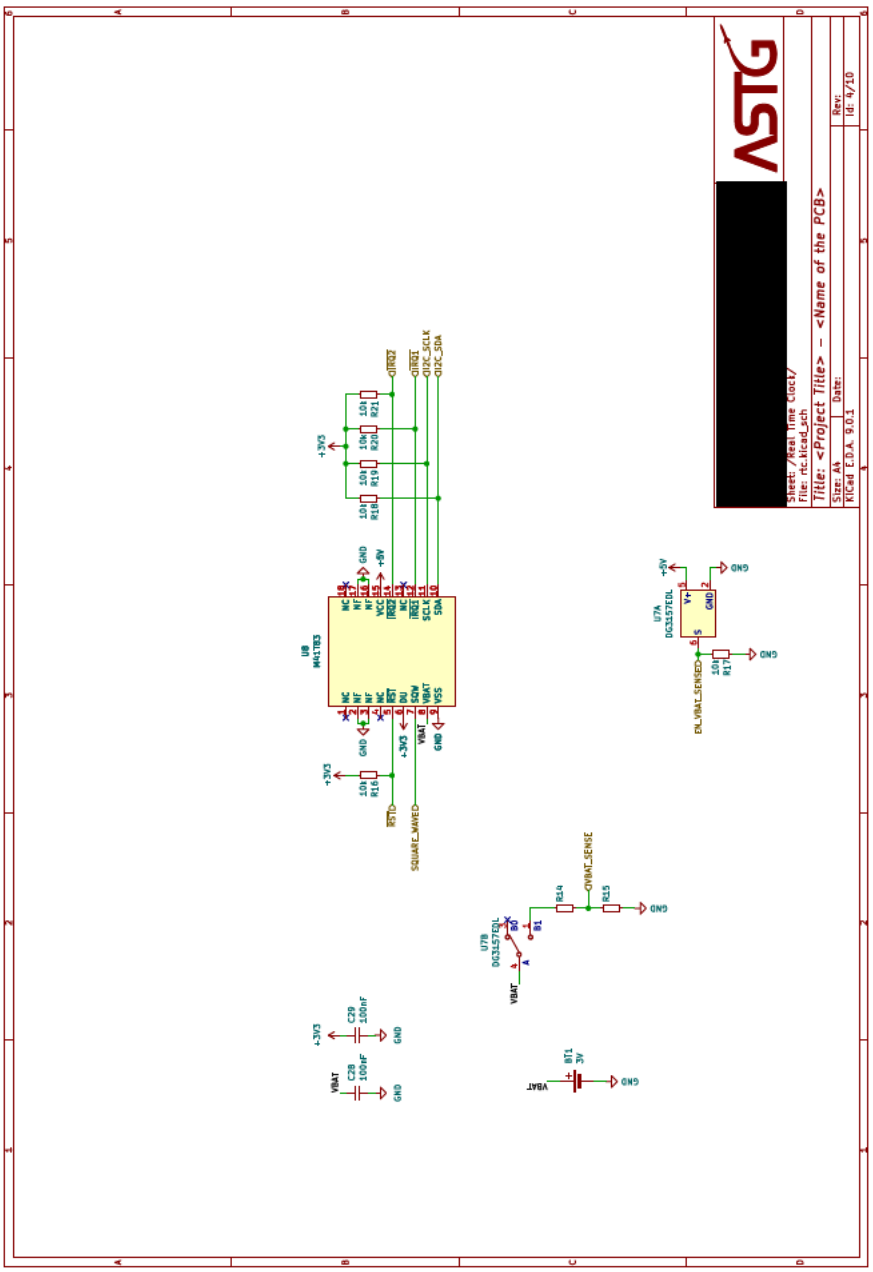
Size: A4	Date:	Rev:
KiCad E.D.A. 9.0.1		Id: 5/5

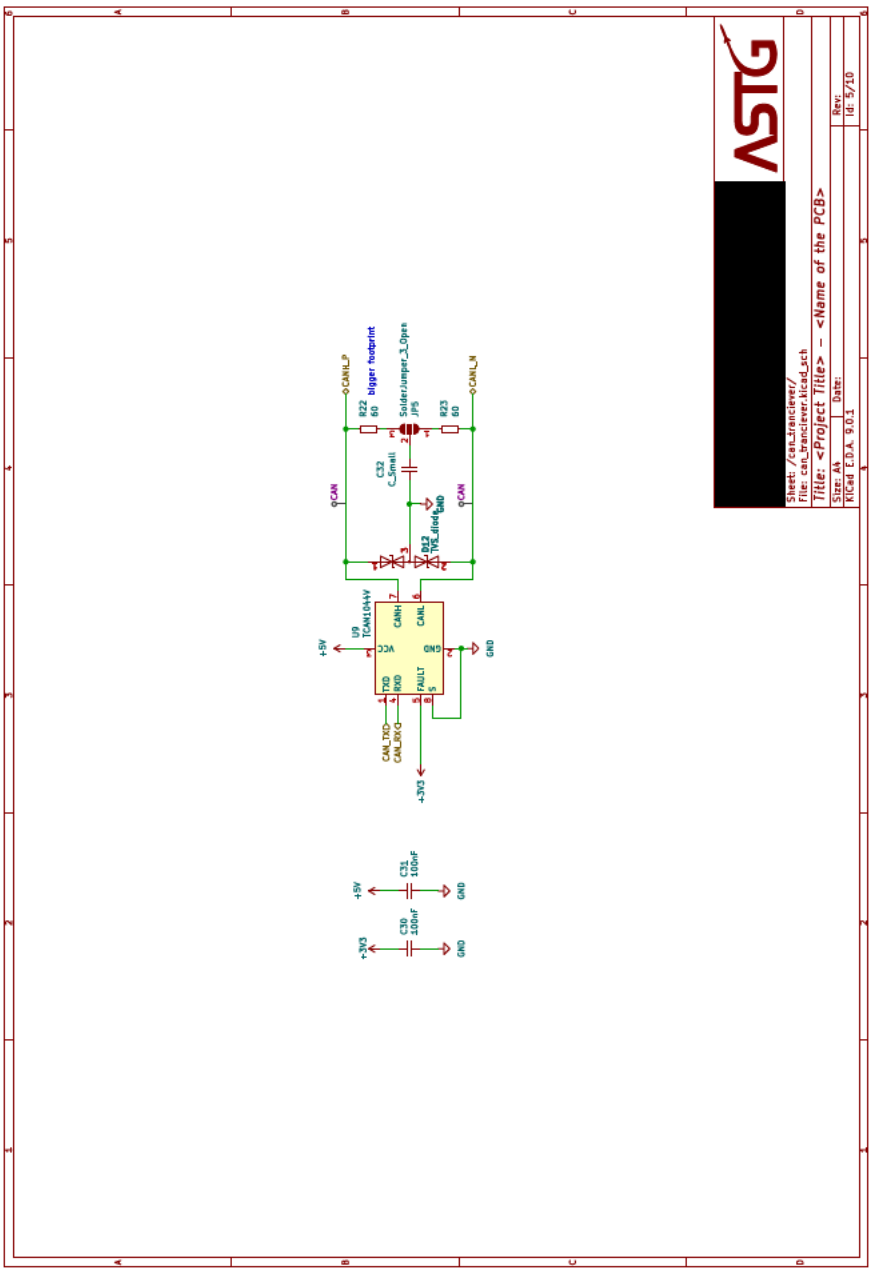

Debug Jumpers
SPI_CLK_debug
JP2
Sensor Debug CLK
SPI_CLK
SPI_CLK_
SPI_SDI_debug
JP4
Sensor Debug SDI
SPI_SDI
SPI_SDI_
SPI_SDO_debug
JP6
Sensor Debug SDO
SPI_SDO
SPI_SDO_
SPI_NSS_1_debug
JP8
Sensor Debug NSS1
SPI_NSS_1
SPI_NSS_1_
SPI_NSS_2_debug
JP10
Sensor Debug NSS2
SPI_NSS_2
SPI_NSS_2_
SPI_NSS_3_debug
JP12
Sensor Debug NSS3
SPI_NSS_3
SPI_NSS_3_
Sensor Extension Board x Main FLI Connector
J6
Conn_02x10_Top_Bottom
+3V3
GND
U9
74HC138
SPI_NSS_1
SPI_NSS_2
SPI_NSS_3
CS01
CS02
CS03
CS04
CS05
CS06
CS07
CS08
Power LED
R2
110
D2
grn
J4
Sensor Debug
SPI_SDO_debug
SPI_NSS_1_debug
SPI_NSS_3_debug
SPI_CLK_debug
SPI_SDI_debug
SPI_NSS_2_debug
H2
MountingHole_Pad
H4
MountingHole_Pad
ASTG
Sheet: /Connectors B/
File: connections.kicad_sch
Title: ISPIDA – Sensor Board
Size: A4
Date:
Rev:
KiCad E.D.A. 9.0.1
Id: 6/5

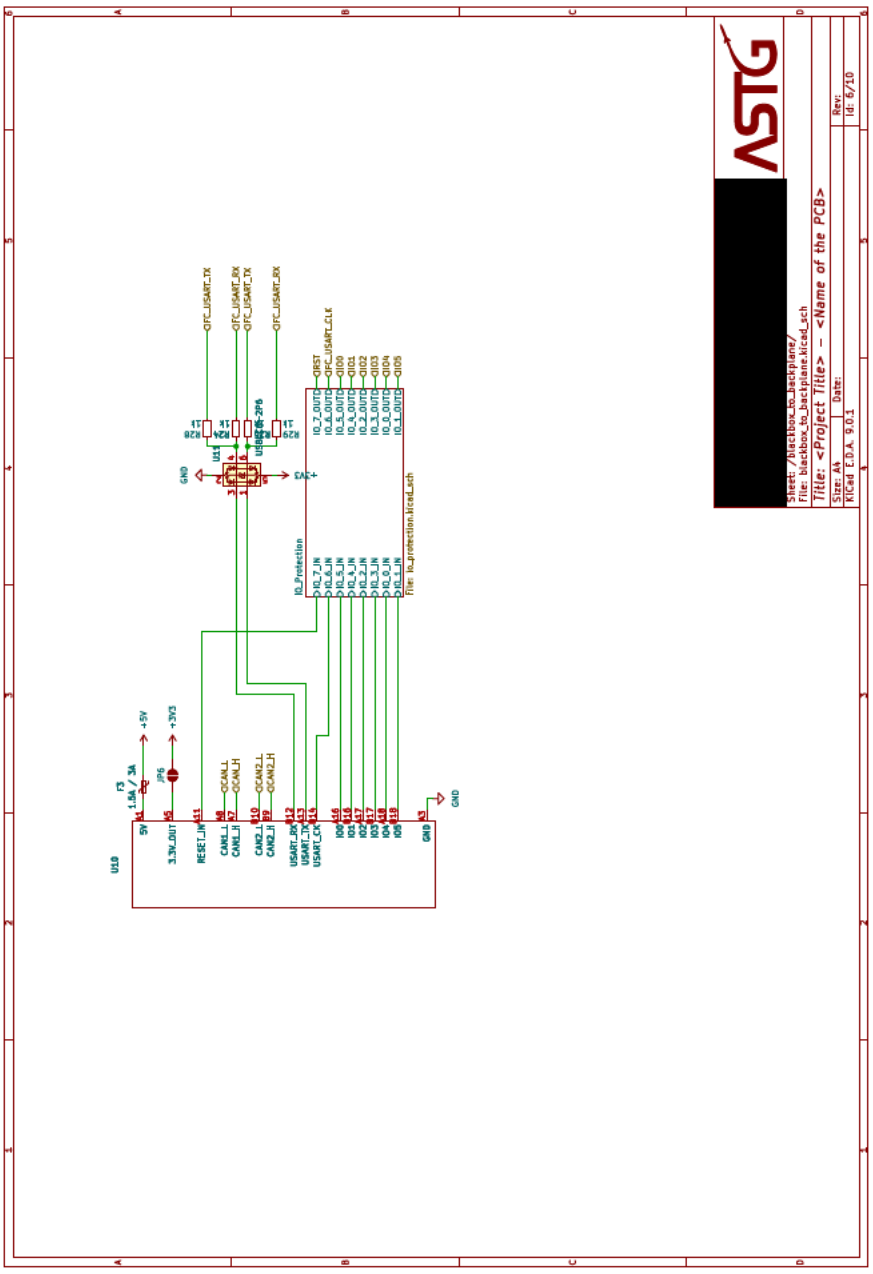

Storage
CAN
RTC
Power Conversion
USB Breakouts
Decoupling Caps
Boot Switch
Reset
LEDs
JTAG
IC1
STM32H745ZIT3
Power LEDs
RxTx Comunication
UART Comm
Sheet: /
File: ispida-blackbox-pcb.kicad_sch
Title: <Project Title> - <Name of the PCB>
Size: A3
Date: 2025-01-04
Rev:
KiCad E.D.A. 9.0.1
Id: 1/10

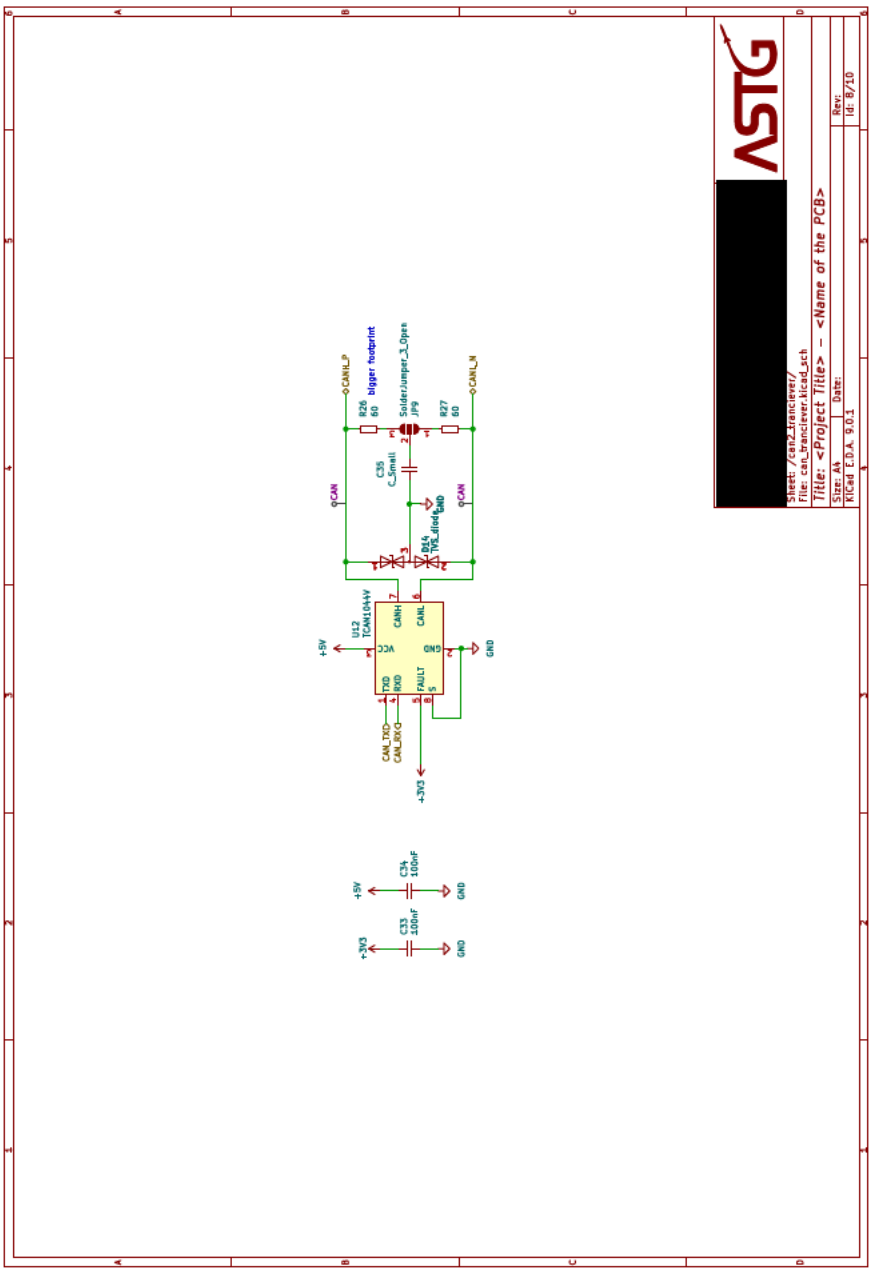

ASTG
Sheet: /usb_c/
File: usb_c.kicad_sch
Title: <Project Title> - <Name of the PCB>
Size: A4
Date:
Rev:
KiCad E.D.A. 9.0.1
Id: 2/10
+5V
F1
1.5A / 34.5534
D11
R13
470
D10
F14
USB_CC1
USB_CC2
USB_D-
USB_D+
U5
USBLC6-2P6
U4
USBLC6-2P6
R11
5k1
R12
5k1
J3
USB_C_Receptacle_USB2.0_16P
VBUS
CC1
CC2
D-
D+
SBU1
SBU2
GND
SHIELD

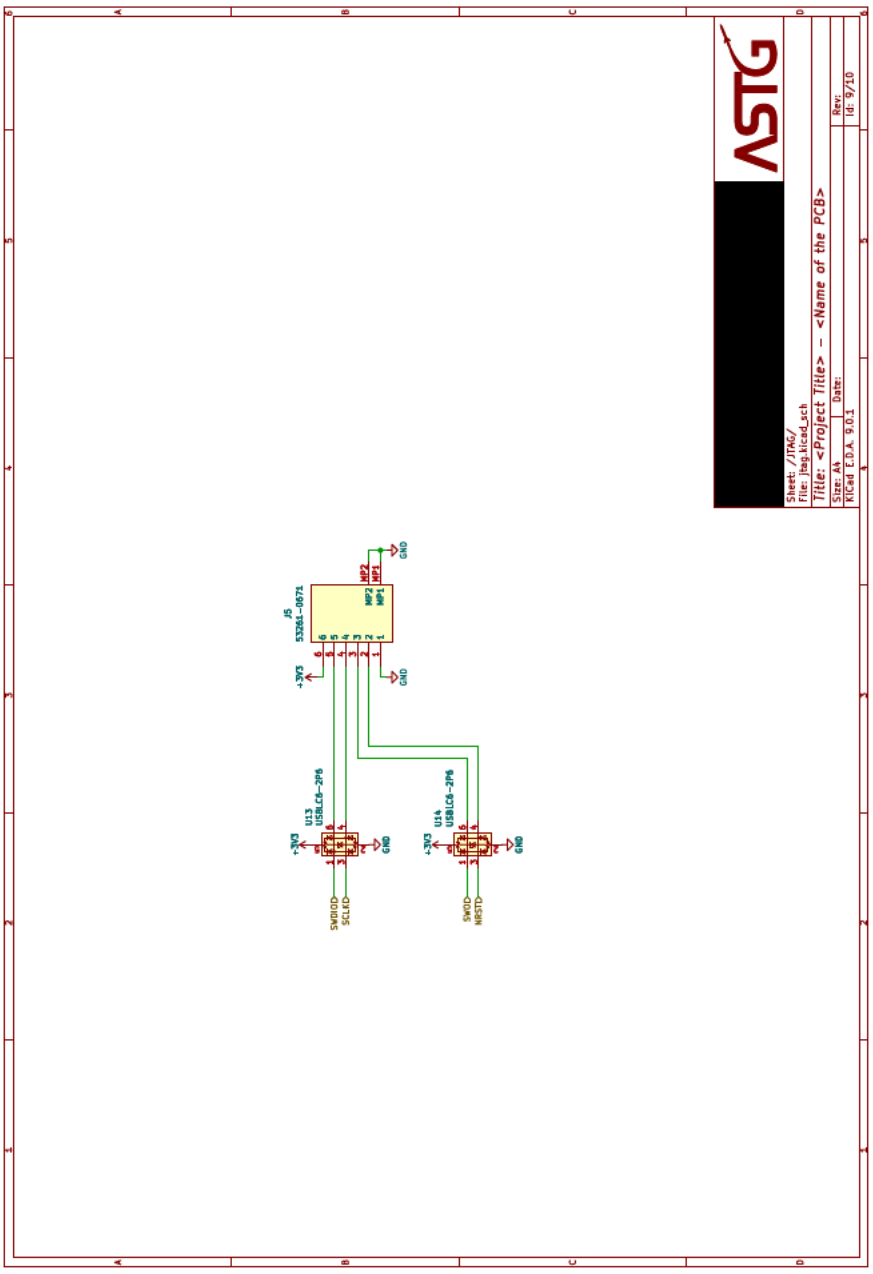

ASTG
[redacted]
Sheet: /USB_A/
File: usb_A.kicad_sch
Title: <Project Title> - <Name of the PCB>
Size: A4
Date:
Rev:
KiCad E.D.A. 9.0.1
Id: 3/10
USB_A_D+
USB_A_D-
USBLC6-2P6
U5
GND
PWR_FLAG
+5V
F2
0.3A/0.6A
J4
USB_A
VBUS
D+
D-
GND
PM45
PWR_FLAG
GND

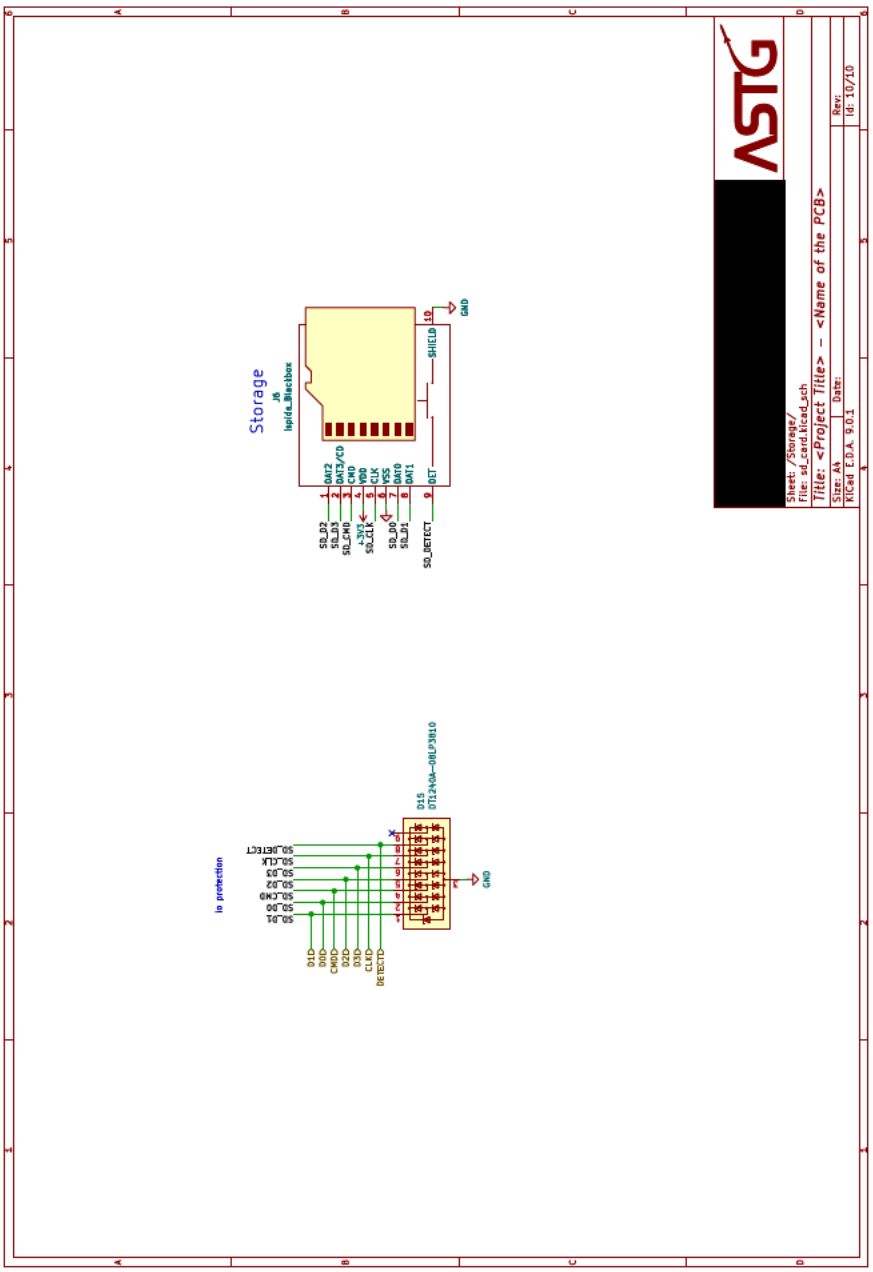

ASTG
[redacted]
Sheet: /Real Time Clock/
File: rtc.kicad_sch
Title: <Project Title> - <Name of the PCB>
Size: A4
Date:
KiCad E.D.A. 9.0.1
Rev:
Id: 4/10
U8
M41T83
U7A
DG3157EDL
U7B
DG3157EDL
BT1
3V
C29
100nF
C28
100nF
R16
10k
R17
10k
R18
10k
R19
10k
R20
10k
R21
10k
R14
R15
+3V3
+5V
GND
VBAT
IRQ2
CLOCK_SCLK
CLOCK_SDA
RSTO
SQUARE_WAVED
EXL_VBAT_SENSED
CVBAT_SENSE

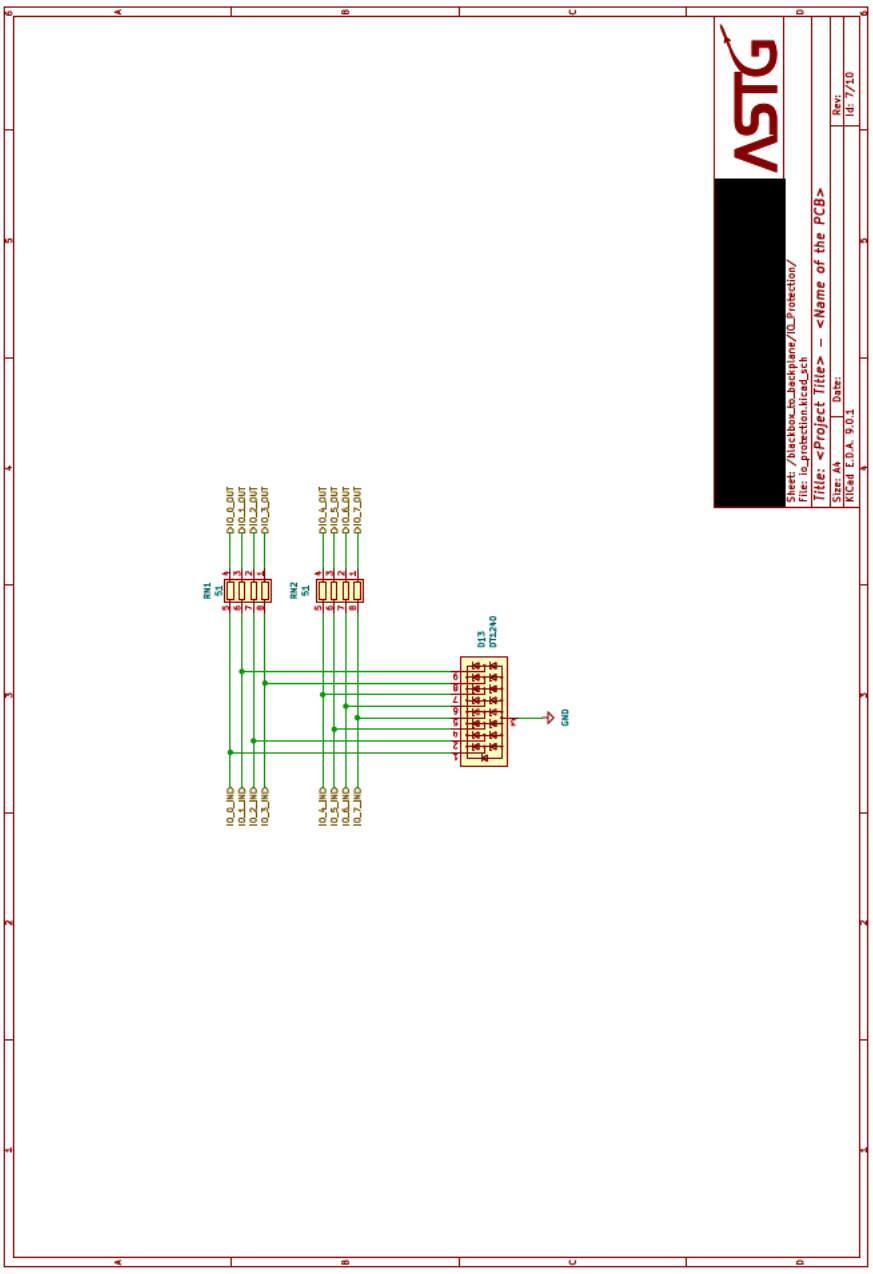

CANH_P
R22
60
bigger footprint
Solder Jumper_3_Open
JP5
R23
60
CANH_N
C32
C_Small
CAN
CAN
D12
TVS_diode
U9
TCAN1044V
CANH
CANL
VCC
GND
TXD
RXD
FAULT
+5V
GND
CAN_TXD
CAN_RXD
+3V3
C31
100nF
C30
100nF
+5V
GND
+3V3
GND
ASTG
Sheet: /can_transciever/
File: can_transciever.kicad_sch
Title: <Project Title> - <Name of the PCB>
Size: A4
Date:
KiCad E.D.A. 9.0.1
Rev:
Id: 5/10

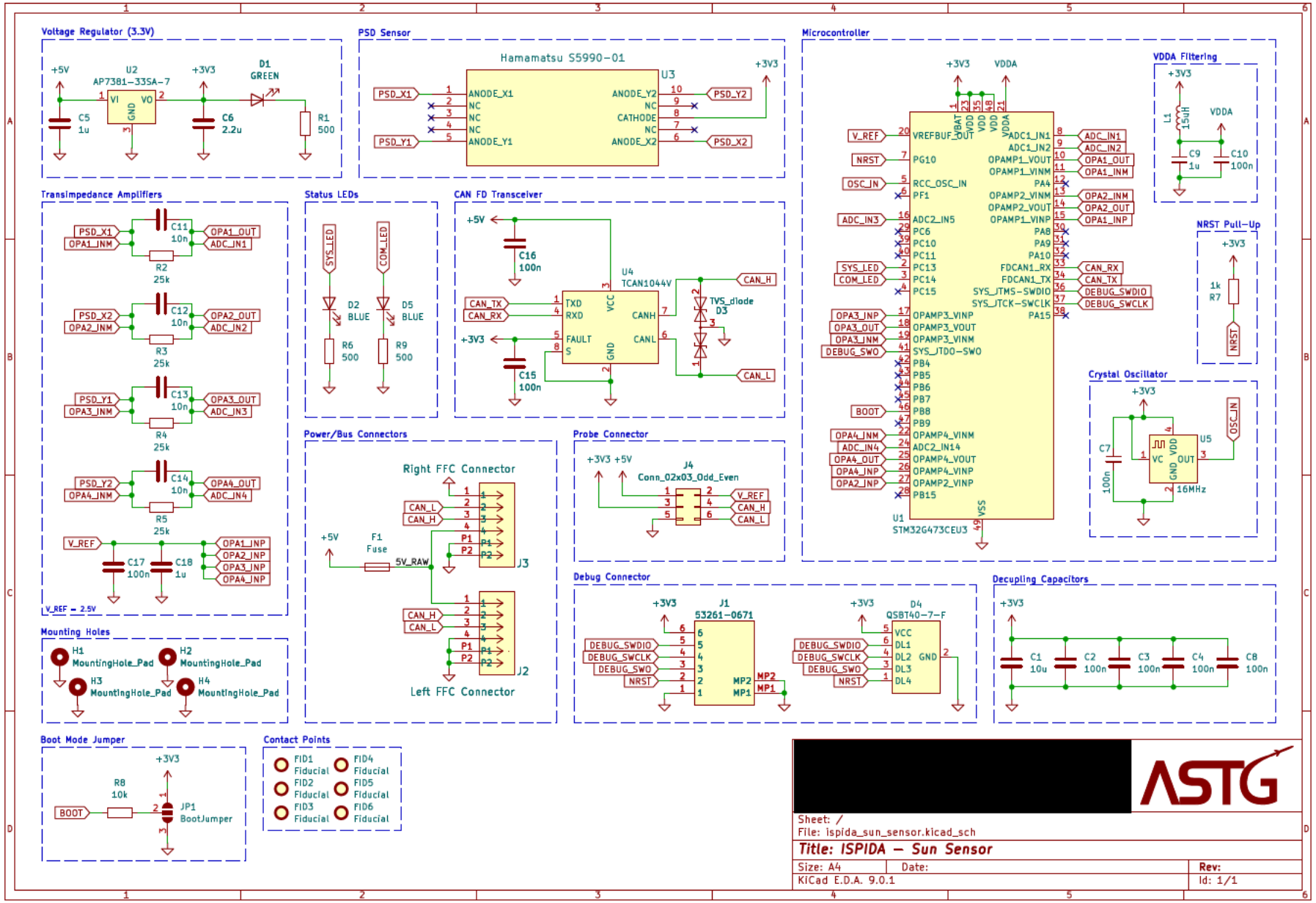

ASTG
[redacted]
Sheet: /blackbox_bc_backplane/
File: blackbox_bc_backplane.kicad_sch
Title: <Project Title> - <Name of the PCB>
Size: A4
Date:
Rev:
KiCad E.D.A. 9.0.1
Id: 6/10
IO_Protection
Title: io_protection.kicad_sch
U10
GND
+5V
+3V3

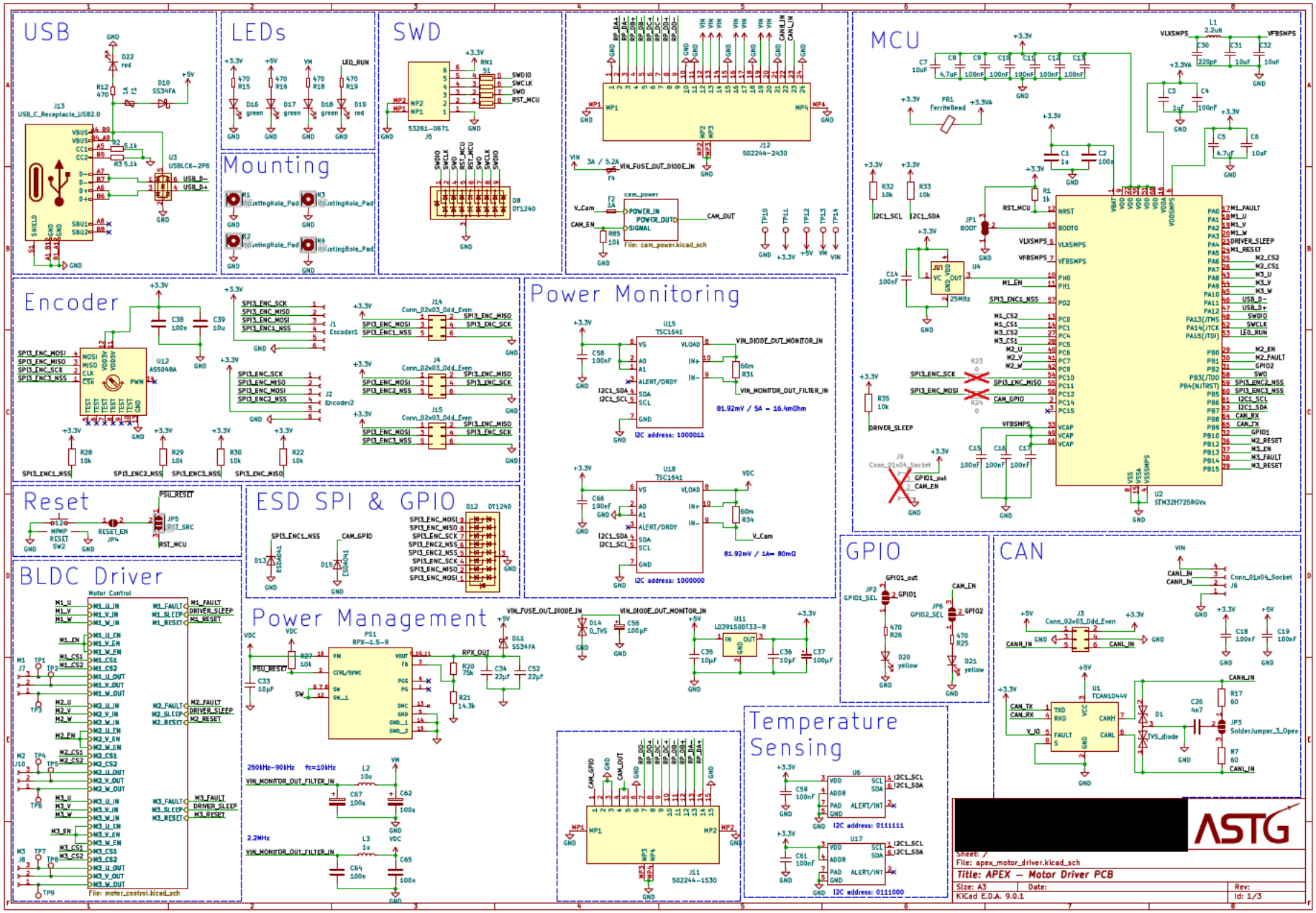

CANH_P
CANH_N
R26
60
bigger footprint
Solder Jumper_3_Open
JP9
R27
60
C35
C_Small
CAN
CAN
GND
D4
TVS_diode
U12
TCAN1044V
CANH
CANL
VCC
GND
TXD
RXD
FAULT
+5V
GND
CAN_TXD
CAN_RXD
+3V3
C34
100nF
C33
100nF
+5V
GND
+3V3
GND
Sheet: /can2_transciever/
File: can_transciever.kicad_sch
Title: <Project Title> - <Name of the PCB>
Size: A4
Date:
KiCad E.D.A. 9.0.1
Rev:
Id: 8/10

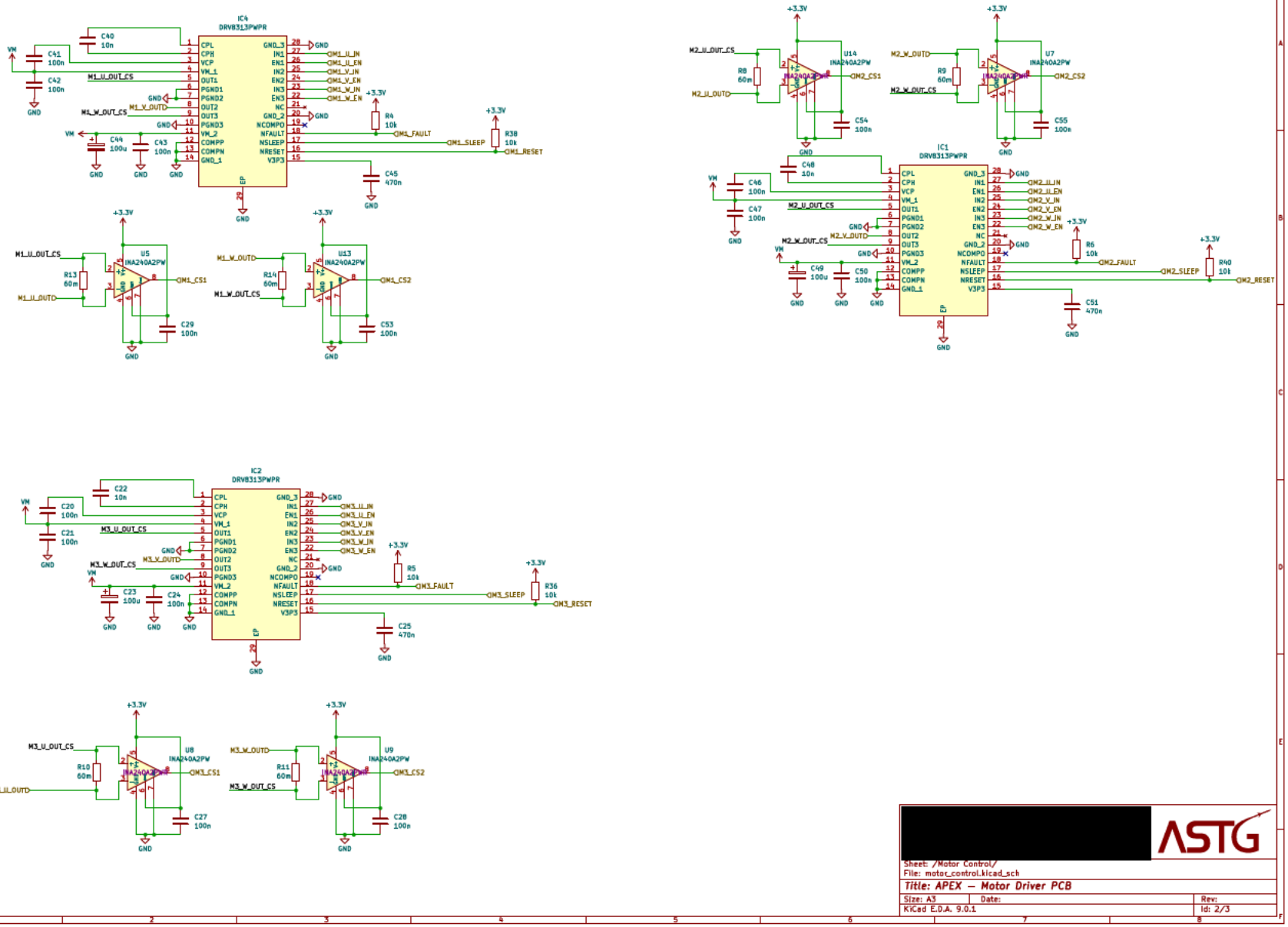

ASTG
Sheet: /JTAG/
File: Jtag.kicad_sch
Title: <Project Title> - <Name of the PCB>
Size: A4
Date:
Rev:
KiCad E.D.A. 9.0.1
Id: 9/10
J5
533661-0671
MP2
MP1
GND
+3V3
U13
USBLC6-2P6
U14
USBLC6-2P6
SWDIOD
SCLKD
SWDIO
NRSTD

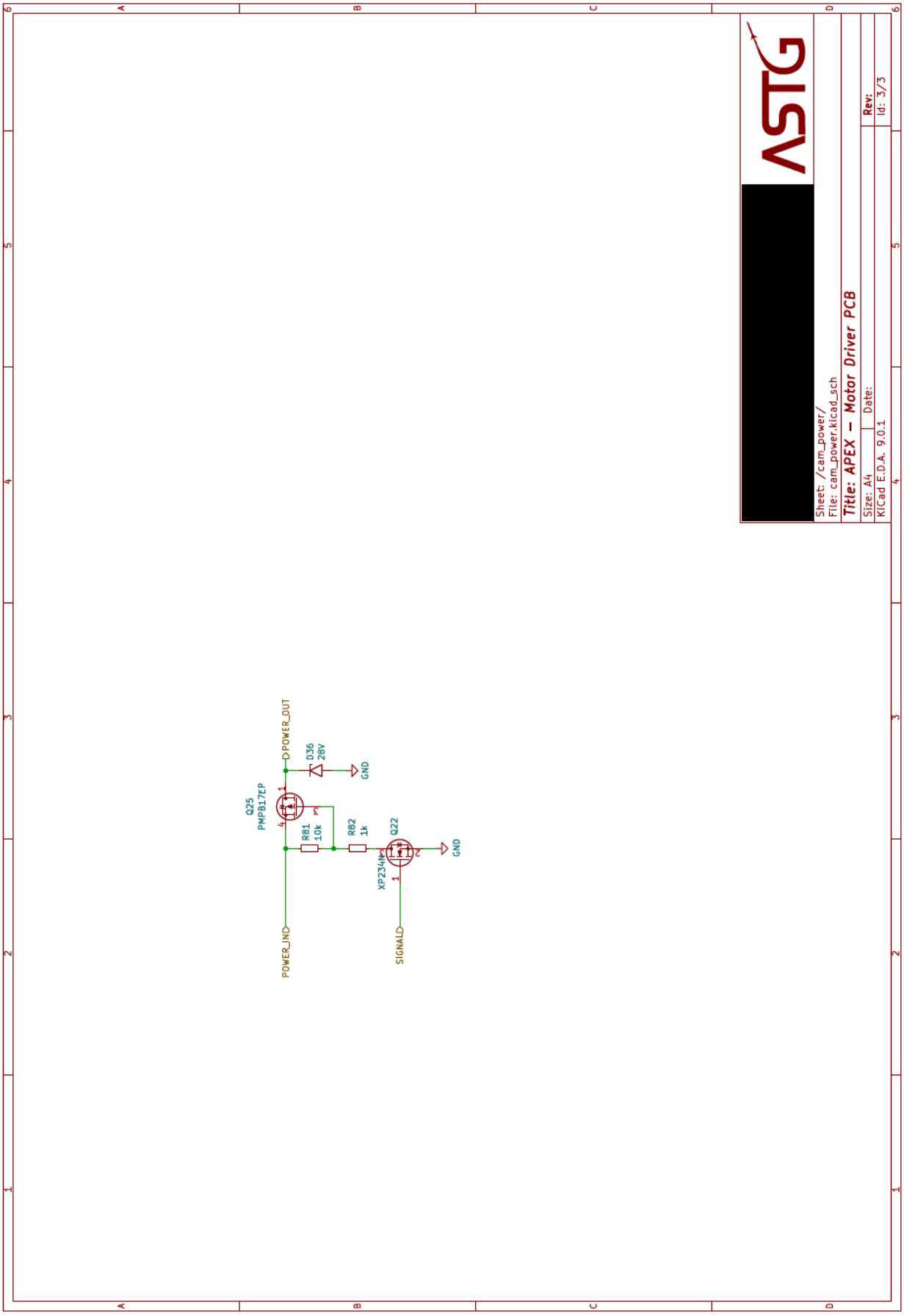

Storage
SD_D2
SD_D3
SD_CMD
+3V3
SD_CLK
SD_D0
SD_D1
SD_DETECT
SHIELD
GND
Io protection
D15
GND
Sheet: /Storage/
File: sd_card.kicad_sch
Title: <Project Title> - <Name of the PCB>
Size: A4
Date:
Rev:
KiCad E.D.A. 9.0.1
Id: 10/10

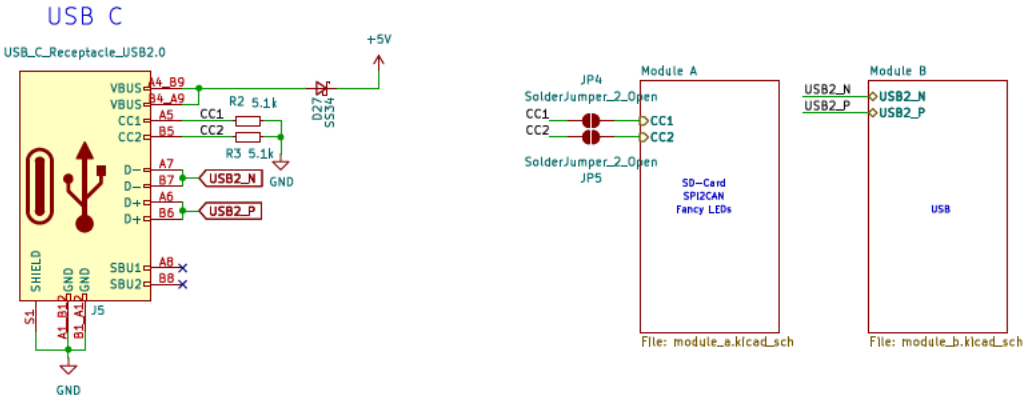

ASTG
Sheet: /blackbox_backplane/IO_Protection/
File: io_protection.kicad_sch
Title: <Project Title> - <Name of the PCB>
Size: A4
Date:
Rev:
KiCad E.D.A. 9.0.1
Id: 7/10
RN1
51
RN2
51
D13
DT1240
IO_0_OUT
IO_1_OUT
IO_2_OUT
IO_3_OUT
IO_4_OUT
IO_5_OUT
IO_6_OUT
IO_7_OUT
IO_0_IND
IO_1_IND
IO_2_IND
IO_3_IND
IO_4_IND
IO_5_IND
IO_6_IND
IO_7_IND
GND


Voltage Regulator (3.3V)
U2
AP7381-33SA-7
C5 1u
C6 2.2u
D1 GREEN
R1 500
PSD Sensor
Hamamatsu S5990-01
U3
PSD_X1
PSD_Y1
PSD_X2
PSD_Y2
Microcontroller
U1
STM32G473CEU3
VDDA Filtering
L1 15uH
C9 1u
C10 100n
NRST Pull-Up
R7 1k
Crystal Oscillator
U5
16MHz
C7 100n
Transimpedance Amplifiers
R2 25k
R3 25k
R4 25k
R5 25k
C11 10n
C12 10n
C13 10n
C14 10n
C17 100n
C18 1u
V_REF = 2.5V
Status LEDs
D2 BLUE
D5 BLUE
R6 500
R9 500
CAN FD Transceiver
U4
TCAN1044V
C16 100n
C15 100n
TVS_diode D3
Power/Bus Connectors
Right FFC Connector
Left FFC Connector
J3
J2
F1 Fuse
5V_RAW
Probe Connector
J4
Conn_02x03_Odd_Even
Debug Connector
J1
53261-0671
D4
QSBT40-7-F
Decupling Capacitors
C1 10u
C2 100n
C3 100n
C4 100n
C8 100n
Mounting Holes
H1 MountingHole_Pad
H2 MountingHole_Pad
H3 MountingHole_Pad
H4 MountingHole_Pad
Boot Mode Jumper
R8 10k
JP1 BootJumper
Contact Points
FID1 Fiducial
FID2 Fiducial
FID3 Fiducial
FID4 Fiducial
FID5 Fiducial
FID6 Fiducial
ASTG
Sheet: /
File: ispida_sun_sensor.kicad_sch
Title: ISPIDA – Sun Sensor
Size: A4
Date:
Rev:
KiCad E.D.A. 9.0.1
Id: 1/1


USB
LEDs
SWD
Mounting
MCU
Encoder
Power Monitoring
Reset
ESD SPI & GPIO
BLDC Driver
Power Management
GPIO
CAN
Temperature Sensing
ASTG
Title: APEX – Motor Driver PCB
KiCad E.D.A. 9.0.1


IC4
DRV8313PWPR
C40 10n
C41 100n
C42 100n
C44 100u
C43 100n
C45 470n
R4 10k
R38 10k
M1_U_OUT_CS
M1_W_OUT_CS
M1_V_OUTD
M1_FAULT
M1_SLEEP
M1_RESET
U5
INA240A2PW
U13
INA240A2PW
R13 60m
R14 60m
C29 100n
C53 100n
M1_U_OUT_CS
M1_W_OUT_CS
M1_U_OUTD
M1_CS1
M1_CS2
IC2
DRV8313PWPR
C22 10n
C20 100n
C21 100n
C23 100u
C24 100n
C25 470n
R5 10k
R36 10k
M3_U_OUT_CS
M3_W_OUT_CS
M3_V_OUTD
M3_FAULT
M3_SLEEP
M3_RESET
U8
INA240A2PW
U9
INA240A2PW
R10 60m
R11 60m
C27 100n
C28 100n
M3_U_OUTD
M3_W_OUTD
M3_CS1
M3_CS2
U14
INA240A2PW
U7
INA240A2PW
R8 60m
R9 60m
C54 100n
C55 100n
M2_U_OUT_CS
M2_W_OUT_CS
M2_U_OUTD
M2_W_OUTD
M2_CS1
M2_CS2
IC1
DRV8313PWPR
C48 10n
C46 100n
C47 100n
C49 100u
C50 100n
C51 470n
R6 10k
R40 10k
M2_V_OUTD
M2_FAULT
M2_SLEEP
M2_RESET
+3.3V
GND
VM
Sheet: /Motor Control/
File: motor_control.kicad_sch
Title: APEX – Motor Driver PCB
Size: A3
Date:
Rev:
KiCad E.D.A. 9.0.1
Id: 2/3


ASTG
Sheet: /cam_power/
File: cam_power.kicad_sch
Title: APEX – Motor Driver PCB
Size: A4
Date:
Rev:
KiCad E.D.A. 9.0.1
Id: 3/3
POWER_OUT
D36
28V
GND
Q25
PMPB17EP
R81
10k
R82
1k
Q22
XP234N
GND
POWER_IND
SIGNALD



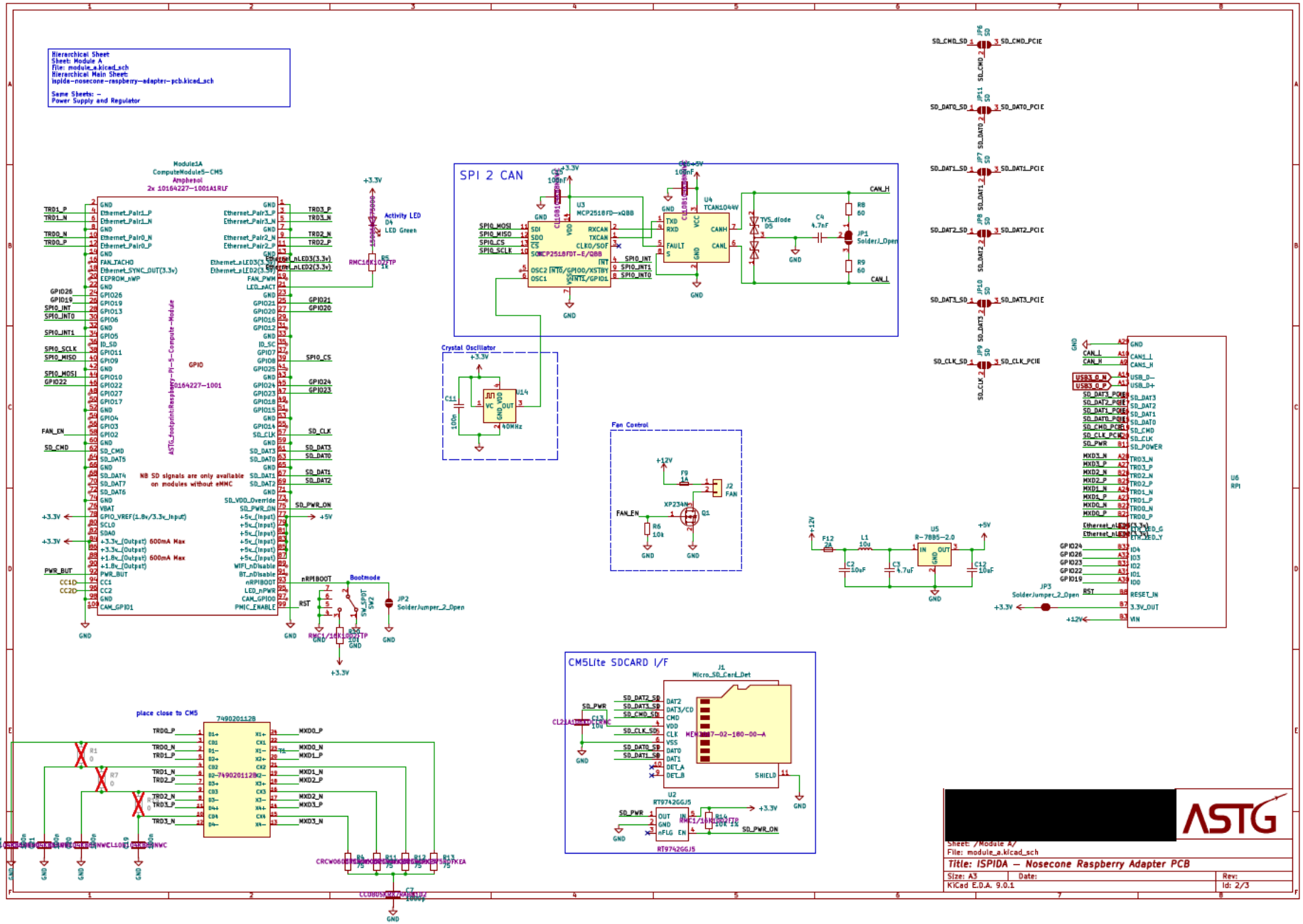
[redacted]

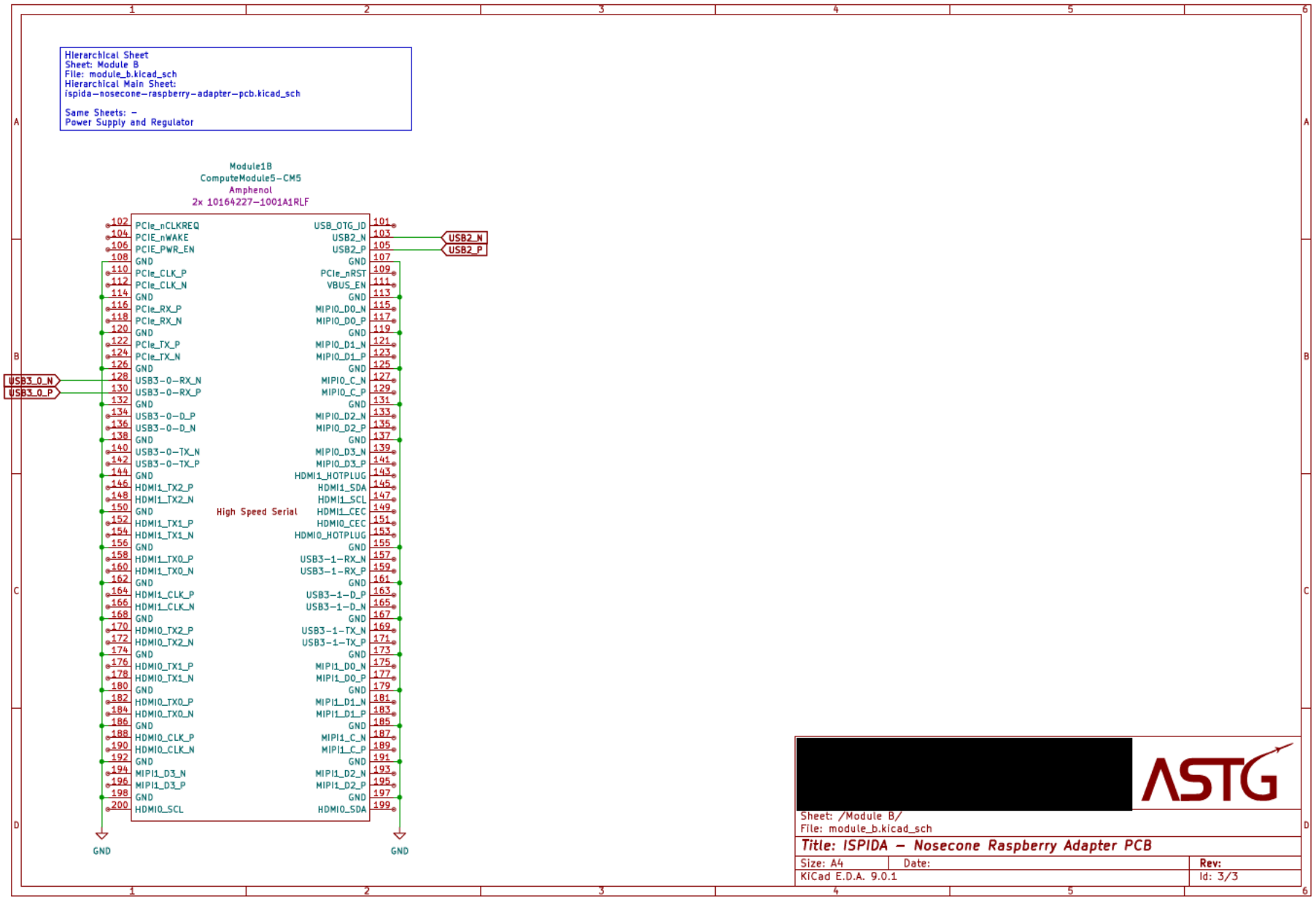
ASTG

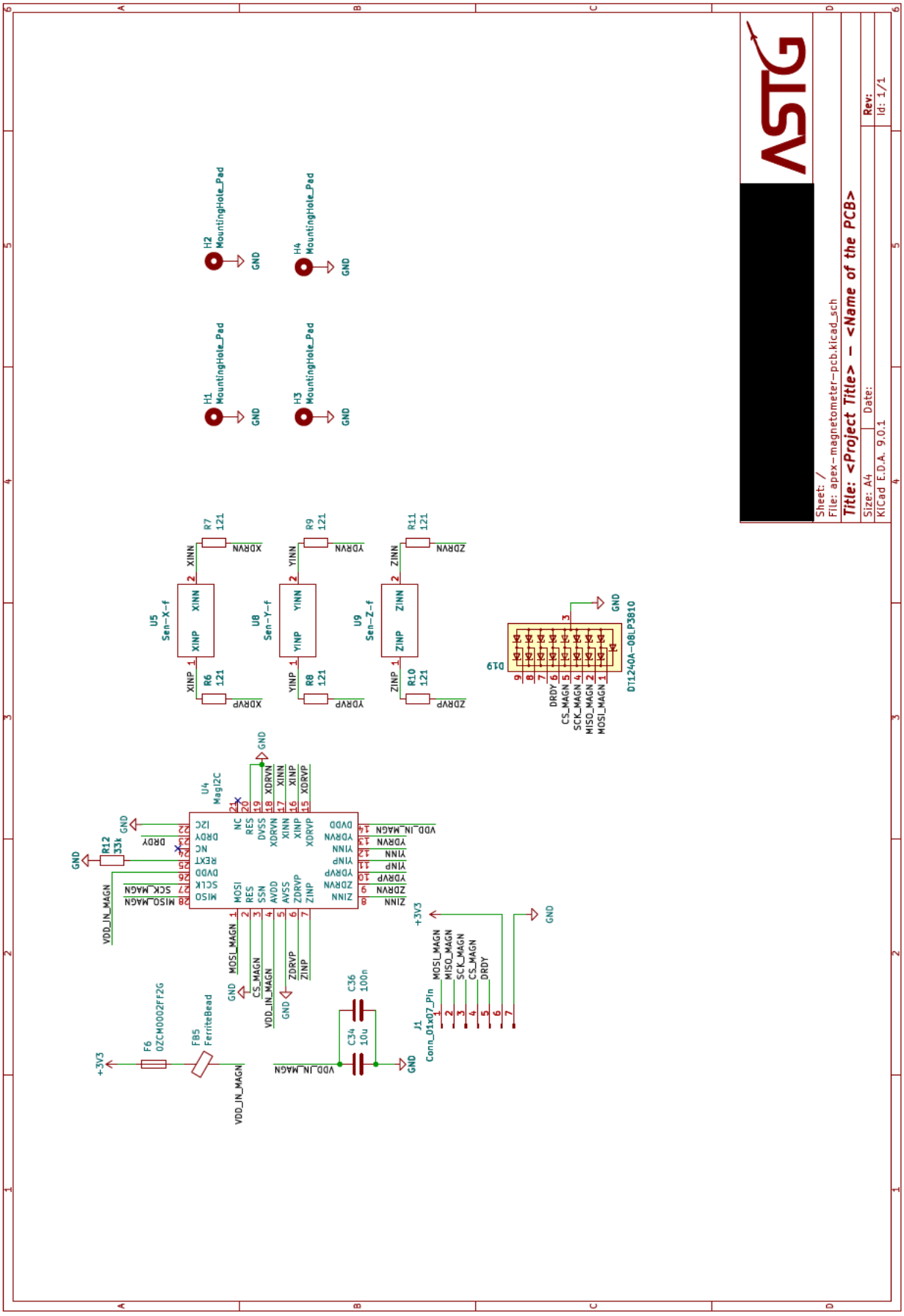
Sheet: /
File: ispida-nosecone-raspberry-adapter-pcb.kicad_sch

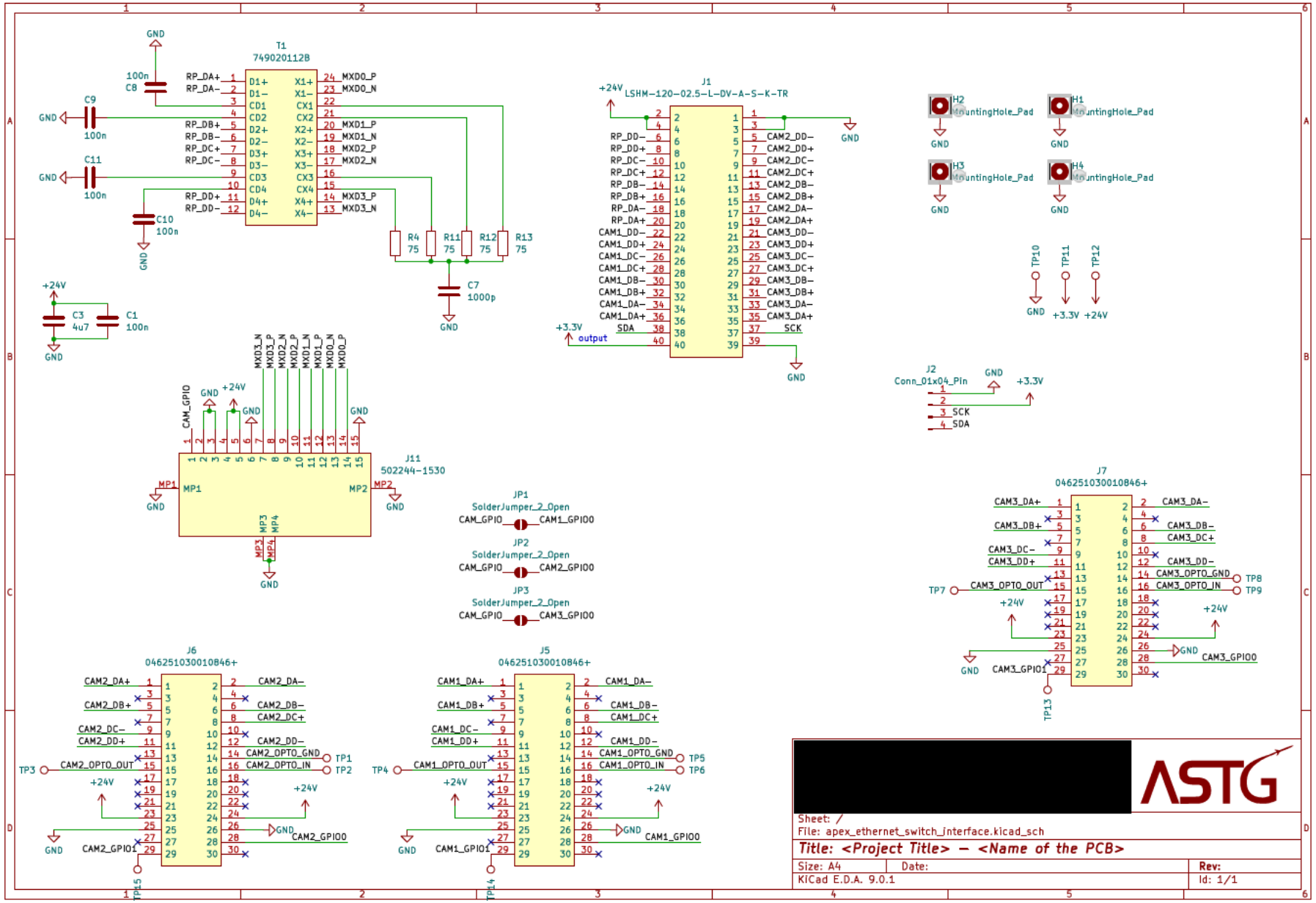
Title: ISPIDA - Nosecone Raspberry Adapter PCB

Size: A4	Date: 2025-04-17	Rev:
KiCad E.D.A. 9.0.1		Id: 1/3


Hierarchical Sheet
Sheet: Module A
File: module_a.kicad_sch
Hierarchical Main Sheet:
ispida-nosecone-raspberry-adapter-pcb.kicad_sch
Same Sheets: -
Power Supply and Regulator
Module1A
ComputeModule5-CM5
Amphenol
2x 10164227-1001A1RLF
SPI 2 CAN
Crystal Oscillator
Fan Control
CM5Lite SDCARD I/F
place close to CM5
7490201128
Activity LED
D4
LED Green
Bootmode
nRPIBOOT
NB SD signals are only available on modules without eMMC
U6
RPI
Micro_SD_Card_Det
RT9742GGJ5
Sheet: /Module A/
File: module_a.kicad_sch
Title: ISPIDA — Nosecone Raspberry Adapter PCB
Size: A3
Date:
Rev:
KiCad E.D.A. 9.0.1
Id: 2/3


Hierarchical Sheet
Sheet: Module B
File: module_b.kicad_sch
Hierarchical Main Sheet:
ispida-nosecone-raspberry-adapter-pcb.kicad_sch
Same Sheets: -
Power Supply and Regulator
Module1B
ComputeModule5-CM5
Amphenol
2x 10164227-1001A1RLF
High Speed Serial
USB2_N
USB2_P
USB3_0_N
USB3_0_P
GND
Sheet: /Module B/
File: module_b.kicad_sch
Title: ISPIDA - Nosecone Raspberry Adapter PCB
Size: A4
Date:
Rev:
KiCad E.D.A. 9.0.1
Id: 3/3


H2
MountingHole_Pad
GND
H4
MountingHole_Pad
GND
H1
MountingHole_Pad
GND
H3
MountingHole_Pad
GND
U5
Sen-X-f
U8
Sen-Y-f
U9
Sen-Z-f
R7
121
R9
121
R11
121
R6
121
R8
121
R10
121
XDRVN
YDRVN
ZDRVN
XDRVP
YDRVP
ZDRVP
XINN
YINN
ZINN
XINP
YINP
ZINP
D19
DT1240A-08LP3810
DRDY
CS_MAGN
SCK_MAGN
MISO_MAGN
MOSI_MAGN
U4
Mag12C
R12
33k
VDD_IN_MAGN
+3V3
F6
0ZCM0002FF2G
FB5
FerriteBead
C34
10u
C36
100n
J1
Conn_01x07_Pin
Sheet: /
File: apex-magnetometer-pcb.kicad_sch
Title: <Project Title> - <Name of the PCB>
Size: A4
Date:
Rev:
KiCad E.D.A. 9.0.1
Id: 1/1


T1
749020112B
C8 100n
C9 100n
C11 100n
C10 100n
R4 75
R11 75
R12 75
R13 75
C7 1000p
C3 4u7
C1 100n
J1
LSHM-120-02.5-L-DV-A-S-K-TR
H1 MountingHole_Pad
H2 MountingHole_Pad
H3 MountingHole_Pad
H4 MountingHole_Pad
TP10
TP11
TP12
J2
Conn_01x04_Pin
J11
502244-1530
JP1 SolderJumper_2_Open
JP2 SolderJumper_2_Open
JP3 SolderJumper_2_Open
J7
046251030010846+
J6
046251030010846+
J5
046251030010846+
TP1
TP2
TP3
TP4
TP5
TP6
TP7
TP8
TP9
TP13
TP14
TP15
ASTG
Sheet: /
File: apex_ethernet_switch_interface.kicad_sch
Title: <Project Title> — <Name of the PCB>
Size: A4
Date:
Rev:
KiCad E.D.A. 9.0.1
Id: 1/1

C.4 PCB - Layout

C.5 Datasheets

Specification Fuse Head 1W1A PP overmolded

Specification:

Bridge resistance:	1,0 +/- 0,2 Ω
No-fire current:	≤ 1,0 A / 5min
All-fire current:	≥ 5A / 50ms
All-fire impuls (10mF; Bruceton methode):	≤ 1,0 W
Stray voltage:	2000 pulses, 2Hz, 100mA, 300ms duration
Helium leakage rate:	> 1x10-6 ccm/s @ 1atm diff. pressure
TTFP:	< 5ms @ 5A
ESD immunity:	500pF / 500 Ω / ± 25kV (0,6 Joule)
Pressure after ignition (3.5 ccm bomb):	25 – 45 bar (mean value)

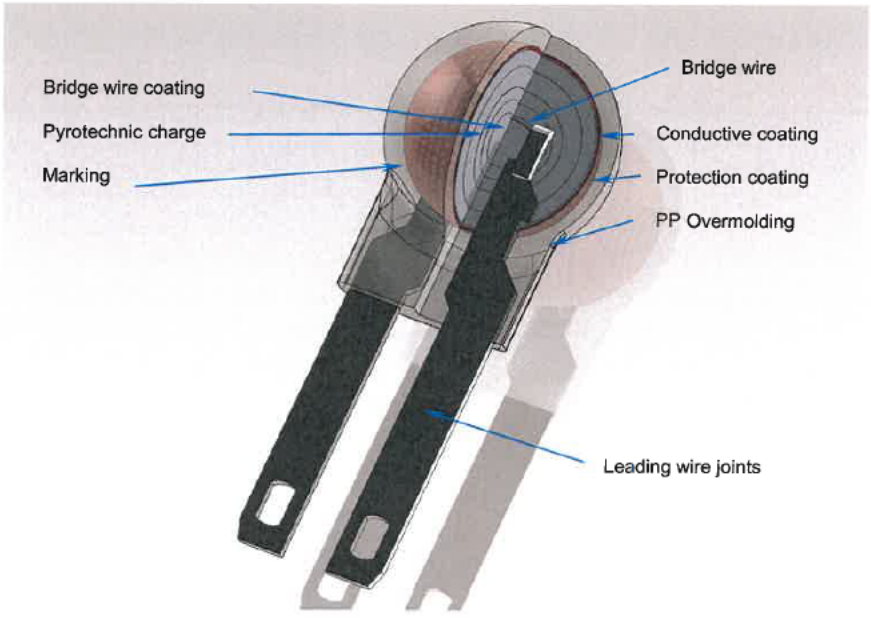
Temperature data:

Use temperature range:	-40°C	to	+85°C
Storage temperature (shelf life 10 years):	-40°C	to	+71°C

The ballistic function is given down to -40°C; it is on the users responsibility, to compile the wire coating material to the demands in the application.

Geometric Properties (see also drawing 6019303 B00):

Total length:	14,0 mm ± 0,40 mm (ca. 8mm overmolded)
Max. width (Head):	6,2 mm ± 0,20 mm
Width (pair of Legs):	4,15 mm ± 0,15 mm



"All data provided on this data sheet is intended as a non-binding guideline only. Any warranty is excluded. A certain suitability or possible use of the products may not be construed or deducted from this data. A guarantee or any warranty in this regard is therefore excluded in any case. Furthermore, our General Terms and Conditions of Sale, Delivery and Service are applicable."

Appendix D: Checklists

For Checklists please contact Team APEX via the Aerospace Team Graz.

Appendix E: Detailed Test Reports

E.1 Minimal Prototype Test

This section details the verification and validation protocol executed on the initial physical manifestation of the gimbal system. The test campaign comprises two primary focus areas: functional articulation verification and micro-vibration characterization. The fundamental objective is to establish an early baseline for the structural, mechanical, and electrical subsystems prior to integration with high-fidelity optical components.

Test ID	1
Test Name	Minimal Prototype Functionality and Kinematic Test
Verified item	Mechanical prototype assembly utilizing mass/inertia simulators in lieu of the final optical subsystem flight hardware.
Test description	Empirical evaluation of the actuation dynamics, closed-loop control, and mechanical locking/unlocking mechanisms of the Gimbal System. The assembly includes the primary structural frame, hold-down and release mechanisms, localized actuation components, and the preliminary wire harness.
Expected Result	**Success:** Unrestricted kinematic movement across all designated rotational degrees of freedom (DoF) matching operational envelope requirements, alongside 3 consecutive, flawless mechanical unlocking cycles. **Partial Success:** Consistent actuation across all axes with minor angular positioning deviations, or minor mechanical resistance noted during a subset of the unlocking cycles.
Obtained results	The multi-axis gimbal structure was actively controlled across all three independent rotational axes. Uniform motion was achieved within the structurally and electronically defined boundary limits without binding.
Overall conclusion	**Successfully Verified** — The structural integrity, kinematic boundaries, and primary actuation mechanisms conform to initial design criteria.

Test ID	16
Test Name	Gimbal-Induced Structural Vibration Test
Verified item	Integrated Minimal Prototype Assembly
Test description	Dynamic actuation of the integrated gimbal system across various angular velocity profiles, utilizing ultra-sensitive acceleration sensors rigidly mounted to the base plate to characterize and quantify induced micro-vibrations and structural resonance.
Expected Result	**Success:** Measured structural vibrations induced into the base interface remain strictly below the allowable threshold of $5 \times 10^{-5}\,\mathrm{g_{rms}}$ across the critical frequency spectrum of 0 to 25 Hz. **Partial Success:** Qualitative and quantitative ground-based assessment shows no major tactile or audible structural oscillations during unconstrained, non-isolated bench testing throughout the full spatial range of motion.
Obtained results	During non-isolated ambient ground laboratory testing, no severe macro-vibrations or abnormal acoustic resonances were detected across the operating spectrum. However, precision micro-g verification remains unquantified due to ambient facility noise floor limitations.
Overall conclusion	**Partially Verified** — Qualitative structural stability is validated for nominal operations; high-fidelity isolation testing is required for quantitative compliance.

Overview and Test Objectives

The primary objective of this experimental campaign is to validate the low-level mechatronic architecture of the gimbal assembly. This specifically encompasses the hardware-in-the-loop interoperability of the dedicated motor-driver board, the brushless/stepper direct-drive motors, and the high-resolution absolute angular encoders.

Furthermore, this test serves as a critical verification checkpoint for the firmware embedded within the motor-driver microcontroller. Key focal points include assessing command-tracking latency, validating the state-machine transitions between locked and active states, and empirically tuning the Proportional-Integral-Derivative (PID) feedback loop parameters to optimize angular stiffness and minimize settling time.

Setup, Instrumentation, and Test Procedure

To guarantee safety and isolate low-level mechatronic variables, the gimbal prototype was configured in a decoupled laboratory environment mimicking flight-representative electrical interfaces, though omitting the primary flight-computer command stack. Primary electrical power was provided by a regulated laboratory DC power supply set to a nominal 24 V bus voltage, incorporating overcurrent protection to safeguard the driver electronics.

The onboard firmware was explicitly refactored for this test sequence to execute a pre-programmed, simultaneous multi-axis path generation algorithm. This script commands the gimbal to break away smoothly from its mechanical hold-down position and traverse a multi-point angular coordinate grid.

For the execution of Test 16 (Vibration Characterization), the hardware setup was mounted on a low-friction rotary platform. The induced vibration, generated by the commutation of the different motors and induced torques, were visually assessed.

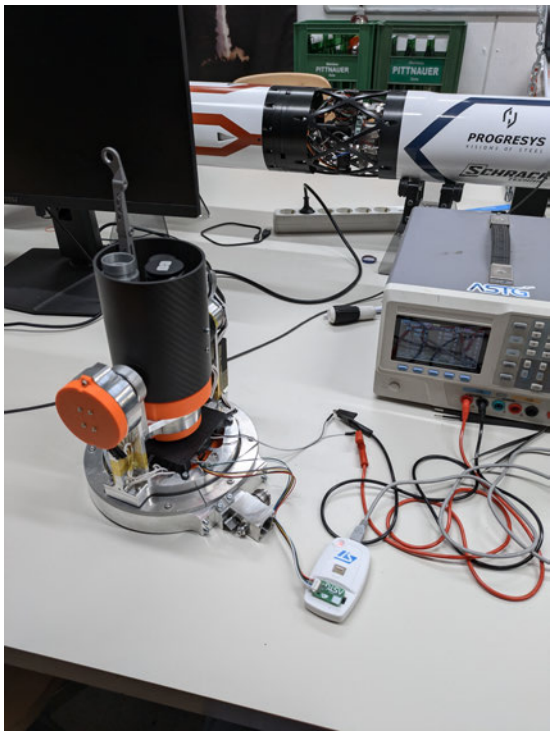


Figure E.1.1: Experimental test setup displaying the decoupled minimal prototype, localized sensor positioning, and 24 V electrical power interface.

Analysis of Results and Requirements Verification

During the execution of the motion profiles, all three rotational axes demonstrated reliable and repeatable angular translation. A comprehensive sweep of angular velocities was performed to identify the upper performance boundaries of the physical assembly.

Up to an angular velocity of 60 deg/s, the control loops maintained exceptional tracking performance. However, when driving the system at velocities exceeding 60 deg/s, a noticeable phase lag was introduced into the tracking error. This resulted in an angular position discrepancy that violated the strict pointing allocation requirement of $\pm 1°$, thereby establishing an operational velocity ceiling for this specific tuning configuration. Nonetheless, this performance envelope completely satisfies the baseline requirement **P-11**.

The dynamic acceleration profiles successfully demonstrated compliance with requirement **P-10**, comfortably reaching the mandated acceleration target of 120 deg/s^2 without causing overcurrent trips or rotor slippage. Additionally, the geometric range-of-motion constraints dictated by requirements **P-7**, **P-8**, and **P-9** were fully verified. The integrated cable-reels and service loops accommodated the extreme angular displacements without introducing parasitic mechanical torque or risking physical binding.

Overall Conclusion and Next Steps

In summary, the Minimal Prototype Test successfully achieved its primary engineering milestones. The mechatronic control loop is stable under nominal operating conditions, and the structural integrity of the gimbal frame is sufficient to handle the dynamic loads of multi-axis slewing.

To achieve full verification for Test 16, future testing iterations must transition to a clean, vibration-isolated optical bench using a high-fidelity data acquisition system (DAQ). This will

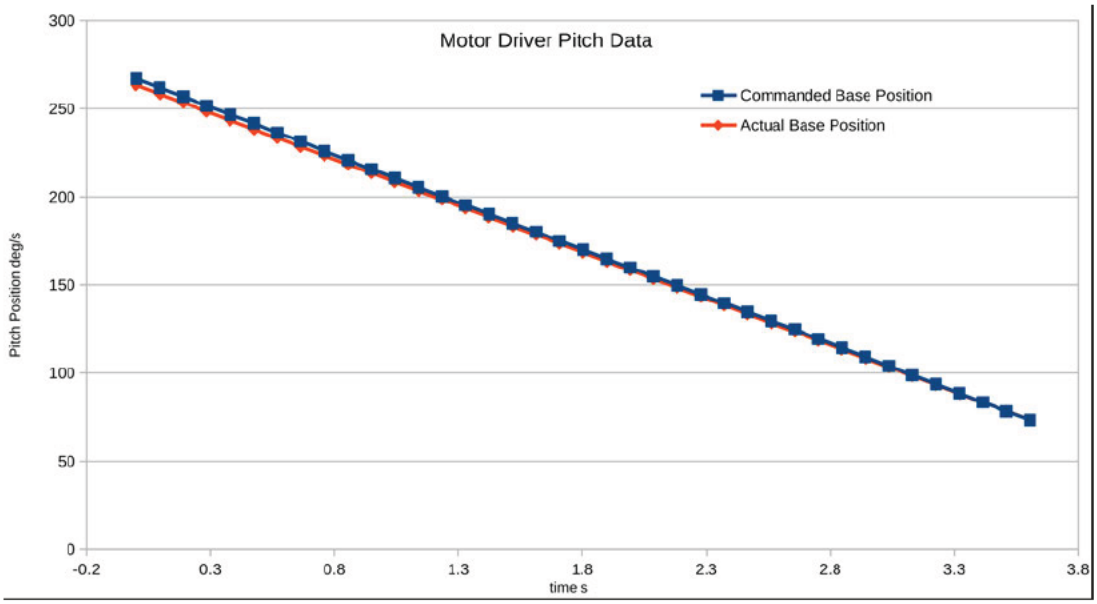


Figure E.1.2: Empirical Pitch Axis time-series data extracted from the motor-driver telemetry, illustrating angular command tracking, error residuals, and steady-state stability.

allow for the precise mapping of micro-vibration spectra against the designated g_{rms} limit lines. The PID parameters will also be further iterated to suppress the tracking lag observed during high-velocity maneuvers.

E.2 Optical Filter Transmissivity Degradation due to Vacuum Outgassing

Test ID	02
Test Name	Optical Filter Transmittance Degradation due to Vacuum Outgassing
Verified item	Optical Color Filter
Test description	Measure transmissivity before and after the filter is placed in a sustained vacuum in order to determine the effect of outgassing on filter transmissivity
Expected Result	**Sucess:** Measureable effect, but not critically strong **Partial Sucess:** No measurable effect would necessitate further tests to confirm
Obtained results	Transmissivity degradation was obtained to be $6.3\,\% \pm 0.7\,\%$ after 1 h in a vacuum equivalent to an altitude of 51 km
Overall conclusion	Successfully verified

Overview

This test was conducted to assess the risk of signal degradation due to the filter signal degradation due to the deposition of outgassing material during the exposition to the vacuum condition in the vacuum environment of the upper atmosphere. The test is considered successful if the degradation can be measured with statistical significance over a given number of measurements.

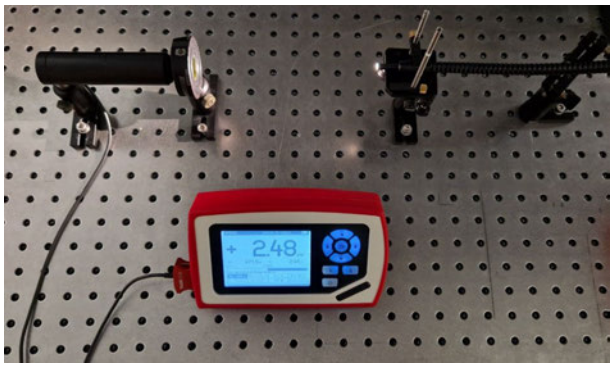


Figure E.2.3: Measurement Setup

Setup and Procedure

Figure E.2.3 shows the setup for measuring the transmittance of the filter, with the power meter at the bottom, the photodiode sensor at the left, the filter right next to it and the white light source at the right. After each measurement with a filter, the filter was removed for a reference measurement. The filter mounting ensured that the filter is in the same position for every measurement, whereas the angle was rather hard to determine precisely. This is one of the reasons for there being 20 measurements, it allows to average over the results, minimizing the effect of an inconsistent angle adjustment.

The filter was transported to the vacuum chamber after the first round of measurements in a sealed, padded container. The filter was left in the vacuum chamber for 60 min at a pressure equivalent to an altitude of 51 km. The vacuum chamber, in addition to containing the filter, was sealed with a rubber tube. Also, there are traces of different hydrocarbons on the inside of the chamber, meaning that there was enough outgassing potential. The same transportation conditions apply for the way back.

Overall Conclusion

Sub-Test ID	2
Date	13.01.2025
Location	Physics Institute at the University of Graz
Checklists	Applicable checklists for setup and procedure
Environment	Controlled Lab Environment at 22 °C

Observation

Immediately, a clear divide is visible in Figure E.2.4, while the compared reference measurements in Figure E.2.5 are very close.

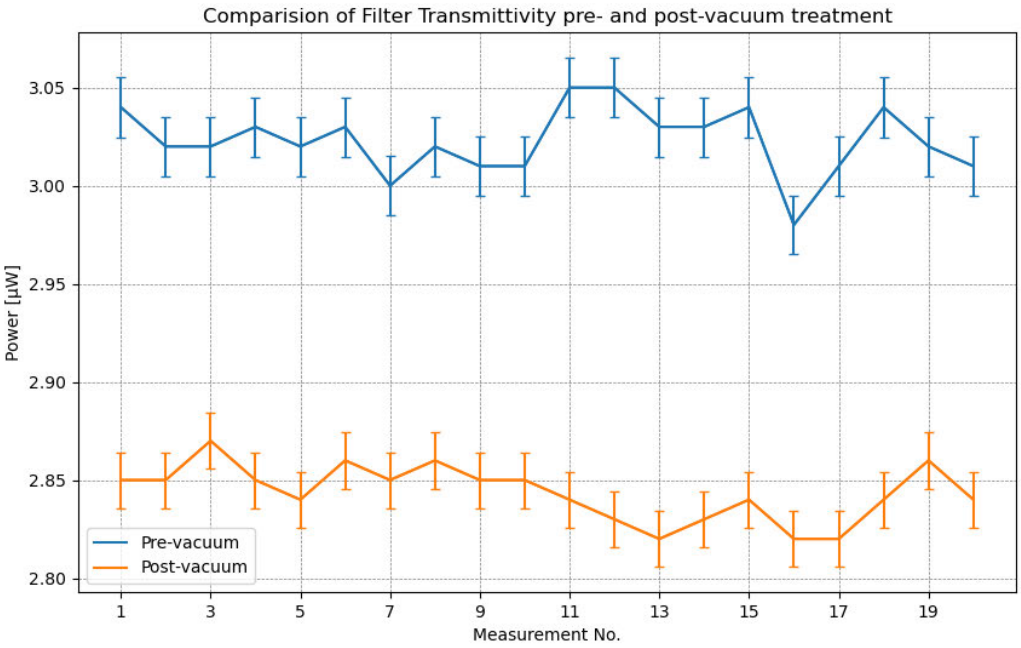


Figure E.2.4: Directly Measured Power

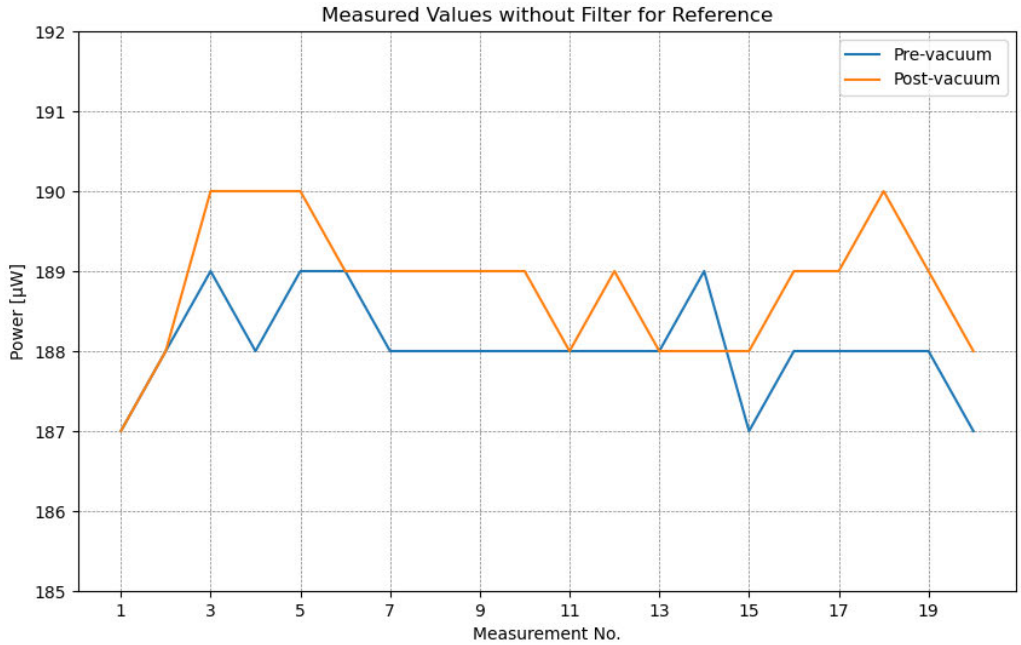


Figure E.2.5: Reference Measurements without Filter

Evaluation

The ratio of measured power between the cases with and without filter was calculated before and after the vacuum treatment, see Figure E.2.6. The relative difference between those ratios can be averaged to 6.3 % ±0.7 %, with the uncertainty being the standard deviation.

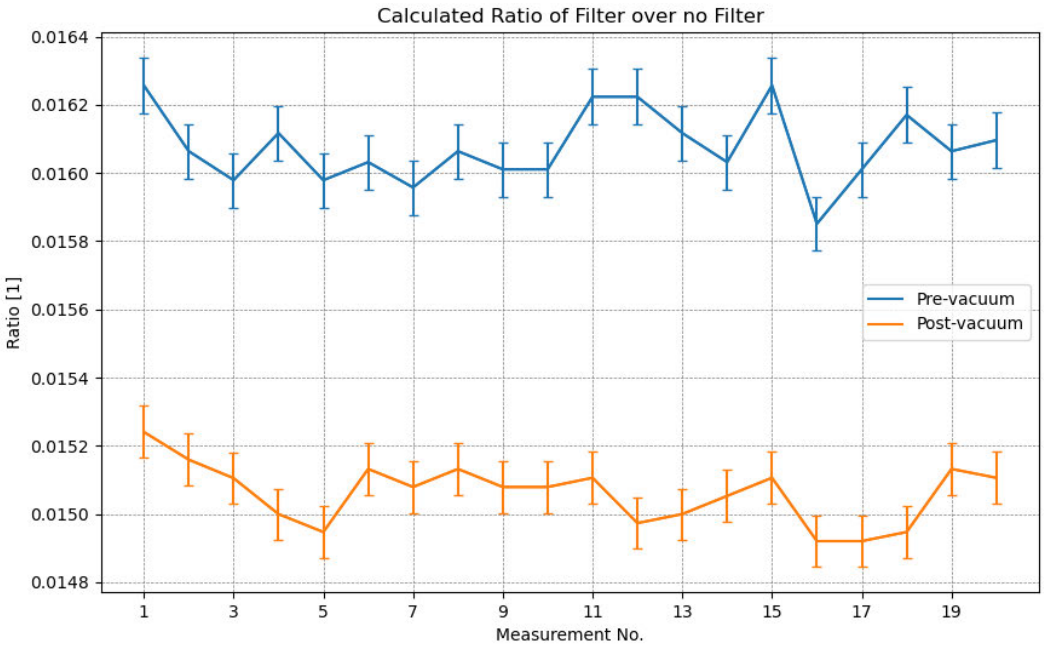


Figure E.2.6: Ratio of Power without Filter over with Filter

Conclusion

In this test, the transmittivity degradation was measured to be 6.3 % ± 0.7 %. This suggests that outgassing material was deposited onto the filter during the exposure to vacuum. While the source of the deposited material could have been from the vacuum chamber itself, it is conservative to think that it came from the filter holder. Thus, a similar degradation could occur during flight. The measurement procedure as such can not be used to determine any fogging of the filter that dissipates within a short span of time. This would require a measurement while inside the vacuum. Additionally, this measurement can not rule out the effects of dust that might have settled on the filter, which might also have played a smaller role even though the filter was transported in a casing and the laboratory generally has a low amount of dust. The filter was cleaned afterwards using a lens cleaning tissue, and appeared to have removed the deposited material, as the transmissitivity was restored to its original value.

E.3 Locking Tests

Test ID	03
Test Name	Unlocking
Verified item	Prototype without optical subsystem, but stands in for optical subsystem
Test description	Repeated unlocking tests under various load types and amounts
Expected Result	**Success :** At least 3 consecutive unlockings of the Gimbal System. At least one of them must be with both ignitors firing simultaneously, and one with only one ignitor firing. **Partial Success:** -
Obtained results	Summary in a few sentences of the overall result of the test.
Overall conclusion	Successfully verified

Test ID	27
Test Name	Pyrotechnic Pin Puller Test
Verified item	Pin Puller
Test description	Test the Pin puller deployment with loads above the expected value
Expected Result	**Success :** At least 3 consecutive unlockings, with no solid parts larger than 10mm^3 escaping the pin puller. At least one of them must be with both igniters firing simultaneously, and one with only one ignitor firing **Partical Success:**-
Obtained results	Tested successfully with both 2 and 1 ignitor, no soot could be observed on paper towels aligned with potential exit paths.
Overall conclusion	Successfully verified

Test ID	28
Test Name	Pin Puller Reaction Force Test
Verified item	Prototype without optical subsystem, but stand in for optical subsystem
Test description	Test the reaction force created by the Pin puller with the whole gimbal. To measure this, the gimbal is suspended on a wire at its center of mass or placed on a slippery surface.
Expected Result	**Success :** The force created by the pin puller is quantified of below a limit of 1 Ns. **Partical Sucess:**-
Obtained results	Retired, as the impulse exerted during other tests by the pin puller on the system was deemed small enough to not result in excessive unwanted tumble rate during the flight of the system.
Overall conclusion	Retiered

Test ID	30
Test Name	Unlocking Vacuum Test
Verified item	Prototype without optical subsystem, but stands in for optical subsystem
Test description	The Unlocking of the Gimbal is tested in a (near) vacuum environment.
Expected Result	**Success :** Unlocking is demonstrated in a vacuum environment of 10 Pascal after being there for 120 s. At least 2 consecutive successful tests **Partical Success:** -
Obtained results	Tested in the Vacuum chamber with success at a pressure of ≈20 mbar. Could not fulfill the vacuum requirement of 10 Pa.
Overall conclusion	Partially verified

Overview

Tested is the locking system of the APEX Payload.

Setup and Procedure

The gimbal is assembled, and the cameras are replaced with mass dummies. A full description of the setup will follow in the modification chapter of the subtest.

Overall Conclusion

This test is ongoing, as not all to be tested requirements could be verified as of 09.11.2025.

Sub-Test ID	27_01
Date	20.09.2025
Location	Aerospace Team Graz Test site
Checklists	charge cup checklist
Environment	20 °C ,outside

Introduction

The locking was tested in a dry - run without the locking arm. The casting process of the charge cups was tested, as well as the tightness of the system regarding smoke and sparks.

Modifications

Only the locking without the gimbal was tested. Three tests were conducted with the aluminium muffler and different muffler fillings. The charge cups were filled and cured following the charge cup checklist.

In the first test, only fleece from plastic was placed in the muffler, tightly rolled. The ignitors in the charge cup were fired sequentially.

In the second test, a central screw was used as an endstop for the locking pin, without any additional 3d print as an attenuator. Around the Screw, fleece was tightly rolled. Both igniters were fired at the same time.

In the third test, a central screw without a 3d print was used as an endstop. Both at the bottom and top of the muffler circles from fleece sandwiched a roll of fleece around the central screw. The top circles also covered the central screw, acting as an additional buffer.

Observation

Figure E.3.7 shows the locking during the first test before the firing, after the first firing, and after the second firing. Figure E.3.8 shows the muffler and muffler filling post-firing.

Figure E.3.9 shows the locking during the second test before the firing and after the firing. Figure E.3.10 shows the muffler and muffler filling post-firing.

Figure E.3.11 shows the locking during the third test before the firing and after the firing. Figure E.3.12 shows the muffler and muffler filling post-firing.

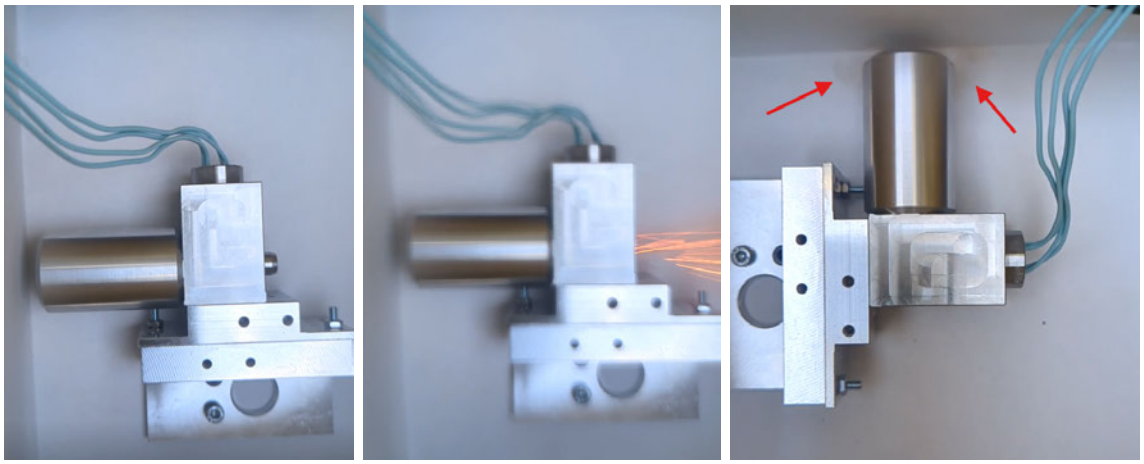


Figure E.3.7: Locking before the first test, during the first firing, and second firing. As no hard endstop is used, the locking bolt is allowed to retract enough to move past its seal, allowing sparks to escape as seen in the middle image. After adding additional material (rubber filament and extra fleece) it appears to push the pin forward sufficiently to seal the system during the second firing, as only smoke escaping through the muffler can be observed.



Figure E.3.8: Muffler and Fleece after the firing. Visible is the charred fleece on the surface facing the pyro chamber.

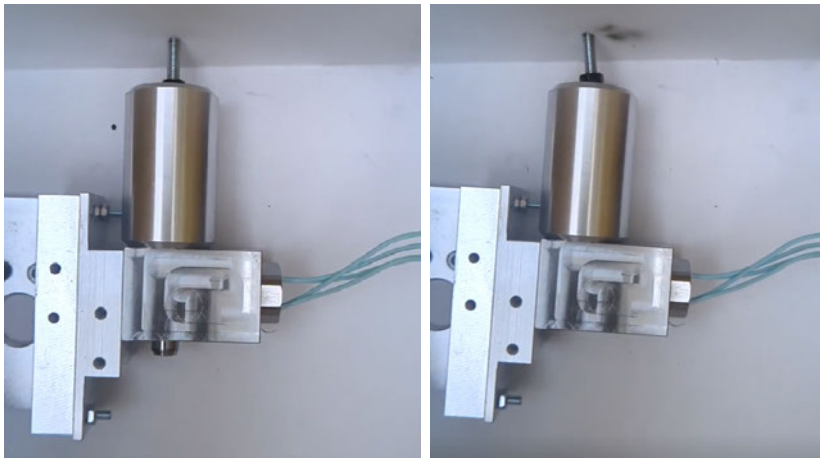


Figure E.3.9: Locking before the second test and after. The force of both ignitor firing at the same time bent both the screw and the bottom of the muffler.

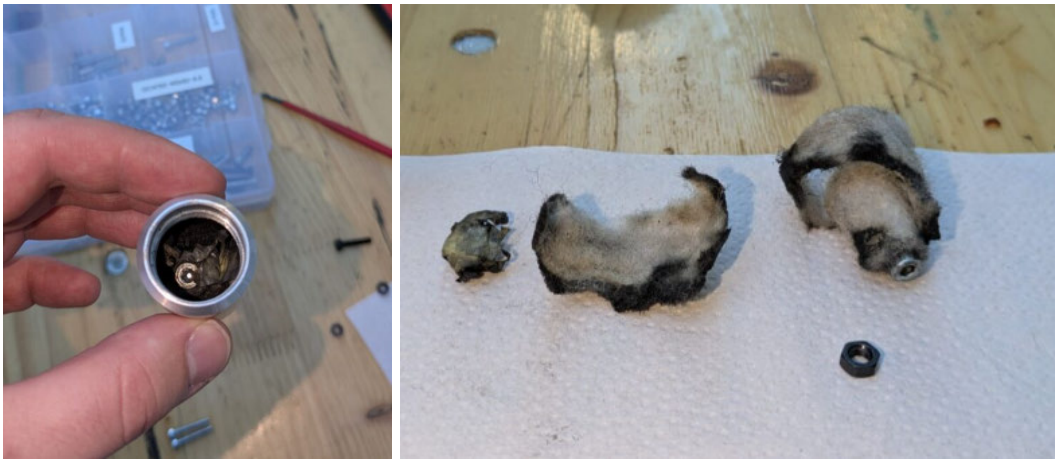


Figure E.3.10: Muffler and Fleece after the firing. Visible is the charred fleece on the surface facing the pyro chamber.

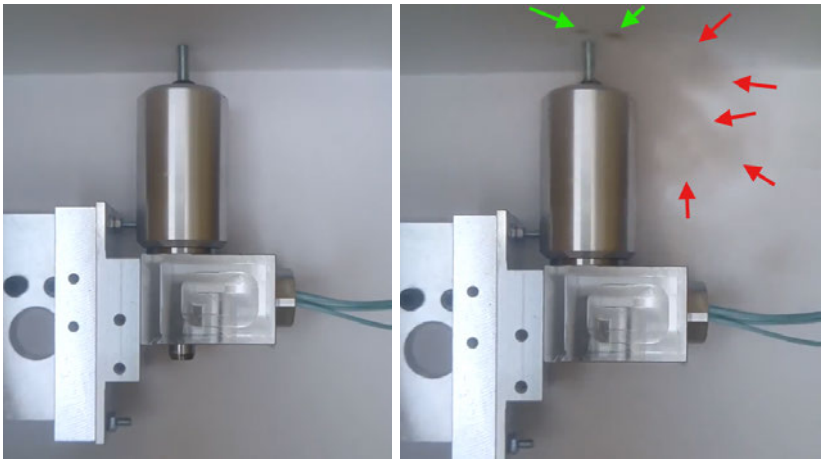


Figure E.3.11: Locking before the third test and after. The green arrows point to spots where soot penetrated through the fleece, and the red arrows point to the penetrated smoke cloud.

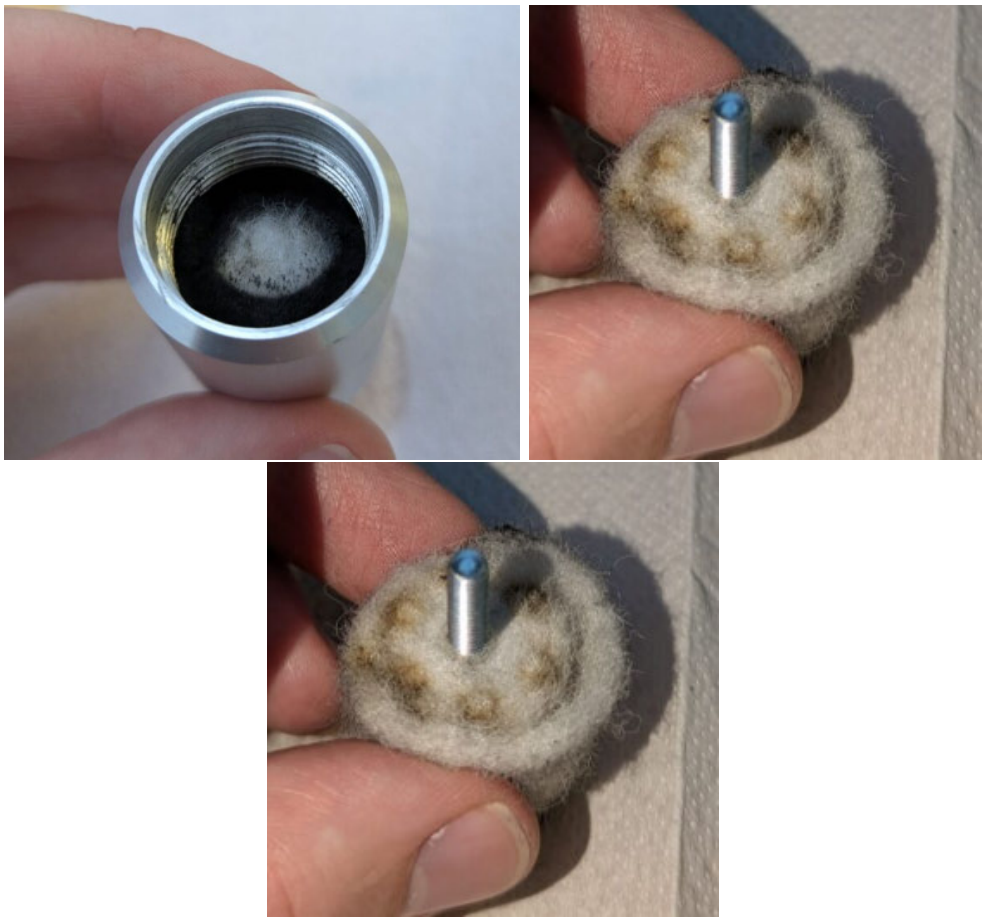


Figure E.3.12: Muffler, Fleece and Locking housing after the firing. Visible is the charred fleece on the surface facing the pyro chamber, and the overmold of the ignitors left behind in the locking housing.

Evaluation

During the first test, the missing endstop resulted in a failure of the forward o-ring, resulting in the expulsion of sparks. Using an Endstop, as in the second and third tests, mitigated this problem. The packing tightness of the fleece majorly impacts the amount of escaping from the muffler, as was expected. Especially when used only as a roll, gases can easily move along the side of the walls. The addition of circular pads appears to mitigate this problem. The second test showed the need for a crash structure in front of the endstop to avoid damage to the muffler and the pin.

Conclusion

The first subtest of the locking can be deemed a success. Gasses escaped only through the designed path over the muffler when an endstop was correctly employed. Improvements in the muffler filling can likely be made by changing the composition of the filter.

Sub-Test ID	27_02
Date	28.09.2025
Location	Aerospace Team Graz Test Side
Checklists	Charge Cup Checklist
Environment	Warm and Moist, above 20°C

Introduction

This test focused on the locking system with the gimbal and improvements in the filling of the charge cups. as well as actuation under more-than-expected load.

Modifications

In this test, the locking was tested with the full gimbal except the optical subsystem, which was replaced with weight representative dummies. Used were the aluminium muffler and the 3D-printed plastic locking grooves.

Three tests were conducted that differed in the number of charges fired and the initial temperature. All three tests were conducted with the same muffler filling of a steel screw as an endstop, surrounded by a plastic tube that protruded about 3 mm over the screw and acted as a dampener for the pin. Around the plastic tube was a stack of 1 sheet of a hyperfine filter from a vacuum cleaner, 2 sheets of plastic fleece, and a roll of plastic fleece.

For the first test, both ignitors in the charge cup were fired at the same time; for the second and third, only one ignitor was fired at a time. For the third test, the whole gimbal and the not-inserted charge cup were chilled in a freezer for roughly one hour to around -15 °C. They were assembled in the test box, and the firing occurred at roughly -10° material temperature.

For each test, the locking screws of the locking arm were pretorqued first to 0.25 Nm (Pin puller side) then 0.2 Nm (Rotating plate side) then again 0.25 (Pin Puller side)

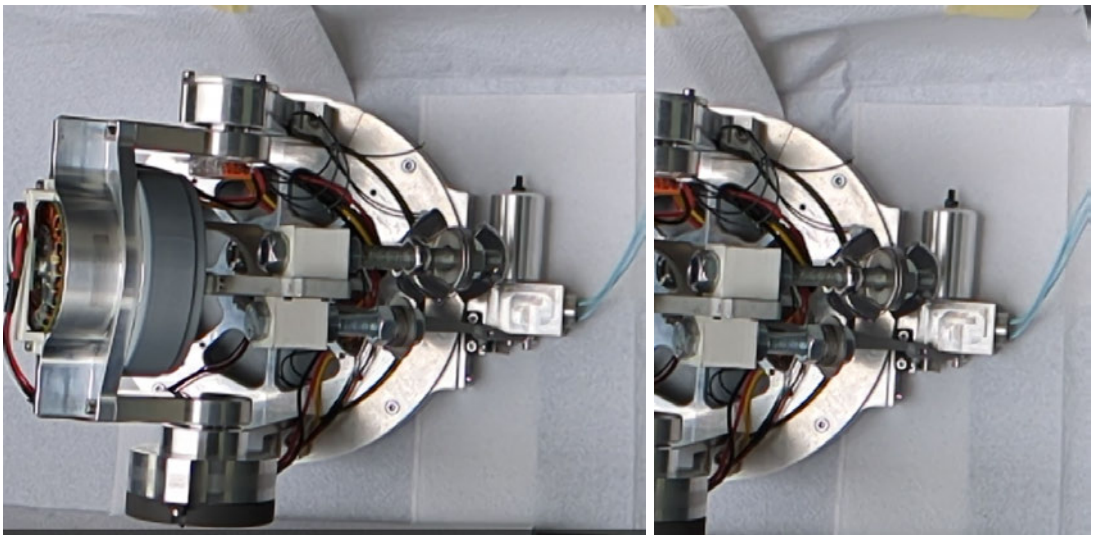


Figure E.3.13: The gimbal prior (left) and shortly after the firing during the first test. Visible is the paper towel being moved by the shock wave in the upper third of the right image, but no smoke, soot, or sparks were observable.

Observation

Figure E.3.13 shows the locking during the first test before the firing, and after the first firing. Figure E.3.14 shows the muffler, muffler filling, and charge cup post-firing.

Conclusion

The actuation system successfully operated under worst-case conditions, demonstrating adequate performance with a single actuator under approximately 50% higher load than the anticipated operational requirements. The fleece material demonstrated limited reusability and should be considered a consumable. While the muffler contents proved effective for noise and soot reduction, installation was time-intensive and may require process optimization. Measured noise levels remained well below hearing hazard thresholds. No immediate design modifications are necessary.

Sub-Test ID	30_1
Date	cc
Location	Aerospace Team Graz Test site
Checklists	Locking test checklist
Environment	22°C ,inside

Vacuum test Introduction

This test was conducted in order to ensure no unforeseen results occur when the locking mechanism is fired in a vacuum.

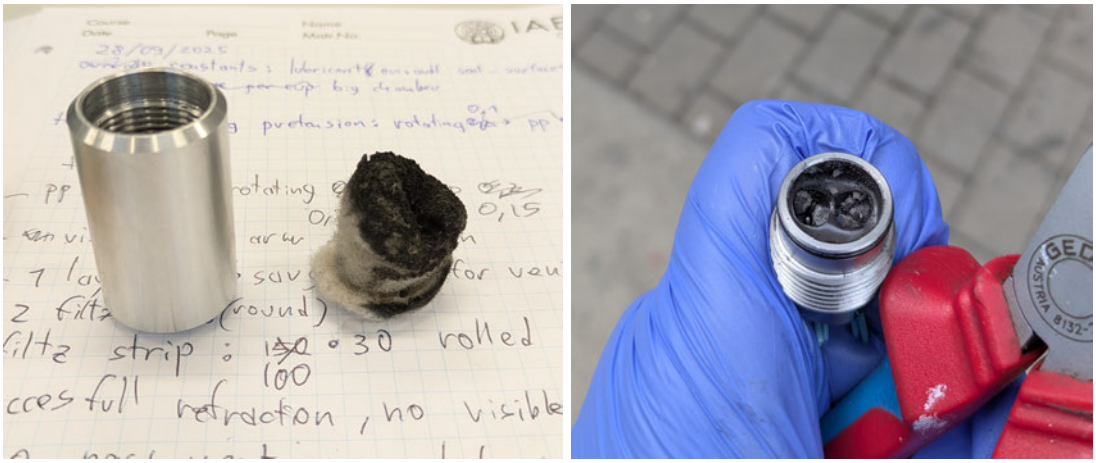


Figure E.3.14: Muffler, Fleece, and charge cup after the firing. Visible is the charred fleece on the surface facing the pyro chamber in the left image. In the right image, the holes with the wires where the ignitors have been can be seen. The resin used for the casting is chared but undamaged.

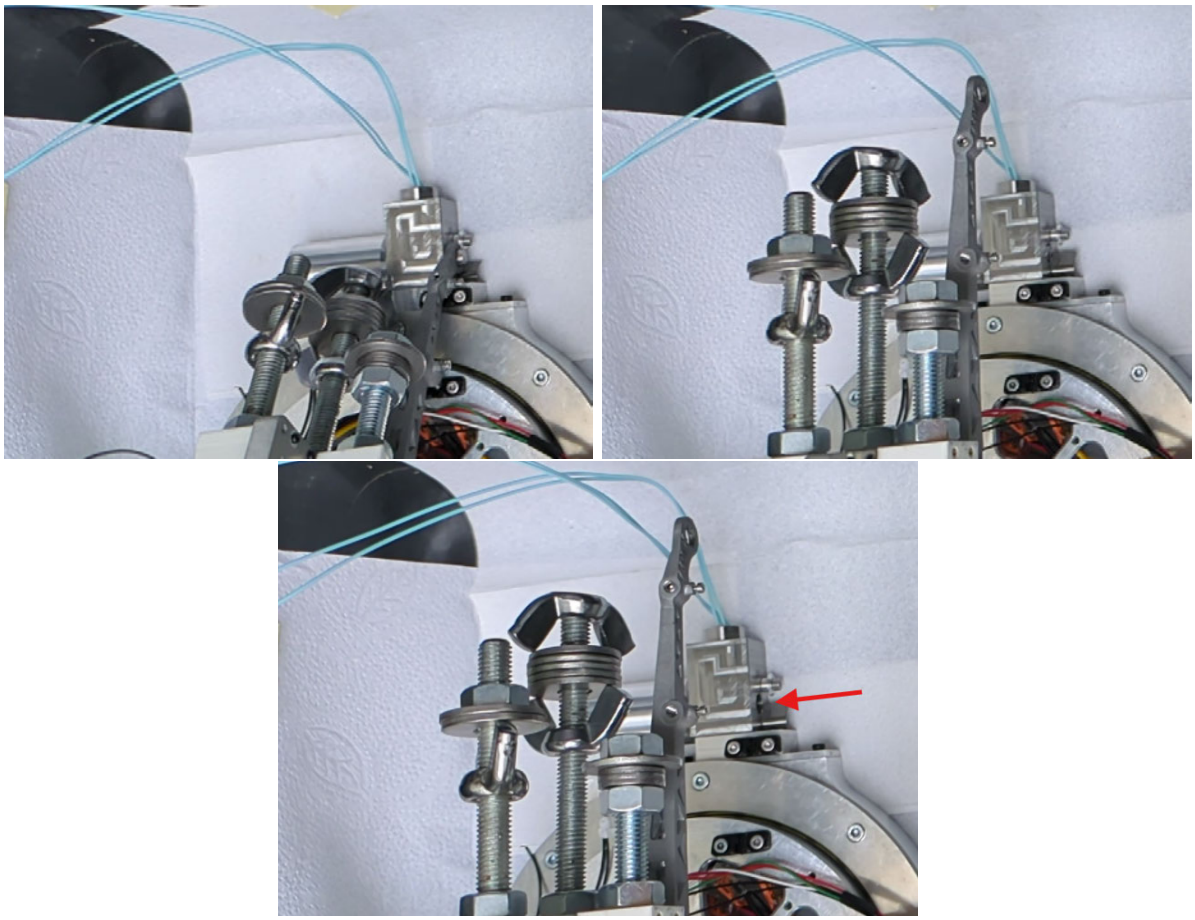


Figure E.3.15: The gimbal prior (left) and shortly after the firing during the first test. Visible is the paper towel being moved by the shock wave in the upper third of the right image, but no smoke, soot, or sparks were observable.



Figure E.3.16: Muffler and Fleece after the firing. Visible is the charred fleece on the surface facing the pyro chamber.

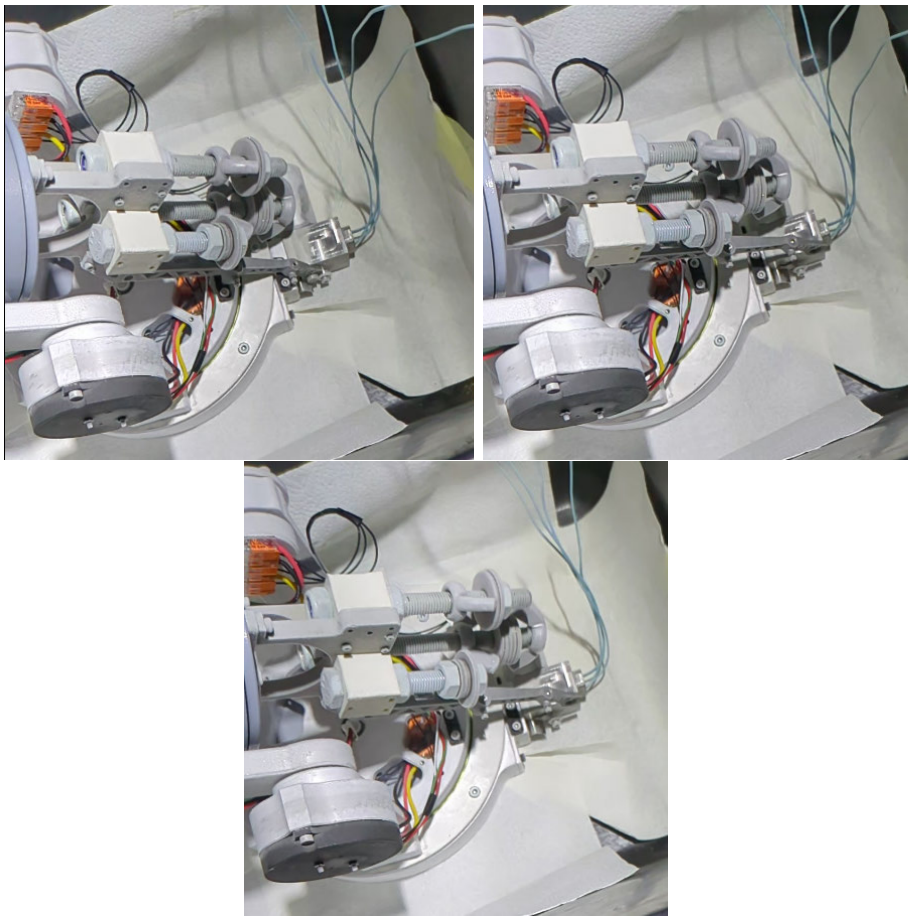


Figure E.3.17

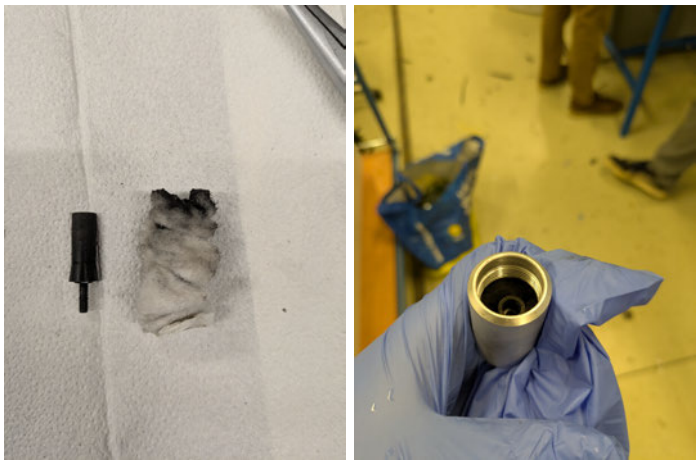


Figure E.3.18: Muffler and Fleece after the firing. Visible is the charred fleece on the surface facing the pyro chamber.

Modifications

Apart from regular locking testing procedure, the the assembled gimbal with prepared pin puller are placed in a cylindrical container (about 0.1 cubic meters in volume) with a pyro cable pasthrough, digital pressure sensor, and vacuum pump. There were two separate firings; Test 1: - the locking mechanism is prepared as per checklist (without bulkhead due to spatial restriction).

- Charge cup with two charges inserted, with a only a single charge connected to cable pass-through

- the vacuum chamber is closed and vacuum pump actuated, targeting a pressure read of 10 Pa or lower

- after bottoming out the possible vacuum, no actions except observing any occurrences

- valve to vacuum pump is closed

- First charge is fired, observe smoke generated

- Open valve to re pressure the chamber, take out and refurbish pin puller (inspect, clean, lubricate, pretension)

- Charge cup with the one remaining charge is inserted, with a only a single charge connected to cable pass-through

-the vacuum chamber is closed and vacuum pump actuated, targeting a pressure read of 100 millibar or lower

- after bottoming out the possible vacuum, no actions except observing any occurrences

- valve to vacuum pump is closed

- Second charge is fired, observe smoke generated



Figure E.3.19: Inserting gimbal (top) and closed vacuum chamber, with valves. pump, and pressure sensor display sitting on chamber lid (bottom)

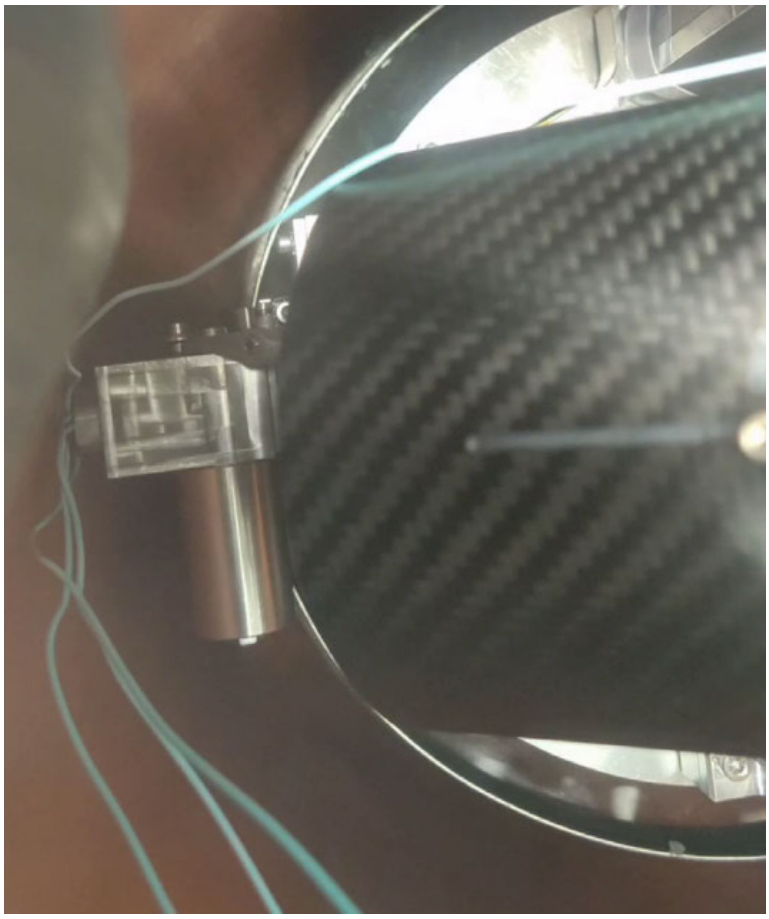


Figure E.3.20: Video screen capture before firing of first test

Observation

Test 1: Minimum pressure pressure observed before firing: 21.9 millibar (at perceived equilibrium), above targeted max. vacuum pressure of 10 Pa.

Visual observations: Successful unlocking observed, very brief misty smoke (barely visible)

Auditory observations: Two very quiet sequential sounds; one at the moment of firing, second when locking arm taps against vacuum chamber wall.

This graph depicts measured vacuum chamber pressure over time.

Test 2: Minimum pressure pressure observed before firing: 23.3 millibar (at perceived equilibrium), above targeted max. vacuum pressure of 10 Pa. Observations are the same as the first test.

This graph depicts measured vacuum chamber pressure over time. There was seemingly problem with the readings, as they stop before the pressure drops down. If the values are reliable, the readings end at 40 millibar pressure,. while still rising.

Evaluation

According to measurements: After firing, the measured pressure increased by about 6 millibar over the course of 10 seconds. Peak pressure might be slightly higher due to time steps of about 200 milliseconds. If another vacuum test is done, the vacuum pump should be disconnected to eliminate possible interference.

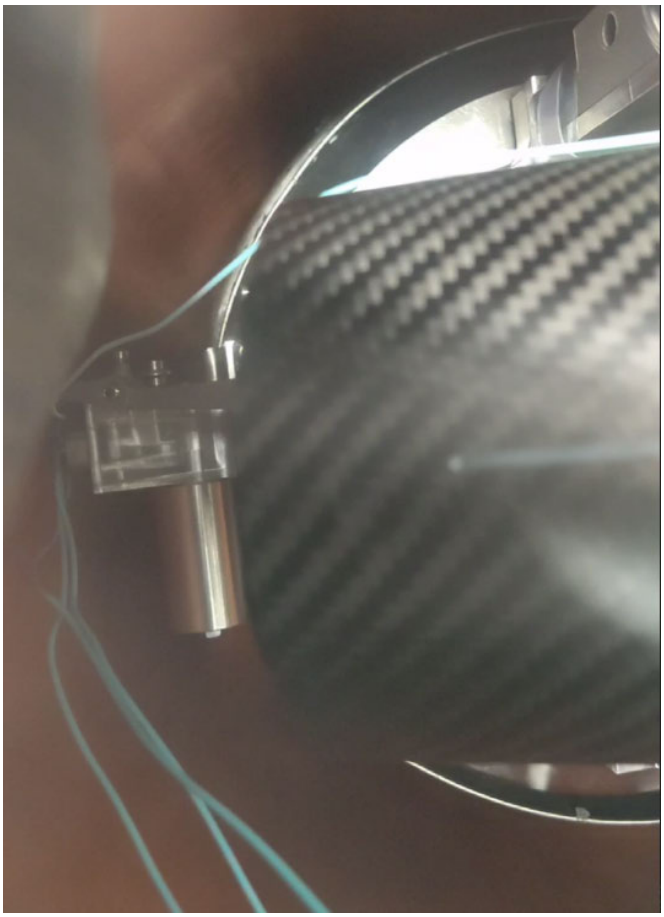


Figure E.3.21: Video screen capture after firing of first test

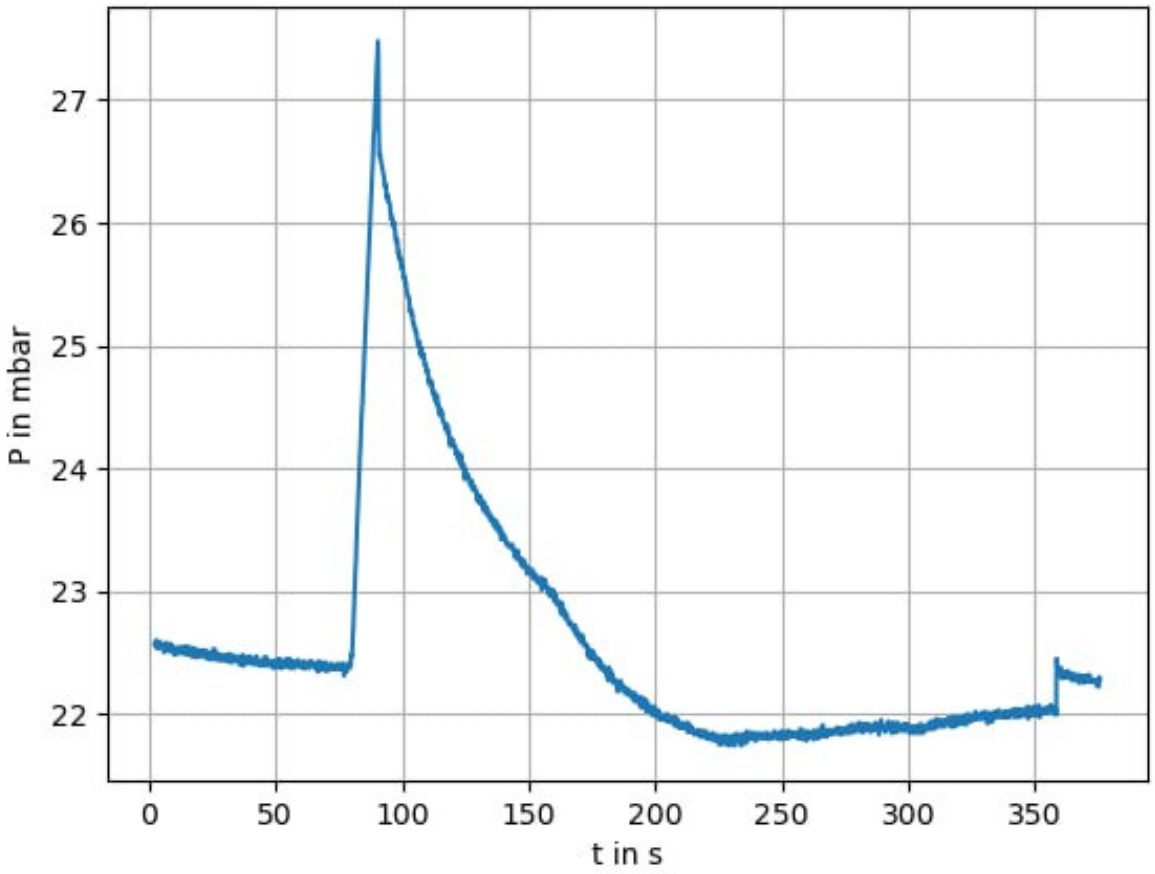


Figure E.3.22: Measured pressure over time

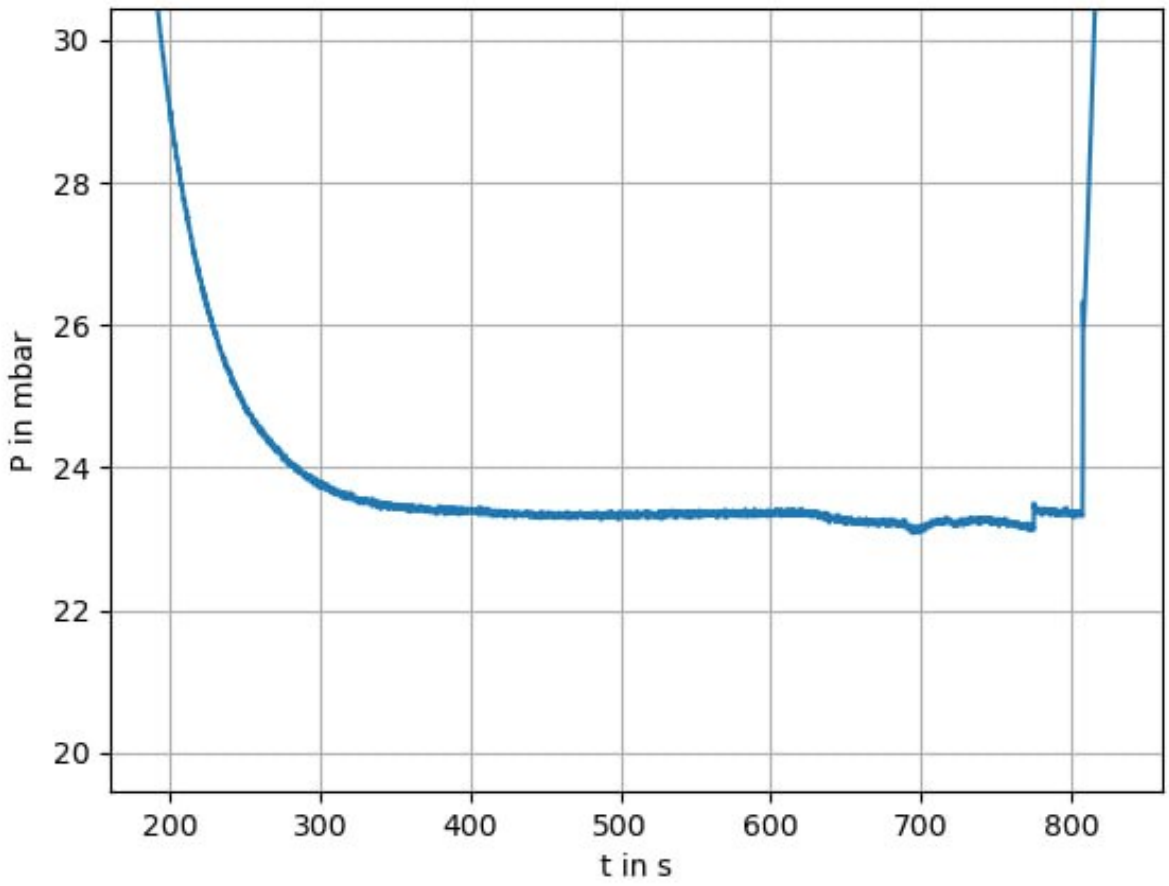


Figure E.3.23: Measured pressure over time



Figure E.3.24: Updated Muffler design post testing. The red arrows indicate the additional Pad used to dampen the impact. The green arrow points at the orange Bolt retainer, which sheered of (as intended) and planted itself in the dampener due to the involved forces.

Conclusion

Successful unlocking in vacuum No modificastions to the setup are needed, however if another vaccuum test is done it should be with two charges and disconnected pump to observe performance of any effects of modificastions to the pin puller muffler.

Sub-Test ID	03_01
Date	01.03.2026
Location	Aerospace Team Graz Test site
Checklists	Locking test checklist
Environment	22°C ,inside

Introduction

During the bench test the Pinpuller failed resulting from excess energy of the bolt combined with lack of energy absorption causing the pin to shoot back. A quick fix was to increase the locking pin travel distance, but to ensure function it was desired to ensure the pin would bounce back.

Modifications

Adding 10x10x3 mm material which converts impact energy into heat.

Observation

2 successful unlocking and 3-4 mm margin measured to where a relocking event might happen. Figure E.3.24 shows the muffler after testing.

Evaluation

Consistent reduction of locking pin ”bounce back” which was measured using the coverage of soot on the pin, Using the imprint of the bolt on the stopper as evidence that there was contact.

Conclusion

This iteration would ensure sufficient enegy to unlock, and mitigation excess energy to ”Re-lock”

E.4 Mass Measurement

Test ID	4
Test Name	Mass test
Verified item	Complete Prototype
Test description	Measuring the weight of the entire assembly
Expected Result	**Sucess:** The assembly has a mass of less than 7.5 kg **Partial Sucess:-**
Obtained results	The mass of APEX without nosecone adapter was weight at 6.22 kg
Overall conclusion	Successfully verified

Test ID	6
Test Name	Center of mass test
Verified item	Complete Prototype
Test description	Measurement of the center of gravity of the whole assembly on all rotational axes
Expected Result	**Sucess:** The centers of masses are within 20 mm of the respective axes of rotation. **Partical Sucess:-**
Obtained results	Retired as CAD - Model Data verified with weight measurement of sub component provided a sufficient approximation of the center of mass.
Overall conclusion	Retired

Overview

The Gimbal and its components were weight to ensure the the total mass of the APEX experiment (without nosecone adapter) is below 7.5 kg.

Setup and Procedure

The Apex experiment was weight with the Nosecone Adapter, and the mass of the Adapter (4.45 kg subtracted from the measured weight (10.67 kg

Overall Conclusion

The mass of the APEX payload was measured at 6.22 kg.

E.5 Vibration Test

Test ID	8
Test Name	Shaker Test
Verified item	Gimbal without Carbon Tube
Test description	Vehicle level 1 Sine and Random Vibrations, with frequency search befor and after. In thrust axis. Vehicel level 1 Random Vibrations, with frequency search befor and after. In lateral axis.
Expected Result	**Sucess:** No shift of eigenfrequency during testing **Partial Sucess:** Minor shift in eigenfrequency
Obtained results	14Hz loss for thrust axis. No frequenzy loss for lateral axis.
Overall conclusion	Successful

Overview

This test validates the structural integrity of critical Apex payload components under simulated launch conditions. Vehicle Level 1 sine and random vibrations are applied in the thrust axis, followed by random vibrations in the lateral axis. Frequency searches are conducted before and after each vibration sequence to detect structural changes. The test is considered successful if: (1) all components remain intact without physical damage, and (2) frequency shifts remain within acceptable limits, indicating no significant structural degradation. The test concludes after completing all vibration profiles and confirming these success criteria are met.

Setup and Procedure

The gimbal is mounted on an adapter to allow rotation for measurement in all axes. The positions of the two accelerometers were attached to the gimbal according to Figure E.5.25 and were chosen as follows:

1. Near the cameras, where, according to the ANSYS simulation, the stress and movement are highest.
2. On an arm near the motor; this is not a high-stress position, but it serves as a reference.

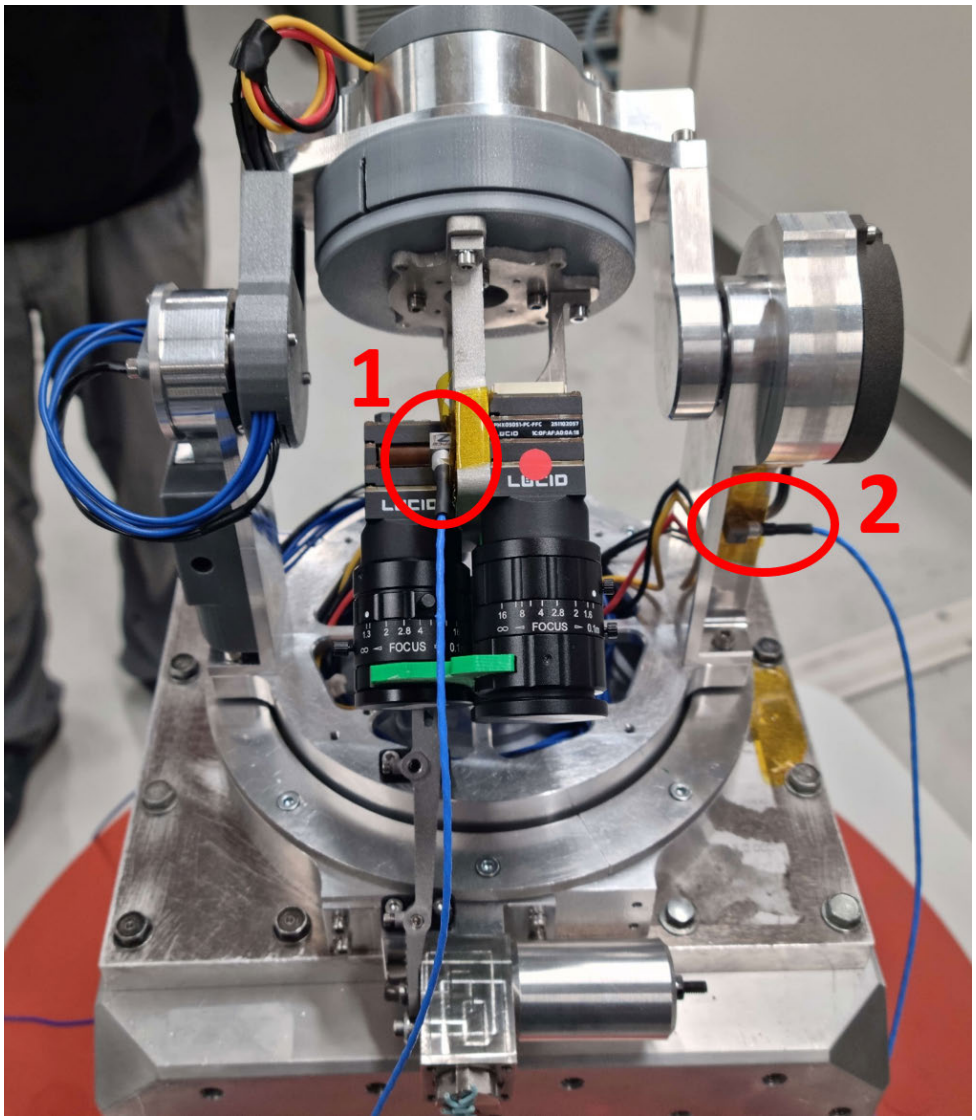


Figure E.5.25: Position of accelerometers

Overall Conclusion

The vibration test campaign successfully validated the gimbal structure's ability to withstand Vehicle Level 1 launch conditions across all axes. Three iterative tests were conducted to address identified design weaknesses: The initial tests (08_01 and 08_02) revealed significant eigenfrequency shifts (20 Hertz - 25 Hertz) due to insufficient screw tightening torque and the absence of locking mechanisms. Post-test inspection confirmed screw loosening, particularly for the M2 camera fasteners and locking mechanism counter-screws. The final test (08_03) incorporated corrective measures: doubled tightening torque aligned with steel-on-steel specifications and installation of toothed washers. Results demonstrated minimal frequency shift (14 Hertz) in the thrust axis and virtually no change in lateral axes, confirming structural integrity. Two design issues require resolution before flight: (1) M2 camera screws will be secured with thread-locking adhesive and proper washers, and (2) locking mechanism clearance will be increased to prevent jamming. The gimbal structure is successfully verified for flight, contingent upon implementing the identified corrective actions.

Sub-Test ID	08_01
Date	20.10.2025
Location	Silicon Austria
Checklists	2025_10_20_APEX_Shaker_Test_Silicon_Austria
Environment	20°C, Silicon Austria Lab

Introduction

This test evaluates the structure by simulating the vibrations experienced during launch to reveal if any components become loose or break.

The test parameters, Vehicle Level 1, were taken from the REXUS manual.

Modifications

The test parameters for the sine vibration demand two profiles over the frequency range. However, the shaker could not combine both profiles into a single test sequence. Therefore, we only simulated the second profile, which is 144 Hz to 2000 Hz. Since the first eigenmode is at 241 Hz, it was decided that this was not an issue.

Observation

During the test, nothing became visibly loose or broke down. However, there was a drop in the eigenfrequency of the first mode.

Evaluation

The following plots show the measurements of the resonance search from the two sensors before and after the test.

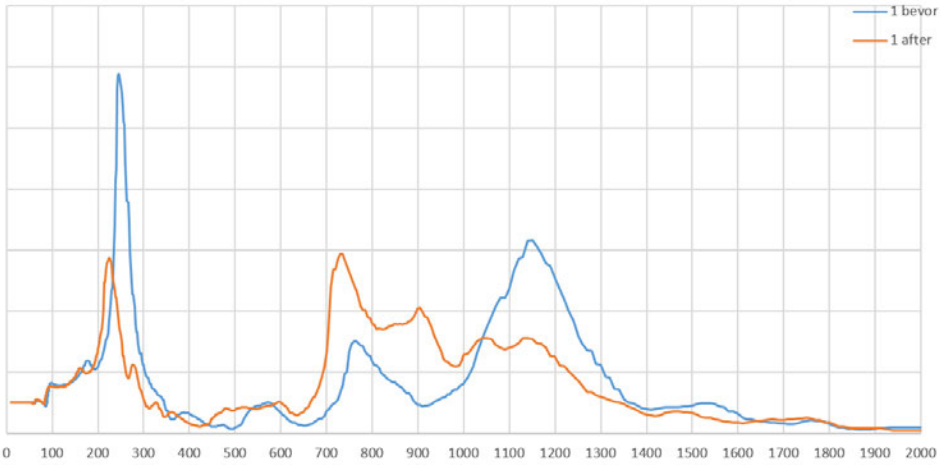


Figure E.5.26: Frequency search, before and after of sensor 1 (Cam)

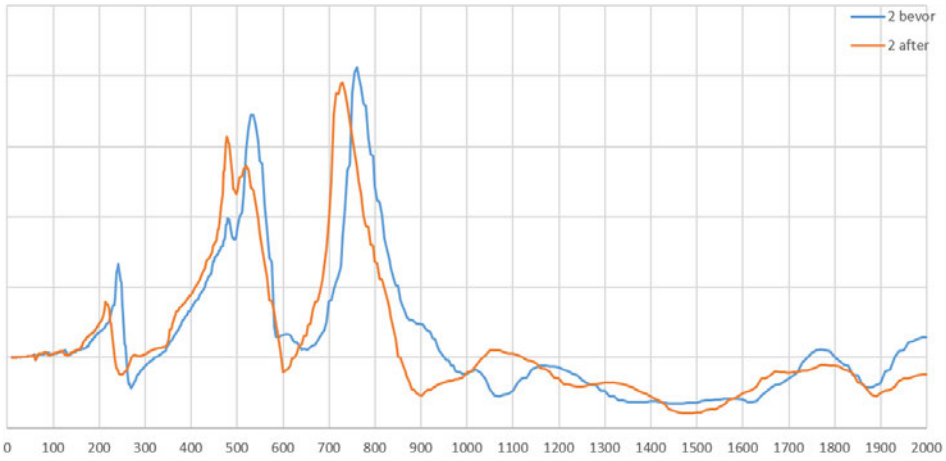


Figure E.5.27: Frequency search, before and after of sensor 2 (Arm)

As shown in Table Table 4.7, the first eigenmode is at 238 Hz, which matches the ”before” measurement from sensor 1. However, a clear shift in the eigenfrequencies is evident.

Conclusion

The results indicate a decrease in frequency of approximately 20 Hertz for most modes. This shift is likely attributable to the use of a low screw tightening torque, combined with the absence of lock washers.

Sub-Test ID	08_02
Date	20.10.2025
Location	Silicon Austria
Checklists	2025_10_20_APEX_Shaker_Test_Silicon_Austria
Environment	20°C, Silicon Austria Lab

Introduction

A subsequent vibration test was conducted immediately after the previous one. For this test, only the locking mechanism was re-tightened, as it was hypothesized that its initial loosening, potentially due to omitted counter-screws, was the primary cause of the observed frequency shift. No other screws were adjusted.

Observation

During the test, nothing became visibly loose or broke down. However, there was a drop in the eigenfrequency of the first mode.

Evaluation

The following plots show the measurements of the resonance search from the two sensors before and after the test.

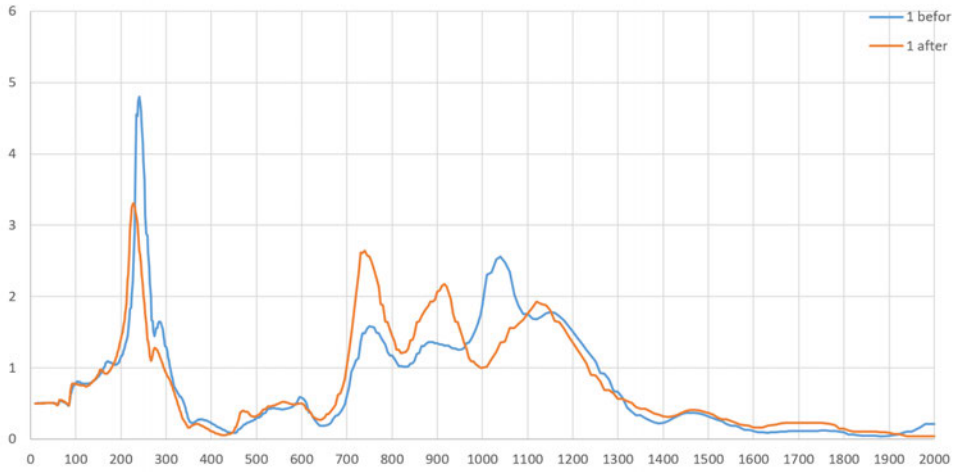


Figure E.5.28: Frequency search, before and after of sensor 1 (Cam)

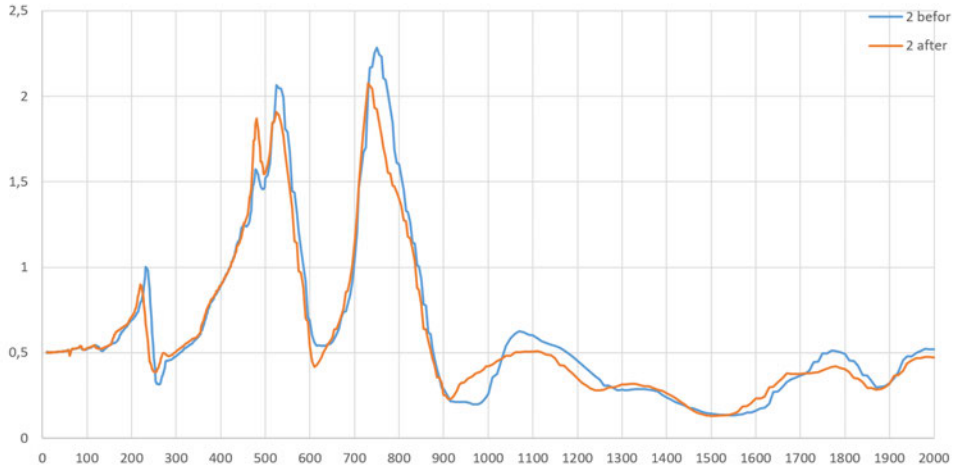


Figure E.5.29: Frequency search, before and after of sensor 2 (Arm)

The results from the second test show a less significant frequency shift, with some modes exhibiting no shift at all.

Conclusion

Initial analysis of the data suggested that the counter-screws of the locking mechanism were the primary cause of the frequency shift.

However, post-test disassembly revealed that other screws had also experienced a reduction in their tightening torque, although they had not come entirely loose. In contrast, several of the M2 screws securing the cameras to the gimbal were found to be completely loose.

Sub-Test ID	08_03
Date	04.11.2025
Location	Silicon Austria
Checklists	2025_10_20_APEX_Shaker_Test_Silicon_Austria
Environment	20°C, Silicon Austria Lab

Introduction

Following the results of the previous tests, the following design flaws were addressed. First, all screws were tightened to approximately double the initial torque, now aligning with the recommended steel-on-steel tightening torque. Additionally, toothed washers were installed to secure the fasteners further.

For this test, all axes were tested consecutively without retightening any screws or re-securing the locking system between runs.

Observation

During the test, nothing became visibly loose or broke down. However, there was a drop in the eigenfrequency of the first mode.

Evaluation

The first two plots show the results of the resonance search in the Z direction (thrust axis).

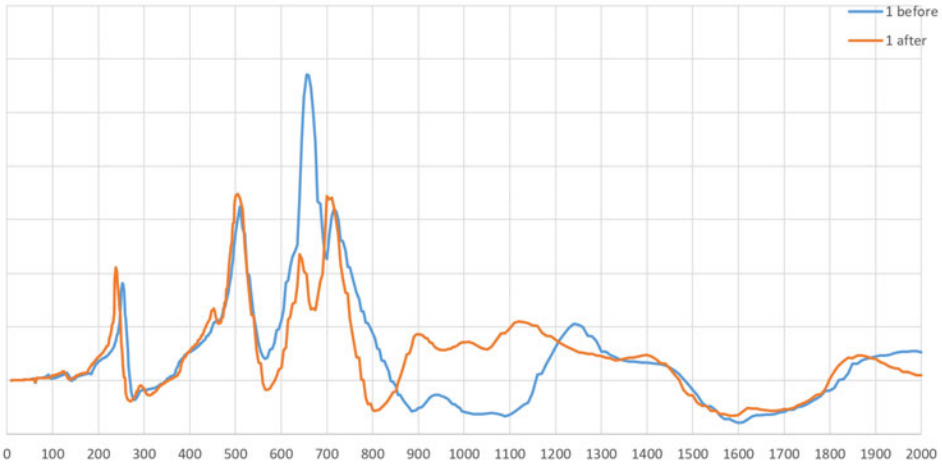


Figure E.5.30: Frequency search Z axis, before and after of sensor 1 (Cam)

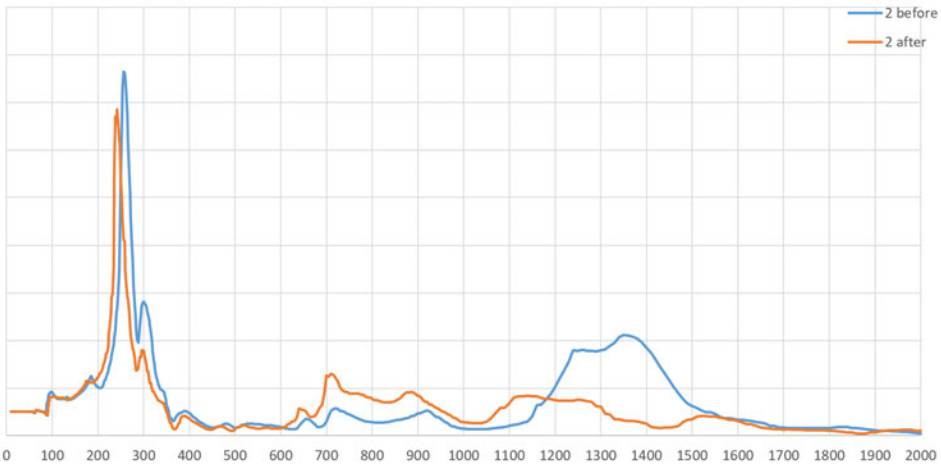


Figure E.5.31: Frequency search Z axis, before and after of sensor 2 (Arm)

During this test, the eigenmodes for the thrust axis exhibited minimal shift following the sine and random vibration tests.

The next two plots show the results of the resonance search in the X direction (lateral axis).

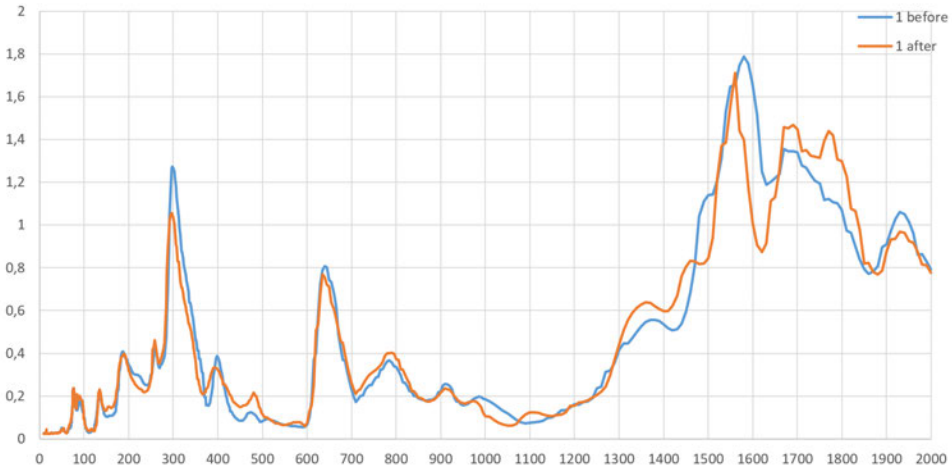


Figure E.5.32: Frequency search X axis, before and after of sensor 1 (Cam)

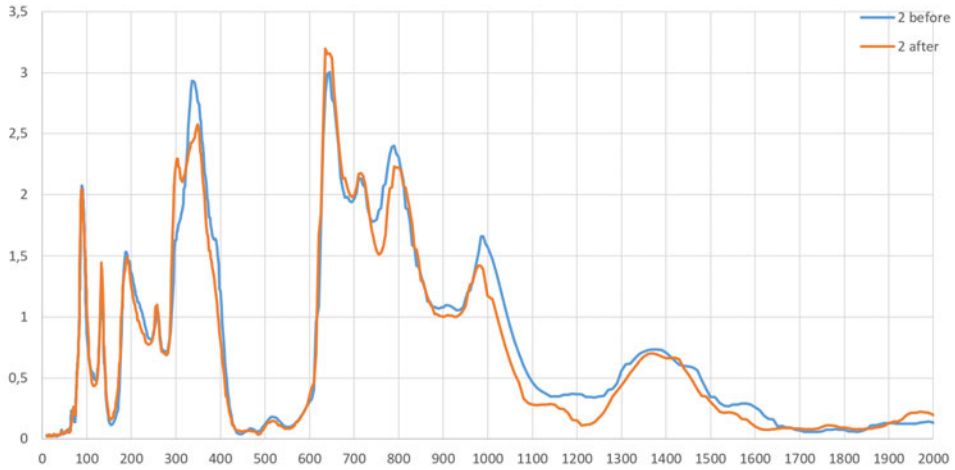


Figure E.5.33: Frequency search X axis, before and after of sensor 2 (Arm)

The last two plots show the results of the resonance search in the Y direction (lateral axis).

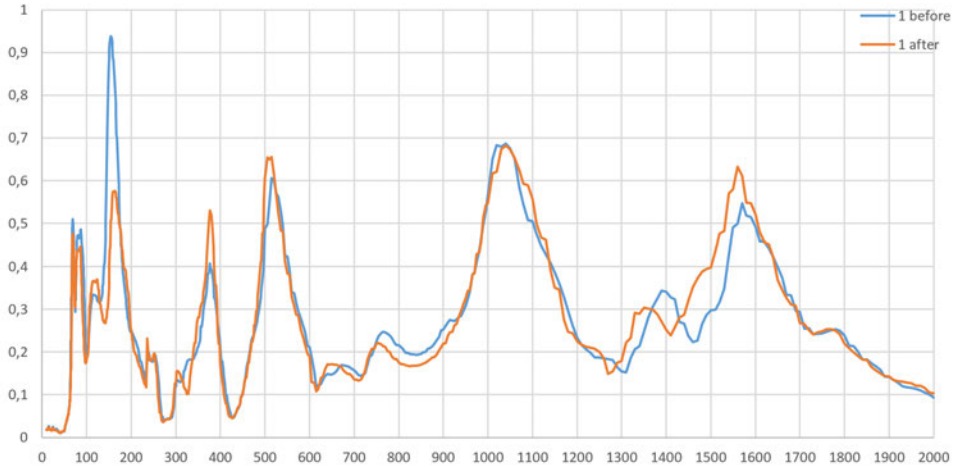


Figure E.5.34: Frequency search Y axis, before and after of sensor 1 (Cam)

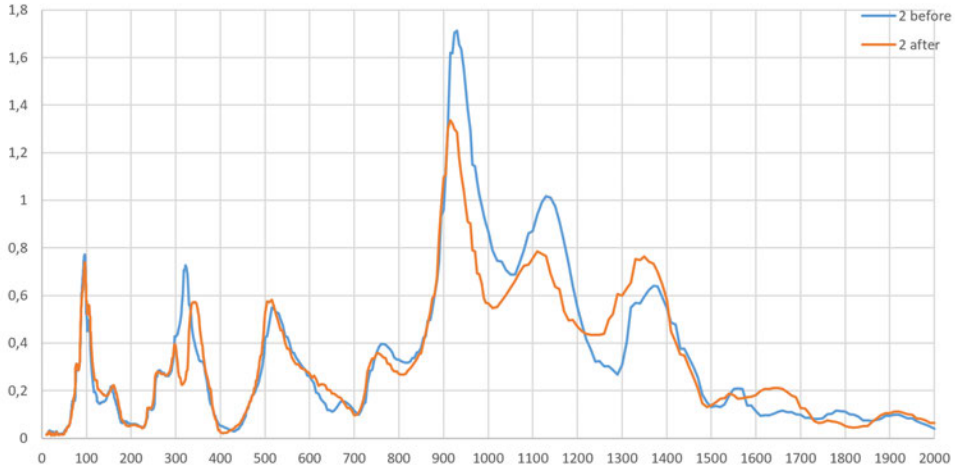


Figure E.5.35: Frequency search Y axis, before and after of sensor 2 (Arm)

For the lateral axis, virtually no frequency change occurred.

Conclusion

The final vibration test is concluded successfully. This is based on the observation that the eigenfrequencies exhibited minimal change for the thrust axis and no change for the lateral axis.

During disassembly, no screws were found to be loose except for the problematic M2 camera screws, which showed a reduction in tightening torque. The cause of this loosening is attributed to an improvised fastening solution. Standard M2 toothed washers were unavailable and were substituted with a combination of M2 washers and M3 toothed washers. For the flight configuration, thread-locking adhesive will be used in addition to the correct washers to prevent this issue.

A separate issue involved the locking mechanism jamming. This was caused by a stopper that was fitted too tightly. The solution is to increase the clearance for the locking arm's movement.

Sub-Test ID	08_04
Date	12.12.2025
Location	ZARM Bremen
Checklists	2025_10_20_APEX_Shaker_Test_Silicon_Austria
Environment	20°C, ZARM Bremen

Introduction

This verification test consists of vibration testing performed at Vehicle Level 2. Successful completion of these tests will provide the necessary clearance for flight.

Modifications

Since the testing took place in a different laboratory, the experimental setup was adjusted. For this phase, the entire module was tested rather than the isolated gimbal. Consequently, the sensor mounting locations were modified to accommodate the full-scale assembly, as illustrated in the following image.

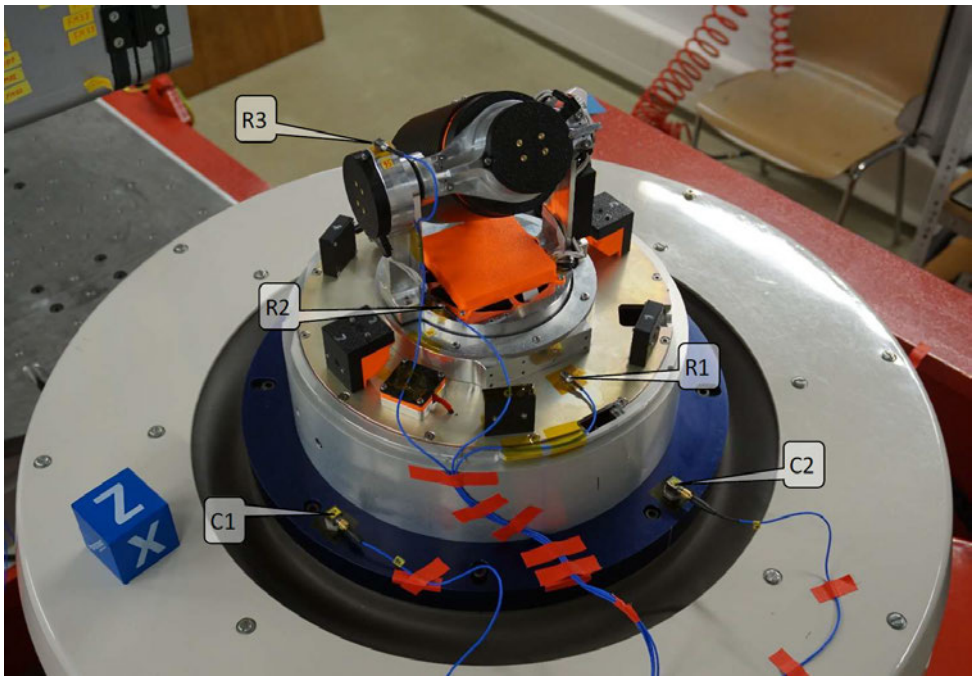


Figure E.5.36: Sensor location

The test procedure also differed for this setup. The sequence consisted of an initial resonance search, followed by sine vibration, a second resonance search, random vibration, and a final resonance search.

Observation

During the initial attempt, the data indicated a loose component, which required an interruption of the test. Upon inspection, it was discovered that the bulkhead screws were not torqued to the required specifications. After re-tightening these screws, the test was restarted.

Evaluation

The following results were recorded for the three sensors:

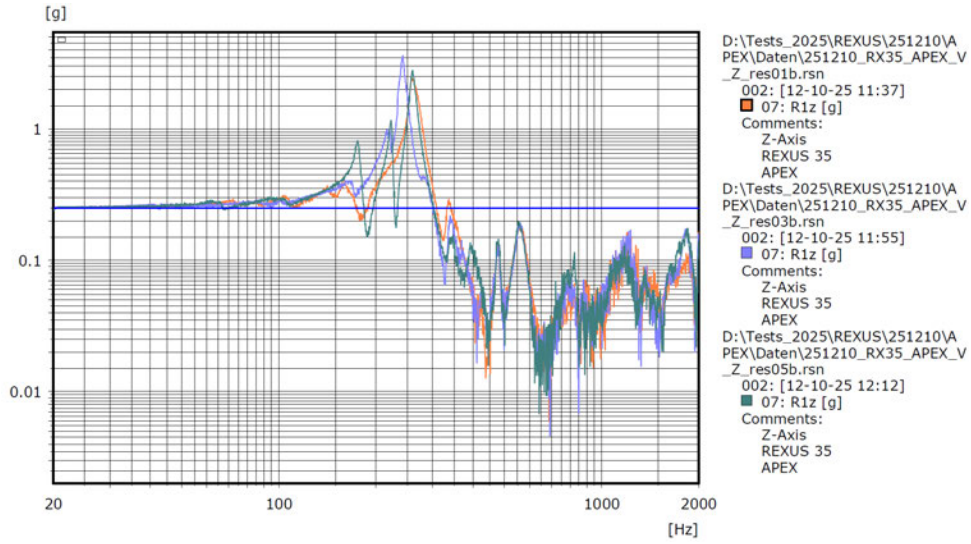


Figure E.5.37: Resonance survey compare, R1 in z-axis

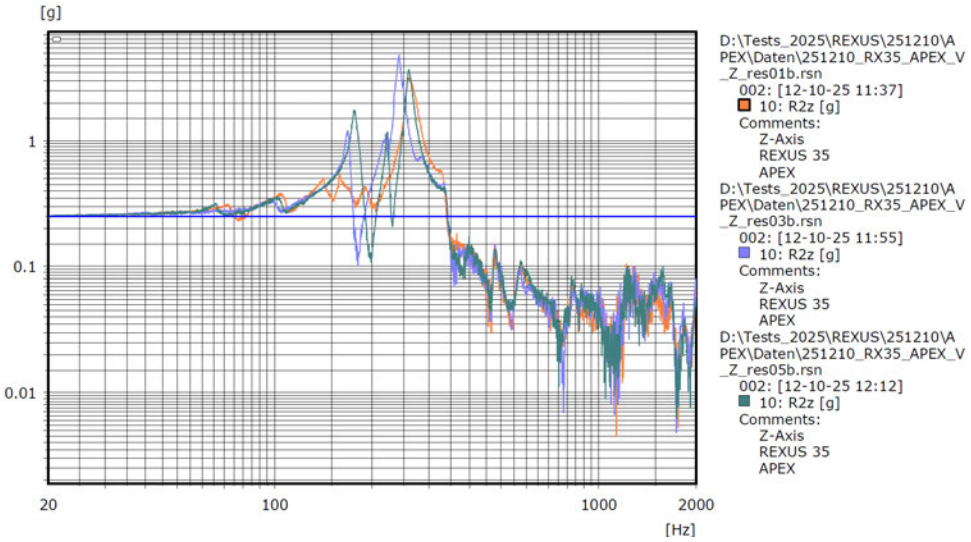


Figure E.5.38: Resonance survey compare, R2 in z-axis

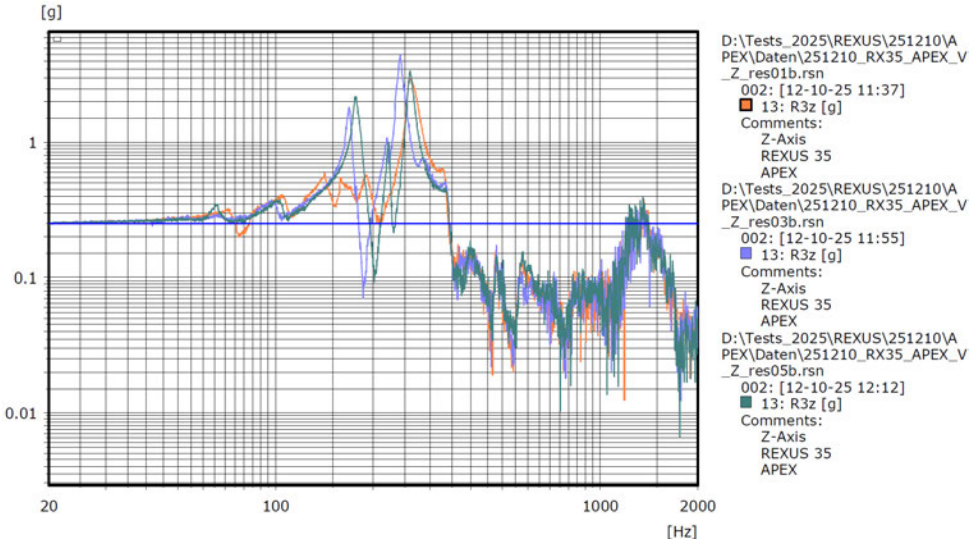


Figure E.5.39: Resonance survey compare, R3 in z-axis

Conclusion

Based on the results, a frequency shift was observed between the first and second resonance searches, which initially suggested a loosening of components. However, after the random vibration and final search, the frequency returned to its original value, resulting in no overall frequency loss between the first and last searches.

This behavior may be explained by the presence of moving parts with ball bearings, which likely shifted slightly during the sine vibration and returned to their original positions during the random vibration. Consequently, the test was considered a success, and the gimbal was cleared for flight.

E.6 Attitude Determination Test and Area Pointing Test

Test ID	10
Test Name	Attitude Determination
Verified item	the whole experiment (system level test)
Test description	The PCB with sensors has the Attitude Determination Software running while the PCB is being moved.
Expected Result	**Success:** The attitude is calculated correctly every 20 ms. **Partial Success:** -
Obtained results	The Attitude Determination system was verified for a few distinct static directions with a simulated sun (flash light). No dynamic tests were successfully performed.
Overall conclusion	Partially verified
Authority	Michael Zweimüller

Test ID	11
Test Name	Area Pointing
Verified item	the whole experiment (system level test)
Test description	We define an area the gimbal shall observe and check if the software keeps pointing towards this area while the sensors detect movement.
Expected Result	**Success:** The system successfully points towards goal area while moving the system. **Partial Success:** -
Obtained results	The Area pointing was tested for a few distinct static directions with a simulated sun (flash light), in wich the camera pod pointed in the expected direction. No dynamic tests were successfully performed. The pointing accuracy was not measured.
Overall conclusion	Partially verified
Authority	Felix Arch

Overview

The goal of this test was to test the pointing capability of the Gimbal and the associated ADS system of APEX. Due to delays in hardware completion and problems in software development, this test could be only done proper during the launch campaign in March 2026.

Setup and Procedure

This test was performed with the full APEX system. The tests were performed with a simulated launch sequence. During the test, predefined settings for the Sun, magnetic field, and aurora were entered, allowing the expected gimbal movement to be predicted and used to verify the correct operation of the algorithm. The Sun was simulated with a flash light (see Figure E.6.40

The gimbal was initially kept in an unlocked state while positioned as it would be during flight when locked. After the system was set to the PRE LAUNCH state, the REXUS signals were triggered in the same sequence expected during the actual flight. The experiment went into the correct states during this.

Once the experiment received the SOE signal, the gimbal moved to the expected orientation, captured an image, and then returned to its base position. This process repeated continuously until the SODS signal was received, at which point power to the motors was cut.

Overall Conclusion

The tests showed that for a static setup with the sun simulator illuminating one sun sensor the observation pipeline worked. Due to limited strength of the flashlight (and the lack of direct sun during the launch campaign at ground level), only direct illumination of the sun sensors could be tested. This meant no angles between sun sensors and no dynamic tests. Due to limited time, the pointing accuracy of the gimbal during these observations was not measured.

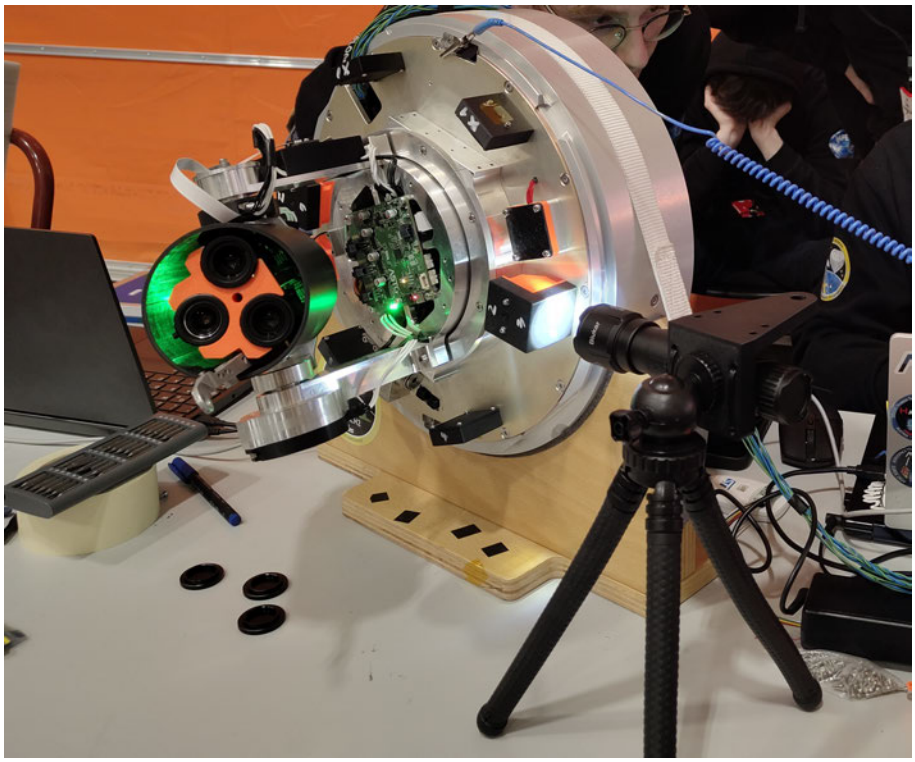


Figure E.6.40: Vertical test setup for the Gimbal pointing test. Test were performed both in horizontal and vertical configuration

E.7 Long Duration Test

Test ID	12
Test Name	Long Duration Test
Verified item	complete prototype
Test description	The Electronics and Software undergo a multiple hour long duration test.
Expected Result	**Success:** The Avionics system is powered for at least 2 hours without failure. **Partical Success:-**
Obtained results	The experiment ran during testing for more than 45 minutes uninterrupted. A longer test was deemed unnecessary because of the missions duration.
Overall conclusion	Successfully verified

Overview

In order to avoid failures and bugs that only surface rarely, long time testing was conducted.

Setup and Procedure

The complete prototype was connected via an external power supply and run for 45 minutes.

Overall Conclusion

No failures and bugs attributed to a long runtime (i.e. they are either extremely rare or are linked to a runtime overrun) were detected. This formulation is chosen as some tests included bugs, but those were linked to procedures (i.e. starting the motor controller).

E.8 Flight Simulation

Test ID	13
Test Name	Flight Simulation
Verified item	Kalman Filter and Attitude Determination
Test description	The Attitude Determination Framework was tested using simulated test-data under different sensor configurations and noise and bias levels.
Expected Result	**Sucess:** The Kalman Filter shall be able to determine the attitude of the bodyframe within an error-margin of below 1°.
Obtained results	The Kalman Filter was able to determine the attitude of the bodyframe within an error-margin of below 1°.
Overall conclusion	Successfully verified
Authority	Felix Arch

Overview

This test is based on the attitude determination results presented in the Master's thesis by Arch [16]. In that work, a simulation framework was used to generate synthetic sun sensor, gyroscope, and magnetometer measurements, which were processed by a Multiplicative Extended Kalman Filter (MEKF) to estimate the quaternion relating the ECI frame to the body frame. The outputs provided in the thesis are used here to provide verification evidence for the attitude determination algorithm.

Setup and Procedure

The setup and procedure used in this test are identical to those described in the author's Master's thesis [16].

Overall Conclusion

This section provides the overall conclusion of the conducted validation. Since only one test run was performed, no comparative conclusions across multiple tests are applicable.

Sub-Test ID	13
Date	November 2025
Location	Graz
Supervisor	Felix Arch
Checklists	N/A
Environment	N/A (Simulation)

Observation

The Multiplicative Extended Kalman Filter (MEKF) consistently estimated the spacecraft attitude with high accuracy across all simulated test cases. The simulation scenarios included variations in sensor noise levels and bias conditions for the sun sensor, gyroscope, and magnetometer measurements.

In all cases, the filter was able to correctly reconstruct the attitude, with the estimation error remaining below approximately 1° after convergence. No divergence of the filter was observed under the tested conditions.

Representative results are shown in Arch [16].

E.9 Data Storage Endurance

Test ID	14
Test Name	Data Storage Endurance
Verified item	Blackbox data storage endurance
Test description	The storage medium is exposed to sub-zero temperatures (approximately -10°C to -15°C) for 30 minutes and snow submersion-like conditions to simulate post-landing recovery conditions.
Expected Result	**Success:** All stored data remains intact and fully retrievable after exposure to all test conditions without corruption or loss.
Obtained results	Summary in a few sentences of the overall result of the test.
Overall conclusion	Successfully verified

Overview

This test verifies data integrity under expected post-landing environmental conditions. The storage medium is subjected to sub-zero temperatures and snow submersion to simulate realistic recovery scenarios. The test is considered successful if all stored data can be fully retrieved without corruption or loss after completing all three exposure conditions. The test concludes only after verifying complete data recoverability.

Setup and Procedure

We save a image on the storage medium inside the blackbox and seal the electronics from moisture.

1. We coat the black-box electronics with liquid petroleum jelly as shown in 1) of Figure E.9.41
2. We let it get back to room temperature as shown in 2) of Figure E.9.41
3. We submerge the the blackbox in room temperature tap water for 5 minutes as seen in 3) of Figure E.9.42
4. We remove the blackbox from the waterbath and place it in a commercial freezer for 30 min at $-18\,°C$ in 4) of Figure E.9.42

5. The blackbox is left at room temperature for 20 minutes, and its connectors are cleaned with isopropanol in order to effectively dry the electrical contact points as shown in 5) of Figure E.9.43.
6. The storage medium is inserted into a computer and the reference file is opened as shown in 6) of Figure E.9.43.

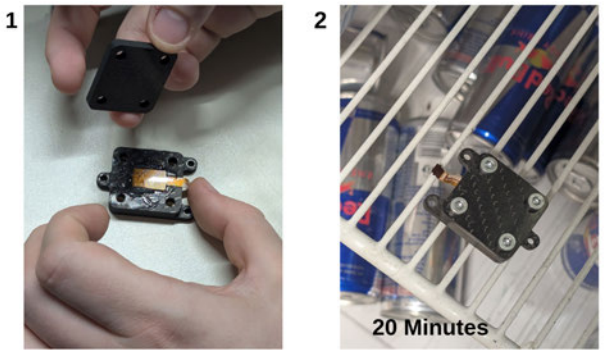


Figure E.9.41: Partial test setup. Image 1 shows the open blackbox housing filled with liquid petroleum jelly for waterproofing the electronics. Image 2 shows how the blackbox spend 20 minutes at 4 °C in the refrigerator to regain firmness.

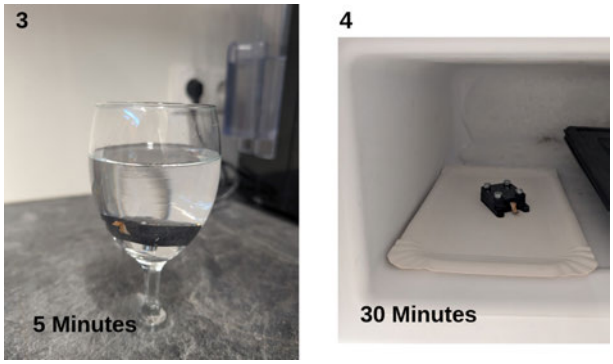


Figure E.9.42: Partial test setup. Image 3 shows the blackbox being submerged in room temperature tap water, and Image 4 shows how the blackbox spend 5 minutes fully submerged in water.

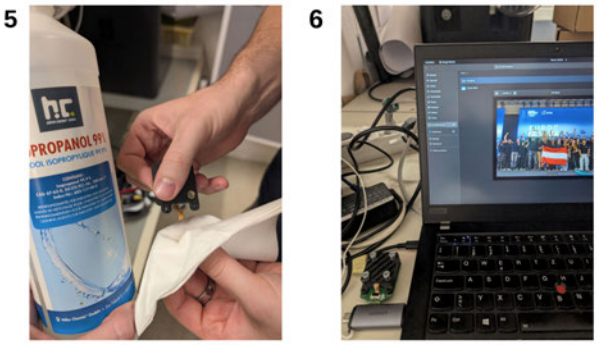


Figure E.9.43: Partial test setup. Image 5 shows the blackbox connectors being cleaned with isopropanol, and Image 6 shows how the blackbox was connected to a computer after the test with the image opened from it.

Overall Conclusion

The environmental survivability test partially validated the data storage system's resilience under recovery conditions. The storage medium was successfully exposed to sub-zero temperatures and a snow submersion-like environment, with all data remaining intact and fully retrievable after these conditions.

Sub-Test ID	14_01
Date	09.11.2025
Location	ASTG Office
Checklists	Not applicable
Environment	Not applicable

Introduction

This test is meant to validate the resilience of the black box and the storage medium within against expected environmental conditions after landing.

Modifications

No modifications were made to conduct this test.

Observation

The blackbox showed no obvious structral differences during or after the test. The data stored on the medium was intact and no change in behavior after the test could be determined.

Evaluation

The storage medium was subjected to submersion in water and following sub-zero temperatures (approximately $-10\,°C$ to $-15\,°C$) for 30 minutes. Post-test data retrieval confirmed data integrity with no file corruption or read errors detected.

Conclusion

The black box data storage successfully withstood cold temperature and snow submersion-like conditions with no structural damage or data loss. The storage system is adequately protected for post-landing recovery scenarios.

E.10 System Alignment Test

Test ID	15
Test Name	System Alignment Test
Verified item	Gimbal without Carbon Tube
Test description	Test the alignment of the System with static pointing
Expected Result	**Success :** The science cameras are aligned within 1° and the reference camer shall be aligned whithin 5° with the science cameras **Partial Success:**Cameras align to the camera housing
Obtained results	Measuring of Camera housing alignments are within 1° of the camera holder plate
Overall conclusion	Partially successful

Overview

The primary objective of this test was to ensure that the cameras were aligned parallel to one another. During the planning phase, several alignment methods were considered; however, significant space constraints within the setup limited the available options.

To address this issue, a try square was utilized. The tool was positioned against the top of the camera housing structure. Using this reference it ensured that every camera was positioned at a 90° angle relative to the same reference structure.

Setup and Procedure

To ensure the cameras were aligned parallel to one another, a try square was first placed against the top surface of the camera housing structure. Using this tool as a guide, several vertical lines were drawn downward at each of the three camera positions. Specifically, between one and five lines were marked in close proximity to indicate the intended location for the edge of each camera.

Once these reference lines were established, the cameras were mounted to the structure and positioned according to the markings, as can be seen in **??**. This method allowed for the cameras to be precisely aligned and secured using the scribed lines as a visual reference, ensuring they remained perpendicular to the top of the housing and therefore parallel to each other.

Overall Conclusion

The alignment method provided a practical solution despite the spatial constraints that prevented the use of external measurement tools. By utilizing the scribed reference lines, the orientation of each camera was verified visually. Over a reference length of 25 mm, the alignment between the camera edges and the markings could be assessed with high precision by the naked eye, ensuring the cameras remained parallel with each other. A verification of the alignment with images taken by the cameras was not performed prior to flight due to time constrains during campaign.

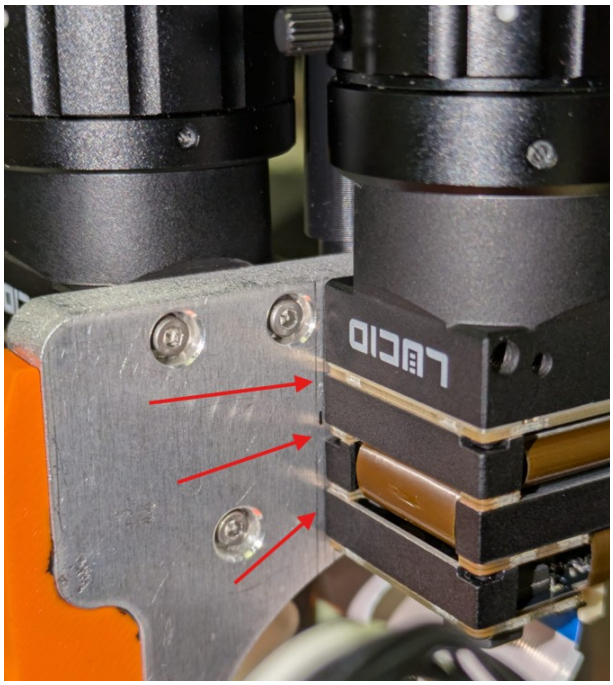


Figure E.10.44: Marking on the Camera Holder (indicated with red arrows) to show to allow the alignment of the cameras to a common parallel line.

E.11 Optical Polarization Test

Test ID	18
Test Name	Optical Polarization Test
Verified item	Optical Subsystem
Test description	The angle, intensity and degree of polarization is measured in an optical setup
Expected Result	**Success :** The Degree of Linear Polarization is resolved with a resolution of 1% at 2-sigma, **Partial Success:-**
Obtained results	The spectrum of the Filter was measured wit a spectrometer. Other parameters or a combination of spectral and polarization measurement were not performed due to a lack in time. This was deemed acceptable, as the optical subsystem is COTS.
Overall conclusion	Partially verified

Overview

The goal of this test was to verify the capabilities of the optical subsystem.

Setup and Procedure

The camera is mounted with the lens and the filter and illuminated with light of known spectrum and polarization.

Table E.11.1: Filter measured for their spectrum. The central savelength and FWHM are as stated by the manufacturer

Filter IDs	Product Nr	Central Wavelength (nm)	FWHM (nm)
F1,F2	FBH560-10	560	10
F3,F4	FBH630-10	630	10
F5	FBH550-40	550	40
F6	FBH630-30	630	40

Overall Conclusion

The spectrum of the filter was measured and verified to be within specification of the manufacturer. The spectrum of the small bandwidth filter (FWHM of 10 nm) were found to be to close to the spectral lines observed to ensure a reliable observation, therefor the filters were switched to the 40 nm broad variants. This was especially important as the shift of the wavelength of the filter depending on the incident angle needed to be considered.

Sub-Test ID	18_01
Date	03.02.2026
Location	University of Technology Graz
Checklists	n.A.
Environment	indoor

Introduction

In this test, the spectrum of the filters used was measured to verify their central wavelength and range.

Modifications

For this test, only the Filters were used in combination with a Thorlabs FTS spectrometer (InterferometerSerial;M00532595) and a white light source. The Items were placed in optical holders and loosely aligned on an optical table. For the angle measurement, the filter was turned by hand while a ruler was used for alignment. An error of $\pm 5°$ are to be assumed as a minimum. The spectrum of the white light source was measured as a reference before and after the measurement of all filters.

Table E.11.1 shows the central wavelength and FWHM as stated by the Manufacturer.

Observation

Figure E.11.45 shows the transmissivity curves measured during the experiment. The curves are already normalized by the refrence spectra taken of the white light source prior and after the experiment. As the right plot in Figure E.11.46 shows, the variation of the white light source prior and after the experiment is on average below 2.5 %.

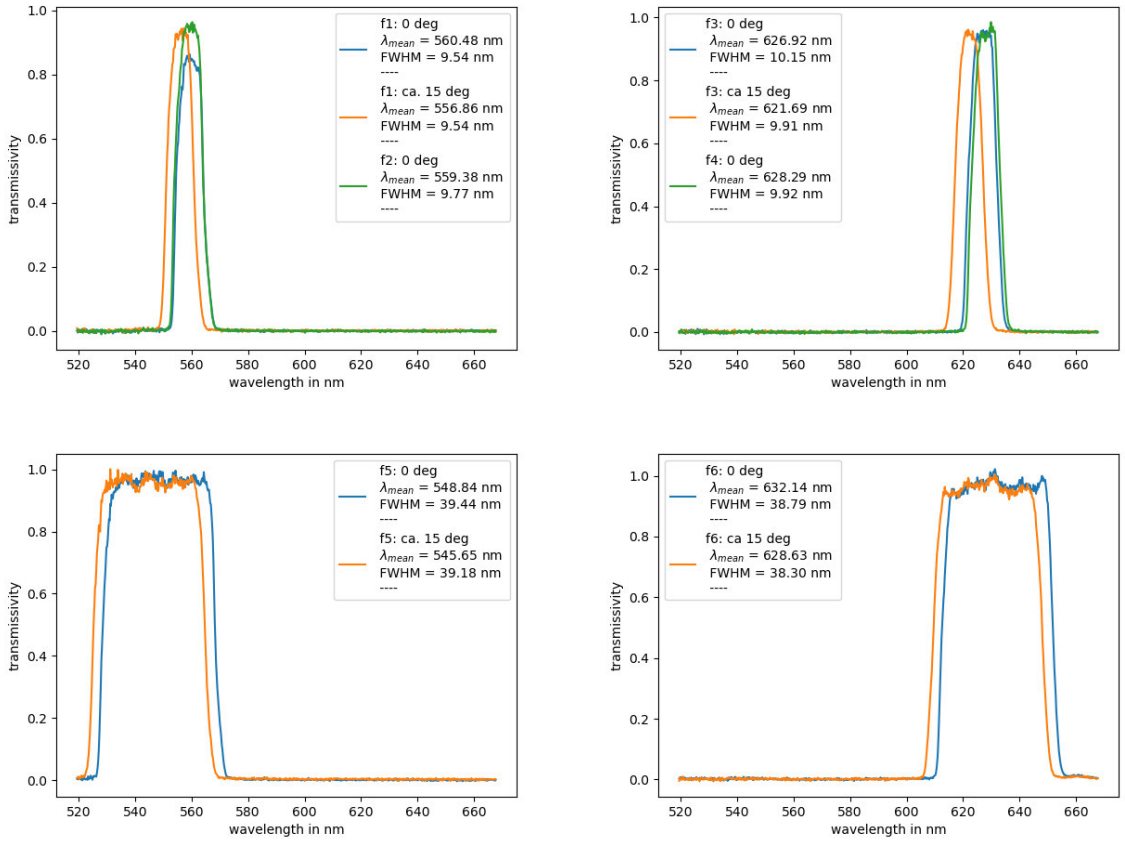


Figure E.11.45: Measured filter transmissivity of the 6 band pass filter. For each filter type, one measurement was performed with a tilted filter to roughly 15°. The measured spectra are already normalized with the reference spectrum taken prior to the measurements.

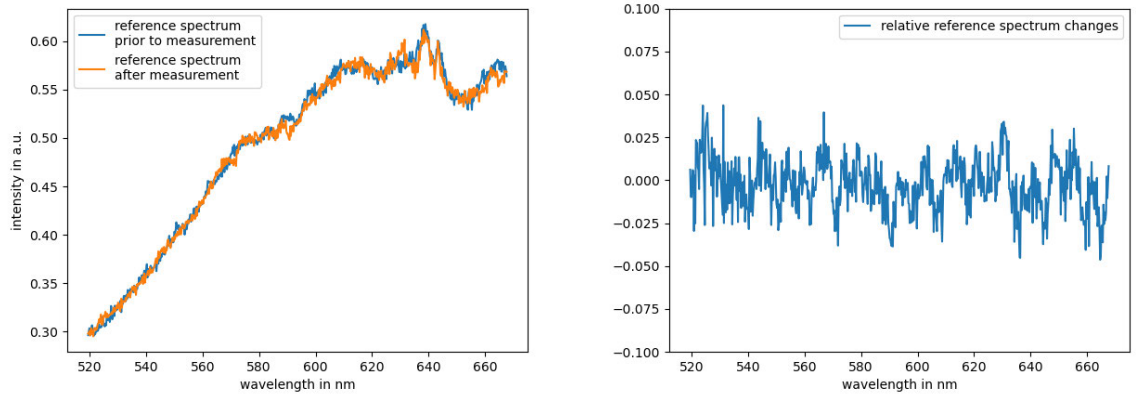


Figure E.11.46: The left image shows the reference spectra of the white light source prior and after the measurements, the right image the relative changes of the reference spectra.

Evaluation

The label in Figure E.11.45 show the central wavelength λ_{mean} calculated as the mean value of the shown curves and the FWHM. The FWHM was calculated as the maximum distance between the points of the measurement above half the maximum value within the measured range.

The measured values are in good agreement with the manufacture values, who states an accuracy of $\pm 0.5\,\%$, which equates to a $\Delta\lambda_{mean}$ of 2.8 nm for the 560 nm filter, 2.75 nm for the 550 nm filter and 3.15 nm for the 630 nm. The measured FWHM also agree with the values of the manufacturer.

Turning the filters for about 15° resulted in all cases in a reduction in the center wavelength λ_{mean}, as was expected. Due to the inaccuracy of the tilting, these measurements can be used as a trend, but not to accurately model the angle dependency. Nevertheless the experiment showed, that for the 10 nm band-pass filter the shift can be significant enough to bring the center wavelength out of the filter range. This impacts especially the red measurement at 630 nm as the spectral line is in the center of the filter range. The effect on the green spectral line 557 nm is lower, as it is already shifted towards the lower end, thus remains in the range of the filter.

Conclusion

We measured the transmission curves of six filter. The measurement showed, that the filters are within manufacturer specification. But, due to the shift with increasing angle of incidence, it was discovered that using the 10 nm band-pass filter has the danger of the spectral line falling out of the measurement range. For the flight, the filter where therefore changed to the 40 nm filter.

E.12 Gimbal Camera Test

Test ID	19
Test Name	Gimbal Camera Test
Verified item	Subsystem and flight hardware test
Test description	Long time exposure of the science cameras is tested in conjunction with the short time exposure of the reference camera
Expected Result	**Sucess:** Long time exposures of 3 seconds for both science cameras are possible in conjunction with 10 Hz exposures of the reference camera **Partial Sucess:** -
Obtained results	Simultaneous initialization and operation of polarization and reference cameras were validated across both subsystem and flight hardware levels. Metadata latency was identified during flight hardware testing. Due to project timing constraints, mitigation strategies remain recommended for future implementations.
Overall conclusion	Succesfully verified

Overview

This test evaluates the simultaneous operation of both science cameras alongside the reference camera. The test is considered a success if all three cameras are initialized and controlled concurrently, with image data successfully written to the SD card without errors or data loss.

Setup and Procedure

The camera subsystem is interfaced with a Raspberry Pi via an Ethernet switch. Control commands for image acquisition are dispatched from the Raspberry Pi to the cameras concurrently. The resulting image data is written to the SD card for persistent storage.

During the test, the reference camera was operated in continuous mode with an acquisition interval of 0.1 s (10 Hz). In contrast, the polarization camera was triggered manually with a fixed exposure time of 3 s. A new acquisition was re-triggered immediately upon the completion of each frame.

Following the conclusion of the test, a manual verification is performed to inspect the datasets for completeness and potential errors.

Overall Conclusion

The simultaneous initialization and operation of all three cameras were demonstrated, validating the system's capability to operate in the final flight configuration. While metadata latency was observed, it did not impact data integrity during testing. However, it indicates a risk of potential image loss if high-frequency acquisition cycles encounter buffer bottlenecks. To ensure operational reliability in future projects, the implementation of multithreading to decouple acquisition from storage, alongside comprehensive I/O optimization, is strongly recommended.

Sub-Test ID	19_01
Date	21.02.2026
Location	ASTG Solder Lab
Checklists	-
Environment	Room temperature

Introduction

The initial test was conducted at the subsystem level, comprising only the cameras and the Raspberry Pi. This stage focused specifically on validating the simultaneous operation of the camera units.

Modifications

Since the test was conducted exclusively at the subsystem level, acquisition commands were entered directly via the Raspberry Pi terminal rather than being dispatched via CAN bus. Additionally, due to the unavailability of one polarization camera at the time of testing, the setup was modified to include one polarization camera and the reference camera.

Due to an update in requirements during the development phase, the exposure time for the polarization camera was adjusted from 6 seconds to 3 seconds. This modification ensures that the test conditions align with the operational exposure times designated for the flight mission.

Observation

The reference camera experienced a buffer overflow error whenever the exposure time exceeded 0.1 sec. This resulted in dropped frames. When the exposure time was configured below the 0.1 sec threshold, the reference camera operated reliably without data loss.

Evaluation

The polarization camera operated as expected, with no issues regarding command execution or image storage.

The anomalies observed with the reference camera at exposure times exceeding 0.1 s are directly linked to the sampling frequency. The camera operates at a frame rate of 10 Hz (1 frame every 0.1 s). If the exposure time is >0.1 s, the camera is still busy integrating the current frame when the subsequent acquisition command arrives. Because the hardware is still occupied, it cannot process the new trigger, resulting in a Buffer Overflow error and the command being ignored. Once the previous acquisition cycle is complete, the camera resumes normal operation and can process incoming commands again.

If the exposure time is shorter than the 0.1 s frame period, this timing conflict does not occur, and the reference camera operates normally. By maintaining an exposure time below this threshold, the system can process every command without errors.

Conclusion

The successful concurrent operation of one polarization camera and the reference camera was confirmed, verifying that both systems can be initialized and controlled simultaneously. While a technical limitation was identified regarding the reference camera's behavior at exposure times exceeding its 10 Hz sampling frequency, this has been diagnosed as a command-timing conflict rather than a hardware failure.

To ensure stable operation in continuous mode, the reference camera configuration must strictly adhere to the following timing constraint: the exposure time must always be shorter than the selected frame period. Failure to maintain this margin will result in command overlaps and subsequent data loss due to buffer overflows.

«««< HEAD Sub-Test ID	19_02
Date	04.03.2026
Location	Kiruna / SSC Space Center
Supervisor	Rolando Unger
Checklists	-
Environment	Room Temperature
======= Sub-Test ID	Replace with Test_ID that is best answere
Date	Date of test execution
Location	Location where test has been conducted
Checklists	Applicable checklists for setup and procedu
Environment	Temperature, Humidity and Weather
»»»> 364aeb8 (rm team member names: list and test reports)	

Introduction

This test evaluated the simultaneous operation of both polarization science cameras alongside the reference camera using the final flight hardware and CAN bus command transmission.

Modifications

Due to an update in requirements during the development phase, the exposure time for the polarization camera was adjusted from 6 seconds to 3 seconds. This modification ensures that the test conditions align with the operational exposure times designated for the flight mission.

Observation

A timing discrepancy was observed in the image metadata. Specifically, the image timestamps were delayed relative to the actual acquisition triggers.

Evaluation

The flight hardware test confirmed that all three cameras can be initialized and controlled concurrently via the CAN bus. Command execution, image acquisition, and storage to the SD card functioned as intended.

However, a timing delay exists between the end of the exposure period and the timestamp assigned to the saved file. This occurs because the system remains occupied with processing and writing data, creating a measurable lag. This issue was likely amplified by the simultaneous operation of all three cameras, which significantly increased the volume of data being written to the SD card at the same time. While this did not affect image data integrity during the test, it presents a potential risk: if the system is occupied with a previous write operation when a new command arrives, the buffer may become blocked, leading to data loss in high-frequency operational scenarios.

Conclusion

The successful concurrent operation of the polarization and reference cameras via flight hardware and the CAN bus was confirmed. Although the system demonstrated robust command execution, metadata latency was identified due to the current processing architecture.

As project timing constraints prevented the implementation of mitigation strategies, these should be prioritized for future projects. Specifically, decoupling acquisition from storage processes through multithreading is recommended to ensure the main control loop remains responsive during I/O operations. Furthermore, optimizing the storage pipeline throughput—by utilizing high-speed media and refined file system parameters—will help eliminate processing bottlenecks and prevent potential data loss.

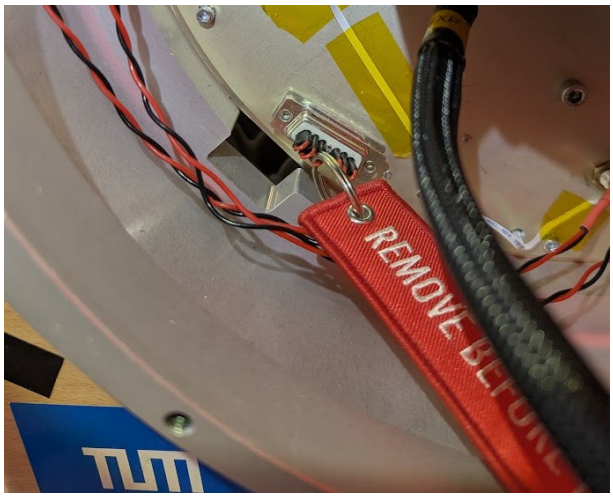


Figure E.13.47: Short-circuit connector with ”remove before flight”-tag

E.13 Arming Test

Test ID	23
Test Name	Arming Test
Verified item	Complete Prototype
Test description	Test pyro short circuiting.
Expected Result	**Success:** Pyro channel is short-circuited when ”remove before flight”-tag is inserted and open when the tag is removed **Partial Success:-**
Obtained results	The short circuit resistance of the short circuit connector was measured at below 0.1 Ohm
Overall conclusion	Successfully verified

Overview

The aim of this test was to verify the working of the short-circuit system.

Setup and Procedure

As the short-circuit system consists of a Sub-D connector with shorted Pins and an attached ”remove before flight”-tag (see Figure E.13.47), the test boiled down to a measurement of the resistance. This was done with cables inserted into the pyro-connector, which were stripped and the ohm meter attached. The measure of resistance between pairs of pins was below 0.1 Ω (due to limitations of the ohmmeter used, which could not resolve smaller values), the resistance between random pins around 3.3 Ohm.

Overall Conclusion

The test showed that a device with a ”remove before flight”-tag could be inserted into the system to short-circuit the pyro during installation.

E.14 Power Supply Test

Test ID	24
Test Name	Power Supply Test
Verified item	the whole experiment
Test description	Test the power supply of the whole system for endurance.
Expected Result	**Success :** The power supply does not collapse during testing. Current, voltage and power limits are not exceeded. Request for Radio Scilence is accepted
Obtained results	Measuring of the voltages and currents during operation showed no peaks or crashes in the power supply. Input voltages between 24 and 36V were accepted without issues. Mean power draw at 28W.
Overall conclusion	Successfully verified
Authority	Michael Zweimüller

Overview

This test verifies Requirements D-12, D-14, D-15, D-16, D-17, D-18, D-19 and the general electrical qualification. The test consists of two subtests. The first one is the unofficial to prepare for the official test conducted by MORABA.

Setup and Procedure

For the setup, the entire experiment is placed on the bench. Additional components needed for the test include a lab bench supply, the REXUS Service Module (or the simulator for the preparation test), and the mission control setup consisting of a laptop and the Serial Data Cable. To verify some requirements, measurement devices are needed, including a multimeter and an oscilloscope. A full timeline is performed to measure the maximum and mean power and current draw during operation.

Overall Conclusion

Although no official report is available at the time of writing, the official test concluded successfully with no anomalies detected.

Supply voltages from 24 to 36V were tested. Current draw never spiked significantly over 1A. Mean power from the service line was 28W. Voltage feedback ripple was only measured at the official benchtest.

E.15 Blackbox Test

Test ID	26
Test Name	Blackbox Test
Verified item	Complete Prototype
Test description	Test to see if the scientific as well as the experiment blackbox work is intended.
Expected Result	**Sucess:** Both blackboxes are able to write data with the desired speeds. **Partial Sucess:**-
Obtained results	During launch operations, neither the scientific data blackbox nor the flight computer blackbox were able to recorded data
Overall conclusion	Not verified

Overview

In this test the writing and retrieving of data from the scientific and flight computer black box is tested and confirmed.

Setup and Procedure

For the set up, the complete prototype is supplied externally with power. A test program is run to actuate the motors while taking observations with the cameras. The data of this test is stored on the black boxes.

Overall Conclusion

The blackbox only recorded data that itself tried to send to the mission control. Additionally, no packets were send to the mission control from it. This shows that the CAN-bus setup of the blackbox was faulty and needs revision.

E.16 Thermal Convection Test

Test ID	31
Test Name	Thermal Convection Test
Verified item	Complete Prototype
Test description	The Gimbal is covered by a chamber simulating the nosecone volume, while the bottom of the module is thermally isolated against the ground below. Prelaunch Tests are done to test thermal increase of air temperature until it stabilizes
Expected Result	**Success:** The air temperature at the module interfaces does not exceed the ambient temperature by more than 10 °C. Ambient Temperature for the Test is assumed with 20°C. **Partial Success:**-
Obtained results	The Avionics system was run for extended period of time with a closed bottom without a noticeable increase in temperature. Test was performed without temperature measurement.
Overall conclusion	Partially verified

Overview

This test is meant to verify, that the temperature produced by the APEX Payload, especially the AVI Box underneath the Bulkhead cannot negatively impact other experiments. The air temperature at the module interfaces does not exceed the ambient temperature by more than 10 °C.

Setup and Procedure

The APEX experiment was placed on a rubber mat and run for an extended time (>30 min, exceeding the nominal 10 min power on time on the launch pad). The temperature was checked by lifting the Module and feeling the escaping air.

Overall Conclusion

The temperature of the air felt in the nosecone adapter module as well as the temperature of the nosecone adapter where not noticeable above ambient temperature.

Appendix F: Analysis and Simulation

Analysis ID 1: Target Region and Resolution

- Requirements: F-1 and P-3
- see: Appendix F.2 and Section 1.1

Analysis ID 2: Reference Footage

- Requirement: F-4
- see: Section 4.5.14

Focal length reference camera: 8.5 mm. With 128.6 mm sensor: FOV 60.6° Focal length science camera: 16 mm. With 61.4 mm sensor: FOV 30.9°

Analysis ID 3: Locking

- Requirement: F-9
- see: Appendix F.4

Analysis ID 4: Degree of Linear Polarization

- Requirement: P-1
- see: Appendix F.2 and Section 1.1

Analysis ID 5: Motor speed

- Requirement: P-10, P-11
- see: Appendix F.5

Analysis ID 6: Mass and Center of Mass

- Requirement: D-1, D-9
- see: Table 4.1

Analysis ID 7: Structural

- Requirement: D-2, D-3, D-4
- see: Sections 4.4.5 and 4.4.6 and Appendix F.6

Analysis ID 8: Batteries

- Requirement: D-13
- see: Section 4.7

Analysis ID 9: Thermal

- Requirement: D-44, D-46, D-48
- see: Appendix F.1

Analysis ID 10: Initial Attitude Determination

- Requirement: P-5

The initial attitude estimation is done by utilizing the QUEST algorithm. With this estimate, the Kalman filter is initialized and provides continuous attitude estimations throughout the experiment. The initial estimate has the purpose of shortening the time of convergence of the Kalman filter.

Analysis ID 11: Blackbox writing speed

- Requirement: P-13

The data sheet for the SD - Card used, a SFSD256GN1AM1TB-E-VG-211-STD (`https://www.digikey.at/de/products/detail/swissbit/SFSD256GN1AM1TB-E-VG-211-STD/20414369?gclsrc=aw.ds&gad_source=1&gad_campaignid=20265439570&gbraid=0AAAADrbLljOrA7skITHfX176XPJAY7jT&gcli EAIaIQobChMIj_2owIDjkAMVya-DBx0drQFSEAQYAyABEgL6XfD_BwE`) lists a writing speed of 39 MBytes/s. The expected maximum image size of the experiment cameras is 5MB per shot, with 4 images taken for every exposure - one for every polarization angle. Therefore, for each exposure of the reference cameras, an approximate image data stream of 20MB per camera is expected. Due to the nature of the experiment and the exposure conditions, the two experiment cameras will work with long exposure times, meaning they will not transmit data every second. The expected maximum image size of the reference camera is 6MB per shot, taking images with a short exposure time.

Due to the differing exposure times of the three cameras, simultaneous data transmission throughout the entire duration of the experiment is not expected. As a result, the available writing speed of 39 MB/s is considered sufficient to handle the data flow. Additionally, each camera is equipped with an internal image buffer of 128 MB, which provides temporary storage capacity and further mitigates the risk of data loss during high-load periods.

F.1 Thermal Analysis

The thermal simulation was conducted using Ansys with the following parameters:

- **Initial Temperature**: 240 K
- **Time**: 100 s
- **Thermal Energy of Motors**: 63 W
- **Thermal Energy of Cameras**: 3 W
- **Radiation**:
  - **Emissivity**: 0.2 (milled aluminum)
  - **Ambient Temperature**: 200 K
- **Solar Radiation**: 1360 W/m^2

The solar radiation illumination was applied to the back of the camera module, which is representative of a scenario where the camera are pointed towards the night-side of Earth. During operation, the cameras will face away from the sun, positioning the sun behind the gimbal.

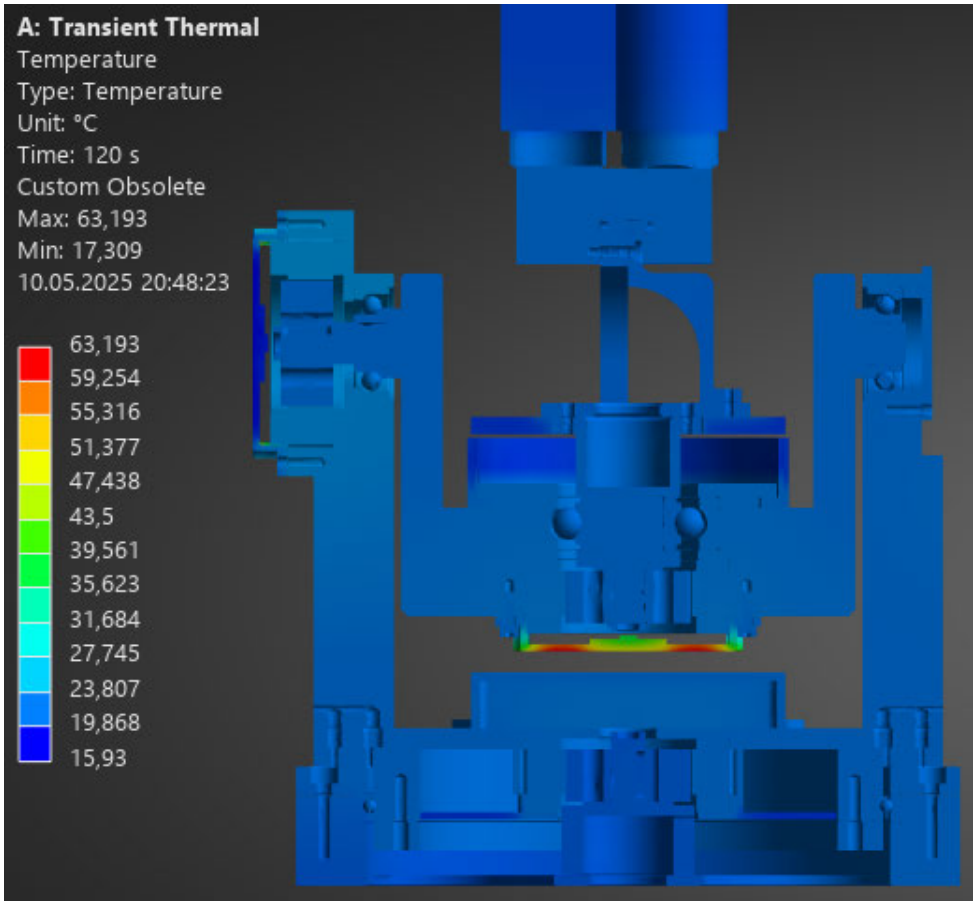


Figure F.1.1: Cross-section of the Thermal simulation in Ansys

F.2 Aurora Simulation

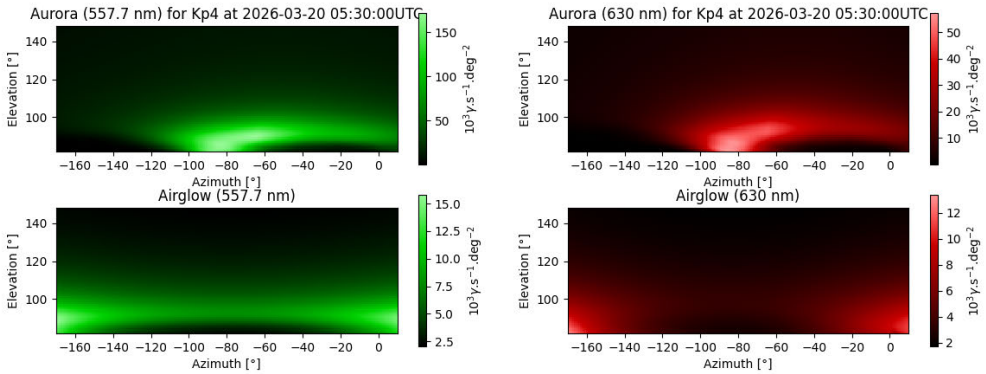


Figure F.2.2: Simulated Field of View for Aurora (top row) and Airglow (bottom) for 2026-03-20 05:30 UTC for the green (left) and red (right) emission lines. Horizontal axis is the viewing angle, measured anticlockwise from north. Brightness is given in photons per second per viewing angle

The scientific mission aims to observe and measure aurora emissions at 630 nm (red line) and 557.7 nm (green line) using rocket-borne instrumentation deployed at an altitude of 80 km above Kiruna, Sweden (67.89°N, 21.08°E). Multiple line-of-sight viewing angles, ranging from -40° to -85°, measured anti-clockwise from north, were simulated to estimate the aurora activity across different atmospheric regions and altitude layers. Figure F.2.2 shows a simulated field of view for aurora and airglow, looking west at 05:30 UTC on 2026-03-20 at an altitude of 80 km.

The earliest launch time is based on the separation of the Sun and the Earth to be 10° at a minimum. The end of the preferred launch window is based on the error for the degree of polarization (Q/I ratio) signal. Figure F.2.3 shows the conditions where we have the lowest error in green ($< 0.3\%$ for the 557.7 nm line, $< 0.5\%$ for the 630.0 nm line). The larger cutoff for the error of the red line has been chosen because, according to ground based observations the degree of polarization is stronger for the red line. For these conditions the fulfillment of all our scientific objectives is possible. The yellow and orange conditions it will be possible to fulfill our scientific results with some larger errors. In the red zones we can only fulfill our technical objectives and cannot collect useful data about aurora polarization, only airglow. The earliest possible launch time (marked as blue dotted lines in Figure F.2.3) are based on the angle of the Sun (see Appendix F.3).

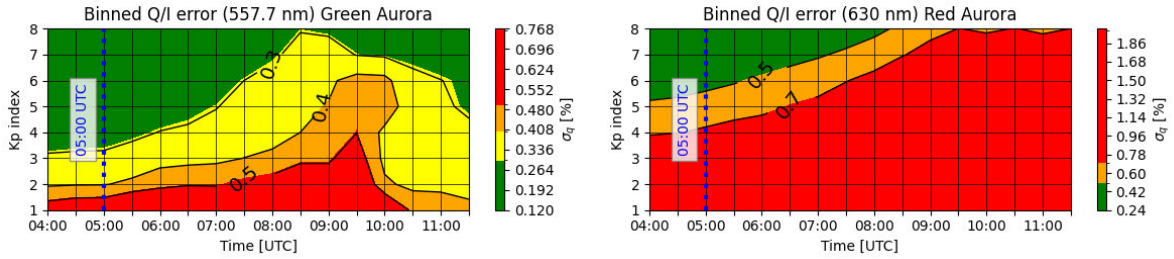


Figure F.2.3: Expected observation errors on 2026-03-20. Horizontal axis shows time (UTC), vertical axis shows Kp index. Blue dotted line shows the earliest possible start time based on the sun.

The Aurora model is based on [9]. The airglow model is based on atmospheric profiles from the NRLMSISE-00 and International Reference Ionosphere models.

F.3 Launch Time Analysis

- Earth's weather impacts the experiment only by changing the error induced by the albedo of Earth on the Sun sensors
- Maintaining above-zero temperature prior to launch is important to minimize the risk of condensation on and inside the optical elements (fogging up).
- In order for the sun sensors to perform nominally, the Sun needs to be high enough above Earth's horizon. This sets the lower bound for the launch time. The upper bound is given by the blind spot produced by the rocket-body in case of a straight flight along the center of the launch corridor.

Launch Window determination

We base the optimal launch window estimation on the Sun's elevation angle and the distance of the rocket to the terminator line. The sun sensor needs to be able to distinguish clearly between the Sun and its reflection on the surface albedo of Earth. The start time of the estimated optimal launch window is determined by the time when the Sun's elevation is at 10° degrees above the horizon, accounting for the shift according to the dip angle at a height of 80 km. The horizon dip angle accounts for the fact that an elevated observer can see farther along Earth's curved surface.

$$r_{observer} = \frac{a * (1 - e^2)}{1 - e^2 * sin(lat_{observer})^2} \tag{F.1}$$

Where $a = 6378137.0$ describing the semi-major axis (m) and $e = \sqrt{2 * f - f^2}$ with a flattening factor $f = 1/298.25722$.

$$\theta_{horizon} = \sqrt{\frac{2 * h_1}{(r_{observer} + h_1)}} \tag{F.2}$$

This angle determines whether the Sun is geometrically above the horizon, affecting whether parts of the line of sight (LOS) are illuminated. The start time is determined by the time t where:

$$-\theta_{horizon} + 10° < \alpha_{alt,Sun}(t) \tag{F.3}$$

The end time of the estimated window is determined by the maximum LOS, based on the formula

$$r_{max,LOS} = \sqrt{(r_{Earth} + h_1)^2 - r_{Earth}^2} + \sqrt{(r_{Earth} + h_2)^2 - r_{Earth}^2} \tag{F.4}$$

where h_1 is the height of the spacecraft at the time of the observation and h_2 is the height of the aurora. With this formula, we gain a radius around the launch site that determines the maximum distance at which we can still observe the aurora at a certain height h_2. We draw a circle around the European Space and Sounding Rocket Range in Kiruna, Sweden (67.86°N, 21.08°E) at an altitude h_1 of 80 km. Based on Equation (F.4), the simulated aurora targets are analyzed at altitudes h_2 of either 80 km 90 km or 100 km . We additionally vary the aurora latitudes, simulating a broad observational arc. We determine the longitude of the target from the latitudes (60°N, 65°N, and 70N°) and $r_{max,LOS}$ (2025 km, 2087 km, 2146 km) depending on h_2, using geodesic calculations that account for Earth's curvature.

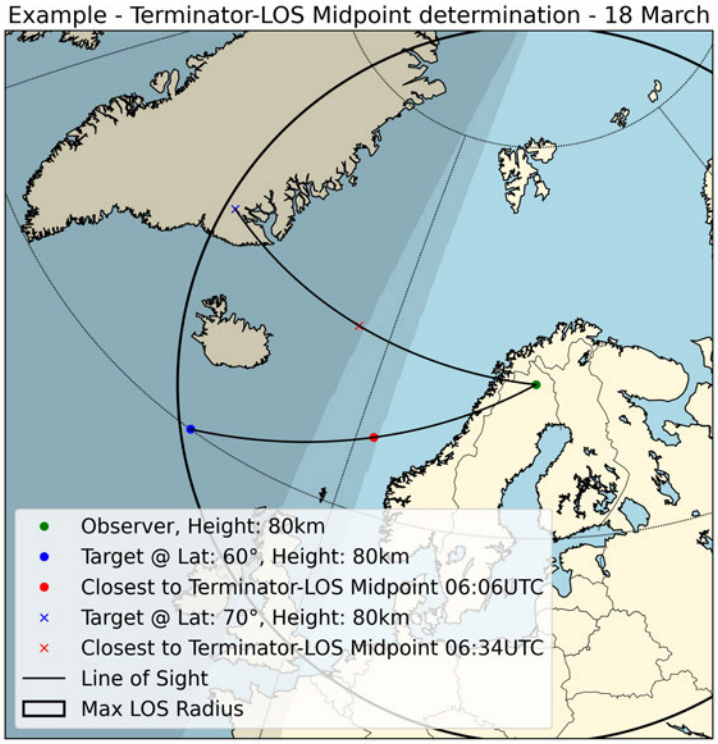


Figure F.3.4: Map view of the terminator on March 18th for two determined observation window end times. The circle with radius $r_{observer}$, describes the maximum LOS from the observer. The blue cross and point mark the closest crossings of the LOS with the circle at different target latitudes. The red cross and point denote the times when the terminator cuts the length of the LOS line approximately in half.

The resulting line-of-sight (LOS) path between the apogee and the target location as illustrated for 60°N and 70° at 80km in Figure F.3.4. The time when the terminator cuts this LOS path approximately in half, we define as the preliminary end time for the optimal launch window. To estimate this time day between 1. March to 30. April, the code simulates sunlight conditions along the LOS path every minute from 02:00 to 10:00 UTC. It divides the LOS into 100 segments and, for each time step, calculates the Sun's position relative to every segment using astronomical solar data. The result is a day fraction—the proportion of the LOS that lies in sunlight. The goal is to find the time each day when this fraction is closest to 0.5.

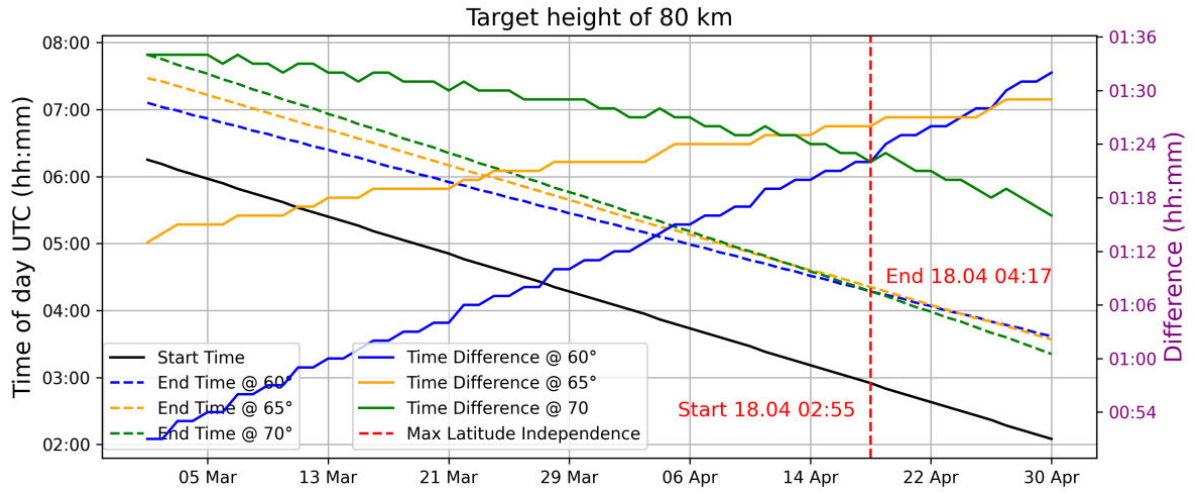


Figure F.3.5: Launch window estimation for a target at 80 km height. For the x-axis we plot the a daily time-range of 1. March to 30. April. On the black y-axis we show the time of day in UTC, with the solid black line marking the time when the sun rises 10° above the horizon at 80 km. The dashed lines on the black y-axis at the times when the terminator line splits the LOS vector between observer and target approximately in half. The purple y-axis shows the differences between the start and end time for the different latitudes. The vertical red dashed line shows the day of least difference depending on the target longitude, annotated with the start and end times at this day.

The resulting estimated launch window end times and differences to the start times are plotted in Figure F.3.5 for three target latitudes at 80 km height. We estimate the optimal launch date during the specified range based on the minimal difference between the determined start and end times. For all simulated heights and latitudes, that date is estimated to be the 18th of April. Indicated by the red dashed line and the annotated times, we estimate that the launch window increases by three minutes with every 10 km increase in target height. Based on these simulated results we estimate optimal launch window for early March between 06:15 UTC and 07:56 UTC and between 02:05 UTC and 03:28 UTC in late April. The durations of the estimated optimal launch windows range from 52 to 97 minutes.

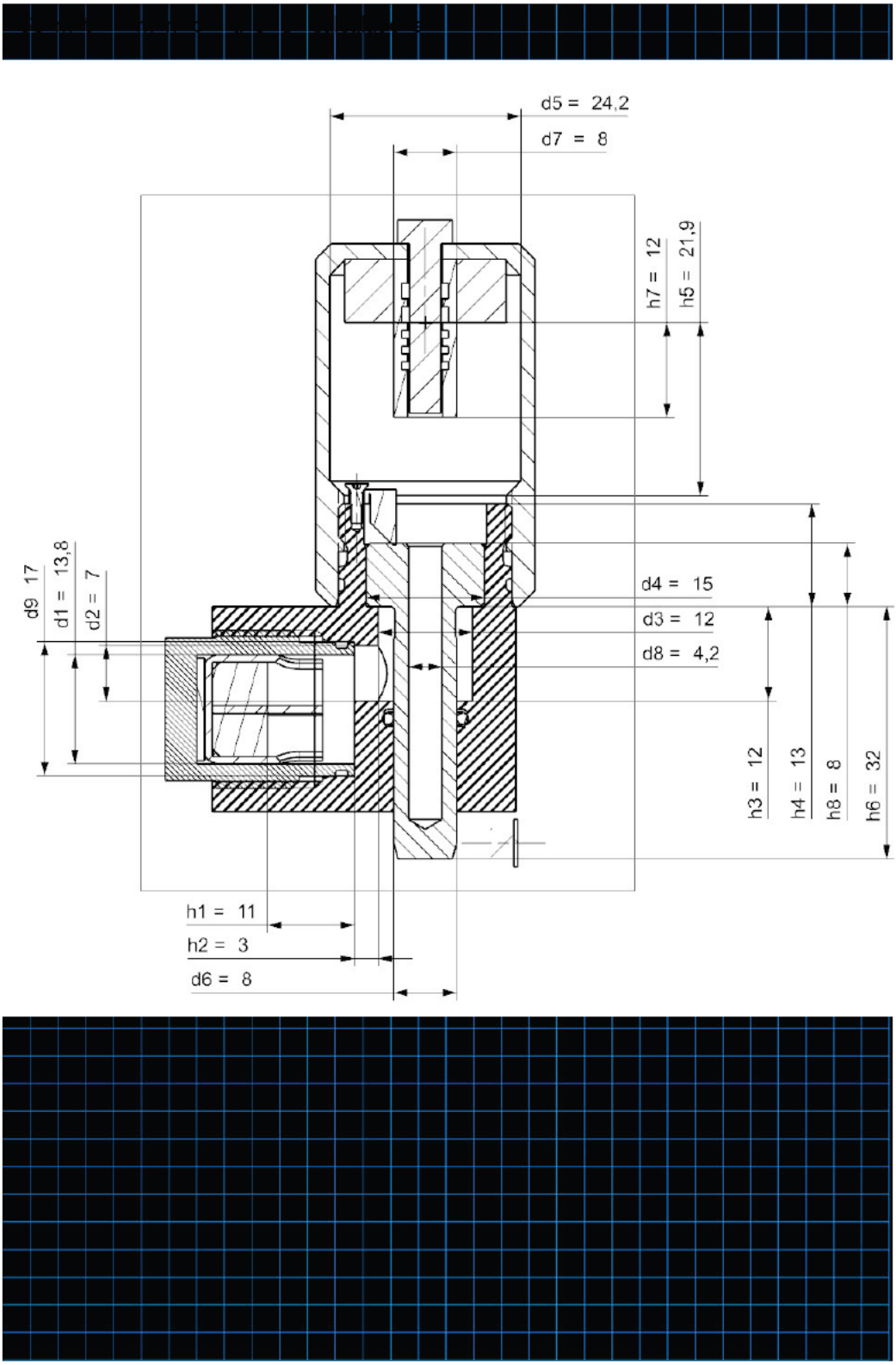
We base our start times of the launch window on this analysis. The end times are based on aurora analysis Appendix F.2.

F.4 Pin Puller Calculations

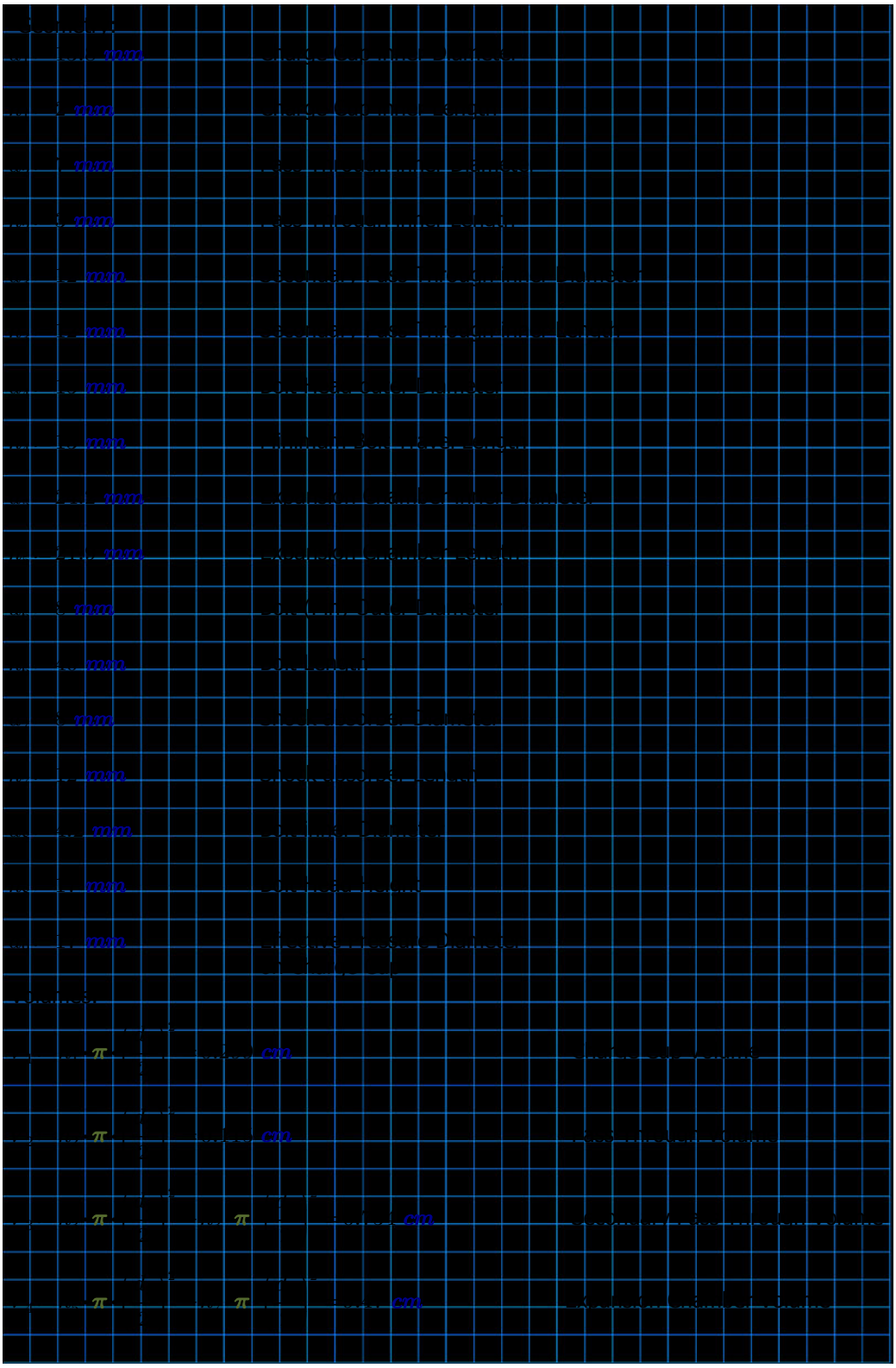
These are the relevant calculations for the Pin Puller concerning safety and function

Approach for safety calculations As the charge cup is the part with thinnest wall thickness and axial stress is larger than thread sheer and hoop stress; The calculation focuses on the part of the charge cup sticks out from the housing and has outer thread (M20), This weak point has been confirmed by FEM analysis.

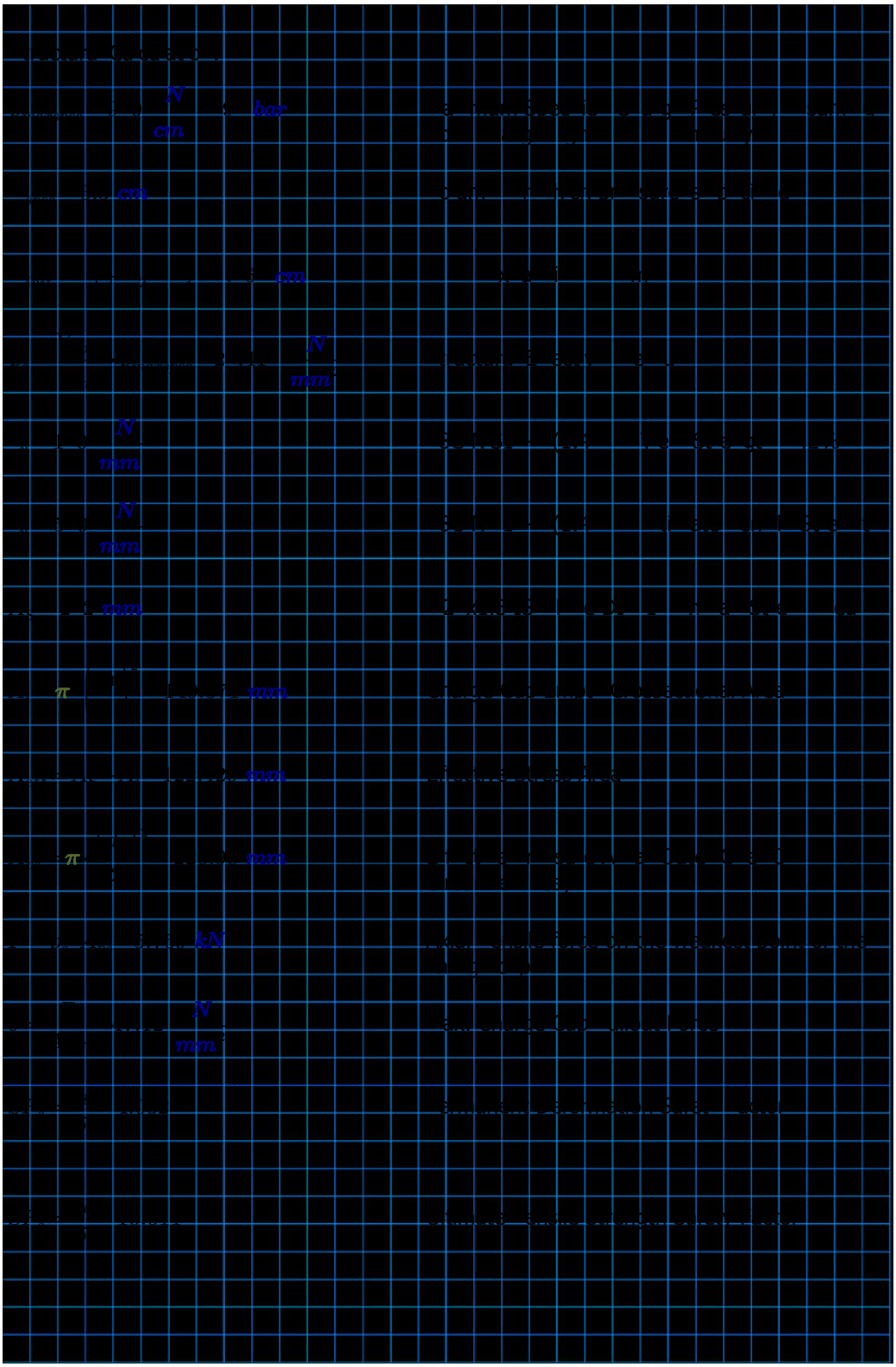
Approach for Operational Calculations The following points have been considered: Effective pullout force of the pin, and the friction it has to overcome; being pretension on the locking arm and O-ring seal friction.



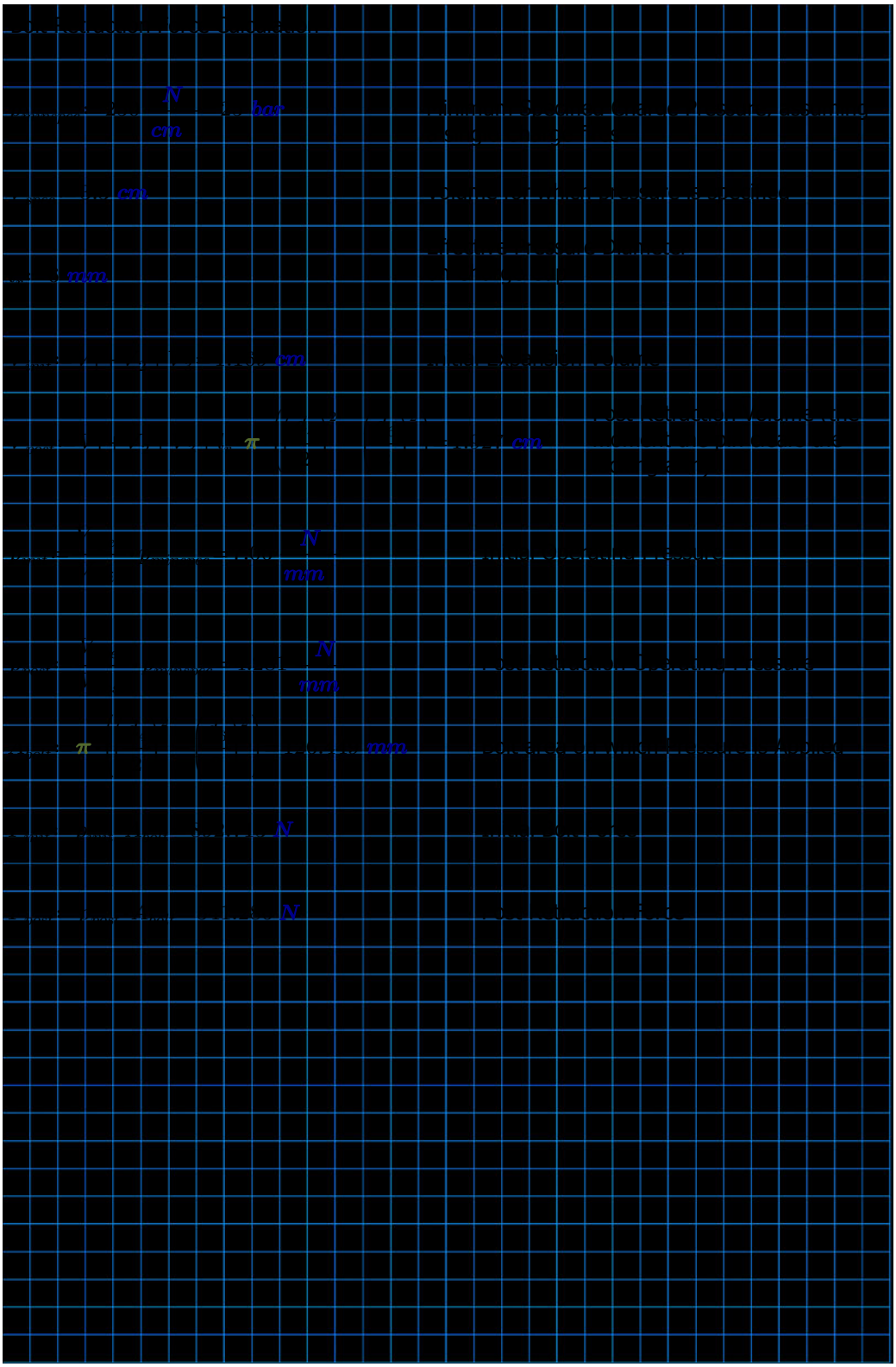
Mit PTC Mathcad Express erstellt. Weitere Informationen finden Sie unter www.mathcad.com.



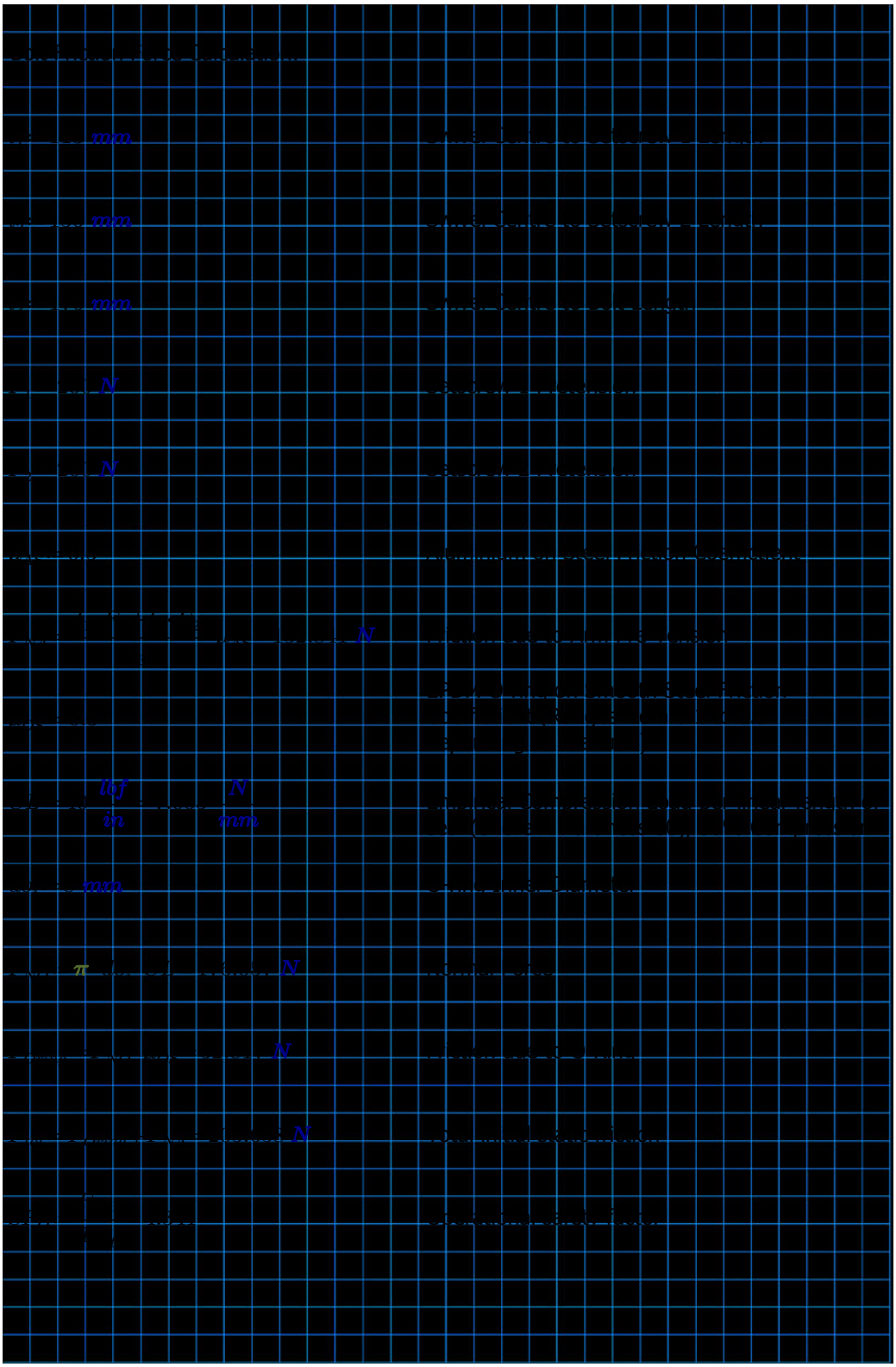
Mit PTC Mathcad Express erstellt. Weitere Informationen finden Sie unter www.mathcad.com.



Mit PTC Mathcad Express erstellt. Weitere Informationen finden Sie unter www.mathcad.com.



Mit PTC Mathcad Express erstellt. Weitere Informationen finden Sie unter www.mathcad.com.



Mit PTC Mathcad Express erstellt. Weitere Informationen finden Sie unter www.mathcad.com.

F.5 Motor Speed Calculations

Motor accelerations

Bearing friction
Moment of Inertia Data from CAD
Moment of Inertia estimations
Torque of the Motors in real working condition
acceleration values

Bearing friction

$f_r := 0.001$ Frictional coefficient (typicalvalue; Source)

$P_{environmental} := 0\ N$ Bearing load= 0 because the rocket moves with constant speed in a microgravital environment and the centre of mass of the assembly is centred on the rotational axis of the rocket.

$d_m := 58\ mm$ mean bearing diameter

$$M_{friction} := f_r \cdot P_{environmental} \cdot d_m$$

$M_{friction} = 0\ J$

Friction caused by preloading the bearings

$P_{preload} := 150\ N$ Preload of the bearing

$$M_{pre} := f_r \cdot P_{preload} \cdot d_m$$

$M_{pre} = \left(8.7 \cdot 10^{-3}\right)\ J$

Moment of inertia from CAD

Subassembly 1(cameras): 411 kg*mm*mm
Subassembly 2: 4731 kg*mm*mm
Subassembly 3 (position with highest m.i. is assumed): 12528 kg*mm*mm

Moment of inertia estimations

All Subassemblies are simulated with homogenic or thin walled cylinders

Subassembly 1: homogenic cylinder with r=45mm and m=0.64kg rotated around length axis
Subassembly 2: homogenic cylinder with r=45mm l=200mm and m=1.4kg rotated around the radial axis
Subassembly 3: m.i. of subassembly 2 plus thin walled cylinder with r=90mm and m=1.4kg rotated around length axis

$I_{\text{homogene cylinder length axis}}$=m*r*r $I_{\text{homogene cylinder radial axis}}$=0.5*m*r*r
$I_{\text{thin walled cylinder length axis}}$=1/12*(3*r*r*L)

Subassembly 1= 650 kg*mm*mm
Subassembly 2= 6143 kg*mm*mm
Subassembly 3= 18050 kg*mm*mm

Torque of the motors

RI-60 has a maximum torque of 0,57 Nm at 5.6 ampers. Maximum available during mission is 0.6 ampers. The torque of the motor and the available amperege is linearly correlated, so the

$$I := 0.5\ \boldsymbol{A}$$
$$k_t := 0.102\ \boldsymbol{N}\cdot\frac{\boldsymbol{m}}{\boldsymbol{A}}$$
$$t := I \cdot k_t$$

Acceleration values

$$\alpha := \frac{t - M_{pre}\cdot(2)}{I}\cdot\frac{180}{\pi}$$

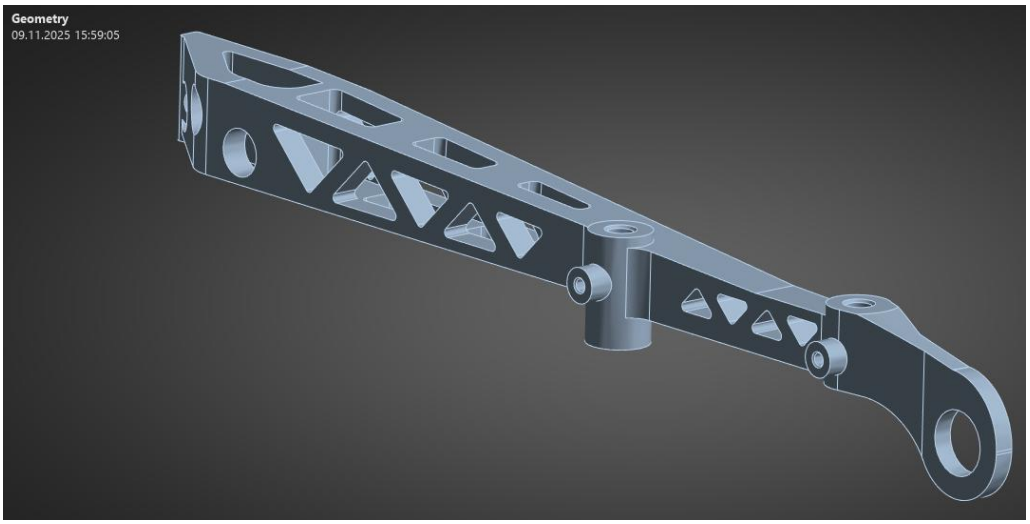
Table of results with current values

	with M.i. from CAD	with M.i from estimations
Subassembly 1:	5850 1/s*s	3700 1/s*s
Subassembly 2:	400 1/s*s	308 1/s*s
Subassembly 3:	192 1/s*s	133 1/s*s

F.6 FEMA Reports

Report – Analytical Strength Assessment
Document Number PRO_FEA_01 Revision 01

01_Locking_Arm
APEX



Aerospace Team Graz - ASTG
Inffeldgasse 16b, 8010 Graz
info@astg.at
www.astg.at

	Name	Department	Date
Created	[redacted]	ASTG PRO	24.03.2025

This Version replaces all previous versions.

© Aerospace Team Graz - ASTG, 2025

1 Introduction

This report is used to document the analytical strength assessment for the component “01_Locking_Arm” used in project “APEX”. This analytical strength assessment report is valid for components and assemblies: “01_Locking_Arm” (Rev. Date 1.08.2025) and is based on the load assumptions: “Specified pre-tensioning of the screw´s” (Rev. Date 1.08.2025).

“Ansys” software package is used for the creation of this analytical strength assessment report.

All coordinates and directions of forces and torques, if not indicated otherwise, refer to an orthogonal coordinate system with its center on the tip of the rocket. Z direction is direction of travel.

2 Description of the FEA model

The structure of the FEA model is shown below.

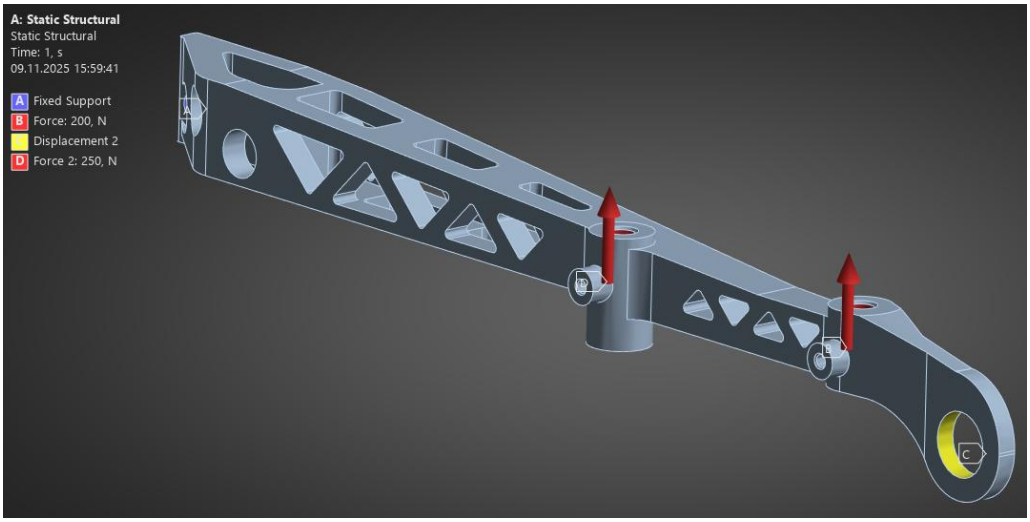


Figure 1: FEA model

A description of the applied boundary conditions and calculated load sets is listed in tables below:

Table 1: Applied boundary conditions

Name	Type	Locked DOF	Description
A	Fixed	6	Interface to connected Part
C	Displacement	2	Interface to pin, Movement along pin axis

Table 2: Calculated load sets

Name	Unit	Value	Description
B	N	200	Screw Pre-tension Force
D	N	250	Screw Pre-tension Force

3 Strength assessment parameters

The strength assessment is carried out using local stresses and simplified assessment rule.

Cyclic degree of utilization

$$a_{BK} \approx \frac{\sigma_v \cdot j_{dyn}}{R_m \cdot f_w} \leq 1$$

σ_v equivalent stress
j_{dyn} cyclic safety factor
R_m ultimate stress
f_w alternating strength factor

Static degree of utilization

$$a_{SK} \approx \frac{\sigma_v \cdot j_{stat}}{R_p \cdot K_p} \leq 1$$

σ_v equivalent stress
j_{stat} static safety factor
R_p yield stress
K_p plastic notch factor

Notice: For the rocket the „fatigue assessment" can be done according to static, but with $K_p = 1$.

A strength assessment task always comprises a load set and set of assessment parameters. The performed strength assessment tasks are listed in the following table:

Table 3: Summary of Simplified assessment Tasks

Task	Load set	Assessment type
Double the expected Force	B	Simplified Assessment Static

The applied assessment and material parameters are listed in tables below:

Table 4: Input parameters for tasks according to Simplified assessment

Parameter	Description	Unit	Value	Tasks
j_{stat}	Static safety factor	-	1	Double the expected pressure
K_p	Plast. notch factor	-	1	Double the expected pressure

Table 5: Material parameters for "Aluminum EN AW 6082 T6"

Parameter	Description	Unit	Value	Source
R_p	Yield stress	MPa	260	Material standard

4 Results

Under the assumptions concerning boundary conditions described in this document, the component shows sufficient resistance against cyclic and proof loads. For all applied assessment rules, the most severe occurring results are listed in the table below.

Table 6: Result Summary

Assessment rule	Loads assessed	Design parameter	Max. value	Limit
Simplified assessment	B	a_{SK}	0,39	≤ 1

Results for A – Degrees of utilization on the structure

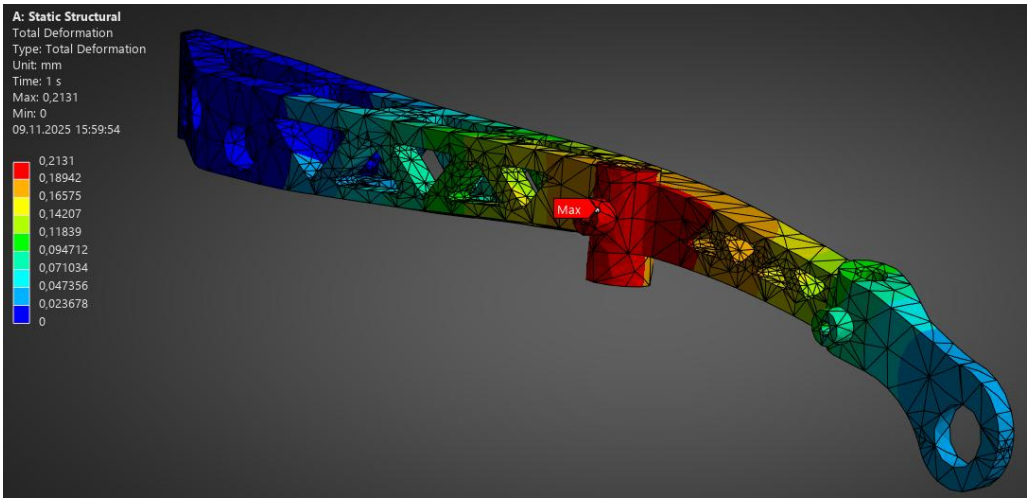


Figure 2: Degrees of utilization - Deformation

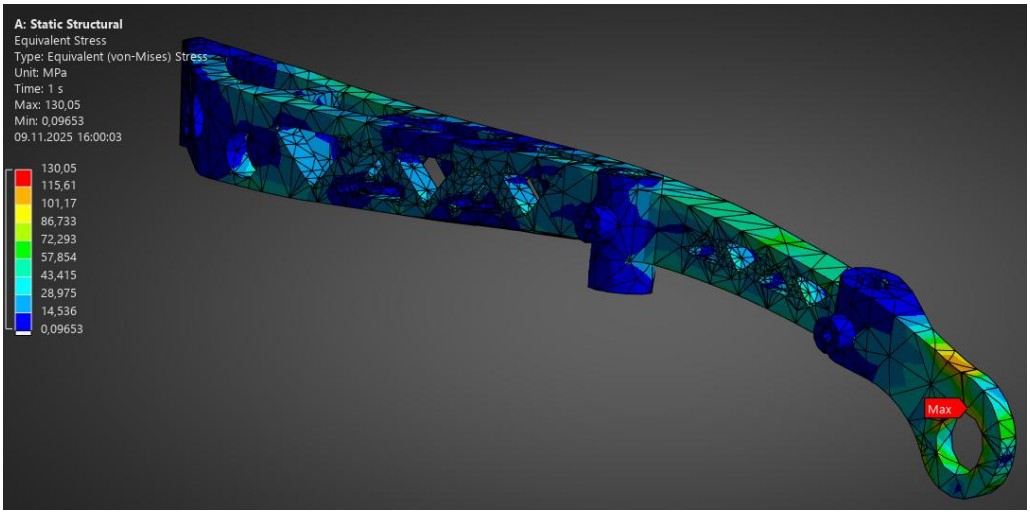
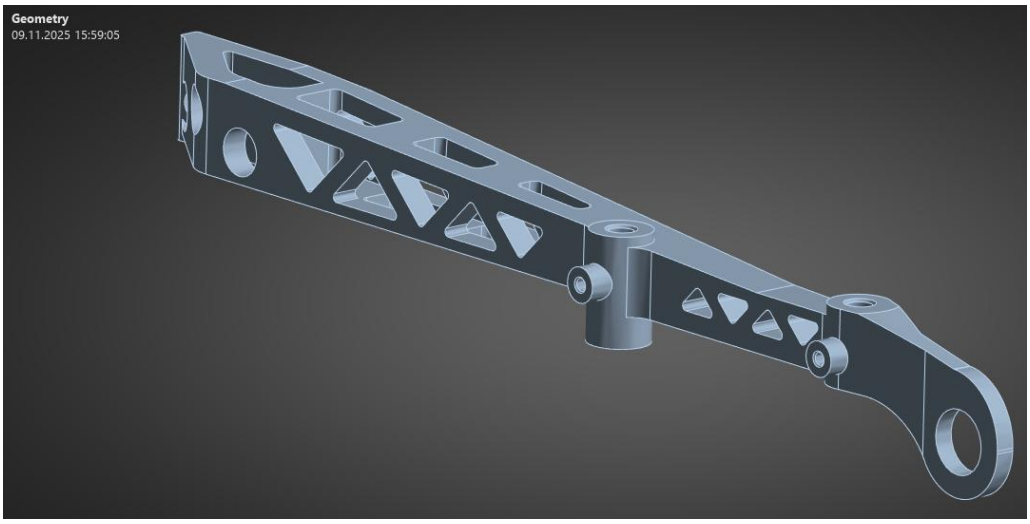


Figure 3: Degrees of utilization –Equivalent Stress

Report – Analytical Strength Assessment
Document Number PRO_FEA_01 Revision 01

01_Locking_Arm
APEX



Aerospace Team Graz - ASTG
Inffeldgasse 16b, 8010 Graz
info@astg.at
www.astg.at

	Name	Department	Date
Created	[redacted]	ASTG PRO	24.03.2025

This Version replaces all previous versions.

© Aerospace Team Graz - ASTG, 2025

1 Introduction

This report is used to document the analytical strength assessment for the component "01_Locking_Arm" used in project "APEX". This analytical strength assessment report is valid for components and assemblies: "01_Locking_Arm" (Rev. Date 1.08.2025) and is based on the load assumptions: "Specified pre-tensioning of the screw´s. In addition, with a rotating Force" (Rev. Date 1.08.2025).

"Ansys" software package is used for the creation of this analytical strength assessment report.

All coordinates and directions of forces and torques, if not indicated otherwise, refer to an orthogonal coordinate system with its center on the tip of the rocket. Z direction is direction of travel.

2 Description of the FEA model

The structure of the FEA model is shown below.

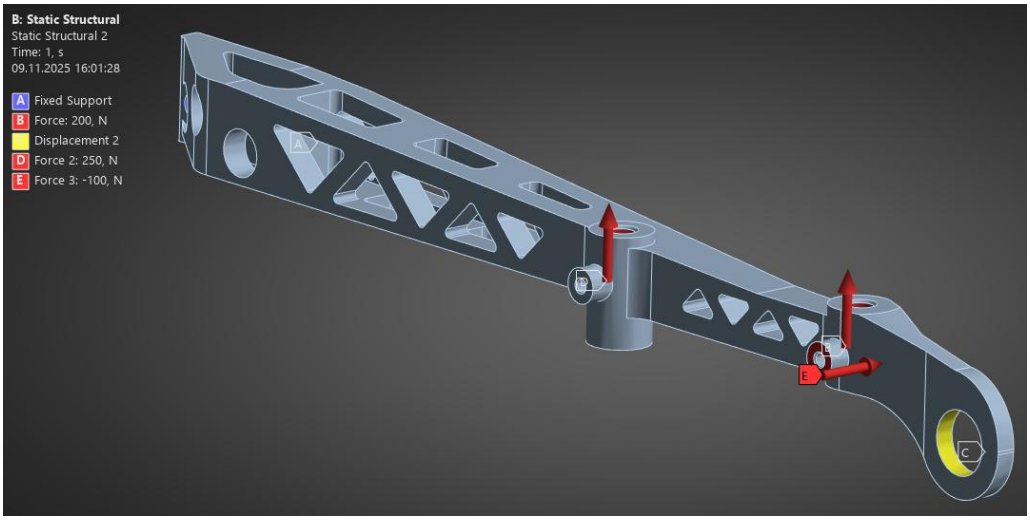


Figure 1: FEA model

A description of the applied boundary conditions and calculated load sets is listed in tables below:

Table 1: Applied boundary conditions

Name	Type	Locked DOF	Description
A	Fixed	6	Interface to connected Part
C	Displacement	2	Interface to pin, Movement along pin axis

Table 2: Calculated load sets

Name	Unit	Value	Description
B	N	200	Screw Pre-tension Force
D	N	250	Screw Pre-tension Force
E	N	100	Side Force due to Rotation

3 Strength assessment parameters

The strength assessment is carried out using local stresses and simplified assessment rule.

Cyclic degree of utilization

$$a_{BK} \approx \frac{\sigma_v \cdot j_{dyn}}{R_m \cdot f_w} \leq 1$$

σ_v equivalent stress
j_{dyn} cyclic safety factor
R_m ultimate stress
f_w alternating strength factor

Static degree of utilization

$$a_{SK} \approx \frac{\sigma_v \cdot j_{stat}}{R_p \cdot K_p} \leq 1$$

σ_v equivalent stress
j_{stat} static safety factor
R_p yield stress
K_p plastic notch factor

Notice: For the rocket the „fatigue assessment" can be done according to static, but with $K_p = 1$.

A strength assessment task always comprises a load set and set of assessment parameters. The performed strength assessment tasks are listed in the following table:

Table 3: Summary of Simplified assessment Tasks

Task	Load set	Assessment type

Double the expected Force	B, D, E	Simplified Assessment Static

The applied assessment and material parameters are listed in tables below:

Table 4: Input parameters for tasks according to Simplified assessment

Parameter	Description	Unit	Value	Tasks
j_{stat}	Static safety factor	-	1	Double the expected pressure
K_p	Plast. notch factor	-	1	Double the expected pressure

Table 5: Material parameters for "Aluminum EN AW 6082 T6"

Parameter	Description	Unit	Value	Source
R_p	Yield stress	MPa	260	Material standard

4 Results

Under the assumptions concerning boundary conditions described in this document, the component shows sufficient resistance against cyclic and proof loads. For all applied assessment rules, the most severe occurring results are listed in the table below.

Table 6: Result Summary

Assessment rule	Loads assessed	Design parameter	Max. value	Limit
Simplified assessment	B	a_{SK}	0,70	≤ 1

Results for A – Degrees of utilization on the structure

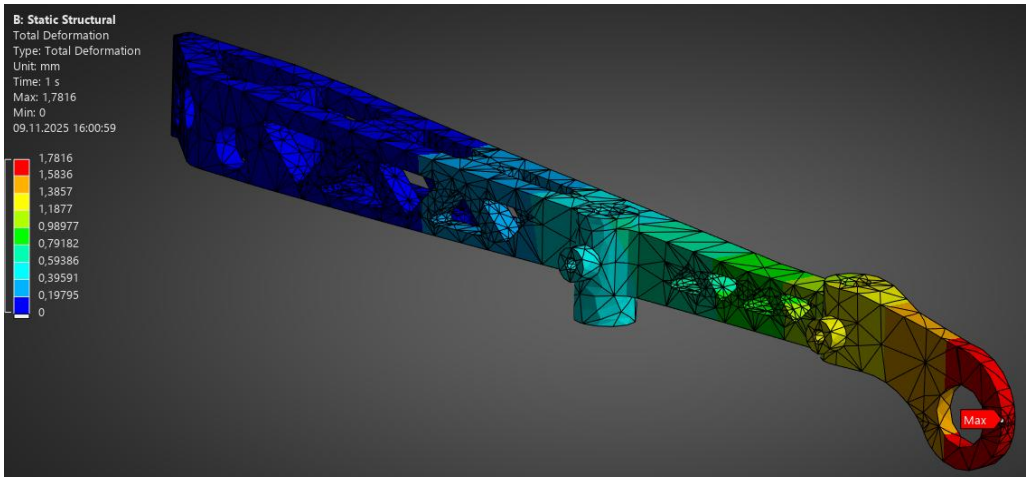


Figure 2: Degrees of utilization - Deformation

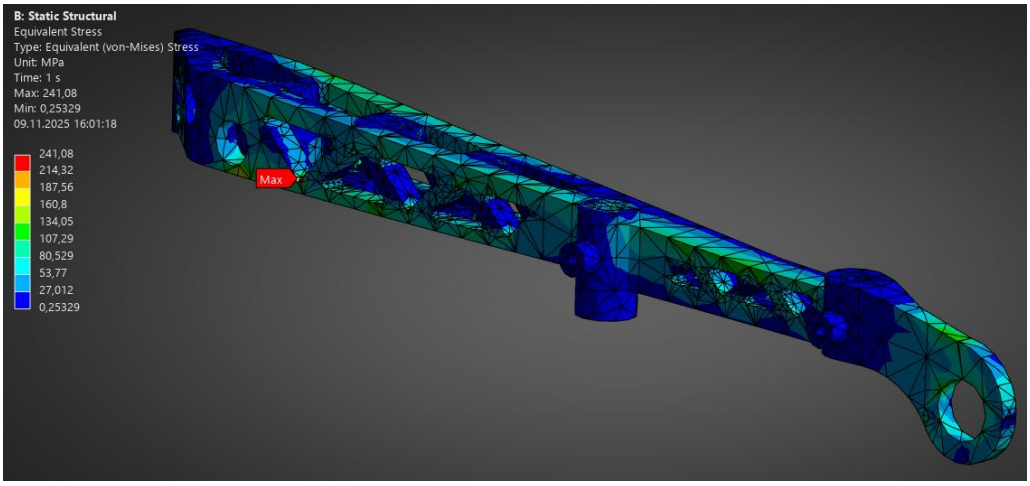
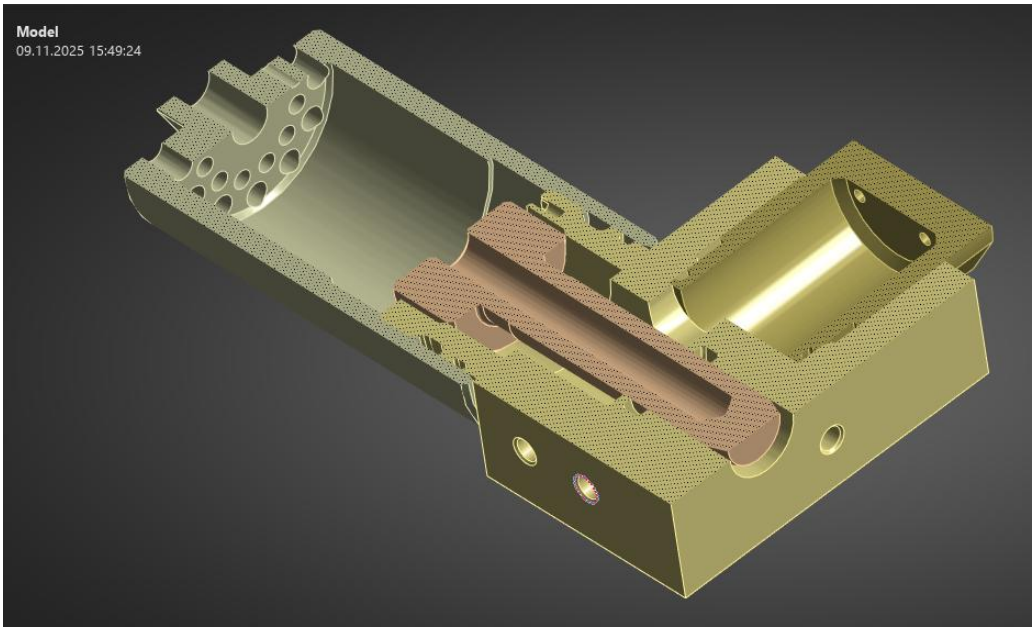


Figure 3: Degrees of utilization –Equivalent Stress

Report – Analytical Strength Assessment
Document Number PRO_FEA_01 Revision 01

01_Locking_V01
APEX



Aerospace Team Graz - ASTG
Inffeldgasse 16b, 8010 Graz
info@astg.at
www.astg.at

	Name	Department	Date
Created	[redacted]	ASTG PRO	09.11.2025

This Version replaces all previous versions.

© Aerospace Team Graz - ASTG, 2025

1 Introduction

This report is used to document the analytical strength assessment for the component “01_Locking_ V01” used in project “APEX”. This analytical strength assessment report is valid for components and assemblies: “01_Locking_V01” (Rev. Date 23.10.2025) and is based on the load assumptions: “Maximum specific charge pressure, assuming both charges ignite simultaneously with the given volume. (Appendix F)” (Rev. Date 23.10.2025).

“Ansys” software package is used for the creation of this analytical strength assessment report.

All coordinates and directions of forces and torques, if not indicated otherwise, refer to an orthogonal coordinate system with its center on the tip of the rocket. Z direction is direction of travel.

2 Description of the FEA model

The structure of the FEA model is shown below.

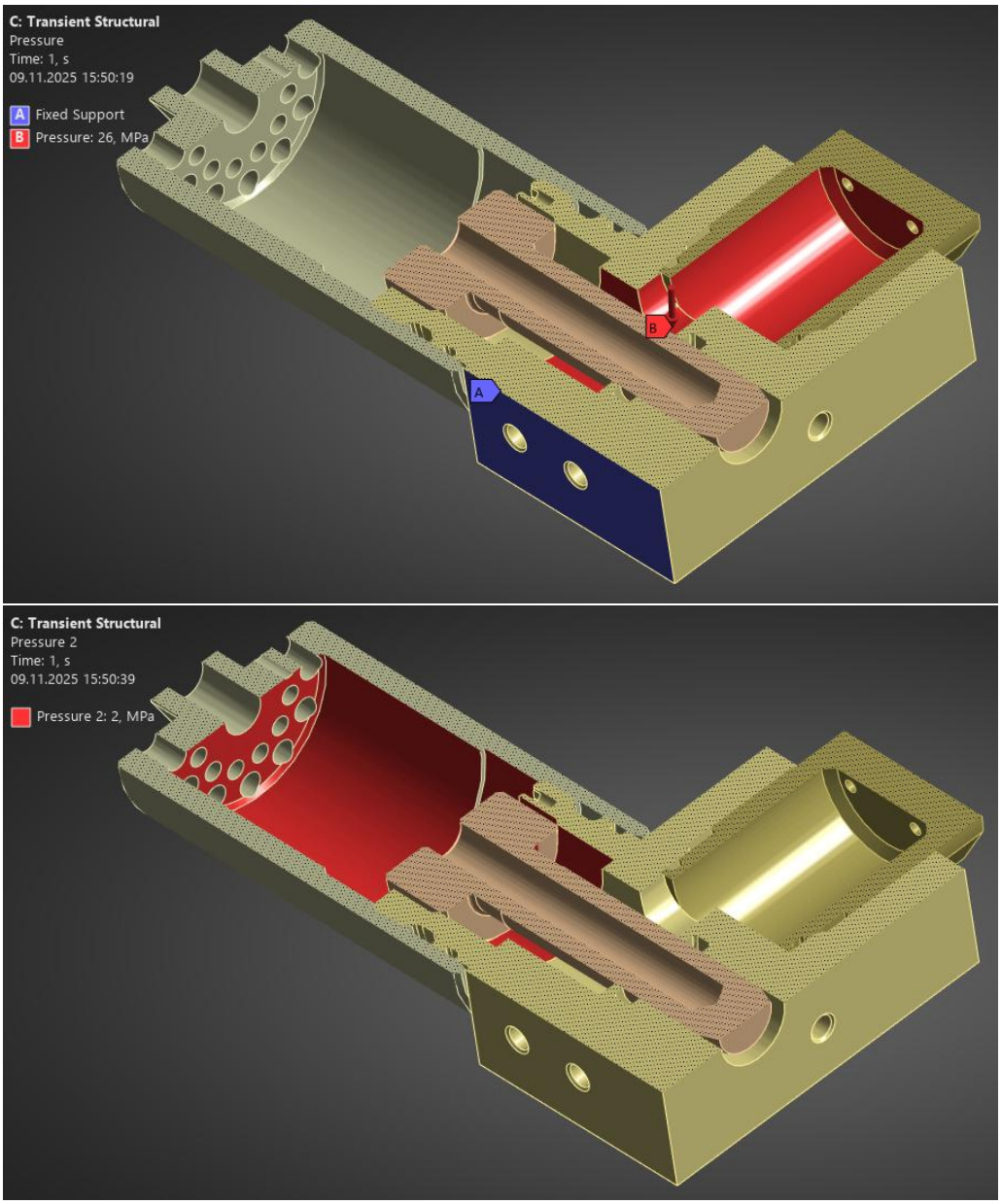


Figure 1: FEA model

A description of the applied boundary conditions and calculated load sets is listed in tables below:

Table 1: Applied boundary conditions

Name	Type	Locked DOF	Description
A	Fixed	6	Interface to connected Part

Table 2: Calculated load sets

Name	Unit	Value	Description
B	MPa	26	Compressed Chamber
C	MPa	2	Extended Chamber

3 Strength assessment parameters

The strength assessment is carried out using local stresses and simplified assessment rule.

Cyclic degree of utilization

$$a_{BK} \approx \frac{\sigma_v \cdot j_{dyn}}{R_m \cdot f_w} \leq 1$$

σ_v equivalent stress
j_{dyn} cyclic safety factor
R_m ultimate stress
f_w alternating strength factor

Static degree of utilization

$$a_{SK} \approx \frac{\sigma_v \cdot j_{stat}}{R_p \cdot K_p} \leq 1$$

σ_v equivalent stress
j_{stat} static safety factor
R_p yield stress
K_p plastic notch factor

Notice: For the rocket the „fatigue assessment" can be done according to static, but with $K_p = 1$.

A strength assessment task always comprises a load set and set of assessment parameters. The performed strength assessment tasks are listed in the following table:

Table 3: Summary of Simplified assessment Tasks

Task	Load set	Assessment type
Double the expected Presure	B, C	Simplified Assessment Static

The applied assessment and material parameters are listed in tables below:

Table 4: Input parameters for tasks according to Simplified assessment

Parameter	Description	Unit	Value	Tasks
j_{stat}	Static safety factor	-	1	Double the expected pressure
K_p	Plast. notch factor	-	1	Double the expected pressure

Table 5: Material parameters for "1.4301 / Aisi 304"

Parameter	Description	Unit	Value	Source
R_p	Yield stress	MPa	190	Material standard

4 Results

Under the assumptions concerning boundary conditions described in this document, the component shows sufficient resistance against cyclic and proof loads. For all applied assessment rules, the most severe occurring results are listed in the table below.

Table 6: Result Summary

Assessment rule	Loads assessed	Design parameter	Max. value	Limit
Simplified assessment	B	a_{SK}	0,71	≤ 1

Results for A – Degrees of utilization on the structure

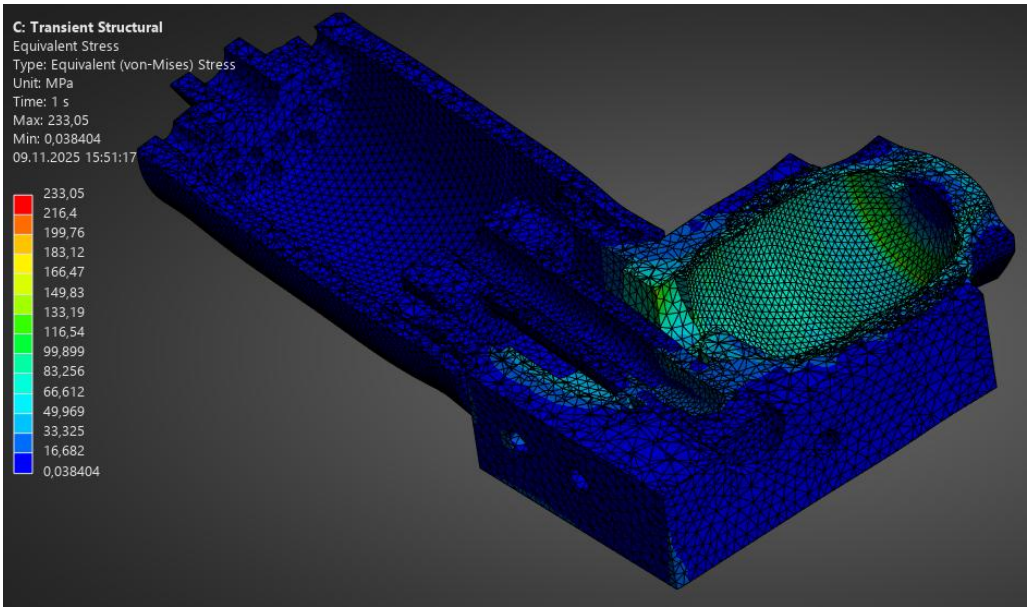


Figure 2: Degrees of utilization - Overview

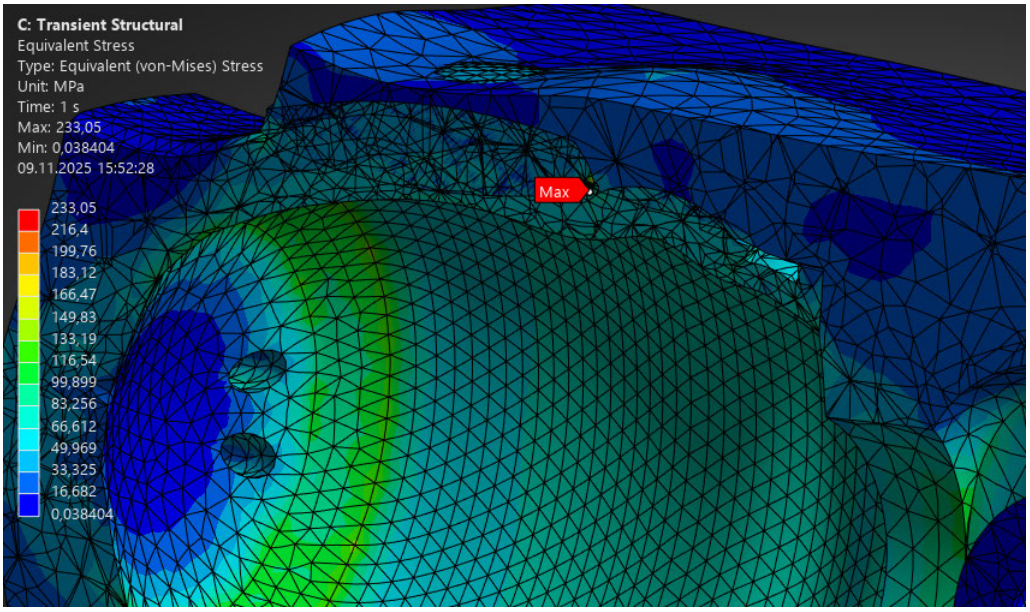
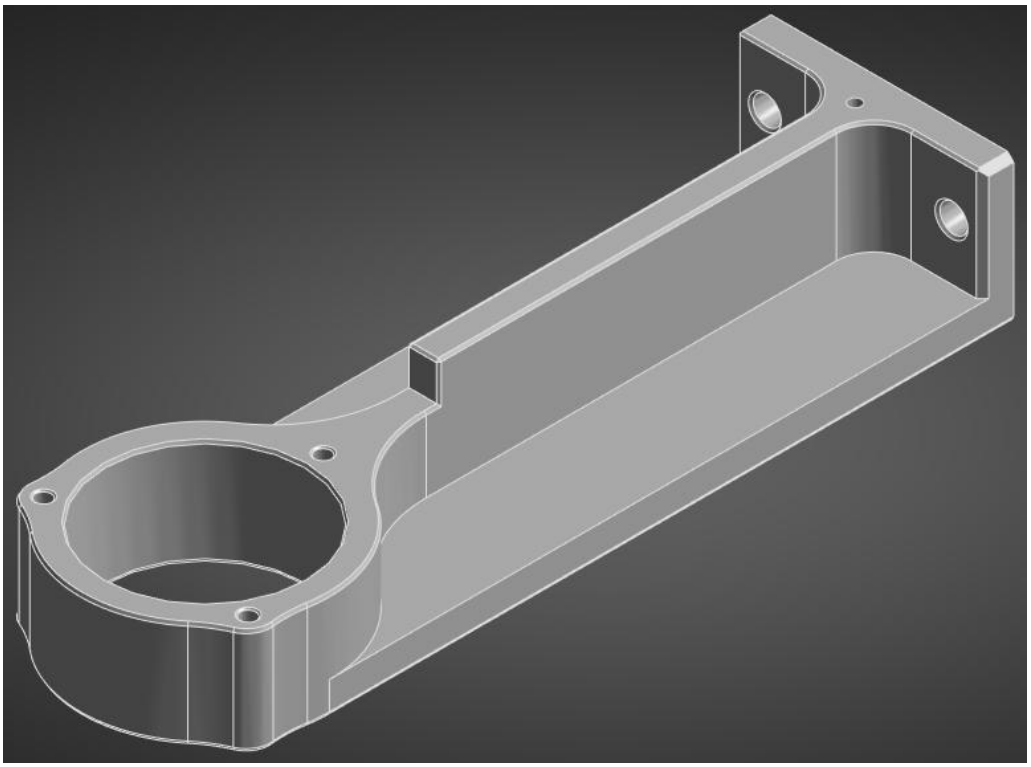


Figure 3: Degrees of utilization - Detail

Report – Analytical Strength Assessment
Document Number PRO_FEA_01 Revision 01

01_Rotating_BearingArm_V01
APEX



Aerospace Team Graz - ASTG
Inffeldgasse 16b, 8010 Graz
info@astg.at
www.astg.at

	Name	Department	Date
Created	[redacted]	ASTG PRO	24.03.2025

This Version replaces all previous versions.

© Aerospace Team Graz - ASTG, 2025

1 Introduction

This report is used to document the analytical strength assessment for the component "01_Rotating_BearingArm_V01" used in project "APEX". This analytical strength assessment report is valid for components and assemblies: "01_Rotating_BearingArm_V01" (Rev. Date 24.03.2025) and is based on the load assumptions: "Pre-tensioning of the bearings with 300N" (Rev. Date 24.03.2025).

"Ansys" software package is used for the creation of this analytical strength assessment report.

All coordinates and directions of forces and torques, if not indicated otherwise, refer to an orthogonal coordinate system with its center on the tip of the rocket. Z direction is direction of travel.

2 Description of the FEA model

The structure of the FEA model is shown below.

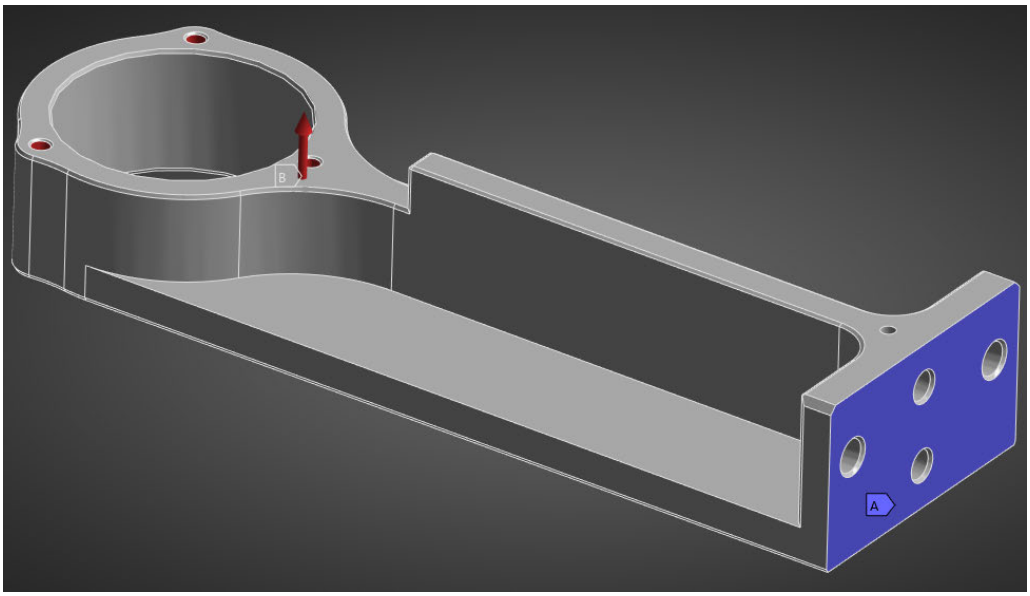


Figure 1: FEA model

A description of the applied boundary conditions and calculated load sets is listed in tables below:

Table 1: Applied boundary conditions

Name	Type	Locked DOF	Description
A	Fixed	6	Interface to connected Part

Table 2: Calculated load sets

Name	Unit	Value	Description
B	N	300	Bearing Preload Force

3 Strength assessment parameters

The strength assessment is carried out using local stresses and simplified assessment rule.

Cyclic degree of utilization

$$a_{BK} \approx \frac{\sigma_v \cdot j_{dyn}}{R_m \cdot f_w} \leq 1$$

σ_v	equivalent stress
j_{dyn}	cyclic safety factor
R_m	ultimate stress
f_w	alternating strength factor

Static degree of utilization

$$a_{SK} \approx \frac{\sigma_v \cdot j_{stat}}{R_p \cdot K_p} \leq 1$$

σ_v	equivalent stress
j_{stat}	static safety factor
R_p	yield stress
K_p	plastic notch factor

Notice: For the rocket the „fatigue assessment" can be done according to static, but with $K_p = 1$.

A strength assessment task always comprises a load set and set of assessment parameters. The performed strength assessment tasks are listed in the following table:

Table 3: Summary of Simplified assessment Tasks

Task	Load set	Assessment type
Double the expected Force	B	Simplified Assessment Static

The applied assessment and material parameters are listed in tables below:

Table 4: Input parameters for tasks according to Simplified assessment

Parameter	Description	Unit	Value	Tasks
j_{stat}	Static safety factor	-	1	Double the expected pressure
K_p	Plast. notch factor	-	1	Double the expected pressure

Table 5: Material parameters for "Aluminum EN AW 6082 T6"

Parameter	Description	Unit	Value	Source
R_p	Yield stress	MPa	260	Material standard

4 Results

Under the assumptions concerning boundary conditions described in this document, the component shows sufficient resistance against cyclic and proof loads. For all applied assessment rules, the most severe occurring results are listed in the table below.

Table 6: Result Summary

Assessment rule	Loads assessed	Design parameter	Max. value	Limit
Simplified assessment	B	a_{SK}	0,23	≤ 1

Results for A – Degrees of utilization on the structure

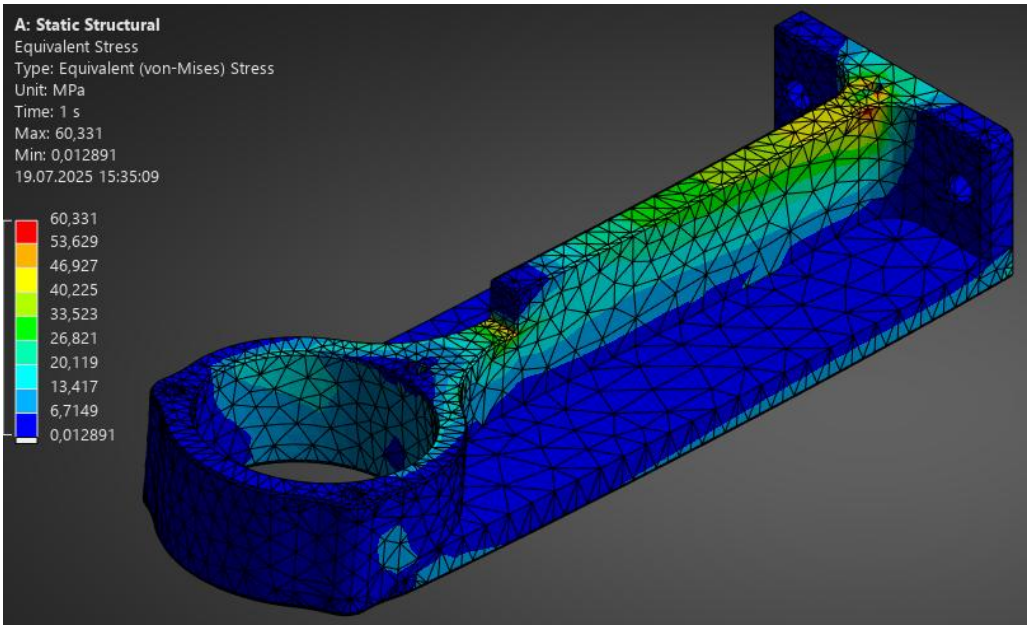


Figure 2: Degrees of utilization - Overview

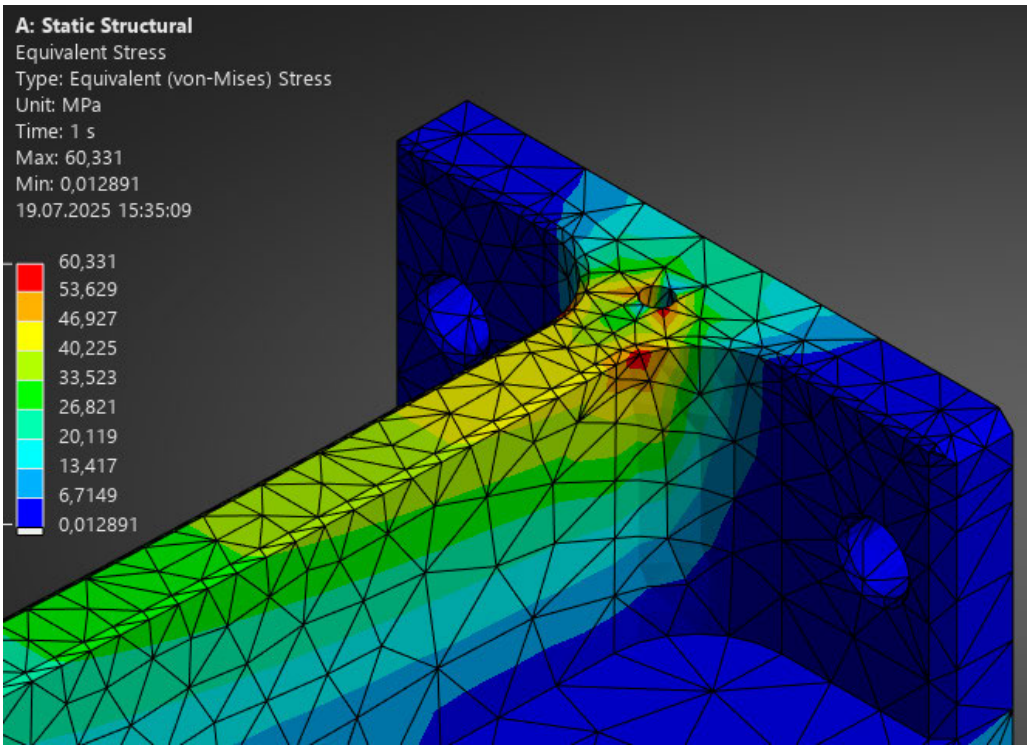
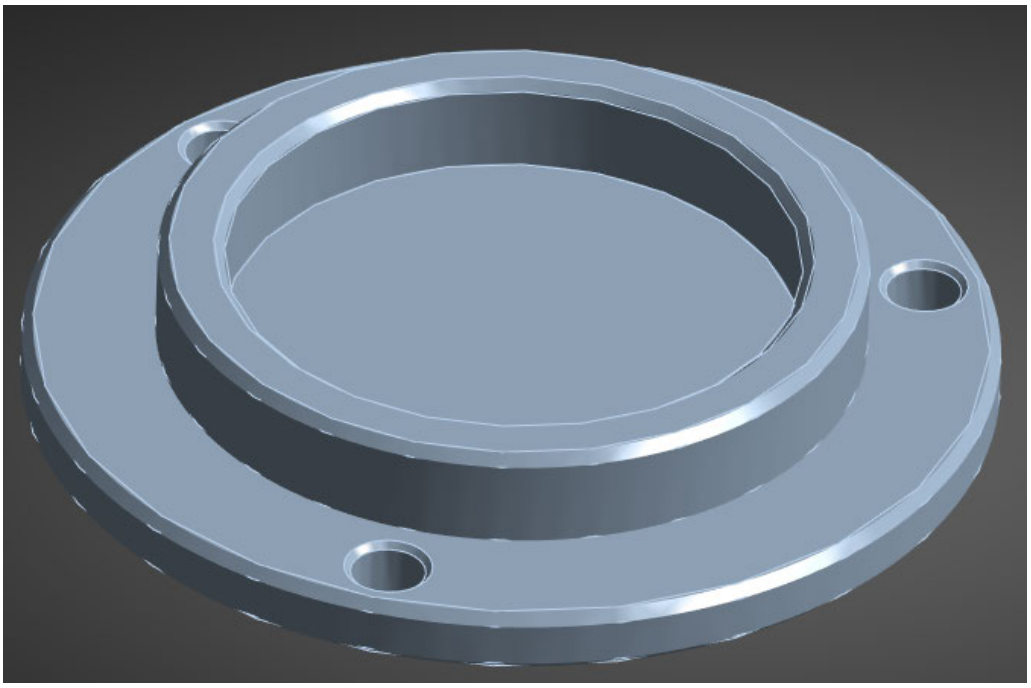


Figure 3: Degrees of utilization - Detail

Report – Analytical Strength Assessment
Document Number PRO_FEA_01 Revision 01

01_Rotating_BearingClampSmall_V01

APEX



Aerospace Team Graz - ASTG
Inffeldgasse 16b, 8010 Graz
info@astg.at
www.astg.at

	Name	Department	Date
Created	Alexander Kallinger	ASTG PRO	24.03.2025

This Version replaces all previous versions.

© Aerospace Team Graz - ASTG, 2025

1 Introduction

This report is used to document the analytical strength assessment for the component "01_Rotating_BearingClampSmall_V01" used in project "APEX". This analytical strength assessment report is valid for components and assemblies: "01_Rotating_BearingClampSmall_V01" (Rev. Date 24.03.2025) and is based on the load assumptions: "Pre-tensioning of the bearings with 300N" (Rev. Date 24.03.2025).

"Ansys" software package is used for the creation of this analytical strength assessment report.

All coordinates and directions of forces and torques, if not indicated otherwise, refer to an orthogonal coordinate system with its center on the tip of the rocket. Z direction is direction of travel.

2 Description of the FEA model

The structure of the FEA model is shown below.

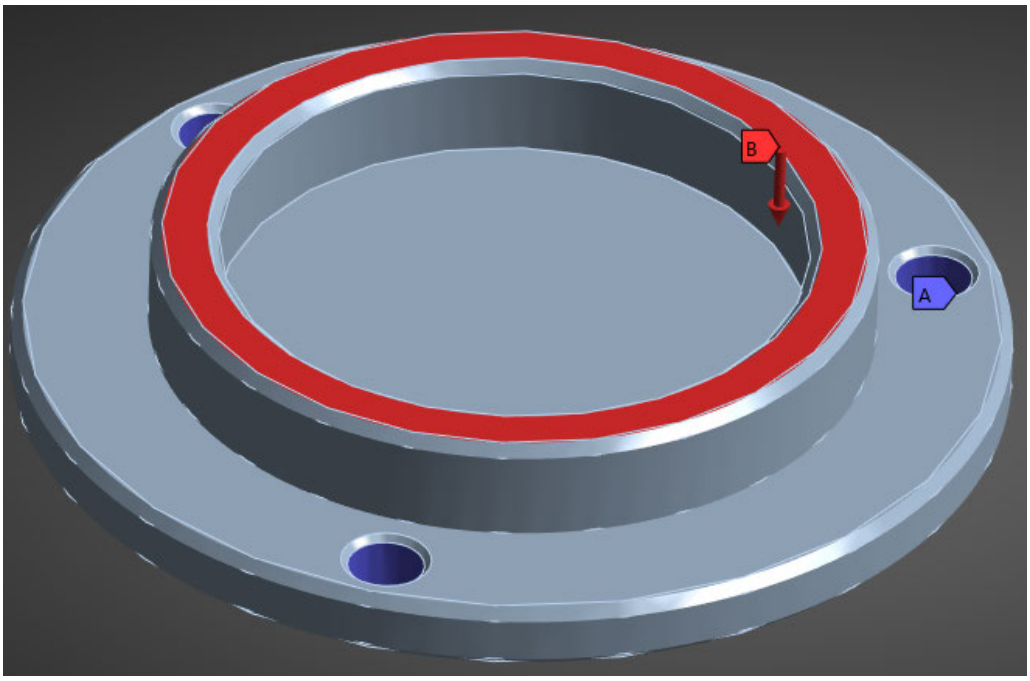


Figure 1: FEA model

A description of the applied boundary conditions and calculated load sets is listed in tables below:

Table 1: Applied boundary conditions

Name	Type	Locked DOF	Description
A	Fixed	6	Interface to connected Part

Table 2: Calculated load sets

Name	Unit	Value	Description
B	N	300	Bearing Preload Force

3 Strength assessment parameters

The strength assessment is carried out using local stresses and simplified assessment rule.

Cyclic degree of utilization

$$a_{BK} \approx \frac{\sigma_v \cdot j_{dyn}}{R_m \cdot f_w} \leq 1$$

σ_v	equivalent stress
j_{dyn}	cyclic safety factor
R_m	ultimate stress
f_w	alternating strength factor

Static degree of utilization

$$a_{SK} \approx \frac{\sigma_v \cdot j_{stat}}{R_p \cdot K_p} \leq 1$$

σ_v	equivalent stress
j_{stat}	static safety factor
R_p	yield stress
K_p	plastic notch factor

Notice: For the rocket the „fatigue assessment" can be done according to static, but with $K_p = 1$.

A strength assessment task always comprises a load set and set of assessment parameters. The performed strength assessment tasks are listed in the following table:

Table 3: Summary of Simplified assessment Tasks

Task	Load set	Assessment type
Double the expected Force	B	Simplified Assessment Static

The applied assessment and material parameters are listed in tables below:

Table 4: Input parameters for tasks according to Simplified assessment

Parameter	Description	Unit	Value	Tasks
j_{stat}	Static safety factor	-	1	Double the expected pressure
K_p	Plast. notch factor	-	1	Double the expected pressure

Table 5: Material parameters for "Aluminum EN AW 6082 T6"

Parameter	Description	Unit	Value	Source
R_p	Yield stress	MPa	260	Material standard

4 Results

Under the assumptions concerning boundary conditions described in this document, the component shows sufficient resistance against cyclic and proof loads. For all applied assessment rules, the most severe occurring results are listed in the table below.

Table 6: Result Summary

Assessment rule	Loads assessed	Design parameter	Max. value	Limit
Simplified assessment	B	a_{SK}	0,13	≤ 1

Results for A – Degrees of utilization on the structure

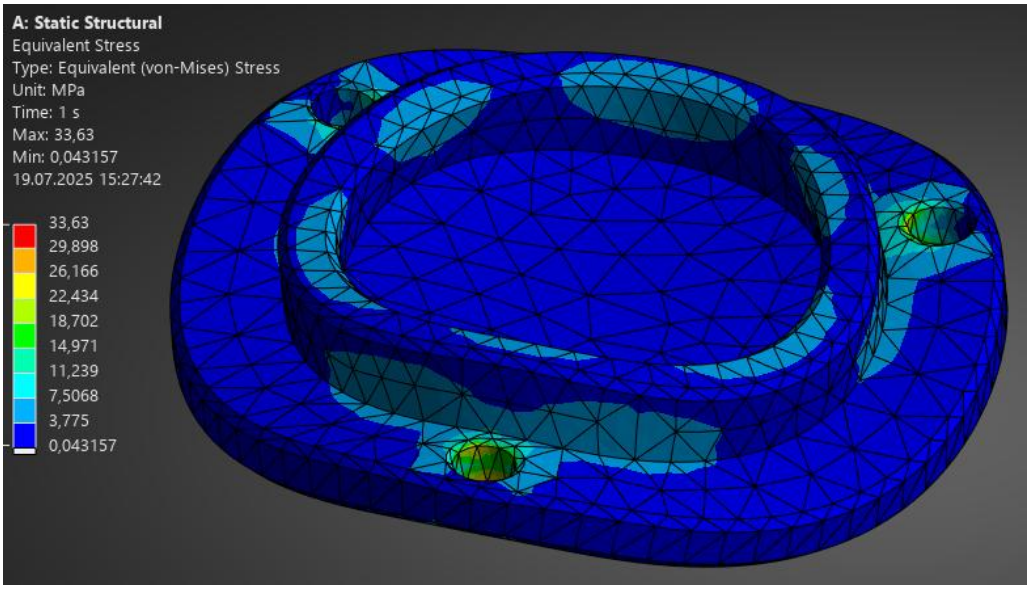
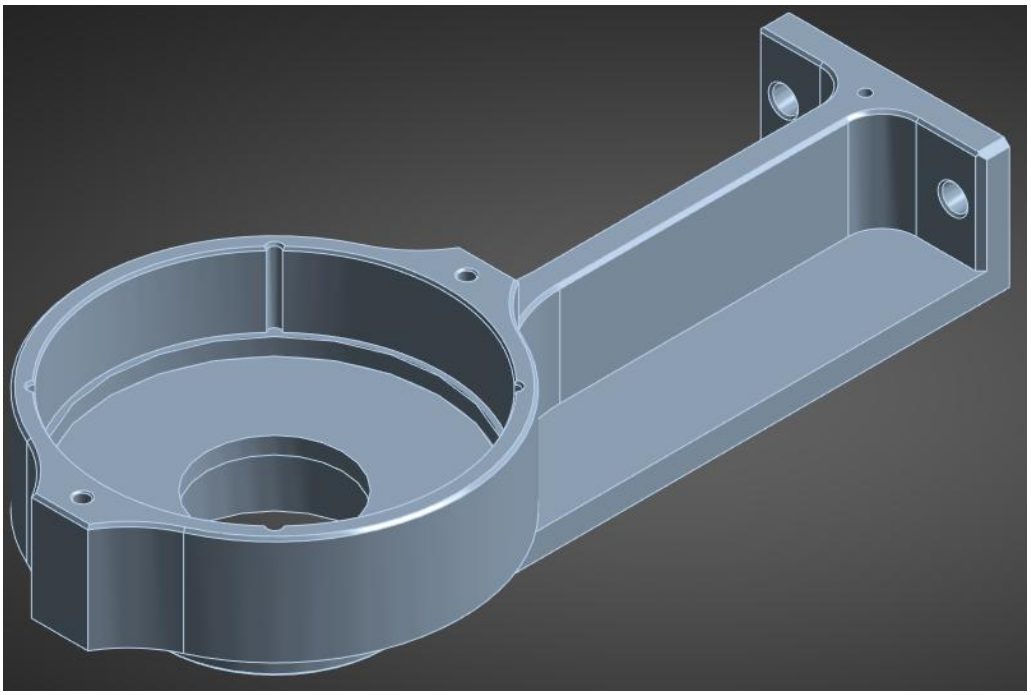


Figure 2: Degrees of utilization - Overview

Report – Analytical Strength Assessment
Document Number PRO_FEA_01 Revision 01

01_Rotating_MotorArm_V01
APEX



Aerospace Team Graz - ASTG
Inffeldgasse 16b, 8010 Graz
info@astg.at
www.astg.at

	Name	Department	Date
Created	Alexander Kallinger	ASTG PRO	24.03.2025

This Version replaces all previous versions.

© Aerospace Team Graz - ASTG, 2025

1 Introduction

This report is used to document the analytical strength assessment for the component "01_Rotating_MotorArm_V01" used in project "APEX". This analytical strength assessment report is valid for components and assemblies: "01_Rotating_MotorArm_V01" (Rev. Date 24.03.2025) and is based on the load assumptions: "Pre-tensioning of the bearings with 300N" (Rev. Date 24.03.2025).

"Ansys" software package is used for the creation of this analytical strength assessment report.

All coordinates and directions of forces and torques, if not indicated otherwise, refer to an orthogonal coordinate system with its center on the tip of the rocket. Z direction is direction of travel.

2 Description of the FEA model

The structure of the FEA model is shown below.

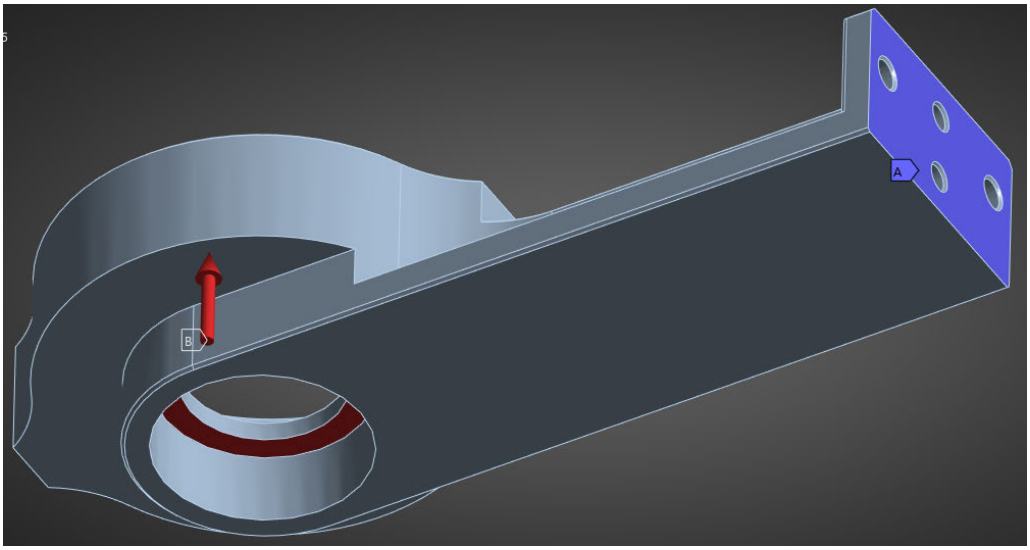


Figure 1: FEA model

A description of the applied boundary conditions and calculated load sets is listed in tables below:

Table 1: Applied boundary conditions

Name	Type	Locked DOF	Description
A	Fixed	6	Interface to connected Part

Table 2: Calculated load sets

Name	Unit	Value	Description
B	N	300	Bearing Preload Force

3 Strength assessment parameters

The strength assessment is carried out using local stresses and simplified assessment rule.

Cyclic degree of utilization

$$a_{BK} \approx \frac{\sigma_v \cdot j_{dyn}}{R_m \cdot f_w} \leq 1$$

σ_v	equivalent stress
j_{dyn}	cyclic safety factor
R_m	ultimate stress
f_w	alternating strength factor

Static degree of utilization

$$a_{SK} \approx \frac{\sigma_v \cdot j_{stat}}{R_p \cdot K_p} \leq 1$$

σ_v	equivalent stress
j_{stat}	static safety factor
R_p	yield stress
K_p	plastic notch factor

Notice: For the rocket the „fatigue assessment" can be done according to static, but with $K_p = 1$.

A strength assessment task always comprises a load set and set of assessment parameters. The performed strength assessment tasks are listed in the following table:

Table 3: Summary of Simplified assessment Tasks

Task	Load set	Assessment type
Double the expected Force	B	Simplified Assessment Static

The applied assessment and material parameters are listed in tables below:

Table 4: Input parameters for tasks according to Simplified assessment

Parameter	Description	Unit	Value	Tasks
j_{stat}	Static safety factor	-	1	Double the expected pressure
K_p	Plast. notch factor	-	1	Double the expected pressure

Table 5: Material parameters for "Aluminum EN AW 6082 T6"

Parameter	Description	Unit	Value	Source
R_p	Yield stress	MPa	260	Material standard

4 Results

Under the assumptions concerning boundary conditions described in this document, the component shows sufficient resistance against cyclic and proof loads. For all applied assessment rules, the most severe occurring results are listed in the table below.

Table 6: Result Summary

Assessment rule	Loads assessed	Design parameter	Max. value	Limit
Simplified assessment	B	a_{SK}	0,23	≤ 1

Results for A – Degrees of utilization on the structure

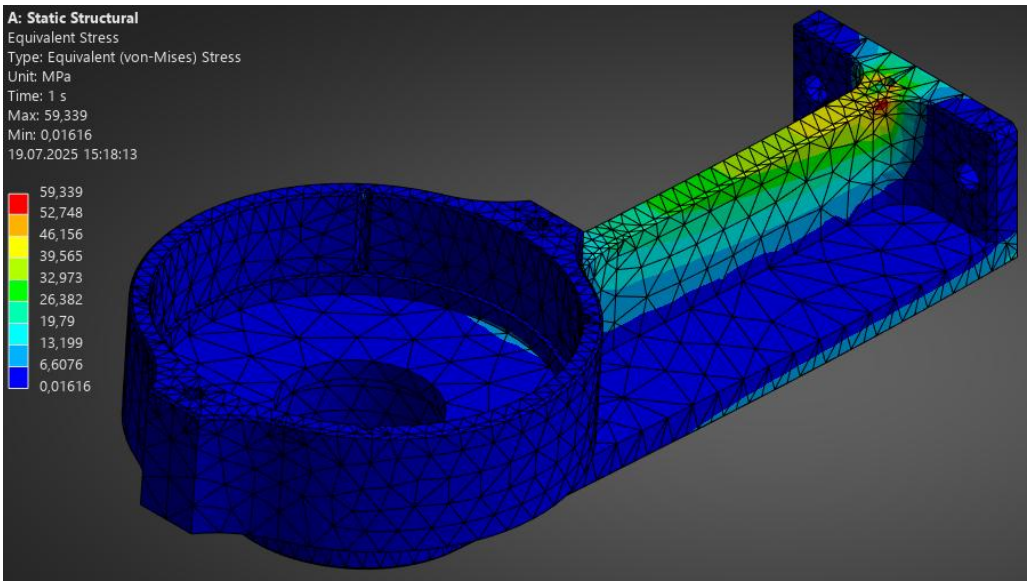


Figure 2: Degrees of utilization - Overview

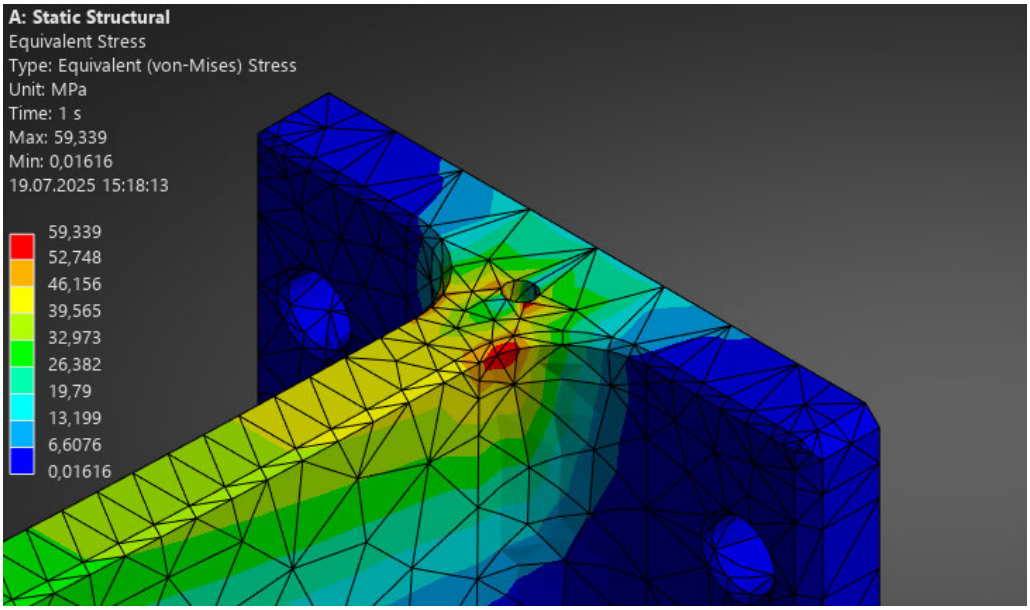
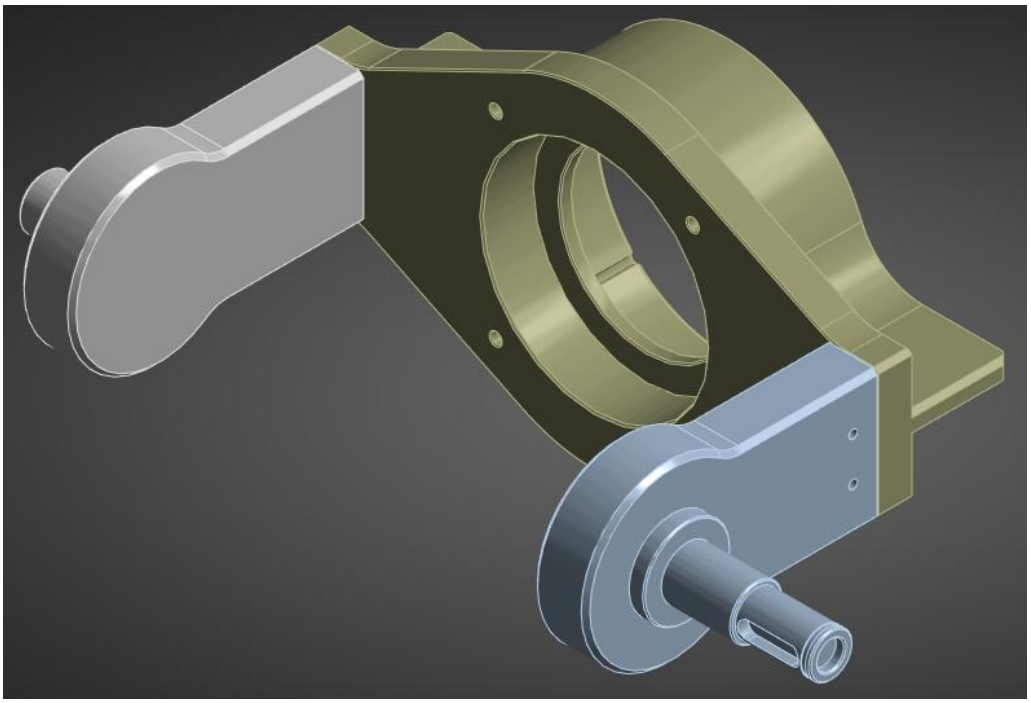


Figure 3: Degrees of utilization - Detail

Report – Analytical Strength Assessment
Document Number PRO_FEA_01 Revision 01

01_Swivel_A_V01
APEX



Aerospace Team Graz - ASTG
Inffeldgasse 16b, 8010 Graz
info@astg.at
www.astg.at

	Name	Department	Date
Created	Alexander Kallinger	ASTG PRO	24.03.2025

This Version replaces all previous versions.

© Aerospace Team Graz - ASTG, 2025

1 Introduction

This report is used to document the analytical strength assessment for the component “01_Swivel_A_V01” used in project “APEX”. This analytical strength assessment report is valid for components and assemblies: “01_Swivel_A_V01” (Rev. Date 24.03.2025) and is based on the load assumptions: “Pre-tensioning of the bearings with 300N” (Rev. Date 24.03.2025).

“Ansys” software package is used for the creation of this analytical strength assessment report.

All coordinates and directions of forces and torques, if not indicated otherwise, refer to an orthogonal coordinate system with its center on the tip of the rocket. Z direction is direction of travel.

2 Description of the FEA model

The structure of the FEA model is shown below.

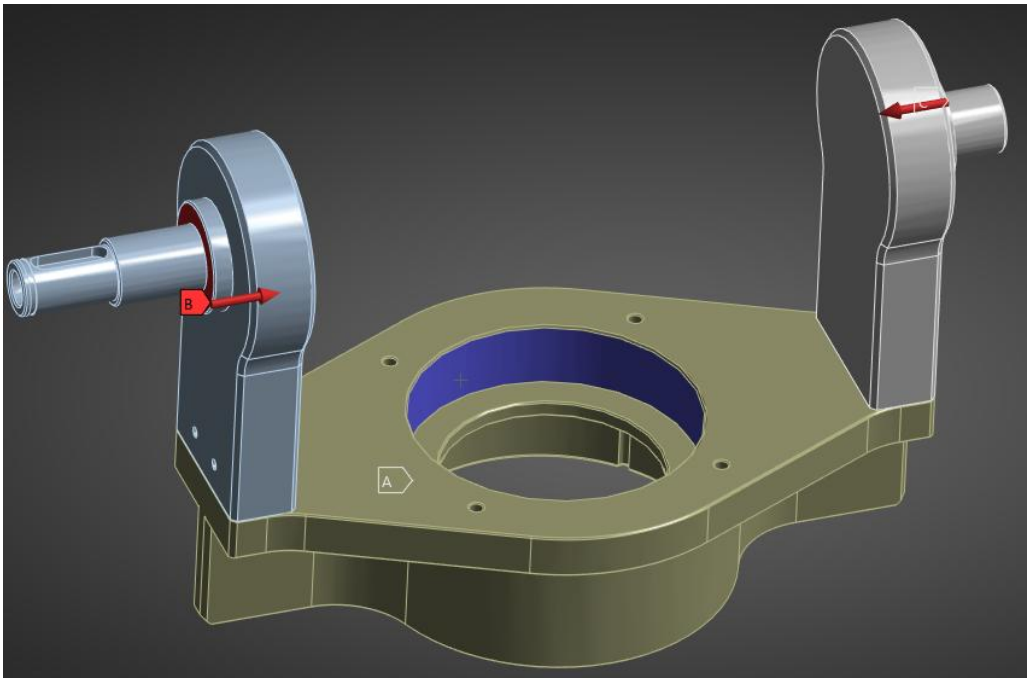


Figure 1: FEA model

A description of the applied boundary conditions and calculated load sets is listed in tables below:

Table 1: Applied boundary conditions

Name	Type	Locked DOF	Description
A	Fixed	6	Interface to connected Part

Table 2: Calculated load sets

Name	Unit	Value	Description
B	N	300	Bearing Preload Force
C	N	300	Bearing Preload Force

3 Strength assessment parameters

The strength assessment is carried out using local stresses and simplified assessment rule.

Cyclic degree of utilization

$$a_{BK} \approx \frac{\sigma_v \cdot j_{dyn}}{R_m \cdot f_w} \leq 1$$

σ_v	equivalent stress
j_{dyn}	cyclic safety factor
R_m	ultimate stress
f_w	alternating strength factor

Static degree of utilization

$$a_{SK} \approx \frac{\sigma_v \cdot j_{stat}}{R_p \cdot K_p} \leq 1$$

σ_v	equivalent stress
j_{stat}	static safety factor
R_p	yield stress
K_p	plastic notch factor

Notice: For the rocket the „fatigue assessment" can be done according to static, but with $K_p = 1$.

A strength assessment task always comprises a load set and set of assessment parameters. The performed strength assessment tasks are listed in the following table:

Table 3: Summary of Simplified assessment Tasks

Task	Load set	Assessment type
Double the expected Force	B	Simplified Assessment Static

The applied assessment and material parameters are listed in tables below:

Table 4: Input parameters for tasks according to Simplified assessment

Parameter	Description	Unit	Value	Tasks
j_{stat}	Static safety factor	-	1	Double the expected pressure
K_p	Plast. notch factor	-	1	Double the expected pressure

Table 5: Material parameters for "Aluminum EN AW 6082 T6"

Parameter	Description	Unit	Value	Source
R_p	Yield stress	MPa	260	Material standard

4 Results

Under the assumptions concerning boundary conditions described in this document, the component shows sufficient resistance against cyclic and proof loads. For all applied assessment rules, the most severe occurring results are listed in the table below.

Table 6: Result Summary

Assessment rule	Loads assessed	Design parameter	Max. value	Limit
Simplified assessment	B, C	a_{SK}	0,17	≤ 1

Results for A – Degrees of utilization on the structure

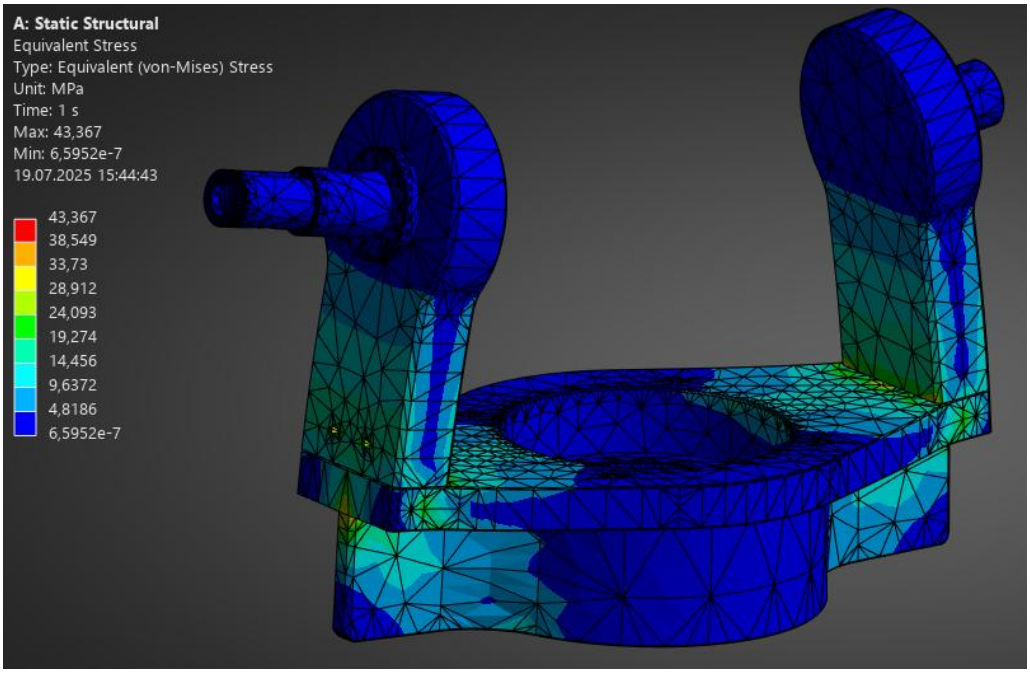


Figure 2: Degrees of utilization - Overview

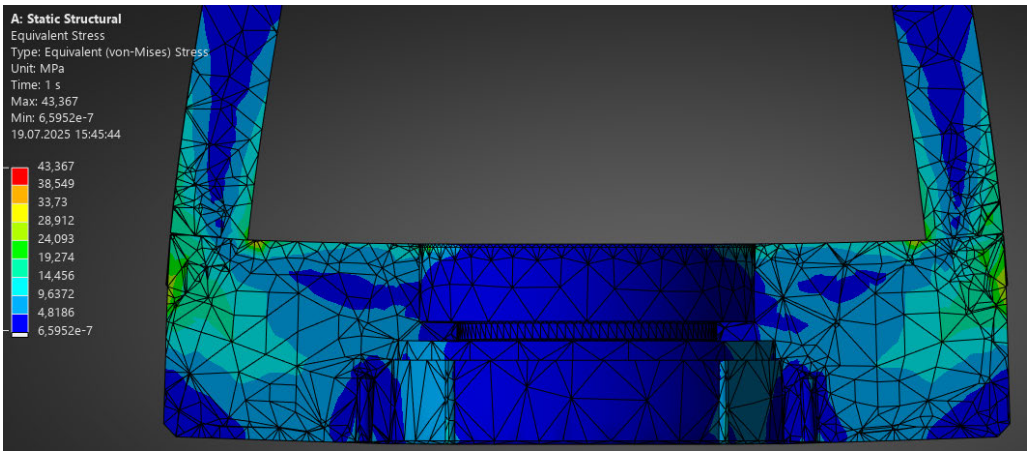
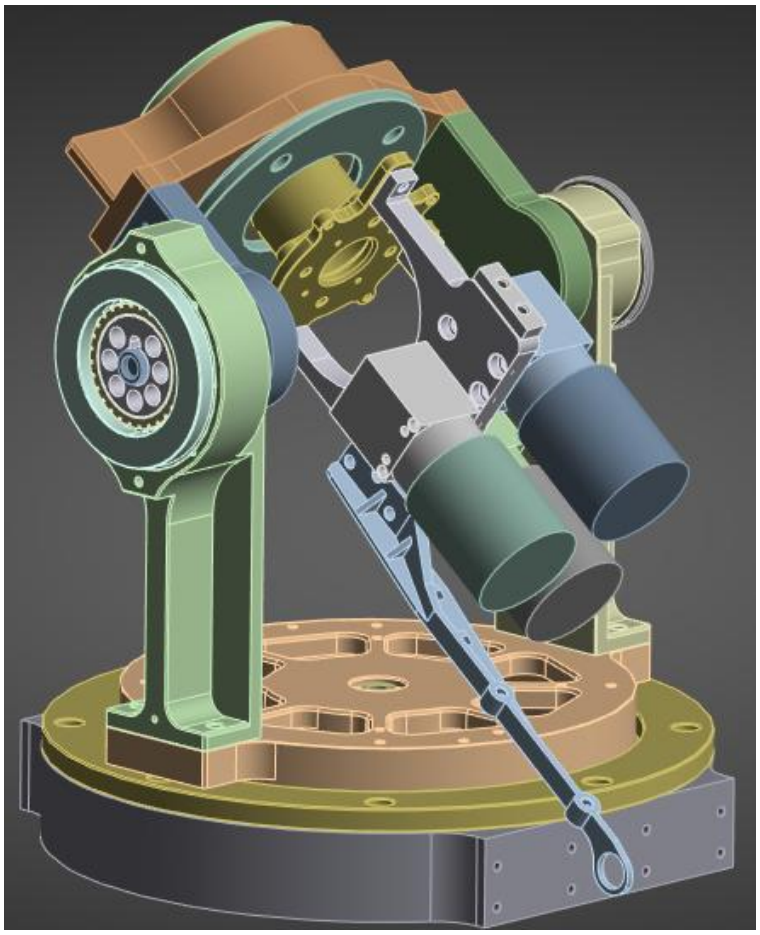


Figure 3: Degrees of utilization - Detail

Report – Analytical Strength Assessment
Document Number PRO_FEA_01 Revision 01

00_Gimbal_Assembly_V01
APEX



Aerospace Team Graz - ASTG
Inffeldgasse 16b, 8010 Graz
info@astg.at
www.astg.at

	Name	Department	Date
Created	Alexander Kallinger	ASTG PRO	13.05.2025

This Version replaces all previous versions.

© Aerospace Team Graz - ASTG, 2025

1 Introduction

This report is used to document the analytical strength assessment for the component “00_Gimbal_Assembly_V01” used in project “APEX”. This analytical strength assessment report is valid for components and assemblies: “00_Gimbal_Assembly_V01” (Rev. Date 13.05.2025) and is based on the load assumptions: “Vehicle Level one sine-vibrations. According to REXUS-Manual table 10-2.” (Rev. Date 26.11.2021).

“Ansys” software package is used for the creation of this analytical strength assessment report.

All coordinates and directions of forces and torques, if not indicated otherwise, refer to an orthogonal coordinate system with its center on the tip of the rocket. Z direction is direction of travel.

2 Description of the FEA model

The structure of the FEA model is shown below.

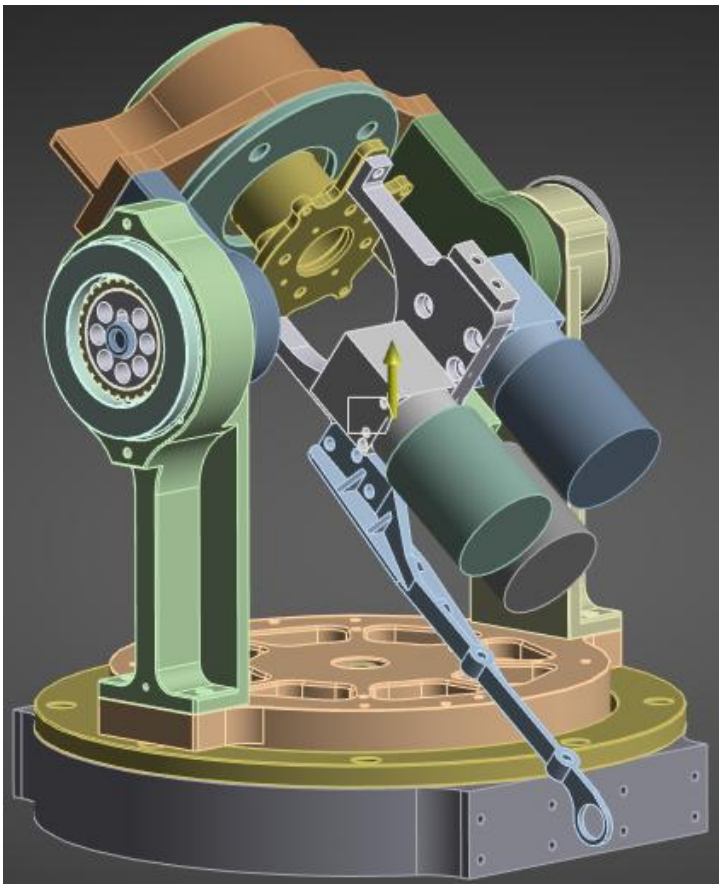


Figure 1: FEA model

A description of the applied boundary conditions and calculated load sets is listed in tables below:

Table 1: Eigenfrequencies

Name	Unit	Value	Description
Mode 1	Hz	237,65	Eigenfrequency from Modal
Mode 2	Hz	268,48	Eigenfrequency from Modal
Mode 3	Hz	308,44	Eigenfrequency from Modal
Mode 4	Hz	400,97	Eigenfrequency from Modal
Mode 5	Hz	546,42	Eigenfrequency from Modal
Mode 6	Hz	682,38	Eigenfrequency from Modal

Table 2: Calculated load sets

Name	Unit	Value	Description
B	mm/s²	68646,55	7g in Z 20-2000Hz

3 Strength assessment parameters

The strength assessment is carried out using local stresses and simplified assessment rule.

Cyclic degree of utilization

$$a_{BK} \approx \frac{\sigma_v \cdot j_{dyn}}{R_m \cdot f_w} \leq 1$$

σ_v equivalent stress
j_{dyn} cyclic safety factor
R_m ultimate stress
f_w alternating strength factor

Static degree of utilization

$$a_{SK} \approx \frac{\sigma_v \cdot j_{stat}}{R_p \cdot K_p} \leq 1$$

σ_v equivalent stress
j_{stat} static safety factor
R_p yield stress
K_p plastic notch factor

Notice: For the rocket the „fatigue assessment" can be done according to static, but with $K_p = 1$.

A strength assessment task always comprises a load set and set of assessment parameters. The performed strength assessment tasks are listed in the following table:

Table 3: Summary of Simplified assessment Tasks

Task	Load set	Assessment type
Double the expected Acceleration	B	Simplified Assessment Static

The applied assessment and material parameters are listed in tables below:

Table 4: Input parameters for tasks according to Simplified assessment

Parameter	Description	Unit	Value	Tasks
j_{stat}	Static safety factor	-	1	Double the expected pressure
K_p	Plast. notch factor	-	1	Double the expected pressure

Table 5: Material parameters for "Aluminum EN AW 6082 T6"

Parameter	Description	Unit	Value	Source
R_p	Yield stress	MPa	260	Material standard

4 Results

Under the assumptions concerning boundary conditions described in this document, the component shows sufficient resistance against cyclic and proof loads. For all applied assessment rules, the most severe occurring results are listed in the table below.

Table 6: Result Summary

Assessment rule	Loads assessed	Design parameter	Max. value	Limit
Simplified assessment	B, Mode 1	a_{SK}	0,08	≤ 1
Simplified assessment	B, Mode 2	a_{SK}	0,11	≤ 1
Simplified assessment	B, Mode 3	a_{SK}	0,20	≤ 1
Simplified assessment	B, Mode 4	a_{SK}	0,05	≤ 1
Simplified assessment	B, Mode 5	a_{SK}	0,05	≤ 1
Simplified assessment	B, Mode 6	a_{SK}	0,02	≤ 1

Results B, All Modes – Degrees of utilization on the structure

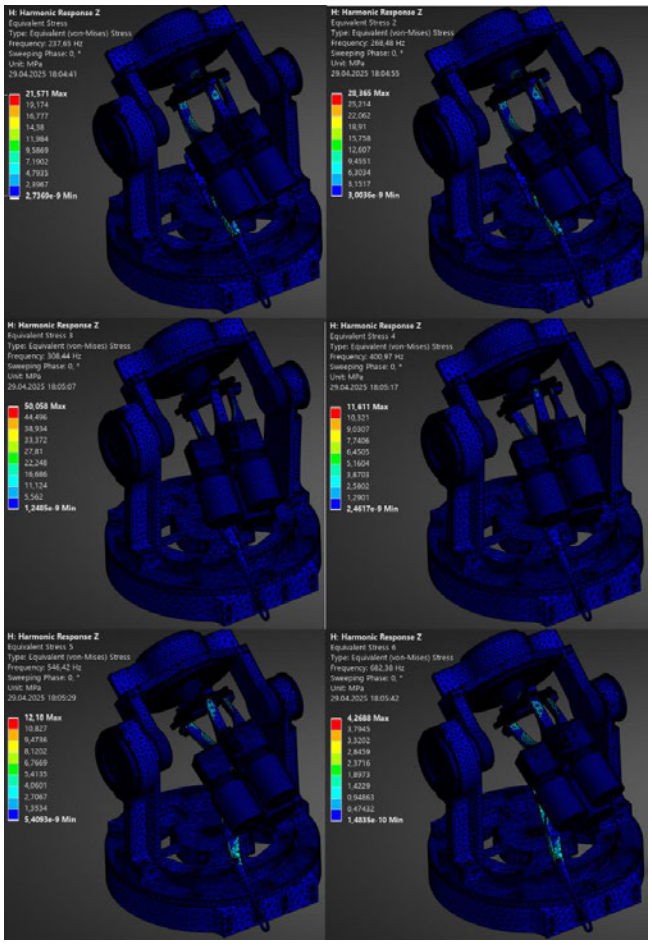
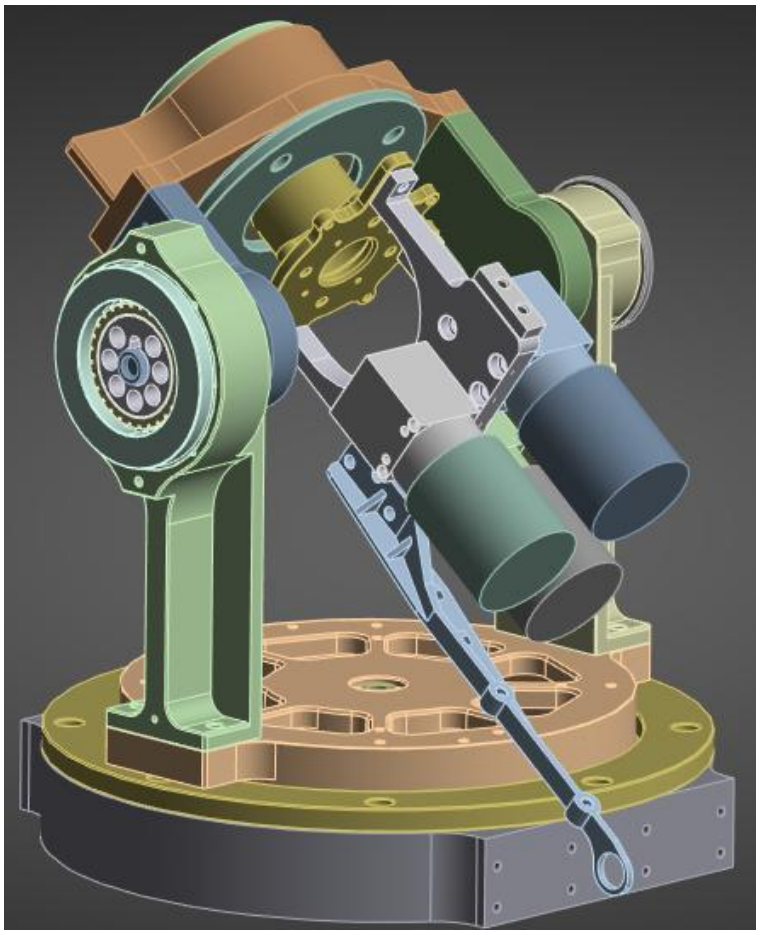


Figure 2: Degrees of utilization - Overview

Report – Analytical Strength Assessment
Document Number PRO_FEA_01 Revision 01

00_Gimbal_Assembly_V01
APEX



Aerospace Team Graz - ASTG
Inffeldgasse 16b, 8010 Graz
info@astg.at
www.astg.at

	Name	Department	Date
Created	Alexander Kallinger	ASTG PRO	13.05.2025

This Version replaces all previous versions.

© Aerospace Team Graz - ASTG, 2025

1 Introduction

This report is used to document the analytical strength assessment for the component “00_Gimbal_Assembly_V01” used in project “APEX”. This analytical strength assessment report is valid for components and assemblies: “00_Gimbal_Assembly_V01” (Rev. Date 13.05.2025) and is based on the load assumptions: “Vehicle Level one random-vibrations. According to REXUS-Manual table 10-2.” (Rev. Date 26.11.2021).

“Ansys” software package is used for the creation of this analytical strength assessment report.

All coordinates and directions of forces and torques, if not indicated otherwise, refer to an orthogonal coordinate system with its center on the tip of the rocket. Z direction is direction of travel.

2 Description of the FEA model

The structure of the FEA model is shown below.

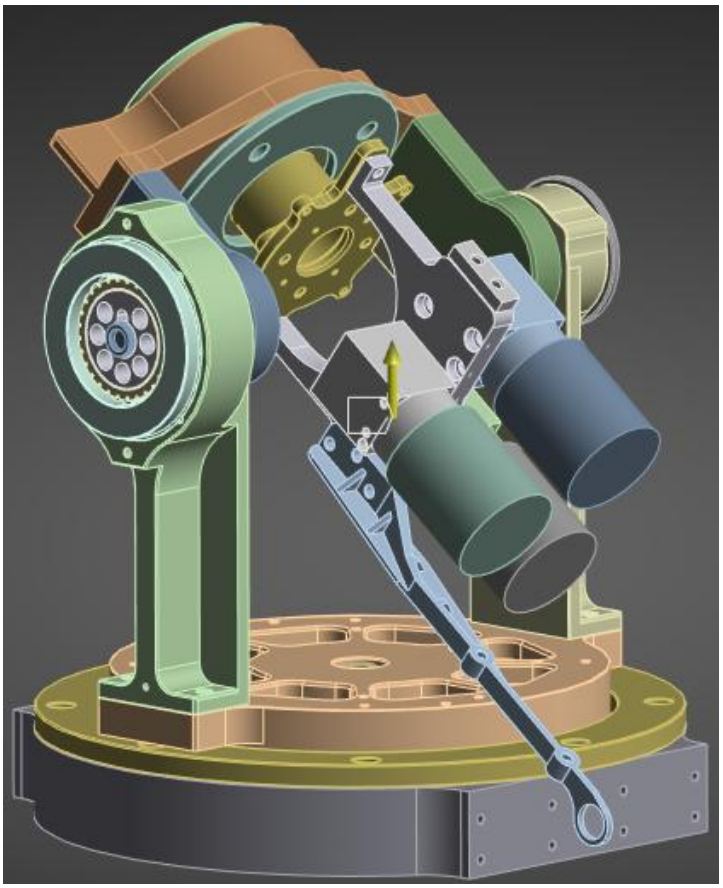


Figure 1: FEA model

A description of the applied boundary conditions and calculated load sets is listed in tables below:

Table 1: Calculated load sets

Name	Unit	Value	Description
PSD G Acceleration X	g²/Hz	0,029	At 20-2000Hz
PSD G Acceleration Y	g²/Hz	0,029	At 20-2000Hz
PSD G Acceleration Z	g²/Hz	0,051	At 20-2000Hz

3 Strength assessment parameters

The strength assessment is carried out using local stresses and simplified assessment rule.

Cyclic degree of utilization

$$a_{BK} \approx \frac{\sigma_v \cdot j_{dyn}}{R_m \cdot f_w} \leq 1$$

σ_v equivalent stress
j_{dyn} cyclic safety factor
R_m ultimate stress
f_w alternating strength factor

Static degree of utilization

$$a_{SK} \approx \frac{\sigma_v \cdot j_{stat}}{R_p \cdot K_p} \leq 1$$

σ_v equivalent stress
j_{stat} static safety factor
R_p yield stress
K_p plastic notch factor

Notice: For the rocket the „fatigue assessment" can be done according to static, but with $K_p = 1$.

A strength assessment task always comprises a load set and set of assessment parameters. The performed strength assessment tasks are listed in the following table:

Table 2: Summary of Simplified assessment Tasks

Task	Load set	Assessment type
Double the expected Acceleration	PSD G Acceleration X, Y, Z	Simplified Assessment Static

The applied assessment and material parameters are listed in tables below:

Table 3: Input parameters for tasks according to Simplified assessment

Parameter	Description	Unit	Value	Tasks
j_{stat}	Static safety factor	-	1	Double the expected pressure
K_p	Plast. notch factor	-	1	Double the expected pressure

Table 4: Material parameters for "Aluminum EN AW 6082 T6"

Parameter	Description	Unit	Value	Source
R_p	Yield stress	MPa	260	Material standard

4 Results

Under the assumptions concerning boundary conditions described in this document, the component shows sufficient resistance against cyclic and proof loads. For all applied assessment rules, the most severe occurring results are listed in the table below.

Table 5: Result Summary

Assessment rule	Loads assessed	Design parameter	Max. value	Limit
Simplified assessment	PSD G Acceleration X	a_{SK}	0,45	≤ 1
Simplified assessment	PSD G Acceleration Y	a_{SK}	0,27	≤ 1

Simplified assessment	PSD G Acceleration Z	a_{SK}	0,37	≤ 1

Results B, All Modes – Degrees of utilization on the structure

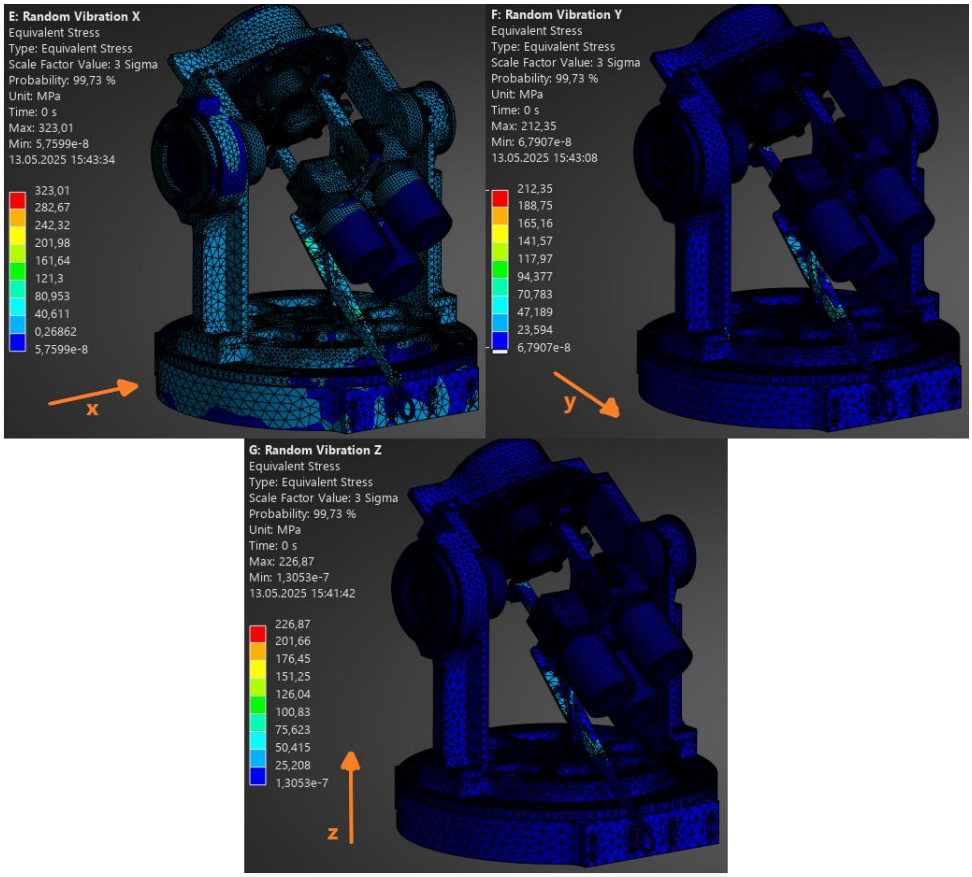


Figure 2: Degrees of utilization – Overview

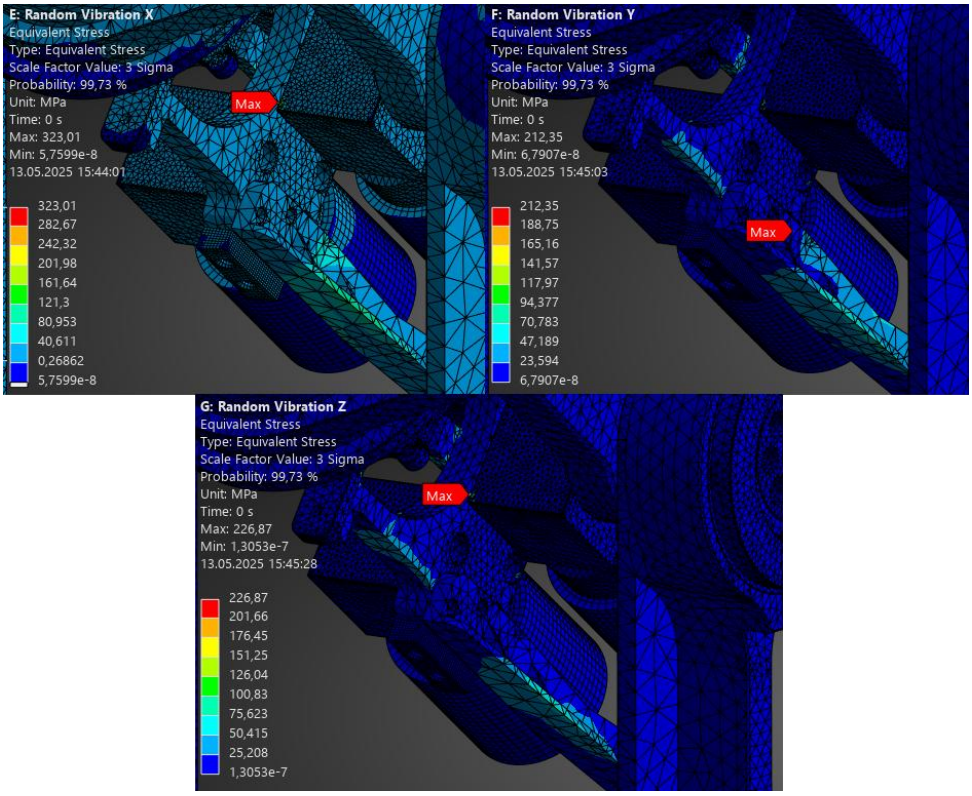


Figure 3: Degrees of utilization – Detail (Max Error)

List of Figures

E.1.1 Experimental test setup displaying the decoupled minimal prototype, localized sensor positioning, and 24 V electrical power interface. 257

E.1.2 Empirical Pitch Axis time-series data extracted from the motor-driver telemetry, illustrating angular command tracking, error residuals, and steady-state stability. 258

E.2.3 Measurement Setup 259

E.2.4 Directly Measured Power 260

E.2.5 Reference Measurements without Filter 260

E.2.6 Ratio of Power without Filter over with Filter 261

E.3.7 Locking Test 1 264

E.3.8 Post locking test 1 264

E.3.9 Locking Test 2 264

E.3.10 Post locking test 2 265

E.3.11 Locking Test 3 265

E.3.12 Post locking test 3 266

E.3.13 Locking Test 1 268

E.3.14 Post locking test 1 269

E.3.15 Locking Test 2 269

E.3.16 Post locking test 2 270

E.3.17 Locking Test 3 270

E.3.18 Post locking test 3 271

E.3.19 Vacuum Setup1 272

E.3.20 Vacuum Setup2 273

E.3.21 Vacuum Setup2 274

E.3.22 Vacuum Setup2 275

E.3.23 Vacuum Setup3 276

E.3.24 Updated Muffler design post testing. The red arrows indicate the additional Pad used to dampen the impact. The green arrow points at the orange Bolt retainer, which sheered of (as intended) and planted itself in the dampener due to the involved forces. 277

E.5.25 Position of accelerometers 280

E.5.26 Frequency search, before and after of sensor 1 (Cam) 281

E.5.27 Frequency search, before and after of sensor 2 (Arm) . . . 282
E.5.28 Frequency search, before and after of sensor 1 (Cam) . . . 283
E.5.29 Frequency search, before and after of sensor 2 (Arm) . . . 283
E.5.30 Frequency search Z axis, before and after of sensor 1 (Cam) . . . 284
E.5.31 Frequency search Z axis, before and after of sensor 2 (Arm) . . . 285
E.5.32 Frequency search X axis, before and after of sensor 1 (Cam) . . . 285
E.5.33 Frequency search X axis, before and after of sensor 2 (Arm) . . . 286
E.5.34 Frequency search Y axis, before and after of sensor 1 (Cam) . . . 286
E.5.35 Frequency search Y axis, before and after of sensor 2 (Arm) . . . 286
E.5.36 Sensor location . . . 288
E.5.37 Resonance survey compare, R1 in z-axis . . . 289
E.5.38 Resonance survey compare, R2 in z-axis . . . 289
E.5.39 Resonance survey compare, R3 in z-axis . . . 290
E.6.40 Gimbal pointing Test . . . 292
E.9.41 Partial test setup. Image 1 shows the open blackbox housing filled with liquid petroleum jelly for waterproofing the electronics. Image 2 shows how the blackbox spend 20 minutes at 4 °C in the refrigerator to regain firmness. . . . 295
E.9.42 Partial test setup. Image 3 shows the blackbox being submerged in room temperature tap water, and Image 4 shows how the blackbox spend 5 minutes fully submerged in water. . . . 295
E.9.43 Partial test setup. Image 5 shows the blackbox connectors being cleaned with isopropanol, and Image 6 shows how the blackbox was connected to a computer after the test with the image opened from it. . . . 295
E.10.44 Marking on the Camera Holder (indicated with red arrows) to show to allow the alignment of the cameras to a common parallel line. . . . 298
E.11.45 Measurement of filter transmissivity . . . 300
E.11.46 Reference Spectrum . . . 300
E.13.47 Short-circuit connector with ”remove before flight”-tag . . . 305

F.1.1 Thermal Simulation . . . 311
F.2.2 Simulated FOV . . . 311
F.2.3 Simulated Observation Errors 2026-03-20 . . . 312
F.3.4 Example of the optimal launch window end time estimation. . . . 314
F.3.5 Estimated optimal launch window for targets at 80 km. . . . 315

List of Tables

E.11.1 Filter measured for their spectrum. The central savelength and FWHM are as stated by the manufacturer 299